Past Climate
in South Am
Surrounding

From the Last Glac
to the Hol

Volume

Edited
FrançoiseVimeux, Fl
and Myriam

Past Climate Variability in South America and Surrounding Regions

Developments in Paleoenvironmental Research

VOLUME 14

Aims and Scope:
Paleoenvironmental research continues to enjoy tremendous interest and progress in the scientific community. The overall aims and scope of the *Developments in Paleoenvironmental Research* book series is to capture this excitement and document these developments. Volumes related to any aspect of paleoenvironmental research, encompassing any time period, are within the scope of the series. For example, relevant topics include studies focused on terrestrial, peatland, lacustrine, riverine, estuarine, and marine systems, ice cores, cave deposits, palynology, isotopes, geochemistry, sedimentology, paleontology, etc. Methodological and taxonomic volumes relevant to paleoenvironmental research are also encouraged. The series will include edited volumes on a particular subject, geographic region, or time period, conference and workshop proceedings, as well as monographs. Prospective authors and/or editors should consult the series editor for more details. The series editor also welcomes any comments or suggestions for future volumes.

For futher volumes:
http://www.springer.com/series/5869

Past Climate Variability in South America and Surrounding Regions

From the Last Glacial Maximum to the Holocene

Edited by

Françoise Vimeux

Institut de Recherche pour le Développement and Laboratoire des Sciences du Climat et de l'Environnement, Gif-sur-Yvette Cedex, France

Florence Sylvestre

Institut de Recherche pour le Développement and Centre Européen de Recherche et d'Enseignement des Géosciences de l'Environnement, Aix-en-Provence Cedex 4, France

Myriam Khodri

Institut de Recherche pour le Développement and Laboratoire d'Océanographie et du Climat, Gif-sur-Yvette Cedex, France

Springer

Editors
Françoise Vimeux
Institut de Recherche pour le Développement
HSM (CNRS, IRD, UM1, UM2) and IPSL/LSCE (CEA, CNRS, UVSQ)
CE Saclay, Orme des Merisiers
Bât. 701
91191 Gif-sur-Yvette
France
francoise.vimeux@lsce.ipsl.fr

Florence Sylvestre
Institut de Recherche pour le Développement
CEREGE (Université Aix-Marseille, CNRS, IRD)
Europôle de l'Arbois
BP 80
13545 Aix-en-Provence
France
sylvestre@cerege.fr

Myriam Khodri
Institut de Recherche pour le Développement
IPSL/LOCEAN (CNRS, IRD, UPMC, MNHN)
Boîte 100
4 place Jussieu
75252 Paris
France
myriam.khodri@ird.fr

ISBN 978-90-481-2671-2 e-ISBN 978-90-481-2672-9
DOI 10.1007/978-90-481-2672-9

Library of Congress Control Number: 2009926893

Cover illustration: Full disk image pair centered on South America. The images were made from a combination of AVHRR, NDVI, Seawifs, MODIS, NCEP, DMSP and Sky2000 catalog data, Photo credit: Image courtesy Nasa

Printed on acid-free paper

Springer is part of Springer Science+Business Media (www.springer.com)

Acknowledgments

We wish to thank all of the contributing authors. We are very pleased with the outcome of this book and we hope that the authors are as proud as we are.

All chapters benefited from a peer-review process. We would like to thank all the referees that dedicated time and efforts to make this book a valuable reference:

Mark Abbott, Emmanuel Chapron, John Chiang, Benjamin Lintner, Francisco Cruz, Valerio de Patta Pilar, Ricardo de Pol-Holz, Christine Delire, Laurent Dezileau, René Garreaud, Dominique Genty, William Gosling, Martin Grosjean, Simon Haberle, Henry Hooghiemstra, Vincent Jomelli, Meredith Kelly, Zhengyu Liu, Bryan Mark, Valérie Masson-Delmotte, Sarah Metcalfe, Christa Placzek, Antje Schwalb, Daniel Sigman, Christine Vallet-Coulomb, Mathias Vuille, Cathy Whitlock, Martin Williams.

Preface

South America is a unique place where a number of past climate archives are available from tropical to high latitude regions. It thus offers a unique opportunity to explore past climate variability along a latitudinal transect from the Equator to Polar regions and to study climate teleconnections. Most climate records from tropical and subtropical South America for the past 20,000 years have been interpreted as local responses to shift in the mean position and intensity of the InterTropical Convergence Zone due to tropical and extratropical forcings or to changes in the South American Summer Monsoon. Further South, the role of the Southern Hemisphere westerly winds on global climate has been highly investigated with both paleodata and coupled climate models. However the regional response over South America during the last 20,000 years is much more variable from place to place than previously thought. The factors that govern the spatial patterns of variability on millennial scale resolution are still to be understood.

The question of past natural rates and ranges of climate conditions over South America is therefore of special relevance in this context since today millions of people live under climates where any changes in monsoon rainfall can lead to catastrophic consequences.

We thus propose contributions that deal with tropical, temperate and high latitudes climate variability in South America with different type of archives and proxies on various timescales from the Last Glacial Maximum to the last thousand years. South America also offers a unique opportunity to examine climate fluctuations at various altitudes. The originality of this work is that it offers both observations and modelling works: we present contributions that aim at documenting paleoclimate histories and modelling studies are also included to help shed light on the relevant processes.

This book stems out from a 2006 Fall meeting American Geophysical Union (San Francisco, USA) session dealing with both overview and original researches on *Past climate variability from the last glacial maximum to the Holocene in South America and surrounding regions*. The 16 chapters in this volume are organized into three major parts. Part I, including 6 chapters, attempts at drawing a consistent picture for the Last Glacial Maximum in South America. Part II contains 4 chapters dealing with modern and past tropical and extra-tropical teleconnections with South America relying on both models and low to high latitudes ice core data comparison.

The third part of this book, containing the last 6 chapters, describes some aspects of the Holocene climate variability and specifically the southernmost part of South America which has been the subject of a growing attention during the recent years.

Contents

Part I Can We Draw a Robust Picture of Last Glacial Maximum Climate Conditions in South America?

1 Moisture Pattern During the Last Glacial Maximum in South America 3
Florence Sylvestre

2 Orbital and Millennial-Scale Precipitation Changes in Brazil from Speleothem Records 29
Francisco W. Cruz, Xianfeng Wang, Augusto Auler, Mathias Vuille, Stephen J. Burns, Lawrence R. Edwards, Ivo Karmann, and Hai Cheng

3 Chronologies of the Last Glacial Maximum and its Termination in the Andes (∼10–55°S) Based on Surface Exposure Dating 61
Roland Zech, Jacqueline Smith, and Michael R. Kaplan

4 Vegetation and Fire at the Last Glacial Maximum in Tropical South America 89
Francis E. Mayle, Michael J. Burn, Mitchell Power, and Dunia H. Urrego

5 Re-evaluation of Climate Change in Lowland Central America During the Last Glacial Maximum Using New Sediment Cores from Lake Petén Itzá, Guatemala 113
Mark B. Bush, Alexander Y. Correa-metrio, David A. Hodell, Mark Brenner, Flavio S. Anselmetti, Daniel Ariztegui, Andreas D. Mueller, Jason H. Curtis, Dustin A. Grzesik, Catherine Burton, and Adrian Gilli

6 Glacial to Holocene Paleoceanographic and Continental Paleoclimate Reconstructions Based on ODP Site 1233/GeoB 3313 Off Southern Chile 129
Frank Lamy and Jérome Kaiser

Part II The High Latitudes-Tropics and Tropics-Tropics Teleconnections over the Last Deglaciation and Last Glacial Maximum

7 Teleconnections into South America from the Tropics and Extratropics on Interannual and Intraseasonal Timescales . . 159
Alice M. Grimm and Tercio Ambrizzi

8 South American Climate Variability and Change: Remote and Regional Forcing Processes 193
Kerry H. Cook

9 Sensitivity of South American Tropical Climate to Last Glacial Maximum Boundary Conditions: Focus on Teleconnections with Tropics and Extratropics 213
Myriam Khodri, Masa Kageyama, and Didier M. Roche

10 Similarities and Discrepancies Between Andean Ice Cores Over the Last Deglaciation: Climate Implications 239
Françoise Vimeux

Part III Characteristics of the Holocene Climate. Focus on Global Events: Are They Widespread, Comparable and Synchroneous in South America?

11 Mid-Holocene Climate of Tropical South America: A Model-Data Approach 259
Pedro L. Silva Dias, Bruno Turcq, Maria Assunção F. Silva Dias, Pascale Braconnot, and Tatiana Jorgetti

12 Millennial-Scale Ecological Changes in Tropical South America Since the Last Glacial Maximum 283
Dunia H. Urrego, Mark B. Bush, Miles R. Silman, Alexander Correa-Metrio, Marie-Pierre Ledru, Francis E. Mayle, Gina Paduano, and Bryan G. Valencia

13 The Nature and Origin of Decadal to Millennial Scale Climate Variability in the Southern Tropics of South America: The Holocene Record of Lago Umayo, Peru 301
Paul A. Baker, Sherilyn C. Fritz, Stephen J. Burns, Erik Ekdahl, and Catherine A. Rigsby

14 Hydrological Variability in South America Below the Tropic of Capricorn (Pampas and Patagonia, Argentina) During the Last 13.0 Ka 323
Eduardo L. Piovano, Daniel Ariztegui, Francisco Córdoba, Marcela Cioccale, and Florence Sylvestre

15 Climate Change in Southern South America During the Last Two Millennia 353
Christopher M. Moy, Patricio I. Moreno, Robert B. Dunbar, Michael R. Kaplan, Jean-Pierre Francois, Ricardo Villalba, and Torsten Haberzettl

16 The Little Ice Age in Southern South America: Proxy and Model Based Evidence 395
Inka Meyer and Sebastian Wagner

Index 413

Contributors

Tercio Ambrizzi University of São Paulo, São Paulo, Brazil, ambrizzi@model.iag.usp.br

Flavio S. Anselmetti Eawag, Ueberlandstrasse 133, P. O. Box 611, 8600 Duebendorf, Switzerland, Flavio.Anselmetti@eawag.ch

Daniel Ariztegui Section of Earth Sciences, University of Geneva, 1205 Geneva, Switzerland, daniel.ariztegui@terre.unige.ch

Augusto Auler Instituto do Carste, Rua Kepler 385/04, Belo Horizonte, MG 30360-240, Brazil, aauler@terra.com.br

Paul A. Baker Duke University, Division of Earth and Ocean Sciences, Durham, NC 27708 USA, pbaker@duke.edu

Pascale Braconnot IPSL/ LSCE, Laboratoire des Sciences du Climat et de L'Environnement, Point courrier 129. CE Saclay, Orme des Merisiers, 91191 Gif sur Yvette cedex France, pascale.braconnot@lsce.ipsl.fr

Mark Brenner Department of Geological Sciences and Land Use and Environmental Change Institute (LUECI), University of Florida, Gainesville, FL 32611, USA, brennerl@ufl.edu

Michael J. Burn Department of Geography and Geology, The University of the West Indies, Mona Campus, Kingston 7, Jamaica, michael.burn@uwimona.edu.jm; School of GeoSciences, University of Edinburgh, Drummond Street, Edinburgh EH8 9XP, UK

Stephen J. Burns Department of Geosciences, Morrill Science Center, University of Massachusetts, Amherst MA 01003, USA, sburns@geo.umass.edu

Catherine Burton Department of Biological Sciences, Florida Institute of Technology, 150 W. University Blvd, Melbourne, FL, 32901, USA, cburton@fit.edu

Mark B. Bush Department of Biological Sciences, Florida Institute of Technology, 150 W. University Blvd., Melbourne, FL 32901, USA, mbush@fit.edu

Hai Cheng Department of Geology and Geophysics, University of Minnesota, Minneapolis, MN 55455, USA, cheng021@umn.edu

Marcela Cioccale Universidad de Chilecito, La Rioja, Argentina, mcioccale@hotmail.com

Kerry H. Cook Department of Geological Sciences, Jackson School of Geosciences, 1 University Station C1100, The University of Texas at Austin, Austin, TX 78712 USA, kc@jsg.utexas.edu

Francisco Córdoba CICTERRA-CONICET, Universidad Nacional de Córdoba, Av Velez Sarsfield 1611, X5016GCA, Córdoba, Argentina, franciscocordoba@efn.uncor.edu

Alexander Correa-Metrio Department of Biological Sciences, Florida Institute of Technology, 150 W. University Blvd, Melbourne, FL, 32901, USA, acorrea@fit.edu

Francisco W. Cruz Instituto de Geociências, Universidade de São Paulo, Rua do Lago, 562, CEP 05508-080, São Paulo-SP, Brazil, cbill@usp.br

Jason H. Curtis Department of Geological Sciences and Land Use and Environmental Change Institute (LUECI), University of Florida, Gainesville, FL 32611, USA, curtisj@ufl.edu

Robert B. Dunbar Department of Environmental Earth System Science, 450 Serra Mall, Braun Hall (Bldg. 320), Stanford University, Stanford, CA 94305-2115 USA, dunbar@stanford.edu

Lawrence R. Edwards Department of Geology and Geophysics, University of Minnesota, Minneapolis, MN 55455, USA, edwar001@umn.edu

Erik Ekdahl University of Nebraska, Department of Geosciences, Lincoln, NE 68588 USA, EEkdahl@waterboards.ca.gov

Jean-Pierre Francois Seminar für Geographie und ihre Didaktik, Universität zu Köln, Gronewaldstraße 2 D-50931, Köln, Germany; Department of Ecological Sciences and Institute of Ecology and Biodiversity, Universidad de Chile, Las Palmeras 3425, Ñuñoa, Santiago, Chile, geofrancois@gmail.com

Sherilyn C. Fritz University of Nebraska, Department of Geosciences, Lincoln, NE 68588, USA, sfritz2@unl.edu

Adrian Gilli Department of Geological Sciences and Land Use and Environmental Change Institute (LUECI), University of Florida, Gainesville, FL 32611, USA; Geological Institute, Swiss Federal Institute of Technology, ETH, 8092 Zurich, Switzerland, adrian.gilli@erdw.ethz.ch

Alice M. Grimm Federal University of Paraná, Department of Physics, Curitiba, Paraná, Brazil

Dustin A. Grzesik Department of Geological Sciences and Land Use and Environmental Change Institute (LUECI), University of Florida, Gainesville, FL 32611, USA, GrzesikD@ufl.edu

Torsten Haberzettl Institut des sciences de la mer de Rimouski (ISMER), University of Québec at Rimouski, 310, allée des Ursulines, Rimouski, Québec, G5L 3A1, Canada, torsten.haberzettl@uqar.qc.ca

David A. Hodell Department of Geological Sciences and Land Use and Environmental Change Institute (LUECI), University of Florida, Gainesville, FL 32611, USA, hodell@ufl.edu

Tatiana Jorgetti National Laboratory of Scientific Computing and Institute of Astronomy, Geophysics and Atmospheric Sciences, University of São Paulo, Rua do Matão 1226, Cidade Universitária, 05508-090, São Paulo, SP, Brazil, tatiana.jorgetti@model.iag.usp.br

Masa Kageyama IPSL, Laboratoire des Sciences du Climat et de l'Environnement (LSCE), UMR 1572 (CEA-CNRS-UVSQ), CE Saclay, Orme des Merisiers, Bât. 701, 91191 Gif-sur-Yvette Cedex, France, masa.kageyama@lsce.ipsl.fr

Jérome Kaiser GeoForschungZentrum (GFZ) Potsdam, Telegrafenberg, 14473 Potsdam, Germany, kaiserj@gfz-potsdam.de

Michael R. Kaplan Lamont-Doherty Earth Observatory of Columbia University, 61 Route 9 W – PO Box 1000, Palisades, NY 10964, USA, mkaplan@ldeo.columbia.edu

Ivo Karmann Instituto de Geociências, Universidade de São Paulo, Rua do Lago, 562, CEP 05508-080, São Paulo-SP, Brazil, ikarmann@usp.br

Myriam Khodri Institut de Recherche pour le Développement, IPSL/LOCEAN (CNRS, IRD, UPMC, MNHN), Boîte 100, 4 place Jussieu, 75252 Paris, France, myriam.khodri@ird.fr

Frank Lamy Alfred-Wegener-Institut (AWI) Bremerhaven, P.O. Box 120161, 27515 Bremerhaven, Germany, frank.lamy@awi.de

Marie-Pierre Ledru Institut de Recherche pour le Développement (IRD), UMR 203 ISEM Montpellier, France, Marie-Pierre.Ledru@ird.fr

Francis E. Mayle School of GeoSciences, University of Edinburgh, Drummond Street, Edinburgh, EH8 9XP, UK, Francis.Mayle@ed.ac.uk

Inka Meyer Marum – Centre for Marine Environmental Sciences University of Bremen, Bremen, Germany, minka@marum.de

Patricio I. Moreno Department of Ecological Sciences and Institute of Ecology and Biodiversity, Universidad de Chile, Las Palmeras 3425, Ñuñoa, Santiago, Chile, pimoreno@uchile.cl

Christopher M. Moy Department of Geological and Environmental Sciences, 450 Serra Mall, Braun Hall (Bldg. 320), Stanford University, Stanford, CA 94305-2115 USA, moyc@stanford.edu

Andreas D. Mueller Geological Institute, Swiss Federal Institute of Technology, ETH, 8092 Zurich, Switzerland, andreas.mueller@erdw.ethz.ch

Gina Paduano Department of Biological Sciences, Florida Institute of Technology, Melbourne, FL 32901, USA, drgmp11@yahoo.com

Eduardo L. Piovano CICTERRA-CONICET, Universidad Nacional de Córdoba, Av Velez Sarsfield 1611, X5016GCA, Córdoba, Argentina, epiovano@efn.uncor.edu

Mitchell Power School of GeoSciences, University of Edinburgh, Drummond Street, Edinburgh, EH8 9XP, UK; Curator Garrett Herbarium, University of Utah, Utah Museum of Natural History, Salt Lake City, UT 84112, USA, Mitch.Power@ed.ac.uk; mitchell.power@geog.utah.edu

Catherine A. Rigsby Department of Geological Sciences, East Carolina University, Greenville, NC 27858 USA, rigsbyc@mail.ecu.edu

Didier M. Roche IPSL, Laboratoire des Sciences du Climat et de l'Environnement (LSCE), UMR 1572 (CEA-CNRS-UVSQ), CE Saclay, Orme des Merisiers, Bât. 701, 91191 Gif-sur-Yvette Cedex, France, didier.roche@lsce.ipsl.fr

Miles R. Silman Department of Biology, Wake Forest University, Winston Salem, NC 27109, USA, silmanmr@wfu.edu

Maria Assunção F. Silva Dias National Laboratory of Scientific Computing and Centro de Previsão de Tempo e Estudos Climáticos (CPTEC), Rodovia Presidente Dutra, Km 40, SP-RJ 12630-000, Cachoeira Paulista, SP, Brasil, mafdsdia@model.iag.usp.br

Pedro L. Silva Dias LNCC, National Laboratory of Scientific Computing and Institute of Astronomy, Geophysics and Atmospheric Sciences, University of São Paulo, Av. Getulio Vargas, 333, Quitandinha 25651-075. Petrópolis, RJ, Brazil, pldsdias@iag.usp.br

Jacqueline Smith Department of Physical and Biological Sciences, The College of Saint Rose, Albany, New York, USA, smithj@strose.edu

Florence Sylvestre CEREGE, Université Aix-Marseille, CNRS, IRD, Europôle méditerranéen de l'Arbois, BP 80, 13545 Aix-en-Provence cedex 4, France, sylvestre@cerege.fr

Bruno Turcq IPSL/LOCEAN, Laboratoire d'Océanographie et du Climat: Expérimentation et Approches Numériques (UPMC/CNRS/IRD/MNHN), Institut de Recherche pour le Développement, 32 av Henri Varagnat, 93143 Bondy cedex, France, bruno.turcq@ird.fr

Dunia H. Urrego Department of Biological Sciences, Florida Institute of Technology, 150 West University Blvd., Melbourne, FL 32901, USA, durrego@fit.edu

Bryan G. Valencia Department of Biological Sciences, Florida Institute of Technology, Melbourne, FL 32901, USA, bguido@fit.edu

Ricardo Villalba Instituto Argentino de Nivología, Glaciología y Ciencias Ambientales (IANIGLA-CONICET), C.C. 330, (5500) Mendoza, Argentina, ricardo@lab.cricyt.edu.ar

Françoise Vimeux Institut de Recherche pour le Développement (IRD), Laboratoire Hydrosciences Montpellier (HSM) and Laboratoire des Sciences du Climat et de l'Environnement (LSCE), CE Saclay, Orme des Merisiers, Bât. 701, 91191 Gif-sur-Yvette Cedex, France, Francoise.Vimeux@lsce.ipsl.fr

Mathias Vuille Department of Earth and Atmospheric Sciences, University at Albany, Albany, USA, mathias@atmos.albany.edu

Sebastian Wagner Institute for Coastal Research, GKSS Research Center, Geesthacht, Germany, sebastian.wagner@gkss.de

Xianfeng Wang Department of Geology and Geophysics, University of Minnesota, Minneapolis, MN 55455, USA, wang0452@umn.edu

Roland Zech Geographical Institute, University of Bern, Switzerland, Roland.Zech@giub.unibe.ch

Part I
Can We Draw a Robust Picture of Last Glacial Maximum Climate Conditions in South America?

Chapter 1
Moisture Pattern During the Last Glacial Maximum in South America

Florence Sylvestre

Abstract The Last Glacial Maximum (LGM) is still an exciting period of time for investigating ecosystem responses to climate changes since it corresponds to a steady state in a glacial world with maximum global expansion of ice-sheets, CO_2 concentrations half those of today, temperatures up to 5°C cooler in the tropical lowlands, and precipitation regimes differed from today. South America is an ideal place to study these changes since climatic conditions during the LGM remain a matter of debate. There is general agreement that the temperature was cooler than today, but there is no consensus about moisture conditions, especially over tropical latitudes. This paper reviews terrestrial and near-shore marine records from South America between 10°N and 50°S during the LGM. Records are selected for their chronological control, their continuity around the LGM and their regional representativeness.

This review aims to show how regional climates of the sub-continent have responded to orbital forcing as opposed to other global glacial boundary conditions, and how they are related to positions of the Intertropical Convergence Zone (ITCZ) and of the westerly belt. A clear pattern emerges for the northern and the southern latitudes, which were respectively drier and wetter, but in the tropical lowlands the pattern remains unclear. The characterization of this area is of particular interest because of the central role played by atmospheric convection centred on the Amazon basin. Modeling experiments argue for drier LGM tropical conditions but several lines of evidence contradict these results. Currently, moister conditions are explained by a glacial boundary forcing mechanism implying a southern shift of the ITCZ and a reinforcement of the South American summer monsoon (SASM), bringing more humidity to the tropical Andes as far as southern Brazil. This hypothesis may explain a large portion of the ecosystem responses during the LGM, but does not account for all observed changes. Paucity of site reconstructions (e.g. in the Amazon basin), and lack of quantitative paleoclimatic responses derived

F. Sylvestre (✉)
CEREGE, Université Aix-Marseille, CNRS, IRD, Europôle méditerranéen de l'Arbois, BP 80, 13545 Aix-en-Provence cedex 4, France
e-mail: sylvestre@cerege.fr

F. Vimeux et al. (eds.), *Past Climate Variability in South America and Surrounding Regions*, Developments in Paleoenvironmental Research 14,
DOI 10.1007/978-90-481-2672-9_1,

from proxies to environmental conditions could partly explain the observed discrepancies. Regional responses of mosaic environmental ecosystems to a generally cooler temperature could be involved, without any need to invoke precessionnal and extra-tropical influences.

Keywords South America · Last Glacial Maximum (LGM) · Paleoclimates · Moisture pattern

1.1 Introduction

Since the international CLIMAP project (1981), a general consensus exists that the Last Glacial Maximum (LGM) climate was much colder, and for the most part, more arid than today. Currently available evidence suggests that intertropical areas probably cooled by 1–3°C in the surface ocean, and by about 4–6°C at moderate altitude on the continents (COHMAP 1988). Since then, from data and models, there is agreement that the tropics were cooler during the LGM, even if the magnitude of the cooling is not spatially uniform. For instance, Central America and northern South America cooled by 5–6°C, whereas regions peripheral to the Indian Ocean (southern and eastern Africa, India and Indonesia) cooled by 2–3°C (Farrera et al. 1999). Coupled atmosphere-ocean-sea-ice simulations suggest that the tropics and subtropics were considerably drier at the LGM than today (Shin et al. 2003). However, several paleoclimatic reconstructions based on proxy data contradict these findings and for several areas, moisture conditions remain a matter of debate. South America illustrates particularly this feature where climate conditions during the LGM are still highly documented by proxy data (Wang et al. 2004; Ledru et al. 2005; Cruz et al. 2005, 2006a, b; Wang et al. 2006; Fritz et al. 2007; Hodell et al. 2008), and investigated by both GCMs coupled and atmosphere-only versions (Shin et al. 2003; Wainer et al. 2005), and regional climate model (Cook and Vizy 2006; Vizy and Cook 2007).

Through this debate, the main question investigated by paleoclimatologists concerns the preferred location of the marine Atlantic Intertropical Convergence Zone (ITCZ) and the continental convection over the Amazon basin. In 1997, Bradbury commented that “to account for dry conditions during full and late glacial periods, the ITCZ is supposed to have resided farther north by South American workers (Martin et al. 1997) and farther south by North American workers”. More recently, Ti/Fe records off the coast of Venezuela showed the role of the North Atlantic sea surface temperature at millennial and orbital time-scales on the tropical hydrologic cycle (Peterson et al. 2000; Haug et al. 2001). This study suggests that a southerly mean position coincided with cooler north Atlantic sea surface temperature and reduced precipitation in the northern tropics; whereas during warm periods, the northern tropics were wetter and associated with weakened wind strength and a more northerly ITCZ position (Peterson et al. 2000; Peterson and Haug 2006). The reverse pattern is observed in the southern hemisphere tropics (Arz et al. 1998; Jennerjahn et al. 2004; Wang et al. 2004; Jaeschke et al. 2007). Both atmospheric

general circulation models (AGCMs) alone or coupled to a slab ocean explored these observations and suggested that the expansion or contraction of land- and sea-ice during the LGM or during millennial events can lead to a displacement of the ITCZ and produce precipitation asymmetries over tropical latitudes (Chiang et al. 2003; Claussen et al. 2003; Chiang and Bitz 2005).

Moreover this hypothesis dealing with the glacial boundary forcing is not exclusive from others mechanisms. Although less drastic than in the North (Petit et al. 1999; Alley 2004), cooling in Southern Hemisphere high latitudes has also played a central role in global climatic changes during the last glacial period. Model simulations suggest that the expansion of circum-Antarctic sea-ice has had a much stronger influence than Northern Hemisphere sea-ice, possibly because of its far greater areal extent (Chiang et al. 2003; Chiang and Bitz 2005). Antarctic sea-ice expansion reinforces the southern hemisphere meridional temperature gradients and forces the southern hemisphere oceanic and atmospheric frontal zones to move equatorward (Stuut et al. 2004; Stuut and Lamy 2004). Mechanisms originated from the tropics could also exert an influence on the climate. Variability in the precession-driven monsoon intensity (Ivanochko et al. 2005), tropical sea-surface temperatures (Visser et al. 2003), methane emission in tropical wetlands (Chappellaz et al. 1993; Severinghaus et al. 1998) and El Niño-Southern Oscillation (ENSO) mechanism (Cane 2005) may have had significant effects in high latitudes.

Testing these hypotheses for continental South America during the LGM is of particular interest. The LGM is defined by the lowest sea level and maximum ice volume (Mix et al. 2001). This time period has been the theatre of considerable debate for continental South America, especially for the tropical latitudes where moisture patterns showed distinct regional differences (Sylvestre et al. 1998; Baker et al. 2001a, b; Sylvestre 2002; Ledru et al. 2005; Smith et al. 2005a; Wang et al. 2006; Cruz et al. 2006a, b; Fritz et al. 2007; Hodell et al. 2008). Moreover, climatologists increased our knowledge about the present-day climate system of South America, describing the seasonal cycle of precipitation dominated by the South American Monsoon (SASM), its interannual variability and the remote forcing mechanisms acting over the system giving to the paleoclimatologists some keys for understanding the climatic changes at different time-scales during the past (Lenters and Cook 1997; Noguès-Paegle et al. 2002; Garreaud et al. 2003; Cook and Vizy 2006; Vera et al. 2006; Vizy and Cook 2007; Garreaud et al. in press; Cook, Chapter 8 of this volume).

The objectives of this paper are to review the best-dated terrestrial and near-shore marine paleoclimatic records from South America during the LGM. A detailed description of individual records is beyond the scope of this paper. The present review aims at highlighting the moisture pattern emerging from a set of well-dated sites representative of the main climatic regions of the continent. This review investigates a variety of terrestrial archives (pollen data, lake sediments and shorelines, speleothems and cores deposits, fluvial, periglacial and glacial deposits), as well as ice and near-shore marine cores. Records are selected for their chronological control, their continuity around the LGM and their regional representativeness. The reconstructions cannot provide accurate quantitative information about changes in

the magnitude or seasonality of rainfall. In most case studies, they offer observation-based evidence about whether the past climate was wetter or drier than the present day. This review is organized around the regions defined by their moisture sources. Throughout this manuscript, all ages are given in calendar ages, using Calib 5.01 (Reimer et al. 2004) or the polynomial equations of Bard et al. (1998) when original references provide ^{14}C ages. This review proceeds as follows. Section 1.2 summarizes the major contemporary climate features of South America. Figure 1.1 presents the modern settings of the South American continent summarizing the major features of the climatic system. This figure also shows the selected sites cited in the text, called S1, S2…, and listed in Table 1.1 with their main characteristics. Section 1.3 presents evidence for regional paleoclimate changes during the LGM, and discusses discrepancies, if any, between records of proxies. Figure 1.2 shows the main paleoclimatic characteristics of each selected sites, interpreted as wetter or drier conditions than today and summarizes the major paleoclimatic forcing mechanisms discussed in the following section. Section 1.4 identifies recent progress and unresolved questions about key paleoclimatic issues.

1.2 Modern Climate

By its continental mass extension across the equator from about 10°N to 55°S, South America displays a large distribution from tropical to extratropical climates. This distribution is defined by several regional and remote factors, in primary order the shape and the topography of the continent (e.g. the Andes mountains, the Amazon rain forest). Its vicinity to the surroundings oceans and its relationships between sea surface temperature (SST) anomalies in association with El Nino/Southern Oscillation (ENSO), the Pacific Decadal Oscillation (PDO), the Antarctic Annular Modes, or the North Atlantic oscillation (NAO) constitute also significant impacts on the climatic variability over the continent (Garreaud et al. in press).

Today, the seasonal precipitation cycle over South America is dominated in tropical latitudes by a monsoon-like system, the South American Summer Monsoon (SASM) (Zhou and Lau 1998; Barros et al. 2002; Noguès-Paegle et al. 2002; Vera et al. 2006) which involved two main components: (i) a near equatorial one associated with the Atlantic Convergence Zone (ITCZ) and convection over Amazonia, and (ii) a subtropical one associated with the South Atlantic Convergence Zone (SACZ) and related features over southeast South America (30/32°S) (Fig. 1.1). These features are connecting through a large-scale atmospheric circulation comprising a low-level jet (Vera et al. 2006). This low-level jet (LLJ) originating in the northern part of South America at the foot of the Andes, is driven by the Chaco Low to provide moisture for subtropical latitudes (Noguès-Paegle and Mo 1997; Labraga et al. 2000). Over that region, the seasonal development of the SACZ results of the confluence of the low-level jet moisture transport with the northeasterly winds coming from the South Atlantic High and the mid-latitude westerly flow on the southern boundary of the South Atlantic High (Saulo et al. 2000). Noguès-Paegle

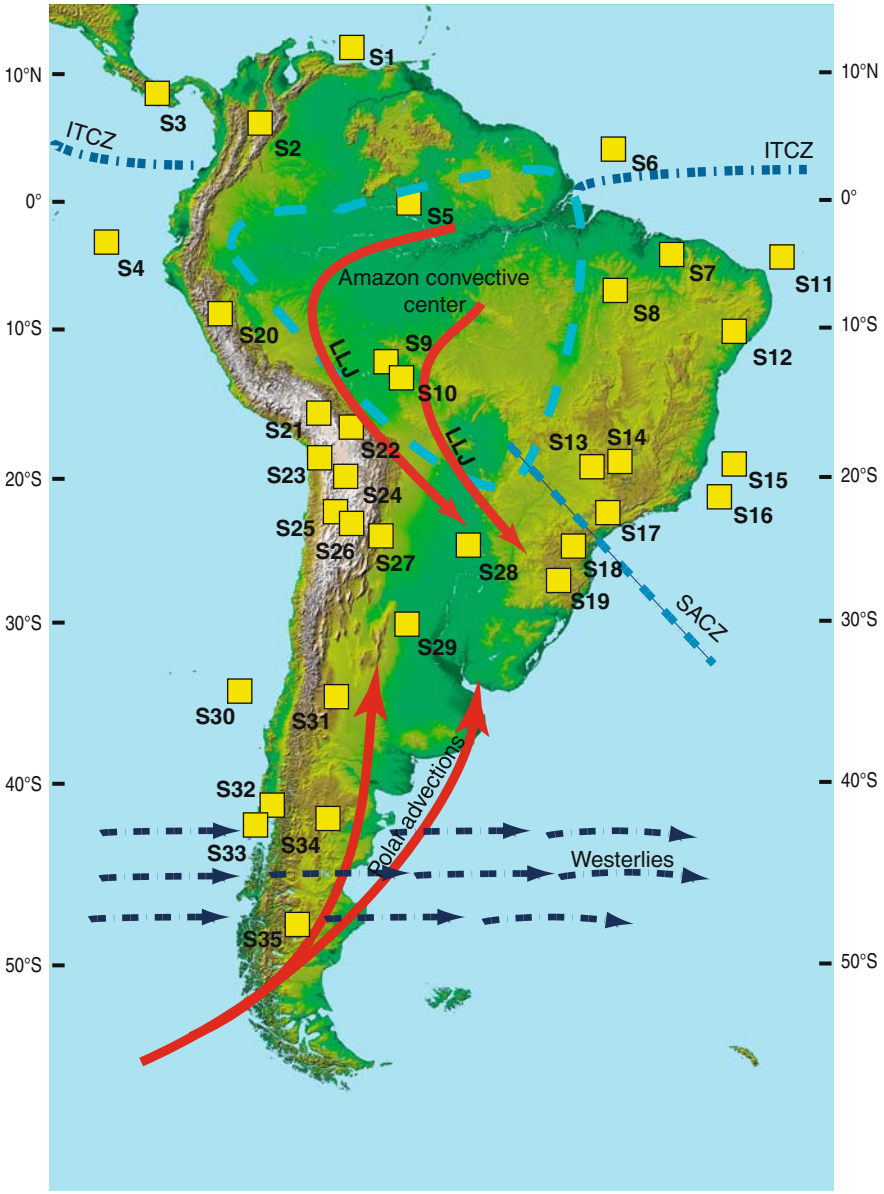

Fig. 1.1 Present-day South America: physical characteristics of the continent with the location of the major atmospheric features of the climatic system (ITCZ, Amazon convection, SACZ, LLJ, Westerlies) and location of the selected sites (S1, S2. . . . are listed in Table 1.1 for names and main characteristics)

Table 1.1 Site name, coordinates (latitude, longitude, elevation), location, archives and original references

N°	Site	Latitude	Longitude	Elevation (m.a.s.l.)	Country	Archives	References
S1	Cariaco	10°40′N	65°W	_	Venezuela	Marine core	Peterson et al. 2000; Haug et al. 2001
S2	Fuquene	5°45′N	73°77′W	2580	Columbia	Lake	Van Geel and Van der Hammen 1973
S3	El Valle	8°45′N	81°20′W	500	Panama	Lake	Bush et al. 1992
S4	Tr 163-31	3°23′S	83°21′W	–	Ecuador	Marine core	Heusser and Shackelton 1994
S5	Pata	0°16′N	66°41′W	300	Brazil	Lake	Colinvaux et al. 1996
S6	ODP site 932	5°12′N	47°1.8′W	–	Brazil	Marine core	Haberle and Maslin 1999
S7	Caço	2°58′S	43°25′W	120	Brazil	Lake	Sifeddine et al. 2003
S8	Carajas	6°35′S	49°30′W	700–800	Brazil	Lake	Sifeddine et al. 2001
S9	Lake Bella Vista	13°37′S	61°33′W	600–900	Bolivia	Lake	Burbridge et al. 2004
S10	Lake Chaplin	14°24′S	61°04′W	600–900	Bolivia	Lake	Burbridge et al. 2004
S11	GeoB3104-1	3°40′.0′S	37°43.0′W	–	Brazil	Marine core	Arz et al. 1999
S12	Bahia TBV-TBR	10°10′S	40°50′W	500	Brazil	Speleothems	Auler and Smart 2001; Wang et al. 2004
S13	Lake Serra Negra	19°S	46°57′W	1170	Brazil	Lake	DeOliveira 1992
S14	Salitre	19°S	46°46′W	1050	Brazil	Lake	Ledru 1993
S15	GeoB 3229-2	19°38′S	38°43′W	–	Brazil	Marine core	Behling et al. 2002
S16	GeoB 3202-1	21°37′S	39°58′	–	Brazil	Marine core	Behling et al. 2002
S17	Colônia	23°52′S	46°42′W	900	Brazil	Lake	Ledru et al. 2005
S18	St8 Santana Cave	24°31′S	48°43′W	500	Brazil	Speleothems	Cruz et al. 2006b
S19	Botuverá Bt2	27°13′S	49°09′W	250	Brazil	Speleothems	Cruz et al. 2006a; Wang et al. 2006
S20	Huascaran	9°06′S	77°36′W	6048	Peru	Ice core	Thompson et al. 1995

Table 1.1 (continued)

N°	Site	Latitude	Longitude	Elevation (m.a.s.l.)	Country	Archives	References
S21	Titicaca	16-17°50′S	68°50′–70′W	3815	Bolivia	Lake	Ybert 1992; Barker et al. 2001
S22	Illimani	16°37′S	67°46′W	6350	Bolivia	Ice core	Ramirez et al. 2003
S23	Sajama	18°06′S	68°53′W	6542	Bolivia	Ice core	Thompson et al. 1998
S24	Coipasa-Uyuni	20°S-	17°W	3653	Bolivia	Lake	Sylvestre et al. 1999; Baker et al. 2001; Fritz et al. 2004
S25	Salar de Atacama	23°30′S	68°25′W	2300	Chile	Lake	Bobst et al. 2001
S26	Lakes Lejia/Miscanti	23°44′S	67°46′W	4140	Chile	Lake	Grosjean 1994; Grosjean et al. 2001
S27	Santa Maria basin/Quebrada del Torro	25°S	66°W	2000	Argentina	Lake/landslide	Trauth and Strecker 1999; Trauth et al. 2000
S28	Alto Parana	22°43′S	53°10′W	250–320	Argentina	Fluvial deposits	Stevaux 2000
S29	Mar Chiquita	30°S	62°W	72	Argentina	Lake	Piovano et al. 2002
S30	GeoB 3302-1	33°S	73°W	–	Chile	Marine core	Lamy et al. 1999
S31	Salinas Bebedero	33°33′S	66°75′W	380	Argentina	Lake	Gonzalez 1994; Gonzalez and Maidana 1998
S32	Chilean Lake District	39–42°S	73–74′W	50–70	Chile	Lake	Heusser 1989; Markgraf 1989; Moreno et al. 1999
S33	Huelmo site	41°30′S	73°00 W	10	Chile	Lake	Massaferro et al. 2009
S34	Cari Laufquen	41°13′S	69°42′W	800	Argentina	Lake	Galloway et al. 1988
S35	Cardiel	49°S	71°25′W	276	Argentina	Lake	Stine and Stine 1990

and Mo (1997) describe an intraseasonal meridional seesaw of dry and wet conditions over tropical and subtropical South America in which SACZ and low-level stream intensify alternatively. Weak SACZ is accompanied by enhanced rainfall over northern Argentina and southern Brazil. These positive rainfall anomalies are supported by a strong vertically integrated southward moisture flux at about 35°S–60°W that shifts eastward to about 40°W for the opposite phase of the seesaw in accordance with an eastward displacement of the Atlantic high. An intensified SACZ is associated with enhanced streamflows to the north (the Parana and Paraguay) and diminished flows to the south (the Uruguay and Negro) (Robertson and Mechoso 2000). This north-south separation is probably related with the anomalously warm sea surface temperatures (SSTs) over tropical and subtropical South Atlantic that strengthens the low-level meridional temperature gradient, intensify the South Atlantic High and consequently the trade-winds (Robertson et al. 2000).

At inter-annual to decadal and longer time-scale variability, changes in ITCZ position and intensity affect continental Amazonian convection through large-scale ascent and low level convergence of the trade winds (Robertson and Mechoso 2002). The variability in Atlantic cross-equatorial SST gradients, from inter-annual to decadal timescales, results from local and remote processes (ENSO, NAO) (Noguès-Paegle et al. 2002; Garreaud et al. in press). Changes in SACZ position and intensity are reflected in SST anomalies over the southwest Atlantic (Barros et al. 2000; Robertson et al. 2000). Large intrinsic inter-annual variability of the SACZ is modulated by ENSO, and imprinted on the Atlantic SST.

Another important climatic feature is the non periodic incursions of polar outbreaks east of the Andes, near the ground that reach tropical latitudes, and generate important drop in temperature, high pressures and could produced important rains (Garreaud 2000; Marengo and Rogers 2001). These surges occur mainly during the winter but their impact on the precipitation is even greater during summer (Garreaud and Wallace 1998).

The southern latitudes of the continent (∼45°S) are characterized by the influence of the southern westerlies. Resulting from the interplay between the Pacific high-pressure cell and the polar low-pressure belt, south of 45°S, the cyclonic activities of the westerlies is permanent throughout the year providing high precipitation. Northwards, during winter, when Antarctic sea ice expands and the Humboldt Current is strengthened, the equator-to-pole temperature gradient is steepest and the Polar Front shifts northward by about 7° of latitude. North of 34°S, the strong influence of the subtropical high pressure belt is one of the main reasons for extreme aridity in this area. Northward penetration of atmospheric perturbations from the westerlies is possible when the southeast Pacific anticyclone is weakened or moves equatoward, allowing penetration of westerly storm tracks to latitudes as far north as 31°S. In the Andes, winter rains reach further north (Vuille and Amman 1997). During summer, the Pacific anticyclone shifts southward, impeding the northward migration of the westerlies.

1.3 Evidence of Regional Paleoclimatic Changes

1.3.1 Northern South America

Varved sediments from the Cariaco basin off the coast of Venezuela (S1) preserve an exceptionally high-resolution record of hydrologic variability through the last glacial cycle (Hughen et al. 1996; Peterson et al. 2000). The basin is situated near the northern limit of the modern seasonal range of the ITCZ and thus experiences a large rainfall cycle, which results in deposition of laminated sediments. Deposition of dark-coloured varves (summer rainy season/weaker easterlies/ITCZ north) and light plankton-rich varves (dry winter season/strong northeasterlies/ITCZ south) provide evidence that significantly cooler and more arid conditions prevailed on the northern margin of the continent during the LGM.

The lake records are consistent with glacial aridity in this region and in neighbouring Central America (Bradbury et al. 2001). Sites include Lake Fuquene and El Abra Valley region, Colombia (S2; van Geel and van der Hammen 1973; van der Hammen and Hooghiemstra 2000), and Lake El Valle, Panama (S3; Bush and Colinvaux 1990). A pollen record of equatorial Andean vegetation from a near-shore marine core collected 300 km west of Ecuador revealed an extended dry and cool glacial period (S4; Heusser and Shackelton 1994).

These data provide a consistent picture of enhanced glacial aridity in northern South America.

1.3.2 Amazon Basin

In the Amazon basin, the pattern is more complex. Some studies indicate biome stability under a persistently wet, cooler climate (Colinvaux et al. 2000). Pollen records from Lake Pata (S5; Colinvaux et al. 1996) and from ODP site 932 (S6) in the mouth of the Amazon (Haberle and Maslin 1999) attest to forest stability and imply that moisture availability remained sufficiently high to support tropical rain forest through the LGM. But Ledru et al. (1998) suggest in their re-evaluation of the Colinvaux et al. (1996) pollen record that the climate was drier during the LGM over this region. Furthermore, they suggest that there was a hiatus or interruption in the observed sediment record for this time period due either to an absence of sedimentation and/or erosion of previously deposited sediments. In Northeastern Brazil (Nordeste), a semiarid region today, the full glacial sediments in Lake Caçó (S7) were dominated by non-arboreal pollen elements indicating a dry climate associated with high quartz contents caused by strong aeolian sand transport (Sifeddine et al. 2003). At Serro dos Carajás (S8), a hiatus in sedimentation is mentioned between ca. 23.6 and 15.2 ka, suggesting lake desiccation and a very dry interval (Absy et al. 1991; Sifeddine et al. 1994). In the southwestern limit of Amazonia, Lake Bella Vista (S9) shows a major sedimentary hiatus spanning the LGM whereas in Lake Chaplin (S10) pollen records characterized savannas and seasonally dry semideciduous forests (Burbridge et al. 2004). However, off Fortaleza (S11), Arz et al.

(1999) reported elevated concentrations of Ti and Fe in sediments of the last glacial period. These are attributed to increased river runoff and more humid conditions. Pollen spectra from the same core demonstrate that these increases in the transport of terrigenous material reflect short wet intervals (38.2, 28.2 ka) in a generally dry LGM context (Behling et al. 2000). Wetter LGM conditions in Nordeste are also indicated by travertine and speleothem deposits from local caves (S12; Auler and Smart 2001; Wang et al. 2004).

1.3.3 Southern Brazil

In this region, from pollen records, the climate was markedly drier as indicated by the replacement of the *Araucaria* and cloud forests by grassland (Behling and Hooghiemstra 2001; Behling 2002). The pollen record of Serra Negra (S13) shows alternating cold and warm conditions, suggesting a time-transgressive mosaic of different forest types reflecting a very cold climate with alternating moister and drier phases for the period ca. 40–17 ka (DeOliveira 1992). A possible hiatus in the record during this period, including the full glacial time, cannot be excluded (Ledru et al. 1998). At Salitre (S14), an 11 000 year gap was detected between 33.6 and 19.8 ka (Ledru et al. 1998). These colder and drier conditions in this area have been confirmed by the analysis of the pollen content from off-shore marine cores drilled in the drainage areas of two major SE Brazilian rivers, the Rio Doce and the Rio Paraiba do Sul (S15–S16; Behling et al. 2002). More recently, the Colônia site (S17) offers a long record spanning the 140,000 years (Ledru et al. 2005, 2009). First interpreted as wet (Ledru et al. 2005), the LGM in this record has been re-interpreted as a rainforest regression period (Ledru et al. 2009). In view of its poorly constrained chronology, this record needs more investigation.

Nevertheless, the available pollen data suggesting cooler and drier conditions contradict the results inferred from stalagmite records (S18–S19; Cruz et al. 2006a, b; Wang et al. 2006) from Santana and Botuverá caves.

1.3.4 Central Andes: Peru, Bolivia and North Chile

In the Peruvian and Bolivian Andes, the temperature and moisture patterns are clearer. The LGM is recorded in the northern Bolivian Altiplano in long sediment cores recovered from both deep and shallow areas of Lake Titicaca (S21). Cores from the deepest part of Lake Titicaca show that it was deep and fresh from before 25 to 15 ka (Baker et al. 2001a). From the shallower part, sedimentological and palynological studies show that the level of the lake was 17 m below its outlet between ca. 24.7 and 21.2 ka (Wirmann et al. 1992; Ybert 1992). In the southern Bolivian Altiplano, the LGM is recorded in cores recovered from the centers of the Coipasa and Uyuni salars (S24). From the salar of Coipasa, a high-resolution diatom study showed that this basin was filled by a shallow salt lake between 24.6 and 20.9 ka,

implying more humid conditions than today (Sylvestre et al. 1998; Sylvestre 2002). This shallow phase is confirmed by ^{14}C datings from deposits on the margin of the salar of Uyuni, defining the "Sajsi Lake cycle" between 24 and 20.5 ka (Placzek et al. 2006). From a long-core drilled in the salar of Uyuni, natural γ-radiation measurements show that the basin was filled continuously between 26.1 and 14.9 ka (Baker et al. 2001b).

Three continuous ice core records from the high Andes, Huascaran (S20, Thompson et al. 1995), Nevado Illimani (S22, Ramirez et al. 2003) and Sajama (S23, Thompson et al. 1998) date back to the last glacial stage. The paleoclimatic information is principally deduced from the isotopic composition ($\delta^{18}O$ and δD) of the ice. These three records reveal a regionally coherent transition from glacial to modern climate conditions north of 20°S. The isotopic records reach full glacial conditions at about 20–18 ka. From low full glacial isotope values, both the Huascaran and Illimani isotope values rise to a pronounced early Holocene optimum then decline progressively to modern values (Thompson et al. 1995; Ramirez et al. 2003). The Sajama record differs from the other two ice cores because it shows a rapid change at the end of the LGM, marked by the isotopically most enriched values in the entire record (Thompson et al. 1998). Thompson et al. (1995, 1998, 2000) have interpreted this as a temperature proxy, using the slope of the classical isotope temperature relationship for high latitudes of about 0.7‰/°C. They estimated an 8–12°C temperature change at high elevation for the tropics. But several studies have demonstrated that in tropical regions, the atmospheric cycle of water isotopes is much more complex and atmospheric temperature variations are not entirely related to condensation (Pierrehumbert 1999; Hoffmann 2003; Vimeux et al. 2005). Based on a modern calibration (e.g. isotopic composition of monthly precipitation), it was demonstrated that local temperature and rainout effect have no control on δD variations which are mainly explain by the moisture transport history and the air masses distillation along their trajectory (Vimeux et al. 2005). This study also shows that during the LGM, from the base to the top of the Andes at the tropical latitude, less than 10% of the isotopic variation is explained by temperature change, mostly is supported by wetter conditions along air masses trajectory (Vimeux et al. 2005).

For the tropical Andes, there are several studies of late Quaternary moraines and fluvio-glacial deposits reviewed by in different papers, Clapperton (1993), Klein et al. (1999), Heine (2000), Smith et al. (2005b), Zech et al. (2008) and Smith et al. (2008). But the chronology consists mostly of minimum limiting ages. It is difficult to know if the glacial reconstructions are Late Glacial, LGM, or even pre-LGM in age. From Central America to the Central Andes, a pronounced glacial period is observed before 28 ka. Some studies show an earlier deglaciation than in the Northern Hemisphere at ~22–19.5 ka (Seltzer et al. 2002). Others studies suggest a glacial period comprising the pre-LGM to the Late Glacial. This is particularly the case of the Ecuadorian Andes where deposits of "full glacial" age date broadly between 38.7 and 11.1 ka (Clapperton 1993). In the Peruvian and Bolivian Andes, a new chronology based on 106 beryllium-ages indicates that glaciers reached their greatest extent in the last glacial cycle ~34 ka and were retreating by ~21 ka (Smith

et al. 2005a). This full glacial period is disrupted by a glacial retreat between 22.4–18.2 ka followed by a second glacial period (18.2–14.2 ka) during the deglaciation (Servant et al. 1995). Others studies involving the surface exposure dating method suggest that the LGM in Bolivia occurred between 20 and 25 ka (Zech et al. 2008). Based on a regional study of ELA depression in the southern tropical Andes (8–22°S), including a glacier mass balance and adjusted for a sea-level fall of −120 m a.s.l., a glacial maximum temperature value is estimated at 4.7±0.8°C (Porter 2001).

In North Chile, the situation is more controversial. In this area, a long continuous record from the Salar of Atacama show an extended wet period from 53.4 to 15.3 ka, with a maximum wet phase from 26.7 to 16.5 ka (S25; Bobst et al. 2001). At higher elevations, east of the Salar de Atacama, Messerli et al. (1993), Geyh et al. (1999) and Grosjean et al. (2001) have investigated certain small lakes. Earlier works on a 4 m-long section from Laguna Lejía (S26) showed freshwater lake deposits in a basin now occupied by a saline lake (Grosjean 1994). The dating of this lake section has been controversial because of the reservoir correction needed for carbonate sediments and aquatic organic matter. More recent dating with reservoir corrections place the beginning of the Laguna Lejía lake sequence at 15.5–14 ka (Geyh et al. 1999). A second 10 m-long section from Laguna Miscanti (S28) with the same dating problem showed an initial shallow freshwater lake (ca. 25.9 ka) (Grosjean et al. 2001). This lake disappeared during the extremely dry conditions of the LGM. These Altiplano lakes do not record the pre-LGM and LGM wet interval evident in the Salar de Atacama (26.7–16.5 ka). A paleoclimate record was also obtained from rodent middens and palaeowetland deposits from the Tilomonte area, few kilometers southeast of the Salar de Atacama (Betancourt et al. 2000). Rodent middens of LGM and late glacial age are rare and they are entirely absent from 35 to 22 ka. These deposits appeared only between 16.2 and 10.5 ka and are interpreted as periods with elevated water tables and wetter climates. Once again, there is a discrepancy with the record of the Salar de Atacama.

The chronology of the glacial history in Northern Chile remains uncertain (Zech et al. 2008). An overview including the glacier reconstruction between 18° and 29°S suggests that in the north (18°–25°S), the glaciations occurred during the Late Glacial times when convective precipitation during the austral summer increased (Ammann et al. 2001). To the south (∼27–29°S), the age of the glaciations are highly speculative too, but probably "pre-LGM" and "post-LGM" suggesting that under the control of the precipitation in this latitude, the conditions during the full-LGM were too arid (Zech et al. 2008).

1.3.5 Central Plains of Argentina

From the central plains of the Argentina (25°S–30°S), we have very few well-dated sites. One study based on a reliable chronology of large landslides in narrow valleys and accompanying lacustrine phases shows two wet phases concentrated in

two time periods during late Quaternary times (S27; Trauth and Strecker 1999; Trauth et al. 2000). The earlier cluster is dated between 40.4 and 29.3 ka, while the younger cluster is dated after 5.6 ka. The late Pleistocene cluster includes a series of landslides in two basins ("Quebrada del Toro", "outlet of the Santa Maria Basin"). In addition, multiple landslides near Villa Vil and the Quebrada del Tonco, as well as a paleo-lake near La Poma, may also have occurred during this time period. A geomorphological study of alluvial deposits from the Upper Parana River indicates drier conditions between ca. 40 and 8.9 ka, with a thermoluminescence dating at 23,540±2240 yr associated with intensive eolian activity in a forest-free environment (S28; Stevaux 2000). Preliminary results from a long lacustrine core covering the last full glacial stage from the Lake Mar Chiquita (S29) indicates a low lake-level suggesting drier conditions during the LGM (Piovano et al. 2008). Although data are sparse, it seems that the LGM in this area was more arid than today.

1.3.6 Southern South America

In this region, the paleoenvironmental studies have been driven by the question concerning the latitudinal position of the Southern Hemisphere westerlies during the last glaciation (Heusser 1989; Markgraf 1989; Lamy et al. 1999; Stuut and Lamy 2004; Lamy et al. 2004). From the western part of the continent, this question has been investigated by documenting the LGM precipitation regimes from records in the Chilean Lake District (S32; 39–42°S). Cold and dry climate have been inferred from Canal de Chanchán (40°56′S, 72°52′W) and Canal de la Puntilla (40°57′S, 72°54′W) based on the predominance of grasses and Compositae in pollen records (Heusser 1974, 1981; Markgraf 1983, 1984, 1987, 1989). However, a cold and wet climate have been proposed from Canal de Chanchan based on fossil beetle assemblages (Hoganson and Ashworth 1992) which has been confirmed by pollen analysis (Moreno 1997; Moreno et al. 1999). A recent chironomid and pollen records from the Huelmo site (S33; Massaferro et al. 2009) suggests equally cold and wet conditions during the LGM. A radiocarbon chronology based on glacial deposits from the Chilean Lake District and the Isla Grande do Chiloé show that the piedmont glacier lobes achieved maxima at 17.5, 24.7, 27, 31.5, 34.5 and >38.8 ka in a cold and wet environment suggesting that mean summer temperatures were 4°C to 5°C below present values (Lowell et al. 1995). This inference accords with results from a coupled ice sheet/climate numerical model showing a lowering of 6°C (Hulton et al. 2002).

Comparable advances have been recognized in the Strait of Magellan (Clapperton 1993). Finally, extensive analyses of changes in terrigenous sediment input along the central and northern Chilean margin from marine cores (30; 33°S) show that the glacial climates (28–18 ka) were generally cold and humid with a cold semi-arid interval between 26 and 22 ka (Lamy et al. 1998, 1999, 2000). Consistent with terrestrial climate reconstructions, the paleoceanographic reconstructions

suggest a ∼5° latitudinal northward shift of both oceanographic and atmospheric circulations systems (Lamy and Kaiser 2009).

From the eastern part of the Andes, in the Pampas plains, two paleolimnological studies from Salinas del Bebedero (S31; 33°S) and from Cari Laufquen (S34; 41°S) show high stands between 23.6 and ca. 15.2 ka, and between 21.7 and 15.2 ka, respectively (González 1994; Galloway et al. 1988). Further south, in southern Patagonia, at 49°S, Lake Cardiel (S36) was characterized by intermediate to low lake levels at 23.5 ka and by transgressive lake deposits with a minimum age of 36.5 ka, and possibly related strandlines, indicating a very high level preceding the full glacial period (Stine and Stine 1990).

1.4 Discussion

The focus on the LGM is of particular interest in revealing how ecosystems have responded to different global boundary conditions compared with present; namely, maximum global expansion of ice-sheets, CO_2 concentrations half those of today, lowered temperatures and changing precipitation regimes. In the context of cooler conditions, this review derived from paleodata records reveals several interesting results and helps to clarify several questions concerning the moisture pattern that prevailed during the LGM over the continent and near-shore areas of South America.

From the northern latitudes of the continent, a clear pattern is evident with prevailing drier conditions; strong evidence of wetter conditions over a large range of latitudes covering the southern half of South America argue for the equatoward displacement of the westerlies. The prolonged debate over whether or not the LGM westerlies were displaced equatoward (Heusser 1989) or poleward (Markgraf 1989), although constrained by evidence from glacier fluctuations (Clapperton 1993; Lowell et al. 1995), marine cores (Lamy et al. 1999) and modeling studies (Hulton et al. 2002) seems resolved in favour of a northward shift. However, a recent study using four coupled ocean-atmosphere simulations evidences any significant shift in the westerly circulation during the LGM (Rojas et al. 2008). In the subtropical areas, it is still difficult to clarify a pattern due to the paucity of the paleoclimatic reconstructions, but the available data converge towards a drier pattern during the LGM. The pattern is also clear in the tropical Andes where wetter conditions seem to have prevailed during the LGM, except in North Chile where paleodata are still controversial and further investigations will need a more rigorous dating strategy.

Finally, the major questions addressed by this review are highlighted by the equivocal moisture pattern in the tropical lowlands (e.g. Amazon basin, Nordeste, Southern Brazil). More humid conditions are documented on the Atlantic margin of the continent (e.g. Amazon Fan, Nordeste) and in the Amazon basin, whereas an “arid corridor” is observed from Lake Caço to the lowlands of Bolivia. This unclear situation is partly due to the paucity of LGM records, with most located on the periphery of the basin (except Lake Pata) and so not necessarily reflective of the entire Amazon ecosystem. Conflicting discussions concerning the interpretation of the pollen spectra, their significance and paleoclimatic inferences are still

continuing (see discussion by Mayle et al., Chapter 4 of this volume). Global coupled atmosphere-ocean models simulate drier conditions under tropical latitudes (Farrera et al. 1999; Shin et al. 2003). Some of them simulate a global mean LGM specific humidity 10% less than the present-day simulation (Bush and Philander 1998). Some regional model climate experiments point to a reduction of 25%–35% in total annual rainfall in most parts of the basin (Cook and Vizy 2006). Even if there is no pollen data to support a savanna-dominated Amazon basin, both data and models suggest a substantial reduction of the rainforest coverage. Characterizing the LGM ecosystems in the Amazon basin is of high interest given the central role of convection in this basin and the re-distribution of vapour water at the tropical scale. The pattern is also conflicting in the tropical lowlands of southern Brazil. The speleothem records suggest humid conditions (Cruz et al., Chapter 2 of this volume) whereas pollen records point to a complete dominance of grasslands over forests due to colder and dryer conditions (Behling 2002; Ledru et al. 2009). In this region, it is difficult to invoke the paucity of the records because there are several (e.g. Behling 2002). The discrepancy between these records could be related to the response of the proxies to changes in environmental conditions. For instance, in the context of the LGM, lowered atmospheric CO_2 concentrations, in combination with a longer dry season, caused expansion of dry forests and savannas. Several questions are raised by this conflicting reconstruction and need to be investigated, in the sense that the location of these sites would clarify the intensity and role of the SACZ during the LGM, a question still poorly addressed.

What does it mean in term of climatic mechanisms? Figure 1.2 summarizes the possible climate forcing mechanisms discussed in the following paragraphs. In South America, past changes in tropical rainfall are currently explained by climate forcing mechanisms acting on both orbital and millennial time-scales, such as insolation precession (Clement et al. 2004) and land/sea-ice coverage in the northern Hemisphere (Chiang et al. 2003; Chiang and Bitz 2005). These mechanisms have an impact on the tropical Atlantic and the adjacent land, changing low-level moisture convergence and convective activity throughout much of tropical South America. Precessional forcing, with its characteristic 20 kyr cycle and its importance in modulating tropical monsoons, has been demonstrated by climate modeling (Kutzbach and Liu 1997) and empirical studies (Baker et al. 2001; Bush et al. 2002; Wang et al. 2004; Cruz et al. 2005). Even if it is impossible to adapt a purely local perspective to understand the climate system's response to precessional forcing, an atmospheric general circulation model demonstrated that the center of convection over land, especially over South America, is weakened (Clement et al. 2004). In the precessional case, the most striking mechanism is the land-sea temperature contrast, resulting in a general shift of precipitation from land to ocean (Clement et al. 2004).

From the glacial boundary forcing point of view, during the last glacial period, a reduction in Atlantic overturning induces sea ice expansion in the North Atlantic and a southward displacement of the intertropical convergence zone (ITCZ) (Chiang et al. 2003; Chiang and Bitz 2005). This may cause a shift in the tropical hydrologic cycle, as seen in the Cariaco Basin (Peterson et al. 2000) and northeastern

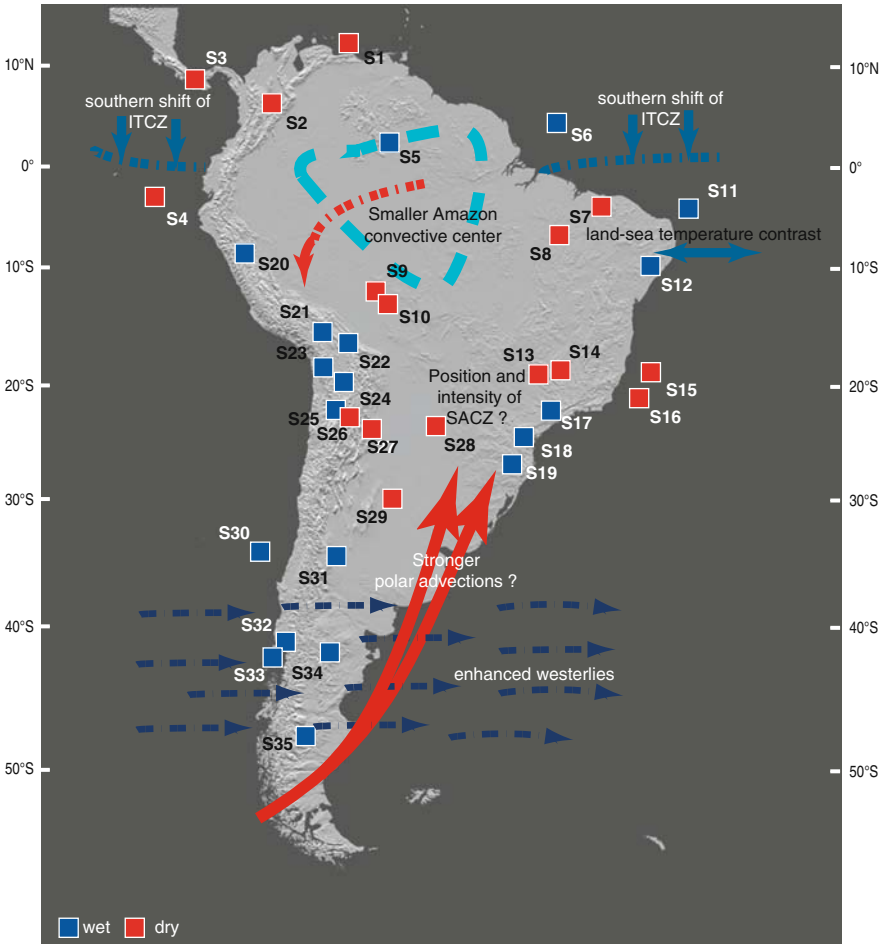

Fig. 1.2 South America during the LGM: main paleoclimatic characteristics (wet/dry) from the selected sites and potential paleoclimatic scenarios showing forcing mechanisms

Brazil (Wang et al. 2004). Southward ITCZ migration during millennial-scale stadial events may have caused meridional asymmetry in the Hadley circulation. A southward shift of the zonal-mean Hadley cell would change meridional moisture transport through intense ascending air masses in southern low latitudes and increased subsidence in the northern tropics and subtropics (e.g. Clement et al. 2004; Chiang and Bitz 2005). This hypothesis would probably explain a large portion of environmental changes observed during the LGM in South America as inferred by paleoproxies; for instance, the drying in the northern tropics, and the wetter conditions in the central Andes and in southeastern Brazil. It has been suggested that the LGM cooling in the tropical Atlantic increased the land/sea contrast that drives the South American monsoon, increasing rainfall rates and the specific humidity

of the low-level flow into the Andes and consequently the moisture inputs to subtropical Brazil (Baker et al. 2001a; Cruz et al., Chapter 2 of this volume). But, in Amazonia, both data and models suggest a substantial reduction of the rainforest coverage (Mayle et al., Chapter 4 of this volume). The paradox of a drier Amazon synchronous with wetter Andes, particularly since the moist air masses come from the north tropical Atlantic via the Amazon basin has been potentially explain by a mechanism involving a delayed onset of Amazon convection during austral spring (Cook and Vizy 2006). It is also interesting to note that the lake-level increasing during the LGM in the tropical Andes (e.g. Bolivian Altiplano) is not too large as inferred for the following period, during the Late-Glacial times (e.g. Tauca phase; Sylvestre et al. 1999; Placzek et al. 2006). Local parameters (e.g. hydrological control) and lower evaporation favoured by low temperature could partly explain the presence of water in Bolivian lakes during the LGM. Finally, the "glacial boundary" hypothesis is certainly particularly suitable during the colder millennial-scale stadial events (e.g. Heinrich events). But during the LGM, cooling in the tropics was not as large as observed during Heinrich events. Bard et al. (2000) noted that the LGM was a rather mild period in the subtropical Atlantic, with SST on the order of 13°C or only 5°C lower than present.

Now considering the extra-tropics forcings, at the time of the LGM, polar ice cores shows that both southern and northern hemispheres had minima in temperatures. Consequently stronger pole-equator temperature gradients on both sides of the equator were able to prevent large seasonal shifts of a weakened ITCZ. Further south, the diameter of the atmospheric circumpolar vortex increased and induced an increase in the intensity of the circulation: mid-latitude westerlies were able to extend northwards because of a weakened ITCZ and consequently the subtropical high shifted equatorward inducing changes in seasonal precipitation (Wainer et al. 2005). Lamy et al. (2009) propose that the displacement of the westerlies could have been ∼5° of latitude until the present southern margin of the Atacama Desert (∼27°N). Subtropical latitudes of the continent experienced drier conditions, which could be related to a location of the descending branch of the Hadley cell, whereas relatively moist climatic conditions in Bolivia at the Salar de Uyuni may have been related to outbreaks of polar air reaching the altitude of the Bolivian Altiplano during the winter (Sylvestre 2002). Southeastern Brazil may have been subject to influxes of polar air, explaining drier and cooler conditions inferred from the pollen data.

1.5 Conclusion

This review of diverse paleoclimate archives from South America during the LGM indicates a clear pattern for the northern and southern latitudes, drier and wetter respectively, whereas in the tropical lowlands, the pattern is still unclear. Resolving this issue is of particular interest because of the central role played by atmospheric convection centred over the Amazon basin. Whereas modeling experiments

suggest drier tropical conditions during the LGM, other evidence appears to contradict these results. Currently, these moister conditions are explained by a glacial forcing mechanism implying a southern shift of the ITCZ and a reinforcement of the SASM, leading to more humidity in the tropical Andes reaching southern Brazil. This hypothesis may explain a large portion of the ecosystem responses during the LGM, but would not account for all changes observed. For instance, the discrepancy between paleoproxies in southern Brazil asks the question about the position and the intensity of the SACZ. Precessionnal and extra-tropical mechanisms also exert an influence. Moreover, regional expressions and responses to global forcing mechanisms need to be better investigated. Certainly, the data resolution, the spatial coverage and the lack of quantitative estimations of climatic parameters produced by the paleoenvironmental studies are as much as limitations for deciphering the forcing mechanisms explaining the environmental changes. Improvements and sustaining efforts are needed in this way. Climate models could also help, providing a better representation of the mosaic regional response of the continental environment, and including feedback processes involving vegetation, water vapor and changes in the concentration of atmospheric CO_2. This kind of approach is necessary, and could be approximated by integrative steps of intermediate models.

Acknowledgments Paleoclimate works at the CEREGE is supported by the French Research National Agencies (IRD, CNRS). I acknowledge M. Williams, F. Vimeux, M. Khodri and two anonymous reviewers for the improvements of the manuscript, comments and discussions. I thank J.-J. Motte for his advices on the figure drawing.

References

Absy ML, Cleef A, Fournier M et al (1991) Mise en évidence de quatre phases d'ouverture de la forêt dense dans le sud-est de l'Amazonie au cours des 60 000 dernières années. Première comparaison avec d'autres régions tropicales. Comptes Rendus Académie des Sciences Paris 312:673–678

Alley RB (2004) GISP2 Ice Core Temperature and Accumulation Data. IGBP PAGES/World Data Center-A for Palaeoclimatology, Data Contribution Series #2004-01, NOAA/NGDC Palaeoclimatology Program, Boulder CO, USA

Ammann C, Jenny B, Kammer K, Messerli B (2001) Late Quaternary glacier response to humidity changes in the arid Andes of Chile (18–29°S). Palaeogeogr Palaeoclimatol Palaeoecol 172:313–326

Arz HW, Patzold J, Wefer G (1998) Correlated millennial-scale changes in surface hydrography and terrigenous sediment yield inferred from Last-Glacial marine deposits off Northeastern Brazil. Quat Res 50:157–166

Arz HW, Patzold J, Wefer G (1999) The deglacial history of the western tropical Atlantic as inferred from high resolution stable isotope records off northeastern Brazil. Earth Planet Sci Lett 167:105–117

Auler AS, Smart PL (2001) Late Quaternary paleoclimate in semiarid Northeastern Brazil from U-series dating of travertine and water-table speleothems. Quat Res 55:159–167

Baker PA, Seltzer GO, Fritz SC et al (2001a) The history of South American tropical precipitation for the past 25,000 years. Science 291:640–643

Baker PA, Rigsby CA, Seltzer GO et al (2001b) Tropical climate changes at millennial and orbital timescales on the Bolivian Altiplano. Nature 409:698–700

Bard E, Arnold M, Hamelin B et al (1998) Radiocarbon calibration by means of mass spectrometric 230Th/234U and 14C ages of corals. An updated data base including samples from Barbados, Mururoa and Tahiti. Radiocarbon 40:1085–1092

Bard E, Rostek F, Turon JL, Gendreau S (2000) Hydrological impact of Heinrich events in the subtropical Northeast Atlantic. Science 289:1321–132

Barros V, Gonzales M, Liebman B, Camilloni I (2000) Influence of the South Atlantic convergence zone and South Atlantic sea surface temperature on interannual summer rainfall variability in Southeastern South America. Theor Appl Climatol 67:123–133

Barros V, Doyle M, González M et al. (2002) Climate variability over subtropical South America and the South American monsoon: a review. Meteorological 27:33–58

Behling H, Arz HW, Pätzold J, Wefer G. (2000) Late Quaternary vegetational and climate dynamics in northeastern Brazil, inferences from marine core GeoB 3104-1. Quat Sci Rev 19:981–994

Behling H, Hooghiemstra H (2001) Neotropical savanna environments in space and time: Late Quaternary interhemispheric comparisons. In: Markgraf V (ed) Interhemispheric Climate Linkages, Academic Press, San Diego

Behling H (2002) South and southeast Brazilian grasslands during Late Quaternary times: a synthesis. Palaeogeogr Palaeoclimatol Palaeoecol 177:19–27

Behling H, Arz HW, Pätzold J, Wefer G (2002) Late Quaternary vegetational and climate dynamics in southeastern Brazil, inferences from marine cores GeoB 3229-2 and GeoB 3202-1. Palaeogeogr Palaeoclimatol Palaeoecol 179:227–243

Betancourt JL, Latorre C, Rech JA, Quade J, Rylander KA (2000) A 22,000-Year record of monsoonal precipitation from Northern Chile's Atacama desert. Science 289:1542–1546

Bobst AL, Lowenstein TK, Jordan TE et al (2001) A 106 ka paleoclimate record from drill core of the Salar de Atacama, northern Chile. Palaeogeogr Palaeoclimatol Palaeoecol 173:21–42

Bradbury JP (1997) Sources of glacial moisture in Mesoamerica. Quat Int 43/44:97–110

Bradbury JP, Grosjean M, Stine S, Sylvestre F (2001) Full and Late Glacial lake records along the PEP1 transect: their role in developing interhemispheric paleoclimate interactions. In: Markgraf V (ed.) Interhemispheric Climate Linkages, Academic Press, San Diego

Bush ABG, Philander SGH (1998) The role of ocean-atmosphere interactions in Tropical cooling during the Last Glacial maximum. Science 279:1341–1344

Bush MB, Colinvaux PA (1990) A long record of climatic and vegetation change in lowland Panama. J Veg Sci 1:105–119

Bush MB, Miller MC, De Oliveira PE, Colinvaux PA (2002) Orbital forcing signal in sediments of two Amazonian lakes. J Paleolimnol 27:341–352

Bush MB, Correa-Metrio A, Hodell DA et al (2009) Re-evaluation of climate change in Lowland Central America during the Last Glacial Maximum using new sediment cores from Lake Petén Itzá, Guatemala. In: Vimeux F, Sylvestre F, Khodri M (eds) Developments in paleoenvironmental research. Springer, Dordrecht, The Netherlands

Burbridge RE, Mayle FE, Killeen TJ (2004) Fifty-thousand-year vegetation and climate history of Noel Kempff Mercado National Park, Bolivian Amazon. Quat Res 61:215–230

Cane MA (2005) The evolution of El Niño, past and future. Earth Planet Sci Lett 230:227–240

Chappellaz J, Blunier T, Raynaud D et al (1993) Synchronous changes in atmospheric CH4 and Greenland climate between 40 and 8 kyr BP. Nature 366:443–445

Chiang JCH, Biasutti M, Battisti DS (2003) Sensitivity of the Atlantic ITCZ to conditions during Last Glacial Maximum. Paleoceanography 18:doi:10.1029/2003PA000916

Chiang JCH, Bitz M (2005) Influence of high latitude ice cover on the marine Intertropical Convergence Zone. Clim Dyn 25:477–496

Clapperton CM (1993) Quaternary and Geomorphology of South America. Elsevier Science, Amsterdam, 779 pp

Claussen M, Ganopolski A, Brovkin V et al (2003) Simulated global-scale response of the climate system to Dansgaard/Oeschger and Heinrich events. Clim Dyn 21:361–370

Clement AC, Hall A, Broccoli AJ (2004) The importance of precessional signals in the tropical climate. Clim Dyn 22:327–341

CLIMAP Project members (1981) Seasonal reconstructions of Earth's surface at last glacial maximum. Geological Society of America, Map and Chart Series, C-36, 18 pp.
COHMAP (1988) Climatic changes of last 18,000 years: observations and model simulations. Science 241:1043–1052
Colinvaux PA, De Oliveira PE, Moreno JE et al (1996) A long pollen record from lowland Amazonia: forest and cooling in glacial times. Science 274:85–88
Colinvaux PA, De Oliveira PE, Bush MB (2000) Amazonian and neotropical plant communities on glacial time-scales: the failure of the aridity and refuge hypotheses. Quat Sci Rev 19:141–169
Cook KH, Vizy EK (2006) South American climate during the Last Glacial Maximum: Delayed onset of the South American monsoon. J Geophys Res – Atmos 111 D02110. doi:10.1029/2005JD005980
Cruz FWJ, Burns SJ, Karmann I et al (2005) Insolation-driven changes in atmospheric circulation over the past 116,000 years in subtropical Brazil. Nature 434:63–66
Cruz FWJ, Burns SJ, Karmann I et al (2006a) A stalagmite record of changes in atmospheric circulation and soil processes in the Brazilian subtropics during the Late Pleistocene. Quat Sci Rev 25:2749–2761
Cruz FWJ, Burns SJ, Karmann I et al (2006b) Reconstruction of regional atmospheric circulation features during the late Pleistocene in subtropical Brazil from oxygen isotope composition of speleothems. Earth Planet Sci Lett 248:494–506
Cruz FW, Wang X, Aulter A, et al (2009) Orbital and millenial-scale precipitation change in Brazil from speleothem records. In: Vimeux F, Sylvestre F, Khodri M (eds) Developement in Paleoenvironmental Research. Springer, Dordrecht, The Netherlands
DeOliveira PE (1992) A palynological record of late Quaternary vegetational and climatic change in southeastern Brazil. Ph.D thesis. The Ohio State University, Columbus, 238 pp.
Farrera I, Harrison SP, Prentice IC et al (1999) Tropical climates at the Last Glacial Maximum: a new synthesis of terrestrial palaeoclimate data. I. Vegetation, lake-levels and geochemistry. Clim Dyn 15:823–856
Fritz SC, Baker PA, Seltzer GO et al (2007) Quaternary glaciation and hydrologic variation in the South American tropics as reconstructed from the Lake Titicaca drilling project. Quat Res 68:410–420
Galloway RW, Markgraf V, Bradbury JP (1988) Dating shorelines of lakes in Patagonia, Argentina. J South Amer Earth Sci 1:195–198
Garcin Y, Williamson D, Taieb M, et al (2006) Centennial to millennial changes in maar-lake deposition during the last 45,000 years in tropical Southern Africa (Lake Masoko, Tanzania). Palaeogeogr Palaeoclimatol Palaeoecol 239:334–354
Garreaud RD (2000) Cold air incursions over subtropical South America: mean structure and dynamics. Mon Weather Rev 128:2544–2559
Garreaud RD, Wallace JM (1998) Summertime incursions of mid-latitude air into tropical and subtropical South America. Mon Weather Rev 126:2713–2733
Garreaud RD, Vuille M, Clement AC (2003) The climate of the Altiplano: observed current conditions and mechanisms of past changes. Palaeogeogr Palaeoclimatol Palaeoecol 194:5–22
Garreaud RD, Vuille M, Compagnucci R, Marengo J. Present-day South American climate. Palaeogeogr Palaeoclimatol Palaeoecol, in press
Gersonde R, Crosta X, Abelmann A, Armand L (2005) Sea-surface temperature and sea ice distribution of the Southern Ocean at the EPILOG Last Glacial Maximum - a circum-Antarctic view based on siliceous microfossil records. Quat Sci Rev 24:869–896
Geyh MA, Grosjean M, Nunez L, Schotterer U (1999) Radiocarbon reservoir effect and the timing of the Late-Glacial/Early Holocene humid phase in the Atacama desert (Northern Chile). Quat Res 52:143–153
González MA (1994) Salinas del Bebedero Basin (República Argentina). In: Kelts K, Gierlowski-Cordesch E (eds.) Global Inventory of Lake Basins. Cambridge University Press
Grosjean M. (1994) Paleohydrology of the laguna Lejía (north Chilean Altiplano) and climatic implications for late-glacial times. Palaeogeogr Palaeoclimatol Palaeoecol 109:89–100.

Grosjean M, van Leeuwen JFN, van der Knaap WO et al (2001) A 22,000 ^{14}C year BP sediment and pollen record of climate change from Laguna Miscanti (23°S), northern Chile. Glob Planet Change 28:35–51

Haberle SG, Maslin MA (1999) Late Quaternary vegetation and climate change in the Amazon based on a 50,000 year pollen record from the Amazon fan, ODP Site 932. Quat Res 51: 27–38

Haug GH, Hughen, KA, Sigman DM et al (2001) Southward migration of the Intertropical Convergence Zone through the Holocene. Science 293:1304–1308

Heine K. (2000) Tropical South America during the Last Glacial Maximum: evidence from glacial, periglacial and fluvial records. Quat Int:72, 7–21

Heusser CJ (1974) Vegetation and climate of the southern Chilean lake district during and since the last Interglaciation. Quat Res 4:190–315

Heusser CJ (1981) Palynology of the last interglacial–glacial cycle in mid-latitudes in central Chile. Quat Res 16:293–321

Heusser CJ (1989) Southern Westerlies during the Last Glacial Maximum. Quat Res 31:423–425

Heusser CJ., Lowell TV, Heusser LE et al (1996) Full-glacial-lateglacial palaeoclimate of the Southern Andes: evidence from pollen, beetle, and glacial records. J Quat Sci 11:173–184

Heusser LE, Shackelton NJ (1994) Tropical climatic variation on the Pacific slopes of the Ecuadorian Andes based on a 25,000-year pollen record from deep-sea sediment core Tri 163–31B. Quat Res 42:222–225

Hodell DA, Anselmetti F, Ariztegui D et al (2008) An 85-ka record of climate change in Lowland Central America. Quat Sci Rev 27:1152–1165

Hoffmann G. (2003). Taking the pulse of the tropical water cycle. Science 301:776–777.

Hoganson JW, Ashworth AC (1992) Fossil beetle evidence for climatic change 18,000–10,000 years B.P. in South-Central Chile. Quat Res 37:101–116

Huguen KA, Overpeck JT, Peterson LC, Trumbore S (1996) Rapid climate changes in the tropical Atlantic region during the last deglaciation. Nature 380:51–54

Hulton NRJ, Purves RS, McCulloch RD et al (2002) The last Glacial Maximum and deglaciation in southern South America. Quat Sci Rev 21:233–241

Ivanochko TS, Ganesshram RS, Brummer GJA et al (2005) Variations in tropical convection as an amplifier of global climate change at the millennial scale. Earth Planet Sci Lett 235:302–314

Jaeschke A, Ruehlemann C, Arz H, Heil G, Lohmann G (2007) Coupling of millennial-scale changes in sea surface temperature and precipitation off northeastern Brazil with high latitude climate shifts during the last glacial period. Paleoceanography 22:PA4206. doi: 10.1029/2006PA001391

Jennerjahn TC, Ittekkot V, Arz HW et al (2004) Asynchronous terrestrial and marine signals of climate change during Heinrich events. Science 306:2236–2239

Klein AG, Seltzer GO, Isacks BL (1999) Modern and last local glacial maximum snowlines in the Central Andes of Peru, Bolivia, and Northern Chile. Quat Sci Rev 18:63–84

Kull C, Hänni F, Grosjean M, Veit H (2003) Evidence of an LGM cooling in NW-Argentina (22°S) derived from a glacier climate model. Quat Int 108 3–11

Kutzbach JE, Liu Z (1997) Response of the African monsoon to orbital forcing and ocean feedbacks in the middle Holocene. Science 278:440–443

Labraga JC, Frumento O, López M (2000) The atmospheric water vapor cycle in South America and the tropospheric circulation. J Clim 13:1899–1915

Lamy F, Hebbeln D, Wefer G (1998) Late Quaternary precessional cycles of terrigenous sediment input off the Norte Chico, Chile (27.5 degrees S) and palaeoclimatic implications. Palaeogeogr Palaeoclimatol Palaeoecol 141:233–251

Lamy F, Hebbeln D, Wefer G (1999) High-resolution marine record of climatic change in mid-latitude Chile during the last 28,000 years based on terrigenous sediment parameters. Quat Res 51:83–93

Lamy F, Klump J, Hebbeln D, Wefer G (2000) Late Quaternary rapid climate change in northern Chile. Terra Nova 12:8–13

Lamy F, Kaiser J, Ninnemann U et al (2004) Antarctic timing of surface water changes off Chile and patagonian ice sheet response. Science 304:1959–1962

Lamy F, Kaiser J. (2009) Glacial to Holocene paleoceanographic and continental paleoclimate reconstructions based on ODP Site 1233/GeoB 3313 off southern Chile. In: Vimeux F, Sylvestre F, Khodri M (eds) Developments in Paleoenvironmental Research. Springer, Dordrecht, The Netherlands

Ledru MP, Bertaux J, Sifeddine A, Suguio K (1998) Absence of last glacial maximum records in tropical lowland forests. Quat Res 49:233–237

Ledru MP, Rousseau DD, Cruz JFW et al (2005) Paleoclimate changes during the last 100 ka from a record in the Brazilian atlantic rainforest region and interhemispheric comparison. Quat Res 64:444–450

Ledru MP, Mourguiart P, Riccomini C (2009) Related changes in biodiversity, insolation and climate in the Atlantic rainforest since the last interglacial. Palaeogeogr Palaeoclimatol Palaeoecol 271:140–152

Lenters JD, Cook KH (1997) On the origin of the Bolivian high and related circulation features of the South American climate. J Atmos Sci 54:656–677

Liu Z, Yang H (2003) Extratropical control of tropical climate, the atmospheric bridge and oceanic tunnel. Geophys Res Lett 30:1230. doi: 10.1029/2002GL016492

Liu Z (2006) Glacial Thermohaline circulation and climate: forcing from the North or South? Adv Atmos Sci 23:199–206

Lowell TV, Heusser CJ, Andersen BG et al (1995) Interhemispheric correlation of Late Pleistocene glacial events. Science 269:1541–1549

Markgraf V (1983) Late and postglacial vegetational and paleoclimatic changes in subantarctic, temperate, and arid environments in Argentina. Palynology 7:43–70

Markgraf V (1984) Late Pleistocene and Holocene vegetation history of temperate Argentina: Lago Morenito, Bariloche. Diss Bot 72:235–254

Markgraf V (1987) Paleoenvironmental changes at the northern limit of the subantarctic Nothofagus forest, Lat 37°, Argentina. Quat Res 28:119–129

Markgraf V (1989) Reply to Heusser's 'Southern Westerlies during the Last Glacial Maximum'. Quat Res 31:426–432

Marengo JA, Rogers JC (2001) Polar air outbreaks in the Americas assessments and impacts during modern and past climates. In: Markgraf V (ed) Interhemispheric Climate Linkages, Academic Press

Martin L, Bertaux J, Corrège T et al (1997) Astronomical forcing of contrasting rainfall changes in tropical South America between 12,400 and 8,800 cal. yr B.P. Quat Res 47:117–122

Massaferro JI, Moreno PI, Denton GH et al (2009) Chironomid and pollen evidence for climate fluctuations during the Last Glacial Termination in NW Patagonia. Quat Sci Rev 28:517–525

Mayle FE, Burn MJ, Power M, et al (2009) Vegetation and fire at the last Glacial Maximum in tropical South America. In: Vimeux F, Sylvestre F, Khodri M (eds) Developments in Paleoenvironmental Research. Springer, Dordrecht, The Netherlands

Messerli B, Grosjean M, Bonani G et al (1993) Climate change and natural resource dynamics of the Atacama Altiplano during the last 18,000 years: a preliminary synthesis. Mou Res Dev 13:117–127

Mix A, Bard E, Schneider R (2001) Environmental processes of the ice age: land, oceans, glaciers (EPILOG). Quat Sci Rev 20:627–657

Moreno PI (1997) Vegetation and climate near Lago Llanquihue in the Chilean Lake District between 20 200 and 9500 ^{14}C yr BP. J Quat Sci 12:485–500

Moreno PI, Lowell TV, Jacobson GL, Denton GH (1999) Abrupt vegetation and climate changes during the last glacial maximum and last termination in the chilean Lake District: a case study from Canal de la Puntilla (41°S). Geogr Ann 81 A:285–311

Nogués-Paegle J, Mo KC (1997) Alternating wet and dry conditions over South America during summer. Mon Weather Rev 125:279–291

Nogués-Paegle J, Mechoso CR, Fu R et al (2002) Progress in Pan American CLIVAR Research: understanding the South American Monsoon. Meteorologica 27:3–30
Peterson LC, Haug GH, Hughen KA, Rohl U (2000) Rapid changes in the hydrologic cycle of the tropical Atlantic during the Last Glacial. Science 290:1947–1951
Peterson LC, Haug GH (2006) Variability in the mean latitude of the Atlantic Intertropical Convergence Zone as recorded by riverine input of sediments to the Cariaco Basin (Venezuela). Palaeogeogr Palaeoclimatol Palaeoecol 234:97–113
Petit JR, Jouzel J, Raynaud D et al (1999) Climate and atmospheric history of the past 420,000 years from the Vostok ice core, Antarctica. Nature 399:429–436
Pierrehumbert RT (1999). Huascaran $\delta^{18}O$ as an indicator of tropical climate during the Last Glacial Maximum. Geophys Res Lett 26:1345–1348
Placzek C., Quade J., Patchett PJ (2006). Geochronology and stratigraphy of late Pleistocene lake cycles on the southern Bolivian Altiplano: implications for causes of tropical climate change. Geol Soc Am Bull 118:515–532
Piovano E, Ariztegui D, Córdoba F et al (2008) Reconstrucciones paleohidrologicas en la región pampeana (Programa paleo-pampas). XII Argentine Meeting of Sedimentology, XIIRAS, Buenos Aires, Argentina
Porter SC (2001) Snowline depression in the tropics during the last Glaciation. Quat Sci Rev 20:1067–1091
Ramirez E, Hoffman G, Taupin JD et al (2003) A new Andean deep ice core from Nevado Illimani (6350 m), Bolivia. Earth Planet Sci Lett 212:337–350
Reimer PJ, Baillie MGL, Bard E et al (2004) IntCal04 terrestrial radiocarbon age calibration, 0–26 cal kyr BP. Radiocarbon 46:1029–1059
Robertson AW, Mechoso CR (2000) Interrannual and interdecadal variability of the South Atlantic Convergence Zone. Mon Weather Rev 128:2947–2957
Robertson AW, Mechoso CR, Young-Joon K (2000) The influence of Atlantic Sea surface temperature anomalies on the North Atlantic Oscillation. J Clim 13:122–138
Robertson AW, Mechoso CR (2002) Links between the Atlantic Ocean and south American climate variability. Exchanges 25:1–4
Rojas M, Moreno P, Kageyama M et al (2008) The southern westerlies during the last glacial maximum in PMIP2 simulations. Clim Dyn. doi10.1007:s00382-008-0421-7
Saulo AC, Nicolini M, Chou SC (2000) Model characterization of the South American low-level flow during the 1997–1998 spring-summer season. Clim Dyn 16:867–881
Seltzer GO, Rodbell DT, Baker PA et al. (2002). Early warming of tropical South America at the Last Glacial-Interglacial transition. Science 296:1685–1686
Servant M, Fournier M, Argollo J et al (1995) La dernière transition glaciaire/interglaciaire des Andes tropicales sud (Bolivie) d'après l'étude des variations des niveaux lacustres et des fluctuations glaciaires. Comptes Rendus Académie des Sciences Paris 320:729–736
Severinghaus JP, Sowers T, Brook EJ et al (1998) Timing of abrupt climate change at the end of the Younger Dryas interval from thermally fractionated gases in polar ice. Nature 391:141–146
Shin SI, Liu Z, Otto-Bliesner B et al (2003) A simulation of the Last Glacial Maximum using the NCAR-CCSM. Clim Dyn 20:127–151
Sifeddine A, Fröhlich F, Fournier M et al (1994) La sédimentation lacustre indicateur de changements des paléoenvironnements au cours des 30 000 dernières années (Carajas, Amazonie, Brésil). Comptes Rendus Académie des Sciences Paris 318:1645–1652
Sifeddine A, Albuquerque ALS, Ledru MP et al (2003) A 21 000 cal years paleoclimatic record from Caçó Lake, northern Brazil: evidence from sedimentary and pollen analyses. Palaeogeogr Palaeoclimatol Palaeoecol 189:25–34
Smith JA, Seltzer GO, Farber DL et al (2005a) Early local Last Glacial Maximum in the Tropical Andes. Science 308:678–681
Smith JA, Seltzer GO, Rodbell DT, Klein AG (2005b) Regional synthesis of last glacial maximum snowlines in the tropical Andes, South America. Quat Int 138–139:145–167

Smith JA, Mark BG, Rodbell DT (2008) The timing and magnitude of mountain glaciations in the tropical Andes. J Quat Sci 23:609–634

Stevaux JC (2000) Climatic events during the Late Pleistocene and Holocene in the Upper Parana River: correlation with the NE Argentina and South-Central Brazil. Quat Int 72:73–85

Stine S, Stine M (1990) A record from Lake Cardiel of climate change in southern South America. Nature 345:705–707

Stuut JBW, Crosta X, Van der Borg K, Schneider R (2004) Relationship between Antarctic sea ice and southwest African climate during the late Quaternary. Geology 32:09–912

Stuut JBW, Lamy F (2004) Climate variability at the southern boundaries of the Namib (southwestern Africa) and Atacama (northern Chile) coastal deserts during the last 120,000 yr. Quat Res 62:301–309

Sylvestre F, Servant-Vildary S, Servant M (1998) Le Dernier Maximum glaciaire (21 000–17 000 14C ans B.P.) dans les Andes tropicales de Bolivie d'après l'étude des diatomées. Comptes Rendus Académie des Sciences Paris 327:611–618

Sylvestre F, Servant M, Servant-Vildary S et al (1999) Chronology of lake-level changes in the South Bolivian Altiplano (18–23°S) during Late-Glacial and early Holocene times. Quat Res 51:54–66

Sylvestre F (2002) A high resolution diatom-reconstruction between 21 and 17 kyr B.P. from the southern Bolivian Altiplano. J Paleolimnol 27:45–57

Thompson LG, Mosley-Thompson E, Davis ME et al (1995) Late Glacial stage and Holocene tropical ice core records from Huascaran, Peru. Science 269:46–50

Thompson LG, Davis ME, Mosley-Thompson E et al (1998) A 25,000-year tropical climate history from Bolivian ice cores. Science 282:1858–1864

Thompson LG (2000) Ice core evidence for climate change in the tropics: implications for our future. Quat Sci Rev 19:19–35

Trauth MH, Strecker MR (1999). Formation of landslide-dammed lakes during a wet period between 40,000 and 25,000 yr B.P. in northwestern Argentina. Palaeogeogr Palaeoclimatol Palaeoecol 153:277–287

Trauth MH, Ricardo AA, Haselton KR et al (2000). Climate change and mass movements in the NW Argentine Andes. Earth Planet Sci Lett 179:243–256

Van der Hammen T, Hooghiemstra H (2000) Neogene and Quaternary history of vegetation, climate, and plant diversity in Amazonia. Quat Sci Rev 19:725–742

Van Geel B, Van der Hammen T (1973) Upper Quaternary vegetational and climatic sequence of the Fuquene area (Eastern Cordillera Colombia). Palaeogeogr Palaeoclimatol Palaeoecol 14:9–92

Vera C, Higgins W, Amador J et al (2006) Towards a Unified View of the American Monsoon Systems. J Clim 19:4977–5000

Vimeux F, Gallaire R, Bony S et al (2005) What are the climate controls on δD in precipitation in the Zongo Valley (Bolivia): implications for the Illimani ice core interpretation. Earth Planet Sci Lett 240:205–220

Visser K, Thunnel R, Stott L (2003) Magnitude and timing of temperature change in the Indo-Pacific warm pool during deglaciation. Nature 421:152–155

Vizy EK, Cook KH (2007) Relationship between Amazon and high Andes precipitation. J Geophys Res – Atmos 112 (D7):Art. No. D07107

Vuille M, Ammann C (1997) Regional snowfall patterns in the high, arid Andes. Clim Change 36:413–423

Wainer I, Clauzet G, Ledru MP et al (2005) Last Glacial Maximum in South America: paleoclimate proxies and model results. Geophys Res Lett 32. doi:10.1029/2004GL021244.

Wang X, Auler AS, Edwards RL et al (2004) Wet periods in northeastern Brazil over the past 210 kyr linked to distant climate anomalies. Nature 432:740–743

Wang X, Auler AS, Edwards R et al (2006) Interhemispheric anti-phasing of rainfall during the last glacial period. Quat Sci Rev 25:3391–3403

Wirrmann D, Ybert JP, Mourguiart P (1992) A 20,000 years palaeohydrological record from Lake Titicaca. In: Dejoux C, Iltis A (eds) Lake titicaca, a synthesis of limnological knowledge. Kluwer Academic Publishers, Dordrecht

Ybert JP (1992) Ancient lake environments as deduced from pollen analysis. In: Dejoux C, Iltis A (eds) Lake Titicaca, a synthesis of limnological knowledge. Kluwer Academic Publishers, Dordrecht

Zhou J, Lau KM (1998) Does a monsoon climate exist over South America? J Clim 11:1020–1040

Zech R, May JH, Kull C et al (2008) Timing of the late Quaternary glaciations in the Andes from ~15 to 40°S. J Quat Sci 23:635–647

Chapter 2
Orbital and Millennial-Scale Precipitation Changes in Brazil from Speleothem Records

Francisco W. Cruz, Xianfeng Wang, Augusto Auler, Mathias Vuille, Stephen J. Burns, Lawrence R. Edwards, Ivo Karmann, and Hai Cheng

Abstract Paleorainfall variability on orbital and millennial time scales is discussed for the last glacial period and the Holocene, based on a multi-proxy study of speleothem records from Brazil. Oxygen isotope ($\delta^{18}O$) records from Botuverá and Santana caves, precisely dated by U-series methods, indicate stronger summer monsoon circulation in subtropical Brazil during periods of high summer insolation in the southern hemisphere. In addition, variations in Mg/Ca and Sr/Ca ratios from speleothems confirm that this monsoon intensification led to an increase in the long-term mean rainfall during insolation maxima. However, they also suggest that glacial boundary conditions, especially ice volume buildup in the northern hemisphere, promoted an additional displacement of the monsoon system to the south, which produced rather wet conditions during the period from approximately 70 to 17 ka B.P., in particular at the height of the Last Glacial Maximum (LGM).

These $\delta^{18}O$ records, together with speleothem growth intervals from northeastern Brazil, have also revealed new insights into the influence of the northern hemisphere millennial-scale events on the tropical hydrological cycle in South America. This teleconnection pattern is expressed by an out-of-phase relationship between precipitation changes inferred from speleothem records in Brazil and China, particularly during Heinrich events and the Younger Dryas. We argue that the pronounced hemispheric asymmetry of moisture is a reflection of the impact of meridional overturning circulation conditions on the position and intensity of the intertropical convergence zone (ITCZ).

Keywords Speleothems · Brazil · Stable isotopes · Trace elements · South American monsoon · Insolation

F.W. Cruz (✉)
Instituto de Geociências, Universidade de São Paulo, Rua do Lago, 562, CEP 05508-080, São Paulo-SP, Brazil
e-mail: cbill@usp.br

F. Vimeux et al. (eds.), *Past Climate Variability in South America and Surrounding Regions*, Developments in Paleoenvironmental Research 14,
DOI 10.1007/978-90-481-2672-9_2,

2.1 Introduction

Speleothems, secondary carbonate cave formations, have become key geological records for the reconstruction of regional to large-scale atmospheric circulation patterns associated with changes in precipitation regimes during the late Pleistocene and Holocene. Relatively long, high-resolution and well-dated oxygen isotope records from speleothems have provided important clues regarding the relationship between the hydrologic cycle of the (sub)tropical climate system and atmospheric/oceanic temperature variations recorded in northern hemisphere ice/marine cores during Dansgaard/Oeschger (D/O) and Heinrich (H) events (Dansgaard et al. 1993; Grootes and Stuiver 1997; NGRIP members 2004). These millennial-scale events occur as abrupt rainfall-related $\delta^{18}O$ changes, which interrupt the generally precession-driven tendency, as seen for example in speleothem records from China (Wang et al. 2001; Yuan et al. 2004). The same events are also responsible for most of the rainfall variability seen at full glacial times in the Indian/East African monsoon or in Eastern Mediterranean regions (Burns et al. 2003; Bar-Matthews et al. 2003).

Despite the increased knowledge about climate variations on millennial and orbital time-scales, the impacts of D/O, H-events and summer insolation on regional- and large-scale tropical atmospheric circulation patterns are not yet fully understood. Ti-Fe records off the coast of Venezuela (Peterson et al. 2000; Haug et al. 2001) and Brazil (Arz et al. 1998; Jennerjahn et al. 2004) provide some of the best evidence of how changes in sea surface temperature during D/O and H-events affected the tropical hydrological cycle in South America. For instance, an out of phase relationship, characterized by positive fluctuations in the tropical hydrological cycle of northern (southern) parts of South America, are observed in the former (latter) events, respectively. These observations have motivated paleoclimate simulations employing both coupled and atmospheric general circulation models (GCMs) (Chiang et al. 2003; Claussen et al. 2003; Chiang and Bitz 2005). Results from these experiments suggest that the expansion or contraction of land- and sea-ice during the Last Glacial Maximum (LGM) or during millennial events can lead to a displacement of the intertropical convergence zone (ITCZ) and produce precipitation asymmetries over tropical South America. However, Clement et al. (2004) argue that precessional forcing induces a stronger tropical hydrologic response than glacial boundary conditions.

Speleothems, together with other well-dated high-resolution paleoclimate records from low latitudes, especially from continental regions, can serve as a crucial test for these model experiments. In particular, models can help us understand how climate signals from high-latitude, millennial-scale events are transmitted through the tropical Atlantic to continental South America, ultimately affecting summer monsoon rainfall. Furthermore the high–low latitude phase-relationship and the exact timing of abrupt climate events in the southern hemisphere need to be assessed. Finally, it is also essential to document the relative geographic importance of the various forcings, as both summer insolation and millennial-scale events are thought to impact moisture transport and precipitation over the Amazon Basin

and the tropical Andes (Seltzer et al. 2000; Baker et al. 2001a). Monsoon precipitation is antiphased between the two hemispheres on seasonal timescales, due to the seasonality of solar heating and related changes in the strength of the hemispheric Hadley cells (Dima and Wallace 2003; Biasutti et al. 2003). However, there is a need for further paleoclimate studies to reconstruct the precipitation patterns in South America and their related forcings.

Speleothem-based paleoclimate studies are a relatively late addition to the rapidly growing body of literature concerning past climates in South America. Carbonate (limestone, dolomite) areas – and thus caves suitable for speleothem growth – occur throughout South America, from ~10° latitude north to ~36° latitude south (Auler 2004), encompassing a wide range of climatic zones and all major biomes such as equatorial Amazon rainforest, semi-arid caatinga, central Brazilian savannas, Chaco swamplands, Atlantic rainforest, Andean grasslands and montane forests, and Patagonian pampas. South American speleothems have allowed new insights on regional precipitation and atmospheric circulation changes. They provide us with important archives for addressing paleoclimatic issues, such as the relative roles played by summer insolation and the glacial boundary conditions in shaping precipitation patterns (Fig. 2.1) within areas affected by the South American Summer Monsoon or the ITCZ (Wang et al. 2004, 2006, 2007a, b; Cruz et al. 2005a, 2006, 2007).

This chapter presents robust climate correlations of speleothem records in Brazil with contemporaneous records in South America and in the northern latitudes. The comparisons are based on independent chronologies as opposed to simply "wiggle matching". This study is organized as follows: Section 2.2 reviews the spatiotemporal variability of stable isotopes in precipitation over South America and describes the results of modern calibration studies based on $\delta^{18}O$ and elemental ratios of cave drip waters. Section 2.3 presents Brazilian speleothem records and evaluates the most likely climate factors affecting their past $\delta^{18}O$, Mg/Ca and Sr/Ca variations. Section 2.4 discusses precipitation variability in Brazil on millennial and longer time-scales from the last glacial period through the Holocene, summarizes possible climate forcings and shows how speleothem records reflect changes in regional to large-scale atmospheric circulation.

2.2 Climate Signals Recorded in Brazilian Speleothems

2.2.1 Climate Variability in South America Based on $\delta^{18}O$ in Precipitation

The stable isotopic composition of precipitation ($\delta^{18}O$ and δD) and its spatiotemporal variability over the South American continent have been the subject of a large number of observational, modeling and paleoclimatic studies. Early work focused on data made available through the network maintained by the International Atomic Energy Agency – Global Network of Isotopes in Precipitation (IAEA-GNIP). This database allowed for preliminary analyses of questions related to water recycling

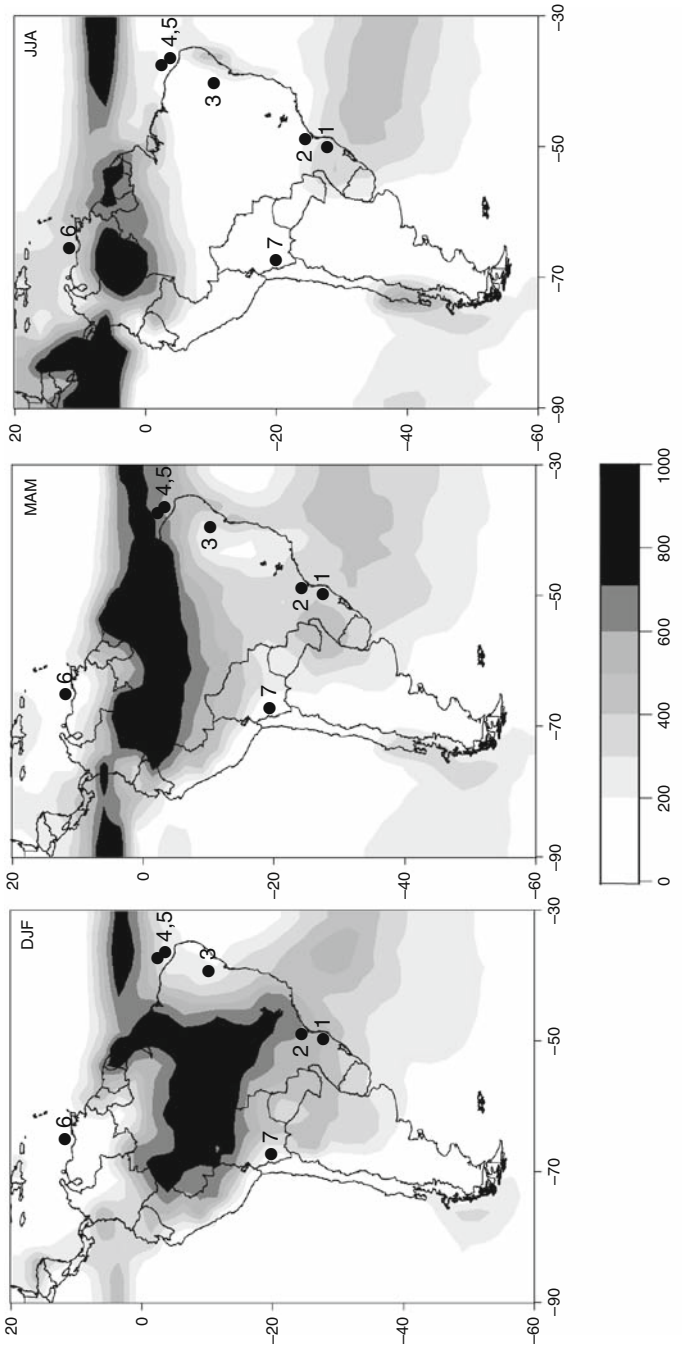

Fig. 2.1 Long-term mean (1979–2000) Climate Prediction Center Merged Analysis of Precipitation (CMAP, Xie and Arkin 1997) seasonal precipitation totals (in mm) for December-February (*left*), March-May (*middle*) and June-August (*right*). Precipitation over SE Brazil in DJF is related to the southward expansion and intensification of the South American summer monsoon, while in JJA precipitation is of extratropical nature and associated with midlatitude cyclonic activity over the South Atlantic. Precipitation in NE Brazil is mainly associated with the southern most position of the Intertropical convergence zone in MAM. Numbers in figure indicate locations mentioned in text: 1 – Botuverá Cave, 2 – Santana cave, 3 – Toca da Boa Vista cave, 4 – Marine cores GeoB 3104-1/GeoB 3911-3, 5 – Marine cores GeoB 3911-3, 6 – Cariaco Basin, 7 – Salar de Uyuni

and the evapotranspiration flux over the Amazon basin. It was observed that the isotopic depletion along an east–west trajectory was much lower than what one would expect based on a Rayleigh type law, despite intense rainout along the trajectory (Salati et al. 1979; Gat and Matsui 1991). This phenomenon can be explained by the intense water recycling taking place over the basin, largely accomplished through transpiration, which is a non-fractionating process, constantly recharging the atmosphere with relatively enriched water vapor. Only about 40% of the moisture flux returning to the atmosphere is isotopically light due to direct evaporation from lakes, rivers and forest canopy (Gat and Matsui 1991; Victoria et al. 1991). As a result the inland gradient of $\delta^{18}O$ in meteoric waters across the Amazon basin from the Atlantic coast to the Andes is much smaller than on other continents. Nonetheless, the long-range transport of moisture from the tropical Atlantic across the Amazon basin toward distant places such as the tropical Andes or subtropical South America leads to a clear depletion in heavy isotopes that can be traced to the degree of rainout upstream (Garcia et al. 1998; Vimeux et al. 2005; Vuille and Werner 2005). Once air masses reach the Andes, a much stronger depletion takes place with increasing altitude ("altitude effect"), due to progressive adiabatic cooling and condensation of atmospheric vapor as air masses are lifted along the Andean slopes (Gonfiantini et al. 2001).

The increasing number of stable isotopic paleorecords (ice cores, speleothems, records from lake and tree ring cellulose, etc.) emerging from South America have fueled the debate over the climatic controls on stable isotopes on interannual and longer time scales. Initially much of the attention was focused on ice core records from the tropical Andes, where the ancient composition of meteoric waters is directly preserved. Grootes et al. (1989) developed a simple transport model, trying to explain the inverse temperature-$\delta^{18}O$ seasonality observed on Quelccaya ice cap, Peru. Subsequent studies, however, showed that the more depleted $\delta^{18}O$ values during the austral summer are caused by an intensified hydrological cycle, where small-scale deep convection leads to the preferential removal of isotopically enriched molecules, thereby leaving the remaining water vapor increasingly lighter (Vuille et al. 2003a). The more intense the convective nature of an event, the higher the rainfall amount and the more depleted its isotopic composition. This process also leaves a significant imprint on interannual time scales, with a more enriched stable isotopic composition during dry years, and more depleted values when strong convective activity accompanies the monsoon season (Matsuyama et al. 2005; Vimeux et al. 2005). On average the interannual temporal slope of the $\delta^{18}O$- precipitation relationship ranges between –0.4 and –0.8‰/100 mm (Vuille et al. 2003a). Much of the spatial variability of this slope can be attributed to the different geographic locations, with high-elevation inland locations having much steeper slopes, while slopes at coastal lowland stations are weak.

This dependence of $\delta^{18}O$ on the precipitation amount has been exploited to use $\delta^{18}O$ from meteoric waters to study interannual climate variability over the South American domain, including the influence of El Niño-Southern Oscillation (ENSO) and the South American Summer Monsoon (SASM). Vuille et al. (2003a) performed a comprehensive study on the interannual variability of stable isotopes in

precipitation over South America and its climatic controls, employing both General Circulation Models (GCMs) fitted with stable isotopic tracers as well as observational data from IAEA-GNIP. According to their results, later confirmed by similar studies (Vimeux et al. 2005; Sturm et al. 2007) stable isotopes record interannual variations of the hydrologic cycle, with a strong dependence on the precipitation amount ("amount effect") but are rather insensitive to temperature variability, at least north of ~30°S. In many regions where ENSO significantly influences the precipitation seasonal cycle, the stable isotopic variability therefore also shows a clear ENSO dependence. In most of tropical South America El Niño events are associated with below average precipitation, while precipitation is abundant during La Niña phases. Therefore El Niño years tend to be characterized by more enriched $\delta^{18}O$ values while they are more negative during La Niña (Vuille et al. 2003a). This is the case, for example, over the Amazon basin or at many Andean ice core locations (Henderson et al. 1999; Bradley et al. 2003; Hardy et al. 2003; Hoffmann et al. 2003; Vuille et al. 2003b). Similarly summers with an intense SASM season tend to show a more negative isotopic composition of monsoon precipitation than years where the SASM is weak. However, as shown by Vuille and Werner (2005), ENSO and the SASM are not independent of one another and, depending on the location, tend to either counterbalance or reinforce one another on interannual time scales. Therefore many regions of South America show a weakened relationship between $\delta^{18}O$ of precipitation and monsoon strength, once the SASM signal is decomposed into its ENSO- and non-ENSO-related variance. Southern Brazil is a notable exception to this rule as its isotopic variability appears to be little affected by ENSO and it therefore offers a great potential to study actual monsoon variability (Vuille and Werner 2005). These studies are fundamental for understanding short-term climate variability in high-resolution $\delta^{18}O$ speleothem records. Preliminary results from studies on speleothem layer counting revealed strong near-decadal variability that is correlated to the North Atlantic oscillation index, which imply in a possible oceanic forcing of monsoon rainfall (Soubies et al. 2005).

Southern Brazil is also an instructive example to demonstrate that the isotopic composition at subtropical regions can be significantly affected by atmospheric processes taking place in far away location upstream, within the tropics. Despite almost steady precipitation throughout the year, the isotopic composition of precipitation in southeastern Brazil is significantly more depleted during austral summer, when moisture is transported southward from tropical to subtropical latitudes by the Andean low-level jet (Fig. 2.1). This depletion is caused by the distant moisture source (recycled moisture from the Amazon basin and the tropical North Atlantic) of summer monsoon precipitation, when compared to the close proximity of the oceanic moisture source responsible for winter precipitation (Cruz et al. 2005b). In fact the tail end of depleted summer rainfall at ~30°S, where a sudden change to more depleted winter precipitation takes place, is a faithful recorder of the southernmost extent of the South American monsoon system (Rozanski and Araguás 1995). As suggested by Vuille et al. (2003a) and later confirmed by Cruz et al. (2005a) proxy records along this border are ideally located to investigate past variations in monsoon extent and intensity. The example from southern Brazil serves as an

important reminder that caution should be exercised when interpreting the climatic controls on isotopic variability and that a simple conversion of isotopic values into "precipitation amount" may be misleading when upstream processes associated with deep convection and rainout or the varying influence of different moisture sources are ignored.

2.2.2 *Factors Affecting the Isotopic Composition of Dripwaters and Modern Speleothems*

Interpreting $\delta^{18}O$ of speleothems in terms of changes in isotopic composition of rainfall requires a good understanding of the hydrologic and geologic features that influence the response of $\delta^{18}O$ in the cave seepage waters to the rainfall recharge events.

This is particularly indispensable for relatively deep caves such as Santana and Botuverá (depth > 100 m), in southern/southeastern Brazil, because in this case the short-term $\delta^{18}O$ responses of dripwater feeding speleothems might be attenuated or even totally buffered due to the greater storage capacity and the resulting larger proportion of older reservoir water in the unsaturated karst aquifer right above the cave. Furthermore, speleothems with distinct $\delta^{18}O$ variations might be formed at different levels along the caves or at sites fed by drips with contrasting hydrologic characteristics, which might be produced by different rates of mixing between old and newly infiltrated waters. On the other hand, this problem is minimized in shallow caves in central Brazil, because of a smaller water reservoir in the aquifer above the cave and fast responses of drip waters discharge to rainfall events (Sondag et al. 2003).

A two-year monitoring program performed on soil and cave seepage waters from sampling sites with contrasting discharge values and located at 100 and 300 m below the surface in the Santana Cave System (Fig. 2.2) revealed important information on the temporal variation of the cave water $\delta^{18}O$ (Cruz et al. 2005b). First, a strong evaporative effect on the isotopic composition of soil and epikarstic waters can be ruled out because all the water infiltrating down to the cave conducts falls on the local meteoric water line. In addition, non-evaporative conditions can also be assumed for the cave environment given the approximate similarity of the observed mean cave temperatures of about 19°C in both Botuverá and Santana caves with the predicted values of temperatures obtained through the equation: $T_P = 16.9 - 4.2 (\delta^{18}O_{calcite} - \delta^{18}O_{water}) + 0.13(\delta^{18}O_{calcite} - \delta^{18}O_{water})^2$(Craig 1965).

This suggests favorable conditions for deposition of speleothems close to isotopic equilibrium with their parental water; otherwise an evaporative enrichment of $\delta^{18}O$ in pool waters should be expected. Thus the oxygen isotopic composition of cave water can be primarily related to the rainfall, as evidenced by the similarity between the mean cave water $\delta^{18}O$ (5.34‰) and the annual weighted mean $\delta^{18}O$ of precipitation observed at IAEA stations along the Southern Atlantic coast (Vuille et al. 2003a).

Second, variations in groundwater $\delta^{18}O$ indicate that the climatic signal of recent rainfall events is rapidly transmitted through the relatively deep karst aquifer to

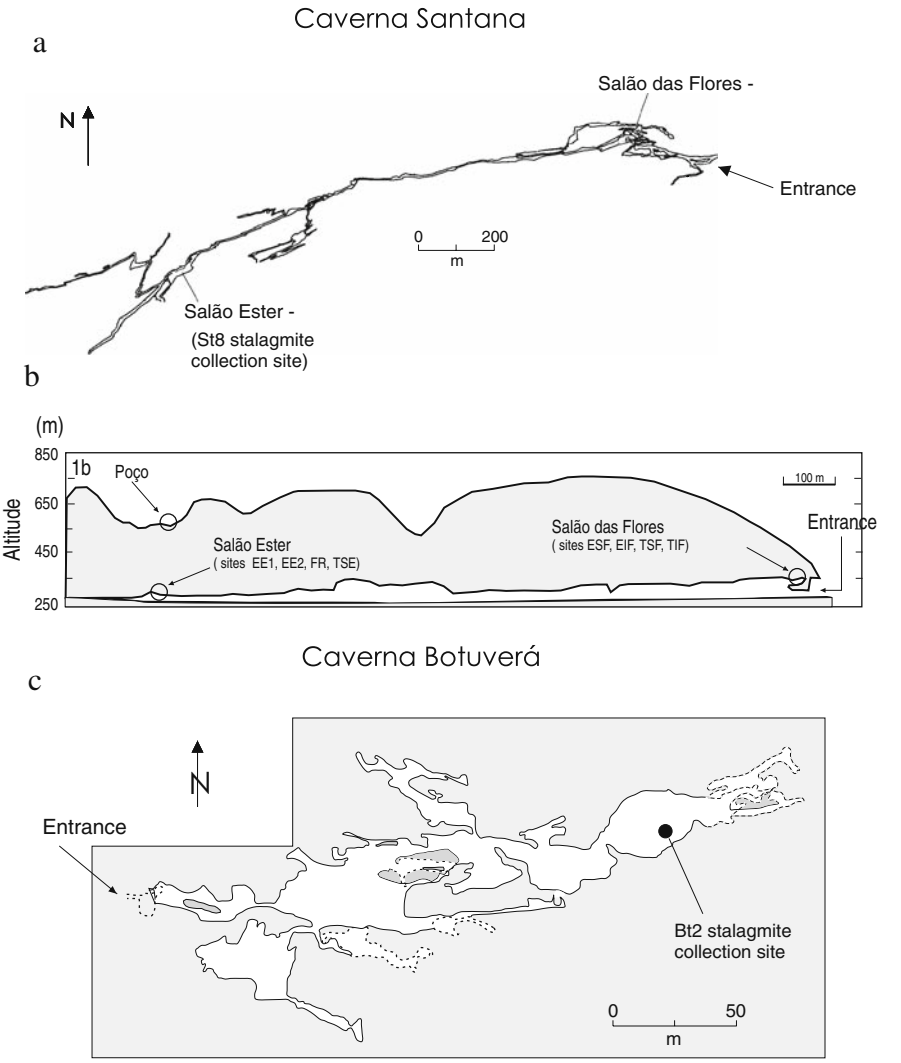

Fig. 2.2 (**a**) Plane view of Santana cave (modified from Viana Jr. 2002); (**b**) Cave longitudinal profile of Santana Cave showing the location of the drip-water monitored sites with depth and distance from entrance; (**c**) Plane view of Botuverá cave (modified from Zilli and Rabelo 2001)

the cave drip waters, regardless of cave location (Fig. 2.3). This is indicated by significant perturbations in the dripwater composition that occur approximately one month after periods of heavy rainfall at the Santana cave site (Cruz et al. 2005b). These $\delta^{18}O$ variations are possibly linked to more enriched rain waters from winter and early spring that are stored in soils and epikarst and later washed down at the peak of the summer rainy season. The lack of $\delta^{18}O$ variations seen in the second year of monitoring is associated with negative anomalies in winter precipitation (Cruz

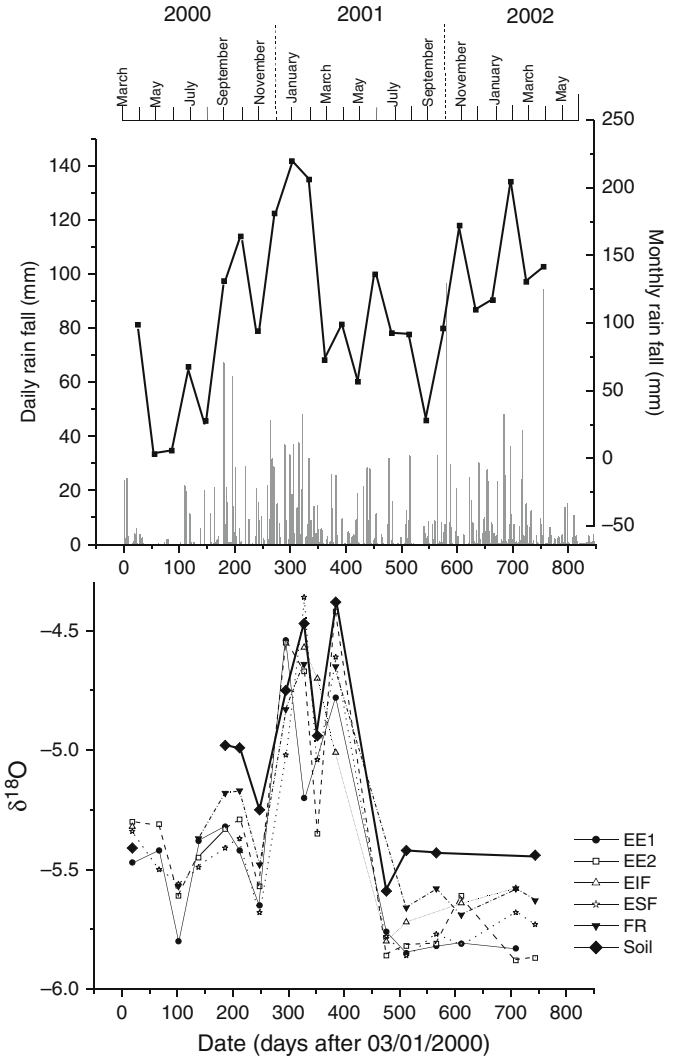

Fig. 2.3 *Top*: Daily and Monthly rainfall amount. *Bottom*: Time series of $\delta^{18}O$ for soil and drip waters at 300 m depth (EE1, EE2, and FR sites) and at 100 m depth (ESF and EIF sites) in Santana cave system

et al. 2005b). In addition, the simultaneous variations in $\delta^{18}O$ among sampling sites also suggest that effective mixing does not significantly influence the response of the drip-water composition to rainfall infiltration; otherwise different responses of infiltrated waters due to variations in aquifer thickness and time of residence should be expected between slow and fast drip flows, as reported in other studies (Ayalon et al. 1998).

These findings indicate that the isotopic composition of drip water is to a large extent influenced by the hydrological regime in which seepage flow occurs during periods of more effective recharge, when the storage capacity in the soil and epikarst zone is exceeded and the water accumulated in the upper parts reaches the whole karst profile in a short time interval. It also implies that CO_2 degassing in stalactite drips is unlikely to be a major factor affecting the isotopic composition of drip waters and consequently the calcite in Santana Cave stalagmites. Otherwise, different responses of infiltrated waters due to variations in time of residence and rate of degassing should be expected between slow and fast dripping speleothems. For example, a relative enrichment in both ^{18}O and ^{13}C caused by a rapid loss of CO_2 from solution has been observed in fast drip stalactites (Johnson et al. 2006; Wiedner et al. 2008).

Calibration studies in caves also provide important information on the relationship between regional climate and the $\delta^{18}O$ of waters forming speleothems. Comparison of cave waters and modern speleothems collected in Santana (24°31′S) and Botuverá (27°13′S) caves reveal a significant meridional gradient in the oxygen stable isotopic composition (Fig. 2.1). The $\delta^{18}O$ of both water and speleothems from Botuverá are more enriched than those from Santana cave by approximately 1‰. The mean $\delta^{18}O$ values in the latter cave are -5.34 ± 0.40‰ (SMOW) and -5.72 ± 0.31‰ (PDB), while in the former cave they are -4.28 ± 0.28‰ (SMOW) and -4.49 ± 0.42‰ (PDB), for drip water and modern speleothems, respectively. These differences in $\delta^{18}O$ have been attributed to changes in the regional rainfall composition as both caves present very close internal temperatures ($\approx$ 19°C) and there is no significant difference in the altitude of the rainfall recharge area. Results suggest that the more enriched values at Botuverá are due to a larger relative contribution of Atlantic moisture and less Amazonian moisture than at Santana. Botuverá has ~20% more precipitation during winter to early spring (July–September, $\delta^{18}O$ mean $\approx$ –3‰) and ~27% less during summer than Santana (December–February, $\delta^{18}O$ mean $\approx$ –7‰).

2.2.3 The Influence of Rainfall Amount on Mg/Ca and Sr/Ca Ratios in Speleothems

Present-day relationships between the Mg/Ca and Sr/Ca ratios of speleothems and climate were studied through a four-year monitoring program of water geochemistry and hydrology performed in the Pérolas-Santana cave system (Karmann et al. 2007). This study evaluated the significance of the commonly reported dissolution and precipitation processes and their possible relationships with changes in rainfall recharge by analysing hydrochemistry and hydrological parameters in different compartments of the cave system such as soil cover, cave drips and rimstone pools and rivers.

It was shown that the ratios of drip water above actively growing speleothems decrease at the height of the wet season, which is driven by the South American Summer Monsoon in the area (from November to February), while it was increasing

during the dry season (from May to August). This relationship was found at drip water sites located in different depths of the cave and with contrasting drip discharges (Fig. 2.4). The most likely process controlling the Ca, Sr and Mg variability in drip waters is the prior calcite precipitation (PCP), which occurs in the unsaturated zone right above the cave (Fairchild et al. 2000; McDonald et al. 2004).

This process is more effective during the dry season when air circulation is enhanced in the upper portions of the karst system due to the low level of the aquifer, which favors the calcite precipitation. PCP increases the Mg/Ca and Sr/Ca ratios because Ca is preferentially incorporated in calcite crystals relative to Mg and Sr as the partitioning coefficients for both Sr ($D_{Sr} = (Sr/Ca)_{calcite}/(Sr/Ca)_{solution}$) and Mg ($D_{Mg} = (Mg/Ca)_{calcite}/(Mg/Ca)_{solution}$) are less than 1 in the low-ionic strength waters (Huang and Fairchild 2001). It affects all the waters in the cave system except the soil and runoff samples because dissolution processes prevail in the epikarstic or surface zone.

Other processes such as groundwater residence time and CO_2 degassing in drip solution are considered less important for the geochemical variations in Santana Cave. The latter has been reported as being an important mechanism, which increases the Mg/Ca and Sr/Ca ratios of the host stalagmite due to progressive removal of C and Ca from a saturated solution during carbonate precipitation in stalactite tips (Johnson et al. 2006). However, the epikarstic waters are always undersaturated with respect to calcite and their variations in Mg/Ca and Sr/Ca ratios differ substantially from those in dripwaters. In addition, simultaneous and relatively rapid variations in the Mg/Ca and Sr/Ca of stalactite drips (Karmann et al. 2007), also observed in $\delta^{18}O$ of water (Cruz et al. 2005b), rule out a major control on trace element ratios by CO_2 degassing (Fig. 2.4). Otherwise a different response of infiltrated water due to variations in time of residence and rate of degassing would be expected between slow and fast drip flow speleothems. Indeed, the elemental ratios are more consistent with variations in rainfall amount than drip discharge and, therefore, can be utilized as a proxy for the past variations of the South American Summer Monsoon. High Mg/Ca and Sr/Ca values are spatially associated with the secondary calcite precipitated in the vadose zone above the cave, which occurs during dry periods, characterized by aquifer low stands.

2.3 Paleoclimatic Changes from Speleothem Records

2.3.1 U/Th Chronology of Speleothems

A major strength of speleothem records is the potential for precise and accurate age control. Carbonate speleothems from tens of years to ~600,000 years are potentially datable by the ^{238}U-^{234}U-^{230}Th disequilibrium techniques (Richards and Dorale 2003). Because solubility of U in groundwater is extremely different from that of Th, a growing speleothem includes U into its crystal lattice but incorporates negligible ^{230}Th (Gascoyne 1992). If the crystal lattice remains a closed system with respect

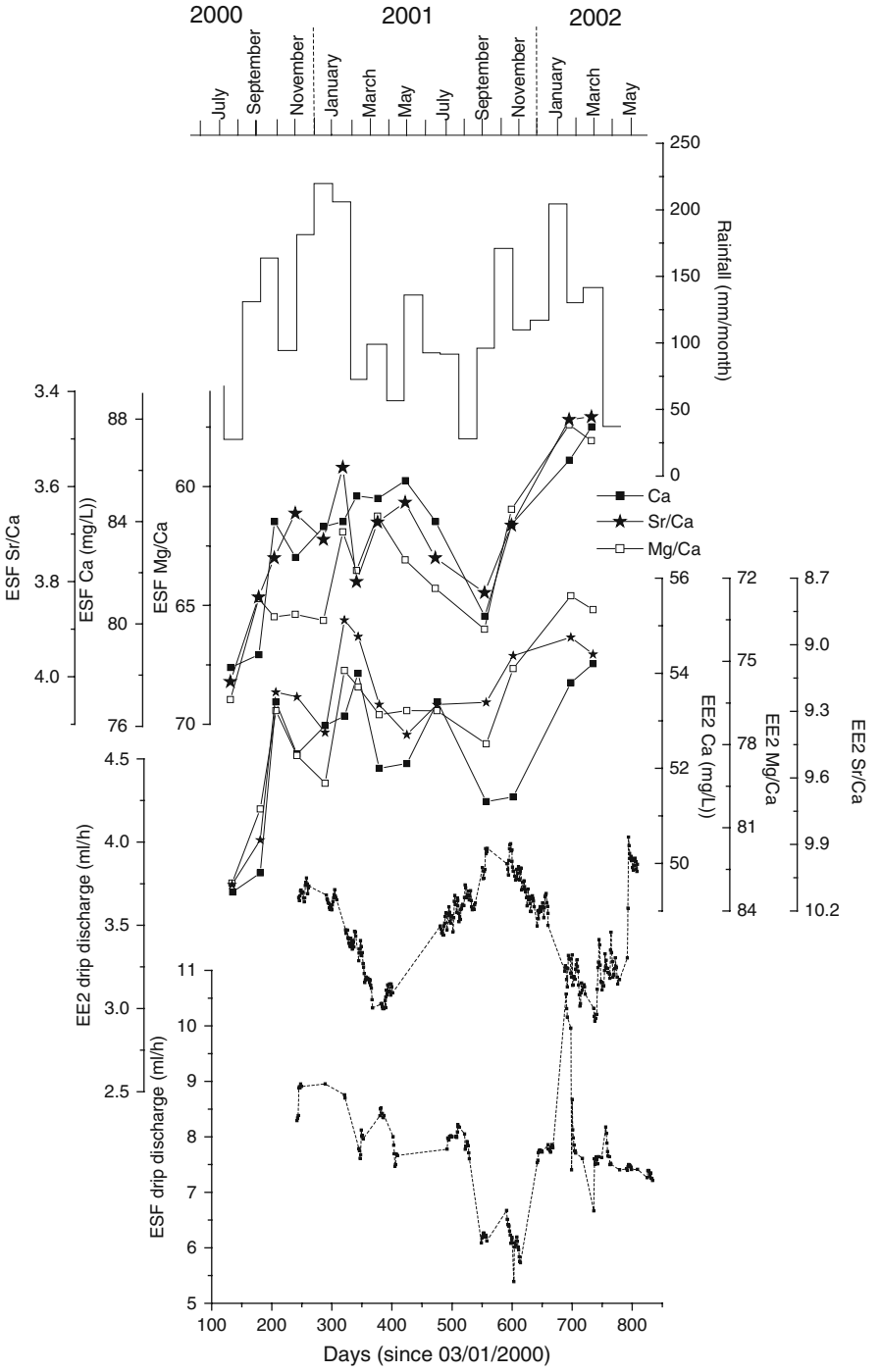

Fig. 2.4 Comparison between Ca, Sr/Ca, Mg/Ca and drip discharge variations at ESF and EE2 sites located 100 and 300 m below the surface in Santana cave, respectively

to the loss or gain of U and Th, the age of a speleothem can be calculated through measurement of radioactive production and decay of their isotopes in the system (Edwards et al. 1987).

Mass spectrometry has largely replaced traditional alpha counting methods for measuring U and Th isotopes on speleothem samples (Edwards et al. 1987; Li et al. 1989). Recently, technical improvements have resulted in a further shift from thermal ionisation mass spectrometry (TIMS) to inductively coupled plasma mass spectrometry (ICP-MS) (Shen et al. 2002; Goldstein and Stirling 2003). The ICP-MS method is preferred due to its distinct advantages, such as higher ionization efficiency and faster sample throughput. ICP-MS has particular interest to speleothem work, which benefits from analyzing small samples (e.g. ~100 mg if samples contain ~1.0 ppm U, Richards and Dorale 2003).

Speleothem samples are cut along the growth axis and sub-samples for dating can then be extracted by milling from flat, polished surfaces using a hand-held dental drill. Chemical separation of U and Th is done in a chemical clean room, following the basic procedure described in Edwards et al. (1987). Samples are totally dissolved with concentrated HNO_3 and then equilibrated with a mixed ^{229}Th-^{233}U-^{236}U spike of known concentration and isotopic composition. U and Th are co-precipitated with Fe and separated by an anion exchange column. Concentrated $HClO_4$ is recommended to use to destroy organics. Finally, the samples are either loaded onto rhenium filaments for TIMS or dissolved in weak nitric acid solution for ICP-MS analysis.

U-Th age errors are dominated by the precision of the analytical measurements and basically follow counting statistics. For typical speleothem samples with uranium concentrations of hundreds ppb to a few ppm, high-resolution dating can provide approximately calculated ages of 500±6 year, 10,000±40 year, 50,000±180 year, 120,000±500 year and 500,000±15,000 year (2σ analytical errors, Richards and Dorale 2003). Age accuracy is determined by the initial concentrations of ^{230}Th, which can be constrained by monitoring ^{232}Th and employing isochron techniques (Richards and Dorale 2003). However, initial ^{230}Th may vary in magnitudes even within the same sample (Shen et al. 2008). As a rule of a thumb, it is crucial to select high quality speleothem samples, i.e. high U content and low detrital contamination, for precise age control.

The uranium concentrations of Brazilian speleothem samples vary from tens of ppb to several ppm (Wang et al. 2004, 2006, 2007a; Cruz et al. 2005a, 2006). Most speleothem ages have 2σ analytical errors that correspond to 0.5–1% of the age. The U-Th ages are in correct stratigraphic order within quoted uncertainties and corrections for initial ^{230}Th are generally negligible. The samples' chronologies are further confirmed by the overall replication between the individual stable isotope profiles either in the same cave (Botuverá cave) or from different regions (i.e. Botuverá and Santana caves, Fig. 2.5). The BT2 age model was refined after Cruz et al. (2005a) by incorporating seven ages between 22,000 and 12,000 years ago and six ages between 42,000 and 62,000 years. With multiple samples, the Brazilian speleothem record now continuously covers the last 130,000 years, with a few episodic growths up to 210,000 years ago.

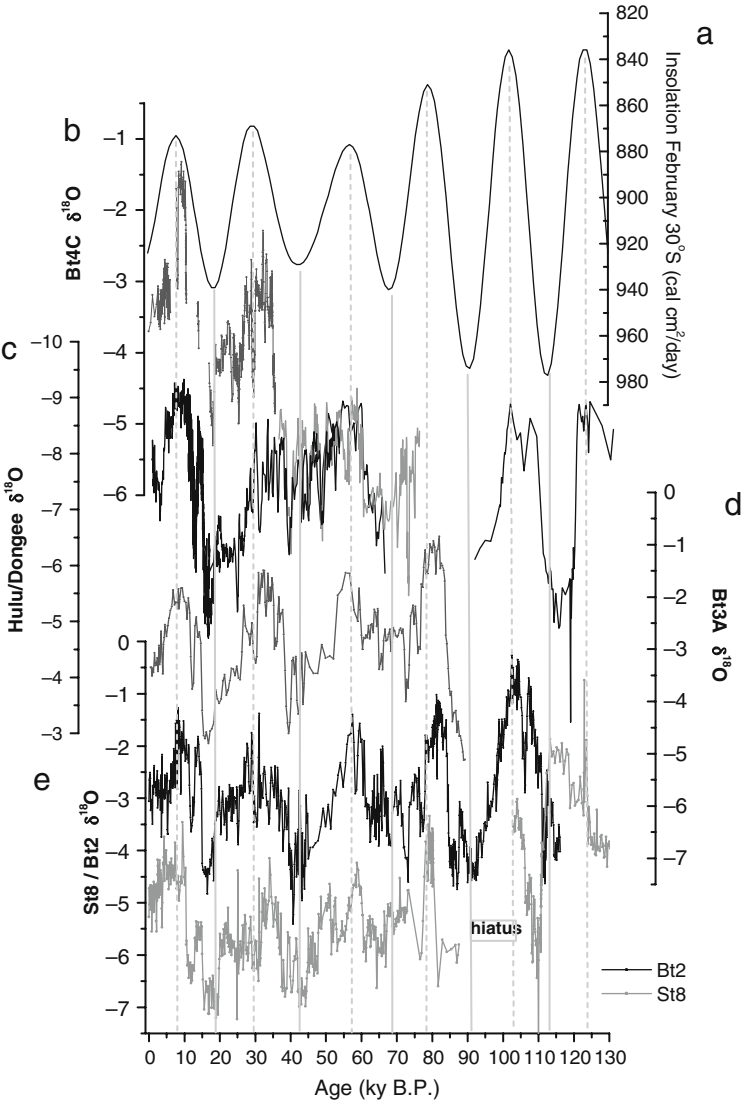

Fig. 2.5 Comparison between (**a**) February insolation at 30ºS (the insolation axis is reversed) and the oxygen isotope ratios of stalagmites; (**b**) BTV4C record from Butuverá cave (Wang et al. 2006); (**c**) Hulu and Dongee records from eastern China (the $\delta^{18}O$ axis is reversed, Wang et al. 2001; Yuan et al. 2004); (**d**) BT3A record from Botuverá cave (Wang et al. 2007a); (**e**) BT2 record and St8 records from Botuverá and Santana caves, respectively (Cruz et al. 2005a, 2006)

2.3.2 Stable Isotope Records

The speleothem isotope records in this study are from stalagmites collected in the Botuverá cave (Bt2, 27°13′24″S; 49°09′20″W) and in the Santana cave (St8, 24°31′51″S; 48°43′36″W), located 300 km apart in southeastern and southern

Brazil, respectively (Fig. 2.1). This set of records, consisting of five stalagmites from Botuverá cave and one from Santana cave, describes changes in the regional precipitation regime in subtropical Brazil over approximately the last 130,000 years (Fig. 2.5). The $\delta^{18}O$ in these records shows an amplitude of more than 4‰, with a mean resolution of 40–60 years for stalagmites Bt4a, Bt4c, Bt21a (Wang et al. 2006), ~150 years for Bt2 and St8 (Cruz et al. 2005a, 2006) and ~370 years for Bt3a (Wang et al. 2007a, b).

All the stalagmites appear to have been deposited in approximate isotopic equilibrium with cave drip water as indicated by the absence of significant correlations between $\delta^{18}O$ and $\delta^{13}C$ along their long axis according to the Hendy test (Mickler et al. 2006. Besides, the relatively large range of variation in $\delta^{18}O$ exclude a significant control by temperature, since the temperature-dependent fractionation between calcite and water is relatively small, –0.24‰/°C (Friedman and O'Neil 1977). The $\delta^{18}O$ variations are also inconsistent with the reported cooler and warmer periods during the last glacial and Holocene, respectively. Therefore, $\delta^{18}O$ variations of these speleothems are primarily related to changes in $\delta^{18}O$ of regional precipitation.

Figure 2.5 presents a comparison of the speleothem $\delta^{18}O$ time series with February insolation at 30°S (the scale for insolation is reversed). The calcite $\delta^{18}O$ shows a striking match with insolation throughout the last glacial period and is characterized by lower $\delta^{18}O$ values coinciding with maxima in insolation for each precessional cycle (periodicity of ~20 ka). However, this cyclicity is not as well defined in St8 as in Botuverá, in particular during the positive phases of summer insolation between 70 and 20 ka. Superimposed on the insolation-driven tendency are abrupt millennial-scale events, recognizable in all stalagmites as secondary fluctuations of 1.5–2‰. They are nearly coincident with one another and with variations seen in Northern Hemisphere paleoclimate records on the same timescale, especially during the so-called Heinrich events (NGRIP 2004). Despite the similarity of the records, the region presents a strong isotopic gradient, characterized by mean values, which are consistently about 2‰ higher at Bt2, when compared with St8.

Past changes in the oxygen isotope ratios are interpreted in terms of shifts in the seasonal balance of precipitation between winter-extratropical versus summer-monsoonal rainfall. This interpretation is supported by observations of the modern isotope climatology, as discussed above. Hence the $\delta^{18}O$ of Brazilian subtropical speleothems is thought to be primarily a function of the rainfall moisture source during the late Pleistocene, which in turn, is connected to the regional atmospheric circulation patterns (Cruz et al. 2005a). Lower values of $\delta^{18}O$ therefore reflect a greater proportion of more depleted SASM rainfall compared to the enriched extratropical rainfall and vice-versa.

2.3.3 Speleothem Growth Intervals

Speleothems can only grow if there is enough seepage water reaching the cave. These conditions are commonly not found in glaciated regions or in arid/semi-arid zones, such as northeastern Brazil (Site 3 in the Fig. 2.1). In these conditions, absence or occurrence of speleothems can be a reliable indicator of past climatic

conditions. In semi-arid northeastern Brazil, home of South America's most extensive cave systems, profuse speleothem deposition occurred in the past. The present semi-arid climate, in which evapotranspiration (~1,400 mm/year) largely exceeds rainfall (~490 mm), does not allow for significant water infiltration and, consequently, speleothem generation. Thus, speleothem growth phases are a clear indicator of wetter conditions than at present at this site.

In addition to speleothems, abundant travertine deposits occur in the area. Travertines are also relict features in the present climate. Since they were generated by bicarbonate-rich shallow spring waters, which only flow when a net regional recharge to groundwater exists, they are also good indicators of past pluvial phases. It should be noted, however, that travertines tend to be a more sensitive paleopluvial feature than speleothems, since they were deposited in streams directly affected by rainfall events. In contrast, an infiltration threshold needs to be overcome in order to activate percolation routes responsible for drip waters forming speleothems. For this reason, travertines might be formed in periods that are not wet enough to promote speleothem growth.

The combined speleothem/travertine record shows a series of short-lived growth intervals (Fig. 2.6). The large majority of speleothems grew very quickly, during highly episodic wet phases as short as several hundred years, with some lasting up to a few thousand years. Last glacial pluvial phases, centered at around ~15.5 ka, 39 ka, 48 ka and additional growth phases between 60 and 74 ka correlate precisely with Heinrich Events recorded in the Northern Hemisphere as well as to high $\delta^{18}O$ recording low monsoon activity in Chinese speleothems (Wang et al. 2004) and to peaks of low $\delta^{18}O$ depicted in southeastern Brazil speleothems (Wang et al. 2006, 2007a) (Fig. 2.6). Pluvial periods in now semi-arid northeastern Brazil are associated with the displacement of the ITCZ, probably representing times when the ITCZ was located south of its present mean position.

2.3.4 Mg/Ca and Sr/Ca Ratios

Mg/Ca and Sr/Ca ratios measured in the Bt2 stalagmite record, presented here as anomalies (departure from total mean), are positively correlated with one another ($r^2 = 0.55$) and show a pattern that is coherent with southern hemisphere summer insolation and stable oxygen isotope ratios during the last 116 ka (Cruz et al. 2005a, Wang et al. 2007a). This pattern is characterized by a general increase in trace element ratios and $\delta^{18}O$ values during low insolation phases and vice-versa. However, there are some significant differences in the long-term variability of trace element ratios throughout the last glaciation (Fig. 2.7). For instance, the positive relationship between Mg/Ca, Sr/Ca and insolation is less clear during periods of lower amplitude insolation changes, such as from 70 to 17 ka or during the Marine Isotope Stages 4 to 2 (Abreu et al. 2003), similar to the $\delta^{18}O$ variations of St8 record (Cruz et al. 2006a).

Elemental ratios of Bt2 have been interpreted as a proxy for local hydrological changes based on evidence for a primary control of Mg/Ca and Sr/Ca ratios

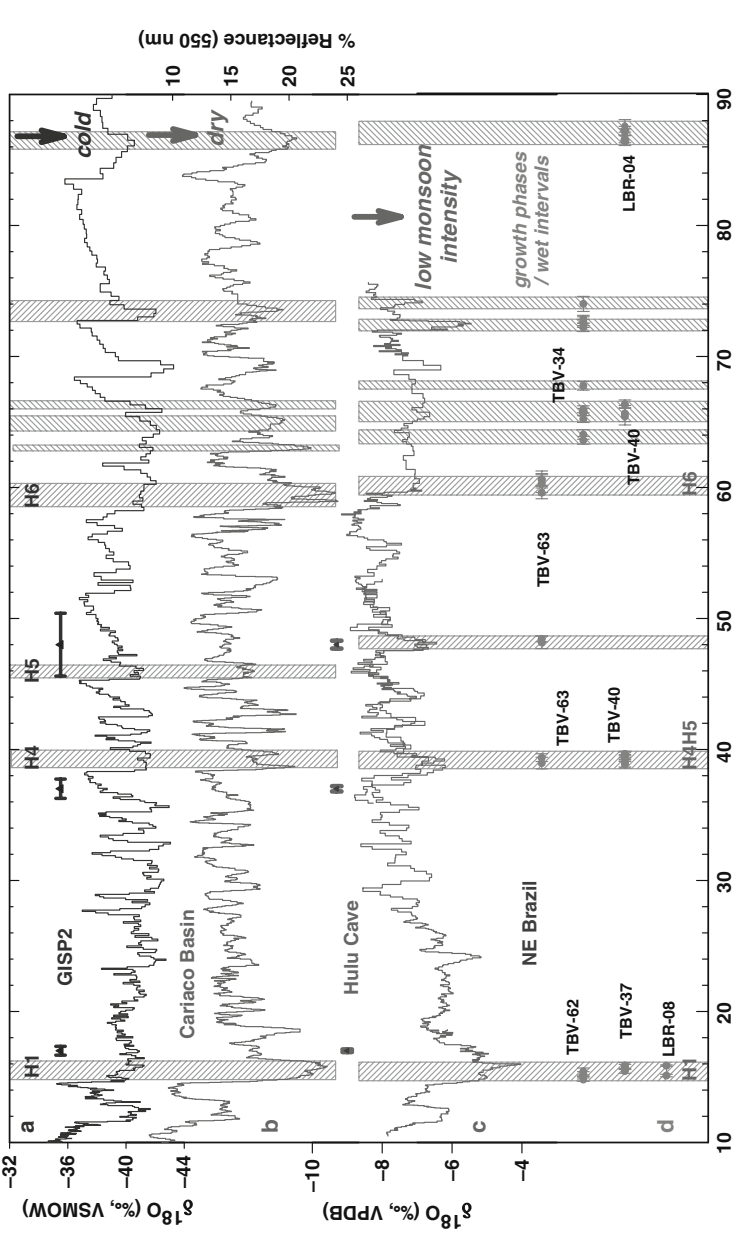

Fig. 2.6 Comparison of the growth patterns of speleothems from northeastern Brazil with events recorded in several Northern Hemisphere palaeoclimate archives; (**a**) $\delta^{18}O$ values of Greenland ice (Grootes and Stuiver 1997); (**b**) Light colour reflectance (*greyscale*) of the Cariaco basin sediments from ODP Hole 1002C5 (Peterson et al. 2000); (**c**) $\delta^{18}O$ values of Hulu cave stalagmites (Wang et al. 2001); (**d**) Speleothem growth patterns in northeastern Brazil. Growth intervals are shown by separated *gray dots* or connections between dots if they are within the same phase. 2σ dating errors (error bars) are typically 0.5–1‰. *Gray hatched vertical bars* indicate possible correlations between four records. Also shown are dating errors for the GISP2 ice core 29 (*black horizontal bars*) and Hulu cave speleothems (*gray horizontal bars*). VSMOW, Vienna standard mean ocean water. VPDB, Vienna PeeDee Belemnite. H1, H4, H5, H6, Heinrich events

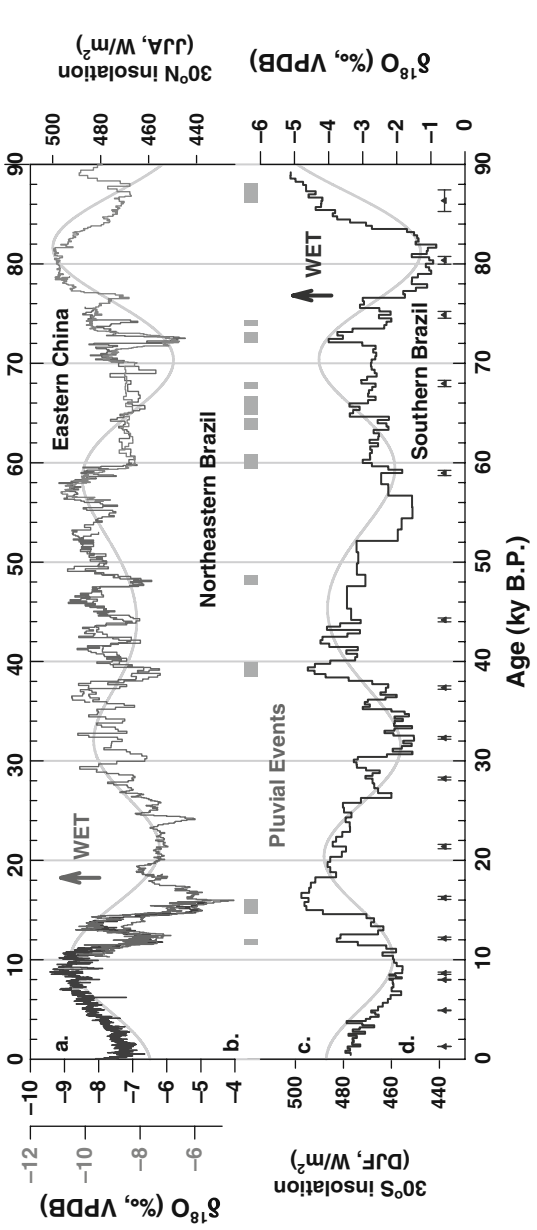

Fig. 2.7 Comparisons of speleothem records: (a) A combined profile of the eastern China $\delta^{18}O$ records (Dongge Cave, Yuan et al. 2004; Wang et al. 2005; Hulu Cave, Wang et al. 2001; and Shanbao Cave, Yongjin Wang and R.L. Edwards, unpublished data). Contemporaneous Dongge and Hulu stalagmites have virtually identical $\delta^{18}O$ values, while Shanbao values are offset by about –1‰, but with a similar pattern to Hulu (see replicated portions); (b) Northeastern Brazil growth periods (Wang et al. 2004); (c) BTV3A from Botuverá cave, Brazil $\delta^{18}O$ record (Caverna Botuverá, Wang et al. 2007a); (d) 2σ age error bars for the BTV3A record. Note scales for speleothem $\delta^{18}O$ are all reversed, increasing downwards. All three chronologies are established independently with uranium-thorium methods, with typical 2σ errors of about 0.5–1%. Also shown are 30°N and 30°S summer insolation (JJA and DJF, respectively, *gray curves*)

by prior calcite precipitation from the modern calibration study in Santana cave. These trace element ratios also show a coherent positive covariation during the last 116 ka and a consistent relationship with the $\delta^{18}O$ of the same stalagmite (Cruz et al. 2007). Furthermore, comparing these ratios with the Bt2 growth rates and $\delta^{13}C$ variations suggest that both growth rates and CO_2 degassing mechanisms are not a major control of the incorporation of Sr and Mg in the calcite (Huang and Fairchild 2001; Treble et al. 2003; Johnson et al. 2006). Thus, the regional climate variability inferred from these elemental ratios can be used as a proxy for mean rainfall amount, which in turn complements the reconstruction of the past activity of South American summer monsoon (SASM) and extratropical rainfall in subtropical Brazil, anchored in the speleothem $\delta^{18}O$ records (Cruz et al. 2005a; Wang et al. 2006; Cruz et al. 2006a; Wang et al. 2007a).

2.4 Discussion

Combined oxygen isotope and trace element records suggest that the past changes in southern Brazil rainfall were mostly led by the convective activity associated with the South American summer monsoon (Cruz et al. 2007; Fig. 2.7). Since the $\delta^{18}O$ of speleothems is directly affected by the isotopic composition of summer rainfall, it can be used to infer the mean location and intensity of the SASM and the South Atlantic convergence zone (SACZ). These features are closely linked to the intensity and location of convective precipitation over the Amazon basin and surrounding regions, because they influence the strengthening or weakening of moisture transport by the Andean low-level jet (ALLJ) from the southern Amazon to the subtropical Atlantic coast (Gan et al. 2004). On the other hand, the speleothem growth phases in northeastern Brazil suggest a direct coupling of regional climate to the mean latitudinal position of the ITCZ (Wang et al. 2004; Fig. 2.6).

To date, the Brazilian speleothem records suggest that past changes in tropical rainfall are associated with climate forcing mechanisms acting on both orbital and millennial time-scales, such as insolation precession and land- and sea-ice coverage in the northern hemisphere (Chiang et al. 2003; Claussen et al. 2003). These mechanisms impact the tropical rainfall distribution by influencing the moisture transport from the tropical Atlantic to the continent, thereby changing low-level moisture convergence and convective activity throughout much of tropical South America.

2.4.1 Long-Term Paleoclimatic Changes

Speleothem $\delta^{18}O$ records have revealed that the variations in the convective intensity within the area affected by SASM/SACZ are dominated by changes in precession-driven solar insolation (Cruz et al. 2005a; Wang et al. 2006, 2007a; Cruz 2006). Insolation determines the north-south displacement of continental convection over South America by favoring moisture convergence over the continent during periods

of increased land-sea temperature contrasts at the solstices (Biasutti et al. 2003). In the past, periods of increased monsoon precipitation in subtropical Brazil occurred in response to enhanced summer solar radiation following the Milankovich ~23 ka precession cycle (Fig. 2.5). Similarly, the speleothem $\delta^{18}O$ records from Hulu and Dongee caves in eastern China (Fig. 2.5) also exhibit an insolation-driven control, which is out of phase with the Brazilian records (Wang et al. 2004; Yuan et al. 2004).

The SASM is reinforced at its southeastern border as the southern hemisphere Hadley cell is strengthened and displaced southward during high insolation phases, thereby increasing the relative contribution of summer monsoonal rainfall to the region. Further evidence for such a monsoon intensification comes from lake records in the Bolivian Altiplano, where similar wet conditions were observed during the last glacial period (Baker et al. 2001a). The comparison between SE Brazil and the Altiplano also holds during the Holocene, when the speleothem isotope records become progressively more negative after 4 ky, concurrent with an increase in summer rainfall on the Altiplano (Seltzer et al. 2000; Baker et al. 2001b; Moreno et al. 2007). At the same time a southward expansion of the Amazon rainforest is observed along its southwestern border (Mayle et al. 2000).

Although the insolation-driven paleo-rainfall, inferred from the Botuverá and Santana speleothem records, appears to be consistent with other available records from the region, it is still necessary to reconstruct each step of the monsoon evolution during the past, in order to elucidate the causal mechanism interconnecting the climate in southern Brazil with the center of deep convection over the Amazon region. To do this, some aspects of the moisture advection from the tropical Atlantic to the Amazon Basin need to be addressed in more detail for the last glacial period.

Unlike the present-day situation, it is difficult to link past low-frequency rainfall oscillations in South America with meridional sea surface temperature (SST) gradients in the tropical Atlantic or SST anomalies in the equatorial Pacific. It is reasonable to assume that the SASM may be intensified because of a more southerly position of the Atlantic Intertropical Convergence Zone (ITCZ) during periods of increased southern hemisphere insolation. However, except for the Holocene part of the Ti-Fe record from the Cariaco Basin (Haug et al. 2001), there is no clear match between summer insolation and hydrological (Arz et al. 1998; Peterson et al. 2000; Jennerjahn et al. 2004) or SST records (Arz et al. 1999, Lea et al. 2003; Weldeab et al. 2006) off the Venezuelan and Brazilian coast. Instead, both hydrological and SST variations in these records are dominated by millennial-scale events, such as Dansgaard-Oeschger- and Heinrich-events (see the discussion in the section below). Thus, it appears that the southeastward displacement of deep continental convection from the Amazon Basin to southeastern and southern Brazil is, at least partially, decoupled from oceanic conditions in the tropical Atlantic on orbital time-scales. Instead it appears as if changes in South American monsoon circulation during the last glacial and the Holocene were dominated by changes in sensible and latent heat transfer over land due to orbitally driven changes in solar radiation, rather than by changes in moisture influx from the Atlantic Ocean, associated with a southward displaced ITCZ (Haug et al. 2001). Indeed recent studies have shown that latent heat release over the Amazon basin is paramount for the development of the upper-level

monsoon circulation, including the Bolivian High (Lenters and Cook 1997), which is associated with the southeastward extension of the SASM into the SACZ region (Zhou and Lau 1998; Gan et al. 2004).

One question, which cannot be answered by looking solely at speleothem $\delta^{18}O$ records, is to what extent an intensification of the SASM increases the long-term mean rainfall amount in southern Brazil. Since $\delta^{18}O$ variations in stalagmites from the Brazilian subtropics record not just monsoonal (60% of annual accumulation today), but also extratropical rainfall (40% of annual accumulation today), they cannot be used to directly infer mean rainfall variations. For example, an increase in the more isotopically depleted monsoon rainfall (today $\sim$ –7‰) might be compensated by a decrease in more enriched extratropical rainfall ($\sim$ –3‰) and thus create a more negative average $\delta^{18}O$ without any change in the total rainfall amount.

Instead changes in rainfall amount can be inferred by the use of Mg/Ca and Sr/Ca ratios, as reported by Cruz et al. (2007) for the last 116 ka based on the Bt2 stalagmite. The comparison with the $\delta^{18}O$ record suggests that increased local rainfall recharge occurred during periods of enhanced monsoon rainfall in the region coincident with high summer insolation phases, as manifested by lower values of both $\delta^{18}O$ and trace element ratios in Bt2 (Fig. 2.7). Conversely, relatively dry conditions, as indicated by higher trace element ratios during low insolation phases, must have been caused by a reduction in summer monsoon rainfall, since a decrease in the isotopically-enriched extratropical winter rainfall would have resulted in more negative $\delta^{18}O$ values in the Bt2 stalagmite. Therefore, this multi-proxy study confirms that the contribution of SASM precipitation is the dominant factor explaining precipitation variations in subtropical Brazil during the last glacial-deglacial period. In addition, the steep north–south gradient in $\delta^{18}O$ of speleothems throughout the region, characterized by more negative values of ST8 (–2‰) as compared to Bt2, indicate a higher relative contribution of SASM precipitation to the north at Santana cave. This gradient is also observed today in cave drip waters and modern speleothems (Cruz et al. 2005b).

There are, however, some significant fluctuations in the long-term variability of trace element ratios from 70 to 17 ka that cannot be explained by summer insolation forcing alone. These departures are characterized by a predominance of negative trace element anomalies despite low-insolation phases, which suggests that rather wet conditions persisted throughout most of the last glacial period due to longer and more intense summertime rainfall. This notion is supported by synchronous negative anomalies in both trace element ratios and $\delta^{18}O$ in Bt2 and St8 (Fig. 2.7). Hence, the weaker correspondence between trace element variations and insolation suggests that other factors must have contributed to the excess of monsoon rainfall during this time period.

Teleconnections from the high northern latitudes under glacial boundary conditions, dominated by extensive land- and sea-ice volume buildup, are a likely factor influencing the monsoon intensification observed in the region between 70 to 17 ka. According to simulations by Chiang et al. (2003) high-latitude glacial conditions are transmitted to the tropics through strengthened northeasterly trades over the North Atlantic, which increase the latent heat flux, in turn causing a progressive cooling

of SSTs from the subtropical (Moreno et al. 2002; Abreu et al. 2003) to the tropical North Atlantic (Lea et al. 2003). As a consequence, this mechanism results in tropical Atlantic meridional SST gradients that favor a southerly displacement of the ITCZ. A more southerly position of the ITCZ, in turn will enhance the moisture flux into the Amazon Basin, ultimately triggering an intensification of the SASM in southern Brazil. This hypothesis is broadly supported by the coincidence of lower trace element ratios in Bt2 with lower SSTs in the subtropical North Atlantic (Abreu et al. 2003), as indicated by heavier $\delta^{18}O$ in planktonic foraminifera during Marine Isotope Stages 4 to 2 (Fig. 2.7). This interpretation is also in agreement with the wettest conditions recorded during the same period in Salar de Uyuni, an area in the Bolivian Altiplano where precipitation equally depends on SASM activity (Fritz et al. 2004).

2.4.2 Millennial-Scale Abrupt Changes in Climate

During the last glacial period, Greenland experienced millennial-scale abrupt climate changes (Dansgaard et al. 1993; Grootes et al. 1993; NGRIP members 2004). As observed in the polar ice cores, temperature could change 7–12°C in decades or less over Greenland, accompanied by dramatic fluctuations of atmospheric methane, sea-salt and dust concentrations (Mayewski et al. 1997; Severinghaus and Brook 1999; Blunier and Brook 2001). Since this discovery, similar events have been identified at many locations around the world (Voelker et al. 2002). Mechanisms of these abrupt climate events, however, are not yet resolved (Broecker 2003). A full understanding of the causes of these climate events requires our knowledge of the spatial and phase relationships between different paleoclimate records.

Recently, there is steadily increasing interest in obtaining records of millennial-scale climate events in speleothems from low-to-mid latitudes (Wang et al. 2001; Spötl and Mangini 2002; Bar-Matthews et al. 2003; Burns et al. 2003; Genty et al. 2003; Drysdale et al. 2007). With high-precision absolute-dated chronology, such studies on speleothems can not only test whether the abrupt climate events were a global phenomenon, but also help to reveal the mechanisms that were responsible for the events. Abrupt climate events have also been identified in different speleothem proxy records from tropical and subtropical Brazil. Indicated by speleothem short growth phases, current semi-arid northeastern Brazil has endured millennial-scale episodic wet periods in the past (Wang et al. 2004). In southeastern and southern Brazil, the speleothem $\delta^{18}O$ records also successfully capture millennial-scale events that are superimposed on the orbital-scale variations during the last glacial period (Cruz et al. 2005a, 2006; Wang et al. 2006, 2007a). The abrupt drop in $\delta^{18}O$ associated with these events is large, with up to 2‰ amplitude. Together with speleothem Mg/Ca and Sr/Ca ratios (Cruz et al. 2007), these suggest that SASM intensity and monsoonal rainfall has undergone abrupt changes in the region during the last glacial period.

Using their individual chronologies, the Brazilian speleothem records can be compared with the contemporaneous records from the northern hemisphere. Wet periods in northeastern Brazil are synchronous with periods of weak East Asian summer monsoons (Wang et al. 2001), cold periods in Greenland (Grootes and Stuiver 1997) and Europe (Genty et al. 2003); Heinrich events in the North Atlantic (Bond et al. 1993) and periods of decreased river runoff to the Cariaco basin (Peterson et al. 2000). The comparison between the Botuverá $\delta^{18}O$ records and the eastern China $\delta^{18}O$ profile also show, within their dating errors (a typical relative 2σ error in age of about 0.5–1%), a remarkable anti-correlation on both orbital and millennial timescales (Fig. 2.8). Throughout the whole profile, the lower Botuverá $\delta^{18}O$ coincides precisely with the higher $\delta^{18}O$ in the eastern China speleothems. However, the opposite is not so evident because no clear increase in the $\delta^{18}O$ of Brazilian speleothems is observed during the warm periods in the northern hemisphere that are coincident with the Daansgard-Oeschger events.

During the last glacial period, an abrupt reduction in the Atlantic overturning induces sea ice expansion in the North Atlantic and a subsequent southward displacement of the intertropical convergence zone (ITCZ) (Chiang et al. 2003; Chiang and Bitz 2005). This may cause an abrupt shift in the tropical hydrologic cycle, as seen in the Cariaco Basin (Peterson et al. 2000) and northeastern Brazil (Wang et al. 2004). Modeling efforts also indicate that weak ocean circulation may result in a positive SST anomaly in the South Atlantic and a weaker pole-to-Equator temperature gradient in the south (Crowley 1992) and the predictions are confirmed by studies of ocean sediment cores (Arz et al. 1998; Rühlemann et al. 1999). As observed today (Robertson and Mechoso 2000; Doyle and Barros 2002; Liebmann et al. 2004), a warm SST anomaly in the western subtropical South Atlantic (WSSA) may stimulate a persistent intense South American Summer Monsoon (SASM) and strong low-level jet (LLJ), which consequently supplies plenty of isotopically depleted precipitation into southern Brazil (Vuille and Werner 2005).

Moreover, analogous to modern seasonal observations in boreal winter (Lindzen and Hou 1988), southward ITCZ migration during millennial-scale stadial events may have caused a meridional asymmetry in the Hadley circulation. A southward shift of the zonal-mean Hadley cell would change meridional moisture transport through intense ascending air masses in the southern low latitudes and increased subsidence in the northern tropics and subtropics. Broadly, the northern low latitudes would be drier and the southern low latitudes wetter, which has been confirmed by recent model results (Clement et al. 2004; Chiang and Bitz 2005). The opposite scenario would have been true during glacial interstadial periods.

We can therefore define an index (speleothem $\Delta\delta^{18}O$) to monitor the displacement history of the mean ITCZ position and the associated strength of the past Hadley circulation. This index is given by the difference of calcite $\delta^{18}O$ values between samples from southern Brazil and eastern China (Table 2.1). As discussed above, low (high) calcite $\delta^{18}O$ values in southern Brazil correspond to high (low) calcite $\delta^{18}O$ values in eastern China. Thus, small (large) speleothem $\Delta\delta^{18}O$ values are linked to North Atlantic cold (warm) temperature, reduced (enhanced) ocean

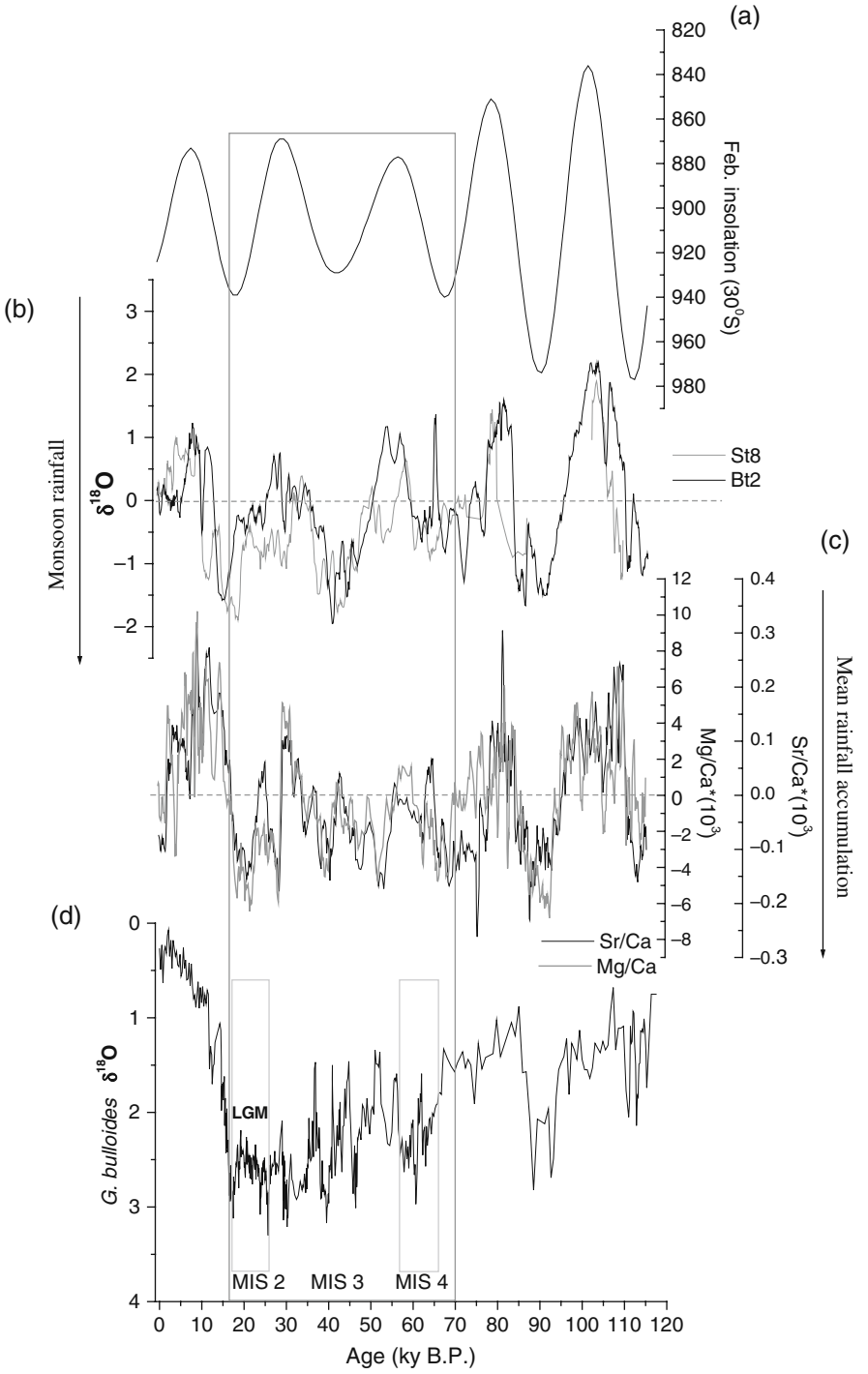

Fig. 2.8 (continued)

Table 2.1 Speleothem $\Delta\delta^{18}O$ index between Southern Brazil and Eastern China

Time window	Eastern China speleothem $\delta^{18}O$ (‰, VPDB)	Southern Brazil speleothem $\delta^{18}O$ (‰,VPDB)	$\Delta\delta^{18}O$ index (‰,VPDB)
Heinrich event 1	~ – 4.9	~ – 4.7	~ 0.2
Early Holocene	~ – 9.3	~ – 1.8	~ 7.5
Today	~ – 7.3	~ – 3.3	~ 4.0

circulation, and a southward (northward) shift of the ITCZ mean position. The North Atlantic circulation is nearly shut down during Heinrich Event 1 (H1) and is substantially strengthened during the early Holocene (McManus et al. 2004). Therefore, we select calcite $\Delta\delta^{18}O$ index values during H1 and the early Holocene as two end members that represent two extreme mean positions of the ITCZ and asymmetries of the Hadley circulation. Today's index value is around 4.0‰, which is close to the average between H1 and early Holocene values of about 0.2 and 7.5‰, respectively. This approach suggests an intermediate state of the mean ITCZ position and weak asymmetry of the Hadley circulation in the modern world.

It is still under extensive debate whether meridional overturning circulation (MOC) changes or tropical air-sea interactions, such as persistent El Niño-Southern Oscillation events (Super-ENSO), have triggered the millennial-scale climate events (Broecker 2003). Phase relationships of these events in Brazilian speleothem records may have implications on their mechanisms. The modern climate in both northeastern and southern Brazil is sensitive to the ENSO phenomenon. For example, modern El Niño events induce drought in northeastern Brazil and high precipitation in southern Brazil (Lau and Zhou 2003). If the modern ENSO behavior does not change substantially with time, the Super-ENSO scenarios may result in opposite rainfall patterns between the two regions. On the other hand, changes in the MOC would cause a latitudinal ITCZ migration and associated changes in the Hadley circulation (Chiang and Bitz 2005). This may cause in-phase precipitation changes in northeastern and southern Brazil on millennial timescales. With their robust chronologies, the Botuverá speleothem $\delta^{18}O$ record can be compared to the record of speleothem growth periods from northeastern Brazil (Wang et al. 2007b). Although the latter may not be a complete data set, a striking positive phase relationship stands out between the two records. For instance, northeastern Brazil speleothem resumes

Fig. 2.8 (continued) (**a**) February insolation at 30°S (the insolation axis is reversed); (**b**) $\delta^{18}O$ anomalies for Bt2 (Cruz et al. 2005a) and St8 (Cruz et al. 2006) stalagmites; (**c**) Mg/Ca and Sr/Ca anomalies for Bt2 stalagmite; (**d**) $\delta^{18}O$ of planktonic foraminifera in the core MD95-2040 from Iberian Margin in North Atlantic (Abreu et al. 2003). Note the predominance of low trace element and more positive values of $\delta^{18}O$ of planktonic foraminifera during the MIS4 to MIS2 (marked with *rectangles*)

growth around 87 ka, 72 ka, 66 ka, 60 ka, 48 ka, 39 ka, 16 ka and 12 ka, when $\delta^{18}O$ values are relatively low in the southern Brazil sample. As both proxies represent regional rainfall changes, this correlation suggests that on millennial timescales, rainfall changes in the two regions are in phase. This relationship is consistent with shifts in the mean ITCZ position, linked to MOC changes, but not with the Super-ENSO mechanism.

2.4.3 Broader Significance of Precipitation Changes Based on Speleothem Records

The speleothem records suggest a new scenario for the paleoclimate in southern Brazil, featuring a predominantly wet last glacial period. These findings have important implications for the inferred paleoenvironmental changes from the pollen records and consequently for the "refugia" hypothesis (Haffer 1997). This is still a highly controversial matter because a considerable number of pollen records point to a complete dominance of grasslands over forests during the last glaciation in subtropical Brazil due to colder and drier conditions (Behling 2002), while other records suggest that an expansion of humid forests occurred during significant parts of this period in agreement with the precipitation changes inferred from speleothems (Ledru et al. 2005). Therefore, the existence of forests "refugia" as a consequence of a large-scale drying during the glacial period needs to be revised, once robust indications of wetter conditions have been found in several areas in South America. An alternative explanation for the changes in tropical biodiversity is the periodic exchange between distinct forests biomes during wet events, such as indicated by the study of paleobotanical remains preserved in travertines, which revealed a rapid expansion of humid forests over caatinga vegetation (dry savanna) in northeastern Brazil during the period coincident with H-events (Wang et al. 2004).

Substantial intensification of the tropical circulation system in subtropical South America at high insolation phases in the southern hemisphere and during cold periods in the Northern Hemisphere (H-events, MIS-4 to MIS-2) recorded in Brazilian speleothems is also important in an attempt to interpret the isotope records from Andean ice-cores and the events of moraine deposition in terms of temperature or precipitation changes (Ramirez et al. 2003; Zech et al. 2007), because an enhancement in the moisture flux and moisture convergence in southern Brazil is likely to affect precipitation in Andes in the same way during the South American summer monsoon season.

2.5 Conclusions

Combined time-series of $\delta^{18}O$ and elemental ratios of speleothems suggest that the long-term variations in mean precipitation in subtropical Brazil during the last glacial period and Holocene are in general modulated by changes in the southern

hemisphere summer insolation. The South American monsoon is intensified at high insolation phases when the transport of low-level tropical moisture from the Amazon Basin to southeastern Brazil is enhanced; most likely due to a more favorable upper-level circulation, established by enhanced latent heat release over the tropics. However, the northern Hemisphere glacial boundary conditions probably played an important role by modulating moisture flux and convergence into the southern hemisphere tropics during austral summer. This impact is documented by the rainfall excess in the region from 70 to 17 ka and especially at the last glacial maximum, as indicated by rather negative anomalies of $\delta^{18}O$, Mg/Ca and Sr/Ca during this period.

Speleothem growth intervals and variations of $\delta^{18}O$ on millennial time-scales indicate significant increases in precipitation both in northeastern and southern Brazil, coincident with Heinrich events in the northern hemisphere. These changes are likely controlled by latitudinal ITCZ displacements, resulting in a hemispheric asymmetry of low-latitude precipitation, as exemplified by the anti-phased relationship between Brazilian and Chinese speleothem records. Furthermore, the similar precipitation response between NE and SE Brazil on millennial timescales implies that abrupt changes in precipitation within tropical South America are linked to climatic conditions in the North Atlantic, through changes in the AMOC and subsequent tropical air-sea feedbacks.

References

Abreu L, Shackleton NJ, Schonfeld J et al (2003) Millennial-scale oceanic climate variability of the Western Iberian margin during the last two glacial periods. Mar Geol 196:1–20

Arz HW, Pätzold J, Wefer G (1998) Correlated millennial-scale changes in surface hydrography and terrigenous sediment yield inferred from last glacial marine deposits off northeastern Brazil. Quat Res 50:157–166

Arz, HW, Patzold J, Wefer G (1999) The deglacial history of the western tropical Atlantic as inferred from high resolution stable isotope records off northeastern Brazil. Earth Planet Sci Lett 167:105–117

Auler AS (2004) South America. In: Gunn J (ed) Encyclopedia of Caves and Karst Science Fitzroy Dearborn, New York

Ayalon A, Bar-Matthews M, Sass E (1998) Rainfall–recharge relationships within a karstic terrain in the Eastern Mediterranean semi-arid region, Israel: $\delta^{18}O$ and δD characteristics. J Hydrol 207:18–31

Baker PA et al (2001a) The history of South American tropical precipitation for the past 25,000 years. Science 291:640–643

Baker PA, Rigsby CA, Seltzer GO et al (2001b) Tropical climate changes at millennial and orbital timescales on the Bolivian Altiplano. Nature 409:698–701

Bar-Matthews M, Ayalon A, Gilmour M et al (2003). Sea-land oxygen isotopic relationships from planktonic foraminifera and speleothems in the Eastern Mediterranean region and their implication for paleorainfall during interglacial intervals. Geochim Cosmochim Acta 67:3181–3199

Behling, H. (2002) South and Southeast Brazilian grasslands during Late Quaternary times: a synthesis. Palaeogeogr Palaeoclimatol Palaeoecol 177:19–27

Biasutti M, Battisti DS, Sarachik ES (2003) The annual cycle over the tropical Atlantic, South America, and Africa. J Clim 16:2491–2508

Blunier T, Brook EJ (2001) Timing of millennial-scale climate change in Antarctica and Greenland during the last glacial period. Science 291:109–112

Bond G, Broeacker WS, Johnsen S et al (1993) Correlations between climate records from North Atlantic sediments and Greenland ice. Nature 365:143–147

Bradley RS, Vuille M, Hardy DR et al (2003) Low latitude ice cores record Pacific sea surface temperatures. Geophys Res Lett 30:1174, doi: 10.1029/2002GL016546

Broecker WS (2003) Does the trigger for abrupt climate change reside in the ocean or in the atmosphere? Science 300:1519–1522

Burns SJ, Fleitmann D, Matter A et al (2003) Indian ocean climate and an absolute chronology over Dansgaard/Oeschger events. Science 301:1365–1367

Chiang JCH, Biasutti M, Battisti DS (2003) Sensitivity of the Atlantic Intertropical Convergence Zone to Last Glacial Maximum boundary conditions. Paleoceanography 18:1094, doi:10.1029/2003PA000916

Chiang JCH, Bitz CM (2005) Influence of high latitude ice cover on the marine Intertropical Convergence Zone. Clim Dyn 25:477–496

Claussen M, Ganopolski A, Brovkin V et al (2003) Simulated global-scale response of the climate system to Dansgaard/Oeschger and Heinrich events. Clim Dyn 21:361–370. doi 10.1007/s00382-003-0336-2

Clement AC, Hall A, Broccoli AJ (2004) The importance of precessional signals in the tropical climate. Clim Dyn 22:327–341

Crowley TJ (1992) North Atlantic deep water cools the southern hemisphere. Paleoceanography 7:489–499

Craig H (1965) The measurement of oxygen isotope palaeotemperatures. In: Tongiorgi E (ed) Stable isotopes in oceanographic studies and palaeotemperatures. Consigleo Nazionale della Ricerche Laboratorio di Geologia Nucleare, Pisa, 3–24

Cruz FW, Burns SJ, Karmann I et al (2005a) Insolation-driven changes in atmospheric circulation over the past 116,000 years in subtropical Brazil. Nature 434:63–66

Cruz FW, Karmann I, Viana Jr. O et al (2005b) Stable isotope study of cave percolation waters in subtropical Brazil: implications for paleoclimate inferences from speleothems. Chem Geol 220:245–262

Cruz FW, Burns SJ, Karmann I et al (2006) Reconstruction of regional atmosphere circulation features during the late Pleistocene in subtropical Brazil from oxygen isotope composition of speleothems. Earth Planet Sci Lett 248:494–506

Cruz FW, Burns SJ, Jercinovic M et al (2007) Evidence of rainfall variations in southern Brazil from trace element ratios (Mg/Ca and Sr/Ca) in a Late Pleistocene stalagmite. Geochim Cosmochim Acta 71:2250–2263

Dansgaard W, Johnsen SJ, Clausen HB et al (1993) Evidence for general instability of past climate from a 250-kyr ice-core record. Nature 364:218–220

Dima IM, Wallace JM (2003) On the seasonality of the Hadley cell. J Atmos Sci 60: 1522–1527

Doyle ME, Barros VR (2002) Midsummer low-level circulation and precipitation in subtropical South America and related sea surface temperature anomalies in the South Atlantic. J Clim 15:3394–3410

Drysdale RN, Zanchetta G, Hellstrom JC et al (2007) Stalagmite evidence for the precise timing of North Atlantic cold events during the early last glacial. Geology 35:77–80

Edwards RL, Cheng JH, Wasserburg, GJ (1987) ^{238}U-^{234}U-^{230}Th-^{232}Th systematics and the precise measurement of time over the past 500,000 years. Earth Planet Sci Lett 81:75–192

Fairchild IJ, Borsato A, Tooth AF et al (2000) Controls on trace element (Sr-Mg) compositions of carbonate cave waters:implications for speleothem climatic records. Chem Geol 166: 255–269

Friedman I, O'Neil JR (1977) Compilation of stable isotope fractionation factors of geochemical interest. In: Data of Geochemistry, United States Geological Survey Professional Paper 440-KK:1–12

Fritz SC, Baker PA, Lowenstein TK et al (2004) Hydrologic variation during the last 170,000 years in the southern hemisphere tropics of South America. Quat Res 61: 95–104

Gan MA, Kousky VE, Ropelewski CF (2004). The South American monsoon circulation and its relationship to rainfall over West-Central Brazil. J Clim 17:47–66

Garcia M, Villalba F, Araguas-Araguas L (1998) The role of atmospheric circulation patterns in controlling the regional distribution of stable isotope contents in precipitation: preliminary results from two transects in the Ecuadorian Andes. In: Proceedings series of International Atomic Energy Agency: isotope techniques in the study of environmental change, Vienna, IAEA-SM 349/7, pp 127–140

Gascoyne M (1992) Palaeoclimate determination from cave calcite deposits. Quat Sci Rev 11: 609–632

Gat JR, Matsui E (1991) Atmospheric water balance in the Amazon basin: an isotopic evapotranspiration model. J Geophys Res 96(D7):13179–13188

Genty D, Blamart D, Ouahdi R, et al (2003) Precise dating of Dansgaard–Oeschger climatic oscillations in western Europe from stalagmite data. Nature 421:833–837

Goldstein SJ, Stirling CH (2003) Techniques for measuring uranium-series nuclides: 1992–2002. In: Bourdon B, Henderson GM, Lundstrom CC, Turner SP (Eds), Uranium-series geochemistry. Rev Mineral Geochem 52:23–57

Gonfiantini R, Roche M-A, Olivry et al (2001) The altitude effect on the isotopic composition of tropical rains. Chem Geol 181:147–167

Grootes PM, Stuiver M, Thompson LG et al (1989) Oxygen isotope changes in tropical ice, Quelccaya, Peru. J Geophys Res 94(D1):1187–1194

Grootes PM, Stuiver M, White JWC et al (1993) Comparison of oxygen isotopic records from the GISP2 and GRIP Greenland ice cores. Nature 366:552–554

Grootes PM, Stuiver M (1997) Oxygen 18/16 variability in Greenland snow and ice with 10^3- to 10^5-year time resolution. J Geophys Res 102:26455–26470

Haffer J (1997) Alternative models of vertebrate speciation in Amazonia: an overview. Biodivers Conserv 6:451–476

Haug GH, Hughen KA, Sigman DM et al (2001) Southward migration of the intertropical convergence zone through the Holocene. Science 293:1304–1308.

Hardy DR, Vuille M, Bradley RS (2003) Variability of snow accumulation and isotopic composition on Nevado Sajama, Bolivia. J. Geophys. Res. 108 (D22):4693. doi: 10.1029/2003JD003623

Henderson KA, Thompson, LG, Lin, P-N (1999) Recording of El Niño in ice core $\delta^{18}O$ records from Nevado Huascarán, Peru. J Geophys Res 104 (D24):31053–31065

Hoffmann G, Ramirez E, Taupin, JD et al (2003) Coherent isotope history of Andean ice cores over the last century. Geophys Res Lett 30. doi:10.1029/2002GL014870

Huang Y, Fairchild IJ (2001) Partitioning of Sr^{2+} and Mg^{2+} into calcite in karst-analogue experimental solutions. Geochim Cosmochim Acta 65:47–62

Jennerjahn TC, Venugopalan I, Arz HW et al (2004) Asynchronous terrestrial and marine signals of climate change during heinrich events. Science 306:2236–2239

Johnson KR, Hu C, Belshaw NS, Henderson GM (2006) Seasonal trace-element and stable-isotope variations in a Chinese speleothem: the potential for high-resolution paleomonsoon reconstruction. Earth Planet Sci Lett 244:394–407

Karmann I, Cruz, FW, Viana Jr. O et al (2007) Climate influence on trace element geochemistry of waters from Santana-Pérolas cave system, Brazil. Chem Geol 244:232–247

Lau KM., Zhou J (2003) Anomalies of the South American summer monsoon associated with the 1997–1999 El Niño-Southern oscillation. Int J Clim 23:529–539

Lea D, Pak DK, Peterson LC et al (2003) Synchroneity of tropical and high latitude temperature over the last glacial termination. Science 301:1361–1364

Lenters JD, Cook KH (1997) On the origin of the Bolivian high and related circulation features of the South American climate. J Atmos Sci 54:656–677

Ledru, MP, Rousseau, DD, Cruz et al (2005) Paleoclimate changes during the last 100 ka from a record in the Brazilian Atlantic rainforest region and interhemispheric comparison. Quat Res, Amsterdam 64:444–450

Li WX, Lundberg J, Dickin AP et al (1989) High-precision mass-spectrometric uranium-series dating of calcite deposits and implications for palaeoclimatic studies. Nature 339:534–536

Liebmann B, Vera CS, Carvalho LMV et al (2004) An observed trend in Central South American Precipitation. J Clim 17:4357–4367

Lindzen RS, Hou AY (1988) Hadley circulations for zonally averaged heating centered off the equator. J Atmos Sci 45:2416–2427

Matsuyama H, Miyaoka K, Masuda K (2005) Year-to-year variations of the stable isotopes in precipitation in February at Cuiaba, located on the northern fringe of Pantanal, Brazil. J Hydrometeorol 6:324–329

Mayewski PA, Meeker LD, Twickler M et al (1997) Major features and forcing of high-latitude Northern Hemisphere atmospheric circulation using a 110,000-year-long glaciochemical series. J Geophys Res 102:26345–26366

Mayle FE, Burbridge R, Killeen TJ (2000) Millennial-scale dynamics of Southern Amazonian rain forests. Science 290:2291–2294

McDonald J, Drysdale R, Hill D (2004) The 2002–2003 El Niño recorded in Australian cave drip waters: implications for reconstructing rainfall histories using stalagmites. Geophys Res Lett 31. doi: 10.1029/2004GL020859

McManus JF, Francois R, Gherardi J-M et al (2004) Collapse and rapid resumption of Atlantic meridional circulation linked to deglacial climate changes. Nature 428:834–837

Mickler PJ, Stern LA, Banner JL, (2006) Large kinetic isotope effects in modern speleothems. Geol Soc Amer Bull 118(1–2):65–81

Moreno A, Nave S, Kuhlmann H et al (2002) Productivity response in the North Canary Basin to climate changes during the last 250 000 yr: a multi-proxy approach. Earth Planet Sci Lett 196:147–159

Moreno A, Giralt S, Valero-Garcés BA et al (2007) A 14 kyr record of the tropical Andes: the Lago Chungará sequence (18°S, northern Chilean Altiplano). Quat Int 161:4–21

NGRIP members (2004) High-resolution record of Northern Hemisphere climate extending into the last interglacial period. Nature 431:147–151

Peterson LC, Haug GH, Hughen KA et al (2000) Rapid changes in the hydrologic cycle of the tropical Atlantic during the last glacial. Science 290:1947–1951

Ramirez E, Hoffmann G, Taupin J et al (2003) A new Andean deep ice core from Nevado Illimani (6350 m), Bolivia. Earth Planet Sci Lett 212:337–350

Richards DA, Dorale JA (2003) Uranium-series chronology and environmental applications of speleothem. In: Bourdon B, Henderson GM, Lundstrom CC, Turner SP (eds) Uranium-series geochemistry. Rev Mineral Geochem 52:407–460

Robertson AW, Mechoso CR (2000) Interannual and interdecadal variability of the South Atlantic Convergence Zone. J Clim 128:2947–2957

Rozanski K, Araguás L (1995) Spatial and temporal variability of stable isotope composition of precipitation over the South American continent. Bull Inst fr études andines 24(3):379–390

Rühlemann C, Mulitza S, Müller PJ et al (1999) Warming of the tropical Atlantic Ocean and slowdown of thermohaline circulation during the last deglaciaiton. Nature 402:511–514

Salati E, Dall'olio A, Matsui E et al (1979) Recycling of water in the Amazon basin: an isotopic study. Water Resources Res 15:1250–1258

Seltzer G, Rodbell D, Burns SJ (2000) Isotopic evidence for Late Glacial and Holocene hydrologic change in tropical South America. Geology 28:35–38

Severinghaus JP, Brook EJ (1999) Abrupt climate change at the end of the Last Glacial Period inferred from trapped air in polar ice. Science 286:930–934

Shen C-C, Edwards RL, Cheng H et al (2002) Uranium and thorium isotopic concentration measurements by magnetic sector inductively coupled plasma mass spectrometry. Chem Geol 185:165–178

Shen C-C, Li K-S, Sieh K et al (2008). Variation of initial^{230}Th/^{232}Th and limits of high U-Th dating of shallow-water corals. Geochimica et Cosmochimica Acta 72(17):4201–4223

Spötl C, Mangini A (2002) Stalagmite from the Austrian Alps reveals Dansgaard–Oeschger events during isotope stage 3: implications for the absolute chronology of Greenland ice cores. Earth Planet Sci Lett 203:507–518

Sondag F, van Ruymbeke M, Soubies F et al (2003) Monitoring present day climatic conditions in tropical caves using an Environmental Data Acquisition System (EDAS). J Hydrol 273: 103–118

Soubies F, Seidel A, Mangin A et al (2005) A fifty-year climatic signal in three Holocene stalagmite records from Mato Grosso, Brazil. Quat Int 135:115–129

Sturm C, Hoffmann G, Langmann B (2007) Simulation of the stable water isotopes in precipitation over South America: comparing regional to global circulation models. J Clim 20: 3730–3750

Treble P, Shelley JMG, Chappell J (2003) High resolution subannual records of trace elements in a modern (1911–1992) speleothem from southwest Australia. Earth Planet Sci Lett 16:141–153

Victoria RL, Martinelli LA, Mortatti J et al (1991) Mechanisms of water recycling in the Amazon basin: isotopic insights. Ambio 20:384–387

Vimeux F, Gallaire R, Bony S et al (2005) What are the climate controls on δD in precipitation in the Zongo Valley (Bolivia)? Implications for the Illimani ice core interpretation. Earth Planet Sci Lett 240:205–220

Voelker AHL and workshop participants (2002) Global distribution of centennial-scale records for Marine Isotope Stage (MIS) 3: a database. Quat Sci Rev 21:1185–1212

Viana O Jr (2002) Hidroquímica, hidrologia e geoquímica isotópica (O e H) da fácies de percolação vadosa autogênica, caverna de Santana, município de Iporanga, Estado de São Paulo. Unpublished Master thesis, Universidade de São Paulo (in Portuguese)

Vuille M, Bradley R.S., Werner M et al (2003a) Modeling δ^{18}O in precipitation over the tropical Americas: 1. Interannual variability and climatic controls. J Geophys Res 108(D6) 4174. doi:10.1029/2001JD002038

Vuille M, Bradley RS, Healy R et al (2003b) Modeling δ^{18}O in precipitation over the tropical Americas: 2. Simulation of the stable isotope signal in Andean ice cores. J Geophys Res 108(D6) 4175. doi:10.1029/2001JD002039

Vuille M, Werner M (2005) Stable isotopes in precipitation recording South American summer monsoon and ENSO variability – observations and model results. Clim Dyn 25:401–413. doi:10.1007/s00382-005-0049-9

Wang YJ, Cheng H, Edwards RL et al (2001) A high-resolution absolute-dated late Pleistocene monsoon record from Hulu Cave, China. Science 294:2345–2348

Wang X, Auler AS, Edwards RL et al (2004) Wet periods in northeastern Brazil over the past 210 kyr linked to distant climate anomalies. Nature 432:740–743.

Wang X, Auler AS, Edwards RL et al (2006) Interhemispheric anti-phasing of rainfall during the last glacial period. Quat Sci Rev 25:3391–3403

Wang X, Auler AS, Edwards RL et al (2007a) Millennial-scale precipitation changes in southern Brazil over the past 90,000 years. Geophys Res Lett 34(23):L 23701

Wang X, Edwards RL, Auler AS et al (2007b) Millennial-scale interhemispheric asymmetry of low-latitude precipitation: speleothem evidence and possible high-latitude forcing. Geophys Monograph Series 173:279–293

Weldeab S, Schneider RR, Kölling M (2006) Deglacial sea surface temperature and salinity increase in the western tropical Atlantic in synchrony with high latitude climate instabilities. Earth Planet Sci Lett 241:699–706

Wiedner E, Scholz D, Mangini A, Polag D, Mühlinghaus C, Segl M (2008) Investigation of the stable isotope fractionation in speleothems with laboratory experiments. Quat Int 187(1): 15–24

Xie P, Arkin PA (1997) Global precipitation: a 17-year monthly analysis based on gauge observations, satellite estimates, and numerical model outputs. Bull Amer Meteor Soc 78:2539–2558.

Yuan DX, Cheng H, Edwards RL et al (2004) Timing, duration, and transitions of the last interglacial Asian Monsoon. Science 304:575–578

Zech R, Kul CH, Kubik P et al (2007) Exposure dating of Late Glacial and pre-Last Glacial Maximum moraines in the Cordon de Doña Rosa, Northern/Central Chile (∼31°S) Climate Past 3:1–14

Zhou J, Lau KM (1998) Does a monsoon climate exist over South America? J Clim 11:1020–1040

Zilli A, Rabelo L (2001) Monitoramento climático do ambiente cavernícola para determinação da capacidade de visitação turística da caverna Botuverá. Relatório final de atividades, Fundação o Boticário de Proteção a Natureza- MacArthur Foundation-Grupo de Estudos Espeleológicos do Paraná. Curitiba-Brasil (in Portuguese).

Chapter 3
Chronologies of the Last Glacial Maximum and its Termination in the Andes (~10–55°S) Based on Surface Exposure Dating

Roland Zech, Jacqueline Smith, and Michael R. Kaplan

Abstract Results of recent studies applying surface exposure dating (SED) along the Andes help to refine existing glacial chronologies and corroborate that glaciation was partly out-of-phase with the global last glacial maximum (global LGM: 24–18 ka). The records indicate an earlier local LGM (30/26 ka, where age pairs reflect present dating uncertainties) in the tropical Andes of Peru and northern Bolivia (apart from the eastern side of the Eastern Cordillera), which might be due to increasingly drier conditions during the course of the last global glaciation. In southern Bolivia, glacier advances occurred synchronously with the paleolake transgression phases Tauca (18–14 ka) and Coipasa (13–11 ka), documenting an intensification and/or southward shift of the tropical circulation. This reflects the high precipitation-sensitivity of glaciers in the arid areas of the Central Andes. Although moraines dating between 18/16 and 15/13 ka are also present in northern Chile (~30°S), the local LGM there occurred as early as ~42/39 ka. Evidence for similar early glacial maxima is found as far south as ~40°S, suggesting that an intensification and/or northward shift of the westerlies at that time provided sufficient moisture. In Patagonia and Tierra del Fuego, glaciation occurred broadly in-phase with the global LGM. At present, systematic methodological uncertainties related to SED as well as different approaches to interpreting scatter in exposure ages limit the utility of exposure ages in resolving dating questions on millennial and shorter timescales.

Keywords Andes · Glaciation · Late Quaternary · Paleoclimate · Surface exposure dating

3.1 Introduction

Glaciers are sensitive recorders of changes in climate, specifically temperature and precipitation. Glacial chronologies derived from dating moraines thus provide

R. Zech (✉)
Geographical Institute, University of Bern, Switzerland
e-mail: Roland.Zech@giub.unibe.ch

F. Vimeux et al. (eds.), *Past Climate Variability in South America and Surrounding Regions*, Developments in Paleoenvironmental Research 14,
DOI 10.1007/978-90-481-2672-9_3,

important complementary information to continuous and high-resolution paleoclimate proxies, such as ice-cores or lake sediments, because they (i) are a direct proxy of former atmospheric conditions and may be very useful for testing independently the validity of temperature and precipitation reconstructions during certain times, (ii) may reach farther back in time than other available archives, (iii) exist on all continents and span virtually all latitudes, and (iv) allow study of changes in atmospheric circulation patterns along regional transects.

The American Cordilleras offer an ideal setting for a glacial transect study: glacial chronologies exist for high northern latitudes in North America, low latitudes but high altitudes in Central America and the tropical and subtropical Andes, and high southern latitudes in Patagonia and Tierra del Fuego in the southernmost Andes. Thus, questions concerning synchrony and asynchrony of regional and interhemispheric climate changes can be addressed, with the goal of improving our understanding of the forcings and mechanisms of the climate system (Markgraf et al. 2000; Markgraf 2001). Clapperton (2000), for example, concluded from a compilation of available chronologies along the American Cordilleras that the main glacial advances were roughly synchronous between the hemispheres and occurred between ca. 28 and 12 ka BP, that is, during marine isotope stage (MIS) 2 (29–14 ka: Lisiecki and Raymo 2005) and the Late Glacial (∼18–12 ka). He emphasized the general importance of Northern Hemispheric insolation, which was at a minimum around 20 ka, compared to Southern Hemispheric insolation, which was at a maximum at the same time (Berger and Loutre 1991). He concluded that globally active feedbacks, including surface albedo and the concentration of water vapor and other greenhouse gases in the atmosphere, were important on orbital timescales. Clapperton (2000) noted, however, that more age control was needed, and that regional differences in glacial chronologies likely reflect past changes and limitations in moisture supply.

This chapter provides an overview of recent research concerning Late Quaternary glacier and climate reconstructions in the Andes, focusing on the local LGM and its termination, and emphasizing studies that have used SED of moraines. Note that we refer to the maximum ice extent during the last glacial cycle (∼130–10 ka) as the local LGM, which may not coincide with the global LGM (∼18–24 ka: Mix et al. 2001). This updated synthesis of studies along the Andean transect provides a foundation for new insights into the forcings and mechanisms responsible for observed regional variations in glacial chronologies. Previous geomorphological and glacial studies (reviewed in Clapperton 1990, 1993, 2000; Ehlers and Gibbard 2004; Smith et al. 2005a) were commonly limited by a lack of organic material for radiocarbon dating, especially in the arid-to-semiarid Central Andes (∼15–35°S).

After a brief overview of the geographical and the modern climatological setting of the Andes, we outline the principles of SED. Our chronological review then covers the southern tropical Andes (Peru: ∼9–11°S, Bolivia: ∼15–16°S), the subtropical Central Andes (Chile: ∼30°S), and Patagonia and Tierra del Fuego (Argentina/Chile: ∼45°S to 55°S) (see Fig. 3.1).

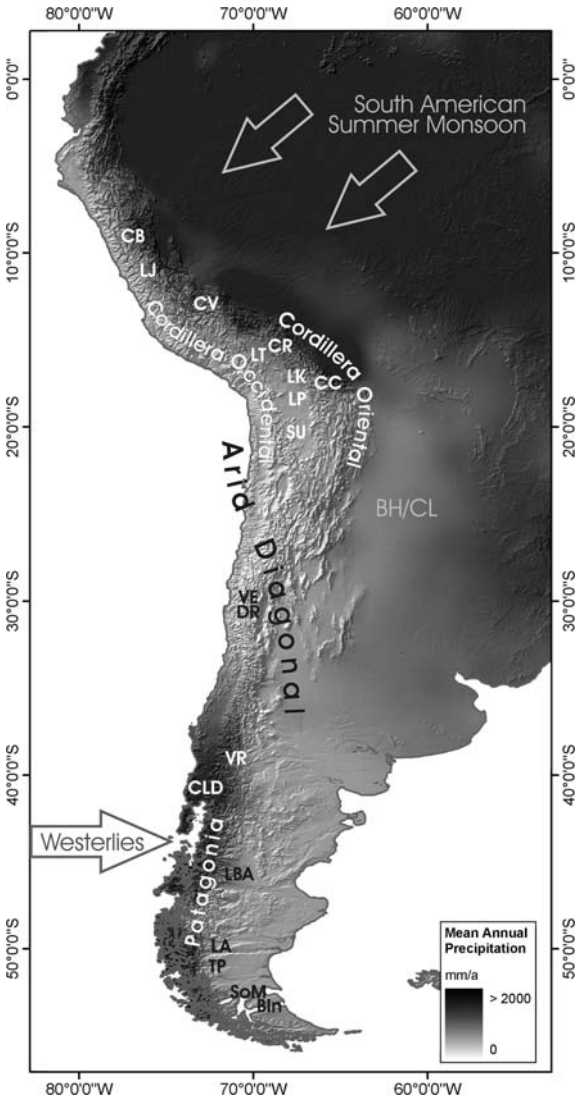

Fig. 3.1 Location of the sites discussed in the text, and mean annual precipiation along the Andes. CB, Cordillera Blanca; LJ, Lake Junin; CV, Cordillera Vilcanota; CR, Cordillera Real; LT, Lake Titicaca; LK, Laguna Kollpa Khota; CC, Cordillera Cochabamba; LP, Lago Poopo; SU, Salar de Uyuni; VE, Valle Encierro; DR, Cordon de Dona Rosa; VR, Valle Rucachoroi; CLD, Chilean Lake District; LBA, Lago Buenos Aires; LA, Lago Argentino; TP, Torres del Paine; SoM, Strait of Magellan; BIn, Bahia Inutil; BH/CL, Bolivian High/Chaco Low

3.2 Geography and Current Climate in the Andes

The mountain chain of the Andes is the dominant landform of South America (Fig. 3.1). The Andes are ~9000 km long and up to 750 km wide, and include the highest mountains on Earth outside Asia (e.g., Cerro Aconcagua: 6962 m). Highest peaks in the southern tropical and subtropical Andes exceed altitudes of 6000 m; ice caps and glaciers are present where the tropical circulation system provides sufficient moisture for snow and ice accumulation (north of ~18°S) (Fig. 3.2). Stretching

Fig. 3.2 Picture from the large right-lateral moraine in Valle San Francisco (dated to ~25/22 ka), Cordillera Real. View looking north with the Ancohuma (6425 m) in the background. Approximately 500 g of rock material is sampled for surface exposure dating from the top centimeters of flat, large, unweathered, and stable boulders. W. Zech for scale

from ~10 to 27°S, the high-elevation Central Andean Plateau (~3500–4100 m) was formed during orogenesis and uplift since ~30 Ma ago (Gregory-Wodzicki 2000; Orme 2007) and separates the Cordillera Occidental to the west and the Cordillera Oriental to the east (Kennan 2000). The Plateau is known as the Altiplano in Peru and Bolivia and as the Puna in NW-Argentina. It is famous for extensive salt pans (e.g., Salar de Uyuni) that are remnants of vast lakes that once occupied the intra-montane basins.

Observational and climate re-analysis data, in combination with climate modelling, have recently led to a better understanding of the complex climate system in the tropical and subtropical Andes (Lenters and Cook 1997; Garreaud et al. 2003; Vuille and Keimig 2004; Garreaud and Aceituno 2007). Precipitation originates primarily from the Atlantic Ocean, and humidity is advected into the Amazon Basin by the north-easterly South American Summer Monsoon (SASM, Zhou and Lau 1998). It is then transported farther south along the eastern slopes of the Andes by the South American Low Level Jet (SALLJ) (Marengo et al. 2004). Deep moist convection, especially during austral summer, is related to distinctive atmospheric pressure systems, known as the near-surface Chaco Low and the tropospheric Bolivian High. Ultimately, upper-tropospheric easterly anomolies, which are modulated by Pacific sea-surface temperatures, transport the humidity to the Cordilleras and onto the Altiplano. We here define the "humid tropical Andes" as those areas where mean annual precipitation (MAP) is typically >700 mm/a. These areas include the Cordillera Oriental north of ~18°S and both the Cordillera Occidental and the Cordillera Oriental north of ~12°S (see Fig. 3.1). Mass-balance studies and observations of equilibrium line altitudes (ELAs) indicate that glaciers tend to become more sensitive to

precipitation than temperature when MAP is <700 mm/a (Seltzer 1990; Kull and Grosjean 2000; Kaser and Osmaston 2002).

In the tropical Andes, a steep precipitation gradient exists from the eastern slopes of the Cordillera Oriental to the more arid Cordillera Occidental, and southward to the dry subtropical Andes. The core of the so-called "Arid Diagonal" (Ammann et al. 2001) crosses the Andes between ~18°S and 27°S (Fig. 3.1), separating regions to the north where moisture is delivered primarily by the tropical circulation from regions farther south where precipitation is delivered mainly by the mid-latitude southern westerlies. Due to the extreme aridity (<100 mm/a) in the Arid Diagonal, no glaciers exist there today, even though peak altitudes (>6000 m) lie above the zero-degree isotherm (Ammann et al. 2001). South of ~27°S, cold frontal events and cold air cut-offs, which are pressure lows that develop in the westerlies frontal system but become isolated (Vuille and Ammann 1997), provide sufficient moisture for glaciers to exist. Although the peak altitudes of the Andes drop from ~6000 m north of 35°S to only ~3000 m farther south, they remain glaciated, because MAP increases considerably (~2000 mm/a at 40°S) (Garreaud and Aceituno 2007) and temperatures decrease.

MAP reaches a maximum at around 50°S, (>5000 mm/a), where the core of the westerlies intersects the Patagonian Andes (~40–55°S). Despite relatively low altitudes (~3000 m), low temperatures and abundant year-round precipitation allow the Northern and Southern Patagonian Ice Fields to exist (~47°S and 49–51°S, respectively), with outlet glaciers reaching sea level on the western side and with extensive lakes surrounded by terminal moraine complexes (e.g., Lago Buenos Aires and Lago Argentino) on the eastern side. A steep west-to-east precipitation gradient characterizes the climate in Patagonia, resulting in extreme aridity on the eastern lee side of the Andes and excellent preservation of the glacial deposits. Southernmost South America (52–55°S) hosts the vast, windy, and steppe-like landscapes known as Tierra del Fuego. Altitudes there are generally <300 m east of the moutains, but the presence of glacial deposits extending as far as the Atlantic coastline testify to the extensive glaciers that once existed. Those paleoglaciers were nourished in the Cordilleras near the Pacific coast, where only a few peaks exceed 1000 m, and today the drowned trough-valleys form a wild fjord landscape.

Moraines that lie beyond modern ice limits all along the Andes from the tropics to Patagonia demonstrate that climate conditions in the past were more favorable for glaciation than are conditions today, either because of lower temperatures or increased precipitation, or both. Several recent studies comparing past and present equilibrium-line altitudes (ELAs) in the Andes (e.g. Klein et al. 1999; Haselton et al. 2002; Mark et al. 2005; Smith et al. 2005a) have emphasized that sound paleoclimatic interpretation of changes in ELA depends on having chronological control in order to correlate and compare glacial extents in different locations. This prerequisite has historically presented a significant challenge, mainly because of the lack of organic material for radiocarbon dating. The proliferation of studies using SED, which allows the exposure times of boulders on moraines and glacially eroded bedrock to be dated directly, promises to greatly expand the number of numerically dated glacial chronologies along the Andes.

3.3 Surface Exposure Dating

3.3.1 Principle

The basis of SED is the accumulation over time of *in-situ* cosmogenic nuclides, which are isotopes that are produced by the interaction of cosmic radiation with the Earth's surface (Gosse and Phillips 2001; Walker 2005). Primary cosmic radiation (mainly protons and α-particles) is thought to be galactic in origin and produced by supernovae. As the charged particles stream toward the Earth, they are deflected by the geomagnetic field, which leads to a specific flux distribution and energy spectrum dependent mainly on the geomagnetic latitude. When cosmic radiation collides with nuclides in the atmosphere (~10 km altitude), a cascade of nuclear reactions results in the formation of secondary cosmic radiation, of which fast and slow neutrons and muons are the components most relevant for SED. Secondary cosmic radiation is attenuated approximately in an exponential manner on its way through the atmosphere to the Earth surface, where it ultimately produces *in-situ* cosmogenic nuclides in the mineral lattice of exposed rocks. The most commonly used cosmogenic nuclide for SED is the radionuclide ^{10}Be (beryllium), most of which is produced by spallation of oxygen in quartz. Other cosmogenic nuclides that have been used for SED include ^{3}He, ^{14}C, ^{21}Ne, ^{26}Al, and ^{36}Cl. Some production reactions may also include neutron capture (e.g., ^{36}Cl).

The accumulation of cosmogenic nuclides follows the equation:

$$N = P.\, t$$

N is the concentration of the cosmogenic nuclide in the target mineral [atoms g^{-1}], P is the production rate [atoms g^{-1} a^{-1}], and t the exposure time [a]. For radioactive nuclides, such as ^{10}Be, the equation takes the decay constant λ into account:

$$N = \frac{P}{\lambda} \cdot (1 - e^{-\lambda t})$$

Determination of the ^{10}Be concentration in quartz (*N*) follows standard laboratory procedures that include (i) separation of quartz, (ii) dissolution of the quartz in hydrofluoric acid after addition of a ^{9}Be carrier, (iii) purification of beryllium by chromatography, (iv) precipitation and oxidation, and (v) accelerator mass spectrometer (AMS) measurement of the ^{10}Be over ^{9}Be ratio (e.g., Kohl and Nishiizumi 1992; Ivy-Ochs 1996; Bierman et al. 2002).

3.3.2 Scaling and Systematic Uncertainties

The rate of production of a cosmogenic isotope in an exposed surface depends on a number of factors (e.g., altitude, latitude, sample thickness) and can vary widely. Accordingly, obtaining robust exposure ages depends heavily on calculating

the production rate with the greatest possible accuracy. Generally, corrections for sample-specific effects such as sample thickness (P follows an exponential depth profile in the upper few decimeters of the rock surface), sample geometry, and topographic shielding are relatively straightforward (Masarik and Reedy 1995; Dunne et al. 1999; Masarik and Wieler 2003; Kubik and Reuther 2007). More complicated, however, are the latitude- and altitude-dependence of the local production rate due to the geomagnetic deflection and the atmospheric attenuation of cosmic radiation. Several scaling systems have been developed to scale a reference production rate (defined at sea level and high latitude, SLHL) to the sampling location (Lal 1991; Stone 2000; Dunai 2001; Desilets and Zreda 2003; Pigati and Lifton 2004; Lifton et al. 2005; Desilets et al. 2006). The reference production rate ($\sim$5.1 atoms a^{-1} g^{-1} SiO_2 for ^{10}Be) can be calculated from calibration sites, where the age of the investigated feature has been determined independently. The reference production rate and calculated exposure ages will differ depending on the choice of the scaling method and calibration site. International efforts are underway to standardize scaling procedures and reduce the systematic age uncertainties to <5% (Balco et al. 2008; CRONUS-Earth and CRONUS-EU projects: www.physics.purdue.edu/cronus and www.cronus-eu.net).

We report all exposure ages herein as "x/y ka", with x being the age calculated using the scaling method of Lal (1991)/Stone (2000) and y being the age calculated using the scaling method of Lifton et al. (2005). For consistency, all exposure ages have been recalculated using the CRONUS-Earth Online Calculator of Balco et al. (2008) (version 2.1, which includes corrections for regional altitude-pressure anomalies) and time-dependent production rates (including corrections for geomagnetic field changes). At high altitudes, the Lal/Stone scaling method generally produces older ages than other scaling methods (e.g., Lifton et al. 2005), primarily because it assumes an altitude-independent energy spectrum of the cosmic radiation, and because it is based on a relatively small neutron flux dataset compared to the other scaling systems. Along the Andes, the scaling-related range of calculated ages for a sample is smallest for the low-altitude, high-latitude sampling locations in Patagonia and greatest at the high altitudes and low latitudes of the tropical and subtropical Andes.

3.3.3 Scatter in Exposure Ages and Geomorphological Uncertainties

Geomorphic processes can result in a range of exposure ages among boulders on a single moraine. Ideally, exposure of a glacially transported and eroded boulder begins at the moment when the boulder is deposited atop the moraine before or as the ice front begins to retreat. In reality, exposure may begin before or after that moment. Exposure ages may overestimate the depositional age of a moraine because of nuclide inheritance, that is, the sampled boulder may have retained cosmogenic isotopes from exposure prior to deposition on the moraine because of incomplete erosion during glacial transport. The probability for inheritance is

typically considered to be low in most settings in non-polar regions (e.g., Shanahan and Zreda 2000; Putkonen and Swanson 2003; Briner et al. 2005). On the other hand, exposure ages may underestimate the real depositional age as a result of various post-depositional, geomorphic processes. Long-lasting ice-decay, denudation of the moraine surface, weathering and erosion of the boulder surface (with loss of accumulated isotopes), and boulder upheaval and toppling all result in exposure ages younger than the depositional age (e.g., Zreda and Phillips 1995; Briner et al. 2005; Zech et al. 2005; Putkonen and O'Neal 2006). Such effects have led some workers (e.g., Farber et al. 2005; Zech et al. 2007b) to use what we refer to as the "oldest age model", whereby the oldest exposure age is considered the best available estimate for the deposition and/or stabilization age of a dated feature, unless stratigraphic inconsistencies indicate inheritance. Other workers, especially those with large datasets that show age clustering, have used plateaus in the distribution of ages, mean ages, or mean square of weighted deviates statistics as the best estimate of depositional age (e.g., Douglass et al. 2006). Different approaches have been used in the study areas along the Andes that are compared in this chapter; we generally present data with the published approach and interpretation and plot all available exposure ages individually to facilitate comparisons.

3.4 Chronologies of the LGM

3.4.1 Exposure Ages from the Tropical Andes of Peru and Bolivia

The first exposure ages from the tropical Andes were published by Smith et al. (2005b, c), who dated more than 140 boulders on moraines from four valleys in the Eastern Cordillera bordering the east side of the Junin Plain (~4100 m, 11°S, central Peru, Figs. 3.1 and 3.3a). Although the summits (4600–4850 m) are currently ice-free, trough valleys and moraines that reach almost to the shores of Lake Junin document the existence of numerous mountain glaciers in the past.

The most extensive moraines, defined as Group D moraines by Smith et al. (2005c), yield exposure ages typically older than ~160/135 ka and clearly predate the last glacial cycle. Exposure ages from the Group C moraines, which are end moraines located approximately half way between the lower and upper ends of the valleys, typically range from 30/27 to 20/18 ka. The Group C moraines thus represent the local LGM in the Junin region during the last glacial cycle and indicate a much less extensive glaciation than earlier glaciations. The Group C moraines were interpreted as evidence for an early local LGM in the tropical Andes (Smith et al. 2005b, c) (Fig. 3.3a, open triangles), as compared to the global LGM. The range of exposure ages from the Group C moraines may reflect the effects of exhumation or other geomorphic processes; the oldest ages on the moraines suggest deposition of the Group C moraines as early as ~30/27 ka in the three west-facing valleys, and ~23/20 ka in the east-facing Collpa Valley. The Group B end moraines are located up-valley from Group C moraines (typically 1–2 km), commonly dam glacial lakes, and typically yield boulder ages between 19/17 and

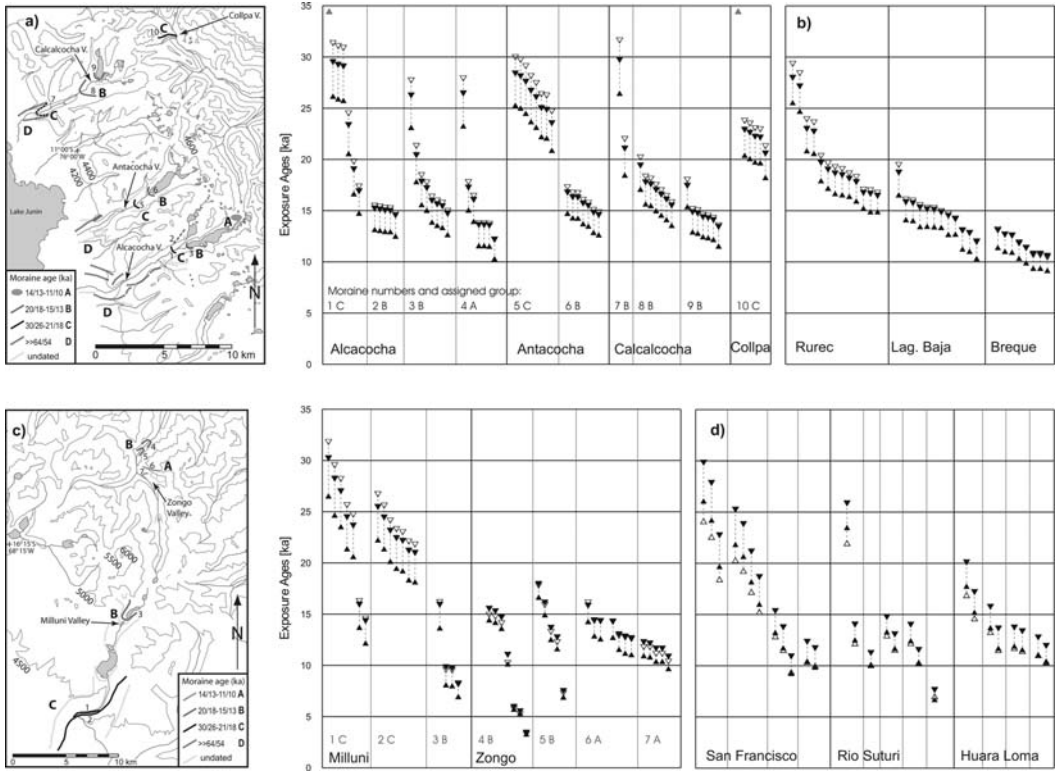

Fig. 3.3 (**a**) Location map and exposure ages of the moraines near Lake Junin, Peru (numbered 1–10, Group C = local LGM, Group B and A = Late Glacial) (Smith et al. 2005b, c). Here and in the following figures the open symbols mark exposure ages as originally published; the *black upward-pointing triangles* are ages calculated according to Lifton et al. (2005), the *downward-pointing triangles* ages according to Lal (1991)/Stone (2000) (time-dependent), both using the online calculator of Balco et al. (2008). (**b**) Exposure ages from the Cordillera Blanca, Peru (Farber et al. 2005). (**c**) Location map and exposure ages of the local LGM and Late Glacial moraines (numbered 1–7) in the Milluni and Zongo Valleys, Bolivia (Smith et al. 2005b, c). (**d**) Exposure ages from the San Francisco Valley, Rio Suturi and Huara Loma, Bolivia (Zech et al. 2007b)

15/13 ka. The Group B moraines have been interpreted as delimiting Late Glacial readvances or stillstands that were followed by rapid deglaciation. Group A samples were obtained from ground moraine and bedrock in the upper reaches of Alcacocha Valley. Ages concentrate between ~14/12 and 12/10 ka, with several older ages (26/23 to 16/14 ka) suggesting that inheritance may have affected some of the samples. Smith et al. (2005b, c) interpreted the Group A ages as indicating rapid deglaciation and ice-free conditions in the main valley after ~14/12 ka.

The hypothesis of an early local LGM was supported by Farber et al. (2005), who conducted a surface exposure study on moraines in four valleys in the central Cordillera Blanca, Peru (~9.5°S). Farber et al. (2005) concluded that glaciers reached their greatest extent during the last glacial cycle ~29 ka (Rurec moraines) and ~16.5 ka (Laguna Baja moraines) (Figs. 3.1 and 3.3b, open triangles). Recalculated ages are ~28/26 and ~16/14 ka, which suggest glacial advances in phase with the west-facing valley glaciers near Lake Junin (Group C and B moraines, respectively). Farber et al. (2005) also dated the Breque moraine in the Rio Negro drainage, which yielded exposure ages of ~13 ka; re-calculated ages are 13/11 ka.

Farther south, in the Cordillera Real (~16°S), Smith et al. (2005b) used SED to date moraines in the Milluni and Zongo Valleys (Figs. 3.1 and 3.3c). Results indicate that moraines in the Milluni Valley correlate with the Group C (local LGM) and Group B moraines from the Junin area. Using the oldest ages as depositional ages suggests that moraine 1 was deposited ~30/26 ka, moraine 2 ~25/22 ka, and the recessional moraine 3 ~16/14 ka. Moraines 1 and 2 are the two crests of what appears to be a compound moraine, with moraine 2 being the outer crest. The younger ages on moraine 2 than moraine 1 are either the result of geomorphic processes, or of a poly-thermal – and thus laterally non-erosive – glacial advance at 25/22 ka overriding the 30/26 ka moraine. In the northeast-facing Zongo Valley, Late Glacial moraines are present down to altitudes ~1000 m lower than the local LGM moraines in the Milluni Valley. The oldest ages on the Zongo Valley Group B moraines are ~15.5/14.5 ka (moraine 4) and ~18/17 ka (moraine 5), and on Group A moraines 16/14 ka (moraine 6) and 12/11 ka (moraine 7). Smith et al. (2005b) proposed that the apparent lack of local LGM moraines, the abundance of Group B and A moraines, and the lower ELAs in the Zongo Valley (Ramage et al. 2005) reflect the effects of shading by the steep valley walls, heavy debris cover, and more abundant orographic precipitation compared to the wider, gently sloping, drier, southwest-facing Milluni Valley.

Zech et al. (2007b) used SED to date sequences of moraines in the Valle San Francisco (~15°S, Cordillera Real) and the Cordillera Cochabamba (~17°S) of Bolivia (Figs. 3.1 and 3.3d). Based on their age calculations, Zech et al. (2007b) suggested that glaciers in the tropical humid Andes reached their maximum extent at ~25–22 ka, that is, in-phase with the global LGM (open triangles in Fig. 3.3d); several Late Glacial moraines were dated to 13–11 ka. Recalculated ages indicate that the local LGM advances in the San Francisco Valley occurred at 30/26 and 25/22 ka, respectively, in phase with the Group C moraines in the Milluni Valley. Recalculated ages for the recessional stages are 15/13 and 12/10 ka, coinciding with the Group B and A moraines in the Milluni and Zongo Valley. Similar Late Glacial

moraines are also found in the Cordillera Cochabamba in the Rio Suturi Valley (15/13 and 14/12 ka) and the Huara Loma Valley (16/14, 14/12 and 13/11 ka), but there the ages of the local LGM moraines are not well constrained (26/23? ka in the Rio Suturi Valley, and 20/18? ka in the Huara Loma Valley).

In summary, exposure ages in the humid tropical Andes of Peru and Bolivia suggest an overall consistent pattern of local LGM advances dated to between 30/27 and 23/20 ka. Late Glacial moraines were deposited between ~17/15 and 12/10 ka.

3.4.1.1 Comparison with Radiocarbon Chronologies

Several reviews have been published recently summarizing the state of knowledge about the glacial history in the tropical Andes with an emphasis on radiocarbon ages (Heine 2004; Mark et al. 2004; Smith et al. 2005a; Seltzer 2007). We will therefore limit our discussion here to (i) the timing of the local LGM, and (ii) the Late Glacial cold reversal.

(i) Radiocarbon ages provide some age constraints for the local LGM in the tropical Andes. Close minimum (basal) radiocarbon ages of 18.5 and 17.4 cal ^{14}C ka BP from the Laguna Casercocha and Comercocha in the Cordillera Vilcanota, Peru, respectively (Goodman et al. 2001; Mark et al. 2002), date the transition of glacial to non-glacial sedimentation to after ~20 ka BP (calibrated ages estimated using www.calpal.de). This agrees well with often cited basal radiocarbon ages (~17 ^{14}C ka, ~20 cal ka BP) reported by Seltzer (1994) from Laguna Kollpa Khota, Bolivia, which have been interpreted to document an early local LGM and an early deglaciation at ~20 cal ka. Sedimentological and isotopic data from Lake Junin and Lake Titicaca (Seltzer et al. 2000, 2002; Baker et al. 2001b) have been interpreted and cited as evidence for an early local LGM (Smith et al. 2005b, c). Zech et al. (2007b) contended that the observed drops in accumulation rates and magnetic susceptibility at ~20 ka do not exclude a local LGM in-phase with the global LGM, but only date the beginning of deglaciation.

Maximum-limiting radiocarbon ages for the local LGM in tropical Peru and Bolivia are scarce. Wright (1984) presented bracketing ages of ~12 ^{14}C ka BP (~14 cal ka BP) and ~24 ^{14}C ka BP (~29 cal ka BP) for clayey sediments in Lake Junin interpreted as glacial outwash. Seltzer et al. (2000) suggested bracketing ages for the local LGM of 21 cal ka BP and ~30 ^{14}C ka BP (~34 cal ka BP), again based on sediment cores from Lake Junin. Maximum-limiting radiocarbon ages of ~33 ^{14}C ka BP (~37.5 cal ka BP) from the San Francisco Valley (Argollo 1980) and bracketing ages of 16.6 and 27 ^{14}C ka BP (19.9 and 31.8 cal ka BP) from Rio Kollpana Valley (Cordillera Cochabamba) (Servant et al. 1981; Servant et al. 1995) are of limited utility because of the lack of information about the sample locations and the geomorphic setting (Smith et al. 2005a). In summary, radiocarbon ages are in general agreement with the LGM chronology derived from SED, but do not help to reduce the remaining systematic uncertainties related to SED.

(ii) Basal radiocarbon ages from glacial lakes (Seltzer et al. 1995; Rodbell and Seltzer 2000; Smith et al. 2005a) indicate that, at least in the southern tropical Andes in Peru and Bolivia, glacial advances slightly predated the Younger Dryas

cold reversal (YD, 12.9–11.6 cal ka) (NGRIP members 2004). The YD is well documented in the North Atlantic region (including glacial re-advances), and most likely related not only to changes in the atmospheric composition and circulation, but also to re-organizations of the ocean circulation (McManus et al. 2004). Glacial re-advances in the southern tropical Andes seem to have coincided instead with the Antarctic Cold Reversal (ACR, 14.5–12.9 cal ka) (Blunier and Brook 2001), which indicates that climate conditions during the YD became either warmer, or drier, or a combination of both. Given that the YD climate signal remains highly controversial both in the tropics and in the southern hemisphere, more precise age control for the glacial advances – particularly along the Andes – is desirable.

SED may hold the potential to address millennial-scale issues like the YD and the ACR in the future, once the systematic uncertainties are better controlled with the help of local high-altitude calibration sites. Calibration sites are deposits, such as moraines, that are precisely and independently dated. One such site may be the Breque moraine in Peru, for which Rodbell and Seltzer (2000) reported tightly bracketing radiocarbon ages of 11.0 ^{14}C ka BP (12.9 cal ka BP) from a peat core up-valley and 11.3 ^{14}C ka BP (13.2 cal ka BP) from organic material below gravel (interpreted as glacial outwash sediments) farther down-valley. The exposure ages of ~13 ka obtained by Farber et al. (2005) for the Breque moraine (Fig. 3.3b) appear to validate the exposure age calculations based on Lal (1991)/Stone (2000) rather than those based on the more recently developed scaling systems (e.g., Lifton et al. 2005). However, the Breque moraine used as a calibration site yields significantly lower reference production rates than other calibration sites from the global data set (Balco et al. 2008), suggesting that the Breque site should be cross-checked and additional calibration sites sought.

3.4.1.2 The Role of Temperature and Precipitation for Glaciation in the Southern Tropical Andes

Although age control for the glacial advances in the southern tropical Andes is still limited, we attempt to interpret the available data from a paleoclimate perspective, with the aim of presenting a model that takes into account the role of temperature and precipitation for glaciation in the different parts of the Andes. Our interpretation is based on the fact that glaciers are sensitive recorders of temperature and precipitation. Precipitation plays an increasingly more important role as climate gets drier and it becomes the dominantly limiting factor for positive glacial mass balances (Kaser and Osmaston 2002; Kull et al. 2003, 2008; Favier et al. 2004).

SED ages from the one dated moraine in the east-facing valley (Collpa Valley) in the Junin region are younger than ages from the Group C moraines in the west-facing valleys. The Collpa Valley moraine may document a glacial advance in response to lower temperatures in phase with the global LGM. In the west-facing valleys, precipitation that was sufficient for glacier growth earlier may have become more limiting for glacier expansion later in the last glaciation due to the rain shadow effects of the growing glaciers to the east. Consequently glaciers in the west-facing valleys reached their maximum positions closer to 30/26 ka rather than during

the temperature minimum of the global LGM, thus preserving the "early LGM" moraines. The same logic may explain the preservation of the Rurec moraine in the Cordillera Blanca and the ~30/26 ka moraines in the San Francisco and Milluni Valleys. The 25/22 ka moraine in the San Francisco Valley indicates the existence of a subsequent glacial advance reaching approximately the same extent as at 30/26 ka. The later advance, more in phase with the global LGM, was mainly triggered by lower temperatures, and limited in extent due to the rain shadow effects at that time and resultant reduced precipitation in west-facing valleys.

Farther to the south and west on the Bolivian Altiplano, modern climate conditions become very dry, and glaciers are dominantly precipitation-sensitive (Seltzer et al. 1995; Kull et al. 2008). This is reflected in the synchrony of the local LGM in the dry southern tropical Andes with lake transgression phases (Clapperton et al. 1997; Clayton and Clapperton 1997): moraines and glacial outwash east of Lago Poopo and north of the Salar de Uyuni intercalate with shorelines that document much higher lake levels on the Altiplano compared to today. The glacial high stands and transgression phases have been dated to ~13.3 ^{14}C ka BP (~16 cal ka BP) and 12–10 ^{14}C ka BP (14–11.5 cal ka BP). Those findings have more recently been corroborated by SED of moraines (Zreda et al. 2001), and by coupled radiocarbon and U-Th dating of the shoreline carbonates Placzek et al. (2006). Whereas results of U-Th dating are in good agreement with radiocarbon dating for the Late Glacial ("Tauca" phase: 18–14 ka, with a maximum at 16 ka; and "Coipasa": 13–11 ka (Placzek et al. 2006)), the existence of the traditionally assumed "Minchin" paleolake on the Altiplano at ~35–30 ka BP and correlative moraines (e.g., Servant and Fontes 1978; Sylvestre et al. 1999) could not be verified. U-Th ages of 120–98 ka from the respective shorelines indicate that (i) re-crystallization and reservoir effects limit the applicability of radiocarbon dating for such old carbonates, and (ii) the earlier transgression phase (now named "Ouki") phase is much older than previously assumed (Placzek et al. 2006).

Paleoclimatically, increased precipitation on the Bolivian Altiplano during the Tauca and Coipasa phase can be attributed to an intensification of the South American Summer Monsoon (SASM, Zhou and Lau 1998), which coincides with a southward shift of the Intertropical Convergence Zone (ITCZ) and an intensification of the Bolivian High. As has been inferred from speleothem data in SE Brazil (Cruz et al. 2005; Wang et al. 2006) and from a sediment core from the Salar de Uyuni on the Altiplano, (Baker et al. 2001a; Fritz et al. 2004), the SASM is controlled by insolation on orbital timescales (with a summer insolation maximum at 20 ka). Additionally, however, Northern Hemispheric temperatures influence the SASM on millennial timescales. Modeling studies show a southward shift of the ITCZ and an intensification of the SASM when the North Atlantic region experiences cooling (Chiang and Bitz 2005; Zhang and Delworth 2005). Accordingly, the Tauca and Coipasa transgression phases and the related glacial advances on the dry Bolivian Altiplano may correlate with Heinrich event 1 (~16 ka) and the YD, respectively.

Seltzer et al. (2002) deduced relatively wet conditions at Lake Junin in Peru until ~16 ka, followed by drying during the Late Glacial, with a return to wetter conditions at the beginning of the Holocene (~11.8 ka). As compared to the Bolivian

Altiplano (i.e., the Late Glacial Tauca and Coipasa transgression phases), this opposite paleohydrological signal may point to a latitudinal shift of the focus of the monsoonal precipitation along the Andes. Other studies, however, emphasize the importance of the upper-tropospheric easterlies for the precipitation in the Andes, which in turn are influenced by the Pacific sea-surface temperatures and more intensive during El Niño phases, at least on annual timescales (Garreaud et al. 2003; Vuille and Keimig 2004; Garreaud and Aceituno 2007).

Better SED age control will eventually allow identification of the regional pattern of glacial (re-)advances on millennial time-scales, thereby helping to refine the complex role of precipitation and temperature for glaciation in the tropics and thus also clarifying the climate forcings and mechanisms involved.

3.4.2 Exposure Ages from the Subtropical Andes

Due to the extreme aridity and the resultant lack of organic material for radiocarbon dating, virtually no age control was available for moraines in the Arid Diagonal until the advent of SED. Zech et al. (2006, 2007a) presented ^{10}Be exposure ages for the Cordon de Dona Rosa (30.7°S, 70.4°W; Figs. 3.1 and 3.4) and from the Valle Encierro (29.1°S, 69.9°W) in Chile.

Trough valleys and moraine remnants are evidence for extensive glacial advances in the past. Attempts to date this earliest glaciation in the Cordon de Dona Rosa were not successful, because erosion and landscape instability led to exposure ages that were stratigraphically far too young and widely scattered (ages omitted from

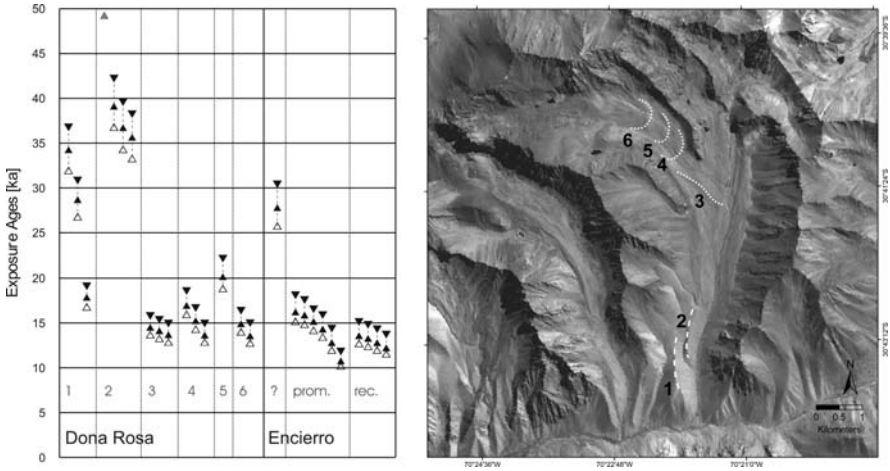

Fig. 3.4 *Left*: Exposure ages from the Cordon the Dona Rosa (numbered 1–6) (Zech et al. 2007a) and the Valle Encierro (? = oldest dated frontal moraine, prom = prominent lateral and frontal moraine, and rec = recessional moraines) (Zech et al. 2006). *Right*: The Cordon de Dona Rosa and sampling locations (Landsat satellite image)

Fig. 3.4). Ages from the oldest morphologically well-preserved moraine (number 1 in Fig. 3.4) are still widely scattered and are most likely too young. More robust dating results came from the stratigraphically younger, sharp-crested latero-frontal moraine (number 2, Fig. 3.4) with a recalculated age estimate of ~42/39 ka (excluding one outlier >100 ka, probably due to pre-exposure). Additional exposure ages were obtained from the catchment farther upstream (moraines 3–6 in Fig. 3.4, with moraine 3 being the farthest downvalley and moraine 6 farthest upvalley). Revised calculations and tentative application of the oldest age model suggest that the age of moraine 6 may be 16/15 ka, and that of moraine 4 may be 19/17 ka. We are hesitant to interpret the age of 22/20 ka from moraine 5 as deposition age, given its position between moraines 6 and 4, and assume that this sample may contain inherited nuclides. Moraine 3, which lies farthest downvalley and was dated to 16/14 ka, may have been affected by post-depositional glacial outwash processes, so stratigraphically these ages are not necessarily inconsistent with the older age of moraine 4.

The Late Glacial chronology in the Cordon de Dona Rosa is consistent with the chronology derived for the Encierro Valley (Zech et al. 2006), where recalculated ages are ~18/16 ka for a prominent latero-fronal moraine, and ~15/13 ka for recessional moraines (Fig. 3.4). One recalculated age of 30/28 ka was obtained from a poorly preserved, older frontal moraine, and probably only serves as a tentative minimum estimate for the deposition age.

Because mass balances are severely limited by precipitation in the arid subtropical Andes at ~30°S, glacier advances there have to be attributed in large part to either an intensification of the SASM, or an increase in winter precipitation due to more northerly and/or intensive westerlies. The ~18/16 and ~15/13 ka glacial advances in the subtropical Andes have been correlated with Late Glacial humid phases on the Bolivian Altiplano (Tauca: 18–14 ka and Coipasa: 13–11 ka), and an intensification of the SASM (Cruz et al. 2005; Wang et al. 2006) at that time (Zech et al. 2006, 2007a). Glacier-climate-modeling corroborates the more important role of summer precipitation for the prominent glacial advance in the Encierro Valley compared to climate conditions there today (Kull et al. 2002). Evidence for increased tropical summer precipitation during the Late Glacial also comes from glacier-climate-modeling in the Cordillera Occidental at ~18 and 22°S (Kull et al. 2008), and from pollen records in rodent middens at ~25°S (from 17 to 11 ka) (Maldonado et al. 2005), but conditions became increasingly arid south of ~28°S during the Late Glacial (Geyh et al. 1999; Grosjean et al. 2001).

The pollen records at ~25°S indicate increased winter precipitation between 40–33 ka and between 24–14 ka (Maldonado et al. 2005), which is roughly consistent with evidence for humid phases 54–38 ka and 28–12 ka in Northern Chile derived from marine sediments (Stuut and Lamy 2004). The early LGM at ~42/39 ka in the Cordon de Dona Rosa may thus have occurred mainly due to increased winter precipitation. During the course of the global LGM, climate conditions became increasingly dry, which explains the limited glacial extent at that time and the preservation of the early local LGM moraines. Unpublished ^{10}Be exposure data from the Valle Rucachoroi in the Argentinean Andes (39°S, R. Zech) show

that the local LGM there also occurred early (~35/35 ka). No moraines with ages indicating deposition during the global LGM have been dated, and ice-free conditions in the Rucachoroi Valley since ~15/15 ka are indicated by ^{10}Be ages on bedrock and boulders.

Detailed radiocarbon glacial chronologies from the Chilean Lake District (CLD) (Lowell et al. 1995; Denton et al. 1999b; Heusser 2003) show that the piedmont glaciers reached maxima at ca. 29.6, 26.9, 23.1, 21.0, 14.9 and 13.9 ^{14}C ka BP (~35, 31, 28, 25, 18 and 17 cal ka BP), with earlier advances being notably more extensive in the northern CLD, whereas in the southern CLD the latest advance overran the older deposits. We interpret this glaciation pattern along Northern and Central Chile as indicating increasingly drier conditions during the course of the last glaciation (from ~40 to 18 ka), and a southward shift of the westerlies probably in response to changing global boundary conditions during the LGM. The latitudinal position of the westerlies during the LGM has been heavily debated because pollen records from Chile and Argentina have been interpreted to indicate both a southward shift and focusing of the westerlies core between 43–45°S (Markgraf 1989; Markgraf et al. 1992) and a northward shift and/or intensification of the westerlies (Heusser 1989; Moreno et al. 1999). This is, however, a slightly different discussion, because we are suggesting decreasing winter precipitation during the course of the LGM and cannot directly make comparisons with the present atmospheric circulation system. Note that lake sediment studies from the Laguna Tagua Tagua in Central Chile (34.5°S) (Valero-Garcés et al. 2005) indicate generally wet conditions from ~40 to 20 ka, and increasingly drier conditions from then on during the Late Glacial, which is in good agreement with deglaciation in Central Chile at that time.

The exact timing of the Late Glacial readvances, both in Northern and Central Chile, and the role temperature and precipitation changes on millennial time-scales require further investigation.

3.4.3 Exposure Ages from the Patagonian Andes and Tierra del Fuego

At the east end of Lago Buenos Aires (LBA), Argentina 46.5°S, a sequence of increasingly older moraines informally named Menucos, Fenix I-V, Moreno, Deseado and Telken was deposited by a large outlet glacier of the Northern Patagonian Ice Field (Figs. 3.1 and 3.5a). Kaplan et al. (2004) dated the Fenix moraine sequence to 23.0–15.6 ka using ^{10}Be, ^{26}Al, and ^{3}He (original data) and the more extensive earlier glaciation (Moreno moraines) to ~150–140 ka (Kaplan et al. 2005). Douglass et al. (2006) more recently refined the chronology (Fig. 3.5b), presenting additional exposure ages and applying mean square of weighted deviates statistics and cumulative frequency plots in order to identify possible outliers. They assigned ages of 22.7±0.9, 21.4±1.9, 19.9±1.1, 17.0±0.8, 15.8±0.6 and 14.4±0.9 ka to the Fenix V to I moraines and the Menucos moraine, respectively (original data, based on the scaling system of Stone (2000) including corrections for geomagnetic fluctuations and atmospheric anomalies, shown as open triangles

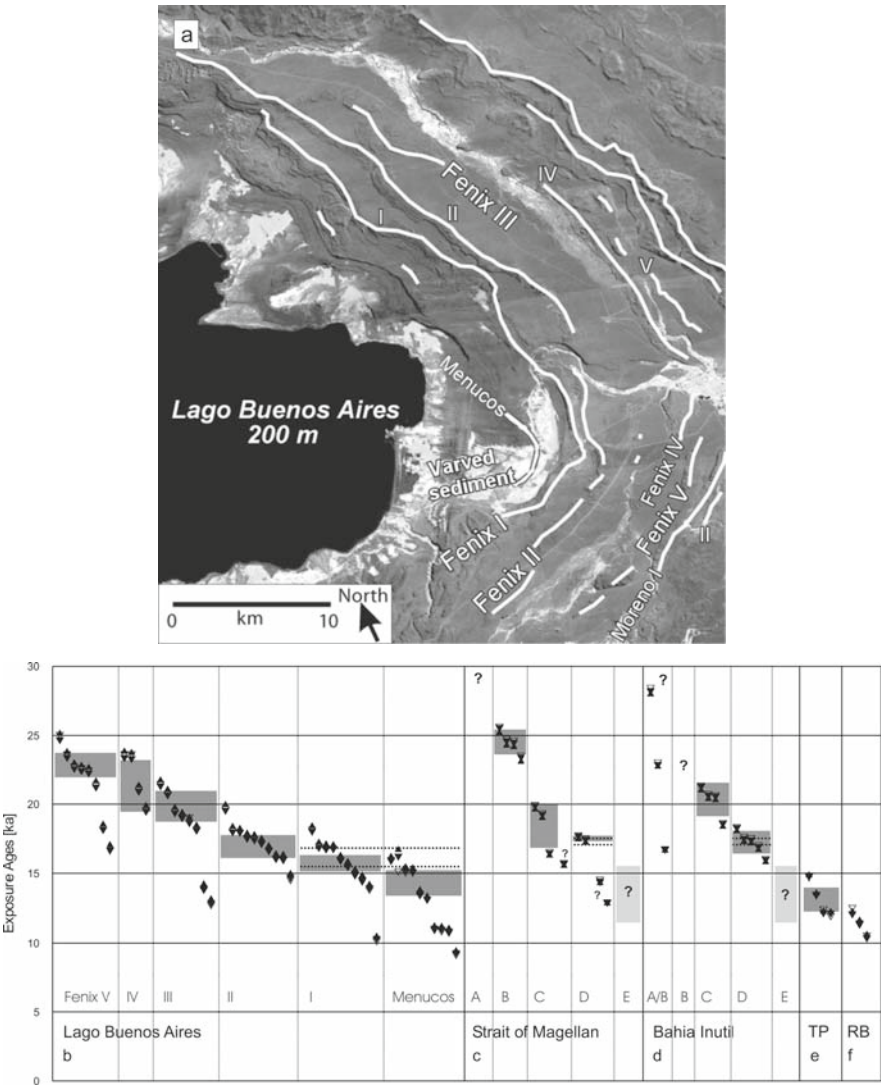

Fig. 3.5 (**a**) Geographical setting and (**b**) exposure ages from the moraines at Lago Buenos Aires (Fenix I-V and Menucos) (Douglass et al. 2006), (**c**) the Strait of Magellan and **(d)**, Bahia Inutil (McCulloch et al. 2005; Kaplan et al. 2008), (**e**) Torres del Paine (TP) (Fogwill and Kubik 2005), and (**f**) from Rio Bayo (RB), Northern Patagonia Ice Field (Glasser et al. 2006). The *dotted horizontal lines* indicate additional radiocarbon age control

and shaded boxes in Fig. 3.5b). Recalculations based on the online calculator of Balco et al. (2008) yield slightly different ages (filled triangles), but the choice of the scaling system has only negligible effects on the exposure ages (<5%) for the low altitudes and mid-latitudes of Patagonia. Additionally, three radiocarbon ages (12.8–14.6^{14}C ka BP, i.e. 15.5–16.9 cal. ka: Kaplan et al. 2004) from carbonate

concretions in varved sediments underlying Menucos till and overlying Fenix I till provide a maximum and minimum age, respectively, and corroborate the exposure age chronologies. Applying the maximum age model to the exposure ages would result in slightly older age estimates for the moraines and better agreement with the radiocarbon ages (Fig. 3.5b), but as the age scatter on individual moraines is generally low, the overall paleoclimatic implications are not affected.

A similar glacial chronology compared to the one at LBA was recently established for southernmost South America [Strait of Magellan (SoM) and Bahia Inutil (BIn): 53–55°S] using a combination of SED, radiocarbon dating, amino acid racemization, and tephrachronology (McCulloch et al. 2005; Kaplan et al. 2008) (Fig. 3.5b). Exposure ages from the moraine stages B, C and D (the labeling follows Bentley et al. 2005) have been interpreted to date the respective glacial advances to 24.6 ± 0.9 ka, 18.5 ± 1.8 and 17.6 ± 0.2 ka in the SoM, and the C and D moraine stages in the BIn to 20.4 ± 1.2 and 17.3 ± 0.8 ka (original data: mean ± 1 standard deviation, open triangles and shaded boxes in Fig. 3.5c and d) (Kaplan et al. 2008). Recalculation using the online calculator of Balco et al. (2008) yields very similar exposure ages (filled triangles), and applying the oldest age model would result in slightly older age estimates for the glacial advances. Numerous radiocarbon dates provide a robust minimum age of 17.0–17.6 cal ka BP (1σ calibrated age range) for deglaciation after stage D both in the SoM and the BIn, and thus corroborate the exposure age chronologies. A Late Glacial stage E reached the head of the SoM and BIn and is radiocarbon-dated to between 15.5 and 11.7 cal ka BP (McCulloch et al. 2005) (light grey boxes in Fig. 3.5c and d).

SED control for the last glacial-to-interglacial transition is also available from Torres del Paine (51°S), Chile (Fogwill and Kubik 2005), where four boulders from a recessional moraine were dated to 13.2 ± 0.8 ka (original data: open triangles in Fig. 3.5e). Glasser et al. (2006) dated a small cirque moraine in a tributary of the Rio Bayo Valley (west of LBA, 46.6°S) to ∼12.5±0.9 ka (one boulder), and a outlet glacier moraine in the Rio Bayo Valley itself to 11.4 ± 0.9 and 10.5 ± 0.8 ka (two boulders, original data: open triangles in Fig. 3.5f). Again, recalculation using the online calculator of Balco et al. (2008) does not affect the interpretation (filled triangles).

The SED results reviewed above show that the local LGM in the Patagonian Andes and Tierra del Fuego occurred at ∼25–23 ka, that is, during MIS 2 and approximately synchronous with the northern hemispheric insolation and temperature minima, and coeval with extensive global ice volume (Denton et al. 1999a; Clapperton 2000; Clapperton and Seltzer 2001; Coronato et al. 2004; Kaplan et al. 2004, 2005). The patterns of multiple glacial advances at LBA, SoM and BIn are in broad agreement with each other, within uncertainties, and all show a successively more limited extent from ∼25 to 18 ka. This trend documents increasing temperatures, and/or reduced precipitation. The latter could have been caused by lee-effects on the eastern side of the Andes due to blocking of moisture from the Pacific by the growing ice-fields. Alternatively, a more northerly position of the westerlies during the LGM at ∼18–20 ka has been suggested, mainly based on palynological and marine sediment records (Heusser 1989; Moreno et al. 1999; Stuut and Lamy 2004; Maldonado et al. 2005). This would be in agreement with the local LGM

in the southern CLD at ~18 ka (Lowell et al. 1995; Denton et al. 1999b; Heusser 2003), but seems to differ with the earlier local LGMs in the northern CLD and further north (Lowell et al. 1995; Denton et al. 1999b; Heusser 2003; Zech et al. 2007a). The apparent discrepancy could be solved by proposing a more focused core of the westerlies, located near the southern CLD at ~18 ka, with the westerlies not providing abundant precipitation towards the north – the scenario that has been suggested earlier by Markgraf (1992). A ~5° southward migration of the westerlies after ~17 ka to their present location at ~48–50°S by 14.3 ka has been inferred based on paleoecological evidence (Moreno et al. 1999; McCulloch et al. 2000; Moreno 2002; Moreno and León 2003). This would have helped facilitate the relatively extensive Late Glacial advances at LBA, SoM and BIn, whereas at latitudes of the CLD glaciers had already retreated from their LGM positions to the highest catchments (Ariztegui et al. 1997; Hajdas et al. 2003; Zech, unpublished SED data).

Although the differences between scaling schemes for latitude and altitude become more negligible in the Patagonian Andes, there is still an uncertainty about the production rate itself (Ackert et al. 2003; Balco et al. 2008). In addition, the scatter in ages for individual moraines (Fig. 3.5) and different approaches to interpreting that scatter (mean ages versus oldest age model) currently limit the possibility of using SED to correlate glacial advances with millennial-scale climate events, such as the YD chron and other northern high-latitude cold Heinrich events.

Based on the precise radiocarbon-dated chronologies in the CLD, Denton et al. (1999a) argued that the synchrony of stepwise warming during deglaciation (at ~17, 14.5 and 11.4 ka) in the southern and the northern hemisphere points to a common atmospheric forcing, including water vapor and/or other greenhouse gases. Lake sediment studies show that the Late Glacial climate reversal in the Cordillera east of the CLD region spans, but its beginning clearly predates, the YD chron (Ariztegui et al. 1997; Hajdas et al. 2003). This likely indicates the influence of the Antarctic climate, which – on millennial timescales – is out of phase with the northern hemispheric signal, possibly due to the south-north heat transfer via the ocean circulation (the so-called bipolar seesaw hypothesis: Broecker 1998; Blunier and Brook 2001). Paleoecological proxies along the Patagonian Andes do not always reveal a consistent picture; some proxies, for example, do not show any evidence for a Late Glacial climate reversal (Ashworth et al. 1991; Bennett et al. 2000; Massaferro et al. 2005). The bulk of the evidence points to climatic variability during this time period, however, which has been interpreted to indicate that towards the southern tip of South America the data are more consistent with Antarctic temperature changes than with those in the northern hemisphere (McCulloch et al. 2000, 2005; Sugden et al. 2005; Turner et al. 2005; Douglass et al. 2006).

3.5 Conclusions

SED provides a powerful tool to date moraines and establish glacial chronologies. Its application worldwide and particularly along the Andean transect during the last

decade indicates the enormous potential for Late Quaternary climate reconstruction. Two current limitations should, however, be kept in mind:

1. Systematic uncertainties due to scaling and the reference production rate can be substantial, particularly at high altitudes and low latitudes, such as in glaciated regions in the tropical Andes. There exposure ages calculated using different scaling methods may differ by as much as 20%. Local calibration sites are therefore greatly needed in order to improve the calculation methods and the resultant glacial chronologies.
2. In some instances the scatter in exposure ages from a specific moraine can make assigning an accurate deposition age challenging and somewhat subjective, but awareness of the underlying causes of scatter helps to reduce its likelihood. Careful sampling protocols can minimize the chance of dating exhumed, eroded, or unstable boulders. Dating multiple boulders from each moraine increases the probability of identifying the true depositional age of the moraine.

Despite these limitations, SED has already improved our understanding of the glaciation history along the Andean transect and the role of changing temperature and precipitation. We summarize the above results again in order to provide a conceptual model and testable hypotheses concerning the glaciation history during the LGM and its termination as follows:

1. On orbital timescales, glaciation in some parts of the southern Andes (tropics and Patagonia) was roughly synchronous with northern hemispheric insolation and temperature minima (i.e., during MIS 2), calling for globally active feedbacks such as the concentrations of water vapor and other greenhouse gases in the atmosphere. Local LGM advances out of phase with the global LGM most likely document limitations in moisture and may reveal changing atmospheric circulation patterns.
2. SED results indicate that glaciers in the tropical Andes reached their local LGM as early as ~30/26 ka. This may be due to increased precipitation early in the course of the last glaciation, followed by increasingly drier conditions on the leeward (western) side of the Cordillera Oriental as ice built up on the windward (eastern) side and caused more effective rain shadow effects. This interpretation would be in agreement with moraines of similar extent as the older ones dated to 25/22 ka on the lee side of the Cordillera, and one moraine dated to 23/20 ka on the eastern slope.
3. Late Glacial moraines were deposited between ~17/15 and 12/10 ka in the tropical Andes, indicating a regional climatic shift that caused stillstands and/or readvances in a number of valleys. Detailed paleoclimatic interpretation of the SED chronologies to extract the respective contributions of reduced temperatures, increased precipitation, and related millennial-scale events and global teleconnections, must await further calibration studies and reduced systematic, methodological uncertainties of SED.

4. In the arid tropical Andes, on the Altiplano, glaciers that are – and presumably were – mainly precipitation-sensitive reached their local LGM during the Late Glacial, synchronous to the lake transgression phases Tauca (18–14 ka) and Coipasa (13–11 ka) (Placzek et al. 2006), caused by an intensification and/or southward shift of the tropical circulation.
5. An intensification and/or southward shift of the tropical circulation also seems to have triggered the Late Glacial advances in Northern Chile at ~30°S (~between 18/16 and 15/13 ka). There, however, the local LGM occurred as early as ~42/39 ka. This advance could have been triggered by an intensification and/or northward shift of the westerlies at that time, because evidence for an early LGM is found as far south as ~40°S in the northern CLD.
6. The westerlies' storm tracks may have been focused near the southern Chilean Lake District at ~18 cal ka BP, which would explain the maximum ice extent there at that time, and the earlier maxima to the north and to the south (~25–23 ka at LBA and SoM). Evidence indicates that the westerlies subsequently shifted south, which may explain, in combination with its more southerly latitude, the relatively extensive Late Glacial advances at LBA, SoM and BIn, whereas the Late Glacial readvances at ~40° were limited to the highest catchments. The coincidence with the proposed southward shift of the tropical circulation at the same time calls for a global latitudinal re-organization of the atmospheric circulation, possibly triggered by cold northern-hemispheric winter temperatures and increasing temperatures recorded in Antarctica.
7. The role of rapid temperature fluctuations for the Late Glacial advances in Patagonia is complex. Radiocarbon-based evidence in southernmost South America suggests that glaciers responded to an Antarctic-like temperature signal (the ACR). If correct, this points to opposite temperatures between the hemispheres on millennial timescales and corroborates the bi-polar seesaw hypothesis.

Acknowledgments We thank INQUA for providing the platform for discussions on "Timing and nature of mountain glacier advances from 5e to YD" during a workshop and fieldtrip to Xining and the Tibetan Plateau, 14–22 September 2006. In particular, we thank Glenn Thackray, Lewis A. Owen, and Chaolu Yi for organization and guiding the workshop and field trip. We thank Meredith Kelly and an anonymous reviewer for their thoughtful and detailed feedback.

References

Ackert RP, Singer BS, Guillou H et al (2003) Long-term cosmogenic 3He production rates from 40Ar/39Ar and K–Ar dated Patagonian lava flows at 47°S. Earth Planet Sci Lett 210:119–136

Ammann C, Jenny B, Kammer K et al (2001) Late Quaternary Glacier response to humidity changes in the arid Andes of Chile (18–29°S). Palaeogeogr Palaeoclim Palaeoecol 172:313–326

Argollo J (1980) Los Pie de Montes de la Cordillera Real entre los Valles de La Paz y de Tuni: Estudio Geologico, Evolution Plio-Cuaternaria. Tesis de Grado, Departamento de Geociencias, Facultad de Ciencias Puras y Naturales, Universidad Mayor de San Andres, La Paz, Bolivia. 100 pp

Ariztegui D, Bianchi MM, Masaferro J et al (1997) Interhemispheric synchrony of late-glacial climatic instability as recorded in proglacial Lake Mascardi, Argentina. J Quat Sci 12:333–338

Ashworth AC, Markgraf V, Villagran C (1991) Late Quaternary climatic history of the Chilean Channels based on fossil pollen and beetle analyses, with an analysis of the modern vegetation and pollen rain. J Quat Sci 6:279–291

Baker PA, Rigsby CA, Seltzer GO et al (2001a) Tropical climate changes at millennial and orbital timescales on the Bolivian Altiplano. Nature 409:698–701

Baker PA, Rigsby CA, Seltzer GO et al (2001b) The history of South American tropical precipitation for the past 25,000 years. Science 291:640–643

Balco G, Stone JO, Lifton NA et al (2008) A complete and easily accessible means of calculating surface exposure ages or erosion rates from 10Be and 26Al measurements. Quat Geochron 3:174–195

Bennett KD, Haberle SG, Lumley SH (2000) The Last Glacial-Holocene transition in southern Chile. Science 290:325–328

Bentley MJ, Sugden DE, Hulton NRJ et al (2005) The landforms and pattern of deglaciation in the Strait of Magellan and Bahia Inutil, southernmost South America. Geogr Ann 87A:313–333

Berger A, Loutre MF (1991) Insolation values for the climate of the last 10 million of years. Quat Sci Rev 10(4):297–317

Bierman PR, Caffee MW, Davis PT et al (2002) Rates and timing of Earth surface processes from in situ-produced cosmogenic Be-10. In: Grew ES (eds) Beryllium: mineralogy, petrology, and geochemistry. Mineralogical Society of America, Washington D.C.

Blunier T, Brook EJ (2001) Timing of millennial-scale climate change in Antarctica and Greenland during the last glacial period. Science 291(5501):109–112

Briner JP, Kaufman DS, Manley WF et al (2005) Cosmogenic exposure dating of late Pleistocene moraine stabilization in Alaska. GSA Bulletin 117(7):1108–1120

Broecker WS (1998) Paleocean circulation during the last deglaciation: a bipolar seesaw? Paleoceanography 13:119–121

Chiang J, Bitz C (2005) Influence of high latitude ice cover on the marine Intertropical Convergence Zone. Clim Dyn 25(5):477–496

Clapperton C (1990) Quaternary glaciations in the Southern Hemisphere: an overview. Quat Sci Rev 9:299–304

Clapperton C (1993) Quaternary geology and geomorphology of South America. Elsevier, Amsterdam

Clapperton C (2000) Interhemispheric synchroneity of Marine Oxygen Isotope Stage 2 glacier fluctuations along the American cordilleras transect. J Quat Sci 15:435–468

Clapperton C, Seltzer GO (2001) Glaciation during marine isotope Stage 2 in the American Cordillera. In: Markgraf V (eds) Interhemispheric climate linkages. Academic Press, San Diego

Clapperton CM, Clayton JD, Benn DI et al (1997) Late Quaternary glacier advances and palaeolake highstands in the Bolivian Altiplano. Quat Int 38–39:49–59

Clayton JD, Clapperton CM (1997) Broad synchrony of a Late-Glacial glacier advance and the highstand of palaeolake Tauca in the Bolivian Altiplano. J Quat Sci 12:169–182

Coronato A, Martinez O, Rabassa J (2004) Glaciations in Argentine Patagonia, southern South America. In: Ehlers J, Gibbard PL (eds) Quaternary glaciations – extent and chronology. Part III: South America, Asia, Africa, Australasia, Antarctica. Elsevier, Cambridge

Cruz FW, Burns SJ, Karmann I et al (2005) Insolation-driven changes in atmospheric circulation over the past 116,000 years in subtropical Brazil. Nature 434:63–66

Denton GH, Heusser CJ, Lowell TV et al (1999a) Interhemispheric linkage of paleoclimate during the last glaciation. Geogr Ann 81:107–153

Denton GH, Lowell TV, Heusser CJ et al (1999b) Geomorphology, stratigraphy, and radiocarbon chronology of Llanquihue drift in the area of the southern Lake District, Seno Reloncavi, and Isla Grande de Chiloe, Chile. Geogr Ann 81 (A):167–229

Desilets D, Zreda M (2003) Spatial and temporal distribution of secondary cosmic-ray nucleon intensities and applications to in situ cosmogenic dating. Earth Planet Sci Lett 206:21–42

Desilets D, Zreda M, Prabu P (2006) Extended scaling factors for in situ cosmogenic nuclides: new measurements at low latitude. Earth Planet Sci Lett 246:265–276

Douglass DC, Singer BS, Kaplan MR et al (2006) Cosmogenic nuclide surface exposure dating of boulders on last-glacial and late-glacial moraines, Lago Buenos Aires, Argentina: interpretive strategies and paleoclimate implications. Quat Geochron 1(1):43–58

Dunai TJ (2001) Influence of secular variation of the geomagnetic field on production rates of in situ produced cosmogenic nuclides. Earth Planet Sci Lett 193:197–212

Dunne A, Elmore D, Muzikar P (1999) Scaling factors for the rates of production of cosmogenic nuclides for geometric shielding and attenuation at depth on sloped surfaces. Geomorphology 27:3–11

Ehlers J, Gibbard PL (eds) (2004) Quaternary glaciations – extent and chronology. Elsevier, Cambridge

Farber DL, Hancock GS, Finkel RC et al (2005) The age and extent of tropical alpine glaciation in the Cordillera Blanca, Peru. J Quat Sci 20(7–8):759–776

Favier V, Wagnon P, Ribstein P (2004) Glaciers of the outer and inner tropics: a different behaviour but a common response to climatic forcing. Geophys Res Lett 31:L16403. doi:10.1029/2004GL020654

Fogwill CJ, Kubik P (2005) A glacial stage spanning the Antarctic Cold Reversal in Torres del Paine (51°S), Chile, based on preliminary cosmogenic exposure ages. Geogr Ann 87A: 403–408

Fritz SC, Baker PA, Lowenstein TK et al (2004) Hydrologic variation during the last 170,000 years in the southern hemisphere tropics of South America. Quat Res 61:95–104

Garreaud R, Vuille M, Clement AC (2003) The climate of the Altiplano: observed current conditions and mechanisms of past changes. Palaeogeogr Palaeoclim Palaeoecol 194 (1–3):5–22

Garreaud R, Aceituno P (2007) Atmospheric circulation and climatic variability. In: Veblen TT, Young KR, Orme AR (eds) The physical geography of South America. Oxford University Press, Oxford

Geyh MA, Grosjean M, Nunez L et al (1999) Radiocarbon reservoir effect and the timing of the late-glacial/early Holocene Humid Phase in the Atacama Desert (Northern Chile). Quat Res 52:143–153

Glasser NF, Harrison S, Ivy-Ochs S et al (2006) Evidence from the Rio Bayo valley on the extent of the North Patagonian Icefield during the Late Pleistocene-Holocene transition. Quat Res 65 (1):70–77

Goodman AY, Rodbell DT, Seltzer GO et al (2001) Subdivision of glacial deposits in southeastern Peru based on pedogenic development and radiometric ages. Quat Res 56:31–50

Gosse JC, Phillips FM (2001) Terrestrial in situ cosmogenic nuclides: theory and application. Quat Sci Rev 20:1475–1560

Gregory-Wodzicki KM (2000) Uplift history of the Central and Northern Andes: a review. GSA Bull 112:1091–1105

Grosjean M, van Leeuwen JFN, van der Knaap WO et al (2001) A 22,000 14C yr BP sediment and pollen record of climate change from Laguna Miscanti 231S, northern Chile. Glob Planet Change 28:35–51

Hajdas I, Bonani G, Moreno PI et al (2003) Precise radiocarbon dating of Late-Glacial cooling in mid-latitude South America. Quat Res 59 (1):70–78

Haselton K, Hilley G, Strecker MR (2002) Average Pleistocene climatic patterns in the southern Central Andes: controls on mountain glaciation and paleoclimate implications. J Geol 110:211–226

Heine K (2004) Late Quaternary glaciations of Bolivia. In: Ehlers J, Gibbard PL (eds) Quaternary glaciations – extent and chronology. Part III: South America, Asia, Africa, Australasia, Antarctica. Elsevier, Cambridge

Heusser CJ (1989) Southern westerlies during the last glacial maximum. Quat Res 31:423–425

Heusser CJ (2003) Ice Age Southern Andes - A Chronicle of Paleoecological Events. Elsevier, Amsterdam

Ivy-Ochs S (1996) The dating of rock surface using in situ produced 10Be, 26Al and 36Cl, with examples from Antarctica and the Swiss Alps. Dissertation ETH No. 11763, Zürich. 197 pp.

Kaplan MR, Ackert RP, Singer BS et al (2004) Cosmogenic nuclide chronology of millennial-scale glacial advances during O-isotope stage 2 in Patagonia. GSA Bull 116(3/4):308–321
Kaplan MR, Douglass DC, Singer BS et al (2005) Cosmogenic nuclide chronology of pre-last glacial maximum moraines at Lago Buenos Aires, 46°S, Argentina. Quat Res 63(3):301–315
Kaplan MR, Fogwill CJ, Sugden DE et al (2008) Southern Patagonian glacial chronology for the Last Glacial period and implications for Southern Ocean climate. Quat Sci Rev 27 (3–4):284–294
Kaser G, Osmaston H (2002) Tropical Glaciers. Cambridge University Press, Cambridge
Kennan L (2000) Large-scale geomorphology of the Andes; interrelationships of tectonics, magmatism and climate. In: Summerfield MA (eds) Geomorphology and global tectonics. John Wiley & Sons, Chichester
Klein AG, Seltzer GO, Isacks BL (1999) Modern and Last Local Glacial Maximum snowlines in the Central Andes of Peru, Bolivia and Northern Chile. Quat Sci Rev 18:63–84
Kohl CP, Nishiizumi K (1992) Chemical isolation of quartz for measurement of in-situ-produced cosmogenic nuclides. Geochim Cosmochim Acta 56:3583–3587
Kubik PW, Reuther AU (2007) Attenuation of cosmogenic 10Be production in the first 20 cm below a rock surface. Nucl Instrum Methods Phys Res B 259(1):616–624
Kull C, Grosjean M (2000) Late Pleistocene climate conditions in the North Chilean Andes drawn from a Climate-Glacier Model. J Glaciol 46:622–632
Kull C, Grosjean M, Veit H (2002) Modeling Modern and Late Pleistocene Glacio-Climatological Conditions in the North Chilean Andes (29–30°). Clim Change 52:359–381
Kull C, Hanni F, Grosjean M et al (2003) Evidence of an LGM cooling in NW-Argentina (22°S) derived from a glacier climate model. Quat Int 108(1):3–11.
Kull C, Imhof S, Grosjean M et al (2007) Late Pleistocene glaciation in the Central Andes: temperature versus humidity control – A case study from the eastern Bolivian Andes (17°S) and regional synthesis. Glob Planet Change. doi: 10.1016/j.gloplacha.2007.03.011
Kull C, Imhof S, Grosjean M et al (2008) Late Pleistocene glaciation in the Central Andes: Temperature versus humidity control—A case study from the eastern Bolivian Andes (17°S) and regional synthesis. Glob Planet Change 60:148–164
Lal D (1991) Cosmic ray labeling of erosion surfaces: in situ nuclide production rates and erosion models. Earth Planet Sci Lett 104:429–439
Lenters JD, Cook KH (1997) On the origin of the Bolivian High and related circulation features of the South American climate. J Atmos Sci 54:656–677
Lifton NA, Bieber JW, Clem JM et al (2005) Addressing solar modulation and long-term uncertainties in scaling secondary cosmic rays for in situ cosmogenic nuclide applications. Earth Planet Sci Lett 239 (1–2):140–161
Lisiecki LE, Raymo ME (2005) A Pliocene-Pleistocene stack of 57 globally distributed benthic d18O records. Paleoceanography 20:PA1003. doi:10.1029/2004PA001071
Lowell TV, Heusser CJ, Andersen BG et al (1995) Interhemispheric correlations of Late Pleistocene glacial events. Science 269:1541–1549
Maldonado A, Betancourt JL, Latorre C et al (2005) Pollen analyses from a 50 000-yr rodent midden series in the southern Atacama Desert (25°30'S). J Quat Sci 20(5):493–507
Marengo JA, Soares WR, Saulo C et al (2004) Climatology of the low-level jet east of the Andes as derived from the NCEP-NCAR reanalyses: characteristics and temporal variability. J Clim 17(12):2261–2280
Mark BG, Seltzer GO, Rodbell DT et al (2002) Rates of deglaciation during the last glaciation and Holocene in the Cordillera Vilcanota-Quelccaya Ice Cap region, southeastern Peru. Quat Res 57:287–298
Mark BG, Seltzer GO, Rodbell DT (2004) Late Quaternary glaciations of Ecuador, Peru and Bolivia. In: Ehlers J, Gibbard PL (eds) Quaternary glaciations – extent and chronology. Part III: South America, Asia, Africa, Australasia, Antarctica. Elsevier, Cambridge
Mark BG, Harrison SP, Spessa A et al (2005) Tropical snowline changes at the last glacial maximum: a global assessment. Quat Int 138–139:168–2001

Markgraf V (1989) Reply to C.J. Heusser's "Southern Westerlies during the Last Glacial Maximum". Quat Res 28:426–432
Markgraf V, Dodson JR, Kershaw AP et al (1992) Evolution of late Pleistocene and Holocene climates in the circum-South Pacific land areas. Clim Dyn 6:193–211
Markgraf V, Baumgartner TR, Bradbury JP et al (2000) Paleoclimate reconstruction along the Pole-Equator-Pole transect of the Americas (PEP 1). Quat Sci Rev 19(1–5):125–140.
Markgraf V (ed) (2001) Interhemispheric climate linkages. Academic Press, San Diego
Masarik J, Reedy RC (1995) Terrestrial cosmogenic-nuclide production systematics calculated from numerical simulations. Earth Planet Sci Lett 136:381–395
Masarik J, Wieler R (2003) Production rates of cosmogenic nuclides in boulders. Earth Planet Sci Lett 216:201–208
Massaferro J, Brooks SJ, Haberle SG (2005) The dynamics of chironomid assemblages and vegetation during the Late Quaternary at Laguna Facil, Chonos Archipelago, southern Chile. Quat Sci Rev 24 (23–24):2510–2522
McCulloch RD, Bentley MJ, Purves RS et al (2000) Climatic inferences from glacial and palaeoecological evidence at the last glacial termination, southern South America. J Quat Sci 15 (4):409–417
McCulloch RD, Fogwill CJ, Sudgen DE et al (2005) Chronology of the last glaciation in the Central Strait of Magellan and Bahia Inutil, southernmost South America. Geogr Ann 87A:289–312
McManus JF, Francois R, Gherardi J-M et al (2004) Collapse and rapid resumption of Atlantic meridional circulation linked to deglacial. Clim Changes 428 (6985):834–837
Mix AC, Bard E, Schneider R (2001) Environmental processes of the ice age: land, oceans, glaciers (EPILOG). Quat Sci Rev 20:627–657
Moreno PI, Jacobson GL, Andersen B et al (1999) Abrupt vegetation and climate changes during the last glacial maximum and the last Termination in the Chilean Lake District: a case study from Canal de la Puntilla (41ºS). Geogr Ann 81A:285–311
Moreno PI (2002) Western Patagonia: a key area for understanding Quaternary paleoclimate at southern mid-latitudes. In: Casassa G, Sepulveda FV, Sinclair RM (eds) The Patagonian icefields. A Unique Natural Laboratory for Environmental and Climate Change Studies. Kluwer Academic/Plenum Publishers, New York
Moreno PI, León AL (2003) Abrupt vegetation changes during the last glacial to Holocene transition in mid-latitude South America. J Quat Sci 18 (8):787–800
NGRIP (2004) High-resolution record of Northern Hemisphere climate extending into the last interglacial period. Nature 431(7005):147–151
Orme AR (2007) The tectonic framework of South America. In: Veblen TT, Young KR, Orme AR (eds) The physical geography of South America. Oxford University Press, Oxford
Pigati JS, Lifton NA (2004) Geomagnetic effects on time-integrated cosmogenic nuclide production with emphasis on in situ 14C and 10Be. Earth Planet Sci Lett 226:193– 205
Placzek C, Quade J, Patchett PJ (2006) Geochronology and stratigraphy of late Pleistocene lake cycles on the southern Bolivian Altiplano: implications for causes of tropical climate change. GSA Bull 118 (5):515–532
Putkonen J, Swanson T (2003) Accuracy of cosmogenic ages for moraines. Quat Res 59:255–261
Putkonen J, O'Neal M (2006) Degradation of unconsolidated Quaternary landforms in the western North America. Geomorphology 75(3–4):408–419
Ramage JM, Smith JA, Rodbell DT et al (2005) Comparing reconstructed Pleistocene equilibrium line altitudes in the tropical Andes of central Peru. J Quat Sci 20:777–788
Rodbell DT, Seltzer GO (2000) Rapid ice margin fluctuations during the Younger Dryas in the Tropical Andes. Quat Res 54:328–338
Seltzer GO (1990) Recent glacial history and paleoclimate of the Peruvian-Bolivian Andes. Quat Sci Rev 9:137–152
Seltzer GO (1994) A lacustrine record of late Pleistocene climatic change in the subtropical Andes. Boreas 23:105–111

Seltzer GO, Rodbell DT, Abbott M (1995) Andean glacial lakes and climate variability since the last glacial maximum. Bulletin de L'Institut Francais d'Etudes Andines 24(3):539–549
Seltzer GO, Rodbell DT, Burns SJ (2000) Isotopic evidence for late Quaternary climatic change in tropical South America. Geology 28:35–38
Seltzer GO, Rodbell DT, Baker PA et al (2002) Early warming of tropical South America at the last glacial-interglacial transition. Science 296:1685–1686
Seltzer GO (2007) Late Quaternary Glaciation in the Tropical Andes. In: Veblen TT, Young KR, Orme AR (eds) The physical geography of South America. Oxford University Press, Oxford
Servant M, Fontes J (1978) Les lacs quaternaires des hauts plateaux des Andes Boliviennes: Premieres interpretations paleoclimatiques. Cah. O.R.S.T.O.M., Ser. Geol 10:9–23
Servant M, Fontes J, Argollo J et al (1981) Variations du regime et de la nature des precipitations au cours des 15 derniers millenaires dans les Andes de Bolivie. Comptes Rendus de l'Academie des Sciences Paris Serie II 292:1209–1212
Servant M, Fournier M, Argollo J et al (1995) La dernière transition glaciaire/interglaciaire des Andes tropicales sud (Bolivie) d'après l'étude des variations des niveaux lacustres et des fluctuations glaciaires. Comptes Rendus de l'Académie des Sciences Paris Série IIa 320:729–736
Shanahan TM, Zreda M (2000) Chronology of Quaternary glaciations in East Africa. Earth Planet Sci Lett 177:23–42
Smith JA, Seltzer GO, Rodbell DT et al (2005a) Regional synthesis of last glacial maximum snowlines in the tropical Andes, South America. Quat Int 138–139:145–167
Smith JA, Seltzer GO, Farber DL et al (2005b) Early local Last Glacial Maximum in the Tropical Andes. Science 308:678–681
Smith JA, Finkel RC, Farber DL et al (2005c) Moraine preservation and boulder erosion in the tropical Andes: interpreting old surface exposure ages in glaciated valleys. J Quat Sci 20 (7–8):735–758
Stone JO (2000) Air pressure and cosmogenic isotope production. J Geophys Res 105: 23753–23759
Stuut J-BW, Lamy F (2004) Climate variability at the southern boundaries of the Namib (southwestern Africa) and Atacama (northern Chile) coastal deserts during the last 120,000 yr. Quat Res 62 (3):301–309
Sugden DE, Bentley MJ, Fogwill CJ et al (2005) Late-Glacial glacier events in southernmost South America: a blend of 'northern' and 'southern' hemispheric climatic signals? Geogr Ann 87 (2):273–288. doi:10.1111/j.0435-3676.2005.00259.x
Sylvestre F, Servant M, Servant-Vildary S et al (1999) Lake-level chronology on the Southern Bolivian Altiplano (18–23 S) during Late-Glacial time and the early Holocene. Quat Res 51:54–66
Turner KJ, Fogwill CJ, McCulloch RD et al (2005) Deglaciation of the eastern flank of the North Patagonian Icefield and associated continental-scale lake diversions. Geogr Ann (A) 87 (2):363–374. doi:10.1111/j.0435-3676.2005.00263.x
Valero-Garcés BL, Jenny B, Rondanelli M et al (2005) Palaeohydrology of Laguna de Tagua Tagua (34°30'S) and moisture fluctuations in Central Chile for the last 46 000 yr. J Quat Sci 20(7–8):625–641
Vuille M, Ammann C (1997) Regional snowfall patterns in the high, Arid Andes (South America). Clim Change 36:413–423
Vuille M, Keimig F (2004) Interannual variability of summertime convective cloudiness and precipitation in the Central Andes derived from ISCCP-B3 data. J Clim 17(17):3334–3348.
Walker M (2005) Quaternary dating methods. Wiley, Chichester
Wang X, Auler AS, Edwards RL et al (2006) Interhemispheric anti-phasing of rainfall during the last glacial period. Quat Sci Rev 25 (23–24):3391–3403
Wright HE Jr (1984) Late glacial and late Holocene moraines in the Cerros Cuchpanga, central Peru. Quat Res 21:275–285

Zech R, Glaser B, Sosin P et al (2005) Evidence for long-lasting landform surface instability on hummocky moraines in the Pamir Mountains from surface exposure dating. Earth Planet Sci Lett 237:453–461

Zech R, Kull C, Veit H (2006) Late Quaternary glacial history in the Encierro Valley, Northern Chile (29°S), deduced from 10Be surface exposure dating. Palaeogeogr Palaeoclimatol Palaeoecol 234 (2–4):277–286

Zech R, Kull C, Veit H (2007a) Exposure dating of Late Glacial and pre-LGM moraines in the Cordillera Dona Rosa, Northern Chile (∼31°S). Climate Past 3:1–14

Zech R, Kull C, Kubik P et al (2007b) LGM and Late Glacial glacier advances in the Cordillera Real and Cochabamba (Bolivia) deduced from 10Be surface exposure dating. Climate Past 3:623–635

Zhang R, Delworth TL (2005) Simulated tropical response to a substantial weakening of the Atlantic thermohaline circulation. J Clim 18 (12):1853–1860

Zhou J, Lau K-M (1998) Does a monsoon climate exist over South America? J Clim 11 (5):1020–1040

Zreda M, Clapperton C, Argollo J et al (2001) Evidence for contemporary lakes and Glaciers in the Southern Altiplano during Late Glacial time. Fifth Iberian Quaternary Meeting (extended abstract), Lisboa, Portugal

Zreda MG, Phillips FM (1995) Insights into alpine moraine development from cosmogenic 36Cl buildup dating. Geomorphology 14(2):149–156

Chapter 4
Vegetation and Fire at the Last Glacial Maximum in Tropical South America

Francis E. Mayle, Michael J. Burn, Mitchell Power, and Dunia H. Urrego

Abstract This chapter aims to review current knowledge of the key vegetation types, and their composition, structure, distribution, and fire regime across the South American tropics during the global Last Glacial Maximum ca. 21,000 cal yr BP (calendar years before present). We do this by synthesising previously published Last Glacial Maximum fossil pollen and charcoal data as well as Last Glacial Maximum vegetation model simulations, in comparison with ecoregion/biome maps of present day vegetation. Both model simulations and empirical data suggest that there were no large-scale differences in major biome distributions between the Last Glacial Maximum and present (notwithstanding the Atlantic forests of SE Brazil), with biome shifts largely associated with ecotonal areas – downslope expansion of montane grasslands in the Andes at the expense of montane forest, and savanna expansion at the expense of rainforest and gallery forest at the Amazon basin margins. However, species composition and structure of these Last Glacial Maximum forests was quite different from those of today. At the Last Glacial Maximum, pollen data show that montane Andean taxa descended into the lowlands to form novel non-analogue forest communities with lowland Amazonian taxa, whilst vegetation model simulations show that carbon limitation caused by low atmospheric CO_2 likely produced forest communities with reduced canopy density and hence lower biomass than present-day forests. These pollen data-model comparisons show that although Amazonia was probably still dominated by closed forest at the Last Glacial Maximum, its carbon store may have been only 50% of present. Most charcoal records show reduced burning during the Last Glacial Maximum compared with today, most likely due to the significantly colder temperatures.

Keywords Charcoal · Last Glacial Maximum · pollen · Quaternary · tropical South America

F.E. Mayle (✉)
School of GeoSciences, University of Edinburgh, Drummond Street, Edinburgh EH8 9XP, UK
e-mail: Francis.Mayle@ed.ac.uk

F. Vimeux et al. (eds.), *Past Climate Variability in South America and Surrounding Regions*, Developments in Paleoenvironmental Research 14,
DOI 10.1007/978-90-481-2672-9_4,

4.1 Introduction

The vegetation in tropical South America during the Last Glacial Maximum ca. 21 cal ka BP (21,000 calendar years before present), has been a topic of great interest and debate for several decades, particularly in Amazonia, concerning the spatial extent of forest versus savanna (Haffer 1969; Haffer and Prance 2001; Colinvaux et al. 2000), and the structural (Cowling et al. 2001) and floristic (Colinvaux et al. 2000) composition of those forests. This focus on the Last Glacial Maximum period in particular stems from interest in how ecosystems responded to the radically different global boundary conditions at the time compared with present; namely, maximum global expansion of ice-sheets, CO_2 concentrations half those of today, lowered temperatures (by 5°C in the tropical lowlands), and differing precipitation regimes (in some areas higher (e.g. Bolivian Altiplano, Baker et al. 2001), and others lower than present (e.g. lowland Bolivia, Mayle et al. 2000)).

The purpose of this chapter is to describe the vegetation and fire regime of tropical South America at the Last Glacial Maximum and how it differed from that of today. This is done by synthesising previously published fossil pollen and charcoal data, together with vegetation model simulations. We then consider the palaeoecological, palaeoclimatic, and carbon cycling implications of these data-model comparisons, and also explore the limitations to our current understanding of Last Glacial Maximum ecosystems, and potential avenues for overcoming these limitations in the future.

4.2 Methods and Approach

We collated previously published pollen data from sites across tropical South America (above 30°S) (Table 4.1), either by obtaining pollen percentage values from the published paper, or from the pollen data spreadsheet from the site analyst (D. Urrego, Consuelo). We retrieved charcoal data from the publicly available Global Fossil Charcoal Database (GCD v. 1) (Power et al. 2008). We stress that the focus here is on the *global* Last Glacial Maximum, when global ice-volume was at its maximum and global sea-levels and atmospheric CO_2 concentrations were at a minimum (120 m below present and 190–200 ppm, respectively). This time period does not equate with the time of maximum glacial expansion in South America, and in fact approximates the onset of deglaciation in the Andes (Seltzer et al. 2002; Smith et al. 2005; Van der Hammen et al. 1980).

Since most fossil pollen and charcoal records have low temporal resolution through the last glacial period, as a result of low sedimentation rates in most lakes during the Pleistocene, we consider a broad temporal window of 6 ka, centred on the Last Glacial Maximum, i.e. 18–24 cal ka BP. This ensures a sufficiently large number of pollen/charcoal samples to obtain as robust and reliable a reconstruction of Last Glacial Maximum vegetation as possible. To obtain insights into the climatic

Table 4.1 Site metadata

Site name	Latitude	Longitude	Elevation (m)	Country	Ecoregion/Regional veg	Investigator
Last Glacial Maximum charcoal records						
Chaplin	−14.4667	−61.0667	200	Bolivia	Madeira-Tapajos moist forest	Burbridge et al. 2004
Titicaca	−16.1344	−69.1553	3810	Bolivia/Peru	Central Andean wet puna	Baker et al. 2001
Siberia 93–1	−17.83333	−64.718889	2920	Bolivia	Cloud forest, open forest, & Puna	Mourguiart and Ledru 2003
Morro de Itapeva	−22.78333	−45.57333	1850	Brazil	Mixture of grassland, Araucaria forest, and Atlantic rainforest	Behling 1997
Catas Altas	−20.083333	−43.36667	755	Brazil	Semi-deciduous tropical forest	Behling and Lichte 1997
Cambara do Sul	−29.0525	−50.101111	1040	Brazil	Prior to settlement: mosaic of Araucaria forest and grassland	Behling et al. 2004
Sao Francisco de Assis	−29.586667	−55.217222	100	Brazil	Lowland campos or grassland	Behling et al. 2005
Lagoa do Caco	−2.970219	−43.267808	120	Brazil	Restinga, cerrado, rainforest	Ledru et al. 2002
Pata	0.2667	−66.0667	300	Brazil	Negro-Branco moist forests	Bush et al. 2002, 2004b
Last Glacial Maximum pollen records						
Salar de Uyuni	−20	−68	3653	Bolivia	Central Andean wet puna	Chepstow-Lusty et al. 2005
Consuelo	−13.95	−68.983333	1360	Peru	Cloud forest	Urrego et al. 2005
Titicaca	−16.1344	−69.1553	3810	Bolivia/Peru	Central Andean wet puna	Baker et al. 2001
Siberia	−17.83333	−64.718889	2920	Bolivia	Cloud forest, open forest, & Puna	Mourguiart and Ledru 2003
Fuquene-3	5.45	−73.766667	2580	Colombia	Eastern Cordillera moist forest	Van der Hammen and Hooghiemstra 2003
Timbio	2.4	−76.6	1750	Colombia	Cauca Valley montane forests	Wille et al. 2000
Amazon Fan	5.201944	−47.018889	0	N/A	Atlantic Ocean	Haberle and Maslin 1999
Lake Pata	0.2667	−66.0667	300	Brazil	Negro-Branco moist forests	Bush et al. 2002, 2004b
Chaplin	−14.4667	−61.0667	200	Bolivia	Madeira-Tapajos moist forest	Burbridge et al. 2004
El Pinal	4.133333	−70.38333	180	Colombia	Llanos	Behling and Hooghiemstra 1999

Table 4.1 (continued)

Site name	Latitude	Longitude	Elevation (m)	Country	Ecoregion/Regional veg	Investigator
Marine Core GeoB 3104–1	−3.666667	−37.716667	0	N/A	Atlantic Ocean	Behling et al. 2000
Volta Velha	−26.066667	−48.633333	5	Brazil	Serra do Mar coastal forests	Behling and Negrelle 2001
Catas Altas	−20.083333	−43.36667	755	Brazil	Semi-deciduous tropical forest	Behling and Lichte 1997
Morro de Itapeva	−22.78333	−45.57333	1850	Brazil	Mixture of grassland, Araucaria forest, and Atlantic rainforest	Behling 1997
Sao Francisco de Assis	−29.586667	−55.217222	100	Brazil	Lowland campos or grassland	Behling et al. 2005
Dragoa	0.270261	−66.687805	300	Brazil	Negro-Branco moist forests	Bush et al. 2004b
Verde	0.292314	−66.678423	300	Brazil	Negro-Branco moist forests	Bush et al. 2004b
Cambara du Sol	−29.0525	−50.101111	1040	Brazil	Prior to settlement: mosaic of Araucaria forest and grassland	Behling et al. 2004
Lagoa do Caco	−2.970219	−43.267808	120	Brazil	Restinga, cerrado, rainforest	Ledru et al. 2002
Last Glacial Maximum sites with Hiatus						
Salitre	−19	−46.766667	970	Brazil	Cerrado savanna	Ledru et al. 1993
Carajas	−6.5	−49.5	800	Brazil	Mato Grosso seasonal forests	Absy et al. 1991; Sifeddine et al. 1994
Serra Negra	−19	−46.75	1170	Brazil	Cerrado savanna	Oliveira 1992
Aguas Emendadas	−15	−47.58	1040	Brazil	Cerrado savanna	Barberi 1994
Itapeva	−22.78333	−45.57333	1850	Brazil	Mixture of grassland, Araucaria forest, and Atlantic rainforest	Behling 1997
Bella Vista	−13.6167	−61.5500	190	Bolivia	Madeira-Tapajos moist forest	Burbridge et al. 2004; Mayle et al. 2000

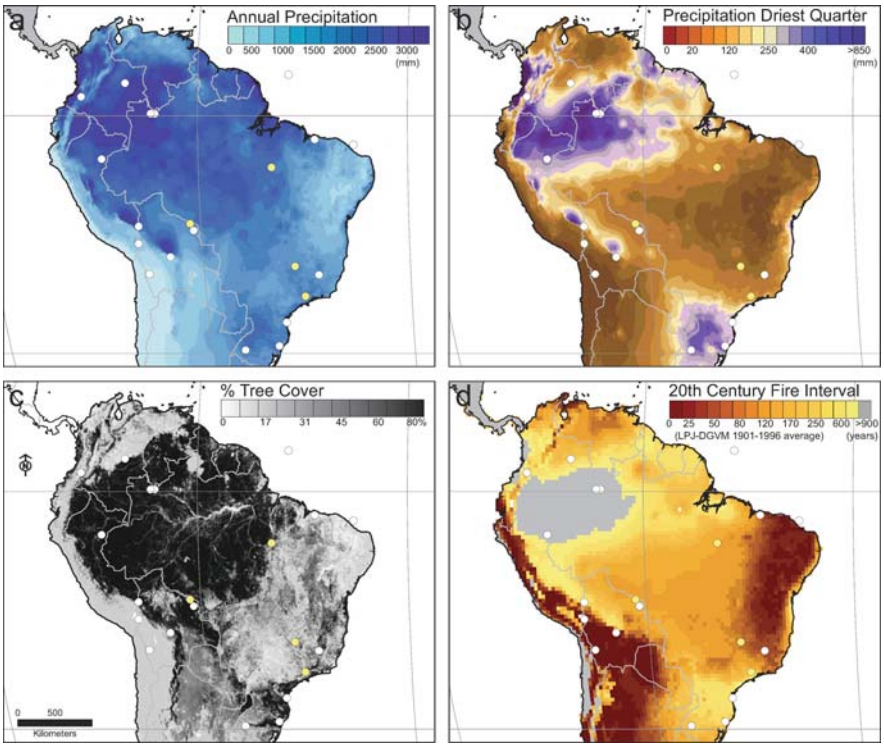

Fig. 4.1 Map showing site locations in relation to present-day rainfall, tree-cover, and fire regime. WorldClim bioclimatic variables (Hijmans et al. 2005) of (**a**) annual precipitation, and (**b**) precipitation of the driest quarter (driest 3 months), characterise present-day climatic variability across the South American tropics. The percent tree cover map (De Fries et al. 2000) (**c**) illustrates the relative forest cover (available biomass). Simulated variations in historical fire-return-intervals using the LPJ-DGVM (Lund–Potsdam–Jena Dynamic Global Vegetation Model) (Thonicke et al. 2001) are shown in panel (**d**). Pollen and charcoal sites are shown by *white circles*. Yellow circles denote sites with a sedimentary hiatus spanning the Last Glacial Maximum

and atmospheric controls upon these Last Glacial Maximum tropical ecosystems, we also consider these empirical data in the light of previously published vegetation model simulations under differing Last Glacial Maximum climatic and CO_2 scenarios.

The locations of the study sites are shown in Figs. 4.1, 4.2, and 4.3, superimposed upon maps of annual and seasonal precipitation (Hijmans et al. 2005), tree cover (De Fries et al. 2000), fire regime (Thonicke et al. 2001), and biomes/ecoregions (Olson et al. 2001), enabling comparisons between modern ecosystems and their environmental setting versus Last Glacial Maximum ecosystem reconstructions. The relative proportions of the most abundant pollen taxa for each site within the 18–24 cal ka BP Last Glacial Maximum window are depicted as colour-coded pie-charts (Fig. 4.2), whilst the inferred Last Glacial Maximum vegetation type is shown

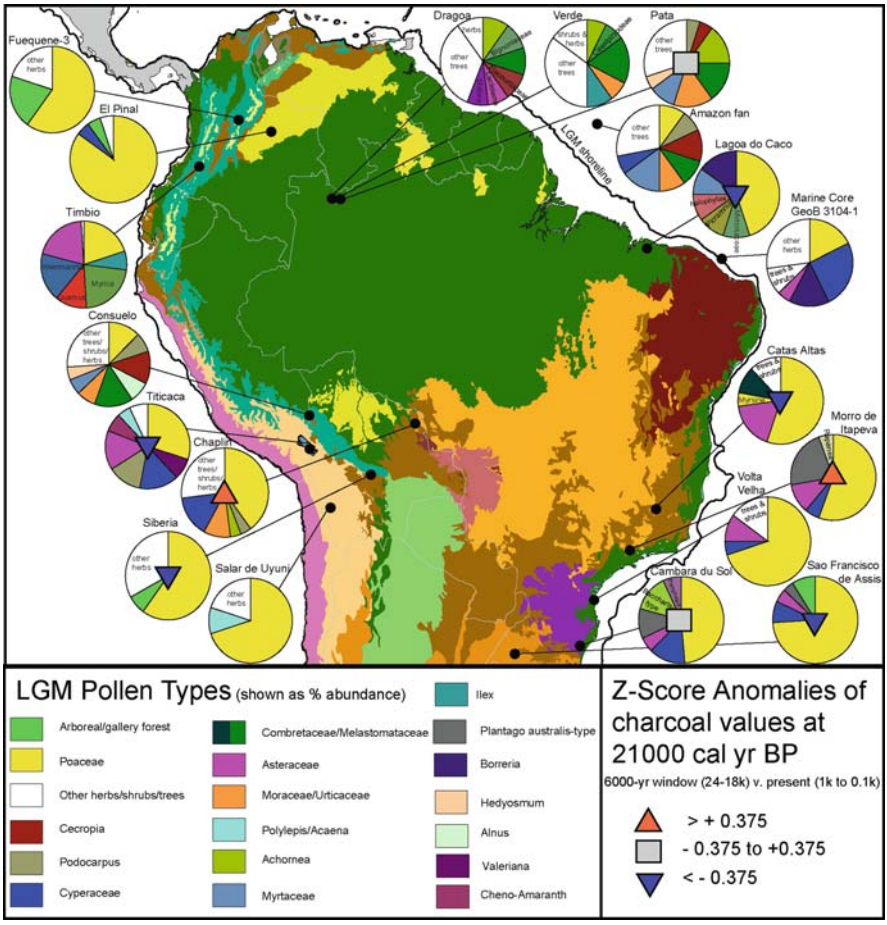

Fig. 4.2 Map showing percentages of most abundant pollen types in Last Glacial Maximum pollen assemblages of sites discussed in the text, depicted as colour-coded pie-charts. Accompanying site meta-data and references are shown in Table 4.1. Last Glacial Maximum charcoal anomalies are shown as *colour-coded triangles* or *squares* in the centre of the pie-charts (see Power et al. 2008 for full details). Last Glacial Maximum pollen and charcoal data are shown in relation to present-day distributions of modern biomes/ecoregions, following Olson et al. (2001), which are colour-coded according to the key in Fig. 4.3. The *black outline* of the map shows the Last Glacial Maximum shoreline of South America, when global sea-level was 120 m below present

as a colour-coded circle at the site location (Fig. 4.3). To obtain an indication of differences in fire regime between the Last Glacial Maximum and present, Z-score charcoal anomalies (showing whether there is more, or less, charcoal in the 24–18 cal ka BP window versus present (1–0.1 cal ka BP)) are depicted as red and blue triangles, respectively, in the centre of the pie-charts, whilst negligible anomalies (or charcoal absence) are shown as grey squares. For full details of how these charcoal anomalies were calculated, see Power et al. (2008).

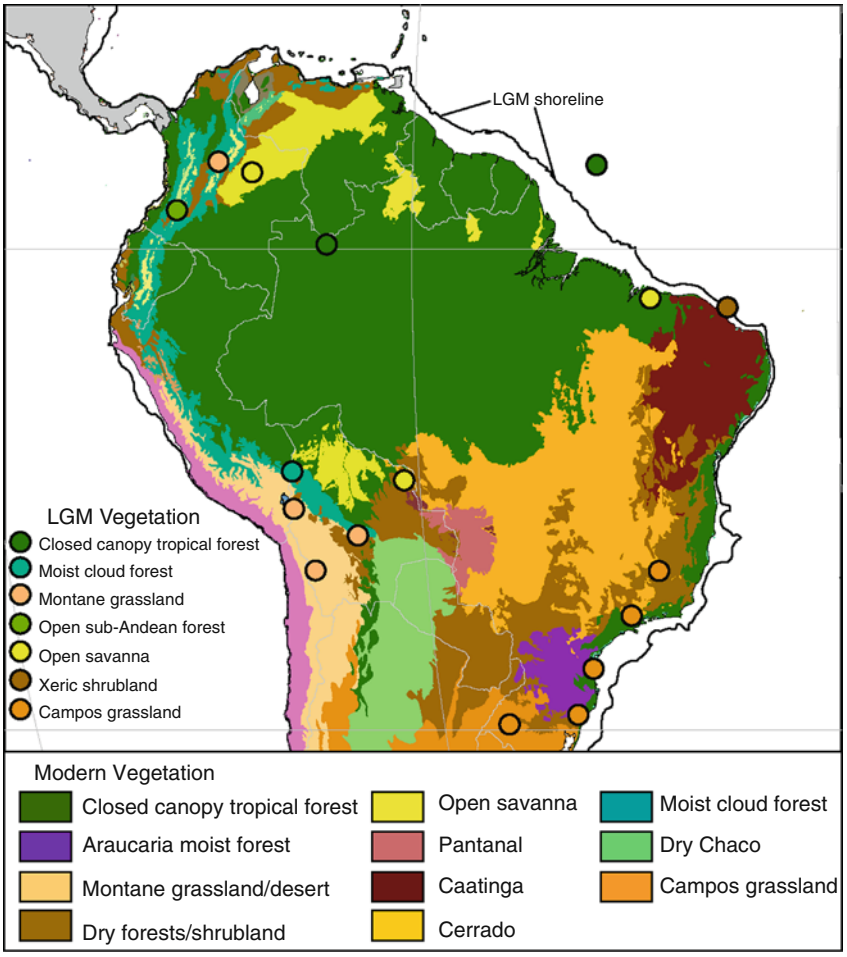

Fig. 4.3 Map showing the pollen-based Last Glacial Maximum vegetation reconstructions for each site, depicted as colour-coded circles at the site locations, in relation to present-day distributions of modern biomes/ecoregions, following Olson et al. (2001). The *black outline* of the map shows the Last Glacial Maximum shoreline of South America, when global sea-level was 120 m below present

4.3 Last Glacial Maximum Pollen-Based Vegetation Reconstructions

Site metadata are shown in Table 4.1, Last Glacial Maximum pollen percentages for each site are shown in Fig. 4.2, and pollen-based Last Glacial Maximum vegetation inferences are shown in Fig. 4.3. Modern ecoregions/biomes are shown in Figs. 4.2 and 4.3.

4.3.1 Andean Records

4.3.1.1 Bolivian Altiplano

The highest elevation pollen sites in the South American tropics are Lake Titicaca and the Salar de Uyuni salt flat in the high Andean Bolivian Altiplano. These sites are well above modern forest-line, surrounded by open, herbaceous puna vegetation. However, surface sample pollen spectra from Titicaca (Paduano et al. 2003) contain a mix of puna, sub-puna, and Andean forest elements, showing that interpretation of pollen records from these sites is complicated by a large wind-blown component of pollen originating from updraft from different vegetation communities of lower elevations of the eastern Andean flank. Other proxy data from both these sites show that Last Glacial Maximum precipitation was greater than present on the Altiplano, causing Titicaca to overflow and turn the Salar de Uyuni into a 130 m deep lake (Baker et al. 2001). The Last Glacial Maximum pollen assemblages (Paduano et al. 2003) are generally similar to those of today (dominated by herbaceous puna elements, especially Poaceae and Cyperaceae), demonstrating that temperatures were too low to support trees. Pollen concentrations of all taxa are extremely low in Last Glacial Maximum assemblages, consistent with an open puna landscape, indicating that occasional increases in *Podocarpus* (40%) and Moraceae (10%) pollen are likely percentage artefacts and due to long-distance dispersal from populations at much lower elevations. However, Chepstow-Lusty et al. (2005) argue that 10% *Polylepis/Acaena* pollen in Last Glacial Maximum sediments of the Salar de Uyuni are indicative of small *P. tarapacana* trees or shrubs growing locally and/or regionally on the Altiplano, rather than long-distance transport from lower elevations. This inference is based on observations of scattered individuals of this tree/shrub (up to 3 m high) growing among the puna on the western slope of Sajama mountain at 4,400 m.

4.3.1.2 Bolivian/Peruvian Cloud Forests

Lake Consuelo and Siberia both occur in the cloud forest on the eastern flank of the Andes, below Titicaca and the Salar de Uyuni, respectively. Siberia is located toward the present upper cloud forest limit, ecotonal with open forest and puna, whilst Consuelo is located toward the present lower cloud forest limit. The modern pollen spectra of Siberia are dominated by arboreal pollen (25–75%), reflecting its cloud forest location (Mourguiart and Ledru 2003). During the Last Glacial Maximum, the low proportion of arboreal pollen at this site (4–10%) and high grass abundance (60%) points to an open herbaceous landscape, with *Alnus* (25%) growing in lower elevation valleys. Although the authors, Mourguiart and Ledru (2003), interpret this open glacial vegetation as indicative of climatic aridity, we agree with Baker et al. (2003) that a more parsimonious explanation is that forest was excluded because of low temperatures, rather than low precipitation. This explanation seems more consistent with well documented high precipitation on the neighbouring Altiplano during the Last Glacial Maximum (Baker et al. 2001) and pollen data from Lake

Consuelo, a lower elevation cloud forest site (Bush et al. 2004a; Urrego et al. 2005). Vegetation modelling studies by Marchant et al. (2002), albeit for the Colombian Andes, corroborate this hypothesis that temperature, rather than precipitation, was the primary control in determining high altitude forest versus grassland.

At Lake Consuelo, the present-day cloud forest is reflected in surface pollen spectra dominated by Moraceae/Urticaceae, *Acalypha*, *Alchornea*, *Celtis*, *Trema*, and *Cecropia*. Although Last Glacial Maximum pollen assemblages also contain these taxa, they differ crucially in the additional presence of higher altitude Andean taxa such as *Alnus, Bocconia, Hedyosmum,* and *Podocarpus*, forming a unique Last Glacial Maximum forest community without modern analogue. Using purpose-designed temperature transfer functions for modern distributional ranges derived from herbarium collections, Bush et al. (2004a) showed that this non-analogue forest assemblage signifies a humid climate that was 5–9°C cooler than present during the Last Glacial Maximum. Furthermore, this pollen record is consistent, not only with evidence from Titicaca and the Salar de Uyuni, but also other glaciological records from the Andes (Seltzer et al. 2002; Smith et al. 2005) which show that the Last Glacial Maximum in tropical South America marks the end of the last glacial stage, with rising temperatures commencing 22 cal ka BP. This transition is marked by the loss of the high-Andean taxa from the Consuelo pollen record.

4.3.1.3 Colombian Montane Forests

The two Colombian sites, Timbio and Fuquene-3, are located in the lower montane and upper montane Andean forest zones, respectively, although the catchments of both sites have long been deforested over recent centuries (Fuquene) and millennia (Timbio). Furthermore, much of the Holocene pollen record of Timbio is missing, making comparisons between Last Glacial Maximum and "natural" vegetation under present climatic conditions problematic for this site. Last Glacial Maximum pollen assemblages at Timbio are dominated by *Ilex*, *Myrica*, *Quercus*, *Weinmannia*, Poaceae, and Asteraceae, pointing to a diverse and open forest with tree species that are today typical of Upper sub-Andean forests. The authors (Wille et al. 2000) argue that the relatively open character of these forests (Poaceae 20%, Asteraceae 20%), together with peaks in *Quercus* and low values of *Podocarpus* pollen, point to relatively dry conditions, whilst presence of taxa such as *Bocconia*, which are today confined to the upper forest limit, are indicative of Last Glacial Maximum temperatures significantly less than present.

The complete Holocene record at Fuquene-3, and its shorter history of human impact, allows for clearer Last Glacial Maximum versus modern vegetation comparisons than at Timbio. Last Glacial Maximum pollen assemblages at Fuquene-3 are characterised by high Poaceae abundance relative to the arboreal taxa *Polylepis/Acaena*, *Alnus*, *Quercus*, and *Weinmannia*, indicative of grass-paramo, especially the peaks in characteristic herbs such as Cruciferae, Caryophyllaceae, and *Jamesonia*. The authors, van der Hammen and Hooghiemstra (2003), infer from these pollen data that the upper forest line was located at ca. 2000 m elevation during the Last Glacial Maximum (ca. 580 m below the lake), signifying a temperature

depression of 7–8°C at the site compared with present. Furthermore, peak abundance of aquatic taxa (e.g. Cyperaceae, *Myriophyllum*, *Ludwigia*) are suggestive of lower lake-levels, and hence drier conditions, compared with present (Van der Hammen and Hooghiemstra 2003).

4.3.2 Lowland Records

4.3.2.1 Amazon Rainforests

Laguna Chaplin (Mayle et al. 2000; Burbridge et al. 2004) and the "Hill of Six Lakes" (Bush et al. 2004b) are the only two localities within the present-day lowland humid evergreen Amazonian forests that have records which span the Last Glacial Maximum. Carajas (Absy et al. 1991) and Bella Vista (Burbridge et al. 2004) also have Amazonian Pleistocene records but have major sedimentary hiatuses spanning the Last Glacial Maximum (Table 4.1).

The three closely neighbouring sites atop the Hill of Six Lakes (Pata, Dragao, and Verde) have Last Glacial Maximum pollen assemblages dominated by forest taxa, with a mix of lowland Amazonian (e.g. *Alchornea*, Combretaceae/Melastomataceae, Moraceae/Urticaceae, Myrtaceae, Caesalpinioideae, Bignoniaceae) and Andean (e.g. *Podocarpus*, *Ilex*, *Weinmannia*) elements. Negligible percentages of herb pollen (< 5% Poaceae) shows that these forests must have had closed canopies. This mix of lowland Amazonian and Andean tree taxa shows that these Last Glacial Maximum forests were without modern analogue and suggests that temperatures were ca. 5ºC below present (Colinvaux et al. 1996). Publication of these Last Glacial Maximum pollen data from Pata over a decade ago (Colinvaux et al. 1996) provided the first convincing evidence to challenge the then widely accepted glacial rainforest refugium hypothesis (Haffer 1969; Haffer and Prance 2001) which proposed that Amazonia was dominated by savanna, instead of forest, during the Last Glacial Maximum under an arid climate. However, Colinvaux himself acknowledged that data from a single locality in an area the size of Europe by no means constituted a sufficiently rigorous test of this refugium hypothesis.

Three years later Haberle and Maslin (1999) published a 40,000-yr Pleistocene history of Amazonian vegetation from a fossil pollen record taken from the Amazon Fan core ODP-932. The Last Glacial Maximum pollen assemblage from this off-shore core is remarkably similar to that of Pata, dominated by a mixture of lowland and Andean forest taxa, indicative of a colder Last Glacial Maximum climate in the lowland basin than present. Since the Amazon Fan collects sediment from the entire Amazon basin, this core potentially provides a much more rigorous test of Haffer's refugium hypothesis. Notwithstanding the peaks in Andean taxa (e.g. *Podocarpus*), the Last Glacial Maximum Fan pollen assemblage is remarkably similar to that of modern samples taken throughout the length of the Amazon river, leading Haberle and Maslin (1999) to infer that the spatial extent of Amazon forest at the Last Glacial Maximum was similar to present and that Haffer's rainforest refugium hypothesis must therefore be unsupported. These results from ODP-932

are corroborated by pollen data from three other Amazon Fan cores (ODP-940A, 944A, and 946A) which also show little palynological difference between glacial and interglacial sediments (Hoorn 1997).

It is clear though, that rainforest cover was at least slightly reduced at the Last Glacial Maximum compared with present, at least at the southern rainforest-savanna ecotone of the basin, as revealed by pollen data from Laguna Chaplin in NE Bolivia (Mayle et al. 2000; Burbridge et al. 2004). This site is presently surrounded by largely undisturbed humid evergreen rainforest, but only 30 km from the ecotone with semi-deciduous dry forests and savannas to the south. Modern surface pollen spectra are characterised by 45% Moraceae and only 3% Poaceae and 6% Cyperaceae, whereas Last Glacial Maximum sediments are dominated by 40% Poaceae, 15% Cyperaceae, and only 10% Moraceae, consistent with open herbaceous savanna. Punyasena et al. (2008) applied a newly developed climate-vegetation model (based on the modern abundance distributions of 154 Neotropical plant families, Punyasena 2008) to the Chaplin and Bella Vista pollen datasets. Their model results strengthen the earlier qualitative climate reconstructions by Mayle et al. (2000), showing that this Last Glacial Maximum savanna community of NE Bolivia was a function of both lower precipitation and lower temperatures, compared with present.

Although there are no pollen data to support a savanna-dominated Amazon basin during the Last Glacial Maximum (or any other period during the Quaternary), the paucity of Last Glacial Maximum records, combined with uncertainty over the palaeoecological significance of these few records, means that our knowledge of Amazonia's ecosystems during the Last Glacial Maximum remains extremely imprecise and a topic of continued debate and speculation. For example, Pennington et al. (2000) cogently argued that Last Glacial Maximum pollen spectra from Pata, interpreted by Colinvaux et al. (2000) and Bush et al. (2004b) as a rainforest signal, albeit with Andean elements, could equally well be interpreted as a predominantly semi-deciduous dry forest signal owing to the fact that most dry forest families are a subset of rainforest families and because most pollen types cannot be identified to species level, thus frustrating attempts to distinguish these ecosystems. The fact that semi-deciduous dry forests grow under similarly dry and seasonal climates as Brazilian *cerrado* savannas means that distinguishing between these two types of tropical forest has important palaeoclimatic (Mayle 2004, 2006; Mayle et al. 2004) implications for Amazonia at the Last Glacial Maximum. Also, the markedly different carbon storage values between rainforest (320 tons C ha^{-1}) and dry forest (260 tons C ha^{-1}) (Adams and Faure 1998) means that determining which of these two forest types dominated the Amazon basin would shed light on the magnitude of its carbon store, with implications for understanding global carbon cycling at the Last Glacial Maximum (Mayle and Beerling 2004; Beerling and Mayle 2006).

Furthermore, the palaeoecological significance of the Amazon Fan pollen record is also controversial, with some (e.g. H. Hooghiemstra, personal communication 2003; Berrio et al. 2000), arguing that rather than reflecting basin-wide vegetation, it may instead be a riparian signal of seasonally-flooded *varzea/igapo* forest lining the Amazonian rivers. If true, the Last Glacial Maximum pollen assemblage from the

Fan would reveal little about the vegetation occupying *terra firme* areas beyond the ribbon of forest lining the rivers, and therefore unsuitable for testing the rainforest refugium hypothesis. Fortunately, recent studies of pollen rain signatures of different kinds of rainforest and dry forest (Gosling et al. 2009, Burn 2008) and advances in Amazon pollen taxonomy have the potential to resolve these uncertainties of interpretation of fossil pollen assemblages. In particular, Burn and Mayle (2008) have shown that, not only can Moraceae and Urticaceae families be palynologically differentiated from one another, but the key tropical forest family Moraceae can also be palynologically separated into its constituent genera, providing the potential for distinguishing between riparian, seasonally flooded evergreen forest versus *terra firme* evergreen forests beyond the rivers.

4.3.2.2 Savanna/Woodland/Thorn-Scrub

El Pinal, Caco, and Marine core GeoB 3104-1 presently have catchments within highly seasonal, dry vegetation types beyond the limits of humid Amazonian forests. Laguna El Pinal (Behling and Hooghiemstra 1999) is located in the centre of the open, grass-dominated *Llanos Orientales* savannas of Colombia, where trees (predominantly *Mauritia* palm) are largely restricted to the lake shore and gallery forests lining rivers. Surface pollen spectra of this site are therefore dominated by Poaceae (65%) and Cyperaceae (12%), gallery forest taxa accounting for only 17% of the pollen sum. During the Last Glacial Maximum the *Llanos* was even more open than today (Poaceae 85%, Cyperaceae 5%, gallery forest 5%), indicative of a drier climate than present.

Lagoa do Caco (Ledru et al. 2002) is located just beyond the present eastern limit of Amazon rainforest, surrounded by an ecotonal mix of *restinga* (coastal steppe vegetation), *cerrado* (woody savanna), and gallery (riparian) forest. The open character of this vegetation is reflected in the high percentages of herbaceous pollen in the surface sample (*Borreria* 5%, Poaceae 30%, halophytes 2%). During the Last Glacial Maximum, vegetation was even more open (*Borreria* 15%, Poaceae 45%, halophytes 10%), pointing to drier conditions than present.

Last Glacial Maximum pollen assemblages from marine core GeoB 3104-1, dominated by the herbs Poaceae, Cyperaceae, *Borreria*, and Asteraceae (Behling et al. 2000), are similar to those from modern surface samples collected from rivers, lakes, and soils across the *caatinga* thorn-scrub dominated landscape of NE Brazil, demonstrating that this xeric vegetation, and its arid climate, also predominated during the Last Glacial Maximum.

4.3.2.3 Atlantic Forests and Campos Grasslands of SE Brazil

Behling and his collaborators have produced pollen-based Quaternary vegetation histories of numerous sites from a range of ecosystems and altitudes across SE Brazil – Volta Velha (Behling and Negrelle 2001): Atlantic evergreen rainforest, 5 m elevation; Catas Altas (Behling and Lichte 1997): semi-deciduous dry forest, 755 m elevation; Morro de Itapeva (Behling 1997): ecotone between cloud forest,

rainforest, dry forest, and *Araucaria forest*, 1850 m elevation; Sao Francisco de Assis (Behling et al. 2005): lowland grassland *Campos*, with riverine gallery forest, 100 m elevation; Cambara do Sul (Behling et al. 2004): *Araucaria* forest with patches of *Campos* grassland, 1040 m elevation.

What is particularly interesting about these pollen records is that, despite the diversity of ecosystems that these sites encompass today (rainforest, dry forest, *Araucaria* forest, grassland *Campos*), they all have Last Glacial Maximum pollen assemblages dominated by herbs (especially Poaceae), indicative of open, high-elevation *Campos* grasslands, which are today restricted, either to elevations over 1000 m, or high latitudes (> 27–28ºS). This has led Behling to infer that Last Glacial Maximum temperatures were ca. 5–7ºC colder than present, whilst peaks in *Eryngium* at Morro de Itapeva and Cambara do Sul are suggestive of drier conditions too.

4.4 Model Simulations of Last Glacial Maximum Vegetation

Our review of previously published Last Glacial Maximum pollen data shows that our knowledge of Last Glacial Maximum vegetation types, distribution, structure, carbon storage, and species composition, across tropical South America remains poorly understood, especially for Amazonia. This arises from the extreme paucity of Last Glacial Maximum pollen records, limitations of pollen taxonomy, and poor knowledge of modern pollen-vegetation relations. Use of vegetation models, forced by Last Glacial Maximum climatic and CO_2 conditions, has the potential to address several of these unresolved issues, and crucially, explore the underlying climatic controls and relative influences of climate versus CO_2.

4.4.1 Colombia

Marchant et al. (2002, 2004, 2006) used the BIOME-3 global vegetation model, developed by Haxeltine and Prentice (1996), to better understand how Colombian Andean and lowland ecosystems responded to glacial-interglacial temperature, precipitation, and atmospheric CO_2 changes. BIOME-3 is a biogeography-based model that predicts the dominance of different plant functional types (PFTs) based on ecophysiological constraints, resource availability, and competition (VEMAP members 1995). Their model outputs were in broad agreement with both the present-day ecoregion maps (Olson et al. 2001, Figs. 4.2 and 4.3) and the Last Glacial Maximum fossil pollen data, although the lowland *llanos* savannas (El Pinal), with their particular edaphic and hydrological conditions, were less accurately simulated (Marchant et al. 2002).

Temperature reduction was found to be the key driver for Last Glacial Maximum grassland expansion in the Bogota basin of the high Andes (2,550 m), whilst Last Glacial Maximum precipitation reduction was largely responsible for expansion of C_4 grasses in the lowland savannas/xeric woodlands (Marchant et al. 2004).

Marchant et al. (2002) examined the interactive effects of climate and CO_2 changes in the Bogota basin, with CO_2, temperature, and precipitation varying between 290–170 ppmV, 4–13°C, and 150–750 mm pa, respectively (these values were chosen to capture the full glacial-interglacial range). Unsurprisingly, low glacial CO_2 values (200 ppm), in combination with low precipitation, caused expansion of C_4 savanna grasses in the lowland savannas, as they would have had a competitive advantage over C_3 trees and shrubs in drought-stressed environments due to their greater water-use-efficiency (Farquhar 1997). However, Marchant et al. (2002) found that high altitude vegetation (as simulated by the BIOME-3 model) was not only affected by temperature reduction, but also CO_2 reduction, with a strong inter-dependence between these two variables. Once temperatures are reduced by at least 5ºC, and atmospheric CO_2 concentrations fall to below 225 ppmV, there is an abrupt biome shift in the Bogota basin from cool evergreen forest to cool grass/shrubland.

These model results are consistent with n-alkane δ^{13} C data from lacustrine sediments, not only from the Bogota basin (Boom et al. 2002), but also Mt. Kenya in Africa (Street-Perrott et al. 1997). These simulations suggest that the climatic and CO_2 conditions of the Last Glacial Maximum caused expansion of both high- and low-altitude grasslands, thereby compressing the altitudinal range of montane forests. Interestingly, the model suggests that these montane forests were largely semi-deciduous dry forests (akin to the xeric woodland scrub biome), a forest type which today has a highly scattered, disjunct distribution within isolated inter-Andean dry valleys (Prado and Gibbs 1993). These simulations therefore support the "Pleistocene Dry Forest Arc" hypothesis proposed by Prado and Gibbs (1993) and Pennington et al. (2000) which states that present-day pockets of montane dry forest constitute Holocene refugia, or remnants, of a more extensive and contiguous Andean dry forest distribution during the Last Glacial Maximum (Note though, that Mayle (2004, 2006) questions the validity of this hypothesis with respect to lowland dry forest biogeographic history in South America).

It is important to note, however, that the wettest, non-seasonal areas of the Colombian lowlands (e.g. Quibdo) remain unchanged as evergreen rainforest with this model, even under maximum temperature, precipitation, and CO_2 reductions (Marchant et al. 2004).

4.4.2 Amazon Basin

Beerling and Mayle (2006) used the University of Sheffield Dynamic Global Vegetation Model (SDGVM) to investigate the separate and interactive effects of climate versus CO_2 upon different parameters of Amazonian ecosystems (vegetation biomass, soil carbon storage, and biome type) between the Last Glacial Maximum and present day (pre-industrial). Model experiments were performed with an annual resolution, to allow the ecosystems within the Amazon Basin to continuously evolve from their initial equilibrium glacial state forwards in time to the present-day, and

at a fine spatial scale (1° lat. × 1° lon.) to capture range shifts in forest distributions. Three transient 21 ka model experiments were performed, designed to assess the separate and interactive effects of changes in climate and CO_2 since the Last Glacial Maximum on Amazonian ecosystems: (i) changing CO_2 and climate (CT), (ii) changing CO_2 and constant pre-industrial climate (C), and (iii) changing climate and a constant pre-industrial CO_2 concentration (T). Their procedure gave a Basin-wide Last Glacial Maximum mean annual temperature decrease of 3–4°C below present and mean annual precipitation reduction of 20% below present, in broad agreement with fossil pollen and other palaeoclimate proxy data. Last Glacial Maximum-present CO_2 changes were obtained from Antarctic ice-core measurements by Indermühle et al. (1999) and Monnin et al. (2001). For full details of the approach see Beerling and Mayle (2006).

The climate and CO_2 experiment simulated dry forest/savanna cover at the Last Glacial Maximum to be 67% greater than today, whilst evergreen rainforest area was 14% below present. The near identical trends in forest cover in experiments CT and T, and contrasting trends in experiment C, indicate that broad-scale changes in lowland Amazonian vegetation distribution between the Last Glacial Maximum and present were primarily driven by climate. Reduced precipitation at the Last Glacial Maximum favoured expansion of the more drought-tolerant deciduous forests/savannas by increasing soil moisture deficits during a longer, more severe dry season (Beerling and Woodward 2001). The geographic patterns of these Last Glacial Maximum versus modern ecosystem changes (Fig. 4.4) match well with the fossil pollen data (Fig. 4.3); i.e. expansion of dry forests/savannas versus

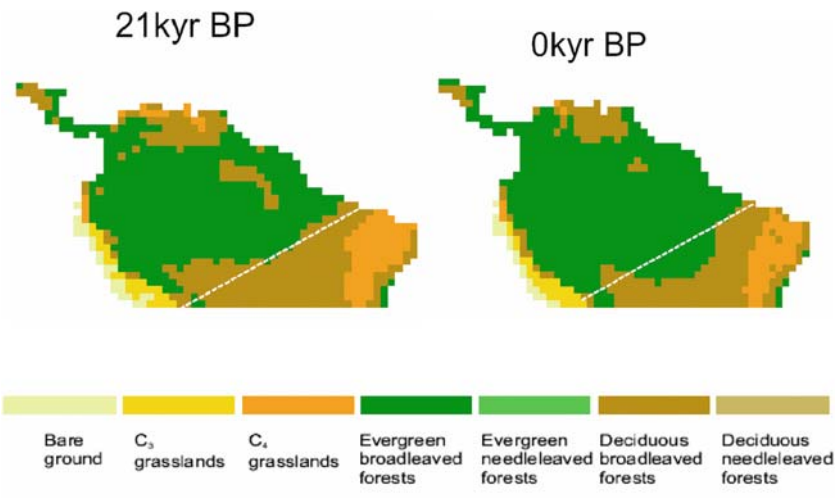

Fig. 4.4 Geographic distributions of Amazonian ecosystems simulated for the Last Glacial Maximum and pre-industrial (present day) using the University of Sheffield Dynamic Global Vegetation model as described in the text. Amazonia is defined as the area north of the diagonal line. Modified from Beerling and Mayle (2006)

evergreen rainforest in ecotonal areas (e.g. Chaplin) compared with present. The dominance of evergreen rain forest throughout most of the Amazon Basin at the Last Glacial Maximum (Fig. 4.4) is also consistent with the "Hill of Six Lakes" (Colinvaux et al. 1996; Bush et al. 2004b) and Amazon Fan (Haberle and Maslin 1999) pollen data (Fig. 4.3). These model simulations therefore do not support the rainforest refugia hypothesis of Haffer (1969) and Haffer and Prance (2001), and also suggest that the dry forest/savanna expansion in the "Dry Corridor" of eastern Amazonia (Fig. 4.4) was insufficient to divide the rain forest into two disjunct areas, as proposed by Bush (1994). These results suggest that a 20% reduction in mean annual precipitation would have been insufficient to disrupt rain forest cover, except in the most seasonal, ecotonal areas, especially since any soil moisture deficits would have been partially offset by reduced evapo-transpiration under a cooler climate.

These process-based vegetation simulations by Beerling and Mayle (2006) suggest that, in contrast to the rather minor climate-driven shifts in ecosystem geographic distribution between the Last Glacial Maximum and present, the low Last Glacial Maximum CO_2 concentrations (180 ppm versus pre-industrial 280 ppm) resulted in Amazonia's total above-ground carbon storage to be only half its pre-industrial value. This 50% reduction in carbon storage relative to present can be attributed to carbon limitation producing rainforests with markedly lower canopy densities and simpler structures than those of today (Fig. 4.5). Rainforest leaf area index (LAI) at the Last Glacial Maximum is simulated to be only 76% of its present-day value (5.25 versus 6.9, respectively). These results are in general

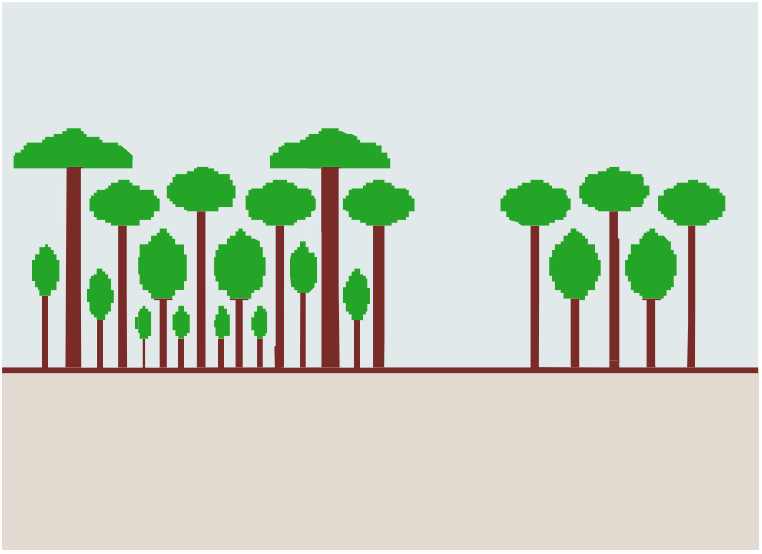

Fig. 4.5 Cartoon depicting hypothetical change in Amazon forest structure (*left*: present-day forests; *right*: Last Glacial Maximum forests). Modified from Cowling (2004)

agreement with those of Cowling (2004) and Cowling et al. (2001, 2004), who also showed that atmospheric CO_2 concentrations were more important than precipitation levels in controlling canopy density (i.e. vegetation structure). For a decrease in 20% precipitation alone, Cowling et al. (2001) simulated an 11% decrease in Basin-average LAI, whereas Last Glacial Maximum CO_2 concentrations alone caused a 34% reduction in LAI. These authors also argue that glacial cooling was likely the key factor responsible for maintaining Last Glacial Maximum Amazon forest cover via its effects in reducing photorespiration and evapotranspiration, which together improve plant carbon and water relations. Cowling et al. (2001) noted that, although their modelling studies simulated a largely forested Amazon basin (consistent with Beerling and Mayle 2006), there was considerable spatial heterogeneity in LAI (forest canopy density) across the basin, leading them to propose an interesting alternative to Haffer's rainforest refugium hypothesis as a mechanism of speciation. Instead of Haffer's model of allopatric speciation via fragmented rainforest populations isolated by open savannas (Haffer 1969), Cowling et al. offer the novel idea that these geographic variations in canopy density (Fig. 4.5) (and hence forest structure and productivity) could potentially have been sufficient to promote neotropical vicariance and thus allopatric speciation if gene pools were isolated. Increasing evidence for sympatric speciation over recent years among different organisms (e.g. Smith et al. 1997) raises the possibility that even if gene pools were not fragmented, environmental gradients associated with differences in forest structure may have been sufficient to promote sympatric speciation.

4.5 Last Glacial Maximum Fires

Although there are relatively few charcoal records for the Last Glacial Maximum (18–24 cal ka BP), most records show a pattern of less-than-present fire. Of the nine Last Glacial Maximum records (18–24 cal ka BP window) where charcoal has been searched for (Fig. 4.2), two sites are either devoid of charcoal or have negligible anomalies, five have significant negative anomalies (i.e. Z-score anomaly <–0.375 versus "present" (1–0.1 cal ka BP)), and two have positive anomalies (Z-score anomaly >+0.375 versus "present"), suggesting greater-than-present fire activity. The positive Last Glacial Maximum charcoal anomalies are unsurprising when one considers the contrasting vegetation at these sites between the Last Glacial Maximum and present. Morro de Itapeva is today surrounded by poorly flammable humid cloud forest, rainforest, and *Araucaria* forest (Figs. 4.2and 4.3), but at the Last Glacial Maximum was surrounded by grassland *Campos* (Fig. 4.3) which would be expected to have a higher fire frequency than the present-day humid forests (notwithstanding the cooler Last Glacial Maximum climate, see below). Likewise, Chaplin is today surrounded by humid evergreen rainforest, which is much less flammable than the open savannas which dominated this site's catchment during the Last Glacial Maximum.

The reduction in fire activity during the Last Glacial Maximum at several other sites can be explained in terms of the differences between modern and Last Glacial

Maximum vegetation and climate linkages. At Catas Altas, one might expect that the Last Glacial Maximum grasslands would have higher fire frequencies than the modern semi-deciduous forests, although grasslands have less fuel (and hence less potential for producing charcoal) than flammable dry forests. An overall reduction in biomass from lower CO_2 and the cooler Last Glacial Maximum climate would have limited fires. Sao Francisco de Assis, Caco, and Titicaca all have similar vegetation types (open and herbaceous) at the Last Glacial Maximum and present-day (Fig. 4.3), suggesting that the reduction in fires during the Last Glacial Maximum is likely a result of the colder than present Last Glacial Maximum climate (at least 5°C less than present). The absence of charcoal from Pata lake samples is consistent with the continued presence of humid rainforest during the Last Glacial Maximum and today. At Cambara do Sul, both the cool Last Glacial Maximum grasslands and cool, humid *Araucaria* forests produced little charcoal, suggesting similar-to-present fire activity.

4.6 Implications and Conclusions

Figure 4.3 shows the reconstructed Last Glacial Maximum vegetation for each pollen site mapped onto the distribution of present-day biomes/ecoregions, illustrating any differences/similarities between Last Glacial Maximum and modern (pre-clearance) vegetation types and their distribution. Although the paucity of sites does not allow for a detailed Last Glacial Maximum vegetation map to be drawn (hence we have not tried to do so!), some interesting conclusions can be made.

4.6.1 Last Glacial Maximum Climate

Despite the much wetter climate of the Altiplano compared with today (Baker et al. 2001), its vegetation during the Last Glacial Maximum was broadly similar to today's (an open herbaceous montane grassland or puna), indicating that temperatures were too low to support trees (e.g. Paduano et al. 2003). Cloud forests below the Altiplano descended downslope (Siberia et al. 2003; Baker et al. 2003) to form non-analogue mixtures of high Andean taxa and cloud forest taxa, demonstrating that temperatures must have been 5–9°C cooler than present (Bush et al. 2004a; Urrego et al. 2005), although precipitation must have been sufficiently high to support cloud forest taxa. A similar temperature depression is evident from the upper montane Colombian forest site, Fuquene-3, inferred from the downslope movement of grass-paramo to occupy the lake catchment during the Last Glacial Maximum (Van der Hammen and Hooghiemstra 2003).

Evidence that the lowland tropics also experienced a temperature reduction of at least 5°C during the Last Glacial Maximum comes from the mixture of Andean and lowland rainforest taxa at the Hill of Six Lakes (Bush et al. 2004b) and Amazon Fan (Haberle and Maslin 1999) sites, as well as presence of open tree-less grassland in

areas of SE Brazil currently occupied by a mix of different types of tropical forests (e.g. Volta Velha, Behling and Negrelle 2001).

Although the Altiplano was significantly wetter than present during the Last Glacial Maximum (Baker et al. 2001), there was greater extent of savannas at the southern lowland Amazon margin (Chaplin, Mayle et al. 2000) and reduction in gallery forests in the Colombian *Llanos* (El Pinal, Behling and Hooghiemstra 1999) signifying reduced precipitation in the lowland tropics compared with present. Strong independent evidence for reduced Last Glacial Maximum precipitation throughout much of the lowland tropics comes from multi-millennial sedimentary hiatuses spanning the Last Glacial Maximum (Ledru et al. 1998) at six sites (Table 4.1). However, the Hill of Six Lakes (Pata, Dragao, and Verde), Amazon Fan, and vegetation modelling simulations together suggest that rainfall remained sufficiently high (under the cooler-than-present Last Glacial Maximum climate) to maintain closed-canopy forest and low fire activity across the Amazon basin. In fact, model simulations by Beerling and Mayle (2006) and Cowling et al. (2001) suggest that the low CO_2 concentrations at the time had a greater impact upon forests than lowered rainfall, through carbon limitation reducing LAI and resulting in forests with simpler structure and lower biomass than those of today.

Simulation of Colombian ecosystems using the BIOME-3 vegetation model (e.g. Marchant et al. 2002) reveals that high and low altitude ecosystems were controlled by differing climatic variables at the Last Glacial Maximum, with temperature being the key control on montane ecosystems, and precipitation the key driver in the lowlands. Furthermore, these authors show that low CO_2 concentrations not only favoured C_4 grass expansion in water-stressed lowland ecosystems (through their greater water-use-efficiency than C_3 trees/shrubs), but also in the high Andes.

4.6.2 Biogeography, Biodiversity, and Carbon Cycling

Considering tropical South America as a whole, the model simulations and fossil pollen data suggest that biome shifts between forest and grassland/savanna between the Last Glacial Maximum and present were not substantial. Biome shifts were largely restricted to ecotonal areas – depression of the Andean tree-line and encroachment of savanna into lowland rainforest. The exception, however, appears to be the Atlantic forests of SE Brazil, where, irrespective of the type of forest surrounding the site today (Table 4.1), all sites within the region are dominated by open *Campos* grasslands at the Last Glacial Maximum (Fig. 4.3), indicating substantial reduction in forest area. This expansion of grassland in SE Brazil points to a 5–7°C lowering of temperatures (Behling 1997), whilst taxa such as *Eryngium* indicate drier conditions. Today, these Atlantic forests receive most of their precipitation from the nearby Atlantic Ocean, but this moisture source would have been reduced during the Last Glacial Maximum due to reduced evaporation associated with lower tropical Atlantic sea-surface-temperatures (Guilderson et al. 1994; Pflaumann et al. 2003), which would account for the cold- and drought-tolerant glacial grasslands. Moreover, these sites were much further inland at the Last Glacial Maximum due to

the 120 m lowering of sea-level (Fig. 4.3), which would perhaps have exacerbated this precipitation reduction.

Given the size of Amazonia's carbon store (10% of global terrestrial carbon stock), its wealth of biodiversity (possibly one third of global biodiversity), and hydrological importance for regional and global climates (Malhi and Phillips 2004), the nature of its ecosystems during the Last Glacial Maximum have naturally been the subject of intense interest and debate. Last Glacial Maximum pollen records from the centre and margin of the basin and the Amazon Fan, considered together with vegetation model simulations, suggest that Amazonia remained largely forested at the Last Glacial Maximum, contradicting the rainforest refugia hypothesis which argues for a savanna-dominated basin with rainforests restricted to isolated refugia (e.g. Haffer 1969; Haffer and Prance 2001). However, these studies suggest that Amazonia's forests have been far from static. The cyclic reassortment of Andean and lowland species (Colinvaux et al. 1996; Bush et al. 2004b), combined with changes in forest structure and canopy density (Cowling et al. 2001), over glacial-interglacial cycles in response to temperature, precipitation and CO_2 changes, means that there would have been great opportunity for population fragmentation and allopatric speciation, which did not require large-scale biome shifts.

In terms of carbon cycling, a key finding of a dynamic vegetation model is that Amazonia remained covered by rainforest at the Last Glacial Maximum but with only half the present-day carbon store (due to reduced canopy density and biomass) (Beerling and Mayle 2006), although we acknowledge that the ability of the model to accurately differentiate between evergreen humid rainforest versus semi-deciduous dry forest is open to question. The model experiments by these authors also show that climate and CO_2 likely had quite distinct and separate effects on tropical ecosystems – Last Glacial Maximum-modern climate change driving biome replacements in ecotonal areas, and CO_2 driving changes in biomass per unit area, irrespective of the vegetation type.

Despite the insights into Last Glacial Maximum ecosystems from these data-model comparisons, large gaps in knowledge remain. Given the diversity of rainforest ecosystems (Olson et al. 2001) and heterogeneity of climatic regimes across Amazonia today (Fig. 4.1), similar, or perhaps greater heterogeneity likely occurred at the Last Glacial Maximum. Consequently, the two Last Glacial Maximum sites currently available from within the Amazon rainforest biome today are insufficient to draw a basin-wide vegetation reconstruction. This is compounded by questions over the interpretation of Last Glacial Maximum pollen assemblages – e.g. evergreen rainforest versus semi-deciduous dry forest (Pennington et al. 2000, with respect to Pata) and regional "terra firme" versus riparian seasonally-flooded rainforest (Burn and Mayle 2008, with respect to the Amazon Fan). Although new pollen rain data and pollen taxonomic advances (Burn 2008; Burn and Mayle 2008) have the potential to resolve some of these issues, the biggest problem is the paucity of Last Glacial Maximum records in the Amazon, due to the river-dominated landscape and predominance of young ox-bow lakes. Perhaps greatest research efforts, with respect to the Last Glacial Maximum environment of Amazonia at least, should

therefore be directed to improving the quality of fully coupled vegetation-climate model simulations.

Acknowledgments We thank Francoise Vimeux and Florence Sylvestre for kindly inviting us to write this chapter, as well as the authors of all the records discussed here, whose research made this chapter possible. We also thank the two referees for their comments and suggestions which improved the paper.

References

Absy ML, Cleef A, Fornier M et al (1991) Mise en evidence de quatre phases d'ouverture dela foret dense le sud-est de l'Amazonie au cours des 60 000 dernieres annees. Premiere comparaison avec d′autres regions tropicales. CR Acad Sci Paris 313:673–678

Adams JM, Faure H (1998) A new estimate of changing carbon storage on land since the last glacial maximum, based on global land ecosystem reconstruction. Glob Planet Change 16–17:3–24

Baker PA, Bush MB, Fritz S et al (2003) Last Glacial Maximum in an Andean cloud forest environment (Eastern Cordillera, Bolivia): comment and reply. Geology: Online Forum: pp. e26. http://www.gsajournals.org/i0091-7613-31-6-e26.html

Baker PA, Seltzer GO, Fritz SC et al (2001) The history of South American tropical precipitation for the past 25,000 years. Science 291:640–643

Barberi M (1994) Paleovegetacao e paleoclima no Quaternario tardio da vereda de Aguas Emendadas, DF. Dissertacao de Mestrado 93, Univ. de Brasilia

Beerling DJ, Mayle FE (2006) Contrasting effects of climate and CO_2 on Amazonian ecosystems since the last glacial maximum. Glob Chan Biol 12:1977–1984

Beerling DJ, Woodward FI (2001) Vegetation and the terrestrial carbon cycle: modelling the first 400 million years. Cambridge University Press, Cambridge

Behling H (1997) Late Quaternary vegetation, climate and fire history from the tropical mountain region of Morro de Itapeva, SE Brazil. Palaeogeog Palaeoclim Palaeoecol 129:407–422

Behling H, Arz HW, Pätzold J, Wefer G (2000) Late Quaternary vegetational and climate dynamics in northeastern Brazil, inferences from marine core GeoB 3104–1. Quat Sci Rev 19:981–994

Behling H, De Patta Pillar V, Girardi Bauermann S (2005) Late Quaternary grassland (Campos), gallery forest, fire and climate dynamics, studied by pollen, charcoal and multivariate analysis of the Sao Francisco de Assis core in western Rio Grande do Sul (southern Brazil). Rev Pal Pal 133:235–248

Behling H, De Patta Pillar V, Orloci L et al (2004) Late Quaternary Araucaria forest, grassland (Campos), fire and climate dynamics, studied by high-resolution pollen, charcoal and multivariate analysis of the Cambara do Sul core in southern Brazil. Palaeogeog Palaeoclim Palaeoecol 203:277–297

Behling H, Hooghiemstra H (1999) Environmental history of the Columbian savannas of the Llanos Orientales since the Last Glacial Maximum from lake records El Pinal and Carimagua. J Paleolimn 21:461–476

Behling H, Lichte M (1997) Evidence of dry and cold climatic conditions at glacial times in tropical SE Brazil. Quat Res 48:348–358

Behling H, Negrelle RRB (2001) Tropical rain forest and climate dynamics of the Atlantic lowland, Southern Brazil, during the Late Quaternary. Quat Res 56:383–389

Berrio JC, Hooghiemstra H, Behling H et al (2000) Late Holocene history of savanna gallery forest from Carimagua area, Colombia. Rev Pal Pal 111:295–308

Boom A, Marchant R, Hooghiemstra H et al (2002) CO_2- and temperature-controlled altitudinal shifts of C_4- and C_3-dominated grasslands allow reconstruction of palaeoatmospheric $p\ CO_2$. Palaeogeog Palaeoclim Palaeoecol 177:151–168

Burbridge RE, Mayle FE, Killeen TJ (2004) Fifty-thousand-year vegetation and climate history of Noel Kempff Mercado National Park, Bolivian Amazon. Quat Res 61:215–230

Burn MJ (2008) Characterisation of Amazonian rainforest ecosystems by their surface pollen spectra. Unpublished PhD thesis, School of GeoSciences, The University of Edinburgh
Burn MJ, Mayle FE (2008) Palynological differentiation between genera of the Moraceae family and implications for Amazonian palaeoecology. Rev Pal Pal. 149:187–201
Bush MB (1994) Amazonian speciation: a necessarily complex model. J Biogeogr 21:5–17
Bush MB, Silman MR, Urrego DH (2004a) 48,000 years of climate and forest change in a biodiversity hot spot. Science 303:827–829
Bush MB, De Oliveira PE, Colinvaux PA et al (2004b) Amazonian paleoecological histories: one hill, three watersheds. Palaeogeog Palaeoclim Palaeoecol 214:359
Chepstow-Lusty A, Bush MB, Frogley MR et al (2005) Vegetation and climate change on the Bolivian Altiplano between 108,000 and 18,000 yr ago. Quat Res 63:90–98
Colinvaux PA, De Oliveira PE, Moreno JE et al (1996) A long pollen record from lowland Amazonia: forest and cooling in glacial times. Science 274:85–88
Colinvaux PA, De Oliveira PE, Bush MB (2000) Amazonian and neotropical plant communities on glacial time-scales: the failure of the aridity and refuge hypotheses. Quat Sci Rev 19: 141–169
Cowling SA (2004) Tropical forest structure: a missing dimension to Pleistocene landscapes. J Quat Sci 19:733–743
Cowling SA, Cox PM, Betts RA (2004) Contrasting simulated past and future responses of the Amazon rainforest to atmospheric change. Phil Trans R Soc B 359:539–548.
Cowling SA, Maslin MA, Sykes MT (2001) Paleovegetation simulations of lowland Amazonia and implications for neotropical allopatry and speciation. Quat Res 55:140
De Fries R, Hansen M, Townshend JRG et al (2000) A new global 1 km data set of percent tree cover derived from remote sensing. Glob Change Biol 6:247–254
Farquhar GD (1997) Carbon dioxide and vegetation. Science 278:1411
Gosling WD, Mayle FE, Tate NJ et al (2009) Differentiation between Neotropical rainforest, dry forest, and savannah ecosystems by their modern pollen spectra and implications for the fossil pollen record. Rev Pal Pal 153:70–85
Guilderson TP, Fairbanks RG, Rubenstone JL (1994) Tropical temperature variations since 20,000 years ago: modulating interhemispheric climate change. Science 263:663–665
Haberle SG, Maslin MA (1999) Late Quaternary vegetation and climate change in the Amazon basin based on a 50,000 year pollen record from the Amazon fan, ODP site 932. Quat Res 51:27–38
Haffer J (1969) Speciation in Amazonian forest birds. Science 165:131–137
Haffer J, Prance GT (2001) Climate forcing of evolution in Amazonia during the Cenozoic: on the refuge theory of biotic differentiation. Amazoniana 16:579–607
Haxeltine A, Prentice IC (1996) BIOME3: an equilibrium terrestrial biosphere model based on ecophysiological constraints, resource availability, and competition among plant functional types. Glob Biogeochem Cycl 10:693–709
Hoorn C (1997) Palynology of the Pleistocene glacial/interglacial cycles of the Amazon Fan (Holes 940A, 944A, and 946A). Proc ODP Scientific Results 155:397–409. College Station, TX (Ocean Drilling Program)
Hijmans RJ, Cameron SE, Parra JL et al (2005) Very high resolution interpolated climate surfaces for global land areas. Int J Climatol 25:1965–1978
Indermühle A, Stocker TF, Joos F et al (1999) Holocene carbon-cycle dynamics based on CO_2 trapped in ice at Taylor Dome, Antarctica. Nature 398:121–126
Ledru M-P, Bertaux J, Sifeddine A et al (1998) Absence of Last Glacial Maximum records in lowland tropical forests. Quat Res 49:233–237
Ledru M-P, Mourguiart P, Ceccantini G et al (2002) Tropical climates in the game of two hemispheres revealed by abrupt climatic change. Geology 30:275–278
Malhi Y, Phillips OL (eds) (2004) Tropical forests and global atmospheric change (theme issue). Phil Trans R Soc B 359:305–555
Marchant R, Boom A, Hooghiemstra H (2002) Pollen-based biome reconstructions for the past 450 000 yr from the Funza-2 core, Colombia: comparisons with model-based vegetation reconstructions. Palaeogeog Palaeoclim Palaeoecol 177:29–45

Marchant R, Boom A, Behling H et al (2004) Colombian vegetation at the Last Glacial Maximum: a comparison of model- and pollen-based biome reconstructions. J Quat Sci 19: 721–732

Marchant R, Berrio JC, Behling H et al (2006) Colombian dry moist forest transitions in the Llanos Orientales – A comparison of model and pollen-based biome reconstructions. Palaeogeog Palaeoclim Palaeoecol 234:28–44

Mayle FE (2004) Assessment of the Neotropical dry forest refugia hypothesis in the light of palaeoecological data and vegetation model simulations. J Quat Sci 19:713–720

Mayle FE (2006) The Late Quaternary biogeographic history of South American seasonally dry tropical forests: insights from palaeoecological data. In Pennington RT, Lewis GP, Ratter JA (eds.) Neotropical savannas and dry forests: plant diversity, biogeography and conservation. Systematics Association special vol. 69. CRC Press, Taylor & Francis, London, pp 395–416

Mayle FE, Beerling DJ (2004) Late Quaternary changes in Amazonian ecosystems and their implications for global carbon cycling. Palaeogeog Palaeoclim Palaeoecol 214:11–25

Mayle FE, Beerling DJ, Gosling WD et al (2004) Responses of Amazonian ecosystems to climatic and atmospheric CO_2 changes since the Last Glacial Maximum. Phil Trans R Soc B 359(1443):499–514

Mayle FE, Burbridge R, Killeen TJ (2000) Millennial-scale dynamics of southern Amazonian rain forests. Science 290:2291–2294

Monnin E, Indermühle A, Dällenbach A (2001) Atmospheric CO_2 concentrations over the last glacial termination. Science 291:112–114

Mourguiart P, Ledru M-P (2003) Last glacial maximum in an Andean cloud forest environment. Geology 31:195–198

Oliveira PE (1992) A palynological record of Late Quaternary vegetational and climatic change in southeastern Brazil. PhD dissertation, Ohio State University, Columbus

Olson DM, Dinerstein E, Wikramanayake ED et al (2001) Terrestrial ecoregions of the world: a new map of life on Earth. Bioscience 51:933–938

Paduano GM, Bush MB, Baker PA et al (2003) A vegetation and fire history of Lake Titicaca since the Last Glacial Maximum. Palaeogeog Palaeoclim Palaeoecol 194:259–279

Pennington RT, Prado DE, Pendry CA (2000) Neotropical seasonally dry forests and Quaternary vegetation changes. J Biogeogr 27:261–273

Pflaumann U, Sarnthein M, Chapman M et al (2003) Glacial North Atlantic: sea-surface conditions reconstructed by GLAMAP 2000. Paleoceanography 18:1065–1093

Power MJ, Marlon J, Ortiz N et al (2008) Changes in fire regimes since the Last Glacial Maximum: an assessment based on a global synthesis and analysis of charcoal data. Clim Dyn 30: 887–907

Prado DE, Gibbs PE (1993) Patterns of species distributions in the dry seasonal forests of South America. Ann Miss Bot Gard 80:902–927

Punyasena SW (2008) Estimating neotropical paleotemperature and paleoprecipitation using plant family climatic optima. Palaeogeog Palaeoclim Palaeoecol 265:226–237

Punyasena SW, Mayle FE, McElwain JC (2008) Quantitative estimates of glacial and Holocene temperature and precipitation change in lowland Amazonian Bolivia. Geology 36(8) :667–670

Seltzer GO, Rodbell DT, Baker PA et al (2002) Early warming of tropical South America at the last glacial-interglacial transition. Science 296:1685–1686

Smith JA, Seltzer GO, Farber DL et al (2005) Early local Last Glacial Maximum in the tropical Andes. Science 308:678–681

Smith TB, Wayne RK, Girman DJ et al (1997) A role for ecotones in generating rainforest biodiversity. Science 276:1855–1857

Street-Perrott FA, Huang Y, Perrott RA et al (1997) Impact of low atmospheric carbon dioxide on tropical mountain ecosystems. Science 278:1422–1426

Thonicke K, Venevsky S, Sitch S et al (2001) The role of fire disturbance for global vegetation dynamics: coupling fire into a Dynamic Global Vegetation Model. Glob Ecol Biogeogr 10: 661–677

Urrego DH, Silman MR, Bush MB (2005) The Last Glacial Maximum: stability and change in a western Amazonian cloud forest. J Quat Sci 20:693–701

Van der Hammen T, Barelds J, De Jong H, De Veer AA (1980) Glacial sequence and environmental history in the Sierra Nevada del cocuy (Colombia). Palaeogeog Palaeoclim Palaeoecol 32: 247–340

Van der Hammen T, Hooghiemstra H (2003) Interglacial-glacial Fuquene-3 pollen record from Colombia: an Eemian to Holocene climate record. Glob Planet Change 36:181–199

VEMAP members (1995) Vegetation/ecosystem modelling and analysis project: comparing biogeography and biogeochemistry models in a continental-scale study of terrestrial ecosystem responses to climate change and CO_2 doubling. Glob Biogeochem Cycl 9:407–437

Wille M, Negret JA, Hooghiemstra H (2000) Paleoenvironmental history of the Popayan area since 27000 yr BP at Timbio, Southern Colombia. Rev Pal Pal 109:45–63

Chapter 5
Re-evaluation of Climate Change in Lowland Central America During the Last Glacial Maximum Using New Sediment Cores from Lake Petén Itzá, Guatemala

Mark B. Bush, Alexander Y. Correa-metrio, David A. Hodell, Mark Brenner, Flavio S. Anselmetti, Daniel Ariztegui, Andreas D. Mueller, Jason H. Curtis, Dustin A. Grzesik, Catherine Burton, and Adrian Gilli

Abstract Glaciological data derived from moraines, and multiproxy data from lake sediment cores (e.g. fossil pollen, diatoms, and isotope data) indicate cooling in the Central American tropics during the last ice age. Contrary to prior inferences, however, new lake core data from Lake Petén Itzá, lowland Guatemala, indicate that climate was not particularly dry on the Yucatan Peninsula during the last glacial maximum (LGM) chronozone, around 23,000–19,000 cal. yr BP. We present pollen and lithologic data from Lake Petén Itzá and an improved chronology for climate changes in lowland Central America over the last 25,000 years. The driest period of the last glaciation was not the LGM, but rather the deglacial period (~18,000–11,000 cal. yr BP). Causes of climate shifts during the last glaciation are ascribed to precessional changes in insolation, the position of the Inter-Tropical Convergence Zone, and southward penetration of polar air masses.

Keywords Pleistocene · Guatemala · Fossil pollen · Petén Itzá · Glaciation · Aridity

5.1 Introduction

High-resolution paleoecological records spanning the last 25,000 years are sparse in Central America. The principal sources of evidence for environmental change have been glaciological data (i.e., moraines) and lake sediment cores that have yielded isotope, fossil pollen, charcoal, and diatom data. It is well known that glaciers descended to lower elevations in high-altitude regions of Central America during the last glacial, broadly coincident with the Last Glacial Maximum (LGM) (Lachniet and Vazquez-Selem 2005). The LGM has been variously defined as the coldest glacial time, the time of lowest sea level, the time of regional maximum ice expansion, and simply as the period about 22,000 years ago (hereafter thousands

M.B. Bush (✉)
Department of Biological Sciences, Florida Institute of Technology Melbourne, FL, 32901, USA
e-mail: mbush@fit.edu

F. Vimeux et al. (eds.), *Past Climate Variability in South America and Surrounding Regions*, Developments in Paleoenvironmental Research 14,
DOI 10.1007/978-90-481-2672-9_5,

of years ago is expressed as ka). However, as these events were not synchronous (Peltier and Fairbanks 2006), we chose to follow the working definition of the LGM chronozone (21± 2 ka) adopted by Mix et al. (2001).

Substantial questions remain regarding Central American climate during the last ice age (1) Did montane and lowland regions experience similar cooling during the LGM? (2) Was the LGM characterized by regional aridity? (3) What climatic processes were responsible for temperature and precipitation changes during the LGM (23–19 ka) and the deglacial (∼18–11 ka)? We address these questions using previous paleoclimate work from Central America and new data from the Lake Petén Itzá Scientific Drilling Project (PISDP).

Lake Petén Itzá lies within the Yucatan Peninsula, an area demonstrated to have extreme sensitivity to climate change. In the 1970s, Edward S. Deevey and colleagues spearheaded an exploration for Pleistocene lake records in the lowlands of Guatemala, culminating in the raising of a long core from Lake Quexil (Deevey et al. 1983). This 19.7-m core (Quexil 80-1) was drilled in 29 m of water and had an extrapolated basal age of c. 36 ka. The pre-Holocene chronology of the core from this karst lake was based on a single radiocarbon date (27,450 ± 500 ^{14}C yr BP) from a shell taken at 15.96 m. Importantly, that date was not corrected for hard-water lake error. In the basal section of the core, the pollen indicated vegetation that was more temperate than today and marked by a montane pine-oak forest, suggesting cool-moist conditions with temperatures 4.7–6.5°C lower than present (Leyden et al. 1993, 1994). This section of core was overlain by deposits containing pollen indicative of an *Acacia*-rich scrubland that was initially interpreted, based on peaks of *Juniperus* pollen, to indicate temperatures c. 6.5–8°C lower than today (Leyden et al. 1993, 1994). Replacement of the open-water alga *Botryococcus* during this dry period by the littoral and marsh taxa *Potamogeton*, *Alternanthera*, and *Typha*, suggested that the lake was considerably reduced and may have been ephemeral.

Chemical data, and especially gypsum deposition, reinforced evidence for drying derived from the pollen record during the period attributed to the LGM in core Quexil 80-1. The δ^{13}C values of long-chain n-alkanes (C_{27}, C_{29}, C_{31}) in core Quexil 80-1 were 4‰ greater during the "marshland phase" than those of the early Holocene, indicating a higher proportion of C4 plants in the watershed prior to the Holocene (Huang et al. 2001). Such a shift can indicate the transition from a drought tolerant C4 species to a tree dominated (C3-rich) Holocene landscape. Below, we re-interpret the chronology of climate changes inferred from the Quexil 80-1 core based on correlation to well-dated cores from nearby Lake Petén Itzá.

5.1.1 The Lake Petén Itzá Scientific Drilling Project (PISDP)

Lake Petén Itzá (area = ∼100 km^2, maximum depth = 160 m), the deepest lake in lowland Central America, is located at ∼16°55′N, 89°50′W in the Department of Petén, northern Guatemala (Fig. 5.1). Prior to the most recent drilling efforts, a detailed seismic survey of the basin was made using 3.5-kHz and airgun profiling

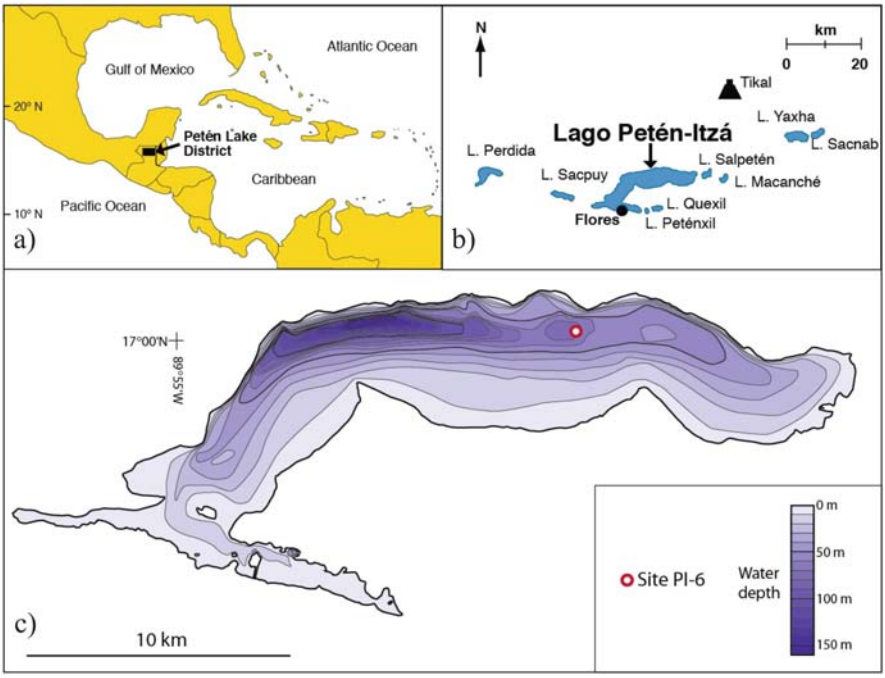

Fig. 5.1 (**A**) Map of the Intra America Seas showing the location of the Department of Petén, northern Guatemala and Cariaco Basin off northern Venezuela. (**B**) Map of the Petén Lake District. (**C**) Bathymetric map of Lake Petén Itzá showing the location of primary and alternate coring sites. Coring location PI-6 is labelled as 6

(Anselmetti et al. 2006). The survey revealed the underlying karst topography and several deep pockets of sediment that became the focus of the coring campaign. Seismic images from the deepest part of the basin indicated possible slumping of deposits from the steep north shore. Consequently, when the GLAD 800 drilling rig was deployed on Lake Petén Itzá, between January and March 2006, a transect of drill sites from the deep to the shallow-water was targeted for coring in order to recover the optimal sediment sequences for paleoenvironmental reconstructions.

Holes were drilled at seven sites in the lake, with multiple holes drilled at six locations (Hodell et al. 2006, 2008). Sediments were generally composed of green or gray lake muds, but in particular sections of the core, white bands of gypsum (calcium sulfate) formed distinct layers. These high-density bands, as well as ash layers and changes in magnetic susceptibility, were used to correlate stratigraphically the multiple cores raised from each drill site. Among the cores, Site PI-6 consisted of three holes that were correlated stratigraphically to provide a continuous 75.9-m-long sediment column.

Chronology of this record was based on 23 AMS ^{14}C dates on terrigenous organic matter and the occurrence of three identifiable ash layers with ages between 53 $\pm$ 3 ka and 84 $\pm$ 0.5 ka (Hodell et al. 2008). The deep ash layer was "fingerprinted"

geochemically by electron microprobe glass analysis. The ash was derived from the Los Chocoyos eruption of the Atitlán Caldera in the Guatemalan highlands that occurred at 84 ka, during Marine Isotope Stage (MIS) 5a (c. 85–78.5 Ka) (Ledbetter 1984). The lithology and chronology of PI-6 are described in detail by Hodell et al. (2008). This core appeared to offer a continuous sedimentary record from 0 to 85 ka.

Glacial-age deposits consisted of interbedded clays and gypsum that were clearly expressed by variations in magnetic susceptibility of the sediment (Fig. 5.2). Authigenic gypsum displayed relatively low magnetic susceptibility values compared with detrital clays, which had high susceptibility values.

Preliminary analyses of cores from Site PI-6 in Lake Petén Itzá revealed that lithology of LGM sediments was dominated by clays thought to have been deposited in deep water under relatively wet climate conditions. In contrast to these clays, gypsum was deposited during lake lowstands. Interbedded gypsum and clay layers were deposited from 45 to 23 ka during MIS 3, and the last deglaciation (~18–11 ka), but gypsum is conspicuously absent from sediments deposited during the LGM (23–19 ka). Thus the last deglaciation was much drier than the LGM. Evidence of a substantially lowered lake level in the late glacial was also revealed in the seismic profiles of Petén Itzá. Transects reveal a wave-cut bench and paleoshoreline buildups ~56 m below modern lake level, suggesting a lowering of lake level by that amount, which is equivalent to an 87% reduction in lake volume (Anselmetti et al. 2006, Hodell et al. 2008).

The fossil pollen record from Petén Itzá reveals that during the LGM regional vegetation was rich in *Myrica*, *Quercus*, and *Pinus* (Fig. 5.2). Charcoal increases in abundance in the LGM compared with MIS 3, an observation consistent with the relatively frequent but low intensity fires documented in pine-oak forests of Mexico (Fule and Covington 1997). Throughout the LGM Poaceae and *Ambrosia* were only c. 10% of the pollen sum, leading us to investigate Mexican montane oak-pine forests as a possible analog.

The Mexican pine-oak vegetation complex spans a large environmental range and further work is needed to refine which modern community most closely approximates the LGM conditions recorded in PI-6. Our initial estimate is consistent with observations made by Leyden et al. (1994) that this LGM pine-oak forest probably formed under conditions that were c. 3-5°C cooler than present.

In the deglacial phase at Petén Itzá, Poaceae increased in abundance, while *Pinus* and *Quercus* declined. The period of northern hemispheric deglaciation was also marked by increased abundances of Amaranthaceae pollen, an indication of fluctuating lake level, similar to that seen in the "marshland phase" of Lake Quexil.

The superior chronology of the new cores from Petén Itzá permits reinterpretation of the poorly-dated record from Quexil 80-1. The montane *Pinus-Quercus* pollen assemblage interpreted by Leyden et al. (1993, 1994) to have been deposited during MIS 3 instead represents the LGM (23–19 ka). Similarly, the postulated LGM flora of xeric thorn scrub, in fact represents the period of maximum aridity during deglaciation (~18–11 ka). During this latter interval, the open water of Lake Quexil was probably replaced by a *Typha* swamp. If this driest period of Lake Quexil is aligned with the driest event in Petén Itzá, then the preceding period,

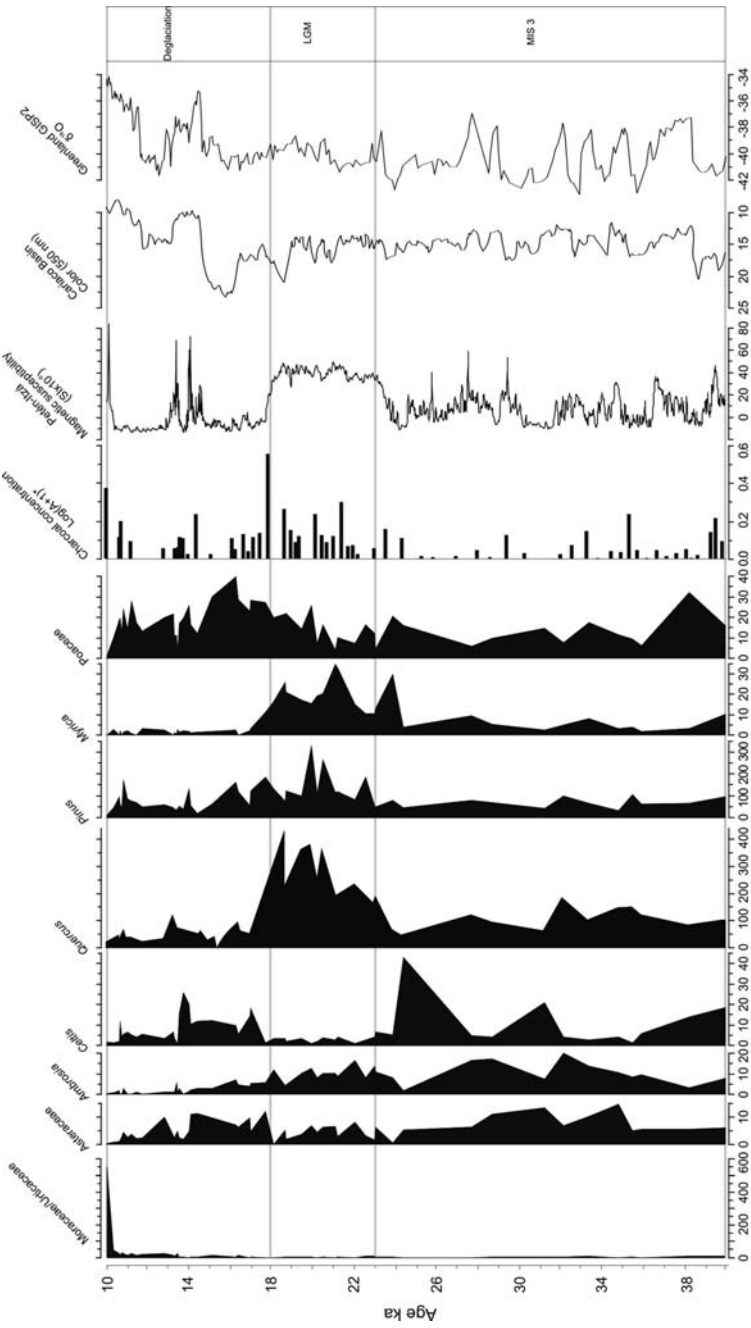

Fig. 5.2 The paleoecological record of core PI-6 from Lake Petén Itzá, Guatemala, 40–10 ka. Percentage data for fossil pollen (*Quercus* and *Pinus* excluded from the pollen sum) of selected taxa, charcoal concentrations, and magnetic susceptibility are shown. Low magnetic susceptibility indicates gypsum deposition and low lake level. Also shown are the $\delta^{18}O$ of the Greenland Ice Core (Grootes et al. 1993) and color reflectance values from the Cariaco Basin (Peterson et al. 2000)

dated to the LGM in Petén Itzá, displays a very similar flora at both sites. The *Pinus-Quercus* assemblage of the LGM could be consistent with a cooling of 3–5°C for the lowlands, whereas the suggestion of a 6.5–8°C cooling (Leyden et al. 1993) for what is now dated to the deglacial phase, will be investigated further as data emerge from the Petén Itzá record.

Near the Pleistocene/Holocene boundary (~12 ka), Petén lakes filled rapidly in response to increased precipitation. Pollen studies demonstrated that the Petén tropical forest arose abruptly after 12.5 ka and was dominant by ~11 ka (Leyden 1984, Leyden et al. 1993, 1994). The Petén Itzá record offered a slightly more refined insight into these events. Transition toward a more "tropical" system began around 18 ka, but though warming, this was also a period of strong drought. Between 15 and 13 ka (the precise boundaries have yet to be established) a climatic oscillation intensified the dry conditions. Between 13 and 11 ka there was gradual change toward more mesic conditions. A mixed community formed in which mesic lowland elements, e.g. Urticaceae/Moraceae, and *Ficus*, coincided with mesic upland taxa, e.g. *Quercus, Pinus, Hedyosmum* and *Alnus*, and xeric lowland indicators, e.g. *Acacia, Bursera* and *Hymenaea*, co-existed. At that time, communities changed rapidly and probably formed a landscape mosaic of vegetation types without modern analog. A major wet event elevated Urticaceae/Moraceae from c. 40 to 60% of the pollen sum between 11 and 10.3 ka (Fig. 5.2), and gypsum deposition terminated about 10.3 ka.

5.2 Did Montane and Lowland Regions Experience the Same Degree of Last Glacial Maximum Cooling?

5.2.1 Glaciological Evidence

At the height of the LGM ice caps developed in montane regions of Central America, South America, and Mexico (Lachniet and Vazquez-Selem 2005, Lachniet 2007). Terminal moraines formed at about 3000 m in the Talamancas of Costa Rica, where glaciers descended below their equilibrium line altitude (Lachniet and Vazquez-Selem 2005). In Guatemala, an ice cap of ~60 km^2 existed on the high plateau, with moraines at elevations of 3470–3600 m (Lachniet 2004). The record of past glacial activity can be used to recreate the glacial equilibrium line altitude (ELA). This measure denotes where the mass balance of the glacier was zero, i.e. where accumulation = ablation. Temperature, local topography, shading, and precipitation can all influence local ELAs. However, if taken regionally, the ELA in combination with the moist air adiabatic lapse rate (lapse rate) can provide an index of past temperature change.

The use of a specific lapse rate to calculate temperature depression during the LGM needs to account for the potential influence of humidity. As air becomes drier, lapse rates increase. Van der Hammen and Hooghiemstra (2000) invoked a Pleistocene lapse rate different from today to suggest that the high Andes may have cooled much more than the Amazon lowlands. However, large changes in lapse rate

are unlikely in a region that receives maritime airflow. Furthermore, given the presence of abundant evapo transpiring vegetation during the LGM (the case for this follows), it is likely that the lapse rate was similar to that of today (Rind and Peteet 1985), i.e. between ~5.5 and 6°C/km.

Applying a 5.6°C/km lapse rate yields a range of estimates for LGM cooling of 4.6–8.5°C (Lachniet and Vazquez-Selem 2005). The low value of 4.6°C for Vaquerías, Mexico, is the minimal cooling estimate, and is similar to other north- or northwest-facing Mexican sites of similar latitude. Only 8 of 25 Mexican sites were reported to have ELAs lowered by <1000 m. Mexican sites facing south and east tended to have ELAs lowered by about 1000–1500 m at the LGM. From these data, it is apparent that peaks above 3200 m often had ice caps, consistent with high-elevation cooling of c. 8°C.

Poor chronological control on the timing of glacial advances made comparisons with other paleoclimate records difficult. In Mexico, a major glacial expansion at c. 151–126 ka, dated using ^{36}Cl exposure was, within the limits of this dating technique, consistent with the glacial maximum of MIS 6 (c.160–132 ka) (Martinson et al. 1987). Other moraines were dated to c. 19–18 ka and 15–14 ka (Vazquez and Givnish 1998), with a last brief expansion at about 10 ka (ibid).

Many moraines, including all those of Guatemala and Costa Rica, remain undated and age estimates rely on correlation with the Mexican moraines that have radiometric ages. Moraine morphology and weathering characteristics are used to infer temporal equivalence of advances. While direct dating of moraine advances has not been possible in Costa Rica, a minimum estimate for deglaciation of c. 12,360–11,240 cal. yr BP is available from basal sediments in a corrie (cirque) lake at 3480 m elevation (Horn 1990).

5.2.2 Palynological Evidence

Evidence of subalpine temperature depression comes primarily from fossil pollen records. Lachner Bog (2400 m elevation) in Costa Rica provided the first long record of vegetation change for Central America (Martin 1964). At that site, pollen of *Quercus* was abundant in sediments beyond the range of bulk radiocarbon dating. During the last glacial, *paramo* grasslands replaced these forests. About 10 ka, grasslands were replaced by *Quercus* forest that has persisted until modern times. The inferred descent of *paramo* grasslands at the LGM (Martin 1964) indicates a minimum displacement of dominant species in these assemblages of at least 600 m. Given a local lapse rate of 5.6°C/km, this descent of grasslands suggests a minimum of 3°C cooling, somewhat less than the 8°C cooling inferred from glaciological studies. However, the grassland signature, at least at the level of detail revealed in Martin (1964), could also be consistent with a cooling of as much as 9°C.

In Panama, the 57-m-long sediment sequence from El Valle provided the first transglacial record for lowland Central America (Bush and Colinvaux 1990). El Valle is a *caldera* whose walls extend to about 1100 m above sea level (masl), whereas the ancient lakebed that forms the floor of the *caldera* lies at 500 masl.

A continuous 130,000-year fossil pollen record from El Valle suggests a descent of *Quercus* forest to the elevation of the *caldera* rim, and in the late glacial, to the *caldera* floor. Between c. 35 and 20 ka, the lake contracted and became a *Typha* swamp. That this record shows no evidence of the wet events of the early Holocene recorded at other Panamanian and Central American locations (Bush et al. 1992), suggests that at least some of the apparent drying may have been a product of hydrarch succession rather than simply climate change. However, the relative importance of hydrarch succession versus climate drying has yet to be tested.

These data are consistent with cooling that would have been sufficient to bring *Quercus* close to the floor of the El Valle crater. As *Quercus* does not currently grow in this portion of Panama and is restricted to elevations above c. 1700 m (Bush 2000), the c. 600–1200 m descent of *Quercus* within the El Valle *caldera* is consistent with c. 3–5°C cooling.

Another insight into Panamanian deglacial climates comes from Lake La Yeguada (650 masl). This lake did not begin to accumulate sediment until c. 16,000 cal. yr BP, at which time *Quercus* had descended and grew near the lake (Bush et al. 1992). Thus the La Yeguada data are consistent with a cooling of c. 5°C within the deglacial period. Together, the La Yeguada and El Valle data indicate that lowland Panama experienced cooling of about 5°C at the LGM (Bush 2002).

The new data from Petén Itzá are consistent with these estimates of lowland cooling. So far, the peak of *Juniperus* pollen described by Leyden et al. (1993, 1994) has not been identified in the analysis of the PI-6 sediment. Leyden et al. (1993, 1994) used *Juniperus* to infer a c. 6.5–8°C cooling in sediments thought to have been deposited during the LGM (now re-assigned to the early deglacial period). Despite the absence of a *Juniperus* peak in PI-6, the presence of what appears to be either a scrub oak or a montane oak-forest community at the LGM is consistent with c. 4–6°C cooling. The cooling in lowland Central America inferred from pollen studies is more extreme than estimates from many tropical, deepwater oceanic records (e.g. Ballantyne et al. 2005, Zhang 2006). In general, a 1–3°C cooling has been suggested for the tropical Atlantic and Pacific. Schmidt et al. (2004) suggested c. 2.5°C cooling for the western Caribbean at the LGM, slightly warmer than Guilderson et al.'s (1994) estimate of a 3–5°C cooling in the shallow waters off Barbados.

Overall, it seems that montane regions cooled about 5–8°C, while the lowlands cooled approximately 5°C, and the oceans cooled somewhat less.

5.3 Was the LGM Characterized by Aridity?

Last Glacial Maximum paleoclimate records from Central and South America remain rare, whereas Holocene records are relatively abundant. As glacial-age aridity was identified in paleoecological studies of the African tropics (Livingstone 1967, 1975), a simplistic model of wet interglacials and dry glacials was applied to

characterize all Neotropical climates. Observations in the early 1990s of millennial-scale climate variability in Greenland ice cores, however, made it apparent that tropical climate variability during the last glacial cycle consisted of periods of both wetter and drier climate (Peterson et al. 2000).

The simple wet-dry dichotomy was also challenged spatially by a regional synopsis from which a pattern of high lake level was inferred at the LGM for the Southwestern USA and western Mexico, whereas low lake stage was observed for Panama and the Yucatan Peninsula (Bradbury 1997). In support of this hypothesis was the observation that many shallow lakes in the lowlands of northern Central America and southeastern Mexico first filled with water in the early Holocene, about 10.5–8 ka (e.g. Leyden 1984, Vaughan et al. 1985, Whitmore et al. 1996). The first appearance of these lakes in the early Holocene is easily explained by a wet phase that followed a late glacial dry phase.

The Petén Itzá data contribute to the growing body of evidence that the LGM itself was not necessarily a dry time in the Neotropics. The clays deposited during the LGM and the presence of a montane *Quercus-Pinus-Myrica* community are consistent with cool conditions relative to today, but with no indication of a marked increase in soil-moisture deficits. Preliminary diatom data for the LGM suggest that lake level was higher than the latter part of MIS 3 or the deglacial period, but lower than the Holocene. As in other locations, it is the early deglacial period that appears to have been the driest time.

Notably, the lake at El Valle deepened at c. 16 ka, broadly coincident with the formation of Lake La Yeguada (Bush and Colinvaux 1990, Bush et al. 1992). At Petén Itzá, where a more detailed record is available, the rising lake levels coincident with the Bølling-Allerød period (14.9–12.8 ka) were punctuated by a dry event during Meltwater Pulse 1A (14.1–13.5 ka; Fairbanks et al. 2005).

5.4 Precession as a Long-Term Driver of Precipitation Change in Central America

Our understanding of the causes of climate change at the LGM is still limited. In particular, Central America is poorly represented in the relatively coarse resolution of most Global Climate Model simulations due to its complex topography and small width. Consequently, our first approximation of climate forcing is based on rather simple assumptions relating insolation to climate. Insolation forcing operates on multi-millennial, orbital time scales with the precession cycle and its harmonics ($\sim$11 and 5.5 ka) (Berger et al. 2006). It cannot directly explain abrupt change at shorter time scales (addressed in Section 5.5).

A readily quantifiable insolation parameter is the precession-driven variability of insolation in the upper atmosphere. Numerous papers point to the importance of precessional rhythms in the Neotropics, especially on patterns of precipitation (e.g. Berger 1978, Hooghiemstra et al. 1993, Bush et al. 2002, Rowe et al. 2002, Clement et al. 2004, Wang et al. 2004, Cruz et al. 2005, Hodell et al. 1991, 2000). It has been

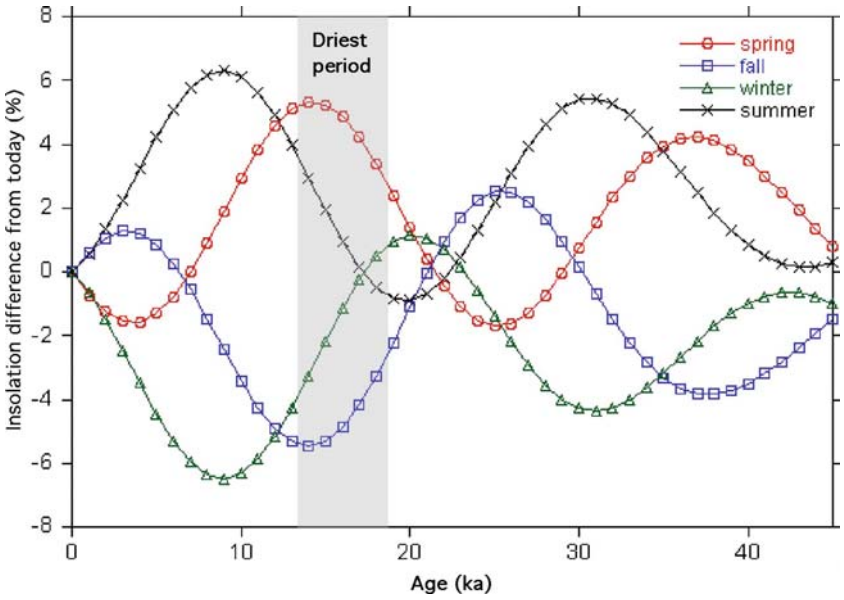

Fig. 5.3 Changes in insolation at 15° N over the last 40,000 years. Amount of insolation received (watts per m^2) for spring (March 21), summer (June 21), autumn (Sept 21), and winter (Dec 21). Data from Analyseries 1.2 (Berger 1992, Paillard et al. 1996)

suggested that increased wet season insolation translates into elevated wet season rainfall, and that high (low) seasonality broadly relates to maximum (minimum) differences in seasonal insolation. Clement et al. (2004) identified the importance of precession to Pleistocene tropical climates, but cautioned that complex land-ocean interactions played an important modifying role.

Here we provide a very simple set of observations regarding precessional changes that may have influenced the climate of Petén over the last 30,000 years. These observations should really be taken as a set of hypotheses to be tested rather than a definitive history. For latitudes between 10° N and 23° N, the seasonal insolation pattern during the LGM was similar to that of today, and characterized by reduced seasonality relative to the deglacial and early Holocene (Fig. 5.3). The onset of wet conditions at the LGM c. 23 ka, coincided with a time of minimum seasonality during which summer insolation was relatively low and winter insolation was relatively high (i.e. similar to today).

We hypothesize that trajectories of insolation change leading up to and out of the LGM were highly significant influences on vegetation and lake levels on the Yucatan Peninsula. The previous peak of seasonal insolation difference (i.e. maximum difference between summer and winter insolation) occurred at c. 31 ka and transitioned to the LGM through an orbital configuration when perihelion occurred during northern hemisphere autumn.

On a regional scale, if summer heating of the ocean induces the northward migration of the Hadley cell, then thermal inertia of the ocean probably caused sea surface temperature (SST) increases to lag insolation. Consequently, wet season precipitation maxima would have lagged insolation maxima. This lag may have reduced summer convective activity during the LGM, but the increased autumn insolation may have prolonged the wet season. We suggest that the net effect of those changes was to produce a less intense, but longer wet season that maintained mesic conditions overall.

In the deglacial precessional transition, perihelion occurred in the northern hemisphere spring. During this period, spring insolation was higher than summer insolation. We hypothesize that weak summer insolation reduced convective activity and caused reduced wet season precipitation. The springtime peak of insolation would have occurred during the dry season, too early in the year for the ocean to have warmed and generated rainfall.

Ecologically, rainfall deficits in the dry season have far more influence on vegetation than equivalent reductions in wet season precipitation, when there is excess moisture in the system. In the Caribbean, the migration of the Inter-tropical convergence zone (ITCZ) results in wet season convective activity and delivers the majority of moisture to the region. The combination of a strengthened dry season and relatively weak ITCZ between c. 16 and 14 ka led to the greatest aridity within the last 50,000 years.

5.5 Short-Term Drivers of Precipitation and Temperature

Superimposed upon the longer-term effects of insolation were the influences of frontal activity, migration of air masses, and ocean currents. All of these factors were influenced by high-latitude (North Atlantic) climate. For example, the cooling that influenced the tropics came about as a consequence of high-latitude ice sheet expansion that influenced atmospheric (e.g. jet streams) and ocean circulation. Indeed the weight of each of these factors may have been different at various times in the past. Clement et al. (2004) isolates glacial boundary conditions from precessional forcing as potential influences on tropical climate. Bush (2002) suggested that the growth of the Laurentide ice mass was responsible for a change in forcing that affected the El Valle record, Panama at c. 45 ka. While we know the limits of that ice sheet and can model its volume, its teleconnective linkages with the tropics remain speculative. Empirical data support the idea that the polar jet was displaced southward or split to flow around the ice mass during the northern hemispheric winter (e.g. COHMAP 1988).

Global Climate Models, supported by empirical paleoclimatic data, indicate that when the meridional overturning circulation (MOC) was weakened (the extreme situation being Heinrich events), heat was retained in equatorial waters of the southern hemisphere. Furthermore, the presence of the northern-hemispheric ice mass, and stronger polar than equatorial cooling, steepened the pole-equator temperature gradient. Under these circumstances, the northern migration of the ITCZ was

weakened, while that of the southern migration was strengthened (Koutavas and Lynch-Stieglitz 2004, Chiang and Bitz 2005).

Modern precipitation over the Yucatan Peninsula is strongly seasonal, with the vast majority arriving in late northern hemispheric summer when the ITCZ lies to the north. We hypothesize that if the ITCZ fails to migrate far northward or its influence is weakened by the southward displacement of the westerlies (Ganopolski et al. 1998) and a steepened temperature gradient, then wet season (May–October) precipitation over Yucatan will be reduced.

The most striking feature of the paleoclimate record from Petén Itzá is that the LGM of the Yucatan Peninsula appears to have been moist, and it was the deglacial period that was driest. We hypothesize that the strengthened incursion of cold polar air masses (today referred to locally as *nortes*) at the LGM, resulted in relatively cool, wet winters.

As the Laurentide ice mass expanded southward, steepening the pole-equator temperature and pressure gradients, outbursts of polar air would likely have penetrated into Central America. Assuming that the weather associated with modern *nortes* was similar in the past, the *nortes* would have brought a rain front, followed by days of cold, dry weather. If the *nortes* penetrated into the Neotropics more frequently than today, and if they started from a more southerly polar jet, they would be expected to have enhanced seasonality in terms of temperature, but reduce soil moisture deficits in the dry season. The same basic mechanism, which promotes a cool, moist, and rather weakly seasonal precipitation system, though in that case fed by westerlies rather than *nortes*, was proposed to explain records from central Mexico (Metcalfe et al. 2007).

Toward the southern end of their range, the principal cooling of *nortes* comes not from air temperature, but from the blockage of insolation by clouds (Marengo and Rogers 2001). Cloudiness (or lack of it) could have moderated or accentuated insolation effects. To date, no models incorporate cloudiness, and although we can calculate insolation at the top of the atmosphere, insolation on the ground could have been very different.

Relatively dry events surrounding the wetter conditions of the LGM may have resulted from a combination of factors. Heinrich events H1 and H2, which bracket the LGM, may have caused reduced precipitation in Petén due to the postulated southward migration of the ITCZ (e.g. Vellinga and Wood 2002). Additionally, reduced incursions of *nortes* after $\sim$18,000 years ago may have contributed to lowered lake levels and a change in vegetation. Drier conditions coincided with increased seasonality in insolation and a change in the vegetation. We hypothesize that a shift to fewer *nortes* resulted in milder, but drier dry seasons. Climate oscillations, including cooler periods of the Oldest Dryas, Older Dryas, and Younger Dryas, as well as intervening warm periods all appear to be present in the Petén Itzá record. The clear representation of events such as the deglacial Meltwater Pulse of c. 14 ka and Heinrich events suggest that the Petén Itzá record is sensitive to fluctuations in the strength of the MOC.

5.6 Conclusions

New data from Lake Petén Itzá sediment cores contribute to our understanding of late Pleistocene Central American paleoclimate, though much still remains to be discovered. The first question we addressed was whether there was cooling in the lowlands equal to that in montane settings at the LGM. Our data suggest that vegetated areas of montane and lowland regions probably both experienced cooling of ~5°C in the LGM. However, ELA estimates for mountaintops suggest that this cooling may have been as great as 8.5°C above c. 3,300 m elevation. Assuming these proxies are reliable, it appears that there was steepening of the thermal gradient on mountainsides, especially above the vegetated zone.

The second question we addressed was whether the LGM was characterized by regional aridity? The Petén Itzá data provide very strong evidence that the LGM was cool, but wet enough to maintain a forest cover, whereas the deglacial ~17–14 ka was markedly drier than today. The deglacial, rather than the Last Glacial Maximum, was the time of maximum aridity in lowland Guatemala, a finding consistent with paleoclimate data from other Central American localities.

In light of these data, we re-interpreted the paleoecological record from Lake Quexil (Leyden et al. 1993, 1994). The pre-Holocene chronology of this core was based on a single ^{14}C date on an aquatic mollusc shell, uncorrected for hardwater lake error. Consequently, the ^{14}C age was too old, and deglacial-age sediments (c. 17,000–15,000 cal. BP) were attributed erroneously to the LGM. The new core from Petén Itzá has 23 ^{14}C dates on terrigenous organic matter and yielded a far superior chronology for investigating climate change in the Central American lowlands.

New pollen data from Lake Petén Itzá indicate that from 23 to 19 ka (i.e. LGM chronozone), the catchment was occupied by a forest rich in oaks and pines that co-existed alongside tropical elements. Whether this forest constituted a no-analog assemblage or a close analog to Mexican pine-oak forests has yet to be determined.

The third question we addressed dealt with the cause(s) of precipitation change in Central America over the last 23,000 years. Although several mechanisms that influenced LGM climate in Central America have been identified, i.e. the southward shift of the westerlies, migration of the ITCZ, precessional insolation variability, cold fronts, SSTs, and cloudiness, the relative importance of each at any given time in the past remains unknown.

We hypothesize that the relatively mesic conditions of the LGM may have been a consequence of more evenly distributed precipitation than that of today, with reduced wet season inputs, but increased dry season moisture availability. A mechanism to account for this pattern and its timing is suggested based upon a combination of orbital forcing and stronger and more frequent cold fronts that brought rain to the region during winter (dry season). There exists a need to generate new, highly-resolved (both temporally and spatially) climate models that portray the Central American region at different times in the past realistically. Until that is achieved, we can provide empirical data on local climate conditions, but must speculate as to their cause.

Table 5.1 Data for Late Quaternary glacial descent in Mexico and Central America. Of 25 Mexican glaciers given in Lachniet and Vazquez-Selem (2005), the extreme cases, i.e. with the greatest and least changes in equilibrium line altitude (ELA) relative to modern, are listed here. Temperature depression during the Last Glacial Maximum, relative to modern, was calculated assuming a lapse rate of 5.6°C/km): Data from Lachniet and Vazquez-Selem (2005)

Location	Latitude °N	Modern ELA (m)	Last Glacial Maximum ELA (m)	Temperature depression (°C)
Vaquerías valley, Mexico	19.20	4970	4146	4.6
Tancítaro, Mexico	19.43	4900	3390 ± 50	8.5
Cuchumatanes ice cap, Guatemala	15.5	4900	3544	7.6
Talari Glacier, Costa Rica	9.47	5000	3489	8.5
Morrenas Glacier, Costa Rica	9.5	5000	3464	8.6

Acknowledgments We thank all individuals who participated in the fieldwork of the Lake Petén Itzá Scientific Drilling Project. We thank the LacCore (National Lacustrine Core Repository), Department of Geology and Geophysics, University of Minnesota-Twin Cities, for their expertise and help in sampling the Petén Itzá core. This project was funded by grants from the US National Science Foundation (ATM-0502030), the Swiss Federal Institute of Technology, the Swiss National Science Foundation, and the International Continental Scientific Drilling Program. We are grateful to William Gosling and Sarah Metcalfe for constructive reviews.

References

Anselmetti FS, Ariztegui D, Hodell DA et al (2006) Late Quaternary climate-induced lake level variations in Lake Petén Itzá, Guatemala, inferred from seismic stratigraphic analysis. Palaeogeogr Palaeoclimatol Palaeoecol 230:52–69

Ballantyne AP, Lavine M, Crowley TJ, Baker PA (2005) Meta-analysis of tropical surface temperatures during the Last Glacial Maximum. Geophys Res Lett 32:L05712 (05714)

Berger A (1978) Long-term variations of daily insolation and Quaternary climatic change. J Atmos Sci 35:2362–2367

Berger A (1992) Astronomical theory of paleoclimates and the last glacial-interglacial cycle. Quat Sci Rev 11:571–581

Berger A, Loutre MF, Mélice JL (2006) Equatorial insolation: from precession harmonics to eccentricity frequencies. Clim Past 2:131–136

Bradbury JP (1997) Sources of glacial moisture in Mesoamerica. Quat Int 43–44:97–110

Bush MB (2000) Deriving response matrices from Central American modern pollen rain. Quat Res 54:132–143

Bush MB (2002) On the interpretation of fossil Poaceae pollen in the humid lowland neotropics. Palaeogeogr Palaeoclimatol Palaeoecol 177:5–17

Bush MB, Colinvaux PA (1990) A long record of climatic and vegetation change in lowland Panama. J Veg Sci 1:105–119

Bush MB, Miller MC, de Oliveira PE, Colinvaux PA (2002) Orbital forcing signal in sediments of two Amazonian lakes. J Paleolimnol 27:341–352

Bush MB, Piperno DR, Colinvaux PA (1992) A 14,300 year paleoecological profile of a lowland tropical lake in Panama. Ecol Monographs 62:251–276

Chiang JCH, Bitz M (2005) Influence of high latitude ice cover on the marine Intertropical Convergence Zone. Climate Dyn. doi: 10.1007/s00382-00005-00040-00385

Clement AC, Hall A, Broccoli AJ (2004) The importance of precessional signals in the tropical climate. Clim Dyn 22:327–341

COHMAP (1988) Climate changes of the last 18,000 years: observations and model simulations. Science 241:1043–1052

Cruz FW Jr, Burns SJ, Karmann I (2005) Insolation-driven changes in atmospheric circulation over the past 116,000 years in subtropical Brazil. Nature 434:63–66

Deevey ES, Brenner M, Binford MW (1983) Paleolimnology of the Peten Lake District, Guatemala. Hydrobiologia 103:211–216

Fairbanks RG, Richard RA, Mortlock A et al (2005) Marine radiocarbon calibration curve spanning 0 to 50,000 years B.P. based on paired $^{230}Th/^{234}U/^{238}U$ and ^{14}C dates on pristine corals. Quat Sci Rev 24:1781–1796

Fule PZ, Covington WW (1997) Fire regimes and forest structure in the Sierra Madre Occidental, Durango, Mexico. Acta Botánica Mexicana 41:43–79

Ganopolski A, Rahmstorf S, Petoukhov V, Claussen M (1998) Simulation of modern and glacial climates with a coupled global model of intermediate complexity. Nature 391:351–356

Grootes PM, Stuiver M, White JWC et al (1993) Comparison of oxygen isotope records from the GISP2 and GRIP Greenland ice cores. Nature 366:552–554

Guilderson TP, Fairbanks RG, Rubenstone JL (1994) Tropical temperature variations since 20,000 years ago: modulating interhemispheric climate change. Science 263:663–665

Hodell DA, Curtis JH, Jones GA et al (1991) Reconstruction of Caribbean climate change over the past 10,500 years. Nature 352:790–793

Hodell DA, Brenner M, Curtis JH (2000) Climate change in the northern American tropics since the last ice age: implications for environment and culture. In: Lentz DL (ed) Imperfect balance: landscape transformations in the Precolumbian Americas. Columbia University Press, New York

Hodell DA, Anselmetti F, Ariztegui D et al (2008) An 85-ka record of climate change in Lowland Central America. Quat Sci Rev 27:1152–1165

Hodell DA, Anselmetti FS, Brenner M et al (2006) The Lake Petén Itzá scientific drilling project. Sci Drill 3:25–29

Hooghiemstra H, Melice JL, Berger A, Shackleton NJ (1993) Frequency spectra and paleoclimatic variability of the high-resolution 30–1450 ka Funza I pollen record (Eastern Cordillera, Colombia). Quat Sci Rev 12:141–156

Horn SP (1990) Timing of deglaciation in the Cordillera de Talamanca, Costa Rica. Clim Res 1:81–83

Huang Y, Street-Perrott FA, Metcalfe SE et al (2001) Climate change as the dominant control on glacial-interglacial variations in C3 and C4 plant abundance. Science 293:1647–1651

Koutavas A, Lynch-Stieglitz J (2004) Variability of the Marine ITCZ over the Eastern Pacific during the Past 30,000 years: regional perspective and global context. In: Diaz HF, Bradley RS (eds) The hadley circulation: present, past, and future. Kluwer Academic Publishers, Germany

Lachniet MS (2004) Late Quaternary glaciation of Costa Rica and Guatemala. In: Ehlers J, Gibbard PL (eds) Quaternary glaciations—extent and chronology, Part III: South America, Asia, Africa, Australia, Antarctica. Elsevier, Amsterdam

Lachniet MS, Vazquez-Selem L (2005) Last Glacial Maximum equilibrium line altitudes in the circum-Caribbean (Mexico, Guatemala, Costa Rica, Colombia, and Venezuela). Quat Int 138–139:129–144

Lachniet MS (2007) Glacial Geology and Geomorphology. In: Bundschuh J, Alvarado G (eds) Central America: geology, resources, and hazards. Taylor & Francis, London.

Ledbetter MT (1984) Tephrochronology of marine tephra adjacent to Central America. Geol Soc Amer Bull 96:77–82

Leyden BW (1984) Guatemalan forest synthesis after Pleistocene aridity. Proc Nat Acad Sci 81:4856–4859
Leyden BW, Brenner M, Hodell DA, Curtis JA (1993) Late Pleistocene climate in the Central American lowlands. In: Swart PK, Lohmann KC, McKenzie J, Savin S (eds) Climate change in continental records. American Geophysical Union, Washington, DC
Leyden BW, Brenner M, Hodell DA, Curtis JA (1994) Orbital and internal forcing of climate on the Yucatan Peninsula for the past ca. 36 ka. Palaeogeogr Palaeoclimatol Palaeoecol 109: 193–210
Livingstone DA (1967) Postglacial vegetation of the Ruwenzori Mountains in equatorial Africa. Ecol Monographs 37:25–52
Livingstone DA (1975) Late Quaternary climate change in Africa. Annu Rev Ecol Syst 6:249–280
Marengo JA, Rogers JC (2001) Polar air outbreaks in the Americas: Assessments and impacts during modern and past climates. In: Markgraf V (ed) Interhemispheric climate linkages. Academic Press, New York
Martin PS (1964) Paleoclimatology and a tropical pollen profile. In: Report of the VIth International Congress on the Quaternary. Paleoclimatological section, Lodz., Warsaw
Martinson DGN, Pisias G, Hays JD et al (1987) Age dating and the orbital theory of the ice ages; development of a high-resolution 0 to 300,000-year chronostratigraphy. Quat Res 27:1–29
Metcalfe SES, Davies J, Braisby JD et al (2007) Long and short-term change in the Patzcuaro Basin, central Mexico. Palaeogeogr Palaeoclimatol Palaeoecol 247:272–295
Mix A, Bard E, Schneider R (2001) Environmental processes of the Ice Age: land, oceans, glaciers (EPILOG). Quat Sci Rev 20:627–657
Paillard D, Labeyrie L, Yiou P (1996) Macintosh program performs time-series analysis. Eos Trans AGU 77:379
Peltier WR, Fairbanks RG (2006) Global glacial ice volume and Last Glacial Maximum duration from an extended Barbados sea level record. Quat Sci Rev 25:3322–3337
Peterson LC, Haug GH, Hughen KA, Röhl U (2000) Rapid changes in the hydrologic cycle of the tropical Atlantic during the Last Glacial. Science 290:1947–1951
Rind D, Peteet D (1985) Terrestrial conditions at the last glacial maximum and CLIMAP sea-surface temperature estimates: are they consistent? Quat Res 24:1–22
Rowe HD, Dunbar RB, Mucciarone DA et al (2002) Insolation, moisture balance and climate change on the South American Altiplano since the Last Glacial Maximum. Clim Change 52:175–199
Schmidt MW, Spero HJ, Lea DW (2004) Links between salinity variation in the Caribbean and North Atlantic thermohaline circulation. Nature 428:160–163
Van der Hammen T, Hooghiemstra H (2000) Neogene and Quaternary history of vegetation, climate and plant diversity in Amazonia. Quat Sci Rev 19:725–742
Vaughan HH, Deevey ES, Garrett-Jones SE (1985) Pollen stratigraphy from two cores in the Peten lake district. In: Pohl M (ed) Prehistoric lowland Maya environment and subsistence economy. Harvard University Press, Cambridge
Vazquez GJA, Givnish TJ (1998) Altitudinal gradients in tropical forest composition, structure, and diversity in the Sierra de Manantlán. J Ecol 86:999–1020
Vellinga M, Wood RA (2002) Global climatic impacts of a collapse of the Atlantic Thermohaline circulation. Clim Change 54:251–267
Wang X, Auler AS, Edwards RL et al (2004) Wet periods in northeastern Brazil over the past 210 kyr linked to distant climate anomalies. Nature 432:740–743
Whitmore TJ, Brenner M, Curtis JH et al (1996) Holocene climatic and human influences on lakes of the Yucatan Peninsula, Mexico: an interdisciplinary, palaeolimnological approach. The Holocene 6:273–287
Zhang R (2006) How cold were the tropics and subtropics at the Last Glacial Maximum? Quat Sci Rev 25:1150–1151

Chapter 6
Glacial to Holocene Paleoceanographic and Continental Paleoclimate Reconstructions Based on ODP Site 1233/GeoB 3313 Off Southern Chile

Frank Lamy and Jérome Kaiser

Abstract ODP Site /GeoB 3313 located at the upper continental slope off southern Chile (41°S) is ideally located to study latitudinal shifts of atmospheric and oceanographic circulation off southwestern South America. Extraordinarily high sedimentation-rates allow for high resolution reconstructions and detailed comparisons of various continental climate and paleoceanographic proxy records within the same archive avoiding problems linked to age model uncertainties. We discuss the major paleoclimatic findings of Site 1233/GeoB 3313 in chronological order from the last glacial to the Holocene within the regional context and explore links to tropical and high southern latitude records. During the last glacial, sea surface temperatures (SSTs) off southern Chile were about 4.5°C colder than today and ~6–7°C colder than during the early Holocene maximum. Deglacial warming started at ~18.8 kyr BP with a ~2-kyr-long increase of nearly 5°C and was followed by relatively stable SSTs until the beginning of a second warming step of ~2°C during the early halve of the Northern Hemisphere Younger Dryas cold period. Maximum warm conditions in the early Holocene (~12–9 kyr BP) were followed by a gradual decline towards modern SSTs in the Late Holocene. The paleoceanographic changes and related regional continental climate variations since the last glacial are primarily controlled by latitudinal shift of both the oceanographic and the atmospheric circulation systems in the southeast Pacific. In general, they appear to be closely linked to changes in the Southern Ocean and Antarctica.

Keywords Continental paleoclimate · Holocene · Last glacial · Paleoceanography · Southeast Pacific · Termination 1

F. Lamy (✉)
Alfred-Wegener-Institut (AWI) Bremerhaven, 27515, Bremerhaven, Germany,
e-mail: frank.lamy@awi.de

F. Vimeux et al. (eds.), *Past Climate Variability in South America and Surrounding Regions*, Developments in Paleoenvironmental Research 14,
DOI 10.1007/978-90-481-2672-9_6,

6.1 Introduction

The Chilean continental margin provides a key region for studying natural variability of globally important atmospheric and oceanic circulation members of the Southern Hemisphere since the last glacial maximum and beyond. These primarily include the Antarctic Circumpolar Current (ACC) approaching South America around 40–45°S and flowing then northward along the continental margin as the Peru-Chile (PCC) or Humboldt Current and the Southern Westerly Wind belt (SWW) (Fig. 6.1). Past changes in the strength and latitudinal position of the ACC and SWW are supposed to play a major role in explaining global climate changes for example through their impact on atmospheric CO_2 contents on a large variety

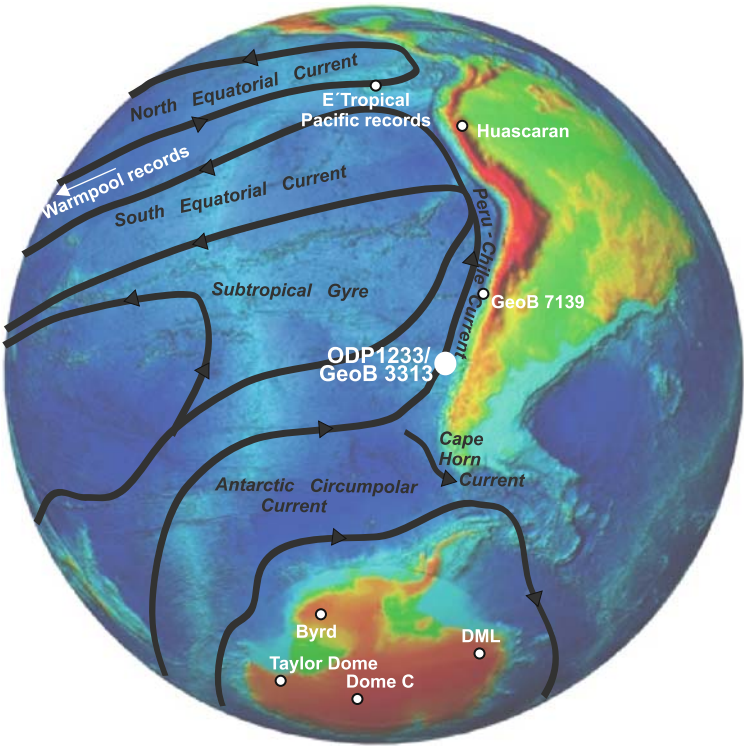

Fig. 6.1 Map of the Pacific and adjacent areas showing major surface currents (after Tomczak and Godfrey (2003)) and the location of marine sediment cores (several cores from the Indo-Pacific warmpool (Stott et al. 2004; Visser et al. 2003); TR163-19 and V21-30 from the eastern tropical Pacific (Koutavas et al. 2002; Lea et al. 2006); GeoB 7139 off north-central Chile (De Pol-Holz et al. 2006); ODP 1233/GeoB 3313 off southern Chile; Antarctic ice-cores (Byrd (Blunier and Brook 2001); Dome C (EPICA Community Members 2004); Dronning Maud Land (DML) (EPICA Community Members 2006); Taylor Dome (Steig et al. 1998)), and the Andean ice-core Huascaran (Thompson et al. 1995) discussed in the paper

of time-scales ranging from decadal to orbital scale (e.g., Toggweiler et al. 2006; Yin 2005).

Compared to other regions of the Southern Hemisphere, marine sediments along the continental margin off Chile have been relatively thoroughly studied after a number of international research cruises during the last decade (e.g., RV SONNE cruises 102 and 156; RV MARION DUFRESNE cruise "Pachiderme" and Ocean Drilling Project (ODP) Leg 202). The presently existing network of sediment cores along the Chilean margin yielded important contributions to improve our understanding of Late Quaternary terrestrial climate changes in Chile (e.g., Hebbeln et al. 2007; Lamy et al. 2001; Lamy et al. 1998b; Lamy et al. 1999; Stuut and Lamy 2004) and the paleoceanography of the adjacent PCC (e.g., Hebbeln et al. 2002; Kim et al. 2002; Mohtadi and Hebbeln 2004). These findings are summarized in two recent review articles (Marchant et al. 2007; Stuut et al. 2006).

Here, we focus on results based on ODP Site 1233 (and site survey core GeoB 3313-1) located at the upper continental slope off southern Chile (41°S) (Fig. 6.1). This site received particular interest because the ~70-kyr-old sequence has been recovered continuously with the Advanced Piston Coring System and extends over ~135 m composite core depth, resulting in unprecedented high sedimentation rates for the South Pacific. The site is ideally located to compare past variations of both surface and deep ocean water masses to high southern latitudes (e.g., Antarctic ice-cores) (Fig. 6.1). Modern SST gradients within the northernmost ACC are very large and intimately linked to the northern margin of the SWW, making this region very sensitive to latitudinal shifts of atmospheric and oceanographic circulation. Furthermore, Site 1233 is located close to the southern Chilean coast (~40 km) and close to the northwestern margin of the glacial Patagonian Ice Sheet (PIS), which occupied a large area of southernmost South America during the last glacial (Fig. 6.2). Thus, this unique location allows detailed comparison of various continental climate and paleoceanographic proxy records within the same archive and therefore avoids problems linked to age model uncertainties. A number of different proxy records from ODP Site 1233 have been published within the past years including alkenone and radiolarian-based sea-surface temperature reconstructions (Kaiser et al. 2007; Kaiser et al. 2005; Lamy et al. 2007; Lamy et al. 2004; Pisias et al. 2006), terrestrial sediment input and pollen-based continental climate studies (Heusser et al. 2006; Kaiser et al. 2007; Lamy et al. 2004; Pisias et al. 2006), and nitrogen isotope analyses (Martinez et al. 2006). The major findings of these studies are summarised in this review article.

6.2 Regional Setting

Site 1233 and gravity core GeoB 3313-1 (41°00′S; 74°27′W) are both located 38 km offshore at 838 m water depth in a small forearc basin on the upper continental slope off Southern Chile (Fig. 6.2) (Mix et al. 2003). The area is characterized by a 30–60 km wide shelf, which becomes significantly wider south of 42°S in the Chilean fjord region (Scholl et al. 1970). The upper continental slope is moderately

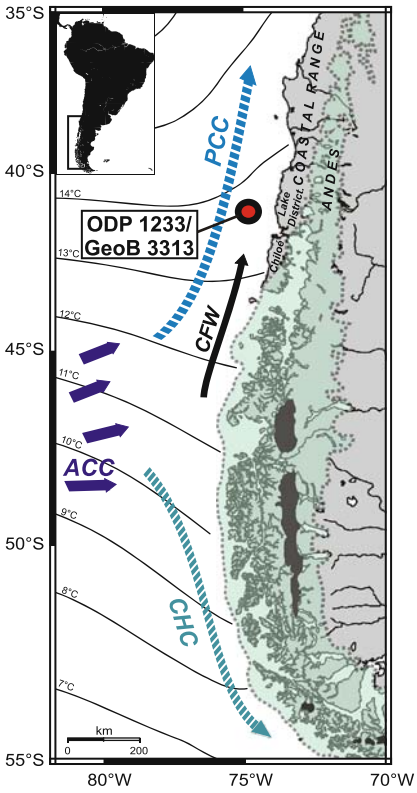

Fig. 6.2 More detailed location of ODP Site 1233/GeoB 3313 off Southern Chile. *Full lines* indicate the modern annual mean SST distribution (data from the NOAA-CIRES Climate Diagnostics Center; http://www.cdc.noaa.gov/index.html) together with a simplified view of the major current systems (PCC=Peru-Chile Current; ACC=Antarctic Circumpolar Current; CHC=Cape Horn Current) and the modern mean position of the Southern Westerly Winds (SWW). Further shown are the location of presently existing Andean icefields (*black areas*) and the limits of the Patagonian Ice Sheet (PIS) during the Last Glacial Maximum as derived from field evidences (*dotted line*)

inclined. Thick sheet-flow turbidites bury the Peru-Chile trench as a bathymetric feature in this region, while turbidity currents are more channelized on the upper slope (Thornburg and Kulm 1987a). Site 1233 is located away from these pathways of major turbidity currents.

The site is located within the northernmost boundary of the Antarctic Circumpolar Current (ACC) at the origin of the Peru-Chile Current (PCC) (Fig. 6.2). The ACC brings cold, relatively fresh, nutrient-rich, Subantarctic Surface Water originating from the region north of the Subantarctic Front. At ~43°S, the ACC splits into the PCC flowing northward and the Cape-Horn Current (CHC) turning towards the south (Strub et al. 1998; Tomczak and Godfrey 2003). The mean annual SST at the coring site is ~14°C and varies between ~11°C in winter and ~16°C in summer, i.e. a seasonal amplitude of ~5°C. Linked to the northern boundary of the ACC, steep latitudinal SST gradients occur just southward of Site 1233, whereas further north the isotherms run more longitudinally marking the cold water advection by the PCC and, to a lesser extent, the effects of increasing coastal upwelling towards the central and northern Chilean margin (Fig. 6.2) (Strub et al. 1998; Tomczak and Godfrey 2003). There, cold waters (11–14°C) coming from the equatorial latitudes

through the Gunther Undercurrent (GUC) are brought to the surface by upwelling. Five main upwelling cells determined by the topography are presently observed off central and northern Chile, at ∼23°, 27°, 30° and 35°–38°S (Strub et al., 1998).

The steepest SST gradient within the ACC is related to the main atmospheric circulation member of the Southern Hemisphere, the SWW (Streten and Zillman 1984). This intense and powerful circulation, annually centered around 50°S, results from the strong thermal gradient and atmospheric pressure difference between cold air masses over Antarctica and the warmer air and water masses in the subtropical regions (Hobbs et al. 1998). In southernmost South America, the SWW and associated storm tracks bring heavy rainfalls, e.g. an annual mean greater than 2000 mm in Puerto Montt (41°S), and prevent upwelling south of 42°S (Strub et al. 1998; Tomczak and Godfrey 2003). Trenberth (1991) has described the modern seasonal fluctuation of the storm tracks associated to the SWW. In summer, the storm track activity can be as strong as in winter, but is located slightly equatorward of its winter position, and is concentrated in a tight band centered around 49–50°S. In winter, storm track activity extends over a broader range of latitudes and is centered ∼2° poleward. The strong SST gradients associated with the ACC are shifted of ∼5° in latitude northward from their summer position.

The proximity of Site 1233 (GeoB 3313) to the Chilean coast allows following changes in the amount and composition of the terrigenous sediment input in response to rainfall changes and variations in the extent of inland glaciation (Fig. 6.2). The modern climate conditions around 41°S are characterized by a humid temperate climate with year round precipitation peaking in austral winter (Miller 1976). The area lies within the transition zone of the summer dry Mediterranean climate north of 37°S and year round humid conditions with heavy precipitation south of 42°S. Rainfall originates from the frontal passages of the SWW and increases strongly to the south making the region very sensitive to latitudinal shifts of the wind belt. Due to the orographic rising of moist Pacific air-masses, rainfall in the Andes is significantly higher than in low elevation areas.

Interannual rainfall variability is strongly linked to the El Niño-Southern Oscillation (ENSO) phenomena and related changes in the strength and position of the Subropical High Pressure cell (STH) (Montecinos and Aceituno 2003; Ruttlant and Fuenzalida 1991). During La Niña events, the STH is consistently strong throughout the year. The storm tracks linked to the SWW remain south of 45°S reducing rainfall in the mid-latitudes. Conversely, the STH is weakened during an El Niño event, allowing an equatorward shift of the SWW and a greater cyclonic activity in the Chilean mid-latitudes. Based on monthly data from weather stations in Chile (30°–41°S) for the 1958–1999 period, Montecinos and Aceituno (2003) have studied the seasonality of ENSO-related rainfall variability. During El Niño events, the precipitations are above the average between 30°–38°S in austral winter and spring. A rainfall deficit is observed from 38° to 41°S in summer, when El Niño development is maximum. Opposite precipitation anomalies characterize La Niña events.

Three main physiographic features (the Coastal Range, the Chilean Longitudinal Valley, and the Andes) characterize the continental hinterland around 41°S

(Fig. 6.2). The Coastal Range with elevations generally below 500 m is dominated by primarily low-grade metamorphic rocks (Thornburg and Kulm 1987b). The Central Valley is filled with up to 4,000 m thick alluvial sediments. The Andes reach elevations of 2,000–3,000 m. The lower parts mainly consist of iron-poor plutonic basement rocks, while the high Andes are dominated by iron-rich basaltic to andesitic volcanics resulting from Pliocene to recent volcanic activity (Thornburg and Kulm 1987b). Various small rivers drain the Coastal Range within the study area. Larger rivers originating in the Andes flow into the ocean north and south of the core position in the region of Puerto Montt. Therefore, terrigenous sediments on the continental slope can be expected to contain both a Coastal Range and Andean source rock signal.

While the modern Patagonian ice-fields are restricted to southernmost Chile (between ~47 and 52°S), during the Last Glacial Maximum (Last Glacial Maximum) the Patagonian ice-sheet (PIS) extended much further north and reached the island of Chiloé directly south of Site 1233 (Fig. 6.2). Therefore, the site is located in an ideal position to monitor PIS extent variations by recording compositional changes in the regional terrigenous sediment input to the continental margin (Kaiser et al. 2007; Lamy et al. 2004). Glacial erosion processes strongly enhanced the glaciofluvial sediment flux from Fe-rich basaltic volcanics in the Andes during the last glacial. Ice-sheet advances provided more Fe-rich material, being subsequently transported to the continental margin by rivers. Another important regional hydrographic feature off southern Chile that can be used to reconstruct past changes in continental freshwater input is the low-salinity surface water tongue originating from the high fresh water supply to the Chilean fjord region (Strub et al. 1998). This low-salinity Chilean Fjord Water mass (CFW) flows northward within 150–200 km off the coast (Fig. 6.2).

6.3 Material and Methods

Site 1233 was drilled during ODP Leg 202 and gravity core GeoB 3313-1 during German R/V Sonne cruise 102 (Hebbeln and Shipboard Scientists 1995; Mix et al. 2003). Five Advanced Piston Corer holes were drilled at Site 1233 to ensure a complete stratigraphic overlap between cores from different holes. Detailed comparisons between high-resolution core logging data performed shipboard demonstrated that the entire sedimentary sequence to 116.4 m below surface (mbsf) was recovered. Based on these data, a composite sequence (the so-called splice) was constructed representing 135.65 m composite depth (mcd). The complete recovered sequence at Site 1233 covers the past ~ 70 kyr whereas ~8-m-long gravity core GeoB 3313-1 extends only back to ~8 kyr BP. We are here discussing data since ~25 kyr BP (thus including the global Last Glacial Maximum (19–23 kyr BP (Mix et al. 2001)), Termination 1, and the Holocene). This interval represents the uppermost ~40 mcd at Site 1233.

Sediments are dominated by terrigenous components (clay and silty clay) with varying but generally small amounts of calcareous and siliceous components.

Respectively, calcium carbonate concentrations and organic carbon contents range from 1 to 11 wt% (average = 5.4 wt%) and from 0.4 to 2.5 wt% (average = 0.9 wt%) (Martinez et al. 2006; Mix et al. 2003). Organic carbon contents are substantially lower between 30 and 40 mcd (0.4–1 wt%) in comparison to the top of the core (up to 2.5 wt%). A number of different studies have been done on Site 1233 including primarily alkenone sea surface temperature (SST) giving an approximation of the annual mean temperature between 0–10 m water depth (e.g., Müller et al. 1998), paleosalinity and paleoproductivity reconstructions as well as terrigenous sediment input parameters (XRF scans, clay mineralogy, grain-sizes) and pollen. Details on the methods can be found in the original publications (Heusser et al. 2006; Kaiser et al. 2007; Kaiser et al. 2005; Lamy et al. 2001; Lamy et al. 2007; Lamy et al. 2004; Lamy et al. 2002; Martinez et al. 2006; Pisias et al. 2006).

The age models for both the younger part of the Site 1233 sequence and gravity core GeoB 3313-1 are based on radiocarbon dating. Core GeoB 3313-1 has been dated by 7 ^{14}C accelerator mass spectrometry (AMS) dates reaching back to ~8 kyr BP (Lamy et al. 2001). This age model has been transferred to the uppermost ~9 mcd of the Site 1233 sequence using magnetic susceptibility and Ca content records (Kaiser et al. 2005). Below, 18 further ^{14}C-AMS dates provide a reliable age model down to 25 kyr BP (Lamy et al. 2007). All radiocarbon ages have been converted to calendar years assuming a constant reservoir age of 400 years (for a detailed discussion see Lamy et al. (2004, 2007)), primarily using the INTCAL04 calibration curve (Reimer et al. 2004). An exception is the interval between ~12,500 to ~14,500 ^{14}C years BP where the INTCAL04 calibration curve is poorly constrained and radiocarbon data from the Cariaco basin (Hughen et al. 2004) and the Northwest Pacific (Sarnthein et al. 2006) suggest the presence of a radiocarbon plateau lasting from ~12,900~ to ~13,300 ^{14}C years BP (~15.7–~17 kyr BP). Therefore, we applied in this interval the CalPal_SFCP_2005 (www.calpal.de) calibration curve which is primarily based on the Cariaco basin record (Hughen et al. 2004) (for details refer to Lamy et al. (2007)). The resulting mean sedimentation rates range between ~1.4 m/kyr in the Holocene to an average of ~2.2 m/kyr during the glacial. These high sedimentation rates are consistent with strong fluvial discharge in response to heavy continental rainfall in southern Chile during the Holocene (Lamy et al. 2001). During the last glacial, the continental hinterland of Site 1233 was extensively glaciated as the PIS advanced towards the north (Denton et al. 1999b) explaining even higher terrestrial input through glacial erosion processes (Lamy et al. 2004).

6.4 Results and Discussion

In the following we discuss the major findings of Site 1233/Geo 3313 in chronological order from the last glacial to the Holocene. In each chapter, we first summarize and review the evidences based on our site, discuss them within the regional framework including other marine records from the Chilean margin and terrestrial data-sets (land-ocean correlations), and finally relate these findings to tropical and high southern latitude records in order to derive larger-scale implications and

pattern. Radiocarbon ages of the other records shown and discussed in this chapter have been calibrated in the same way as our Site 1233 records.

6.4.1 Glacial

6.4.1.1 Regional Aspects

During the last glacial, SSTs off southern Chile were about 4.5°C colder than modern SSTs and ~6–7°C colder than during the early Holocene maximum (Fig. 6.3).The record shows a pronounced millennial-scale variability of 2–3°C over the glacial interval (~45–19 kyr BP) (Kaiser et al. 2005; Lamy et al. 2004). The global Last Glacial Maximum is not well defined in the record. Instead, we observe two millennial-scale SST minima during this interval, one close to 22.5 kyr BP, and a second at ~19 kyr BP directly before the initiation of the deglacial warming (Fig. 6.3) (Lamy et al. 2007). A pollen assemblages study on Site 1233 sediments suggests a significant expansion of subantarctic vegetation type during the last glacial (Fig. 6.4) (Heusser et al., 2006). Based on similar pollen reconstruction onshore, Heusser and Heusser (2006) deduced that summer air temperature (using transfer functions) was around 8–9°C at 41°S during the last glacial, in close agreement with the SST results.

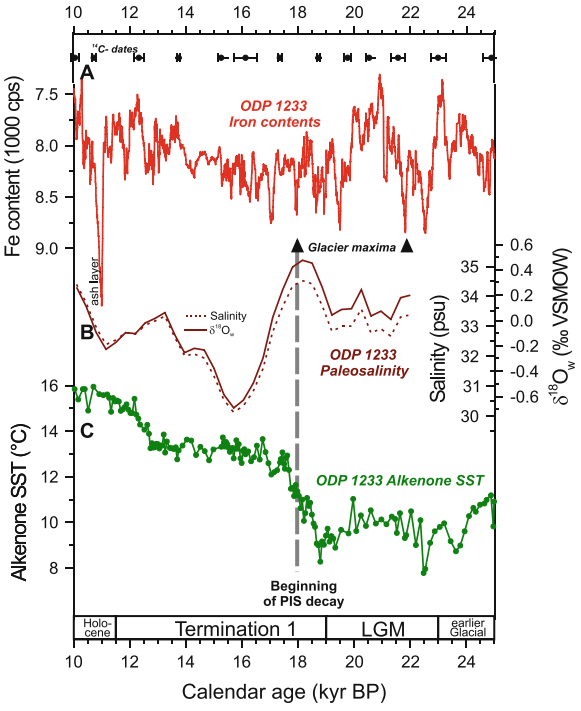

Fig. 6.3 Site 1233 SST record compared to proxy data taken for changes in the extent of the PIS (after Kaiser et al. 2007; Lamy et al. 2004). (A) Iron record (inverted scale), high values indicate ice sheet advances with location of major glacier maxima as dated on land (Denton et al. 1999b; Kaplan et al. 2004). (B) Alkenone SST record (Lamy et al. 2007). (C) Paleosalinity data, *dashed line* indicates beginning of rapid melting after the final PIS maxima at ~17.8 kyr BP

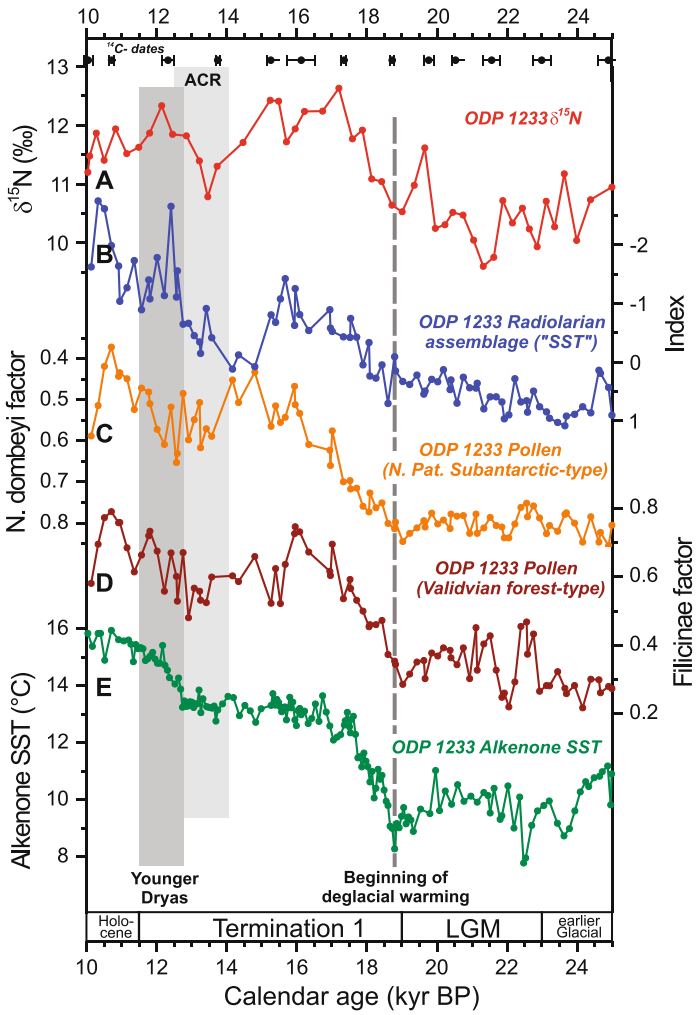

Fig. 6.4 Different paleoenvironmental records from Site 1233 over T1 and the Last Glacial Maximum plotted on the Lamy et al. (2007) timescale. (A) $\delta^{15}N$ record (Martinez et al. 2006). (B) First canonical variates from radiolarian multivariate data sets used as a proxy for SSTs (Pisias et al. 2006). (C) North Patagonian Subantarctic-type pollen (Heusser et al. 2006). (D) Validvian forest-type pollen (Heusser et al. 2006). (E) Alkenone SST record (Lamy et al. 2007)

During the SST minima, the relative abundance of iron in the sediment is increased (Fig. 6.3). However, iron maxima occur several hundred years later than SST minima. These iron maxima have been related to advances of the PIS during the last glacial and the delay interpreted as a lagged response of ice-sheet fluctuations to SST changes in the SE-Pacific (Kaiser et al. 2007; Lamy et al. 2004). Though this pattern is clearer during Marine Isotope Stage 3, a major advance at the eastern

flank of the PIS at ~21.8 kyr BP (Kaplan et al. 2004) fits well to the iron record (Fig. 6.3) (see also 6.4.2). In a recent modeling study of the changes in the Patagonian ice-sheet extent during the Last Glacial Maximum, (Hulton et al. 2002) have shown a good agreement between modelled ice extent and empirical evidence by applying a temperature decrease of 6°C relative to present day which is consistent with our alkenone SST record.

The relative glacial SST cooling observed at Site 1233 appears to be a regional feature at least northward up to 33°S. Glacial SSTs were likewise about 6°C cooler than during the Holocene maximum at ~35°S (Romero et al. 2006) and ~33°S (Kim et al. 2002), whereas a SST record at ~30°S suggests a cooling of only ~3.5°C (De Pol-Holz et al. 2006). However, compared to the modern SST distribution, gradients appear to be enhanced in the southern Peru-Chile current between ~41°S and ~33°S consistent with a northward movement of at least 5° in latitude of the present zone of high SST gradients (Fig. 6.2) linked to the northern margin of the ACC (Kaiser et al. 2005). This is in agreement with modeling results suggesting stronger SST gradients in the mid-latitudes at the Last Glacial Maximum (Shin et al. 2003). This enhanced northward influence of the ACC up to ~33°S during the Last Glacial Maximum has also been suggested in paleoproductivity reconstructions along the Chilean coast as it brings the nutrient source closer to the core site resulting in higher biological productivity (Hebbeln et al. 2002; Mohtadi and Hebbeln 2004). A similar conclusion has been derived from the $\delta^{15}N$ record at Site 1233 (Fig. 6.4) suggesting that the interplay between nutrient demand in the Subantarcitic Zone and latitudinal shifts of hydrologic fronts controlled both the concentrations and the isotopic signature of the remaining nitrate delivered to the southern Chilean margin (Martinez et al. 2006). However, Thorium-230 normalized biogenic flux calculations based on cores off northern Chile suggest regionally varying Last Glacial Maximum paleoproductivity that was higher at ~27°S (Dezileau et al. 2004) and comparable to the Holocene at ~30°S (De Pol-Holz et al. 2007). These different results may be related to the enhanced influence of upwelling in the north that could introduce low latitude climate signals through upwelling of water masses of the GUC as suggested e.g. by the $\delta^{15}N$ record at Site 1234 (36°S) (Robinson et al. 2007).

Extensive analyses of terrigenous sediment input changes along the central and northern Chilean margin suggested a ~5° latitude equatorward shift of the present-day precipitation gradient resulting in semiarid winter-rain climates at the present southern margin of the Atacama Desert (~27°S) (Lamy et al. 1998a; Lamy et al. 1999; Lamy et al. 2000; Stuut and Lamy 2004). This northward shift is consistent with terrestrial climate reconstructions (e.g. review by Heusser (2003)) and substantially enhanced the glacial supply of terrigenous material to the ocean in particular off north-central Chile where the terrigenous glacial accumulation doubled (Hebbeln et al. 2007). Taken together, the paleoceanographic and continental paleoclimate reconstructions suggest a ~5° latitude northward shift of both the oceanographic and the atmospheric circulation systems (northern margin of the ACC and SWW).

6.4.1.2 Link to the High Latitudes

In previous works, we showed that the complete ~70-kyr-long alkenone SST record at Site 1233 closely follows millennial-scale temperature fluctuations as observed in Antarctic ice cores (Kaiser et al. 2005; Lamy et al. 2004). There are however comparatively large absolute dating uncertainties of marine sediments in the earlier part of the last glacial due to increasing uncertainties in radiocarbon dating and calendar year conversion, whereas large amplitude methane fluctuations allow a detailed inter-correlation of Greenland and Antarctic ice-cores (Blunier and Brook 2001; EPICA Community Members 2006). Nevertheless, this methane-based correlation reveals ambiguities over the interval of the Last Glacial Maximum and beginning of Termination 1 where radiocarbon dating errors are relatively small. Consequently, the comparison of our SST data-set to Antarctic ice-core records reveals some offsets around the Last Glacial Maximum (Fig. 6.5). For example, the SST minimum close to 22.5 kyr BP may well correspond to the temperature minimum at ~21.5 kyr BP in the Byrd record (Pacific Sector of Antarctica, Fig. 6.1). As well, the new record from Dronning Maund Land (EPICA Community Members 2006) (DML; Atlantic Sector, Fig. 6.1) shows a millennial-scale warming between ~23.5 and 24.5 kyr BP (Antarctic Isotope Maximum 2) that occurs ~500 years later than a warming shown in the SST data (see 6.4.2. and Lamy et al. (2007) for further discussion of the delay in the Antarctic records).

6.4.1.3 Link to the Tropics

Based on coupled ocean-atmosphere models, Shin et al. (2003) have proposed that the upper ocean circulation in the southern mid- and high-latitudes plays a key role in explaining tropical cooling at the Last Glacial Maximum. This connection could be explained by a transmission of South Pacific SST cooling through the surface ocean via the Eastern Boundary Current system (PCC) and through intermediate water masses towards the tropics (Clark et al. 2004). Such a link has been proposed based on Mg/Ca SST reconstruction near the equator (Lea et al. 2006; Lea et al. 2000) and on the presence of high southern latitude foraminifera species even north of the equator suggesting an intensification of the Peru-Chile Current during the Last Glacial Maximum (e.g., Feldberg and Mix 2003; Martinez et al. 2003).

A direct comparison of our Site 1233 SST record to tropical SST reconstruction is difficult as the records have very different time resolutions and age models. However, some similarities are apparent in particular regarding the comparison to the high resolution eastern tropical Pacific Mg/Ca SST record that reveals some similar features also on millennial time-scales (Lea et al. 2006) (Fig. 6.7). Kaiser et al. (2005) performed a time-slice analysis in order to compare SST gradients along the PCC from 41°S (Site 1233) to just north of the equator (2°N). During the Last Glacial Maximum, the overall mid-latitude-to-equator gradient (2°N–41°S) was ~3°C higher than today. This increase in meridional SST gradients during the Last Glacial Maximum is mainly derived from a relatively strong cooling in the southern and central part of the PCC (41–17°S), with particularly enhanced gradients

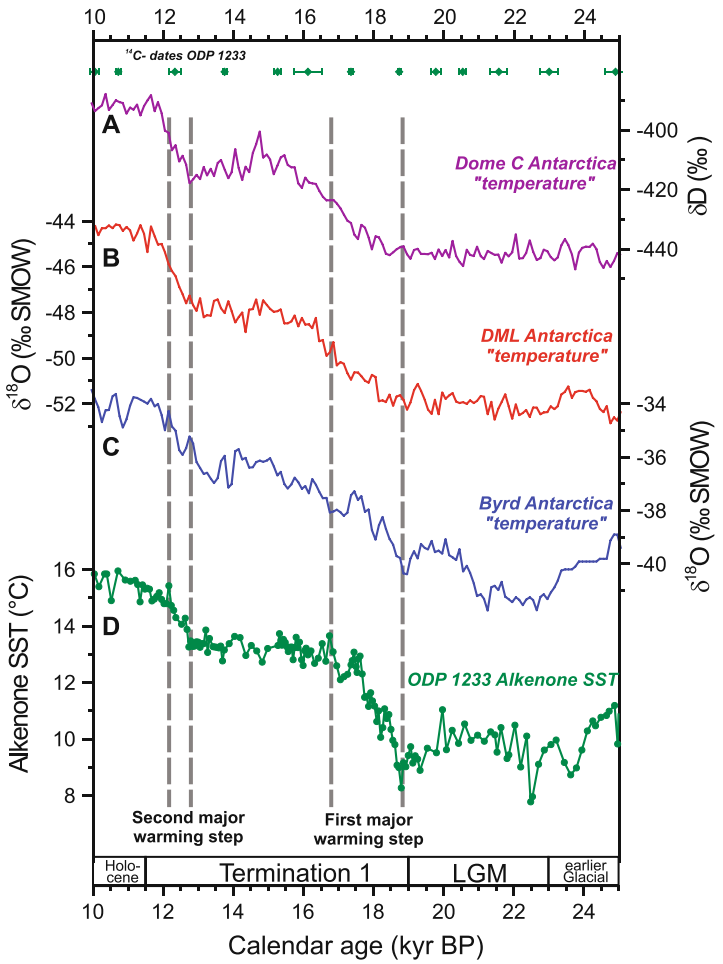

Fig. 6.5 Site 1233 SST record compared to different Antarctic temperature proxy records over the Last Glacial Maximum and T1. (A) Deuterium record from the Dome C ice-core (EPICA Community Members, 2004) (continental site in eastern Antarctica). (B) Oxygen isotope record from the Dronning Maud Land (DML) ice-core (EPICA Community Members, 2006) (coastal site, Atlantic sector). (C) Oxygen isotope record from the Byrd ice-core (Blunier and Brook 2001) (coastal site, Pacific sector). All ice-core records are plotted on the GICC05 displaying 100-years averages. (D) Alkenone SST record from Site 1233 with radiocarbon datings (*top* of panel A)

in the southernmost part between ~33°S and 41°S consistent with a ACC/SWW northward shift of ~5° in latitude in comparison to the present day (see above). In addition, a northward displacement of the SWW (or their northern boundary), as implied by Kaiser et al. (2005) results, would be in agreement with the proposed northward shift of the eastern Pacific STH at the Last Glacial Maximum (Andreasen and Ravelo 1997; Mohtadi and Hebbeln 2004).

6.4.2 Termination 1

The termination of the last ice age (Termination 1; T1) is the last major climate transition of the Earthś recent geological history and is thus crucial for our understanding of modern climate processes and the validation of climate models. Though T1 is very well studied involving numerous proxy records from both marine and terrestrial archives (e.g., Alley and Clark 1999; Clark et al. 1999; Clark et al. 2004; Rinterknecht et al. 2006) as well as modelling studies (e.g., Knorr and Lohmann 2003; Weaver et al. 2003), there are still a number of open questions regarding for example the exact timing and the mechanisms involved in the initiation of deglaciation and the subsequent interhemispheric pattern of the warming. The present picture of climate pattern during T1 is thus largely focussed on high latitude records in particular from Greenland and Antarctic ice-cores that have been synchronised by correlating globally recordable methane fluctuations (e.g., Blunier and Brook 2001; EPICA Community Members 2006; Morgan et al. 2002). However, this correlation reveals ambiguities over the interval of the early deglacial warming in the Southern Hemisphere making the analysis of interhemispheric climate pattern over this important interval more difficult. Site 1233 improves our understanding of the sequence of events over the last termination as it provides exceptional time-resolution and dating accuracy over T1 (Lamy et al. 2007).

6.4.2.1 Regional Aspects

The alkenone SST record of Site 1233 reveals a beginning of deglacial warming at ∼18.8 kyr BP with a ∼2-kyr-long increase of nearly 5°C until ∼16.7 kyr BP (Figs. 6.4and 6.5). Thereafter, temperatures remain comparatively stable until the beginning of a second warming step of ∼2°C between ∼12.7 and ∼12.1 kyr BP. This pattern is consistent with independent SST estimates from Site 1233 based on radiolarian assemblages (Pisias et al. 2006) (Fig. 6.4), that show however a cooling event between ∼13 and 15 kyr BP. Furthermore, the first warming step coincides with a major shift in the $\delta^{15}N$ record from Site 1233 (Fig. 6.4) that has been explained by a southward shift of fronts in the Southern Ocean (Martinez et al. 2006).

Melting of the PIS onshore started significantly later than the initial SST rise as documented by two well-dated glacier maxima in the Chilean Lake District between ∼18.0 to 17.7 kyr B.P. (Denton et al. 1999a) that occurred while SSTs were already increasing rapidly for ∼1,000 years (Fig. 6.3). Additional support for a delayed ice sheet response comes from our reconstruction of paleosalinity over T1 (Lamy et al. 2004) (Fig. 6.3). The substantial decrease in salinities from ∼17.8 to 15.8 kyr B.P. suggests that the PIS was wasting rapidly after the last glacier maxima inferred from terrestrial studies (Denton et al. 1999b). During this period, Fe contents remain high and most likely reflect strong fluvial erosion of the rapidly exposing glacial deposits. Thereafter Fe contents decrease towards the Holocene when they become rainfall-controlled (Lamy et al. 2001). These observations suggest that a substantial time-lag occurs between climate forcing and the PIS response – assuming that the atmospheric system responds roughly synchronously to changes in SSTs which is

reasonable for the extremely maritime climate conditions in southern Chile. The changing time-lag along the record suggests a possible relationship to ice sheet size (see for further details Lamy et al., 2004and Kaiser et al., 2007). The largest lag is observed for the decay of ice after its maximum extent before the deglaciation (Lamy et al. 2004).

Though the general magnitude of ~6–7°C SST warming over T1 is similar to results obtained from land (e.g., reviews by Denton et al. 1999a; Heusser and Heusser 2006), there are differences in the timing between the terrestrial datasets and our marine record. Pollen records from the Lake District and Chiloe Island (Taiquemo) suggest a beginning of warming at ~17.5 kyr BP, i.e. more than 1,000 years later than the initial SST warming. We originally interpreted this lag as being related to the response time of the PIS and the surrounding ecosystems (Lamy et al. 2004). However, there are now pollen records available from Site 1233 (Heusser et al. 2006) that suggest that the beginning of deglacial changes in the pollen records was basically in phase with the initial SST rise (Fig. 6.4). These new data show that pollen characteristic for the North Patagonian Subantarctic vegetation types substantially decreased after ~19 kyr. whereas Valdivian Forest type pollen (primarily ferns) increase (Fig. 6.4). The reasons for the offset between the marine and continental pollen records remain unclear. One possibility is that reservoir ages at the beginning of T1 were substantially higher than present day values that we assumed for Site 1233. As discussed in detail in our previous publications (Kaiser et al. 2005; Lamy et al. 2004), we assume no regional deviation from the global reservoir effect of ~400 years because of the presence of an early Holocene volcanic ash layer at Site 1233 (that has been likewise dated on land) and the position of our site significantly south of the Chilean upwelling zone (Strub et al. 1998) and north of the southern polar front where higher reservoir ages may be expected. Furthermore, our paleosalinity reconstruction fits very well to the land-based evidence for the timing of the rapid PIS decay after ~17.8 kyr BP, that can be taken as a further evidence that the Site 1233 age-model is correct (Fig. 6.3). On the other hand, local conditions may be over-represented at terrestrial sites close to the margins of the PIS (at least before the rapid decay of the ice-sheet) or the records may be incomplete whereas the marine pollen record is reflecting a more integrated regional signal including areas that are not directly affected by the presence of the large ice-sheet.

Another important issue regarding the comparison of our marine to regional terrestrial records are the climate pattern during later Termination 1. Pollen records in the Lake District and on Chiloé Island have been interpreted in terms of a cooling during the Northern Hemisphere Younger Dryas (YD) (e.g., Denton et al. 1999a; Moreno et al. 2001) whereas the alkenone and radiolaria-based SST reconstructions from Site 1233 reveal a clear warming during the YD (Fig. 6.3). However, it has been recently suggested that the deglacial cold reversal in NW Patagonia started earlier (at ~14.7–13.4 kyr BP.), and that the YD interval is rather characterized by fire disturbance (Hajdas et al. 2003; Moreno 2004) that may not necessarily imply cooling. In addition, other paleoenvironmental reconstructions in southern Chile (~40°S to 48°S) based on pollen, glacial morphology, and beetle assemblages did not find evidence of a cooling during the YD epoch either (Ashworth and Hoganson 1993;

Bennett et al. 2000; Glasser et al. 2004). In the lower latitudes, two SST records located at ~35°S (Romero et al. 2006) and ~30°S (De Pol-Holz et al. 2006) present a very similar pattern to ODP Site 1233 with a 1–2°C warming during the YD. Only one SST record at ~33°S shows a cooling over this time-interval (Kim et al. 2002).

The different records from Site 1233 partly suggest a cold reversal between ~14.5 and 12.5 kyr BP, synchronously to the Antarctic Cold Reversal (ACR; 14–12.5 kyr BP; Jouzel et al. 1995). Whereas the alkenone-based SST record shows rather a plateau, the radiolarian assemblage and the pollen records imply a cooling. The $\delta^{15}N$ record suggests a slight northward shift of the Southern Ocean fronts (Fig. 6.4). Recent studies based on glaciers fluctuations in southernmost Chile (46–55°S) evidence a glacial re-advance during this time-interval (see for a review Sugden et al. 2005). Taken together, these results imply a slight northward movement of the atmospheric and oceanographic systems in the southeast Pacific during the ACR.

6.4.2.2 Link to the High Latitudes

A comparison of our SST record to different Antarctic ice-core records suggests a general correspondence in the major temperature trends, particularly the two-step warming over T1 (Fig. 6.5). As in our SST record, in the Pacific Sector of Antarctica, (Byrd ice-core (Blunier and Brook 2001), deglacial warming initiated shortly after 19 kyr BP whereas the new record from Dronning Maund Land (EPICA Community Members 2006) (DML; Atlantic Sector; Fig. 6.5) shows a ~700 years delayed initiation of deglacial warming. In the Dome C record (EPICA Community Members 2004) (continental site, Fig. 6.5), the initial warming starts at about the same time as in the DML record. In general, the deglacial warming as documented in Antarctic ice-cores is substantially more gradual than observed in our SST record where most of the initial warming occurs over a time-interval of only ~1,200 years (~18.8–17.6 kyr BP).

Millennial-scale temperature changes in Antarctica over the last glacial may be consistently explained by the bipolar seesaw concept that suggests an out-of-phase millennial-scale climate pattern between the Northern and Southern Hemisphere during the last glacial (e.g., Stocker 1998). The concept was later extended by including a time constant that describes the thermal storage effect of the Southern Ocean and explains why glacial Antarctic and Greenland temperatures are not strictly anti-correlated but are rather characterised by a lead-lag relationship (Knutti et al. 2004; Siddall et al. 2006; Stocker and Johnsen 2003). The timing of both the initial and the second warming step (12.7–12.1 kyr BP) in the Site 1233 alkenone SST record suggests that the SST response in the mid-latitude SE-Pacific occurred quasi instantaneous to the starting slowdown of the Atlantic Meridional Overturning Circulation (AMOC) (Fig. 6.6). The conceptual model of Stocker and Johnsen (2003) shows such strict antiphase behaviour for the South Atlantic. However, the occurrence of an "immediate" and high amplitude response in our SST record requires a rapid transfer of the Atlantic signal to the SE-Pacific without involving the thermal inertia of the Southern Ocean that contributed to the substantially more

gradual and partly delayed (in case of the DML and Dome C records) deglacial temperature rise seen in Antarctic ice-cores. The most plausible mechanism for this rapid transfer is a seesaw induced change of the coupled ocean-atmosphere system of the ACC and the SWW as indicated by modelling studies (Timmermann et al. 2005). The SST response to a weakening of the AMOC in these and other model simulations (e.g., Knutti et al. 2004; Schmittner et al. 2002) is however much smaller than the initial warming observed at Site 1233 (Fig. 6.6). Apart from the pronounced regional sensitivity of Site 1233 due to strong regional SST gradients, more global forcings such as changes in CO_2 and atmospheric dust explain an important fraction of the deglacial SST rise in the SE-Pacific (Fig. 6.6). In addition, it has been

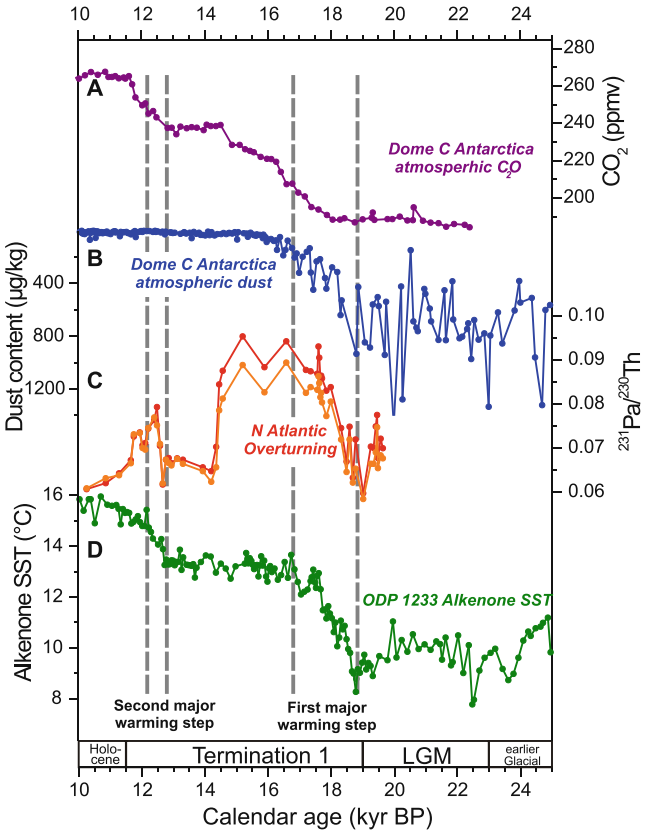

Fig. 6.6 Comparison of Site 1233 SST record to atmospheric dust and CO_2 records based on the Antarctic Dome C ice core and to a North Atlantic record of past changes in the AMOC over T1. (A) CO_2 record from the Dome C ice-core (Monnin et al. 2001) (revised time-scale as in Lamy et al. (2007)). (B) Atmospheric dust content record from the Dome C ice-core (Delmonte et al. 2002) (revised time-scale as in Lamy et al. (2007)). (C) $^{231}Pa/^{230}Th$ record from a subtropical North Atlantic sediment core taken as a proxy for the strength of the AMOC (McManus et al. 2004). (D) Alkenone SST record from Site 1233 (Lamy et al. 2007)

recently suggested that increasing austral-spring insolation combined with sea-ice albedo feedbacks may be responsible for an early SH warming between 19 and 17 kyr BP (Stott et al. 2007)

Assuming that the Site 1233 SST record largely reflects shifts of the coupled ACC/SWW system, the concurrence to atmospheric CO_2 changes over T1 is consistent with the previously suggested important role of such latitudinal shifts in controlling atmospheric CO_2 contents (Ninnemann and Charles 1997; Toggweiler et al. 2006). Based on a general circulation model, Toggweiler et al. (2006) showed that equatorward shifted SWW during the glacial allowed more respired CO_2 to accumulate in the deep ocean. During glacial terminations, the southward moving SWW reduced polar stratification and enhanced upwelling of deepwater masses around Antarctica that would then have released large amounts of the stored CO_2 to the atmosphere (for details see Lamy et al. 2007).

6.4.2.3 Link to the Tropics

The large unknown in most paleoclimate scenarios for Termination 1 is the role of the tropics where in particular tropical Pacific SST changes have large impacts on the hydrological cycle and changes in greenhouse gases (Clark et al. 2004; Palmer and Pearson 2003). An increasing number of high resolution records from the tropics have recently become available (e.g., Lea et al. 2006; Visser et al. 2003). As deglacial warming in some of these records occurred largely in phase with the CO_2 increase as observed in Antarctic ice-cores, they have been interpreted in support for a tropical "trigger" for the deglaciation (Visser et al. 2003). Though a tropical "trigger" (such as changes in ENSO) for the initiation of the last deglaciation can not be strictly excluded, we note that most of the available data could be explained by an initiation in the Northern Hemisphere and associated bipolar seesaw effects (see Lamy et al. 2007 for details). A SST record from the Indo-Pacific Warm Pool shows for example the start of deglacial warming, within dating uncertainties, quasi synchronous with our Southeast Pacific record (Fig. 6.7) but changes are more gradual and the total SST change over T1 is much smaller (Visser et al. 2003). However, very recently Stott et al. (2007) evidenced that during the early deglaciation the deep water originating from the Southern Ocean (the upper Pacific Deep Water) warmed about 1,000 years before the surface water of the western tropical Pacific. Our southeast Pacific two-step warming structure with an intervening "plateau" is visible in the eastern tropical Pacific (Lea et al. 2006) (Fig. 6.7). These similarities may well be explained by a transmission of South Pacific SST warming through the surface ocean via the Eastern Boundary Current system and through intermediate water masses towards the tropics (Clark et al. 2004). In these scenarios, the tropics did not initiate the global warming over T1, but they probably played an important role for a number of positive feedbacks (through affecting e.g. atmospheric water vapour and CO_2 content) finally leading out of the last glacial period.

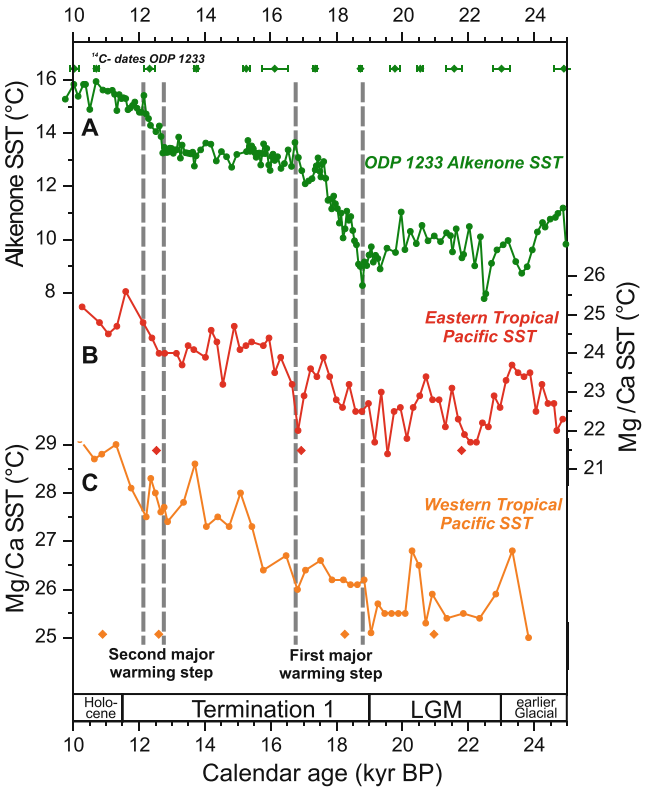

Fig. 6.7 Comparison of Site 1233 SST record to tropical Pacific SST records over T1 (see Fig. 6.1 for site locations). (A) Alkenone SST record from Site 1233 with radiocarbon datings (Lamy et al. 2007). (B) Mg/Ca SST record from the eastern tropical Pacific (Lea et al. 2006) with radiocarbon datings. (C) Mg/Ca SST record from the Indo-Pacific Warm Pool (Visser et al. 2003) with radiocarbon datings

6.4.3 Holocene

6.4.3.1 Regional Aspects

After the second major warming step of T1 from ~12.7 to ~12.1 kyr BP, the alkenone-based SST record from Site 1233 shows maximum warm conditions in the early Holocene (~12–9 kyr BP; Fig. 6.8) (Kaiser et al. 2005). SSTs during this interval were generally between ~15 and 16°C, i.e. ~1–2°C above modern values. Thereafter, temperatures gradually decline reaching the modern SST (~14°C) in the Late Holocene (Fig. 6.8). The early Holocene optimum was not documented in the higher resolution earlier SST record based on core GeoB 3313-1 (Lamy et al. 2002) that only covers the past ~8 kyr (Fig. 6.9). In this record, a secondary middle Holocene warming is observed around 5.5 kyr BP with SSTs generally declining

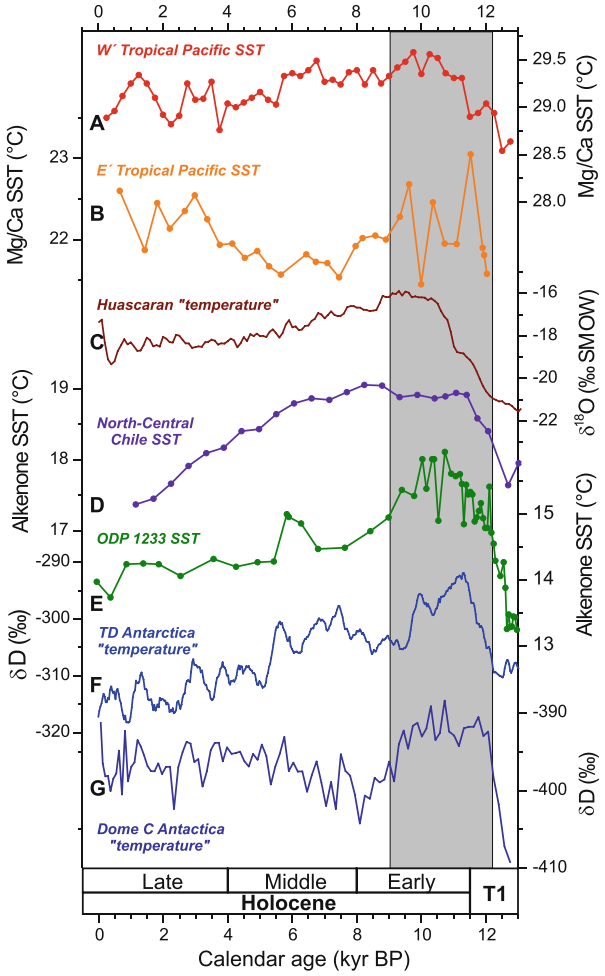

Fig. 6.8 Holocene Site 1233 SST record compared to Antarctic and South American ice core data and (sub)tropical marine data-sets (see Fig. 6.1 for site locations). Gray bar marks early Holocene maximum warm phase as defined at ODP Site 1233 (Kaiser et al. 2005). (A) SST record from the western Pacific Warm Pool (stacked data from several cores as in (Stott et al. 2004)). (B) SST record from the eastern Pacific cold tongue (Koutavas et al. 2002). (C) Huascaran $\delta^{18}O$ record as a proxy for temperature changes in tropical South America (Thompson et al., 1995). (D) SST record from core GeoB 7139-2 off north-central Chile (De Pol-Holz et al. 2006). (E) SST record from ODP Site 1233 (Kaiser et al. 2005; Lamy et al. 2007). (F) δD record from the Taylor Dome ice core as a proxy for western Antarctic temperature (Steig et al. 1998). (G) δD record from the Taylor Dome ice core as a proxy for eastern Antarctic temperature (EPICA Community Members 2004)

afterward towards the late Holocene as in the comparatively low resolution SST record from Site 1233 (Fig. 6.8).

The general middle and late Holocene SST cooling off southern Chile is paralleled by similar trends in continental rainfall and paleosalinity depicted in core

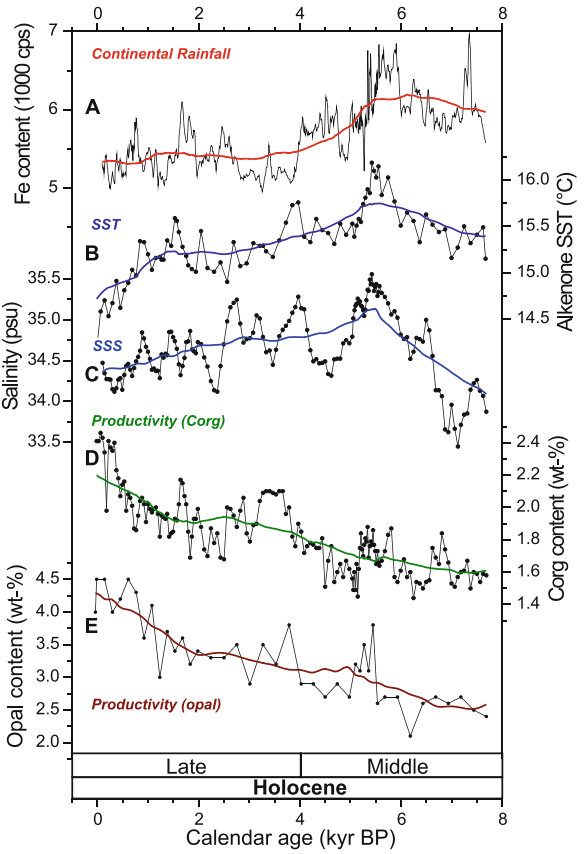

Fig. 6.9 Paleoceanographic and continental paleoclimate records from core GeoB 3313-1 off southern Chile covering the *middle* and late Holocene. *Bold lines* are ~2000-yr moving averages (after Lamy et al. 2002). (A) Iron contents interpreted as a proxy for rainfall and the position of the Southern Westerlies (high iron contents imply increased contribution of iron-rich volcanic Andean source rocks and decreased supply of iron-poor Coastal Range source rocks indicating decreased rainfall (Lamy et al. 2001)) (B) SST record tracing the advection of subpolar water by the ACC. (C) Paleosalinity (SSS) reconstruction (5-point moving average) as a proxy for fresh-water input in the Chilean Fjord region. (D) Corg contents and (E) biogenic opal contents are taken as proxies for paleoproductivity

GeoB 3313-1 (Lamy et al. 2001) (Fig. 6.9). These data show generally drier conditions during the early and middle Holocene and increased precipitation during the late Holocene consistent with regional terrestrial records from Chiloé Island (e.g., Abarzúa et al. 2004) and central Chile (e.g., Jenny et al. 2002; Villagrán and Varela 1990), as well as marine records located further north (Lamy et al. 1999). Similarly, marine productivity (based on organic carbon and opal contents) along the southern part of the PCC was lower during the early and middle Holocene (Fig. 6.9) and increased afterwards, interpreted in terms of latitudinal shifts of the ACC as the main source for nutrients in the PCC system combined with higher input of terrestrial micronutrients (Hebbeln et al. 2002; Lamy et al. 2002). Though paleoproductivity estimates based on contents of biogenic components may be substantially affected by dilution and preservation effects, rather constant Holocene sedimentation-rates and little diagenetic overprint of the organic matter over this time interval (Mix et al. 2003) suggest that they are reliable in this case. Taken together, these long term Holocene trends suggest, as in the glacial, a close coupling

of the main oceanographic (ACC) and atmospheric (SWW) circulation members of the southeast Pacific

The pattern of shorter-term variability on millennial and centennial time-scales is more complex (Lamy et al. 2002). Since it is assumed that past latitudinal shifts of the SWW were likewise connected to latitudinal shifts of the ACC, a southward displacement of the SWW during the Holocene should be associated with higher SSTs and lower productivity comparable to the long-term trend. However, many of the multi-centennial to millennial-scale variations in paleotemperatures and – salinities do not exactly match the reconstructed shifts of the SWW in particular after ~5 kyr B.P (Figs. 6.9and 6.10). The paleoproductivity records from core GeoB 3313-1 (Fig. 6.10) exhibit two century-scale excursions to higher values between 5.5 and 5 kyr BP and shortly after 4 kyr BP which do not exactly coincide with SST minima. Instead, they occur during cooling phases shortly after the two most significant increases in rainfall in the continental hinterland (Fig. 6.10). The Fe record (Fig. 6.10) indicates that these rainfall augmentations terminated the less humid phase of the middle Holocene in southern Chile, pointing to a significant contribution of continent-derived micronutrients which resulted in an increase of marine productivity off southern Chile for several centuries (Lamy et al. 2002) consistent with similar results based on orbital-scale productivity changes in relation to terrigenous micronutrients input off northern Chile (Dezileau et al. 2004)

6.4.3.2 Link to the High Latitudes

The early Holocene optimum depicted at Site 1233 coincides with warm conditions recorded both in the Eastern Antarctic ice cores Dome C and DML (Masson-Delmotte et al. 2004; EPICA Community Members 2004; EPICA Community Members 2006) as well as the Western Antarctic Taylor Dome (Steig et al. 1998), where the maximum warming appears to be restricted to a shorter interval, however (Fig. 6.8). Long-term trends in the ice core records partly deviate as large-scale Antarctic cooling during the Holocene is locally compensated by a decrease of a few tens of metres in the icesheet elevation, in response to the ice-sheet dynamics (Masson-Delmotte et al. 2004). However, there appears to be a consistent multi-centennial-scale temperature pattern in Antarctica over the Holocene (Masson-Delmotte et al. 2004; Masson et al. 2000) with a cyclicity of ~830 years that partly correlates to SST changes as recorded in core GeoB 3313-1 off southern Chile (Fig. 6.10).

6.4.3.3 Link to the Tropics

A SST record off northern mid-latitude Chile (30°S; Fig. 6.8) (De Pol-Holz et al. 2006) displays a slightly delayed optimum warming that lasted longer, i.e. into the middle Holocene, a pattern that likewise appears in the tropical South American ice core record recovered at the Nevado de Huascaran (Fig. 6.8) (Thompson et al. 1995). North of 30°S there are very few sedimentary records along the Chilean margin that cover the Holocene with a reasonable resolution because terrestrial sediment input is minimal off the hyper-arid Atacama Desert. One of the few records

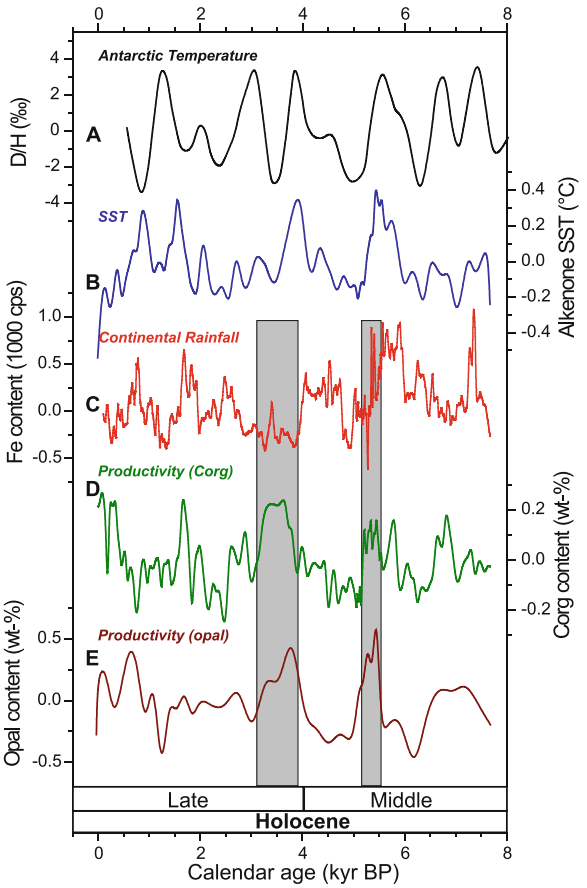

Fig. 6.10 Paleoceanographic and continental paleoclimate records from core GeoB 3313-1 off southern Chile focusing on the millennial to centennial-scale variations compared to Antarctic ice-core records. Data-sets have been detrended by subtracting the long-term trends shown in Fig. 6.5 (after Lamy et al. 2002). (A) Short-term variability in Antarctic temperature shown as the first component of an empirical orthogonal function (EOF) analysis calculated from isotopic records from the Ross sea sector (Byrd and Taylor Dome sites) (Masson et al. 2000). (B) SST record off Chile showing a significant positive correlation ($r = 0.57$, $n = 57$; significant on the 99.9% level after applying a 100 year time-resolution interpolation) to Antarctic temperatures until ca. 2000 B.P. (C) Iron contents of core GeoB 3313-1 indicating rainfall and the position of the SWW. Paleoproductivity proxies (D) Corg content and (E) biogenic opal content. *Vertical gray bars* mark time intervals of century scale increases in paleoproductivity as discussed in the text

comes from core GeoB 7112, located on the continental slope at ~24°S (Mohtadi et al. 2004). Though there is no direct SST proxy record available, several proxy records for marine productivity changes suggest that upwelling intensity was substantially reduced and the advection of warmer subtropical surface was enhanced during the early and middle Holocene. After ~ 5 kyr BP, the pattern reverses, i.e. upwelling became slightly stronger and surface waters were colder, consistent with

the SST record core GeoB 7139 at ~30°S (Fig. 6.8). As observed in most of the Chilean records further south, the variability in the records appears to be higher during the late Holocene, a pattern that may relate to more frequent and stronger El Niño events.

In the tropical Pacific, Holocene paleoceanographic records have been derived from sediment records of the Western Pacific Warm Pool and the Eastern Pacific Cold Tongue (Koutavas et al. 2002; Stott et al. 2004). These are both regions that today are particularly sensitive to SST changes connected to ENSO. While the western Pacific records display a slight (~0.5°C) cooling over the past 10 kyr, the SST record from the cold tongue reveals a broad middle Holocene cooling on the order of 1°C (Fig. 6.8). These data suggest enhanced zonal SST gradients during the middle Holocene that decrease after ~5 kyr, a pattern that would suggest a mean La Niña-like state of ENSO during the middle Holocene and a larger impact of El Niño events during the later part, broadly consistent with marine records from the Peruvian shelf (Rein et al. 2005) and terrestrial data from Equador (Moy et al. 2002). In addition, the western Pacific records show a long-term decrease in salinity over the course of the Holocene that may imply a general change in tropical hydrology, possibly related to a northward shift of the Intertropical Convergence Zone (Stott et al. 2004).

Lamy et al. (2001) suggested that changes in the tropical climate system on multicentennial to millennial-scales largely control rainfall variability in southern Chile as documented in core GeoB 3313-1 by a dominant ~900 years cycle that is likewise found in the Bolivian Sajama ice core record (Thompson et al. 1998). These variations most likely involve changes in the strength of the Hadley Cell over the Southeast Pacific and adjacent South America. On the other hand, the correlation to climate conditions in Antarctica on millennial and multicentennial time-scales reveals a major phase shift at ~4 kyr BP that roughly coincides with the onset of modern ENSO. A shift at the transition from the middle to the late Holocene is also evident in the comparison of the short-term rainfall fluctuations to surface ocean changes (Fig. 6.9) (Lamy et al. 2002). This suggests a mismatch between millennial and multi-centennial-scale variability in atmospheric (SWW) and oceanographic (southern PCC and ACC) circulation patterns during the late Holocene (Fig. 6.10). The proposed explanation is that paleotemperatures in the southern PCC during the late Holocene have probably not been affected by changes in ENSO (Lamy et al. 2002). Modern ENSO-related SST anomalies only reach south to 33°–36°S wheras meteorological studies suggest a strong effect of ENSO on rainfall anomalies both in central and southern Chile (Montecinos and Aceituno 2003).

References

Abarzúa AM, Villagrán C, Moreno PI (2004) Deglacial and postglacial climate history in east-central Isla Grande de Chiloe, southern Chile (43ºS). Quat Res 62:49–59

Alley RB, Clark PU (1999) The deglaciation of the Northern Hemisphere. Annu. Rev. Earth Planet Sci 27:149–182

Andreasen DJ, Ravelo AC (1997) Tropical Pacific Ocean thermocline depth reconstructions for the last glacial maximum. Paleoceanography 12:395–413

Ashworth AC, Hoganson JW (1993) The magnitude and rapidity of the climate change marking the end of the Pleistocene in the mid-latitudes of South America. Palaeogeogr Palaeoclimatol Palaeoecol 101:263–270

Bennett KD, Haberle SG, Lumley SH (2000) The Last Glacial-Holocene Transition in Southern Chile. Science 290:325–328

Blunier T, Brook EJ (2001) Timing of millennial-scale climate change in Antarctica and Greenland during the last glacial period. Science 291:109–112

Clark PU, Alley RB, Pollard D (1999) Northern Hemisphere ice-sheet influences on global climate change. Science 286:1104–1111

Clark PU, McCabe AM, Mix AC, Weaver AJ (2004) Rapid rise of sea level 19,000 years ago and its global implications. Science 304:1141–1144

De Pol-Holz R, Ulloa O, Dezileau L et al (2006) Melting of the Patagonian Ice Sheet and deglacial perturbations of the nitrogen cycle in the eastern South Pacific. Geophys Res Lett 33: L04704

De Pol-Holz R., Ulloa O., Lamy F. et al (2007) Late Quaternary variability of sedimentary nitrogen isotopes in the eastern South Pacific Ocean. Paleoceanography 22(2): PA2207

Delmonte B, Petit J, Maggi V (2002) Glacial to Holocene implications of the new 27000-year dust record from the EPICA Dome C (East Antarctica) ice core. Clim Dyn 18:647–660

Denton GH, Heusser CJ, Lowell TV et al (1999a) Interhemispheric linkage of paleoclimate during the last glaciation. Geografiska Annaler Series a-Physical Geography 81A:107–153

Denton GH, Lowell TV, Heusser CJ et al (1999b) Geomorphology, stratigraphy, and radiocarbon chronology of Llanquihue drift in the area of the southern Lake District, Seno Reloncavi, and Isla Grande de Chiloe, Chile. Geog Ann 81A:167–229

Dezileau L., Ulloa O., Hebbeln D. et al (2004) Iron control of past productivity in the coastal upwelling system off the Atacama Desert, Chile. Paleoceanography 19: PA3012

EPICA Community Members (2004) Eight glacial cycles from an Antarctic ice core. Nature 429:623–628

EPICA Community Members (2006) One-to-one coupling of glacial climate variability in Greenland and Antarctica. Nature 444:195–198

Feldberg MJ, Mix AC (2003) Planktonic foraminifera, sea surface temperatures, and mechanisms of oceanic change in the Peru and south equatorial currents, 0–150 ka BP. Paleoceanography 18: art. no.-1016

Glasser NF, Harrison S, Winchester V, Aniya M (2004) Late Pleistocene and Holocene palaeoclimate and glacier fluctuations in Patagonia. Glob Planet Change 43:79–101

Hajdas I, Bonani G, Moreno PI, Ariztegui D (2003) Precise radiocarbon dating of Late-Glacial cooling in mid-latitude South America. Quat Res 59:70–78

Hebbeln D, Shipboard Scientists (1995) Cruise report of R/V Sonne Cruise SO-102, Valparaiso (Chile) - Valparaiso (Chile). May 09–June 28, 1995. Berichte, Fachbereich Geowissenschaften, Universität Bremen, Bremen

Hebbeln D, Marchant M, Wefer G (2002) Paleoproductivity in the southern Peru-Chile Current through the last 33,000 years. Mar Geol 186:487–504

Hebbeln D, Lamy F, Mohtadi M, Echtler H (2007) Tracing the impact of glacial-interglacial climate variability on erosion of the southern Andes. Geology 35:131–134

Heusser C (2003) Ice age southern andes – a chronicle of paleoecological events. Elsevier Science, Amsterdam

Heusser L, Heusser C (2006) Submillennial palynology and palaeoecology of the last glaciation at Taiquemo (~50,000 cal yr, MIS 2-4) in southern Chile. Quat Sci Rev 25:446–454

Heusser L, Heusser C, Pisias N (2006) Vegetation and climate dynamics of southern Chile during the past 50,000 years: results of ODP Site 1233 pollen analysis. Quat Sci Rev 25: 474–485

Hobbs JE, Lindesay JA, Bridgman HA (1998) Climates of the southern continents: present, past and future. John Wiley & Sons Ltd, Chichester

Hughen K, Lehman S, Southon J et al (2004) C-14 activity and global carbon cycle changes over the past 50,000 years. Science 303:202–207

Hulton NRJ, Purves RS, McCulloch RD et al (2002) The Last Glacial Maximum and deglaciation in southern South America. Quat Sci Rev 21:233–241

Jenny B, Valero-Garces BL, Villa-Martinez R et al (2002) Early to Mid-Holocene Aridity in Central Chile and the Southern Westerlies: The Laguna Aculeo Record (34[deg]S). Quat Res 58:160–170

Jouzel J, et al (1995) The 2-Step Shape and Timing of the Last Deglaciation in Antarctica. Climate Dynamics 11(3):151–616

Kaiser J, Lamy F, Hebbeln D (2005) A 70-kyr sea surface temperature record off southern Chile (ODP Site 1233). Paleoceanography 20: PA1146

Kaiser J, Lamy F, Arz HW, Hebbeln D (2007) Dynamics of the millennial-scale sea surface temperature and Patagonian Ice Sheet fluctuations in southern Chile during the last 70kyr (ODP Site 1233). Quat Int 161:77–89

Kaplan MR, Ackert RP, Jr., Singer BS et al (2004) Cosmogenic nuclide chronology of millennial-scale glacial advances during O-isotope stage 2 in Patagonia. Geol Soc Am Bull 116: 308–321

Kim JH, Schneider RR, Hebbeln D et al (2002) Last deglacial sea-surface temperature evolution in the Southeast Pacific compared to climate changes on the South American continent. Quat Sci Rev 21:2085–2097

Knorr G, Lohmann G (2003) Southern Ocean origin for the resumption of Atlantic thermohaline circulation during deglaciation. Nature 424:532–536

Knutti R, Flückiger J, Stocker T, Timmermann A (2004) Strong hemispheric coupling of glacial climate through freshwater discharge and ocean circulation. Nature 430:851–856

Koutavas A, Lynch-Stieglitz J, Marchitto TM Jr, Sachs JP (2002) El Niño-like pattern in ice age tropical Pacific sea surface temperature. Science 297:226–230

Lamy F, Hebbeln D, Wefer G (1998a) Late quaternary precessional cycles of terrigenous sediment input off the Norte Chico, Chile (27.5 degrees S) and palaeoclimatic implications. Palaeogeogr Palaeoclimatol Palaeoecol 141:233–251

Lamy F, Hebbeln D, Wefer G (1998b) Terrigenous sediment supply along the Chilean continental margin: modern regional patterns of texture and composition Geol Rundsch 87:477–494

Lamy F, Hebbeln D, Wefer G (1999) High-resolution marine record of climatic change in mid-latitude Chile during the last 28,000 years based on terrigenous sediment parameters. Quat Res 51:83–93

Lamy F, Klump J, Hebbeln D, Wefer G (2000) Late Quaternary rapid climate change in northern Chile. Terra Nova 12:8–13

Lamy F, Hebbeln D, Rohl U, Wefer G (2001) Holocene rainfall variability in southern Chile: a marine record of latitudinal shifts of the Southern Westerlies. Earth Planet Sci Lett 185: 369–382

Lamy F, Rühlemann C, Hebbeln D, Wefer G (2002) High- and low-latitude climate control on the position of the southern Peru-Chile Current during the Holocene. Paleoceanography 17:1028

Lamy F, Kaiser J, Ninnemann U et al (2004) Antarctic Timing of Surface Water Changes off Chile and Patagonian Ice Sheet Response. Science 304:1959–1962

Lamy F, Kaiser J, Arz HW et al (2007) Modulation of the bipolar seesaw in the southeast pacific during Termination 1. Earth Planet Sci Lett 259:400–413

Lea DW, Pak DK, Spero HJ (2000) Climate impact of late quaternary equatorial pacific sea surface temperature variations. Science 289:1719–1724

Lea DW, Pak DK, Belanger CL et al (2006) Paleoclimate history of Galápagos surface waters over the last 135,000 yr. Quat Sci Rev 25:1152–1167

Marchant M, Cecioni A, Figueroa S et al (2007) Marine geology, oceanography and climate. In: Moreno T, Gibbons W (eds) The geology of Chile. Ecological Society Special Publication, London

Martinez I, Keigwin L, Barrows TT et al (2003) La Nina-like conditions in the eastern equatorial Pacific and a stronger Choco jet in the northern Andes during the last glaciation. Paleoceanography 18:1033

Martinez P, Lamy F, Robinson RR et al (2006) Atypical [delta]15 N variations at the southern boundary of the East Pacific oxygen minimum zone over the last 50 ka. Quat Sci Rev 25: 3017–3028

Masson-Delmotte V, Stenni B, Jouzel J (2004) Common millennial-scale variability of Antarctic and Southern Ocean temperatures during the past 5000 years reconstructed from the EPICA Dome C ice core. Holocene 14:145–151

Masson V, Vimeux F, Jouzel J et al (2000) Holocene climate variability in Antarctica based on 11 ice-core isotopic records. Quat Res 54:348–358

McManus J, Francois R, Gherardi J-M et al (2004) Collapse and rapid resumption of Atlantic meridional circulation linked to deglacial climate changes. Nature 428:834–837

Miller A (1976) The climate of Chile. In: Schwerdtfeger W (ed) World Survey of Climatology. Elsevier, Amsterdam

Mix AC, Bard E, Schneider R (2001) Environmental processes of the ice age: land, oceans, glaciers (EPILOG). Quat Sci Rev 20:627–657

Mix AC, Tiedemann R, Blum P, Shipboard Scientists (2003) Southeast Pacific paleoceanographic transects. Ocean Drilling Program, College Station, TX

Mohtadi M, Hebbeln D (2004) Mechanisms and variations of the paleoproductivity off northern Chile (24°S–33°S) during the last 40,000 years. Paleoceanography 19: PA2023

Mohtadi M, Romero O, Hebbeln D (2004) Changing marine productivity off northern Chile during the past 19 000 years: a multivariable approach. J Quat Sci 19:347–360

Monnin E, Indermuhle A, Dallenbach A et al (2001) Atmospheric CO_2 concentrations over the last glacial termination. Science 291:112–114

Montecinos A, Aceituno P (2003) Seasonality of the ENSO-related rainfall variability in central Chile and associated circulation anomalies. J Clim 16:281–296

Moreno PI (2004) The Last Transition from extreme glacial to extreme interglacial climate in NW Patagonia: regional and global implications. Eos Trans AGU, 85 (47). Fall Meet. Suppl.,

Moreno PI, Jacobson GL, Lowell TV, Denton GH (2001) Interhemispheric climate links revealed by a late-glacial cooling episode in southern Chile. Nature 409:804–808

Morgan V, et al (2002) Relative timing of deglacial climate events in Antarctica and Greenland. Science 297(5588):1862–1864.

Moy CM, Seltzer GO, Rodbell DT, Anderson DM (2002) Variability of El Nino/Southern Oscillation activity at millennial timescales during the Holocene epoch. Nature 420: 162–165

Müller P. J., Kirst G., Ruhland G. et al (1998) Calibration of the alkenone paleotemperature index UK′37 based on core-tops from the eastern South Atlantic and the global ocean (60°N–60°S). Geochim Cosmochim Acta 62:1757–1772.

Ninnemann US, Charles CD (1997) Regional differences in Quaternary Subantarctic nutrient cycling: link to intermediate and deep water ventilation. Paleoceanography 12:560–567

Palmer MR, Pearson PN (2003) A 23,000-year record of surface water pH and PCO2 in the western Equatorial Pacific ocean. Science 300:480–482

Pisias N, Heusser L, Heusser C et al (2006) Radiolaria and pollen records from 0 to 50 ka at ODP Site 1233: continental and marine climate records from the Southeast Pacific: Quat Sci Rev 25:455–473

Reimer PJ, Baillie MGL, Bard E et al (2004) IntCal04 terrestrial radiocarbon age calibration, 26–0 ka BP. Radiocarbon 46:1029–1058

Rein B, Lückge A, Reinhardt L et al (2005) El Nino variability off Peru during the last 20,000 years. Paleoceanography 20: Pa1099

Rinterknecht VR, Clark PU, Raisbeck GM et al (2006) The Last Deglaciation of the Southeastern Sector of the Scandinavian Ice Sheet. Science 311:1449–1452

Robinson R. S., Mix A., Martinez P. (2007) Southern Ocean control on the extent of denitrification in the southeast Pacific over the last 70 ka. Quat Sci Rev 26:201–212.

Romero OE, Kim JH, Hebbeln D (2006) Paleoproductivity evolution off central Chile from the Last Glacial Maximum to the Early Holocene. Quat Res 65:519–525
Ruttlant J, Fuenzalida R (1991) Synoptic aspects of the central Chile rainfall variability associated with the Southern Oscillation. Int J Climatol 11:63–76
Sarnthein M, Kiefer T, Grootes PM et al (2006) Warmings in the far northwestern Pacific promoted pre-Clovis immigration to America during Heinrich event 1. Geology 34:141–144
Schmittner A, Yoshimori M, Weaver AJ (2002) Instability of Glacial Climate in a Model of the Ocean- Atmosphere-Cryosphere System. Science 295:1489–1493
Scholl DW, Christensen MN, Von Huene R, Marlow M, S (1970) Peru-Chile Trench. Sediments and sea-floor spreading. Geol Soc Am Bull 81:1339–1360
Shin SI, Liu Z, Otto-Bliesner B et al (2003) A simulation of the last glacial maximum climate using the NCAR-CCSM. Clim Dyn 20:127–151
Siddall M, Stocker TF, Blunier T et al (2006) Using a maximum simplicity paleoclimate model to simulate millennial variability during the last four glacial cycles. Quat Sci Rev 25:3185–3197
Sudgen DE et al (2005) Late-Glacial glacier events in southernmost South America: A blend of 'Northern' and 'Southern' hemispheric climatic signals? Geografiska Annaler: Series A. Phy Geography 87(2):273–288
Steig EJ, Hart CH, White JWC et al (1998) Changes in climate, ocean and ice-sheet conditions in the Ross embayment, Antarctica, at 6 ka. Ann Glaciol 27:305–310
Stocker TF (1998) Climate change - The seesaw effect. Science 282:61–62
Stocker TF, Johnsen SJ (2003) A minimum thermodynamic model for the bipolar seesaw. Paleoceanography 18:1087
Stott L, Cannariato K, Thunell R et al (2004) Decline of surface temperature and salinity in the western tropical Pacific Ocean in the Holocene epoch. Nature 430:56–59
Stott L, Timmermann A, Thunell R (2007) Southern hemisphere and deep-sea warming led deglacial atmospheric CO_2 rise and tropical warming. Science 318:435–438
Streten NA, Zillman JW (1984) Climate of the South Pacific. In: van Loon H (ed) Climates of the oceans pp 26–429). Elsevier Sci., New York
Strub PT, Mesias JM, Montecino V et al (1998) Coastal ocean circulation off Western South America. In: Robinson AR, Brink KH (eds) The global coastal ocean. Regional studies and syntheses pp 273–315). Wiley, New York
Stuut J-BW, Lamy F (2004) Climate variability at the southern boundaries of the Namib (southwestern Africa) and Atacama (northern Chile) coastal deserts during the last 120,000 yr. Quat Res 62:301–309
Stuut JBW, Marchant M, Kaiser J et al (2006) The late Quaternary paleoenvironment of Chile as seen from marine archives. Geogr Helv 61:135–151
Thompson LG, Mosley-Thompson E, Davis ME et al (1995) Late Glacial stage and Holocene tropical ice core records from Huascaran, Peru. Science 269:46–50
Thompson LG, Davis ME, Mosley-Thompson E et al (1998) A 25,000 year tropical climate history from the Bolivian ice cores. Science 282:1858–1864
Thornburg T, Kulm LD (1987a) Sedimentation in the Chile Trench: depositional morphologies, lithofacies and stratigraphy. Geol Soc Am Bull 98:33–52
Thornburg T, Kulm LD (1987b) Sedimentation in the Chile Trench: petrofacies and provenance. J Sediment Petrol 57:55–74
Timmermann A, Krebs U, Justino F et al (2005) Mechanisms for millennial-scale global synchronization during the last glacial period. Paleoceanography 20:
Toggweiler JR, Rusell JL, Carson SR (2006) Midlatitude westerlies, atmospheric CO2, and climate change during ice ages. Paleoceanography 21: PA1154
Tomczak M, Godfrey JS (2003) Regional Oceanography: an Introduction. Daya Pub., Delhi
Trenberth KE (1991) Storm Tracks in the Southern Hemisphere. J Atmos Sci 48:2159–2178
Villagrán C, Varela J (1990) Palynological evidence for increased aridity on the Central Chilean coast during the Holocene. Quat Res 34:198–207

Visser K, Thunell R, Stott L (2003) Magnitude and timing of temperature change in the Indo-Pacific warm pool during deglaciation. Nature 421:152–155

Weaver AJ, Saenko OA, Clark PU, Mitrovica JX (2003) Meltwater pulse 1A from Antarctica as a trigger of the bolling- allerod warm interval. Science 299:1709–1713

Yin JH (2005) A consistent poleward shift of the storm tracks in simulations of 21st century climate. Geophys Res Lett 32:L18701

Part II
The High Latitudes-Tropics and Tropics-Tropics Teleconnections over the Last Deglaciation and Last Glacial Maximum

Chapter 7
Teleconnections into South America from the Tropics and Extratropics on Interannual and Intraseasonal Timescales

Alice M. Grimm and Tercio Ambrizzi

Abstract This chapter presents the mechanisms and the most important effects of tropics-extratropics and tropics-tropics atmospheric teleconnections with South America on intra-seasonal to interannual time scales. The basis for theoretical understanding of teleconnections is reviewed, as well as the observed Southern Hemisphere interannual and intraseasonal variability. The observed teleconnections with South America are described, indicating linkages between the tropics and extratropics and between different regions in the tropics. Possible mechanisms of these linkages are presented and some teleconnections are analyzed with Influence Functions. Special emphasis is placed on the teleconnections associated with ENSO on interannual time scales and the Madden Julian Oscillation on intraseasonal time scales.

Keywords Teleconnections · South America · ENSO · Madden-Julian Oscillation

7.1 Introduction

The term "teleconnection", which denotes climate anomalies related over distances typically of order 10^3 km, was introduced in a climate context by Angstroem (1935) and has been used to describe remote influences on the variability of large-scale features of atmospheric circulation as well as precipitation and temperature. Teleconnections are often represented as geographically dependent wave-like structures. Although the concept of teleconnections only gained widespread usage with the work of Bjerknes in the late 1960s on global-scale impacts of El Niño-Southern Oscillation (ENSO) (see Bjerknes 1969), aspects of remote climate variability now recognized as teleconnections were appreciated much earlier (e.g., Walker 1923, 1924; Walker and Bliss 1932). While teleconnections can be defined on

A.M. Grimm (✉)
Department of Physics, Federal University of Paraná, Curitiba, Paraná, Brazil
e-mail: grimm@fisica.ufpr.br

F. Vimeux et al. (eds.), *Past Climate Variability in South America and Surrounding Regions*, Developments in Paleoenvironmental Research 14,
DOI 10.1007/978-90-481-2672-9_7,

synoptic time scales, they are typically associated with lower-frequency variability and are often operationally divided into two frequency regimes: intraseasonal and interannual.

Changes in the tropical atmosphere associated with oceanic changes may trigger responses in the global atmosphere via tropical-extratropical and tropical-tropical teleconnections. In this view, the atmosphere acts as a bridge between the oceanic forcing regions and remote oceanic regions (Lau and Nath 1996; Alexander et al. 2002). Teleconnection studies have provided a good example of link between observations, theory and models, as discussed in Hoskins and Pearce (1983) and Trenberth et al. (1998).

In the early 1980s several studies documented teleconnection patterns (e.g., Wallace and Gutzler 1981), associated some of them with tropical sea surface temperature (SST) variability (e.g., Horel and Wallace 1981), and discussed this association in terms of Rossby wave dispersion theory (e.g., Hoskins and Karoly 1981; Webster 1981; Simmons 1982). These seminal works spurred much interest in the relationship between tropical and extratropical low-frequency variability. Several mechanisms were proposed to explain the origin of the extratropical low-frequency variability. Most of the discussion centered on two hypotheses; namely, that the circulation anomalies are either the product of the Rossby wave dispersion from anomalous tropical heat sources or the result of internal atmospheric fluctuations caused by instabilities of the basic state. Observational and modeling studies have pointed to the contribution of both mechanisms acting in concert, as instability mechanisms can modify and amplify Rossby wave propagation. Instability mechanisms may be taken into account in the Rossby wave propagation by specifying a realistic basic state in the vorticity equation model (e.g., Simmons 1982; Branstator 1983). However, Frederiksen and Webster (1988) discussed the need for a unified theory of Rossby wave propagation and 3-D baroclinic instability to explain the observed teleconnections. According to Schubert (1986), the baroclinic conversion of energy can contribute, but barotropic processes are responsible for most of the total energy that the low-frequency anomalies receive from the basic state.

While the traditional view of teleconnections has emphasized extratropical forcing by the tropics, there is an emergent sense that forcing of the tropics by midlatitude variability is also important. Compared to what is known of tropical impacts on the extratropics, the forcing effects of the midlatitudes on the tropics are less well understood. These processes may involve the possible triggering of equatorially trapped waves by stochastic forcing from higher latitudes (Mak 1969) or the forcing of tropical convection by Rossby waves propagating from midlatitudes (e.g., Liebmann and Hartmann 1984) that can even cross the equator through the westerly duct in the equatorial east Pacific or the Atlantic (e.g., Webster and Holton 1982). The results of different studies on tropical-extratropical interaction suggest a "two-way" relationship in which the tropics influence the extratropics and vice-versa (Matthews and Kiladis 1999; Rasmusson and Mo 1993). A more complete understanding of the processes involved in these interactions and the generation of the atmospheric teleconnection patterns may have a profound impact on the improvement of medium and long-range forecasts (Ferranti et al. 1990).

Interest in the effect of teleconnections on South America (SA) climate increased after the strong 1982–1983 El Niño episode, when extreme floods and droughts affected the southern and northern parts of the continent, respectively. This chapter presents the mechanisms and the most important effects of tropics-extratropics and tropics-tropics teleconnections with SA on intra-seasonal to interannual time scales with more emphasis on the dynamical component of the teleconnections. The focus of Section 7.2 is the theoretical understanding and modeling of the tropics-tropics and tropics-extratropics interactions. Sections 7.3 and 7.4 describe observed teleconnections on interannual and intraseasonal time scales, indicating linkages between the tropics and extratropics and different regions in the tropics. Special emphasis is placed on the teleconnections associated with ENSO on interannual time scales and the Madden Julian Oscillation on intraseasonal time scales.

7.2 Mechanisms of Tropics-Tropics and Tropics-High Latitudes Teleconnections

In the tropics, anomalous positive SSTs increase the heat and moisture flux to the atmosphere, enhance low-level convergence, and therefore increase convection. Consequently, the upper-level tropical divergent circulation is enhanced in its zonal (Walker circulation) and meridional (Hadley circulation) components, resulting in anomalous ascent or descent in the branches of these circulations. Stronger upper-level divergence in the tropics and convergence in the subtropics create an anomalous Rossby wave source. The direct effects of the perturbations in the Walker and Hadley cells, as well as the dispersion and propagation of Rossby waves to the extratropics, induce anomalous circulation in the atmosphere, resulting in changes in precipitation, temperature, and even extratropical SSTs. In this section, the climatological Hadley and Walker circulations are described and the theoretical basis of the Rossby wave propagation is presented.

7.2.1 Walker and Hadley Circulation Cells

The Hadley cell was postulated as early as 1686 by Halley to explain the trade winds; later, Hadley (1735) suggested that thermal convection might drive such a circulation. However, it was only at the end of the 20th century that satisfactory quantitative models of this process were developed (e.g., Held and Hou 1980; see also the thorough review by Diaz and Bradley 2004).

The tropical Hadley cell is generally defined as the zonal mean meridional mass circulation in the atmosphere bounded roughly by 30°S and 30°N. It is characterized by equatorward mass transport by the prevailing trade wind flow in the lower troposphere, and poleward mass transport in the upper troposphere, with convergence and ascending motion in the equatorial zone and subsidence in the subtropics. This cell plays an important role in the large-scale circulation, linking the tropics with the

subtropics. The fundamental forces that determine the Hadley circulation are: pressure gradient forces arising from differential radiative heating between the equator and poles and the Coriolis force associated with the Earth's rotation. The primary energy source of the Hadley cell is the latent heat of water vapor released in the Inter-Tropical Convergence Zone (ITCZ). The adiabatic heating due to downward motion in the subtropics maintains the meridional temperature gradient and large-scale eddy motions in midlatitudes (Sasamori 1981). Also, as suggested by Bergman and Hendon (2000), the impacts of atmospheric cloud radiative forcing on the local stability, which in turn influences convection and latent heating of the atmosphere, are non-negligible and should be taken into account. A more recent discussion of the elementary Hadley circulation can be found in Webster (2004).

The Walker circulation comprises longitudinal direct circulation cells in the equatorial atmosphere. The principal energy source of the Walker circulation is also attributed to the release of latent heat in major convection centers associated with the ocean-continent distribution and the sea-surface temperature distribution maintained by the coupled ocean-atmosphere interactions (Sasamori 1981). In the ascending branch of these longitudinal cells convection and the associated release of latent heat lift isobaric surfaces upward in the upper troposphere and create a high pressure region there. The descending branch is located in a tropical region where less or no convection results in lower pressure in the upper troposphere. A longitudinal pressure gradient is established which, by virtue of its equatorial latitude, cannot be balanced by the Coriolis force. Thus a direct zonal circulation is driven in the equatorial plane with countervailing winds at the surface and in the upper troposphere. The adiabatic heating by downward motion in the Walker circulation is probably mostly balanced by radiative cooling (Bjerknes 1969). The strongest Walker cell is the Pacific cell associated with the pressure difference between eastern and western tropical Pacific, with an ascending branch in the climatological strong convection over the western Pacific warm pool and a descending branch over the cold SST in eastern Pacific. Two other smaller cells are also associated with SA, with ascending branch over the highly convective Amazon region, and descending branches over eastern Pacific and Atlantic oceans.

Diagrams of the climatological Hadley and Walker circulations for the Southern Hemisphere summer and autumn seasons (December-January-February, DJF, and March-April-May, MAM, respectively) are depicted in Fig. 7.1. These seasons were chosen because most of the annual total rainfall observed over SA occurs during these periods.

During both DJF and MAM, the ascending branch of the Pacific Walker cell is over the western Pacific Ocean, around 160°E–180°, and the sinking branch is located in the eastern Pacific, close to the west coast of SA (between 120°W to 90°W). Over the equatorial portion of SA (including Ecuador, northern Peru, south-central Colombia, Venezuela and much of the Brazilian Amazon) there is strong ascending motion, with compensatory subsidence reaching the east-central tropical Atlantic Ocean. While the Walker circulation changes little near SA from summer to autumn, the regional Hadley circulation shows important differences between these seasons. During DJF ascending motion is observed from 5°S to 30°S with a

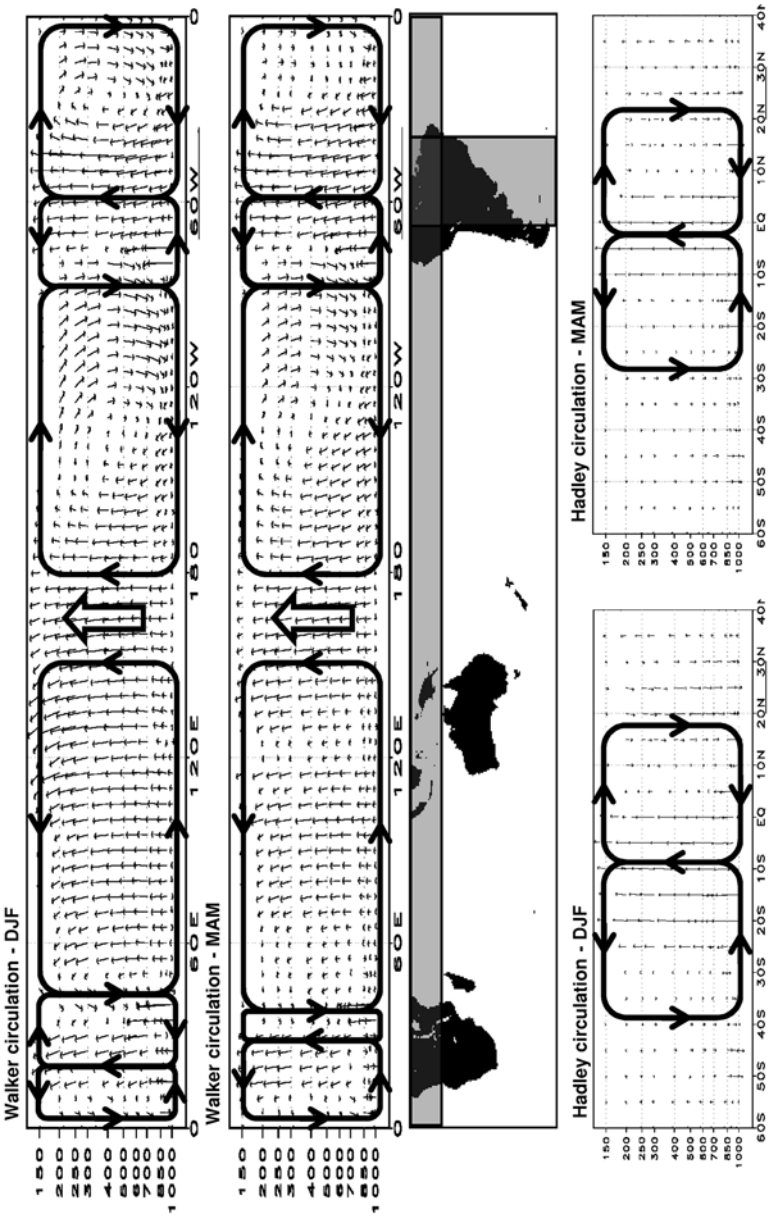

Fig. 7.1 Schematic diagrams of the climatological Walker and Hadley circulations for DJF and MAM, based on wind averages over the latitudinal and longitudinal bands indicated on the map

maximum around 7°S (and a secondary maximum around 20°S). The compensatory descending branches occur over both hemispheres around 20°N and 40°S. This circulation pattern results from the intense convection that occurs over the continent during the austral summer, which reflects the strong monsoon regime that extends into the subtropics of SA. During MAM the ascending motion is nearly centered on the equator. While the descending branch in NH is approximately in the same position as in austral summer, in the SH it is shifted to the north.

It is clear that the seasonal variability of the ascending and descending branches of the regional Walker and Hadley circulations over SA can modulate the rainfall distributions in some regions; further, the intraseasonal and interannual variability of these circulations can significantly affect SA precipitation. The interannual changes associated with ENSO have been intensively studied by many researchers (e.g. Bjerknes 1966, 1969; Arkin 1982; Webster et al. 1998; Philander 1990; Oort and Yienger 1996; Wang 2002; Minobe 2004).

During El Niño (EN) episodes the tropical convection is shifted from western Pacific towards central and east Pacific. Consequently, the Pacific Walker cell is weakened, because the induced anomalous circulation along the equator opposes the climatological circulation. As the anomalous subsidence in the Walker cell associated with anomalous convection over the eastern Pacific occurs over northern SA and Atlantic Ocean, the two smaller cells connected with SA are strongly affected, especially by the weakening of the ascending branch over the Amazon region. The reduction of the convection over this region also reduces the regional Hadley circulation. On the other hand, the Hadley circulation is strengthened over the central/eastern Pacific. During La Niña (LN) episodes the changes are nearly opposite. The perturbations over SA will be analyzed in Section 7.3.2.

The Walker cell variability and associated remote impacts during EN events described above only take in account the dynamical component of the atmospheric circulation. However, as suggested by Chiang and Sobel (2002), impacts from and to the thermodynamics are also important to understanding the teleconnected response to El Niño. Using a single-column model coupled to a slab ocean mixed layer, Chiang and Sobel (2002) investigated the interannual tropical tropospheric temperature (TT) variations during ENSO events. They show evidence that the TT mechanism is applicable to observed SST and precipitation variability in the Tropics outside the ENSO region. In fact, as will be discussed in Section 7.3.2.1, Chiang and Sobel showed that for a given observed TT forcing, the model January-February-March (JFM) averaged precipitation response is correlated to JFM precipitation anomalies in the tropical Atlantic, consistent with previous studies that argue for a dynamical linkage between ENSO and precipitation there via the anomalous Walker circulation (e.g., Ambrizzi et al. 2004 and references therein).

Although the Hadley circulation is referred to in some studies as a global zonally symmetric meridional circulation (e.g. Oort and Yienger 1996; Trenberth et al. 2000; and references therein), and the Walker circulation is considered the zonally asymmetric zonal component of the tropical divergent circulation (Webster 1983), it is possible to analyze their impact and variability on a regional level, though it should be kept in mind that the atmospheric circulations may not be closed cells.

7.2.2 Rossby Wave Propagation

Originally, Rossby (1945) described on a β-plane how a vorticity source in a barotropic atmosphere with a homogeneous westerly basic flow generates a series of ridges and troughs along which the energy is dispersed with the group velocity. The Rossby wave dispersion theory, which still provides the basis for theories of how the tropics influences the extratropics, was later expanded by several authors to more realistic situations. For example, Hoskins et al. (1977) investigated the energy dispersion over a sphere through zonally symmetric basic state, and Simmons (1982) used a realistic zonally asymmetric basic state.

The basic barotropic model to study Rossby wave propagation, with forcing F and damping A, is:

$$\frac{\partial \zeta}{\partial t} + \vec{V}_{\psi} \cdot \nabla \zeta = F + A \tag{7.1}$$

where ζ is the absolute vorticity and $\mathbf{V}_{\psi}$ is the rotational component of the wind. The first two terms govern the dispersion of pure Rossby waves. The forcing term is related with divergence. Many of the studies to be discussed are based on the linear wave theory and usually a stationary Rossby wave is assumed.

In the case of tropical-extratropical interactions, the forcing results from anomalous convection over anomalous tropical SST. Convection anomalies result in anomalous atmospheric heating, mainly due to latent heat release in anomalous precipitation, and this leads to upper-level divergence through the stretching of the air column. Equation (7.1) is solved at a pressure level which is both near to the maximum divergence associated with tropical convection and near an equivalent barotropic level in the extratropics (300–200 hPa).

In the earlier studies $F = -fD$, where f is the Coriolis parameter and D is divergence, and (7.1) is linearized about a zonally symmetric basic state (e.g., Hoskins et al. 1977; Hoskins and Karoly 1981). The resulting wave patterns agreed with certain aspects of the observed responses to tropical ENSO-related convection and those simulated with more complex atmospheric general circulation (AGCM) models: the basic structure and direction of propagation from the tropical forcing, and the stronger teleconnections in winter and weaker in summer (as stronger propagation occurs in stronger westerly flow, but not through easterlies). However, there were also several discrepancies. The principal were: (i) while the tropical forcing is observed in the mean easterlies, the Rossby wave forcing needs to be in mean westerly flow to produce propagation; (ii) this model does not reproduce differences in propagation arising from different longitudes of the forcing, contrary to observed and AGCM-modeled response; (iii) this model response has much weaker amplitude away from the source than the observed response.

Some of these drawbacks can be overcome by relaxing some of the assumptions in this simple model. The use of a realistic basic state, i.e., one that is a function of longitude as well as latitude, can account for the effect of non-uniformities in the basic state on the wave propagation and local instabilities, which allow internal

energy sources to enhance the propagating tropical-stimulated perturbations in the extratropics or to excite internal natural variability modes (e.g., Simmons 1982; Branstator 1983, 1985). Model (7.1) with a climatological basic state was also used by Hoskins and Ambrizzi (1993) and Ambrizzi et al. (1995) to analyze characteristics of the Rossby wave dispersion in terms of preferred propagation paths. They derived the ray path radius of curvature given by the expression

$$r = \frac{K_S^2}{\left(k\frac{dK_S}{dy}\right)} \tag{7.2}$$

where k is the zonal wavenumber, $K_S = \left(\beta^* / \bar{U}\right)^{1/2}$ is the stationary wavenumber, β^* the meridional gradient of absolute vorticity and $\bar{U}$ the mean zonal wind. From a global distribution of K_S, it is possible to indicate preferred propagation paths of Rossby waves.

A step beyond in dealing with the discrepancies between the simple Rossby-wave model simulations and observed tropical-extratropical propagation and in establishing a more realistic relationship between the anomalous tropical heating and the Rossby wave source is using a more complete formulation of the model. From an analysis of the vorticity equation in the upper troposphere, it is possible to neglect the term involving the vertical advection and, after partitioning the horizontal wind into its rotational and divergent components,

$$\overrightarrow{V} = \overrightarrow{V}_\psi + \overrightarrow{V}_\chi$$

and expressing each variable as a sum of a basic state component and a perturbation, such as

$$\zeta = \overline{\zeta} + \zeta'$$

obtain a linearized vorticity equation model by assuming that the perturbations are small compared to the basic state quantities (thereby neglecting products of perturbations):

$$\frac{d\zeta'}{dt} + \bar{\vec{V}}_\psi \cdot \nabla\zeta' + \vec{V}'_\psi \cdot \nabla\bar{\zeta} = F' + A' \tag{7.3a}$$

where

$$F' = -\bar{\zeta}D' - \vec{V}'_\chi \cdot \nabla\bar{\zeta} - \zeta'\bar{D} - \bar{\vec{V}}_\chi \cdot \nabla\zeta' \tag{7.3b}$$

The left hand side of (7.3a) retains the terms necessary to support Rossby wave propagation, but now the Rossby wave source F includes an additional term besides ζD, namely the advection of vorticity by the divergent flow. Sardeshmukh and Hoskins (1988) advocated the importance of this term and Grimm and Silva Dias

(1995a) showed examples of its influence to the Rossby wave propagation. While the Rossby wave source given by $F' = -fD'$ straddles the equator for anomalous equatorial divergence (or convergence), the Rossby wave source given by (7.3b) extends into the subtropical westerly mean flow (from where the waves can propagate efficiently) due to the vorticity advection by the anomalous divergent flow in regions of strong mean vorticity gradients, such as subtropical jets, or to the advection of vorticity perturbations to the subtropics by the climatological divergent circulation in the tropics (see Grimm and Silva Dias 1995a for the relative contributions of each term in (7.3b) for an EN case). Therefore, in this definition of the source, the upper level anomalous divergence does not need to be placed in the subtropics or in particular regions of the tropics in order to produce a nearly realistic extratropical response. Figure 7.2 shows the difference between the responses to an anomalous divergence over the central equatorial Pacific and convergence over western Pacific using $F' = -fD'$ or the expression (7.3b).

Therefore, the local Hadley circulation, through the associated tropical divergent outflow and subtropical convergence, is important in extending part of the Rossby waves source away from the anomalous tropical heating into the subtropics and the westerly mean flow, where the waves can propagate to higher latitudes.

However, even with the more realistic formulation of the model, there is a major problem when studying tropical-extratropical interactions with the aim of determining the regions where tropical heating anomalies contribute to produce certain low-frequency circulation anomalies: the model demands the correct specification of the upper-level divergence associated with the tropical heat sources. Although

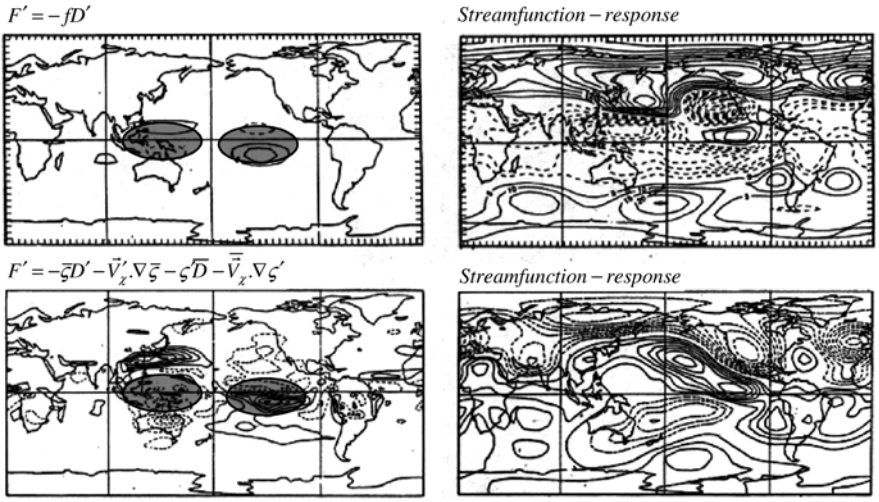

Fig. 7.2 Streamfunction responses (*Right panels*) to the same anomalous divergence in eastern Pacific and anomalous convergence in western Pacific (*indicated by the shaded ellipses in the left panels*), but with different formulations of the Rossby wave source (from Grimm and Silva Dias 1995a, reproduced with permission of the Meteorological Society of Japan)

there is a direct correspondence between upper-level divergence and the tropical heat source, there is not a simple relation with the anomalous upper level convergence, which is as important as the divergence for the rotational response (perturbed convergence in the subtropics is, for example, mainly responsible for the Pacific-North American pattern, PNA, Grimm and Silva Dias 1995a, b). Thus, the correct specification of the anomalous divergence field to achieve certain streamfunction anomalies is very uncertain and small errors or omissions can produce large differences in the response. Apparently insignificant features may have a large impact on the response in remote regions (Grimm and Silva Dias 1995a). Therefore, Grimm and Silva Dias (1995b) proposed the analysis of tropical-extratropical interactions with Influence Functions (IFs) of divergence forcing, which identify the regions where the anomalous upper-level divergence (which is more easily associated with anomalous convection and tropical heating than the vorticity source) has the largest impact on the circulation anomaly around a given point. Therefore, experiments with the barotropic models, which are hardly conclusive when using idealized anomalous divergence fields, can be guided by the indications of the IFs. Model (7.3) was written as

$$\frac{d\zeta'}{dt} + \bar{\vec{V}}_\psi \cdot \nabla\zeta' + \vec{V}'_\psi \cdot \nabla\bar{\zeta} + \bar{\vec{V}}_\chi \cdot \nabla\zeta' + \zeta'\bar{D} - A' = F' \tag{7.4a}$$

with

$$F' = -\bar{\zeta}D' - \vec{V}'_\chi \cdot \nabla\bar{\zeta} \tag{7.4b}$$

where F′ depends only on the anomalous divergence. The stationary version of model (7.4) may be written as:

$$M\psi' = D',$$

with M a linear operator and ψ' the anomalous streamfunction. Then the IF based on divergence forcing is defined by

$$G_D(\lambda,\phi,\lambda',\phi') = M^{-1}\left[\delta\left(\lambda,\phi,\lambda',\phi'\right)\right], \tag{7.5}$$

where $\delta\left(\lambda,\phi,\lambda',\phi'\right)$ is the delta function. Thus the IF $G_D(\lambda,\phi,\lambda',\phi')$ for the target point with longitude and latitude (λ, ϕ) is, at each point (λ', ϕ'), equal to the model response at (λ, ϕ) to an upper-level divergence located at (λ', ϕ'). Maps with contours of IF for a given target point indicate the tropical/subtropical regions in which the anomalous upper-level divergence is most efficient in producing streamfunction anomalies at the target point. Using this tool, Grimm and Silva Dias (1995b) indicated the source regions for several teleconnection patterns. Some of them will be analyzed in following sections.

Manifestations of Rossby wave propagation (and thus indirectly of Hadley and Walker circulation variations) can be seen in low-frequency teleconnection patterns. Large scale tropical convection and global circulation undergo variations on several

time scales and characteristic spatial patterns. The low-frequency variability will be analyzed separately on interannual and intraseasonal (10–120 days) time scales, although some of the variability modes oscillate on both time scales (e.g. Lau et al. 1994; Frederiksen and Zheng 2007). The focus is on the Southern Hemisphere variability modes, although they may be part of global modes. Interannual fluctuations are more geographically dependent, while intraseasonal time scales are less anchored and more zonally oriented wave trains generally localized in the strong westerlies of the subtropical and polar jet.

7.3 Teleconnections with South America on Interannual Time Scales

7.3.1 Southern Hemisphere Observed Interannual Variability

Several observational studies on Southern Hemisphere teleconnection patterns have been carried out with different methods, variables, domains, data sets and periods analyzed (e.g., Mo and White 1985; Mo and Ghil 1987; Kidson 1988, 1999; Ghil and Mo 1991; Kiladis and Mo 1998; Mo 2000; Revell et al. 2001; Frederiksen and Zheng 2007). Although there is some diversity in patterns and explained variances, the interannual low-frequency variability in the SH is dominated basically by three or four features. These are a Southern Hemisphere high latitude mode (HLM, also called Antarctic Oscillation (AAO), or Southern Annular Mode (SAM)), a Rossby wavetrain-like mode, referred to as the Pacific South America mode (PSA), and a Southern Hemisphere meridional wavetrain (MW) pattern (sometimes named South Pacific Wave, SPW), linking western Pacific to the western Atlantic Ocean.

Although there are inter-seasonal differences, several studies have verified that there is some similarity between these patterns in different seasons. For example, Fig. 7.3 shows the variability patterns obtained by Kidson (1999) using data from all months and low-pass filtered with a cut-off of 50-days.

The SAM, the dominant mode on interannual time scales (IA1 in Fig. 7.3), has a strong zonally symmetric component, with out of phase relationship between heights in a zonal band between 55°S and 45°S and heights south of 60°S and in the subtropics, leading to a maximum negative correlation between the anomalous zonal westerlies at about 40°S and 60°S. In its positive phase, it is associated with an equatorward shift of the polar jet. This mode shows a strong connection to ENSO events (Kiladis and Mo 1998; Kidson 1999; Carvalho et al. 2005, and references therein). Enhanced Hadley circulation, driven by strong convection over the central Pacific, strengthens the subtropical jet stream by the large scale meridional flux of westerly momentum. The large anomalies in the extratropical tropospheric zonal wind are brought about by the anomalous rotational circulation forced by perturbed divergence in the subtropics, as the Rossby wave source gets stronger there. The polar jet is weakened and the tendency is for a single

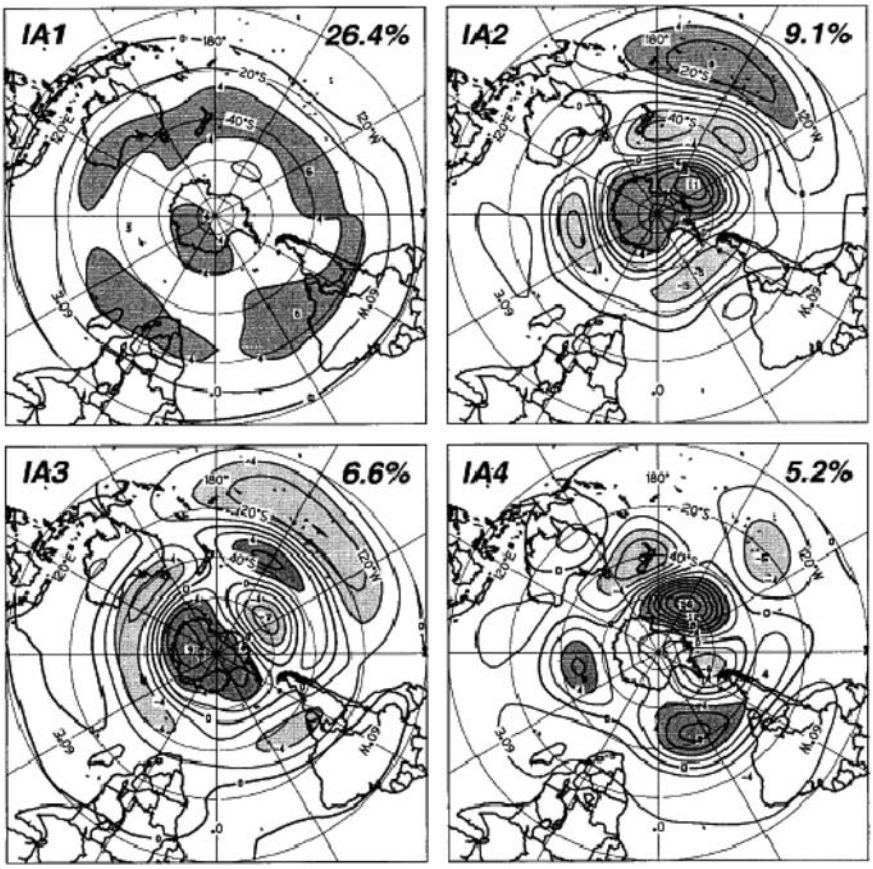

Fig. 7.3 The four leading Empirical Orthogonal Functions of 50-day low-pass filtered 300-hPa streamfunction (from Kidson 1999, reproduced with permission of the American Meteorological Society)

jet, resulting in an equatorward shift of the storm track, which affects southern SA. During cold events approximately opposite anomalies occur and the double jet is more pronounced, as the polar jet gets stronger in subantarctic latitudes (e.g., Kiladis and Mo 1998). Revell et al. (2001) found the strongest upper-level divergence/convergence associated with this mode in the central tropical and subtropical Pacific. Besides the impact of the perturbed Hadley cell and Rossby wave propagation due to anomalous tropical heat sources, it is also necessary to take into account the feedback by the transients in strengthening the westerlies (e.g. Trenberth 1987).

The second and third leading patterns are also connected to ENSO, corresponding to the wave train response that propagates southeastward from the central/western tropical Pacific into the extratropics and then equatorward into SA. (e.g., Kidson 1999; Frederiksen and Zheng 2007). It is referred to as PSA patterns (Mo and Ghil 1987; Mo 2000, and references therein) in analogy to the

Northern Hemisphere PNA pattern (Wallace and Gutzler 1981). These modes seem to originate from the tropics or subtropics, are stronger over the Pacific sector, have wavenumber 3 structure at midlatitudes and are in quadrature, although there is no evidence that this represents a travelling oscillation (Kidson 1988). While one of them seems to originate in tropical central Pacific, the other seems to extend from subtropical western Pacific, which is coherent with the results by Revell et al. (2001). These modes are instrumental in the ENSO impact on southeastern SA. The interannual PSA modes in summer exhibit a much more zonally symmetric structure and weaker magnitude than in other seasons, with less indication of wave train turning northeastward from southern Pacific into subtropical SA and Atlantic Ocean (Kidson 1999; Frederiksen and Zheng 2007). This indicates that the extratropical ENSO teleconnection with southeastern SA in austral summer is weaker, as already suggested in Grimm (2003, 2004).

The fourth leading mode (MW) is a nearly meridional South Pacific wavetrain, with wavenumber 3 (winter) or 4 (summer), extending from Australia into the Atlantic Ocean. It is not related with ENSO, but seems to be connected with anomalous SST east of Australia. It also seems to be a product of Rossby wave dispersion (Karoly et al. 1989). Influence functions of the action centers of this pattern confirm the region between Australia/New Guinea and the Date Line as the region in which upper-level divergence is most efficient in producing the streamfuntion anomalies associated with this mode (not shown).

As seen, a large portion of the interannual variability of the atmosphere in Southern Hemisphere is linked to variations in the tropical oceans, and the most important influence is ENSO. Therefore, the impacts of ENSO will be described in next section.

7.3.2 El Niño/Southern Oscillation Teleconnections with South America

The most important mode of interannual variability of the coupled ocean-atmosphere system is ENSO. Literature on ENSO is extensive, and the reader can find comprehensive reviews in Philander (1990), Diaz and Markgraf (1992), Glantz et al. (1991), Allan et al. (1996) and Trenberth and Caron (2000). Here we will focus on its influence on circulation and precipitation.

The first interannual variability mode of precipitation in SA, which is connected with ENSO, shows the general tendency to opposite ENSO-related anomalies in northern/northeastern and southeastern SA (Fig. 7.4). This leading mode explains 19.0 % of the variance. To calculate the variability modes, precipitation data from about 10,000 stations over most of SA are averaged on a $2.5° \times 2.5°$ latitude-longitude grid. The analyzed period is 1961–2000. These data are obtained mainly from the Brazilian Agência Nacional de Águas (ANA) but also from some other Brazilian agencies and meteorological services of other countries in SA.

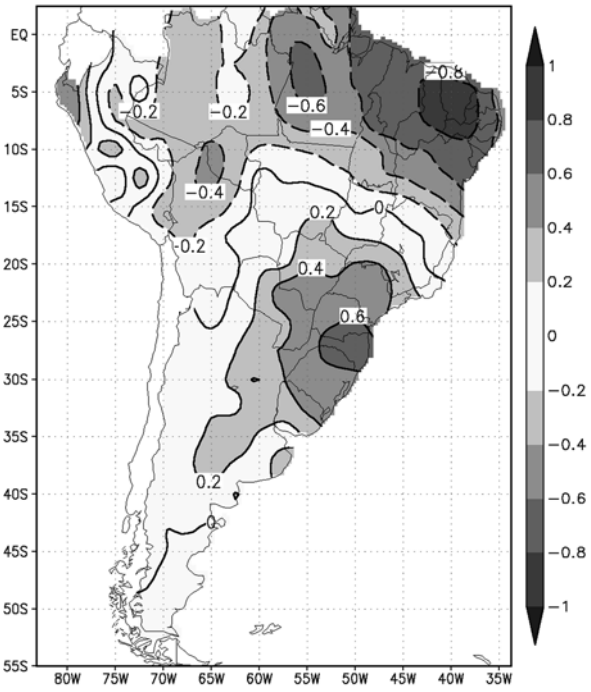

Fig. 7.4 First interannual variability mode of annual rainfall over South America

The anomalous tropical heat sources associated with ENSO events perturb the Walker and Hadley circulation over SA, and generate Rossby wave trains that produce important effects in the subtropics and extratropics of the continent. This response is represented in the leading Empirical Orthogonal Functions (EOFs) of circulation anomalies in Southern Hemisphere (such as the SAM and PSA). It is worth emphasizing that, in spite of the general similarity in the EOF patterns for different seasons, there are significant seasonal differences in these patterns. Therefore, there is some disagreement between the patterns calculated with all months (as in Fig. 7.3) and patterns for one season or month. The ENSO teleconnections described here will focus on the austral spring season, when they are strongest and the largest relative impacts occur.

7.3.2.1 Northern South America and the Tropics-Tropics Teleconnection

Areas located in northern/northeastern SA (including Venezuela, French Guiana, Surinam, Guyana and Brazilian Amazon and Northeast regions) have one of the most consistent ENSO-precipitation relationships (Ropelewski and Halpert 1987, 1989). Several authors (e.g., Kousky et al. 1984; Aceituno 1988; Rao and Hada 1990; Uvo et al. 1998; Souza and Ambrizzi 2002; Grimm 2003, 2004; Poveda et al. 2006; Grimm and Tedeschi 2009) reported observational evidence that EN (LN) episodes are related to deficient (abundant) rainy season in these continental

areas. Ambrizzi et al. (2004) and Magaña and Ambrizzi (2005) have associated ENSO impacts on the seasonal rainfall with the tropical Hadley and Walker regional circulation.

The tropics-tropics teleconnection is instrumental in the impact of ENSO over northern SA. In warm ENSO episodes, warm SST anomalies occur over the tropical central and eastern Pacific (Fig. 7.5). These warm anomalies induce more evaporation, lower sea level pressure, more low-level convergence and more convection in a tropical region with climatological subsidence. The enhanced convection translates into more precipitation, which is represented as negative OLR anomalies in Fig. 7.5. Consequently, there is upper level anomalous divergence over the eastern Pacific and convergence over northern SA (Fig. 7.5), which is associated with the descending branch of a stationary Kelvin wave that inhibits convective activity. The upper-level streamfunction anomalies show the expected pair of antyciclones straddling the tropical anomalous convection (Gill 1980), with a weaker pair of cyclonic anomalies to the east (Fig. 7.5). This anomalous convection over the central/eastern Pacific and its associated tropical circulation perturbs the Walker circulation from its climatological situation (compare Fig. 7.5 with Fig. 7.1) and the Pacific descending branch is shifted from eastern Pacific to northern SA and the increased subsidence over this region is associated with the observed rainfall deficit. Therefore, the Hadley cell is also perturbed (Fig. 7.5). However this canonical El Niño result for a typical episode may be altered by other factors that can modify this pattern, such as anomalous SST in the tropical Atlantic or other inter-episodes differences (Ambrizzi et al. 2004; Magaña and Ambrizzi 2005; Nobre and Shukla 1996).

Many studies have already indicated that the interannual variability of SSTs over the tropical Atlantic has a strong influence on the distribution of rainfall over the tropical Americas (Moura and Shukla 1981; Hasternrath 1984; Nobre and Shukla 1991). In particular, Nobre and Shukla (1996) presented observational evidence that ENSO phenomenon in the Pacific influences atmospheric circulation and SST anomalies over northern tropical Atlantic through atmospheric teleconnection patterns into higher latitudes of the Northern Hemisphere. They suggested that the Pacific-North American pattern (PNA – Horel and Wallace 1981) induces Sea Level Pressure (SLP) of the opposite sign between the Pacific and Atlantic tropical basins. Once SLP anomalies of opposite sign are set over the northern and southern Atlantic, then hemispherically asymmetric trade winds and SST anomalies follow. The observational and modeling studies done by Alexander et al. (2002) have also shown the connection between ocean basins via the "atmosphere bridge".

Besides the dynamics view of the link between the ENSO events in the Pacific and its influence over the Atlantic SSTAs one can also use thermodynamic arguments to explain this association. For example, one suggestion of Chiang and Sobel (2002), and expanded upon in Chiang and Lintner (2005), is that the thermodynamic view of the tropical teleconnection underscores the role of surface-troposphere disequilibrium: in the presence of a warm troposphere (which occurs within weeks after development of El Niño phase Pacific SSTAs because of anomalous temperature propagation via efficient Kelvin wave dynamics), the ocean surface temperature, with its large thermal inertia, initially lags. This produces certain signatures in the

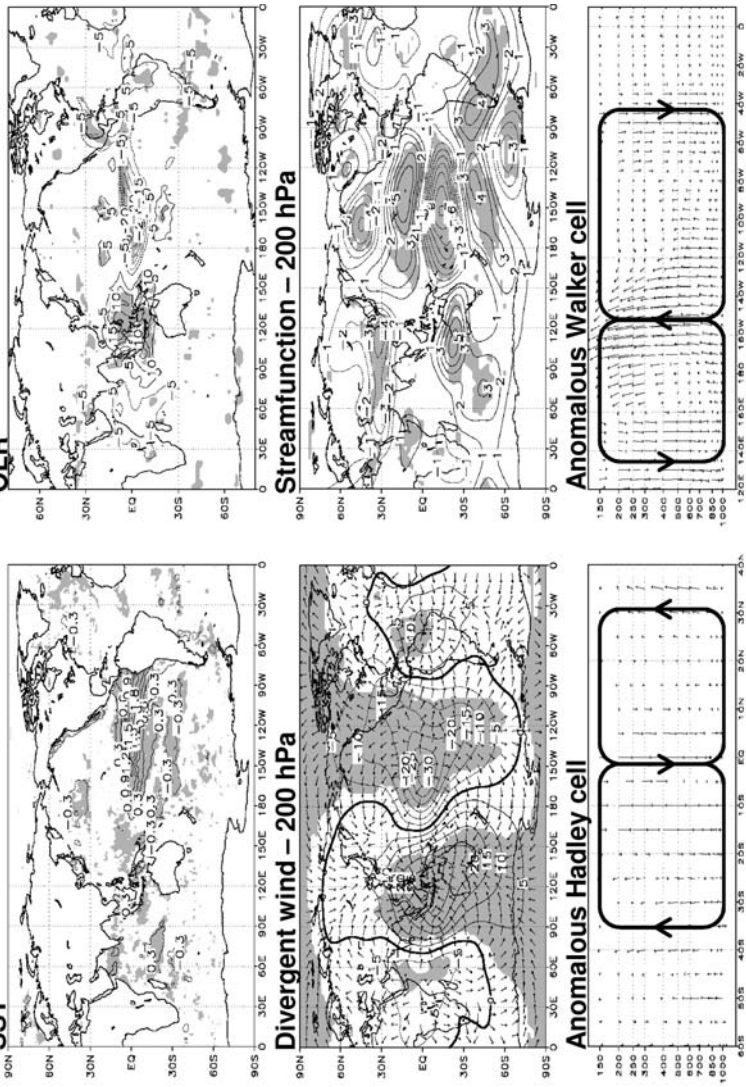

Fig. 7.5 Average anomalous fields associated with El Niño episodes in the austral spring (OND). Regions *shaded in gray* present consistent anomalies with significance level better than 0.10 (After Grimm 2009)

ocean surface flux budget, e.g., latent heating anomalies are initially negative (into the surface) as the surface warms, but the sign of the latent heating anomaly may, at some point, reverse, with positive anomalies acting to limit further surface warming. The way in which latent heating anomalies come about also encompasses both a dynamical effect – i.e., changes associated with low-level windspeed – as well as a thermodynamic effect – the difference in specific humidity at the surface relative to saturation. Chikamoto and Tanimoto (2006) noted that the latter appears to be important to the generation of the Atlantic SST response to El Niño.

The simplified Gill type circulation (Gill 1980) described in this section, i.e., anomalous forced ascent over the Pacific is balanced by compensatory descent elsewhere, is not able to fully explain many of the observed features in the tropical teleconnection where more realistic land-ocean-atmosphere interactions, moist convective dynamics, and inhomogeneous basic states have to be considered (Lintner and Chiang 2007). In fact the "atmospheric bridge" as defined by Lau and Nath (1996) or more recently the "remote tropics" discussed by Lintner and Chiang (2007) indicated the teleconnected dynamical and thermodynamic linkages between warm SST anomalies in the eastern equatorial Pacific and their remote tropical influence. The role of thermodynamics in propagating the ENSO signal to remote Tropics was suggested by the TT mechanism in the work of Chiang and Sobel (2002) and the importance of regionally variable moisture-related processes (e.g., advection and evaporation) in interfering with El Niño-related precipitation changes was studied by Neelin and Su (2005 and references therein).

In summary, as mentioned by Neelin and Su (2005), teleconnection in the tropics, and specially the important impacts on land precipitation are complicated by interactions with convective heating, shortwave and longwave cloud radiative feedbacks (Bergman and Hendon 2000) and land surface feedbacks. The present review has concentrated mostly on the dynamical aspects of the tropics-tropics interaction. However, a general view of the thermodynamic features can be obtained in some of the main studies described above.

7.3.2.2 Southeastern South America and the Tropics-Extratropics Teleconnection

Southeastern SA exhibits a strong and consistent impact of ENSO episodes on precipitation (Ropelewski and Halpert 1987, 1989; Aceituno 1988; Montecinos et al. 2000; Grimm et al. 1998, 2000a; Grimm 2003, 2004). Abundant (deficient) rainfall prevails during EN (LN) episodes, but the signal in precipitation is not uniform throughout an episode, because the atmospheric basic state in which the Rossby waves propagate undergoes seasonal variation. The season of strongest impact is spring, when the Rossby wave propagation is more intense towards subtropical SA, and a PSA-like pattern is more evident in the anomalous fields associated with the Southern Oscillation, as can be seen in Fig. 7.5. (e.g., Trenberth and Caron 2000). The focus of our analysis will be November, the month of strongest impact in spring.

The upper-level circulation anomalies during November of EN episodes show one wave train extending from central Pacific towards the extratropics with a small

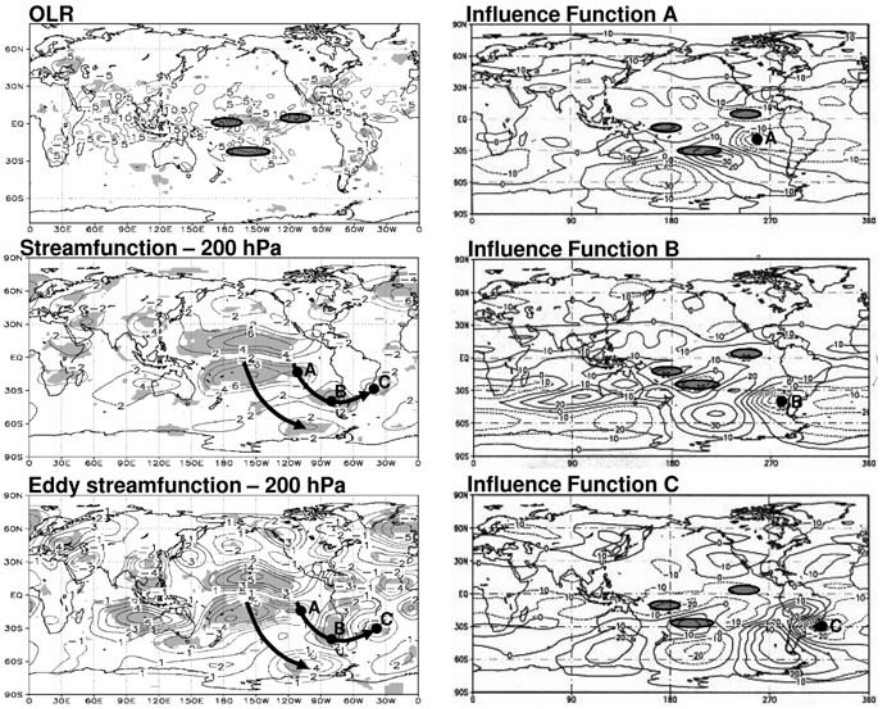

Fig. 7.6 (*Lefts panels*) Average anomalous OLR (with maximum convection over the tropical Pacific and maximum subsidence over the southern Pacific indicated by *shaded ellipses*) and streamfunction (total and without zonal mean) during November of EN episodes. Regions *shaded in gray* present consistent anomalies with significance level better than 0.10. (*Right panels*) Influence functions for the action centers of the wave train extending from eastern Pacific towards SA (*indicated by black circles*), with tropical/subtropical common regions with maximum positive (negative) values indicated by shaded ellipses (After Grimm 2009)

curvature, and another one emerging from the eastern Pacific and then, at the latitude of the subtropical jet, turning northeastward into subtropical SA, coherently with the characteristics of the propagation of a Rossby wave (Fig. 7.6). This wave train produces a cyclonic anomaly over southwest SA, and an anticyclonic anomaly off the eastern coast. This pattern of vertical equivalent barotropic structure favors the strengthening of the subtropical jet over SA, the advection of cyclonic vorticity over southeastern SA, and the transport of northerly warm and moist air into this region, making available the essential ingredients for excessive rainfall: moisture and dynamic lift (Grimm 2003). In LN episodes, the anomalies are nearly opposite, although the patterns are a little shifted; the result is deficient rainfall, with even stronger and more consistent anomalies than in EN (Grimm 2004). Besides the ENSO impact on total monthly rainfall, Grimm and Tedeschi (2009) disclosed an even stronger impact on extreme daily rainfall events, due to the greater sensitivity to ENSO in the heavy rainfall tail of the daily rainfall frequency distribution.

Figure 7.6 shows the influence functions (IFs, Grimm and Silva Dias 1995b) for the action centers of the eastern wave train. They indicate the importance of the anomalous convection (or upper level divergence) over eastern and central tropical Pacific (shown by the near equatorial ellipses) and the anomalous subsidence (or upper level convergence) over subtropical central Pacific (shown by the subtropical ellipse) in generating the streamfunction anomalies of this wave train, as the strongest values in the tropics, common to the three centers, are in these locations. The sign of the IFs is also coherent with the sign of the streamfunction anomaly around each center. For example, in the eastern and central tropical Pacific, the IFs are negative for action centers A and C, coherent with the negative streamfunction anomaly generated around these centers by positive divergence anomalies in those regions; on the other hand it is positive for action center B, coherent with the positive streamfunction anomaly generated around this center. Yet in the subtropics of central Pacific the IFs show opposite sign, indicating that negative divergence anomaly in this region (upper level convergence associated with subsidence) is able to generate streamfunction anomalies of the same sign as those generated by positive divergence anomalies in tropical eastern and central tropical Pacific. Frequently the IFs in the subtropics are stronger than in the tropics, indicating the importance of the compensatory subsidence in the local Hadley cell.

The regions with the strongest common IFs in Fig. 7.6 are also those with the strongest convection anomalies, as indicated by the OLR anomalies, which explains the significant wave train responsible for the consistent precipitation anomalies in southeastern SA. The IFs of the action centers of the western wave train (not shown) indicate the importance of anomalous upper level convergence over Australia as a possible source for this pattern.

A comment is necessary related to the influence function analysis: the large values of the influence functions at middle and higher latitudes do not imply that these regions are important for generating rotational flow by anomalous divergence at upper levels of the troposphere. It simply means that anomalous divergence in these regions is consistent with high values of the streamfunction at the target point. In these latitudes the upper level anomalous divergence is not directly related to anomalous heat sources as in the tropics, but divergence and vorticity are coupled. Thus, more attention is given to the tropics/subtropics, where the anomalous upper level divergence/convergence is directly related to anomalous tropical heat sources and nearly independent of the rotational flow.

From November to January the ENSO signal in rainfall weakens in southern Brazil and Uruguay, and even changes sign in the northern part of this region (see Section 7.3.2.3). However, in austral autumn, especially in April, remote influences are again instrumental in producing above normal rainfall in southeastern SA (Grimm et al. 2000a; Grimm and Tedeschi 2009).

Another example of information given by the IFs is the influence of tropical convection on the circulation in southern SA in winter (July). During winter of EN events there is increased precipitation in southeastern SA, especially when there is increased SST in the eastern Pacific, off the western SA coast. This caused extreme

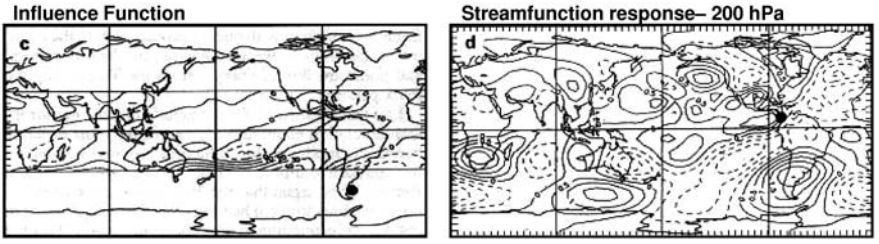

Fig. 7.7 (*Left*) Influence function of a target point in southern SA, indicated by a black circle (from Grimm and Silva Dias 1995b, reproduced with permission of the American Meteorological Society). (*Right*) Streamfunction response to an upper level anomalous divergence centered on the black circle over northern SA

floods in 1983, 1987, 1992, for instance. This enhanced precipitation is associated with a cyclonic anomaly over southern SA (Grimm et al. 2000a) which appears in EN episodes composites for winter (e.g., Karoly et al. 1989; Kiladis and Mo 1998). The IFs for the centers of the winter PSA pattern (not shown) display the right sign for producing the correct positive or negative streamfunction anomalies around each action center and indicate common influence region near the Date Line, and in the subtropics (Grimm and Silva Dias 1995b). It is noteworthy that, besides being influenced by upper level tropical divergence near the Date Line, as the other centers, the circulation around the center in southern SA is connected with the anomalous convection (or upper-level divergence) in eastern tropical Pacific and northern SA (Fig. 7.7, left). Anomalous convection in this region was strong in the EN years with strong winter rainfall anomalies in southern Brazil. Figure 7.7 (right) shows the simulated response to an upper level anomalous divergence in eastern equatorial Pacific/northern SA, featuring the cyclonic anomaly over southern SA. This inter-hemispheric connection, which is not present in austral summer, can enhance winter rainfall in southern Brazil even in non-ENSO years, when there are anomalous heat sources in western equatorial Atlantic and northern SA during the Northern Hemisphere summer.

7.3.2.3 Central-East Brazil and the Influence of Regional Processes During the Summer Monsoon

The Rossby wave tropical-extratropical teleconnection weakens in summer because the atmospheric basic state is not favorable to propagation, as the stronger westerlies are shifted to higher latitudes. There is a reversal of ENSO-related anomalies in central east Brazil (which is part of the SA monsoon core region) and in part of southern Brazil, from November to January, due to surface-atmosphere interactions that are stronger during summer. These processes favor a regional circulation pattern that overcomes the remote influences of spring (Grimm 2003, 2004; Grimm et al. 2007; Grimm and Zilli 2009).

7.4 Teleconnections with South America on Intraseasonal Time Scales

7.4.1 Southern Hemisphere Observed Intraseasonal Variability

The intraseasonal low-frequency variability (10–120 days) in the Southern Hemisphere has also been analyzed in a number of observational studies (e.g., Farrara et al. 1989; Kidson 1991; Ghil and Mo 1991; Mechoso et al. 1991; Lau et al. 1994; Kiladis and Mo 1998; Kidson 1999; Frederiksen and Zheng 2007).

The intraseasonal variability exhibits different behavior for the lower and higher frequency bands within the intraseasonal time-scales. The higher frequency intraseasonal variability (10–30 days), which concentrates much of the intraseasonal variability, is less anchored to the underlying geography. The variability patterns, usually in spatial quadrature, represent zonally oriented eastward (or equatorward) progressing wave trains in the extratropical westerly belt (near 50°S), with nearly equivalent barotropic vertical structure, usually generated by internal barotropic instability. Wavenumbers 3 and 4 are the most frequent (e.g. Kidson 1991, 1999; Berbery et al. 1992; Kiladis and Mo 1998; Frederiksen and Zheng 2007). According to Revell et al. (2001) there is no indication of the forcing of these higher frequency modes coming from the tropics, since the divergence field associated with them is essentially the divergence (convergence) ahead of each trough (ridge). This configuration generates the vorticity tendency needed to hold the upper-level component of a barotropic Rossby wave in check and prevent it being torn apart by the vertical shear in the background zonal wind.

Based on the observational intraseasonal teleconnection patterns for the Northern Hemisphere winter obtained by Hsu and Lin (1992), and applying the Rossby wave theory using simple barotropic models, Hoskins and Ambrizzi (1993) and Ambrizzi et al. (1995) draw diagrams of global teleconnection patterns of intraseasonal variability in the 10–30 day band for austral summer and winter (Fig. 7.8).

Figure 7.8, which is a conceptual diagram of teleconnection pathways obtained from global lag correlation analysis, suggests that the South American continent can be influenced by the passage of the intraseasonal waves in the subtropical and polar jets which may act as wave guides (e.g., Berbery et al. 1992; Hoskins and Ambrizzi 1993; Ambrizzi and Hoskins 1997). It is also indicated that inter-hemispheric propagation and extratropics-tropics interaction can affect the atmospheric circulation over SA, and are dependent of the season. For instance, the wave propagation pattern linking the tropics with the extratropics is clearly observed from the streamfunction 200 hPa map depicted in Fig. 7.6.

In this frequency band the extratropics-tropics interaction is frequent. Troughs and associated frontal zones propagate into the tropical SA from the Southern Hemisphere westerlies, producing cloud band activity over the South Atlantic Convergence Zone (SACZ), connecting extratropics and tropics (e.g., Kiladis and Weickmann 1992a, b, 1997; Liebmann et al. 1999; Todd et al. 2003).

The lower frequency intraseasonal variability (30–120 day) is mainly dominated by the eastward propagating Madden-Julian Oscillation (MJO) on the 30–60 day

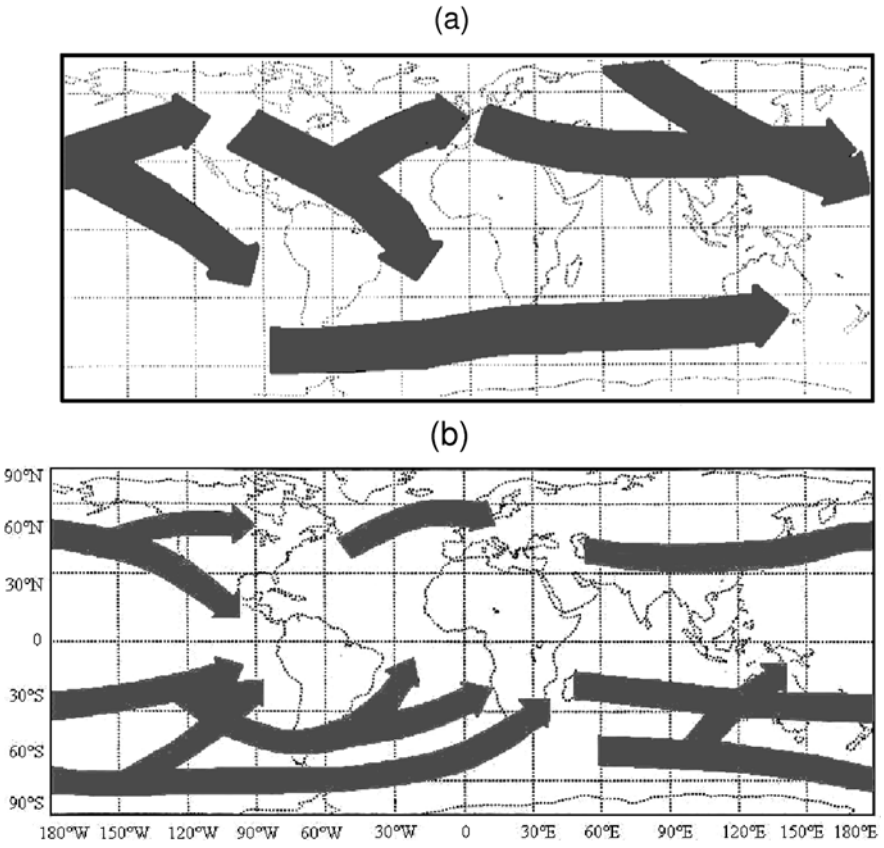

Fig. 7.8 Conceptual diagram of the global teleconnection pathways of intraseasonal influence obtained from lag correlation maps for (**a**) DJF and (**b**) JJA. (After Hoskins and Ambrizzi 1983; and Ambrizzi et al. 1995)

time scale (Madden and Julian 1971). This oscillation dominates the tropical intraseasonal variability, with spatial scale of wavenumber 0 through 2, but also significant extratropical signals are observed during its evolution. The MJO relationships to extratropical intraseasonal variability over the Southern Hemisphere will be analyzed in the following section. The PSA patterns are also present in association with the MJO.

In spite of the differences, there are similarities between the interannual variability patterns described previously and the intraseasonal patterns mentioned above. Both are dominated by the wave 3 and 4 structures and there are fluctuations in similar locations in a broad range of time scales, as in the action centers of the PSA pattern and the MW pattern. The PSA patterns, for example, are present in time-scales ranging from daily (Mo and Ghil 1987), intraseasonal (Ghil and Mo 1991; Mo and Higgins 1998), interannual (Kidson 1988, 1999) to interdecadal

timescales (Garreaud and Battisti 1999). Therefore there can be a periodic amplification/suppression of the stationary waves in those locations (Kiladis and Mo 1998; Frederiksen and Zheng 2007).

7.4.2 Madden-Julian Oscillation (MJO)

There is vast literature on the MJO. Observational and theoretical aspects can be found in Knutson and Weickmann (1987), Lau and Chan (1988), Rui and Wang (1990), Ferranti et al. (1990), Hendon and Salby (1994), Madden and Julian (1994). Here the focus is on the signals related to SA in austral summer, as this is rainy season over most of the continent.

The MJO can be described as a planetary-scale mechanism with disturbances in both tropical deep convection and tropospheric circulation, which propagate eastward in the tropics, taking approximately 30–60 days for a complete cycle around the globe (Madden and Julian 1994), but with related perturbations also in the extratropics.

Observational analysis has disclosed significant intraseasonal variability in the 30–60 day time scales over tropical (Kousky and Kayano 1994; Carvalho et al. 2002; Ferraz 2004; Souza et al. 2005; Souza and Ambrizzi 2006) and subtropical SA, with emphasis on SACZ (Casarin and Kousky 1986; Nogués-Paegle and Mo 1997; Grimm et al. 2000b; Nogués-Paegle et al. 2000; Ferraz 2004; Carvalho et al. 2004; Cunningham and Cavalcanti 2006), which is dynamically linked with MJO events (Kiladis and Weickmann 1992a; Grimm and Silva Dias 1995b). In addition, Jones et al. (2004) reported robust signals of increased frequency of precipitation extremes in the eastern part of SA during active MJO situations.

The intraseasonal variability of summer precipitation (November through March) over SA in the 30–60 day band exhibits two main features: the variability in central-east Brazil and the variability of the SACZ. The first two rotated Empirical Orthogonal Functions (EOFs) represent these features (Fig. 7.9, Ferraz 2004). The first rotated mode (10.6% of the variance) represents oscillations in SACZ, while the second one is concentrated in Central-East Brazil (10.2% of the variance). Both modes also feature anomalies in the subtropical plains of SA that are opposite in sign to those in the main center, but much weaker in magnitude. There is, however, a significant "dipole"-like relationship between precipitation anomalies in Central-East Brazil/SACZ and the subtropics to the south, although with different magnitude in both centers.

The local circulation anomalies associated with the first two modes are consistent with a seesaw pattern in precipitation. In one extreme phase of the first (second) mode, a cyclonic anomaly around 25°S, 45°W (20°S, 50°W) directs the northwesterly moisture flux into SACZ (Central-East Brazil) and decreases the southward transport to southeastern SA. In the opposite phase, an anticyclonic anomaly enhances the moisture flux towards the subtropical plains (In Fig. 7.9, right, the arrows of moisture transport are very similar to the low-level wind). In both modes the positive precipitation anomalies are connected with a cyclonic anomaly

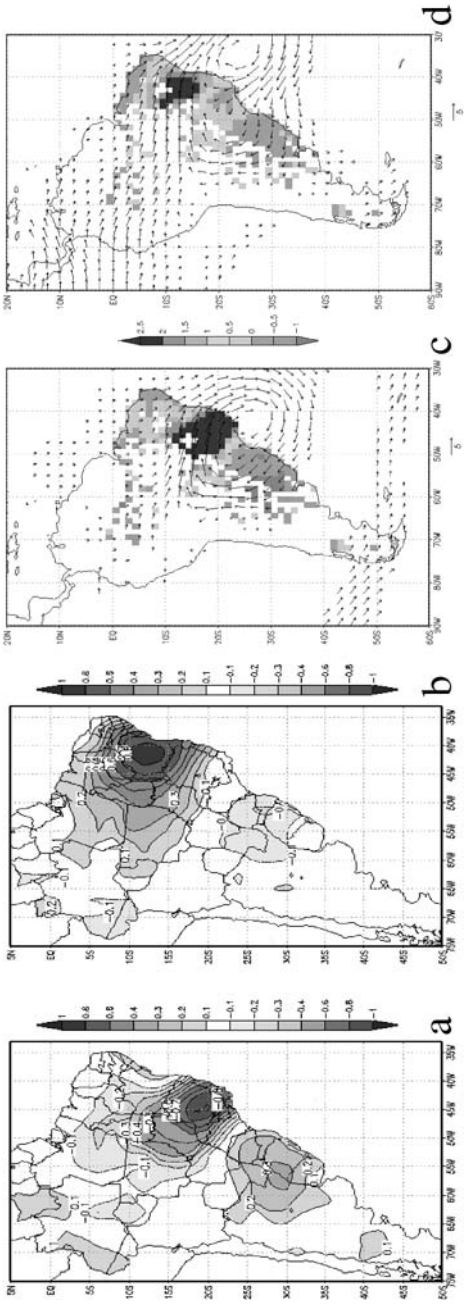

Fig. 7.9 (*Left*) First two rotated modes of intraseasonal variability in the 30–70 day band. (*Right*) Composites of rainfall anomalies and vertically integrated moisture flux for wet phases of these modes in the SACZ and central-east Brazil. Only significant anomalies are represented by arrows (From Ferraz 2004)

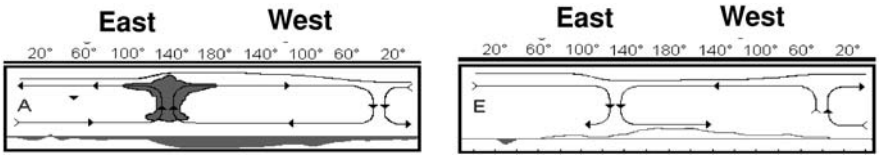

Fig. 7.10 Diagram of the anomalous Walker circulation associated with the phases of the MJO in which there is reduced (*left*) and increased (*right*) rainfall in Central-East Brazil, in the second mode of Fig. 7.9

to the southwest. For the first mode, there is still a connection with an anticyclonic anomaly southwest of this cyclonic anomaly, over southeast Pacific and southern SA, while for the second mode there is a stronger connection with winds in the tropical Pacific.

The first mode seems to be result of a tropical-extratropical interaction, while the second one is probably the product of a tropical-tropical interaction. The low-level circulation connected with these modes in Fig. 7.9 shows that there are no significant winds connected with the first mode in the tropics, but there is a significant connection with the extratropics. The second mode shows opposite behavior, with stronger connection with the tropics, and weaker with the extratropics.

The connection of the second mode with the tropics is stronger when the increased (reduced) convection associated with MJO is over New Guinea and the subsiding (ascending) branch of the anomalous Walker cell is over northern SA, as represented by Madden and Julian (1994), and reproduced in Fig. 7.10. Therefore, enhanced (reduced) convection over central-east Brazil would approximately correspond to reduced (enhanced) convection over New Guinea (corresponds to the first and third panels in the evolution of the MJO convection displayed by Ferranti et al. 1990).

From Fig. 7.10, it is clear that tropics-tropics interaction over South America seems to be important in modulating the precipitation. A further example of the MJO signature is the composite of rainfall anomalies over tropical Brazil keyed to the MJO cycle (Fig. 7.11) presented in Souza and Ambrizzi (2006). A large contribution to the intraseasonal variability over this region can also be due to the interactions with the submonthly variability related to SACZ and ITCZ activity (Souza et al. 2005).

The connection of the first mode in Fig. 7.9 (SACZ mode) to the extratropics is stronger when the convection signal of MJO reaches the SPCZ, enhancing it and shifting it eastward, at the same time that subsidence prevails over Indonesia. IF analysis indicates that the maximum influence in generating the cyclonic anomaly associated with the enhanced SACZ comes from the shifted SPCZ region with subtropical convection over the Pacific Ocean (Fig. 7.12). Anomalous divergence associated with enhanced SPCZ in this phase of MJO is able to generate an extratropical wave train that can stimulate the SACZ by generating the cyclonic anomaly southwest of it (Fig. 7.12, Grimm and Silva Dias 1995b), while opposite effects are associated with the opposite phase of the MJO (these phases correspond

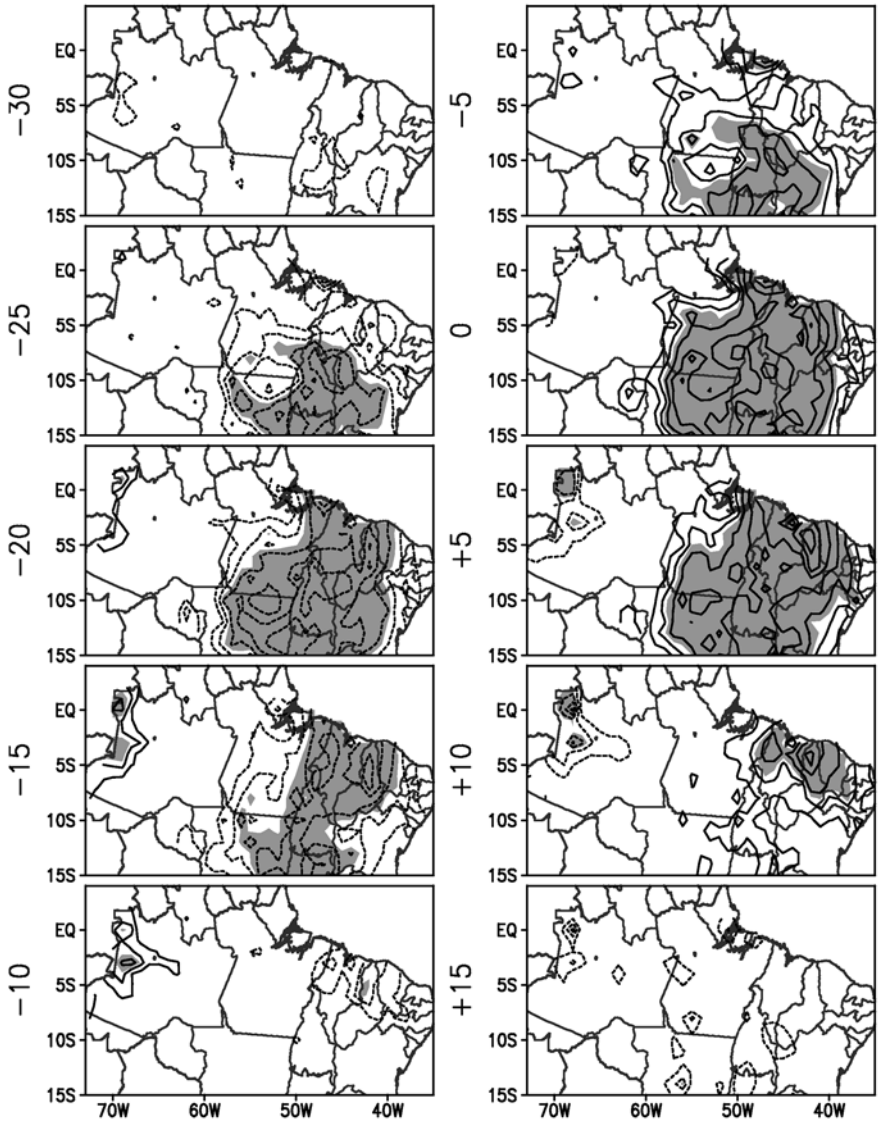

Fig. 7.11 Composites of rainfall anomalies over Tropical Brazil for pentads from day –30 to +15. Nonzero values are contoured every 0.5 mm/day with solid (dashed) contours for positive (negative) anomalies. Shaded areas indicate statistically significant anomalies at 95% local confidence level (After Souza and Ambrizzi 2006)

approximately to the second and fourth panels in the MJO-related OLR evolution displayed by Ferranti et al. 1990). Observational studies confirm this association between enhanced SACZ and an extratropical wave train in the MJO time scale (e.g., Casarin and Kousky 1986; Horel and Jones 1990, Fig. 7.12).

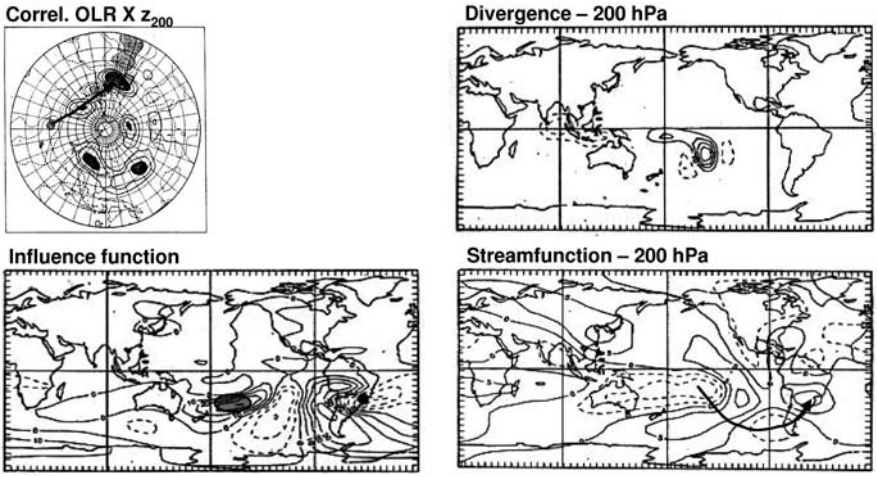

Fig. 7.12 (Upper left) Correlation analysis between OLR at the SACZ and geopotential height at 200 hPa, both filtered to retain only intraseasonal variability (from Jones and Horel 1990). (*Lower left*) Influence function for the target point at the center of the cyclonic anomaly associated with enhanced SACZ, with the region of maximum values indicated by the shaded ellipse. (*Upper right*) Prescribed anomalous divergence at 200 hPa, reproducing the shifted SPCZ at one of the MJO phases, and (*lower right*) resulting streamfunction at 200 hPa (From Grimm and Silva Dias 1995b, reproduced with permission of the American Meteorological Society)

The examples of tropical-extratropical and tropical-tropical teleconnections presented so far described remote influences on the SA circulation and precipitation. However, it is important to mention that SA anomalous tropical convection is also able to excite Rossby wave dispersion, even inter-hemispheric, through the region of climatological upper-level westerlies in the equatorial Atlantic. For example, Grimm and Silva Dias (1995b) show (Fig. 7.13) that the anomalous convection over central-east Brazil (or the SACZ shifted northward) associated with one phase of the MJO generates a wave train that propagates over North Atlantic and Eurasia, which shows reasonable agreement with the composites of streamfunction associated with this phase of the MJO (e.g., Weickmann et al. 1985; Knutson and Weickmann 1987). As this wave train is able to influence convection in the western Pacific/ Indian Ocean

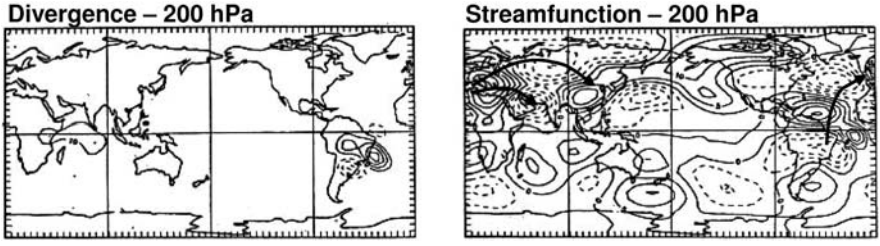

Fig. 7.13 (*Left*) Anomalous divergence at 200 hPa corresponding to enhanced SACZ at one of the MJO phases; (*Right*) resulting streamfunction at 200 hPa (From Grimm and Silva Dias 1995b, reproduced with permission of the American Meteorological Society)

and thus trigger a new pulse of the MJO, there is another dynamical mechanism for explaining the intraseasonal variability associated with the MJO (Grimm and Silva Dias 1995b).

7.5 Final Remarks

Tropical-tropical and tropical-extratropical teleconnections have an important role in generating low-frequency variability of the atmosphere, as demonstrated in many studies. The relationship between tropical anomalous heat sources and atmospheric circulation anomalies provides longer term predictability, which needs to be realized.

Observational and theoretical studies have done much to examine the role of tropical forcing (e.g. review by Trenberth et al. 1998), but several issues remain to be addressed in more detail in order to better understand the interannual and intraseasonal variations derived both from tropical forcing and from boundary forcing or internal variability at higher latitudes. There are a number of factors influencing the teleconnections through the atmosphere, such as the basic atmospheric state, feedback from transients, baroclinic and non-linear effects, feedbacks from induced changes in the underlying surface, such as changes in extratropical SSTs and land surface hydrology. Land-surface processes may be especially important in summer (e.g., Grimm et al. 2007; Grimm and Zilli 2009). Much research is still needed to explore all these issues.

This chapter provides only a brief summary of the main observed teleconnections affecting SA. However, besides ENSO and MJO, there are other possible sources of teleconnections with SA, generating regional patterns of interest, but they may have insufficient variance to be identified by the EOF analyses.

An important issue to be aware of is the dependency of the teleconnections on the basic atmospheric state through which they propagate. Slow variations on interdecadal time scales or longer can affect teleconnections that are effective in present time, shifting the teleconnection patterns and the resulting impacts (e.g., Grimm et al. 2006).

Acknowledgments: The authors thank the two anonymous reviewers for their comments and suggestions. A.M.G. acknowledges the support of CNPq (Brazil) and the European Community's Seventh Framework Programme (FP7/2007-2013) under Grant Agreement N°212492 (CLARIS LPB. A Europe-South America Network for Climate Change Assessment and Impact Studies in La Plata Basin). T.A. was partially supported by CNPq, FAPESP and CAPES.

References

Aceituno P (1988) On the functioning of the Southern Oscillation in the South America Sector Part I: surface climate. Mon Wea Rev 116:505–524

Alexander MA, Bladé I, Newman M et al (2002) The atmospheric bridge: the influence of ENSO teleconnections on air-sea interactions over the global oceans. J Clim 15:2205–2231

Allan RJ, Lindesay J, Parker D (1996) El Niño Southern Oscillation and climate variability. CSIRO Publishing. Collingwood Victoria, Australia, p 405

Ambrizzi T, Hoskins BJ, Hsu HH (1995) Rossby wave propagation and teleconnection patterns in the austral winter. J Atmos Sci 52:3661–3672

Ambrizzi T, Hoskins BJ (1997) Stationary Rossby wave propagation in a baroclinic atmosphere. Quart J Roy Meteor Soc 123:919–928

Ambrizzi T, Souza EB, Pulwarty RS (2004) The Hadley and Walker regional circulations and associated ENSO impacts on the South American Seasonal Rainfall. In: Diaz HF, Bradley RS (eds) The Hadley circulation: present, past, and future. Kluwer Academic Press, Dordrecht

Angstroem A (1935) Teleconnections of climate changes in present time. Geogr Ann 17:242–258.

Arkin A (1982) The relationship between interannual variability in the 200 mb tropical wind field and the Southern Oscillation. Mon Wea Rev 110:1393–1404

Berbery EH, Nogués-Paegle J, Horel JD (1992) Wavelike Southern Hemisphere extratropical teleconnections. J Atmos Sci 49:155–177

Bergman JW, Hendon HH (2000) Cloud radiative forcing of the low latitude tropospheric circulation: linear calculations. J Atmos Sci 57:2225–2245

Bjerknes J (1966) A possible response of the atmospheric Hadley circulation to Equatorial anomalies of ocean temperature. Tellus 18:820–829

Bjerknes J (1969) Atmospheric teleconnections from the Equatorial Pacific. Mon Wea Rev 97: 163–172

Branstator GW (1983) Horizontal energy propagation in a barotropic atmosphere with meridional and zonal structure. J Atmos Sci 40:1689–1708

Branstator GW (1985) Analysis of general circulation model sea-surface temperature anomaly simulations using a linear model. Part I: Forced solutions. J Atmos Sci 42:2225–2241

Carvalho LMV, Jones C, Silva Dias MAF (2002) Intraseasonal large-scale circulations and mesoscale convective activity in tropical South America during TRMM-LBA campaign. J Geophys Res 107(D20):9–19

Carvalho LMV, Jones C, Liebmann B (2004) The South Atlantic Convergence Zone: intensity, form, persistence, and relationships with intraseasonal to interannual activity and extreme rainfall. J Clim 17:88–108

Carvalho LMV, Jones C, Ambrizzi T (2005) Opposite Phases of the Antarctic Oscillation and relationships with intraseasonal to interannual activity in the tropics during the Austral Summer. J Clim 18:702–718

Casarin DP, Kousky VE (1986) Anomalias de precipitação no sul do Brasil e variações na circulação atmosférica. Revista Brasileira de Meteorologia 1:83–90

Chiang JCH, Sobel AH (2002) Tropical tropospheric temperature variations caused by ENSO and their influence on the remote tropical climate. J Clim 15:2616–2631

Chiang JCH, Lintner BR (2005) Mechanisms of remote tropical surface warming during El Niño. J Clim 18:4130–4140

Chikamoto Y, Tanimoto Y (2006) Air-sea humidity effects on the generation of tropical Atlantic SST anomalies during the ENSO events. Geophys Res Lett. doi: 10.1029/2006GL027238

Cunningham CAC, Cavalcanti IFA (2006) Intraseasonal modes of variability affecting the South Atlantic Convergence Zone. Int J Climatol 26:1165–1180

Diaz HF, Markgraf V (eds) (1992) El Niño: Historical and Paleoclimatic aspects of the Southern Oscillation. Cambridge University Press, Cambridge

Diaz HF, Bradley RS (eds) (2004) The Hadley circulation: present, past and future. Kluwer Academic Press, Dordrecht

Farrara JD, Ghil M, Mechoso CR et al (1989) Empirical orthogonal functions and multiple flow regimes in the Southern Hemisphere winter. J Atmos Sci 46:3219–3223

Ferranti L, Palmer TN, Molteni F et al (1990) Tropical-Extratropical interaction associated with the 30–60 day oscillation, and its impact on medium and extended range prediction. J Atmos Sci 47:2177–2199

Ferraz SET (2004) Intraseasonal variability in Brazil and southern South America. PhD Thesis. Department of Atmospheric Sciences, University of São Paulo
Frederiksen JS, Webster PJ (1988) Alternative theories of atmospheric teleconnections and low-frequency fluctuations. Rev Geophys 26:459–494
Frederiksen CS, Zheng X (2007) Variability of seasonal-mean fields arising from intraseasonal variability. Part 3: Application to SH winter and summer circulations. Climate Dyn 28:849–866
Garreaud RD, Battisti DS (1999) Interannual (ENSO) and interdecadal (ENSO-like) variability in the Southern Hemisphere. J Clim 12:2113–2123
Ghil M, Mo K (1991) Instraseasonal oscillations in the global atmosphere. Part II: Southern Hemisphere. J Atmos Sci 48:780–790
Gill AE (1980) Some simple solutions for heat-induced tropical circulation. Quart J Roy Meteor Soc 106:447–462
Glantz M, Katz R, Nicholls N (eds) (1991) Teleconnections linking worldwide climate anomalies. Cambridge University Press, Cambridge
Grimm AM, Silva Dias PL (1995a) Use of barotropic models in the study of the extratropical response to tropical heat sources. J Meteor Soc Jpn 73:765–780
Grimm AM, Silva Dias PL (1995b) Analysis of tropical–extratropical interactions with influence functions of a barotropic model. J Atmos Sci 52:3538–3555
Grimm AM, Ferraz SET, Gomes J (1998) Precipitation anomalies in Southern Brazil associated with El Niño and La Niña events. J Clim 11:2863–2880
Grimm AM, Barros VR, Doyle ME (2000a) Climate variability in Southern South America associated with El Niño and La Niña events. J Clim 13:35–58
Grimm AM, Ferraz SET, Barros VR et al (2000b) Intraseasonal variations of the South American summer rainfall. CLIVAR Exchanges 5(2):13–14
Grimm AM (2003) The El Niño impact on the summer monsoon in Brazil: regional processes versus remote influences. J Clim 16:263–280
Grimm AM (2004) How do La Niña events disturb the summer monsoon system in Brazil? Clim Dyn 22 (2–3):123–138
Grimm AM, Sahai AK, Ropelewski CF (2006) Interdecadal variations in AGCM simulation skills. J Clim 19:3406–3419
Grimm AM, Pal J, Giorgi F (2007) Connection between spring conditions and peak summer monsoon rainfall in South America: role of soil moisture, surface temperature, and topography in Eastern Brazil. J Clim 20:5929–5945
Grimm AM, Tedeschi RG (2009) ENSO and extreme rainfall events in South America. J Clim 22:1589–1609
Grimm AM, Zilli MT (2009) Interannual variability and seasonal evolution of summer monsoon rainfall in South America. J Clim 22:2257–2275
Grimm AM (2009) Variabilidade interanual/ENOS. In: Cavalcanti IFA, Ferreira NJ, Silva Dias MA et al (eds) Tempo e Clima no Brasil, Chapter 22. Editora Offitexto, São Paulo, Brazil (in press)
Hadley G (1735) Concerning the cause of the general trade winds. Philos Trans R Soc Lond 39: 58–62
Halley E (1686) An historical account of the Trade Winds, and Monsoons, observable in the seas between the Tropics, with an attempt to assign the physical cause of the said winds. Philos Trans R Soc Lond 16:153–168
Hasternrath S (1984) Interannual variability and annual cycle: mechanisms of circulation and climate in the tropical Atlantic. Mon Wea Rev 112:1097–1107
Held IM, Hou AY (1980) Nonlinear axially symmetric circulation in a nearly inviscid atmosphere. J Atmos Sci 37:515–533
Hendon HH, Salby ML (1994) The life cycle of the Madden-Julian Oscillation. J Atmos Sci 51:2225–2237
Horel JD, Wallace JM (1981) Planetary-scale atmospheric phenomena associated with the Southern Oscillation. Mon Wea Rev 109:813–829

Horel JD, Jones C (1990) Uma investigação sobre a variabilidade de baixa freqüência da circulação de grande escala sobre a América do Sul. Proceedings of the Brazilian Meteorological Congress, v.2, 539–543, Brazilian Meteorological Society

Hoskins BJ, Simmons AJ, Andrews DG (1977) Energy dispersion in a barotropic atmosphere. Quart J Roy Meteor Soc 103:553–567

Hoskins BJ, Karoly DJ (1981) The steady linear responses of a spherical atmosphere to thermal and orographic forcing. J Atmos Sci 38:1179–1196

Hoskins BJ, Pearce RP (1983) Large-scale dynamical processes in the atmosphere, Academic Press, San Diego

Hoskins BJ, Ambrizzi T (1993) Rossby wave propagation on a realistic longitudinally varying flow. J Atmos Sci 50:1661–1671

Hsu HH, Lin SH (1992) Global teleconnections in the 250 mb streamfunction field during the Northern Hemisphere winter. Mon Wea Rev 120:1169–1190

Jones C, Waliser DE, Lau KM et al (2004) Global occurrences of extreme precipitation and the Madden-Julian oscillation: observations and predictability. J Clim 17:4575–4589

Karoly DJ, Plumb RA, Ting M (1989) Examples of the horizontal propagation of quasi-stationary waves. J Atmos Sci 46:2802–2811

Kidson JW (1988) Interannual variations in the Southern Hemisphere circulation. J Clim 1: 1177–1198.

Kidson JW (1991) Intraseasonal variations in the Southern Hemisphere circulation. J Clim 4: 939–953.

Kidson JW (1999) Principal modes of Southern Hemisphere low-frequency variability obtained from NCEP–NCAR reanalyses. J Clim 12: 2807–2830.

Kiladis GN, Weickmann KM (1992a) Circulation anomalies associated with tropical convection during northern winter. Mon Wea Rev 120:1900–1923

Kiladis GN, Weickmann KM (1992b) Extratropical Forcing of Tropical Pacific Convection during Northern Winter, Mon Wea Rev 120:1924–1939

Kiladis GN, Weickmann KM (1997) Horizontal structure and large scale circulations associated with submonthly convection. Mon Wea Rev 125:1997–2013

Kiladis GN, Mo KC (1998) Interannual and intraseasonal variability in the Southern Hemisphere. Meteorology of the Southern Hemisphere. Meteor Monogr, Am Meteor Soc 49:307–336.

Knutson TR, Weickmann KM (1987) 30–60 day atmospheric oscillations: composite life cycles of convection and circulation anomalies. Mon Wea Rev 115:1407–1436

Kousky VE, Kayano MT, Cavalcanti IFA (1984) A review of the Southern Oscillation: oceanic-atmospheric circulation changes and related rainfall anomalies. Tellus 36A:490–504

Kousky VE, Kayano MT (1994) Principal modes of outgoing longwave radiation and 250-mb circulation for the South American sector. J Clim 7: 131–1143

Lau NC, Nath MJ (1996) The role of the "atmosphere bridge" in linking tropical Pacific ENSO events to extratropical SST anomalies. J Clim 9:2036–2057

Lau KM, Chan PH (1988) Intraseasonal and interannual variations of tropical convection: A possible link between the 40–50 day oscillation and ENSO? J Atmos Sci 45:506–521

Lau KM, Sheu PJ, Kang IS (1994) Multiscale low-frequency circulation modes in the global atmosphere. J Atmos Sci 51:1169–1193

Liebmann B, Hartmann DL (1984) An observational study of tropical-midlatitude interaction on intraseasonal time scales during winter. J Atmos Sci 41:3333–3350

Liebmann B, Kiladis GN, Marengo JA et al (1999) Submonthly convective variability over South America and the South Atlantic Convergence Zone. J Clim 12:1877–1891

Lintner BR, Chiang JCH (2007) Adjustment of the remote tropical climate to El Niño conditions. J Clim 20:2544–2556

Madden RA, Julian PR (1971) Description of a 40–50 day oscillation in the zonal wind in the tropical Pacific. J Atmos Sci 28:702–708

Madden RA, Julian PR (1994) Observations of the 40–50-day tropical oscillation – A Review. Mon Wea Rev 122:814–837

Magaña V, Ambrizzi T (2005) Dynamics of subtropical vertical motions over the Americas during El Niño boreal winters. Atmósfera 18(4):211–233

Mak MK (1969) Laterally driven stochastic motions in the tropics. J Atmos Sci 26:41–64

Matthews AJ, Kiladis GN (1999) The tropical-extratropical interaction between high-frequency transients and the Madden-Julian oscillation. Mon Wea Rev 127:661–677

Mechoso CR, Farrara JD, Ghil M (1991) Intraseasonal variability of the winter circulation in the Southern Hemisphere atmosphere. J Atmos Sci 48:1387–1404

Minobe S (2004) Year-to-year variability in the Hadley and Walker circulations from NCEP/NCAR reanalysis data. In: Diaz HF, Bradley RS (eds) The Hadley circulation: present, past, and future. Kluwer Academic Press, Dordrecht

Mo KC, White GH (1985) Teleconnections in the Southern Hemisphere. Mon Wea Rev 113:22–37

Mo KC, Ghil M (1987) Statistics and dynamics of persistent anomalies. J Atmos Sci 44: 877–901

Mo KC, Higgins RW (1998) The Pacific–South American modes and tropical convection during the Southern Hemisphere winter. Mon Wea Rev 126:1581–1596

Mo KC (2000) Relationships between low-frequency variability in the Southern Hemisphere and sea surface temperature anomalies. J Clim 13:3599–3620

Montecinos A, Diaz A, Aceituno P (2000) Seasonal diagnostic and predictability of rainfall in subtropical South America based on tropical Pacific SST. J Clim 13:746–758

Moura AD, Shukla J (1981) On the dynamics of droughts in northeast Brazil: Observations, theory and numerical experiments with a general circulation model. J Atmos Sci 38:2653–2675

Neelin JD, Su H (2005) Moist teleconnection mechanisms for the tropical South American and Atlantic sector. J Clim 18:3928–3950

Nobre P, Shukla J (1991) Interannual variability of SST and wind stress over the tropical Atlantic and rainfall over Amazon and Northeast Brasil. Fifth Conf. on Climate Variations, Denver, CO, Am Meteor Soc 1:472–475

Nobre P, Shukla J (1996) Variations of Sea Surface Temperature, wind stress, and rainfall over the Tropical Atlantic and South America. J Clim 9:2464–2479

Nogués-Paegle J, Mo KC (1997) Alternating wet and dry conditions over South America during summer. Mon Wea Rev 125:279–290

Nogués-Paegle J, Byerle LA, Mo KC (2000) Intraseasonal modulation of South American summer precipitation. Mon Wea Rev 128:837–850

Oort AH, Yienger JJ (1996) Observed interannual variability in the Hadley circulation and its connection to ENSO. J Clim 9:2751–2767

Philander SG (1990) El Niño and La Niña and the Southern Oscillation. Academic Press, San Diego

Poveda G, Waylen PR, Pulwarty RS (2006) Annual and inter-annual variability of the present climate in northern South America and southern Mesoamerica. Palaeogeogr Palaeoclimatol Palaeoecol 234: 3–27

Rao VB, Hada K (1990) Characteristics of rainfall over Brazil: annual variations and connections with the Southern oscillation. Theor Appl Climatol 42:81–91

Rasmusson EM, Mo K (1993) Linkages between 200 mb tropical and extratropical circulation anomalies during the 1986–1989 ENSO cycle. J Clim 6:595–616

Revell MJ, Kidson JW, Kiladis GN (2001) Interpreting low-frequency modes of Southern Hemisphere atmospheric variability as the rotational response to divergence forcing. Mon Wea Rev 129: 2416–2425

Ropelewski CF, Halpert MS (1987) Global and regional scale precipitation patterns associated with the El Niño/Southern Oscillation. Mon Wea Rev 115:1606–1626

Ropelewski CF, Halpert MS (1989) Precipitation patterns associated with the high index phase of the Southern Oscillation. J Clim 2:268–284

Rossby CG (1945) On the propagation of frequencies and energy in certain types of oceanic and atmospheric waves. J Meteor 2:187–204

Rui H, Wang B (1990) Development characteristics and dynamic structure of tropical intraseasonal convection anomalies. J Atmos Sci 47:357–379

Sardeshmukh PD, Hoskins BJ (1988) The generation of global rotational flow by steady idealized tropical divergence. J Atmos Sci 48:629–650
Schubert SD (1986) The structure, energetics and evolution of the dominant frequency dependent three-dimensional atmospheric modes. J Atmos Sci 43:1210–1237
Sasamori T (1981) Stability of the Walker circulation. J Atmos Sci 39:518–527
Simmons AJ (1982) The forcing of stationary wave motion by tropical diabatic heating. Quart J Roy Meteor Soc 108:503–534
Souza EB, Ambrizzi T (2002) ENSO impacts on the South American rainfall during 1980s: Hadley and Walker circulation. Atmósfera 15:105–120
Souza EB, Kayano MT, Ambrizzi T (2005) Intraseasonal and submonthly variability over the eastern Amazon and Northeast Brazil during the autumn rainy season. Theor Appl Climatol 81:177–191
Souza EB, Ambrizzi T (2006) Modulation of the intraseasonal rainfall over tropical Brazil by the Madden-Julian oscillation. Int J Climatol 26:1759–1776
Todd MC, Washington R, James T (2003) Characteristics of summertime daily rainfall variability over South America and the South Atlantic Convergence Zone. Meteor Atmos Phys 83:89–108
Trenberth KE (1987) The role of eddies in maintaining the westerlies in the Southern Hemisphere winter. J Atmos Sci 44:1498–1508
Trenberth KE, Branstator GW, Karoly D et al (1998) Progress during TOGA in understanding and modelling global teleconnections associated with tropical sea surface temperatures. J Geophys Res 103(C7):14291–14324
Trenberth KE, Stepaniak DE, Caron JM (2000) The global monsoon as seen through the divergent atmospheric circulation. J Clim 13:3969–3993
Trenberth KE, Caron JM (2000) The Southern Oscillation revisited: sea level pressures, surface temperatures and precipitation. J Clim 13:4358–4365
Uvo CRB, Repelli CA, Zebiak SE et al (1998) The relationships between Tropical Pacific and Atlantic SST and northeast Brazil monthly precipitation. J Clim 11:551–562
Walker GT (1923) Correlation in seasonal variations of weather, VIII, A preliminary study of world weather. Mem Indian Meteorol Dep 24:75–131
Walker GT (1924) Correlation in seasonal variations of weather, IX, a further study of world weather. Mem Indian Meteorol Dep 24:275–332
Walker GT, Bliss EM (1932) World weather, V. Mem R Meteorol Soc 106:296–310
Wallace JM, Gutzler DS (1981) Teleconnections in the geopotential height field during the Northern Hemisphere winter. Mon Wea Rev 109:784–812
Wang C (2002) Atmospheric circulation cells associated with the El Niño-Southern Oscillation. J Clim 15:399–419
Webster PJ (1981) Mechanisms determining the atmosphere response to sea surface temperature anomalies. J Atmos Sci 38:554–571
Webster PJ, Holton JR (1982) Cross-equatorial response to middle latitude forcing in zonally varying basic state. J Atmos Sci 39:722–733
Webster PJ (1983) Large-scale structure of the tropical atmosphere. In: Hoskins BJ, Pearce RP (eds) Large-scale dynamical processes in the atmosphere. Academic Press, San Diego
Webster PJ, Magaña VO, Palmer TN et al (1998) Monsoons: processes, predictability, and the prospects for prediction. J Geophys Res 103(C7):14451–14510
Webster PJ (2004) The elementary Hadley circulation. In: Diaz HF, Bradley RS (eds) The Hadley circulation: present, past, and future. Kluwer Academic Press, Dordrecht
Weickmann KM, Lussky GR, Kutzbach JE (1985) Intraseasonal (30–60 day) fluctuations of outgoing longwave radiation and 250 mb streamfunction during northern winter. Mon Wea Rev 113:941–961.

Chapter 8
South American Climate Variability and Change: Remote and Regional Forcing Processes

Kerry H. Cook

Abstract Physical processes that lead to variations in South American climate are discussed. Basic features of the present day South American climatology are presented from modern observations, including a survey of the most prominent circulation and precipitation features and a decomposition of the continental-scale moisture balance, to provide a foundation for considering variability. Our current understanding of regional and remote forcing of South American climate and its variability, with references to Holocene and LGM climate, are reviewed with reference to how the South American monsoon and other features of today's climate operate. The purpose is to support the interpretation of the geological proxy data and a process-based understanding of the paleoclimate record of Holocene and LGM climate variations of the South American climate.

Keywords Climate variability · Moisture balance · Atmospheric circulation · Precipitation distribution

8.1 Introduction

Climate variability is generally divided into two types: internally-generated and externally-forced. The definition of these depends on the system under consideration. If one is thinking of the whole earth climate system, including the atmosphere, oceans, biota, land surface, and cryosphere, the only prominent source of external forcing is changes in insolation, i.e., the solar forcing due to changes in the sun's luminosity or the earth's orbital parameters that is the fundamental cause of the climate's glacial/interglacial oscillation. Here we take as our "climate system" the South American continent, so external (remote) forcing is defined for convenience as any agent of climate variability that originates away from the continent itself, and internal variability is forcing that originates in some way on the continent.

K.H. Cook (✉)
Department of Geological Sciences, Jackson School of Geosciences, The University of Texas at Austin, Austin, TX USA
e-mail: kc@jsg.utexas.edu

F. Vimeux et al. (eds.), *Past Climate Variability in South America and Surrounding Regions*, Developments in Paleoenvironmental Research 14,
DOI 10.1007/978-90-481-2672-9_8,

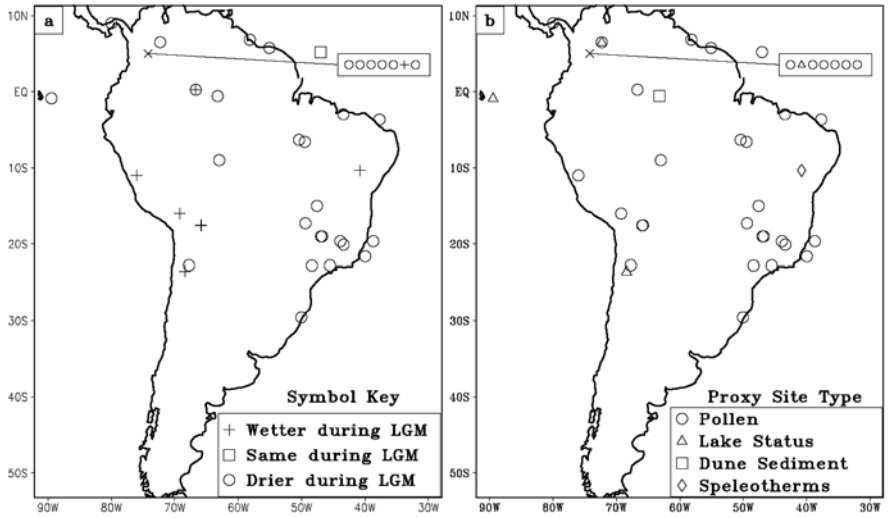

Fig. 8.1 Summary of (**a**) aridity measurements for the LGM in South American and (**b**) the sources used in the aridity reconstructions. See Table 1 in Vizy and Cook (2005) for references

The geological proxy data make it clear that the South American climate was different during the LGM and at times in the Holocene. For example, Fig. 8.1 summarizes information about precipitation and surface temperature distributions over South America during the LGM as reconstructed from pollen, lake levels, ocean cores, speleothems, and plant microfossils. These data indicate levels of aridity, which may be interpreted as plant available moisture, precipitation minus evaporation (see Eq. 8.1), or some other related variable. The reconstructions cannot provide accurate quantitative information about changes in the magnitude or seasonality of rainfall, but they do offer observation-based evidence about whether the past climate was wetter or drier than the present day. The overall pattern indicates drier conditions everywhere on the continent except in the Nordeste and the high Andes, where the climate was wetter than the present day. It is possible that differences in climate between the present day and the LGM have more regional structure in the Andes than in other regions of South America. Sylvestre et al. (1999) suggest higher lake levels in the southern Altiplano, and lower levels in the northern Altiplano, for example. The mean annual temperature was cooler according to the proxy data, by amounts ranging between 2 and 10 K. Certainly this spread is partially due to uncertainties in the reconstructions, but also to the regionality of LGM temperature differences.

Uncertainty about the state of the Amazon basin climate results from difficulties in recovering proxy data from a biologically active region. Attempts are made to evaluate proxy data collected in the dry climate of the high Andes in terms of the climate of the Amazon basin. As summarized in Fig. 8.1, most sites in the Andes indicate wetter conditions during the LGM. Two ideas are discussed. One is that high rainfall levels in the Andes are associated with wet conditions in the Amazon

basin, and the other is that high rainfall levels in the Andes indicate dry conditions in the Amazon basin.

Some of the investigators who reconstruct paleo-lake levels in the high Andes speculate that the higher lake levels reflect wetter LGM conditions in the Amazon basin. Tapia et al. (2003), for example, suggests that a wetter Amazon basin would cause increased moisture transport into the Andes. Baker et al. (2001) hypothesize that LGM cooling in the tropical Atlantic Ocean increases the land/sea contrast that drives the South American summer monsoon, increasing rainfall rates and the specific humidity of the low-level flow into the Andes.

Vizy and Cook (2007) use regional model simulations to explore the dynamical processes that connect high Andes and Amazon precipitation in the present day and LGM climate. They find that the delayed onset of Amazon convection in the LGM during austral spring that causes lower annual rainfall amounts in the Amazon basin is associated with an enhancement of rainfall over the high Andes. The absence of convection over the Amazon in austral spring is associated with stronger zonal geopotential height gradients and the redirection of the low-level flow in the eastern foothills of the Andes. As a result, the flow impinges more directly onto the Andean topography the LGM simulation and transports moisture from the Amazon up into the mountains, enhancing convection over the Andes. This circulation mechanism explains how rainfall in the high Andes increases in conjunction with large-scale drying over the Amazon basin (Fig. 8.1a).

Garreaud et al. (2003) discuss the influence of the upper-level flow on Amazon rainfall. They suggest that climate variations on the Altiplano are closely related to variations in the upper-level circulation on glacial/interglacial time scales as controlled by contrasts in insolation between the Northern and Southern Hemispheres.

To evaluate such possibilities and further develop our understanding of South American climate change, an understanding of remote and regional forcing processes is needed. In the following section, basic features of the present day South American precipitation climatology are presented to provide a foundation for considering variability. The next two sections survey our current understanding of regional and remote forcing of South American climate and its variability, with references to Holocene and LGM climate. The purpose is to leverage our understanding of present day observed and modelled climate processes into a deeper understanding of the Holocene and LGM climates of South America.

8.2 Decomposition of the South American Precipitation Climatology

Figure 8.2 shows the seasonal precipitation climatology for South America. Values plotted over land are from the New et al. (2000) data, at 0.1° latitude × 0.1° longitude resolution compiled from rain gauges. The satellite-derived precipitation climatology from Xie and Arkin (1997) is used to fill in the ocean points

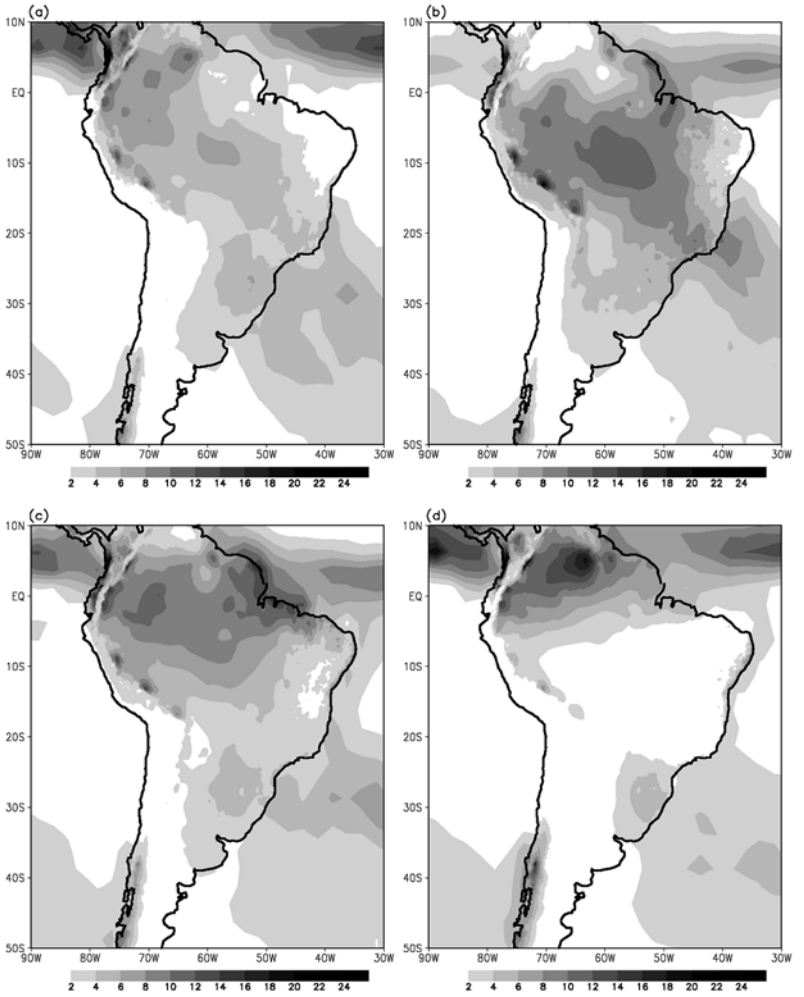

Fig. 8.2 Observed precipitation in mm/day from the CRU 10-minute 1961–1990 (land) and CPC (ocean) climatologies averaged over (**a**) September-October-November, (**b**) December-January-February, (**c**) March-April-May, and (**d**) June-July-August

so the larger-scale structures of the precipitation field are evident even with the discontinuity at the coastline.

Spring monsoons rains begin in the northwestern Amazon basin and spread southward along the foothills of the Andes and eastward into central Amazonia (Fig. 8.2a). The South Atlantic convergence zone (SACZ) begins to form, extending diagonally to the southeast over the South Atlantic Ocean. At the height of the rainy season, represented by the Dec-Jan-Feb mean in Fig. 8.2b, the precipitation maximum is over the central Amazon basin and the SACZ is well developed. High rainfall continues in the western Amazon south of the equator and, especially, along

the eastern slope of the Andes. The rainfall retreats to the north in the fall (Fig. 8.2c), with the withdrawal progressing more slowly than the onset (Marengo et al. 2001). During austral winter (Fig. 8.2d) the maximum rainfall is north of the equator, and the SACZ is barely discernible.

In thinking physically about the South American precipitation climatology and its variability on all time scales, one needs to distinguish between the dynamics of the monsoon and the intertropical convergence zone (ITCZ). The rainfall structures described above are part of the South American monsoon system. Monsoons occur because the heat capacity of land is much smaller than that of the ocean, both because of the differences in material (e.g., water vs. soil) and because of the volume of the material heated by sunlight (e.g., tens of meters of the ocean mixed layer vs. a few centimeters of the land surface). In contrast, ITCZ structures occur because the summer hemisphere is warmer than the winter hemisphere. The monsoon and ITCZ systems may be related and even co-located in certain regions at times but, because the processes that generate them are different, the mechanisms of variability of these two types of circulation and precipitation systems are also different.

South American monsoon and ITCZ precipitation features are clearly separate and distinguishable in all seasons. In each panel of Fig. 8.2, for example, the marine Atlantic ITCZ is in place between the equator and 5°N, and it does not extend far enough west to touch the continent. Unfortunately, many introductory textbooks do not distinguish between the monsoon and ITCZ rainfall and, as a consequence, misrepresent the seasonality of rainfall over South America in terms of excursions of the ITCZ to even 30°S over the continent.

A first-order understanding of the seasonal precipitation climatology shown in Fig. 8.2 is gained by considering the degree to which the South American climatological precipitation and circulation is determined by continentality. The Amazon basin and equatorial precipitation maxima and the SACZ form as the result of the presence of the continent. Interactions between the continental thermal low and the northeasterly trades support the Amazon precipitation maxima, while the SACZ is largely the result of transient activity (i.e., synoptic variations, or weather; Garreaud 2001) and low-level convergence between cyclonic flow about the thermal low and anticyclonic flow about the South Atlantic high. The other precipitation maxima owe their existence to the topography, due to mechanical uplifting along the eastern slopes and to the thermal forcing of vertical motion in the central Andes. Longitudinal structure in SSTs modifies the rainfall distribution, but does not provide a basic generating mechanism over the continent.

Another very fundamental way of thinking about the rainfall climatology is to ask about the sources of the precipitated water. Is the water recycled from the surface, or is it imported and converged by the atmosphere? Each of these methods of delivering precipitating water has its own regional and remote sensitivities, so understanding this basic breakdown for the climatology is essential for identifying the processes of variability (e.g., Brubaker et al. 1993). This idea is expressed mathematically by the moisture balance of an atmospheric column,

$$P = E - \int_{sfc}^{TOA} \nabla \cdot (q\vec{v})dz \tag{8.1}$$

where q is specific humidity and $\vec{v}$ is the horizontal wind vector. In Eq. 8.1, precipitation falling on a unit area, P, is expressed as the sum of the surface evaporation from the area, E, and the atmospheric moisture convergence, $-\nabla \cdot (q\vec{v})$, integrated from the surface to the top of the atmosphere (TOA).[1] If $P > E$, then the atmospheric flow converges water into of the air column.

Due to a lack of observations on the space and time scales needed to establish a climatological moisture balance, it is currently not possible to establish the relative magnitudes of the two terms on the right-hand-side of Eq. 8.1 with high accuracy. To provide corroboration, two sources are used to plot each term in the column moisture budget in Fig. 8.3. Precipitation, evaporation, and the vertically-integrated moisture convergence from the NCEP/NCAR reanalysis[2] climatology (Kalnay et al. 1996) for DJF are displayed in the left column, and results from a high-resolution regional model simulation are displayed in the right column. The reanalysis resolution (i.e., grid spacing) is about 250 km, and the regional model is 60 km. (Please see Cook and Vizy (2008) for more details on this regional model simulation).

Considering the accuracy of the representation of precipitation in the reanalysis and the regional model provides perspective on the accuracy of the estimate of the moisture budget terms. Compared with the observed precipitation for DJF (Fig. 8.2b), the reanalysed precipitation fails to maintain a precipitation maximum over the central Amazon basin and it yields a very dry region to the east of the Andes. The regional model simulation produces a generally more accurate precipitation distribution, but rainfall rates are too high in some regions, especially over the ocean. (Note that the precipitation fields displayed in Figs. 8.2 and 8.3 are presented on their native grids to preserve as much detail as possible. Normally one would interpolate all fields to the same resolution for the comparison.)

In both the reanalysis and the model simulation, evaporation rates are generally smaller than precipitation rates across South America (Fig. 8.3c,d). In the reanalysis, evaporation rates are small where precipitation rates are small, presumably due to dryness of the surface. But precipitation maxima are not reflected as evaporation maxima, presumably because evaporation rates are limited in these regions not by surface moisture levels but by wind speeds or the specific humidity of the overlying

[1] Since this is the balance for the atmospheric column, runoff does not appear in the equation; the redistribution of water on the surface would be accounted for in the evaporation term.

[2] Reanalysis products are not pure observations, but a blend of observed and modelled fields. Considering the variables in Eq. 8.1, precipitation, evaporation, and specific humidity from this reanalysis product are modelled quantities, while winds are the observed values. In certain densely-observed regions such as the U.S., reanalyses that use observed precipitation and specific humidity are being produced, but the accurate observation of evaporation and its assimilation into reanalysis products is currently not done.

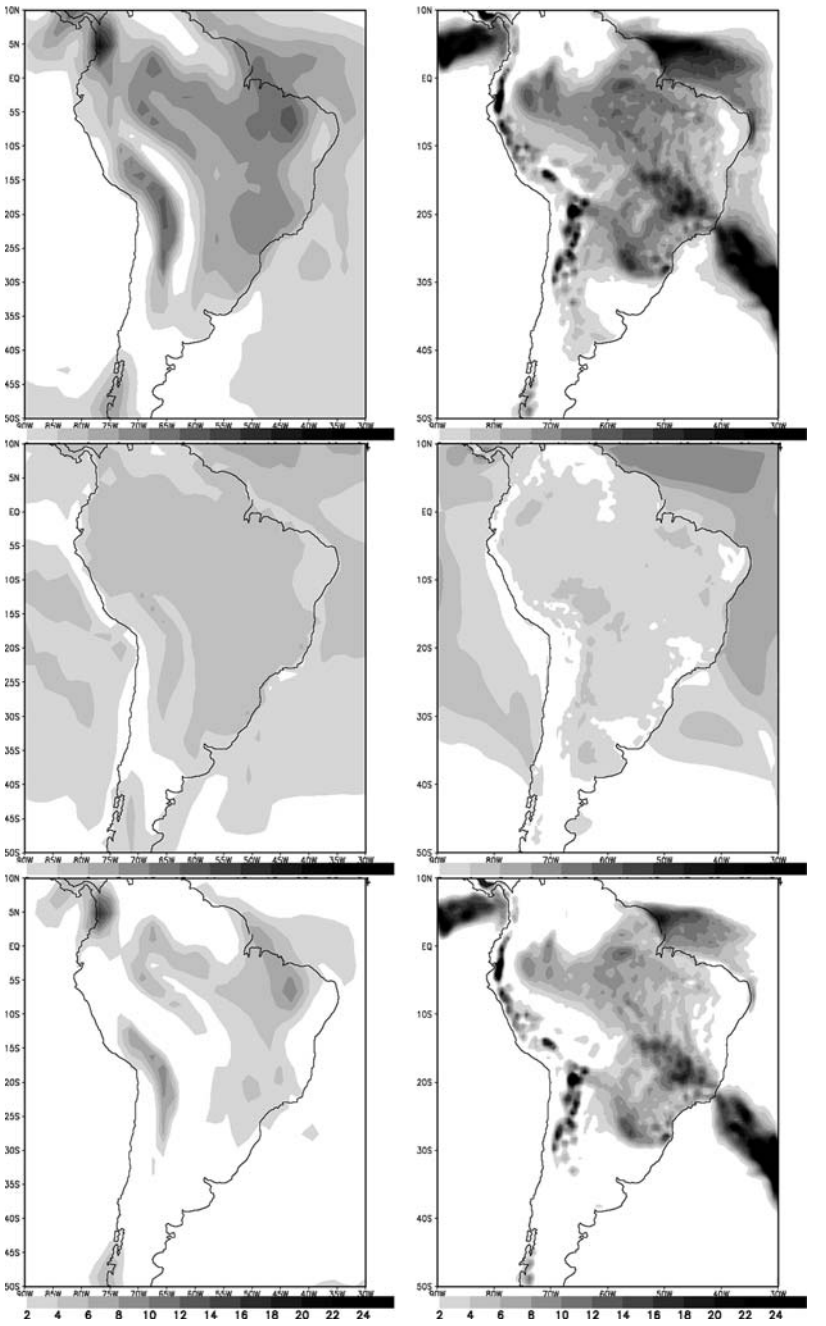

Fig. 8.3 Precipitation, evaporation, and the vertically-integrated moisture flux convergence climatology for DJF from the NCEP reanalysis (respectively; left column) and control simulation from Cook and Vizy (2008; right column)

air. In the regional model simulation, evaporation rates show even less correspondence with precipitation. Evaporation is low in some regions with relatively high rainfall, such as along the subtropical east coast, and high in some relatively low rainfall regions, such as in the western equatorial Amazon.

The precipitation maxima of Fig. 8.3a,b are closely related to maxima in the vertically-integrated moisture convergence (Fig. 8.3e,f). In other words, one cannot ascertain the location of the precipitation maxima by examining the evaporation field – the role of the atmospheric circulation in transporting and converging moisture must be considered.

Figure 8.4a,b display the recycling percent, i.e., evaporation divided by precipitation expressed as a percent, for the reanalysis and the regional model estimates of the moisture budget. A similar pattern emerges in each, with lower recycling percents in wetter regions. In the regional model simulation, recycling percents of 30% and 40% are typical in the central and eastern Amazon. In contract, the western Amazon has much higher recycling of evaporated water, even over 90%.

These differences in the recycling percentages in different regions have implications for climate forcing processes. Regions with a high percentage of recycling, such as the western Amazon, tend to be more sensitive to local and regional forcing factors, such as vegetation, while regions with a low recycling percent, such as the eastern Amazon, are less "self determining" and more sensitive to remote forcing factors that change the circulation and, thereby, the transport and convergence of atmospheric moisture.

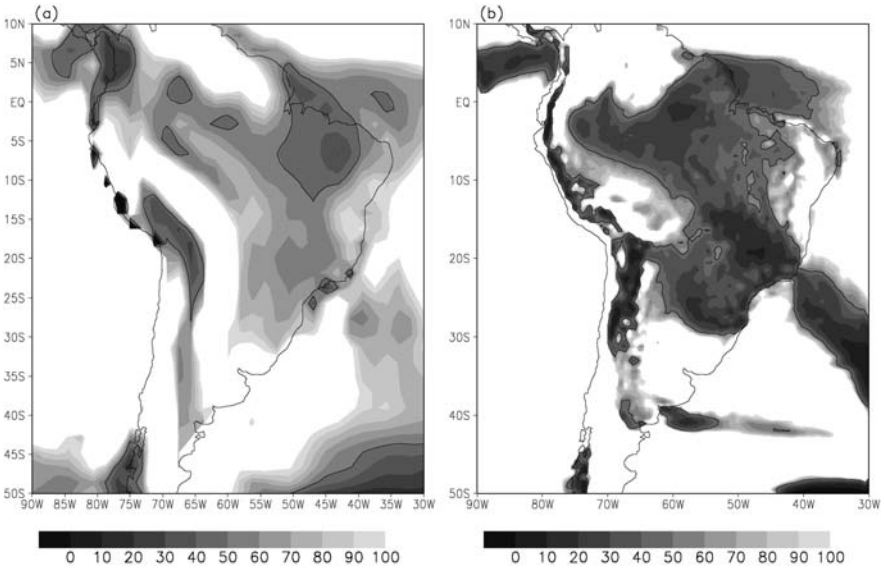

Fig. 8.4 Estimates of the precipitation recycling per cent (defined in text) from the (**a**) NCEP/NCAR reanalysis and (**b**) a regional model simulation [the control simulation in Cook and Vizy (2008)]. Contour interval is 10%, and the 50% level is indicated by a contour line

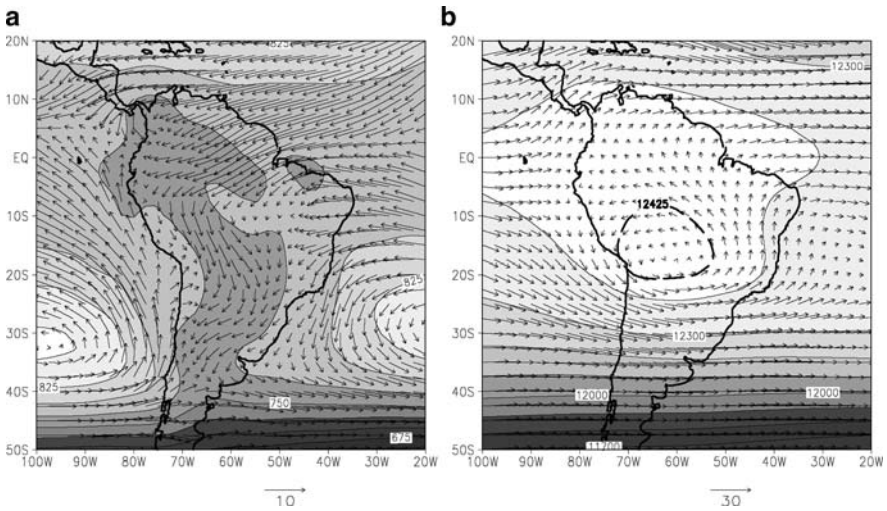

Fig. 8.5 Climatological winds and geopotential heights (gpm) at (**a**) 900 hPa and (**b**) 200 hPa from the NCEP reanalysis. Vector scale is indicated at the bottom in m/s

What circulation features are responsible for this moisture transport and convergence? Figure 8.5a shows DJF geopotential heights and wind vectors at 900 hPa (~ 1 km above the surface) from the reanalysis. The primary moisture support for the warm season precipitation is the flow from the tropical Atlantic across the northeast coast. Close to the equator, where the Coriolis force is small, wind vectors cross geopotential height lines indicating flow moving down the pressure gradient. Farther south, the flow curves anticyclonically (counterclockwise) to parallel the height lines, turning southward to form the South American low-level jet along the eastern flank of the Andes. The cyclonic flow to the east of the Andes between 20°S and 30°S is known as the Chaco low. Note the convergence between the continental circulation and the circulation about the South Atlantic high that forms the SACZ.

In the upper troposphere, at 200 hPa shown in Fig. 8.5b, the main circulation feature is the Bolivian high. Even though the high is located in the vicinity of the Altiplano, it has been show to be the result of condensational heating over the Amazon basin (Lenters and Cook 1995, 1997). The high is shifted to the southwest of the main precipitation maximum so the advection of high planetary vorticity air in the northeastern quadrant of the high can balance the shrinking of relative vorticity in the atmospheric layers above the condensation.

8.3 Regional Forcing of South American Climate Variability

Of fundamental interest for understanding regional variations in South American climate is the degree to which coupling between the atmosphere and land surface introduces variability. When the atmosphere is highly responsive to the land surface, feedback processes through, for example, soil moisture can affect the column

moisture budget (Eq. 8.1) by controlling evaporation, especially in regions with strong recycling (Fig. 8.4). Land surface processes can also exert a more indirect effect on the column moisture balance through controls on surface temperature gradients, since these are directly related to low-level geopotential height fields, the circulation, and moisture convergence. Understanding these processes requires consideration of how the net longwave and shortwave radiative heating of the land surface is partitioned into latent and sensible heat fluxes from the land surface to the atmosphere.

To what extent is land surface/atmosphere coupling important for determining climate variability across South America? This question has been recently addressed in multi-model analyses for boreal summer through controlled GCM simulations and the construction of indices that quantify land surface/atmosphere feedback strength. In the GLACE model comparison analysis (Koster et al. 2006), South America did not emerge as a region with strong land surface/atmosphere coupling in boreal summer. Wang et al. (2007) used a different index to measure soil moisture/atmosphere interactions and found a somewhat higher coupling strength for South America in the subtropics. During austral summer, the land surface-atmosphere coupling strength over the Amazon is found to exert a statistically significant influence on rainfall through controls on sensible heat fluxes in one GCM, but it may not be as strong as the coupling over central North America during boreal summer (Yamada, personal communication).

Xue et al. (2006) find that including vegetation biophysical processes in GCM simulations does not improve the accuracy of the model in capturing the South American precipitation climatology on planetary space scales. This is consistent with the results of Kleidon et al. (2000), who compare extreme simulations in a GCM with desert prescribed everywhere with a prescribed vegetated world. They find little change in the South American climate in the two simulations.

Land surface coupling over South America may operate more prominently on smaller space scales. Zheng et al. (1996) report significant regional drying when they replace the Amazon forest with desert in an atmospheric GCM, suggesting that a dry climate imposed by deforestation may be sustained. Xue et al. (2006) find that vegetation feedbacks can influence the early progression of the monsoon onset through controls on temperature gradients and, thereby, moisture convergence within the atmosphere. Li and Fu (2004) find that the western Amazon is sensitive to land surface/atmosphere feedbacks, but the central and eastern Amazon regions are not, being more closely connected with remote SST forcing. But once convection is triggered, control of the developing monsoon system resides in the large-scale circulation and its connections with the tropical Atlantic.

Several tools are used to study the processes that promote convection. To connect small-scale convection to the larger-scale circulation and distinguish between the roles of temperature and moisture levels in triggering convection, the moist static energy (*MSE*) can be diagnosed. *MSE* is the sum of the sensible, latent, and (geo)potential energy according to

$$\mathrm{MSE} = c_p T + Lq + gz, \tag{8.2}$$

where c_p is the specific heat of air at constant pressure, T is air temperature, L is the latent heat of vaporization of water, q is specific humidity, g is the acceleration due to gravity, and z is height. *MSE* increasing with altitude denotes a stable atmosphere, so increases in low-level *MSE* destabilize the vertical column and promote convection, and decreases in low-level *MSE* discourage convection.

Another process-based diagnostic is the convective inhibition energy, or *CIN*, which is a measure of the energy needed to prevent an air parcel from rising to the level of free convection, given by

$$CIN = \int_{sfc}^{TOA} g\left(\frac{T_v{}^{parcel} - T_v^{env}}{T_v^{env}}\right)dz \tag{8.3}$$

where T_v^{parcel} is the virtual temperature of a rising parcel of air and T_v^{env} is the larger-scale environmental temperature. The vertical (z) integral is taken from the surface to the top of the atmosphere (*TOA*). Any process that increases *CIN* will inhibit convection.

These diagnostic tools help us understand how the vertical atmospheric column becomes convectively unstable. One fundamental question is whether this destabilization is thermally controlled, e.g., through increases in low-level temperature or decreases in temperature at the top of the planetary boundary layer, or hydrologically controlled, e.g., by increasing the low-level moisture content. Another question is whether the destabilizing factors are put in place through land surface/atmosphere interactions.

Fu et al. (1999) analysed observations and a reanalysis to find that the atmosphere over the Amazon is pre-conditioned for the start of the rainy season by moistening of the atmospheric boundary layer and cooling at its top that breaks down dry season temperature inversions and reduces *CIN* (Eq. 8.3). Since seasonal temperature differences are small close to the equator, changes in moisture dominate the seasonal changes in *MSE* (Eq. 8.2). Li and Fu (2004) isolate the role of land surface fluxes in initiating the wet season in Amazonia, and find that the loading of moisture into the lower troposphere from the surface, i.e., evaporation, is a crucial factor that triggers monsoon onset. Cook and Vizy (2006), in contrast, suggest that the early season increases in low-level moisture are more closely tied to advection from the tropical Atlantic.

There is also a variability mode that connects the timing of the monsoon onset and demise with rainfall in subtropical South America. Gonzalez et el. (2002) show that an early start to the monsoon season in the tropics leads to reduced springtime rainfall in southern Brazil, and an early demise in the monsoon favours higher fall precipitation in subtropical South America.

Similar to the Amazon basin, precipitation in the central Andes is greatest in austral summer. The primary source of moisture is easterly flow from the Amazon basin. While sensible heating over the Altiplano warms the lower atmosphere and contributes to a destabilization of the vertical column, the development of deep convection depends on the advection of moisture from the lowlands to the east (Garreaud 1999).

Even though the source of moisture for central Andes (Altiplano) rainfall depends on transport from the continent to the east, variations in high Andes rainfall are also partially controlled by upper-air circulation anomalies. Vuille and Keimig (2004) analyse rain gauge and satellite cloud data along with reanalysed winds and show that easterly upper-level wind anomalies favor wet conditions and westerly winds produce dry conditions. In the northern Altiplano, easterly wind anomalies and wet summers occur when geopotential height gradients between the tropics and middle latitudes are relatively small. But farther south, easterly wind anomalies and wet summers occur along with a repositioning of the Bolivian high. They also find that humidity variations in the lowlands to the east are not correlated with precipitation in the northern Altiplano on interannual time scales, but precipitation in the south is significantly correlated with the low-level moisture content at low levels to the southeast

Co-variability of Amazon and high Andes rainfall is relevant for understanding regional climate forcing on the continent on all time scales. On intraseasonal time scales, Garreaud (1999) finds an anticorrelation between central Andes and Amazon convective cloud amounts. Vizy and Cook (2007) explore the dynamics of this relationship and find that central Andes rainfall rates are sensitive to the orientation of the easterly flow from the lowlands relative to the eastern foothills of the Andes. Anomalously low rainfall in the Amazon basin and the associated high geopotential height anomalies orient the flow more perpendicular to the topography. As a result, more moisture is transported into the central Andes and higher rainfall rates in the central Andes are associated with anomalously low rainfall in the Amazon basin.

On intraseasonal timescales (5–20 days), rainy periods on the Altiplano are associated with three circulation anomalies, namely, extratropical cyclones, cold-core lows, and the westward enhancement of the South Atlantic high (Lenters and Cook 1999). In each case, the primary support for high rainfall rates is moist, poleward flow at low levels along the eastern flank of the central Andes.

Since South America stretches from the tropical Northern Hemisphere through middle latitudes of the Southern Hemisphere, the potential for important regional climate forcing due to extratropical/tropical interactions exists. One known mode of interaction between middle latitudes and subtropical South America comes in the form of cold surges. As documented by Garreaud (2000, 2001), cold surges are equatorward incursions of cold, dry air that move northward along the eastern slopes of the Andes (as well as in other parts of the world) throughout the year. They are associated with freeze events in the winter, and with the generation of deep convection in the warm season.

Li and Fu (2006) note that cold air intrusions from middle Southern Hemisphere latitudes into the Amazon basin play an important role in the rapid progression of the onset of the rainy season from the western Amazon to the southeast (Fig. 8.2a,b). The advancing cold fronts are relatively dry, but they provide a moisture convergence mechanism and destabilize the atmospheric column when they meet warm, moist air over southeastern Brazil. Weaker and less frequent cold air incursions can delay the onset of the monsoon in the southeast even though the large-scale conditions over the continent may be favorable for the initiation of rainfall.

Another mode of climate variability that involves interactions between the tropics and middle latitudes concerns the intensity and position of the SACZ. Nogues-Paegle and Mo (1997) describe a "seesaw" in SACZ intensity on intraseasonal time scales that brings rainfall deficits (abundance) to the subtropics when the SACZ is strong (weak). This variation is associated with a dipole structure of SACZ wind and circulation anomalies (e.g., Lenters and Cook 1999, Barreiro et al. 2002, Gan et al. 2004, Vera et al. 2006, Sturm et al. 2007) that occurs because the SACZ tends to move between two positions. In its northeastern position (sometimes called the "oceanic" position), the Chaco low is located anomalously far south. When the SACZ is shifted to the southwest (the "continental" position), the South Atlantic high is anomalously strong.

Various factors contribute to the oscillation of the SACZ, as if it has two favored positions and when it is perturbed it tends to flip to the other location. These forcing processes include the Madden-Julian oscillation (Paegle et al. 2000, De Souza and Ambrizzi 2006), mid-latitude wave trains (Carvalho et al. 2002), and stationary mid-latitude fronts. Carvalho et al. (2004) explain that when the MJO phase suppresses convective activity over Indonesia and enhances it over the central Pacific, then rainfall is enhanced over northeastern Brazil and the SACZ is in its northeast position. The opposite phase of the MJO brings an opposite response.

Wagner et al. (2007) investigate another mode of climate change related to synoptic activity, namely, the relationship between mid-latitude rainfall and Southern Hemisphere wave activity. They combine simulations using an atmosphere/ocean GCM with a statistical downscaling model to reach regional space scales to study the mid-Holocene (7–4.5 ka) climate of southeastern Patagonia. Precessional forcing changes the seasonality of the Southern Hemisphere waves, but they find only a "moderate" connection to rainfall, with weaker wave activity associated with slightly increased precipitation. These results are contrary to an assumption commonly made in the interpretation of proxy data.

8.4 Remote Forcing of South American Climate Variability

8.4.1 Sea Surface Temperature Forcing

Numerous statistical correlation analyses relate global SST patterns to South American precipitation variability (e.g., Aceituno 1988, Moron et al. 1995, Nobre and Shukla 1996, Marengo et al. 1993, Robertson and Mechoso 2000, Montecinos et al. 2000, Zhou and Lau 2001, Paegle and Mo 2002, Lau and Zhou 2003, and many others), but the physical processes of the relationships are not fully understood.

One basic question is: What is the relative influence of Atlantic and Pacific SST forcing on South American climate variability? The answer is complicated, depending on the region, the season, and the time scales under consideration. Enfield (1996) reports that northern South America is influenced equally by tropical Pacific and tropical North Atlantic SSTs. The influence of South Atlantic SSTAs appears in the Nordeste, and the entire region between Venezuela and the Nordeste showed

sensitivity to antisymmetric configurations of SST anomalies across the equator. Liebmann and Marengo (2001) focus on interannual variability in the Amazon basin, and find strong correlations with tropical Pacific and Atlantic SSTs only in certain regions close to the equator, and only during the transition and dry seasons.

One measure of the relative important of Atlantic and Pacific SSTs on South American rainfall was produced in a study by Fu et al. (2001), who examined the extent to which the seasonality of SSTs in each ocean basin forces the seasonality of rainfall over South America. They find that tropical Atlantic SST anomalies can induce subsidence over the Amazon basin and significantly delay the onset of the monsoon season. Pacific SSTs can enhance the delay by strengthening the subsidence through a Walker circulation, and also through the generation of Rossby waves, but the primary influence is from the Atlantic.

Another complicating factor that arises in assessing the processes of SST forcing on South American climate variability is the fact that Pacific and Atlantic SSTAs are not necessarily independent, and forcing from the Pacific may be mediated through a response in the Atlantic. But Enfield (1996) found that while correlations between North Atlantic SSTs and SSTs in the NINO3 region of the Pacific Ocean explain 25% of the variance of the North Atlantic SSTs, the rainfall correlations between northern South America and North Atlantic SSTs are mostly direct forcing from the North Atlantic, and not an indirect response to ENSO.

Complications notwithstanding, most statistical analyses find significant correlations between regional South America precipitation and Pacific SSTs. The general pattern reported for warm ENSO (El Niño) events includes dry conditions in the north and wet conditions on the Peru and Ecuador coast and in the subtropics (e.g., southern Brazil), with a reversal during cool ENSO events (La Niña).

Grimm (2003) studied the processes that lead to the impact of ENSO warm events on Brazil's summer monsoon on subseasonal time scales. She found that in the early monsoon season, the perturbation of the Walker circulation by El Niño SSTAs places subsidence over the Amazon basin and the generation of Rossby waves generates anticyclonic anomalies in the subtropics. The inflow of moisture from the Atlantic is enhanced, but shifted to the south, bringing dry conditions to the north with wet conditions to the south.

Drying on the Altiplano is an established response to ENSO warm events (e.g., Aceituno 1988, Vuille et al. 2003). A case study of the dry conditions during the 1987 El Nino associates reduced convection on the Altiplano with the presence of a strong cold front over eastern South America and cold, dry air to the west (Lenters and Cook 1999). The characteristic eastward shift of the South Pacific convergence zone during El Nino may be responsible for this enhanced frontal activity in the SACZ (through teleconnections) and, therefore, cool, dry, convectively unfavorable conditions in the central Andes.

The relevance of these Pacific forcing processes for LGM and Holocene climates depends on the history of ENSO events. Coupled ocean/atmosphere GCM simulations are fairly consistent in indicating a weaker ENSO signal at the mid-Holocene

(Otto-Bliesner et al. 2006), but results for the LGM are inconclusive (e.g., Zheng et al. 2008). The overall influence of such interannual variations on the time-mean climate remains a fruitful area for further research.

Atlantic SST forcing may have been a prominent factor in determining the LGCM climate. According to the regional climate modeling studies of Vizy and Cook (2005) and Cook and Vizy (2006), in agreement with much of the geological proxy evidence extracted from Amazonia, annual rainfall was 25–35% lower in the LGM than in the present day throughout the Amazon basin. The primary cause of the annual mean drying in the simulations is a 2–3 month delay in the onset of the summer monsoon, which approximately doubles the length of the dry season. The delayed onset occurs because the low-level inflow from the tropical Atlantic onto the South American continent is drier than in the present day simulation due to reduced evaporation from cooler surface waters, and this slows the springtime buildup of MSE (Eq. 8.2). Thus, hydrological processes rather than thermal processes (e.g., changes in land/sea contrast) dominate. This occurs most fundamentally because of the nonlinearity of the Claussius-Clapeyron relationship. Marengo et al. (2001) report a similar response on intraseasonal time scales, providing an analogy with paleoclimate time scales.

Certainly SST forcing from the Atlantic is important in the drought-prone Nordeste region of Brazil. The primary rainy season there is March-April-May, and it can be interrupted when warm SSTAs in the tropical North Atlantic cause an early shift of the marine Atlantic ITCZ into the Northern Hemisphere (e.g., Nobre and Shukla 1996).

The main influence of South Atlantic SSTAs on South America climate variability comes through an influence on the position and intensity of the SACZ. Doyle and Barros (2002) find that positive (negative) SST anomalies in this region are correlated with weak (strong) SACZ activity, influencing regional rainfall rates in subtropical eastern South America. Barreiro et al. (2002) noted a similar response to South Atlantic SSTs in a modeling study, but there was little effect on continental precipitation. Feedbacks between the SACZ dynamics and the underlying Atlantic SSTs are important for understanding the relationship. According to De Almeida et al. (2007), when warm SSTs intensify the SACZ in austral summer, then the original SST anomalies are reduced by the atmosphere's response.

Several analyses of rainfall trends over South America raise concerns, especially since the trends identified are mostly negative. Zhou and Lau (2001) report a decrease in rainfall from the northwest coast to the southeast subtropics accompanied by increased rainfall over the Nordeste, and suggest that these trends may be related to warming in the southern Atlantic. Costa and Foley (1999) detect a trend of reduced moisture advection into the Amazon basin, and an increase in moisture recycling for 1976–1996. In contrast, Marengo (2004) identifies negative rainfall trends in the Amazon basin as a whole for 1929–1998, with the negative trend in northern Amazonia dominating a positive trend in the south. He associates these trends with more frequent and intense warm ENSO events after 1975.

8.4.2 High Latitude Forcing

As discussed above, tropical/extratropical interactions exert significant influence on South American climate variability, mediated primarily through the dynamics of the SACZ. These processes were included among the regional forcing mechanisms. But there is a recent example of a possible high latitude forcing mechanism that is clearly not related to the mid-latitude portions of the South American continent. Vuille and Milana (2007) note a declining trend in precipitation in subtropical Chile in recent decades, and relate it to trends in SSTs and sea ice in the Amundsen Sea. The mechanism identified for the effect on rainfall in Chile is the production of atmospheric blocking, which redirects the path of storms. Such synoptic-scale processes are very important for establishing the time-mean climate state.

Chiang et al. (2003) and Chiang and Bitz (2005) conducted GCM simulations to study the "meridional mode" of tropical Atlantic variability, manifest by a north/south repositioning of the marine Atlantic ITCZ. These papers explore the relationship of this mode of variability to the specification of sea ice in a GCM. They find that when sea ice is imposed in the North Atlantic in the model, overall cooling of the Northern Hemisphere is sufficient to cause a repositioning of the marine Atlantic ITCZ farther south. While this GCM's resolution of 7.5° (~ 800 km) in latitude and longitude is inadequate for applying the results on regional space scales, we can appeal to known relationships between the position of the Atlantic ITCZ and South American rainfall to extract relevant information from these simulations. The results have implications for the climate of the Nordeste region, where rainfall and its variability on all time scales are known to be closely correlated with the position of the marine Atlantic ITCZ (e.g., Hastenrath and Geischer 1993). Indeed, there is some evidence from the proxy data that the Nordeste was wetter during the LGM (see Fig. 8.1a). The implications for climate over the rest of South America are highly uncertain. In fact, the forcing may well go the other way, since Amazon convection has been observed to generate Kelvin waves that influence the intensity and zonal position of the Atlantic ITCZ (Wang and Fu 2007).

Simulations by Claussen et al. (2003) are also sometimes brought to bear on the problem of LGM and Holocene climate forcing over South America. But, again, this model of intermediate complexity resolving 10° of latitude and 51° of longitude is aimed at studying global-scale climate processes, and it is not useful to apply the results on regional space scales.

8.4.3 Africa and South America: An Intercontinental Teleconnection

The distance between Africa and South America is as close as 3000 km, and each continent generates a large-scale heating anomaly in the summer hemisphere that is associated with circulation anomalies on space scales of 1000s of km. During boreal summer, high surface temperatures over the Sahel and Sahara, accompanied by the West African monsoon farther south, introduce strong, continental-scale

heating of the tropical and subtropical atmosphere. The Amazon heating maximum provides a comparable heat source during austral summer, but with different vertical structure and a somewhat smaller horizontal scale. Dynamical theory (e.g., Matsuno 1966, Gill 1980) suggests that such large-scale tropical heat sources force circulation responses on space scales of thousands of kilometers, meaning that the African heat source can influence the South American precipitation climatology, and vice versa.

Cook et al. (2004) identify various modes of interaction between the two continents' climates and climate variability. The strongest intercontinental teleconnection occurs during austral summer when circulations originated by condensational heating over Africa generate subsidence and significantly suppress rainfall over the Nordeste region of Brazil. This suppression is quadrupled due to regional land surface feedbacks. As a secondary response to the low-level anomalous convergence, rainfall is enhanced on the northern coast and within the SACZ. Zhou and Lau (1998) also discuss possible controls on the low-level flow associated with the surface pressure gradient between the summer low over South America and the relatively high pressure over northern Africa in winter. Cook et al. (2004) find that the mechanisms don't generally act across the equator, but when they do, the cross-equatorial interaction is mediated through the dynamical response over the tropical Atlantic (Hagos and Cook 2005).

The geological record produces evidence of co-variability of African and South America climate. For example, Brown and Johnson (2005) compare cores from Lake Malawi and the Cariacou basin and show that the records are synchronized to some extent on subcentury time scales. This is unlikely to be reflecting a causal relationship, however, but rather a mutual response to the same forcing.

8.5 Concluding Remarks

Our understanding of the processes that lead to climate variability in South America is incomplete, and much exciting and interesting work remains. We should be highly motivated to do so to improve prediction and, thereby, better the lives of people. It is especially important that we produce reliable projections of future climate changes considering the vulnerability of the Amazon rain forests to climate change. Further developing our understanding at the process level so we can carefully interpret the geological record is imperative.

References

Aceituno P (1988) On the functioning of the Southern Oscillation in the South American sector: Surface climate. Mon Weather Rev 116:505–524

Baker PA, Rigsby CA, Seltzer GO et al (2001) Tropical climate changes at millennial and orbital timescales on the Bolivian Altiplano. Nature 409:698–701

Barreiro M, Chang P, Saravanan R (2002) Variability of the South Atlantic convergence zone simulated by an atmospheric general circulation model. J Clim 15:745–763

Brown ET, Johnson TC (2005) Coherence between tropical East African and South American records of the Little Ice Age. Geochem, Geophys, Geosyst 6:Art. No.Q1

Brubaker KL, Entekhabi D, Eagleson PS (1993) Estimation of continental precipitation recycling. J Clim 6:1077–1089

Carvalho LMV, Jones C, Liebmann B (2002) Extreme precipitation events in southeastern South America and large-scale convective patterns in the South Atlantic convergence zone. J Clim 15:2377–2394

Carvalho LMV, Jones C, Liebmann B (2004) The South Atlantic convergence zone: Intensity, form, persistence, and relationships with intraseasonal to interannual activity and extreme rainfall. J Clim 17:88–108

Chiang JCH, Biasutti M, Battisti DS (2003) Sensitivity of the Atlantic Intertropical Convergence Zone to Last Glacial Maximum boundary conditions. Paleoceanography 18:doi:10.1029/2003PA000916

Chiang JCH, Bitz CM (2005) Influence of high latitude ice cover on the marine Intertropical Convergence Zone. Clim Dyn 25:477–496

Claussen M, Ganopolski A, Brovkin V et al (2003) Simulated global-scale response of the climate system to Dansgaard/Oeschger and Heinrich events. Clim Dyn 21:361–370

Cook, KH, Hseih JS, Hagos SM (2004) The Africa/South America intercontinental teleconnection. J Clim 17:2851–2865

Cook KH, Vizy EK (2006) South American climate during the Last Glacial Maximum Delayed onset of the South American monsoon. J Geophys Res 111:Art. No. D02110

Cook KH, Vizy EK (2008) Effects of 21st century climate change on the Amazon rainforest. J Clim 21:542–560

Costa MH, Foley JA, (1999) Trends in the hydrologic cycle of the Amazon basin. J Geophys Res 104:14189–14198

De Almeida RAF, Nobre P, Haarsma RJ, Campos EJ (2007) Negative ocean-atmosphere feedback in the South Atlantic Convergence Zone. Geophys Res Lett 34:Art. No. L18809

De Souza EB, Ambrizzi T (2006) Modulation of the intraseasonal rainfall over tropical Brazil by the Madden-Julian oscillation. Int J Clim 26:1759–1776

Doyle ME, Barros VR (2002) Midsummer low-level circulation and precipitation in subtropical South America and related sea surface temperature anomalies in the South Atlantic. J Clim 15:3394–3410

Enfield DB (1996) Relationships of inter-American rainfall to tropical Atlantic and Pacific SST variability. Geophys Res Lett 23:3305–3308

Fu R, Zhu B, Dickinson RE (1999) How do atmosphere and land surface influence seasonal changes of convection in the tropical Amazon? J Clim 12:1306–1321

Fu R, Dickinson RE, Chen MX, Wang HH (2001) How do tropical sea surface temperatures influence the seasonal distribution of precipitation in the equatorial Amazon? J Clim 14:4003–4026

Gan MA, Kousky VE, Ropelewski CF (2004) The South America monsoon circulation and its relationship to rainfall over west-central Brazil. J Clim 17:47–66

Garreaud RD (1999) Intracontinental connections and circulations: Multiscale analysis of the summertime precipitation over the central Andes. Mon Weather Rev 127:901–921

Garreaud RD (2000) Cold air incursions over subtropical South America: Mean structure and dynamics. Mon Weather Rev 128:2544–2559

Garreaud RD (2001) Subtropical cold surges: Regional aspects and global distribution. Int J Climatol 21:1181–1197

Garreaud RD, Vuille M, Clement AC (2003) The climate of the Altiplano observed current conditions and mechanisms of past changes. Palaeogrogr Paleoclimatol Palaeoecol 194:1–3

Gill AE (1980) Some simple solutions for heat-induced tropical circulation. Q J Roy Meteorol Soc 106:447–462

Gonzalez M, Barros V, Doyle M (2002) Relation between the onset and end of the South American summer monsoon and rainfall in subtropical South America. Clim Res 21:141–155

Grimm AM (2003) The El Nino impact on the summer monsoon in Brazil Regional processes versus remote influences. J Clim 16:263–280
Hagos SM, Cook KH (2005) Influence of surface processes over Africa on the Atlantic marine ITCZ and South American precipitation. J Clim 18:4993–5010
Hastenrath S, Geischer L (1993) Circulation mechanisms related to Northeastern Brazil rainfall anomalies. J Geophys Res 98(D3):5093–5102
Kalnay E, Kanamitsu M, Kistler R et al (1996) The NCEP/NCAR 40-year reanalysis project. Bull Am Meteorol Soc 77:437–471
Kleidon A, Fraedrich K, Heimann M (2000) A green planet versus a desert world: Estimating the maximum effect of vegetation on the land surface climate. Clim Change 44:471–493
Koster RD, Guo ZC, Dirmeyer PA et al (2006) GLACE: The Global Land-Atmosphere Coupling Experiment. Part I Overview. J Hydrometeorol 7:590–610
Lau KM, Zhou JY (2003) Anomalies of the South American summer monsoon associated with the 1997–99 El Nino southern oscillation. Int J Climatol 23:529–539
Lenters JD, Cook KH (1995) Simulation and diagnosis of the regional South American precipitation climatology. J Clim 8:2988–3005
Lenters JD, Cook KH (1997) On the origin of the Bolivian high and related circulation features of the South American climate. J Clim 54:656–677
Lenters JD, Cook KH (1999) Summertime precipitation variability over South America Role of the large-scale circulation. Mon Weather Rev 127:409–431
Li WH, Fu R (2004) Transition of the large-scale atmospheric and land surface conditions from the dry to the wet season over Amazonia as diagnosed by the ECMWF re-analysis. J Clim 17:2637–2651
Li WH, Fu R (2006) Influence of cold air intrusions on the wet season onset over Amazonia. J Clim 19:257–275
Liebmann B, Marengo JA (2001) Interannual variability of the rainy season and rainfall in the Brazilian Amazon basin. J Clim 14:4308–4318
Marengo JA, Druyan LM, Hastenrath S (1993) Observational and modeling studies of Amazonia. Clim Change 23:267–286
Marengo JA, Liebmann B, Kousky VE et al (2001) Onset and end of the rainy season in the Brazilian Amazon Basin. J Clim 14:833–852
Marengo JA (2004) Interdecadal variability and trends of rainfall across the Amazon basin. Theor Appl Climatol 78:79–96
Matsuno T (1966) Quasi-geostrophic motions in the equatorial area. J Meteorol Soc Japan 44: 25–43
Montecinos A, Diaz A, Aceituno P (2000) Seasonal diagnostic and predictability of rainfall in subtropical South America based on tropical Pacific SST. J Clim 13:746–758
Moron V, Bigot S, Roucou P (1995) Rainfall variability in subequatorial America and Africa and relationships with the main sea-surface temperature modes (1951–1990). Int J Climatol 15:1297–1322
New M, Lister D, Hulme M, Makin I (2000) A high-resolution data set of surface climate over global land areas. Clim Res 21:1–25
Nobre P, Shukla J (1996) Variations of sea surface temperature, wind stress, and rainfall over the tropical Atlantic and South America. J Clim 9:2464–2479
Nogues-Paegle J, Mo KC (1997) Alternating wet and dry conditions over South America during summer. Mon Weather Rev 125:279–291
Otto-Bliesner BL, Brady EC, Clauzet G et al (2006) Last Glacial Maximum and Holocene climate in CCSM3. J Clim 19:2526–2544
Paegle JN, Byerle LA, Mo KC (2000) Intraseasonal modulation of South American summer precipitation. Mon Weather Rev 128:837–850
Paegle JN, Mo KC (2002) Linkages between summer rainfall variability over South America and sea surface temperature anomalies. J Clim 15:1389–1407

Robertson AW, Mechoso CR (2000) Interannual and interdecadal variability of the South Atlantic convergence zone, Part II. Mon Weather Rev 128:2947–2957
Sylvestre F, Servant M, Servant-Vildary S et al (1999) Lake-level chronology on the southern Bolivian Altiplano (18–23°S) during Late-Glacial time and the early Holocene. Quat Res 51:54–66
Sturm C, Vimeux F, Krinner G (2007) Intraseasonal variability in South America recorded in stable water isotopes. J Geophys Res 112:Art. No. D20118
Tapia PM, Fritz SC, Baker PA et al (2003) A Late Quaternary diatom record of tropical climatic history from Lake Titicaca (Peru and Bolivia). Palaeogeogr Palaeoclimatol Palaeoecol 194:139–164
Vera C, Higgins W, Amador J et al (2006) Toward a unified view of the American monsoon systems. J Clim 19:4977–5000
Vizy EK, Cook KH (2005) Evaluation of Last Glacial Maximum sea surface temperature reconstructions through their influence on South American climate, J Geophys Res 110 (D11105) doi:10.1029/2004JD005415
Vizy EK, Cook KH (2007) Relationship between Amazon and high Andes rainfall. J Geophys Res 112:Art. No. D07107
Vuille M, Bradley RS, Healy R et al (2003) Modeling delta O-18 in precipitation over the tropical Americas 2. Simulation of the stable isotope signal in Andean ice cores. J Geophys Res 108:Art. No. 4175
Vuille M, Keimig F (2004) Interannual variability of summertime convective cloudiness and precipitation in the central Andes derived from ISCCP-B3 data. J Clim 17:3334–3348
Vuille M, Milana JP (2007) High-latitude forcing of regional aridification along the subtropical west coast of South America. Geophys Res Lett 34:Art. No. L23703
Wagner S, Widmann W, Jones J et al (2007) Transient simulations, empirical reconstructions and forcing mechanisms for the Mid-holocene hydrological climate in southern Patagonia. Clim Dyn 29:333–355
Wang H, Fu R (2007) The influence of Amazon rainfall on the Atlantic ITCZ through convectively coupled Kelvin waves. J Clim 20:1188–1201
Wang GL, Kim Y, Wang DG (2007) Quantifying the strength of soil moisture-precipitation coupling and its sensitivity to changes in surface water budget. J Hydrometeorol 8:551–570
Xie P, Arkin PA (1997) Global precipitation: A 17-year monthly analysis based on gauge observations, satellite estimates, and numerical model outputs. Bull Am Meteorol Soc 78:2539–2558
Xue Y, de Sales F, Li WP et al (2006) Role of land surface processes in South American monsoon development. J Clim 19:741–762
Zheng N, Dickinson RE, Zeng XB (1996) Climatic impact of Amazon deforestation – A mechanistic model study. J Clim 9:859–883
Zheng W, Braconnot P, Guilyardi E et al (2008) The ENSO at 6 ka and 21 ka from ocean-atmosphere coupled model simulations. Clim Dyn 21:745–762
Zhou JY, Lau KM (1998) Does a monsoon climate exist over South America? J Clim 11:1020–1040
Zhou JY, Lau KM (2001) Principal modes of interannual and decadal variability of summer rainfall over South America. Int J Climatol 21:1623–1644

Chapter 9
Sensitivity of South American Tropical Climate to Last Glacial Maximum Boundary Conditions: Focus on Teleconnections with Tropics and Extratropics

Myriam Khodri, Masa Kageyama, and Didier M. Roche

Abstract We explore how the moist deep convection over the Amazonian region responds to glacial forcings compared to the pre-indrustrial climate and how this change might interact with the meridional shift of rainfall over Nordeste, Pacific and Atlantic tropical Oceans. The objective is to assess and investigate the individual contributions of greenhouse gases concentration, ice sheet topography and/or albedo on the hydrological changes over tropical South America and their links to the Hadley and Walker circulations. We employ coupled ocean-atmosphere simulations for the Last Glacial Maximum and sensitivity experiments for each Last Glacial Maximum forcing. We show that the Last Glacial Maximum reduced greenhouse gases alone can explain the observed rainfall changes over tropical South America through the induced increase in tropical and northern extra-tropical dry static stability and altered Hadley circulation. Furthermore, we show that the topography of the North American ice sheet reinforces the equatorward shift of the descending branch of the Hadley cell leading to stronger subsidence and drying over the northern tropics. However, we show that the Laurentide ice sheet has also a significant influence on the simulated enhanced rainfall over Nordeste and Southeastern Brazil via the eastward shift of the Walker circulation, with a mechanism analogous to the atmospheric thermodynamical response to El-Niño conditions.

Keywords Last Glacial Maximum · Teleconnections · South America · Hadley cell · Walker circulation · Inter Tropical Convergence Zone · Ocean atmosphere general circulation model

9.1 Introduction

To date, results obtained from paleoclimate proxies in the Tropics throughout the last glacial, deglacial and Holocene periods have largely been interpreted either in

M. Khodri (✉)
Institut de Recherche pour le Développement, IPSL/LOCEAN (CNRS, IRD, UPMC, MNHN), Boîte 100, 4 place Jussieu, 75252 Paris, France
e-mail: myriam.khodri@ird.fr

F. Vimeux et al. (eds.), *Past Climate Variability in South America and Surrounding Regions*, Developments in Paleoenvironmental Research 14,
DOI 10.1007/978-90-481-2672-9_9,

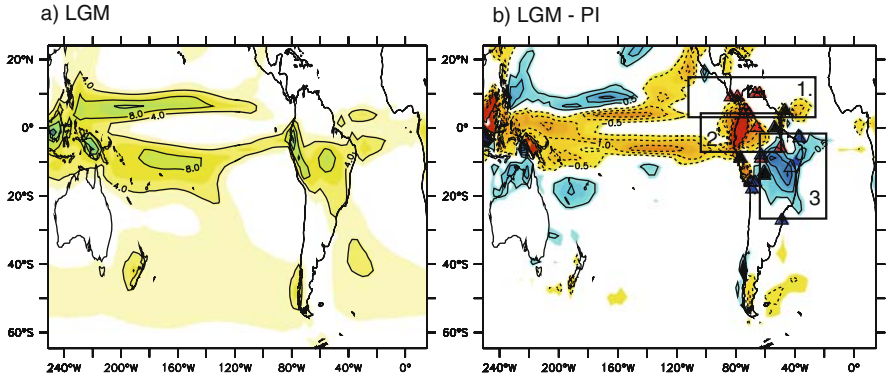

Fig. 9.1 Simulated precipitation during the Last Glacial Maximum by the IPSL-CM4 model and land records of hydrologic change over South America. (**a**) The background map shows Last Glacial Maximum December-January-February-Marsh (DJFM) mean precipitation. Contour interval (CI) is 4 millimeters per day. (**b**) The background map shows Last Glacial Maximum precipitation changes respectively to pre-industrial (PI) conditions during DJFM. CI is 0.5 mm per day. *Blue shading* indicates positive values. *Red symbols* indicate more arid conditions during the Last Glacial Maximum, *black symbols* indicate a hiatus and *blue symbols* more humid conditions compared to present day (Data compilation after Koutavas and Lynch-Stieglitz 2004, see their Fig. 12-3 and Anhuf et al. 2006; The speleothem record in Nordeste and Southeastern Brazil by Cruz et al. 2007 and Wang et al. 2006 are added to the previously cited compilations). Included sites are: Cariaco Basin (Peterson et al. 2000); Laguna el Pinal, Columbia (Behling and Hooghiemstra 1999); Lagoa Pata, Lagoa Gragao, Lagoa Verde (Colinvaux et al. 1996; Santos et al. 2001; Bush et al. 2004); Maicuru (Colinvaux and De Oliveira 2001); Carajas (Absy et al. 1991; Siffedine et al. 2001); Katira (Van der Hammen and Absy 1994); Noel Kempff Laguna Bella Vista (Mayle et al. 2000); Lake Valencia, Venezuela (Leyden 1985); El Valle Lake, Panama (Bush 2002); Lake Fuquene, Colombia (van Geel and van der Hammen 1973); Huascarán, Peru (Thompson et al. 1995); Sajama, Bolivi (Thompson et al. 1998); Illimani, Bolivia (Ramirez et al. 2003); Lake Titicaca, Bolivia (Baker et al. 2001); Lake Pata, Brazil (Colinvaux et al. 1996); ODP 932, Amazon Fan (Haberle and Maslin 1999); GeoB 3912 (Arz et al. 1998); Northeast Brazil (Wang et al. 2004); Southeast Brazil (Cruz et al. 2007)

terms of ENSO-like patterns or as changes in intensity and mean position of the Intertropical Convergence Zone (ITCZ) (e.g. Stott et al. 2002, 2004; Lea et al. 2003; Peterson et al. 2000; Koutavas et al. 2002; Koutavas and Lynch-Stieglitz 2003). For South America (SA) during the Last Glacial Maximum (LGM), 21 000 years Before Present (21 ky, BP) proxy data suggests a picture (Fig. 9.1b, symbols) with: (1) a drier tendency of the northern part of the continent and Central America, (2) a persistence of vegetation in the Amazon Basin, and (3) increased rainfall over southern tropics including the Nordeste, south east Brazil and the Altiplano of Bolivia. Given that the climate of the northern part of SA is affected mostly by the seasonal northward migration of the ITCZ, the LGM hydrology inferred from continental data has been interpreted as a southward shift of the ITCZ on annual mean (Koutavas and Lynch-Stieglitz 2004). Along the same line, Wang et al. (2007), based on speleothem records for the last glacial period, interpret the out of phase relationship between paleorainfall variability in Brazil and Eastern China as a direct response to

the reduced Atlantic meridional overturning circulation (AMOC) and its impact on the ITCZ position.

The seasonal cycle and amplitude of insolation received at the top of the atmosphere at the LGM is close to the present day one. The main LGM forcings are extensive land ice sheets over North America and Eurasia (Peltier 2004) and a reduced atmospheric concentration of greenhouse gases (GHG), notably of the atmospheric CO_2, which decreases by about 80 ppm (Flückiger et al. 1999; Dallenbach et al. 2000; Monnin et al. 2001). Both forcings and feedbacks within the climate system influenced and maintained the LGM climate. Changes in vegetation types might have also played a significant role through their influence on soil moisture variations, land surface albedo and evapo-transpiration (e.g. Kubatzki and Claussen 1998; Levis et al. 1999; Wyputta and McAvaney 2001).

Previous modelling studies have helped quantifying the impact of the land ice sheet and GHG forcings and their feedbacks on the LGM climate. Using atmospheric general circulation models (AGCMs) forced with the CLIMAP proxy-based reconstructions for LGM sea surface temperatures (SSTs), Hansen et al. (1984) have shown that land ice sheets and sea-ice albedo account for most of the LGM cooling. Coupling an AGCM to a slab ocean, other sensitivity studies has quantified the impact of each forcing on the simulated global cooling, revealing in most cases a strong influence of GHG on a global scale while land ice sheets lead to a cooling more restricted to the Northern Hemisphere (e.g. Manabe and Broccoli 1985). On the contrary, Hewitt and Mitchell (1997) relate most of the LGM global cooling to the topography and albedo of the land ice sheets while Felzer et al. (1998) argue for a combination between GHG and land ice influences. More recently, with a coupled ocean atmosphere GCM model (OAGCM), Kim (2004) evaluates that even though the bulk of global SST cooling is indeed due to reduced GHG, a larger cooling in the Northern Hemisphere occurs as response to either GHG and land ice sheets. The OAGCM results show greater cooling in the Northern Hemisphere in response to decreased Atlantic Meridional Overturning (AMOC) and ocean current heat exchange between both hemispheres.

According to tropical proxy data, such LGM global cooling correlates indeed with a reduced thermohaline circulation and with a drier rainy season in many tropical and monsoon regions between approximately 30°N and 5°N while wetter conditions develop in the southern tropics including northeastern Brazil (Nordeste). Chiang et al. (2003), based on paleoclimate observations and using an atmospheric climate model coupled to slab ocean suggest that the present-day "meridional mode" (labelled after Servain et al. 1999) of atmosphere-ocean variability in the tropical Atlantic is a potentially useful model for understanding these paleoclimate changes. The modern "meridional mode" corresponds to an anomalous meridional SST gradient across the equator, a displacement of the ITCZ and cross-equatorial flow toward the warmer hemisphere. The use of the "meridional mode" to explain LGM ITCZ mean position is largely based on the postulate that the dominant modern mode of tropical Atlantic ITCZ variability on inter annual-decadal timescales can link the climates of the tropical and North Atlantic. The marine-ITCZ, a tropical ocean-wide belt of atmospheric intense moist convection nowadays bears a year-round

Northern Hemisphere bias. It is located at the confluence of the northern and southern trades that sustain the rising branch of Hadley cell, is strongly linked to the South American Monsoon System and to the tropical seasonal emergence of cold equatorial SSTs (cold tongues) in the Atlantic and Pacific oceans. In the modern climate, very small interannual changes in tropical Atlantic SSTs (as small as 1°K) linked to NAO or ENSO external forcings explain part of the important ITCZ interannual to decadal variability observed in this ocean. Chiang et al. (2003), Chiang and Bitz (2005, referred herein as CB05) and Broccoli et al. 2006, using AGCMs coupled to a slab ocean, have shown that the Atlantic ITCZ response to LGM boundary forcings is analogous to the present day meridional mode with a southward displacement of the ITCZ. CB05 show that the North Atlantic cooling primarily promoted by the land ice sheets, with a negligible effect of reduced GHG, induces an asymmetric reorganisation of the Hadley circulation, a transfer of humidity toward the Southern Hemisphere through modified equatorial SST gradient and trans-equatorial winds.

Cruz et al. (cf. Chapter 2, this volume), based on this "ITCZ model", argue that the links between the weakening of the East Asian summer Monsoons and the in-phase increased precipitation over Nordeste and in southern Brazil could be initiated by the cooling of North Atlantic Ocean. The authors relate such a cooling either to changes in the AMOC or to the "meridional mode"-like response to LGM forcings in the tropical Atlantic. Even though the "ITCZ model" might indeed provide some elements of explanation for the southward shift of the marine-ITCZ during the LGM, previous modelling results are limited by the absence of a fully interactive ocean and by a missing consistent mechanism for inland precipitation. Over SA, the northern trade winds that feed the monsoons are also strongly linked to moist deep convection processes over the Amazon basin, which could respond on its own right to the LGM forcings. The present day monsoon and ITCZ systems may be related and sometimes vary in pace over certain areas. However, their controlling factors are different and the mechanisms of their variability are also different (cf. Chapter 8, this volume). These aspects are directly of concern for paleoclimate issues since most recently published papers documenting past tropical climate changes tend to confuse the ITCZ dynamics and the monsoon itself.

Using 5 different AGCMs coupled to fully interactive oceans from the PMIP2 data-base (http://pmip2.psce.ipsp.f2, Braconnot et al. 2007), Khodri et al. (2009) have shown that the processes responsible for the LGM South American hydrological changes are independent from their Atlantic Ocean-ITCZ counterpart. In the 5 OAGCMs simulations, an intensification of the Hadley Cell and an equatorward shift of its northern boundary occur, caused by an increased northern hemisphere static stability. A narrower Hadley cell forms at the LGM characterized by a descending northern branch between 10°N and the equator. Such a subsidence explains most of the drying over northern tropical SA (region 1 in Fig. 9.1). This finding contrasts with the "meridional-mode" mechanism found by CB05 with a slab ocean, since in coupled models, the Hadley Cell response does not necessarily rely on a trans-equatorial SST gradient, winds and moisture fluxes. In southern tropical SA (region 2, Fig. 9.1), the drying tendency over the Amazon basin is shown

to be rather due to a strengthening and eastward shift of the Walker circulation. The eastward shift of the Walker circulation appears to be forced by the little cooling in Southeast Central (SEC) Pacific, as compared to the West Pacific Warm Pool (WPWP), reminiscent to an "El-Niño like" pattern. Increased precipitation over the Nordeste and southeastern Brazil (region 3, Fig. 9.1) is then favored since both regions are out of reach of the stabilizing effects of the Walker and Hadley components of the tropical circulation and are located right next to moisture sources (namely the Amazon basin and the South Atlantic) needed to trigger moist convection. The robustness of these physical processes across all models seems to be confirmed by available data over land and over the Pacific Ocean. Over the tropical ocean, recent proxy estimates indeed indicate a relatively uniform cooling of about $1.7 \pm 1°C$ across the tropical oceans (with no trans-equatorial gradient in the Atlantic), while SEC Pacific shows little or no cooling at LGM as compared to modern times (Otto-Bliesner et al. 2009; MARGO Project Members 2009).

Numerous processes could affect the strength and extent of the Hadley cell and Walker circulation during LGM, such as the changes in the tropography and/or albedo of the ice sheets and reduced GHG. We cannot exclude either a specific and more direct response of the moist deep convection over SA to the global mean cooling during the LGM. This chapter builds upon a previous modelling study (Khodri et al. 2009), by using one of the fully coupled PMIP2 OAGCMs used to simulate the LGM climate. The objective is to assess and investigate the individual contributions of GHG concentration, ice sheet topography and/or albedo on the hydrological changes over tropical SA and links to the Hadley and Walker circulations. Here after, we show that the LGM reduced greenhouse gases forcing alone can explain the observed rainfall changes over tropical SA through the induced increase in tropical and northern extra-tropical dry static stability and altered Hadley cell. Furthermore, we show that the topography of Laurentide land ice sheet reinforces the equatorward shift of the northern bound of the Hadley cell leading to stronger subsidence and drying over northern tropics. Finally, we will also show that the Laurentide ice sheet has a significant influence on the simulated enhanced rainfall over Nordeste and Southeastern Brazil via the eastward shift of the Walker circulation.

Section 9.2 describes the model and its applicability to our problem. Section 9.3 describes the results for the full LGM climate. Section 9.4 explores the impact of individual LGM forcings on the Hadley cell, the Walker circulation and tropical moist convection. Discussion and conclusions are given in Section 9.4.

9.2 Model Description and Simulated Thermo-Dynamical Structure of the Atmosphere

9.2.1 The Model and Experimental Set Up

The model simulations analyzed in this chapter rely on the IPSL-CM4-V1 coupled ocean-atmosphere general circulation model developed at the Institut Pierre

Table 9.1 Boundary conditions for the Pre-industrial (PI) and Last Glacial Maximum (LGM) climates

	Ice sheets	Coastlines	CO_2 (ppmv)	CH_4 (ppbv)	NO_2 (ppbv)	Eccentricity	Obliquity (°)	Angular precession (°)
PI	Modern	Modern	280	760	270	0.0167724	23.446	102.04
LGM (21 ky)	ICE-5G	ICE-5G	185	350	200	0.018994	22.949	114.42

Simon Laplace (Marti et al. 2005) that has been extensively used for present, future and past climate studies. It is part of PMIP2 model simulation database for the LGM and preindustrial (PI) conditions (http://www-lsce.cea.fr/pmip2/, Braconnot et al. 2007). In the PMIP2 framework, all model simulations have the same boundary conditions for both the LGM and PI climates (see Table 9.1). Details of the experimental protocols are given in Braconnot et al. (2007). In the coupled ocean-atmosphere experiments analyzed in the present chapter the vegetation is fixed and prescribed to the present day distribution. The control simulation corresponds to a pre-industrial climate with atmospheric trace gases concentrations of 1750 A.D. and the 1950 orbital configuration (the 1750 and 1950 insolation difference is negligible). The LGM boundary conditions correspond to the topography and ice albedo from the ICE-5G data set developed by Peltier (2004). Changes in coastlines due to the decreased sea level induced by the large amount of frozen ice in continental ice-sheets are also taken into account leading to additional land in the Tropics (in the Indonesian Archipelago and between Australia and New Guinea). The specified greenhouse gas concentrations were inferred from the Greenland and Antarctic ice core records (Fluckiger et al. 1999; Dallenbach et al. 2000; Monnin et al. 2001) showing reduced concentrations of atmospheric carbon dioxide (CO_2), methane (CH_4), and nitrous oxide (NO_2) (Table 9.1). Otto-Bliesner et al. (2006a) have shown that LGM decreased greenhouse gases relative to PI resulted in a radiative forcing of the troposphere of –2.8 W m^{-2}. The orbital configuration of 21 ky BP is close to the present day.

In addition to the full LGM climate simulation, four additional sensitivity experiments have been performed (Kageyama et al. in prep), starting from PI conditions and adding in each simulation either: (1) the LGM reduced concentrations of atmospheric GHG (referred herein as LGMGHG); (2) the LGM land ice albedo and topography but with pre-industrial GHG concentrations (referred herein as LANDICE); (3) the topography of the ice sheet only without the corresponding albedo forcing (referred herein as ICETOPO); and (4) the albedo of the land ice distributed over the area of the ice sheet mask but without its topography (referred herein as ICEALB). Table 9.2 summarizes the configurations used in each sensitivity experiment. Each simulation is 500 years long and the last 50 years are used to compute the mean seasonal cycle. To explore the models skills related to the tropical climate, we choose to only examine quantities being useful diagnostics for

Table 9.2 Configuration of the sensitivity experiments to the Last Glacial Maximum forcing parameters

	LGMGHG	LANDICE	ICETOPO	ICEALB
Greenhouse gazes	Last Glacial Maximum	PI	PI	PI
Topography	PI	ICE-5G	ICE-5G	PI
Albedo	PI	ICE-5G	PI	ICE-5G

tropical moist deep convection regions. In the following, we present the simulated large-scale features of tropical precipitations and the thermo-dynamical structure (static stability, stream function, 200 mb velocity potential and divergent winds) of the atmosphere during the southern tropic rainy season (austral summer: December-January-February-March, DJFM). Vimeux and Khodri (2009), have indeed shown that it is the DJFM precipitation changes in the Tropics that imprint the simulated LGM annual response over SA and surrounding tropical oceans.

9.2.2 Simulated Pre-industrial (PI) Climate

We remind the readers that the model configuration is for pre-industrial conditions, which might induce some discrepancies when compared to present day observations. We do not present the results for the full seasonal cycle for the sake of simplicity. The PI model simulation exhibits a realistic seasonal cycle of precipitation and of sea-surface temperature (not shown). Figure 9.2 shows that the overall large-scale characteristics of the tropical precipitation for PI climate are well depicted when compared to the CMAP precipitation data set (Xie and Arkin 1997). Over SA the model does a good job in representing the observed geographical and amplitude characteristics of the austral summer South American Monsoon with precipitation spreading from the northern tropical Atlantic Ocean, into the Amazonian Basin and prolonged to the southeast by the South Atlantic Convergence Zone (SACZ). We note however, a strong positive precipitation bias on the Pacific coast but the overall characteristics of the South American Monsoon are well depicted.

Figure 9.3a and b display the vertical structure of the atmosphere static stability in DJFM for ERA40 and as simulated for PI conditions respectively. Static stability is one of the most fundamental quantities describing the state of the atmosphere. It derives from the vertical equivalent potential temperature (θ) structure of the atmosphere and determines the buoyancy force in the vertical. The vertical buoyancy force can be formalized as follow:

$$\mathrm{d}\omega/\mathrm{dt} = \mathrm{gz}(\gamma - \gamma_\mathrm{d})/\mathrm{T_A}$$

where ω is the vertical motion, γ corresponds to the environmental lapse-rate, γ_d to the adiabatic lapse-rate and $\mathrm{T_A}$ the environmental atmospheric temperature.

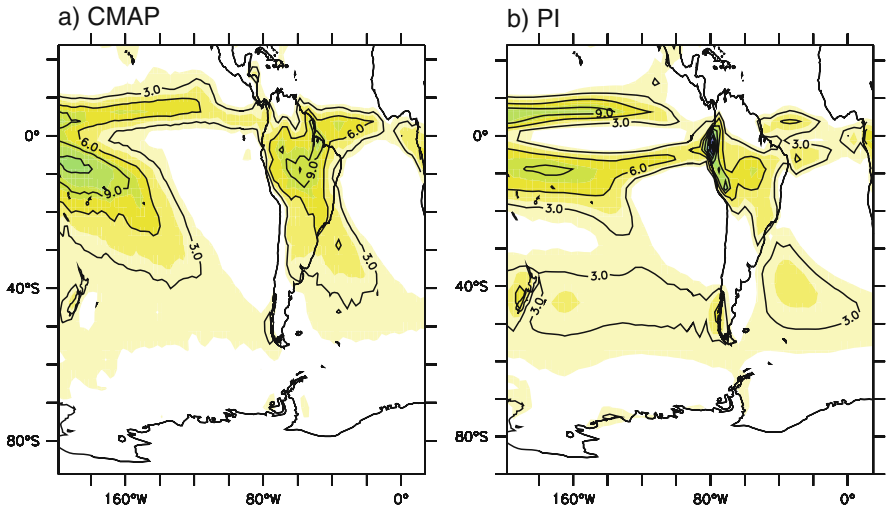

Fig. 9.2 Mean precipitation in DJFM. Colour shading interval is 2 mm per day. *Solid line* interval is 3 mm per day. (**a**) CMAP precipitation data set. (**b**) Model simulated precipitation for pre-industrial conditions

The atmosphere is stable ($d\omega/dt<0$) when $\gamma < \gamma_d$, neutral when $\gamma = \gamma_d$ ($d\omega/dt=0$) and unstable ($d\omega/dt>0$) when $\gamma > \gamma_d$. Using the hydrostatic approximation ($dp/dz = -\rho g$, with ρ being the air density and dp/dz the vertical pressure gradient), the static stability converts to:

$$d\omega/dt = g(\rho_{a-}\rho)/\rho$$

ρ_a is the density of the environment, ρ the density of the moving air parcel and g (ρ_a–ρ) the vertical buoyancy force.

The vertical structure of equivalent potential temperature (θ), plotted on Fig. 9.3a and b, can then be used to estimate the atmospheric static stability against deep convection. The potential temperature of a parcel of air, θ, corresponds to the temperature that the parcel would attain if it were displaced to the surface pressure reference level P_{00} ($\sim$ 1000 mb) in a reversible adiabatic process (i.e. no exchange of heat with the environment atmosphere). It is defined as follow:

$$\theta = T(P_{00}/P)^k, \text{with } k = Rd/C_p,$$

where Rd corresponds to the gas constant for dry air and Cp to the specific heat of air at constant pressure. θ implicitly takes into account the effects of compressibility of the air and it is used to remove the cooling (warming) effects associated to adiabatic processes (compression for dry air). θ therefore allows a direct comparison of air parcels temperature at various levels in the atmosphere. Within tropical moist deep convective regions the moist adiabat assumes that a local heating of an air mass

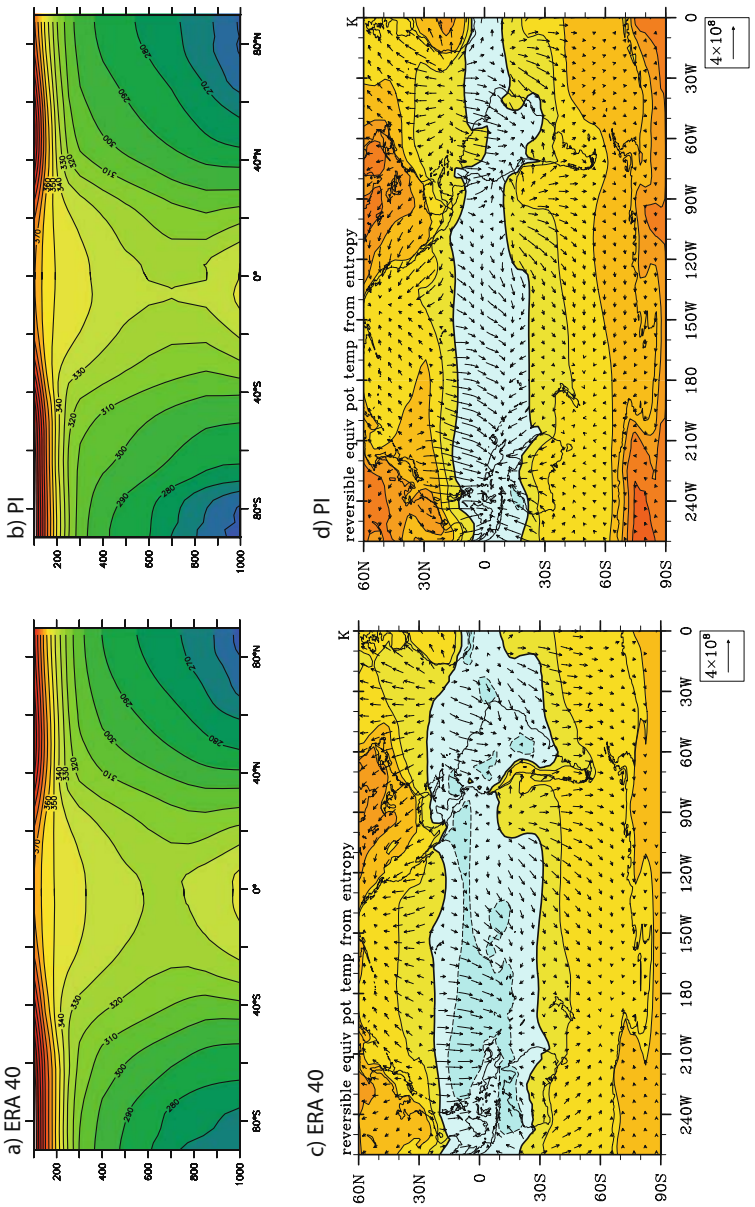

Fig. 9.3 (**a**) Vertical structure of the equivalent potential temperature (θ) in DJFM for (**a**) ERA40 and (**b**) for simulated pre-industrial (PI) conditions. CI is 10 K. Vertical coordinate is pressure in millibar (mb). The *lower panels* show the bulk static stability defined as the difference of θ between the upper troposphere (400 mb) and the surface (1000 mb) for (**c**) ERA40 and (**d**) for simulated pre-industrial (PI) conditions. The *blue shading* indicates negative values and corresponds to regions of minimum stability. Vertically integrated latent heat flux divergence is overlaid as vectors. Unit is J m^{-1} s^{-1}. The reference vector is indicated on the *lower part* of each graph

can destabilize it if it becomes warmer than the surrounding air at the same altitude. Being warmer it expands, which reduces its density ($\rho < \rho_a$), which in turn increases its buoyancy force, so it keeps rising ($d\omega/dt > 0$). When it rises it cools adiabatically (i.e. no exchange of heat between a parcel of ascending air and the environment) at the dry rate (–10°C/km) while the environment cools at the normal rate (–6°C/km). So the air parcel becomes colder until $\rho = \rho_a$ and the buoyancy ($d\omega/dt$) decreases. But if the dew point temperature is reached during the rising, the cooling lapse rate slows down to the wet adiabat lapse rate, which is smaller than the environment lapse rate and the energy released during condensation is used to warm the parcel. The atmosphere remains unstable and the air continues to rise and remains buoyant. At one point, at a certain altitude, the rising air temperature catches up with the temperature of stable air, it looses its extra buoyancy, cease to rise further and the atmosphere becomes stable.

So the static stability can be expressed by $d\theta/dz$, with an unstable atmosphere when $d\theta/dz < 0$, a stable atmosphere when $d\theta/dz > 0$, and a neutral atmosphere with respect to deep convection when $d\theta/dz = 0$. As shown on Fig. 9.3 (upper panels), the uniform vertical profile of θ within the tropics between 30°S and 30°N illustrates that the temperature structure in the tropics is approximately given by the moist adiabat (Xu and Emanuel 1989). Within tropical moist deep convection areas, the warm sea surface temperature promotes strong surface buoyancy explaining the quasi standardization of the vertical temperature profile of θ between 30°S–30°N (dry air following the dry lapse rate), which in fact reflects the surface θ. In addition, as shown in Fig. 9.3a, b, the latitudinal and vertical structure of θ show that moist convection that occurs over tropical warm waters determine upper tropospheric temperatures over mid-latitudes and is important in establishing the static stability from tropical to extra-tropical latitudes.

On Fig. 9.3c, the bulk static stability, defined as the difference of θ between the upper troposphere (400 mb) and the surface (1000 mb) shows that the Tropics bear minimum stability ($d\theta/dz < 0$, minimum vertical gradient of θ) while extra-tropical latitudes are much more stable against convection ($d\theta/dz > 0$, maximum vertical gradient of θ). Interestingly, the model does a fairly good job in representing the thermal structure of the atmosphere even though it underestimates the latitudinal extent of tropical moist deep convective region (blue area, Fig. 9.3d). The model bears a much narrower tropical belt of unstable atmosphere relatively to observations. This difference is probably due to the overall cold SSTs bias of 1 K in the tropics simulated with PI boundary conditions when compared to modern day (Otto-Bliesner et al. 2009, their Fig. 9.2). The vertically integrated divergent latent heat transport is overlaid as vectors on Fig. 9.3c and d. The low-level latent heat divergence from eastern pacific upwelling regions towards the WPWP, illustrating the low level flow of the atmospheric Walker Circulation is well captured in pattern while its strength is underestimated.

The zonally-averaged atmospheric streamfunction displayed on Fig. 9.4a and b features the DJFM Hadley circulation for NCEP and the PI run respectively. Positive (negative) values represent a (counter) clockwise mass flux circulation. The Hadley circulation is constrained by the requirement that diabatic heating in the Tropics

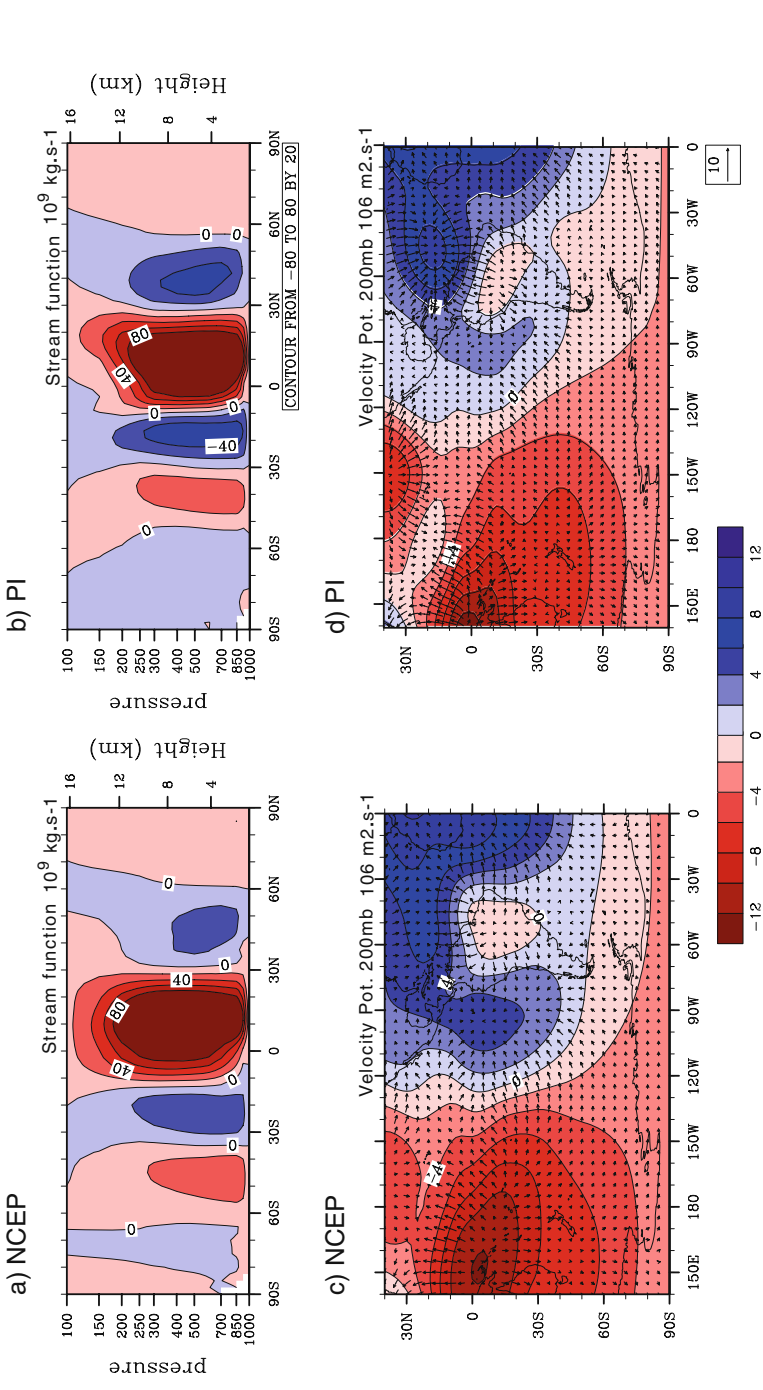

Fig. 9.4 Stream function (10^9kg s^{-1}) in DJFM for (**a**) NCEP reanalyses and (**b**) for the simulated pre-industrial (PI) conditions. *Red (blue) shading* indicates positive clockwise (negative counter clockwise) circulation. Vertical coordinate is pressure in millibar (mb). (**c**) and (**d**) 200 mb velocity potential (10^6m^2 s^{-1}) and divergent winds (m s^{-1}) overlaid as vectors for NCEP reanalyses and for the simulated pre-industrial (PI) conditions. The reference vector is indicated on the *lower part* of each graph. Convergence corresponds to positive (*blue shading*) velocity potential

sustaining the divergent flow in the upper troposphere balances the cooling leading to subsidence in subtropics. The model simulation for PI conditions does a fairly good job in representing the meridional extent and strength of the Hadley cell even though the vertical component of the divergence within the Tropics is weaker than observed. Along the same lines, the 200 mb velocity potential and divergent wind vectors on the lower panels of Fig. 9.4, showing the upper tropospheric large-scale motion, depict the links between the Hadley and Walker circulations and tropical convective regions. The Hadley circulation follows the strong divergent flux from the convective Amazonian basin and WPWP toward the subtropical latitudes of both hemispheres, while divergent winds from the WPWP toward the eastern Pacific illustrates the upper flow of the atmospheric Walker Circulation. The lower panels of Fig. 9.4 confirm the underestimation of the extent and intensity of tropical moist deep convective regions (seen with the bulk of dry static stability, Figs. 9.3c, d) by the IPSL model. Over SA and the WPWP, the area of upper divergent flow (pink and red shading) is smaller than observed.

To sum up, the large-scale features of the thermo-dynamical structure of the PI tropical atmosphere simulated by the model, including its dry static stability, the Walker and Hadley (upper and lower) tropical circulations are underestimated when compared to observations and reanalyses of the present features. This overall weaker tropical circulation could be related to the cold bias in the simulation due to PI conditions.

9.3 Response of Tropical South American Climate to Last Glacial Maximum Forcings

In this section we present the changes in surface temperature gradient, precipitation, dry static stability, zonal and meridional atmospheric circulations in response to the applied LGM forcings. For conciseness, the processes behind the simulated SST changes are not fully developed here and will be the subject of an upcoming paper. Only the impact of the applied forcings on the tropical climate of SA will be discussed.

9.3.1 The Last Glacial Maximum

The simulated surface annual SST changes simulated for the LGM by the IPSL model shows an uniform tropical (15°S–15°N) cooling of about 2.3°K, which compares relatively well to the MARGO estimation of 1.7±1°K (MARGO project members 2009; Otto-Bliesner et al. 2009). Concerning the regional patterns, Otto-Bliesner et al. (2009) have shown that the inter basin and intra basin SST cooling gradients are underestimated by coupled models when compared to MARGO estimations. Here, we have chosen to focus on the sign of changes in surface temperature gradient rather that the net values in order to get a better understanding of

the processes controlling the zonally-asymmetric Walker circulation in the tropical Pacific. Figure 9.5a displays the DJFM surface temperature gradient difference in response to the applied LGM forcings (see caption for details). According to the MARGO proxy data, the SST has greater LGM cooling in the eastern Pacific cold tongue than in the WPWP, which suggests a stronger zonal SST gradient. Observations also indicate that there is little or no cooling over the Pacific subtropical gyres, in the SEC and Northeast Pacific (MARGO project members 2009). For the full LGM simulated climate, on Fig. 9.5a, smaller cooling in the WPWP is found compared to the eastern Pacific cold tongue. Likewise, SEC and North Eastern Central

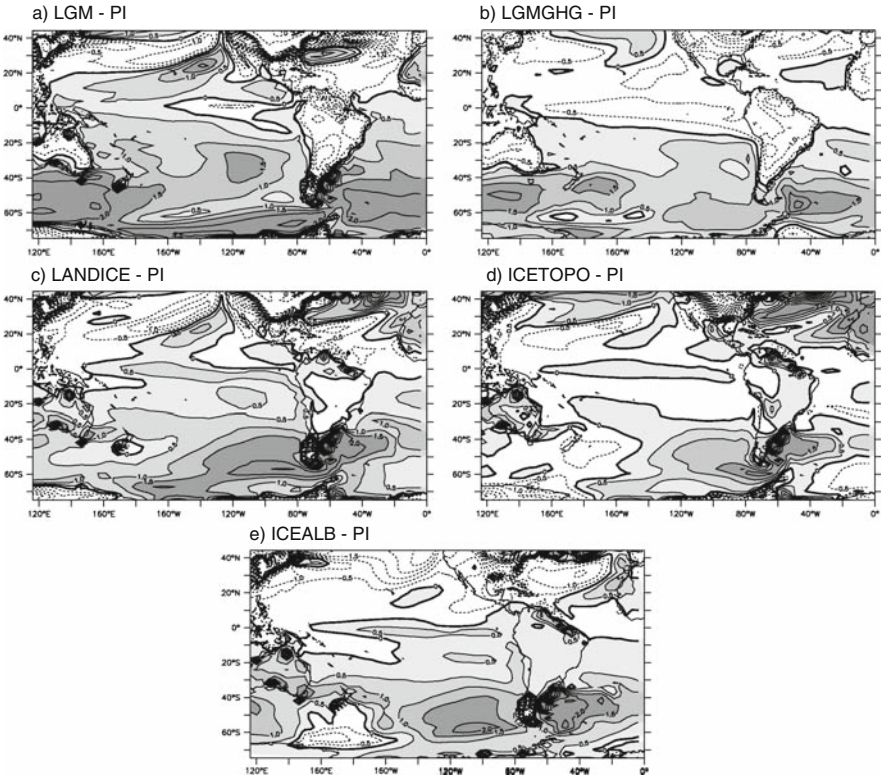

Fig. 9.5 Changes in surface temperature gradient respectively to the pre-industrial simulation. The surface temperature gradient was computed by removing linearly the averaged global surface temperature to each corresponding surface temperature field. The removal of the global average facilitates the comparison of the regional pattern between the sensitivity experiments and PI conditions. This shows the DJFM mean difference between the (**a**) LGM (GHG, orbital, and land ice forcing) and the PI run; (**b**) LGMGHG (GHG only) and the PI run; (**c**) LANDICE (land ice forcing only) and the PI run; (**d**) ICETOPO (land ice topography only) and the PI run; (**e**) ICEALB (land ice albedo only) and the PI run. CI is 0.5 °K and regions above the thick zero line contour are shaded

Pacific bear the least cooling as compared to the abovementioned regions. Reasoning in terms of gradient, the simulated DJFM pattern over the Pacific Ocean might suggest an overall agreement with the MARGO data compilation, even if the amplitude of the changes is weaker. Noteworthy over the Atlantic, the simulated trans-equatorial SST gradient with stronger cooling in the Northern Hemisphere is inconsistent with the MARGO data compilation. This is due to the fact that the PI climate has a relatively weak thermohaline overturning (∼12 sverdrup, Sv) while the LGM has a strong one (∼15 Sv).

Figure 9.6 shows the LGM response in atmospheric static stability (upper panels) and circulation changes (lower panels) simulated by the IPSL model respectively to PI conditions. On Fig. 9.6a, the changes in the vertical structure of the equivalent potential temperature (θ), reveal a robust increase in LGM dry static stability, with the lower tropospheric cooling outpacing the upper troposphere by about 2 K on a global average. The globally cooler and drier LGM climate promotes a contraction of the atmosphere, which becomes denser as evidenced by the lower tropopause

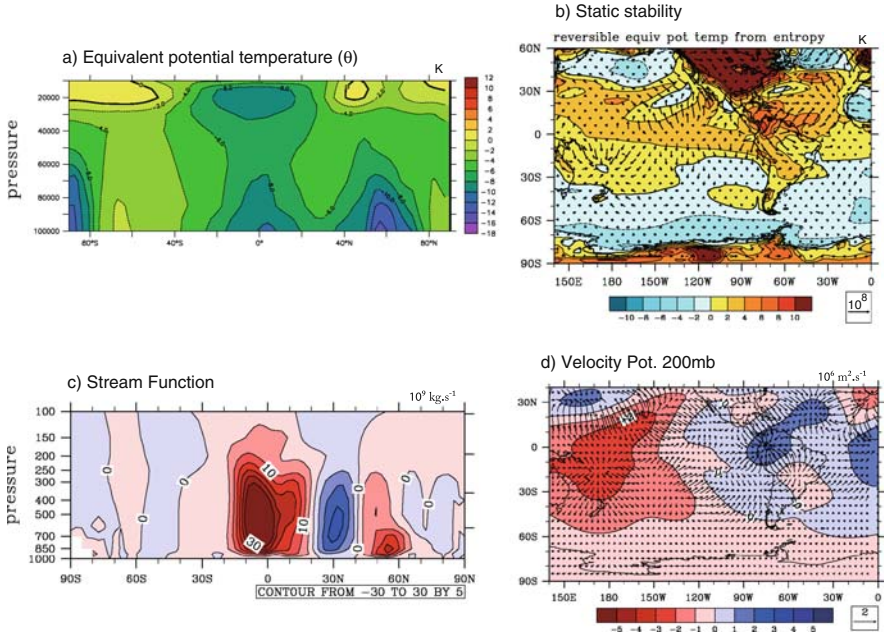

Fig. 9.6 Changes in dry static stability and atmospheric circulation given LGM boundary conditions. This shows the DJFM mean difference between the LGM (GHG, orbital, and land ice forcing) and the PI run. (**a**) Vertical structure of the equivalent potential temperature (θ) (CI 2 °K); (**b**) Bulk static stability (CI 2 °K and the thick line is the zero contour) and vertically integrated latent heat flux divergence overlaid as vectors (J m^{-1} s^{-1}, the reference vector is given on the panel); (**c**) Streamfunction (*red shading* indicates positive values); (**d**) 200 mb velocity potential (CI is $1.10^6 m^2$ s^{-1}) and divergent winds (m s^{-1}, reference vector is given on the panel) overlaid as vectors

Table 9.3 Simulated tropical (15°S–15°N) precipitation, (mm per day) and surface temperature (°k) changes in each simulation respectively to PI conditions

		LGM-PI	LGMGHG-PI	LANDICE-PI	ICETOPO-PI	ICEALB-PI
Precipitation	AN	–0.39	–0.3	0	0.09	0
	DJFM	–0.38	–0.33	0	0.1	0
Surface Temperature	AN	–2.3	–2.2	0.57	1.4	0.2
	DJFM	–2.2	–2.2	0.32	1.4	0.28

height (positive values on Fig. 9.6a). Over tropical latitudes between 15°S and 15°N, this results in a damping of the convective heating of the upper troposphere, explaining the slight tropical mean decrease in precipitation especially over tropical Pacific and northern SA (Fig. 9.1). Despite the slight net precipitation decrease on average over tropical latitudes (Table 9.3), rainfall increases substantially over Nordeste and Southeastern Brazil.

It is worth noting however that a larger thermal stratification occurs over northern extra-tropics (+3.5 °K) as compared to the southern tropics (+0.8 °K) probably because of the presence of large land ice cover in the Northern Hemisphere. An intensification of the Hadley Cell and an equatorward shift of its northern boundary are simulated (Fig. 9.6c). This narrower Hadley cell feeds upon the core of baroclinic eddies developing south of the Laurentide Ice sheet. The resulting stronger subsidence between 10°N and the equator (Fig. 9.6d) then provides a dynamical feedback amplifying the drying tendency seen over northern tropical SA (region 1 in Fig. 9.1). Such an increased Hadley cell circulation seems to be a direct consequence of the increased dry static stability over extra tropical latitudes, which pushes the baroclinic instability zone and the outer limit of the Hadley cell equatorward. This result confirms that tropical circulation may indeed depend on extratropical climate since the boundary condition for the Hadley circulation is constrained by the requirement that diabatic heating in the tropics balances cooling in subtropics. Such extratropic-tropic dependence is stronger at the LGM due to the stronger perturbation of northern extra tropical thermal and dynamical equilibrium.

As expected from the reinforced tropical Pacific zonal SST gradient, a strengthening of the Walker circulation is simulated, as shown by the changes in the 200 mb velocity potential (Fig. 9.6d). The smaller SST cooling over SEC Pacific as compared to the WPWP induces also a positive anomaly in diabatic heating for the atmosphere and is responsible for an anomalous divergence east of 120°W (Fig. 9.6d, pink shading). As a result stronger divergent mass flux from SEC Pacific and stronger subsidence over most of the Amazon basin (Fig. 9.6d, blue shading) are simulated consistently with an eastward extension of the Walker circulation. Overall, the model shows a tendency towards a more "El Niño-like" state in terms of the perturbation of thermal structure of the tropical atmosphere. This is shown by the meridional mean of tropical equivalent potential temperature displayed on Fig. 9.7a,b. The equivalent potential temperature changes simulated at LGM are reminiscent to the tropospheric temperature anomaly in response to an "El Niño-

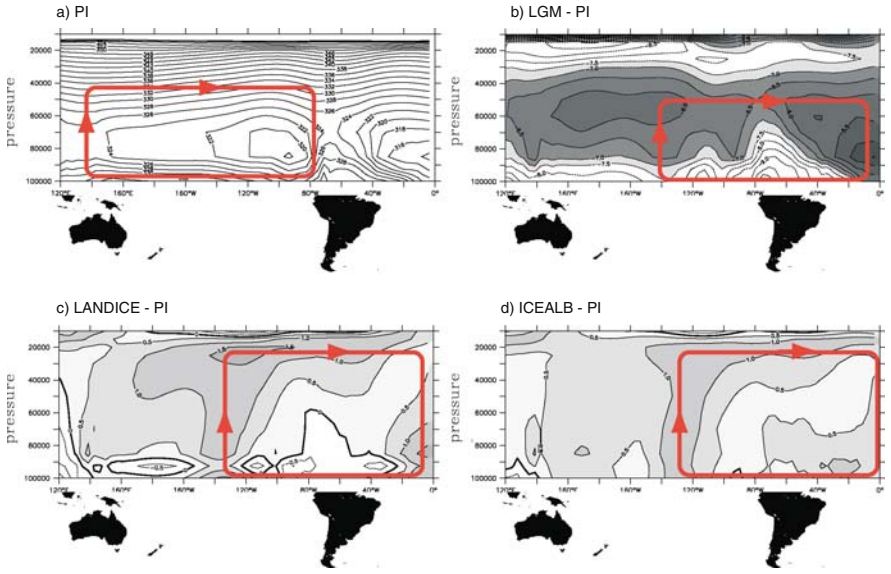

Fig. 9.7 Changes in the tropical (15°S–15°N) meridional mean of dry static stability. This shows the vertical structure of the tropical zonal mean of equivalent potential temperature (θ) in DJFM for (**a**) for the PI run. CI is 2 °K; (**b**) the difference between the LGM (GHG, orbital, and land ice forcing only) and the PI run. Regions above the –7.5 °K contour are shaded; (**c**) the difference between the LANDICE (land ice forcing only) and the PI run; (**c**) the difference between the ICEALB (land ice albedo only) and the PI run. CI is 0.5 °K and regions above the thick zero line contour are shaded. Vertical coordinate is pressure in Pascal (Pa)

like" state, which consists in a widespread warming of upper troposphere compared to lower level, spreading outward from the central Pacific (Wallace et al. 1998; Chiang and Sobel 2002; Su and Neelin 2002). However such an anomalous upper tropospheric warming differs from a canonical "El-Niño-like" state since here it is due to warmer conditions in the SEC Pacific as compared the WPWP. This tropical-tropical teleconnection provides a second mechanism by which the atmospheric column is stabilized (both thermally and dynamically) against deep convection over equatorial SA. As moisture accumulates in the boundary layer over the Amazon to balance the reduced local moist deep convection, a transfer of humidity occurs from the Amazon basin toward the Nordeste and Southeast Brazil. This is well illustrated by the changes in the bulk of static stability and moisture divergence displayed on Fig. 9.6b. The Amazonian moisture is removed by the low-level flow and transferred into the Nordeste and southeastern Brazil where moist convection can occur.

In the following sections, the role played by each LGM boundary condition on the abovementioned physical processes (damping of tropical convective heating, strengthening and contraction of the Hadley cell, strengthening and eastward extension of the Walker circulation) are investigated.

9.3.2 Sensitivity to Last Glacial Maximum Reduced Greenhouse Gases

Figure 9.8a displays the DJFM precipitation changes simulated by the LGMGHG run compared to the PI simulation. While the tropical average is negative (Table 9.3), there is a substantial positive precipitation anomaly occurring along the border of the Amazonian convection zone including the Nordeste and South East Brazil. These features are similar to the full Last Glacial Maximum case (Fig. 9.1) although with a weaker amplitude. The simulated tropical cooling reaches 2.2 °K with reduced GHG, which is nearly equal to the full LGM tropical cooling (Table 9.3).

This suggests that the decreased absorption of infrared radiation induced by lower GHG concentration is mostly responsible for the direct thermo-dynamical adjustment of tropical moist deep convection, as shown on Fig. 9.9a (to be compared with Fig. 9.6a). Indeed the tropical cooling due to reduced GHG, equivalent to the full LGM case, results in a direct atmospheric column drying (low-level specific humidity reduced by about 15%) following the Clausius-Clapeyron relationship and leading to increased tropical dry static stability (Figs. 9.9a, b). Such a tropical atmospheric stabilisation also implies a reduction in water vapor low-level convergence especially over tropical Pacific, which provides amplification for the drying (Fig. 9.9b).

However across the Tropics, the bulk dry static stability anomalies are relatively constant, with positive anomalies spreading between 30°N and 30°S, which therefore do not, on their own, yield insight into the mechanisms for the strong spatial structure in the precipitation signal over tropical SA. Interestingly, reduced

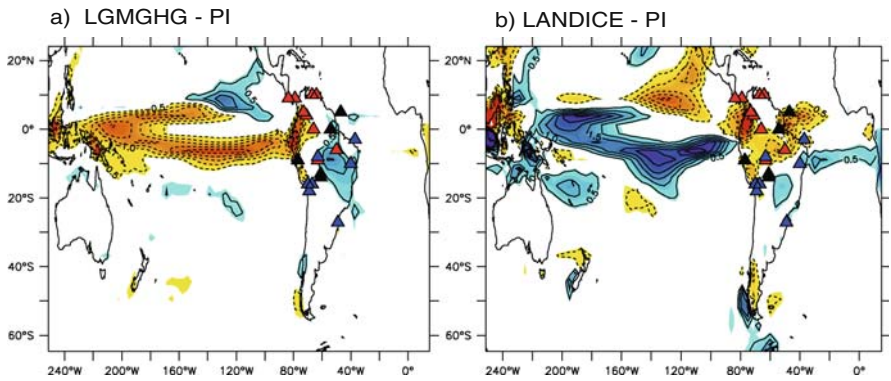

Fig. 9.8 Simulated precipitation changes and land records (symbols) of hydrologic change over South America (see caption of Fig. 9.1). This shows the DJFM mean difference between the (**a**) LGMGHG (GHG only) and the PI run; (**b**) LANDICE (land ice forcing only) and the PI run. CI is 0.5 mm per day. *Blue shading* indicates positive values. *Red symbols* indicate more arid conditions during the Last Glacial Maximum, *black symbols* indicate a hiatus and *blue symbols* more humid conditions compared to present day

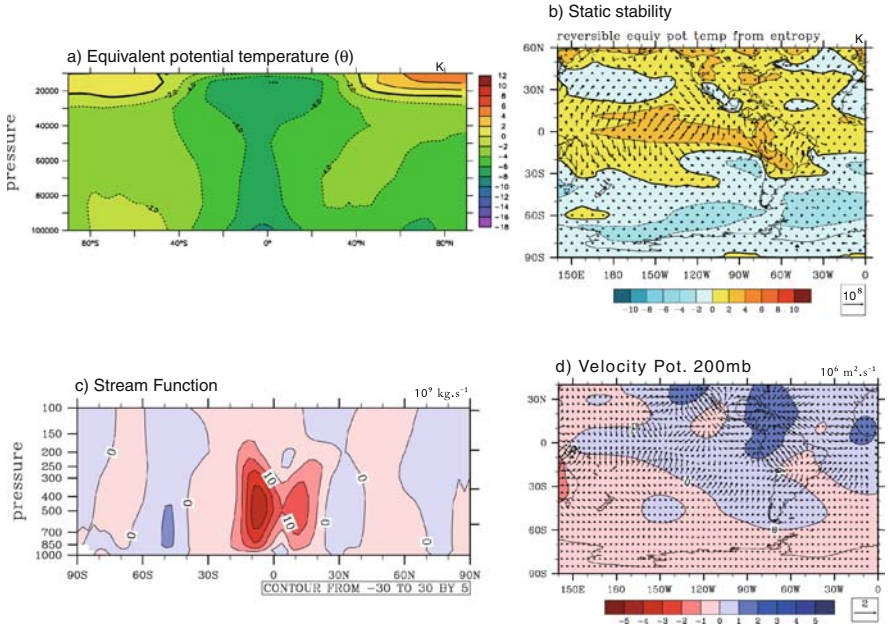

Fig. 9.9 Same as Fig. 9.6 but given LGMGHG (GHG only) boundary conditions

GHG also leads to a stronger cooling of Northern Hemisphere compared to the Southern Hemisphere, due to the presence of more land masses which on average respond more importantly to the radiative cooling that the southern oceans (Fig. 9.5b; Laîné et al. 2009). As a result, the static stability increases more in the Northern Hemisphere as compared to the Southern Hemisphere, which pushes both the baroclinic instability zone and hence the northern boundary of the Hadley cell southward as in the full LGM case (Fig. 9.9c). A robust strengthening of the Hadley cell and subsidence occurring over equatorial and northern SA (Fig. 9.9d, blue shading) provides therefore an amplifying feedback mechanism (in addition to the direct impact of the cooling) for reduced precipitation. These features resemble the mechanism presented by CB05 and Broccoli et al. (2006), relying only on the asymmetric temperature changes between both hemispheres to explain the net southward shift of the Atlantic ITCZ. However in the full LGM and LGMGHG simulation, no southward shift of the Atlantic ITCZ and trans-equatorial moisture transport are reproduced. Instead analysis of the boundary layer moisture budget over the Amazon basin reveals that the accumulation of moisture in the Amazonian boundary layer due to decreased local deep convection is moved by the divergent flow (overlaid latent heat divergent transport on Fig. 9.9b) into the Nordeste and southeast Brazilian coast, where moist instability actually occurs.

The above mentioned physical processes due to reduced GHG alone (radiative tropical cooling and damping of convective mass fluxes, strengthening but limited

expansion of the Hadley cell, transfer of moisture and rainfall from the Amazon basin toward the Nordeste) account for most of the LGM changes over the equatorial Pacific and northern SA. However, the somewhat less pronounced enhanced rainfall over southeast Brazil compared to the full LGM case could be due to the absence of the Walker circulation feedback. This is well illustrated by the overall uniform cooling across the tropical Pacific and the absence of eastward shift of the Walker circulation (Fig. 9.9d). A similar analysis for the simulation taking into account the Northern Hemisphere LGM land ice only as a boundary condition, shows that the mechanism of teleconnection with the central Pacific applies essentially to southern tropical latitudes of SA.

9.3.3 Sensitivity to Last Glacial Maximum Land Ice

On Fig. 9.8b the DJFM precipitation changes simulated in the LANDICE sensitivity experiment reveals a balance between an increased precipitation over the tropical Pacific and a drying tendency over most of tropical SA (Table 9.3). This result confirms that net decreased tropical precipitation during LGM is mostly due to the reduced GHG and induced radiative cooling. Similarly to the full LGM and LGMGHG case however, a hemispheric asymmetry of static stability and limited expansion of the Hadley cell (Fig. 9.10a–c) is simulated. The land ice forcing acts to cool the northern lower troposphere while forcing a southeastward shift of the subtropical jet and western ocean boundary currents (i.e the Atlantic Gulf Stream and

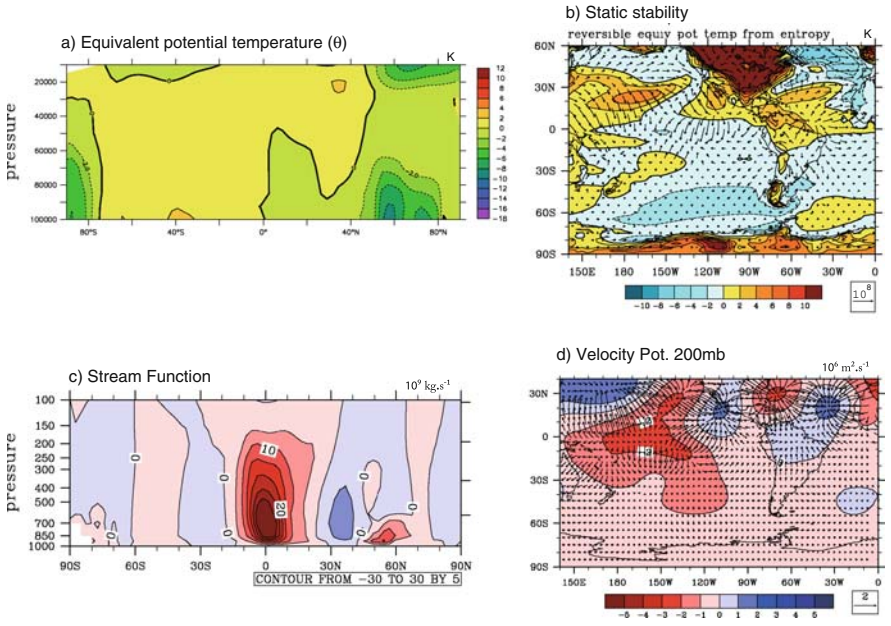

Fig. 9.10 Same as Fig. 9.6 but given LANDICE (land ice forcing only) boundary conditions

the Pacific Kuroshio, not shown) explaining the warmer SST over the subtropical gyres of both hemispheres (Fig. 9.5c). The impact on the bulk dry static stability anomalies across the Tropics and on the Hadley cell subsidence over northern tropical SA is nevertheless much weaker (Fig 9.10b, d) than for the full LGM and LGMGHG cases and is confined north of the equator.

Precipitation changes for southern tropical SA (Fig. 9.8b) appears to be linked to the teleconnection with the central Pacific. Despite the reduced zonal SST gradient and intensity of the Walker circulation, the warmer SEC Pacific sustains an upper tropospheric increase of θ which reaches 1.5 °K over SA (Fig. 9.7c). The resulting eastward shift of the Walker circulation (Fig. 9.10d), amplified atmospheric thermal stratification over southern tropical SA and reduced moisture convergence (Fig. 9.10b), all induce a damping in moist deep convection including most of the Nordeste and southeastern Brazil. Interestingly adding up LGMGHG and LANDICE results (not shown) reveals that the precipitation field obtained is close to the full LGM, which suggests a linear response to both forcings. Reduced GHG and land ice at LGM both contribute to reduced precipitation over northern tropical SA via the Hadley cell thermodynamical adjustments, but the net southeastward shift of the precipitation towards Nordeste and southeast Brazil is amplified when involving "El-Niño like" teleconnection with SEC Pacific and gradient in the boundary layer moisture.

Accordingly when separating the topography from the albedo forcing of land ice, both forcings lead to similar precipitation responses. Increased rainfall over the tropical Pacific is in both cases compensated by drying over tropical SA (Fig. 9.11, Table 9.3). Adding the anomalies due to individual ice albedo and topography forcings does not reproduce the LANDICE precipitation changes (not shown) suggesting a non linear combination of their effects. Indeed while the higher topography barrier in the ICETOPO experiment induces a local thermal stratification over the northern extratropics and a southward shift of the jet stream and of the northern boundary of the Hadley cell, the resulting subsidence over northern SA is weaker

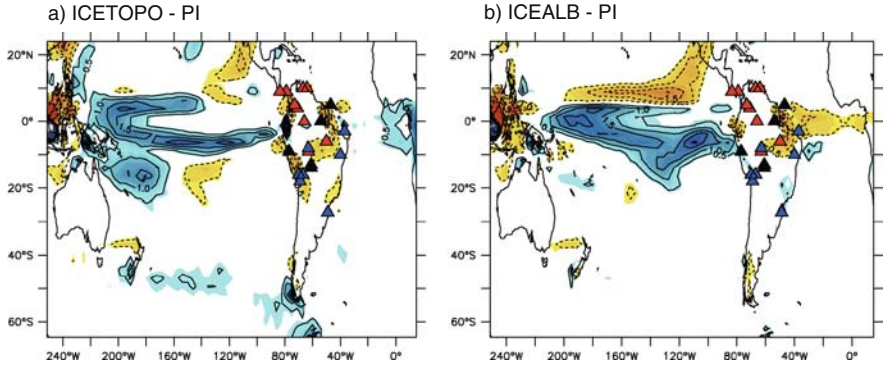

Fig. 9.11 Same as Fig. 9.8 but given (**a**) ICETOPO (land ice topography only) and (**b**) ICEALB (land ice albedo only) boundary conditions

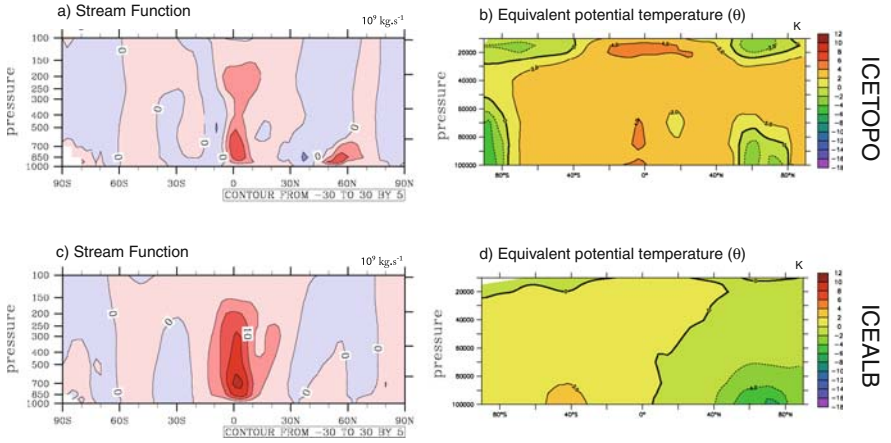

Fig. 9.12 Changes in mean streamfunction and vertical structure of the equivalent potential temperature (θ) in ICETOPO (land ice topography only, *upper panels*) and ICEALB (land ice albedo only, *lower panels*) boundary conditions. This shows the DJFM mean difference to the PI run. In (**b**) and (**d**) CI is 2 °K and the *thick line* is the zero contour. For the streamfunction, the *red shading* indicates positive values

than in LANDICE (Fig. 9.12a, b). This suggests that the dynamical teleconnection alone with the topography of the Laurentide Ice sheet through its influence on the position of the outer boundary of the Hadley cell can explain only part of the drying over northern SA. In the absence of global cooling, the transfer of moist deep convection preferentially occurs towards the tropical Pacific Ocean (as in LANDICE), where abundant moisture supply is not a barrier for convection and even tends to be enhanced by the increased moisture convergence (not shown).

A most interesting result is that in response to the sole ice albedo forcing (unlike in LANDICE or ICETOPO), there is a robust poleward expansion of the Hadley circulation (Fig. 9.12c) despite the inter-hemispheric SST asymmetry and strong surface temperature gradient on the southern limit of the Laurentide Ice sheet (Fig. 9.5e). The ice albedo alone then sustains a strong horizontal gradient in northern static stability, which, in the absence of topographic barrier, pushes the baroclinic instability zone and the northern limit of the Hadley cell poleward (Fig. 9.12c, d). Therefore, in the ICEALB experiment, the Hadley cell subsidence mechanism cannot explain the drying tendency over northern SA. The warm SST in the SEC Pacific however leads to the positive upper tropospheric θ anomaly over tropical SA (Fig. 9.7d), as seen in the LANDICE case. This result confirms that tropospheric warming spreading out from the Pacific and eastward extension of the Walker circulation is the essential mechanism for the drying over equatorial America and is due to the ice albedo.

These results show that the mechanisms of climate change over South America can be broken down between a response to (1) the direct effect on tropical deep

convection of global cooling and associated drying due to reduced GHG (Clausius-Clapeyron relationship); (2) the effect of increased extra-tropical static stability on the Hadley Cell and stronger subsidence over northern tropics due to both reduced GHG and the topography of the ice-sheets; and (3) the influence of SEC Pacific SST positive anomaly, probably due to the land ice albedo, on the strengthening and eastward extension of the Walker circulation.

9.4 Summary and Conclusion

Proxy data over South America for the LGM has been interpreted as a southward shift of the ITCZ, which has been so far linked to a trans-equatorial gradient in the Atlantic Ocean, analogous to the modern day "meridional-mode" mechanism (Chiang et al. 2003; Chiang and Bitz 2005). Here we have explored alternative mechanisms, related to the direct impact of the LGM global cooling and changes in the dry static stability on tropical moist deep convection. We have used a coupled ocean-atmosphere model capable of capturing the thermodynamical structure of the atmosphere and the tropical component of the Hadley and Walker circulations. In each experiment, we have applied either all the LGM forcings, or the individual contributions of greenhouse gases (GHG) concentrations, ice sheet topography and/or albedo to explore the hydrological response over tropical latitudes with a focus on South America.

The dominant forcing for the LGM tropical temperature and precipitation changes is found to be due to the reduced GHG, which explains almost entirely the simulated tropical cooling and drying. The LGM GHG is also responsible for a stronger cooling in the Northern Hemisphere, inducing a stronger overall northern tropical overturning atmospheric circulation. Such a stronger northern component of the tropical Hadley cell appears to be caused by increased extra-tropical static stability. Stronger subsidence over northern tropic then produces an amplification of the northern tropical drying initially due to the direct cooling effect. The boundary layer moisture accumulated in the Amazon basin is then transferred by the low level circulation towards the Nordeste where rainfall increases. The land ice sheet is also able to promote the Hadley cell feedback mostly via the topographic effect on the extra-tropical dry static stability and on the position of the subtropical jets. Our results therefore suggest that the communication between the extra tropics and the tropics is tighter during LGM and does not necessarily rely on the "meridional-mode" mechanism. The Hadley cell response is constrained by the requirement that diabatic heating in the Tropics balances cooling in subtropics. We show that such extratropic-tropic dependence is stronger at the LGM because of the stronger perturbation of northern extra tropical thermal and dynamical equilibrium due to both reduced GHG and land ice sheets. Such a mechanism is potentially useful to explain northern tropical drying and seems to be confirmed by available proxy data. Furthermore the MARGO data compilation indeed suggests a uniform latitudinal cooling across tropical latitudes of the Atlantic Ocean, therefore inconsistent with a "meridional-mode" mechanism.

The role of the ice albedo appears to be nontrivial since, in the absence of the land ice topographic barrier, its influence results in poleward extension of the Hadley cell through the stronger horizontal gradient in static stability. As the topography and albedo influences on the simulated changes are not linear and even lead to opposite responses of the Hadley cell, it is difficult to interpret their respective role in the total land ice forcing. This result sheds some light on the processes that could be at work during the last deglaciation and on the possibility of a threshold from which the land ice sheet would rather favour a northward expansion of the Hadley cell and non-linear shift in the position of tropical drying. Such processes could also be particularly relevant for warm stadials of Dansgaard-Oeschger events or even for the Bølling-Allerød. Paleoproxy records show that warm events over Greenland correspond to a northward shift of the ITCZ as recorded for example by the Cariaco basin sediments north to Venezuela (Peterson et al. 2000). To the extent that Cariaco records can be translated into Amazon convection variations, we suggest that this link could be related to the direct ice sheet impact on the atmosphere. Such an extra-tropical tropical link could work as an additional process to the usually incriminated impact of changes in overturning circulation (Rahmstorf 2002) on the trans-equatorial ITCZ shift. The land ice directly influences the atmospheric circulation in the mid-latitudes and tropics and because of the antagonist effects of its topography and albedo could lead to nonlinear atmospheric circulation responses when it collapses.

We also show that the overall tropical Pacific circulation response to land ice consists in a substantial thermo-dynamical stabilisation of the tropical atmosphere over the Amazon basin, resulting in reduced precipitation. The upper troposphere warming over tropical latitudes spreading out from the South East Central (SEC) Pacific, reminiscent of the one occurring during an El-Niño event, seems to be due to the albedo component alone. We conclude with a cautionary remark related to the realism of the simulated SST changes in the LGM simulations. We reasoned in terms of gradient in order to decipher the processes, evaluate the response of the zonaly-asymmetric Walker circulation and meridional tropical overturning associated with the Hadley cell. We have shown that even though the SST gradient across the Tropics and subtropical Pacific are reminiscent of those observed in MARGO data compilations, the comparison for the Atlantic Ocean is however inconsistent. Sensitivity experiments using an atmospheric only GCM directly forced by the MARGO SST for each season will help in evaluating the realism of processes evidenced here. We did not take into account the biosphere-atmosphere interactions but such interactions would probably have strong implications for the South American Monsoon response to glacial boundary conditions. For this reason biosphere-atmosphere interactions need to be considered in future work.

References

Absy ML, Cleef A, Fournier M, Martin L, Servant M, Sifeddine A, Ferreira da Silva M, Soubiès F, Suguio K, Turcq B, Van der Hammen T (1991) Mise en évidence de quatre phases d'ouverture de la forêt amazonienne dans le sud-est de l'Amazonie au cours des 60000 dernières années.

Premie‘re comparaison avec d’autres régions tropicales. Comptes Rendus de l’Academie des Sciences. Paris 312:673–678

Anhuf D, Ledru MP, Behling H, Da Cruz FW Jr, Cordeiro RC, Van der Hammen T, Karmann I, Marengo JA, De Oliveira PE, Pessenda L, Siffedine A, Albuquerque AL, Da Silva Dias PL (2006) Paleo-environmental change in Amazonian and African rainforest during the Last Glacial Maximum. Palaeogeogr Palaeoclimatol Palaeoecol 239:510–527

Arz HW, Pätzold J, Wefer G (1998) Correlated millennial-scale changes in surface hydrography and terrigenous sediment yield inferred from last-glacial marine deposits off northeastern Brazil. Quat Res 50:157–166

Baker PA, Seltzer GO, Fritz SC, Dunbar RB, Grove MJ, Tapia PM, Cross SL, Rowe HD, Broda JP (2001) The history of South American tropical precipitation for the past 25,000 years. Science 291:640–643

Behling H, Hooghiemstra H (1999) Environmental history of the Colombian savannas of the Llanos Orientales since the Last Glacial Maximum from lake records El Pinal and Carimagua. J Paleolimnol 21:461–476

Bush MB (2002) On the interpretation of fossil Poaceae pollen in the lowland humid neotropics. Palaeogeogr Palaeoclimatol Palaeoecol 177:5–17

Braconnot P, Otto-Bliesner BL, Harrison SP et al (2007) Results of PMIP2 coupled simulations of the mid-holocene and last glacial maximum—part 1: experiments and large-scale features. Clim Past 3:261–277

Broccoli AJ, Dahl KA, Stouffer RJ (2006) Response of the ITCZ to Northern Hemisphere cooling, Geophys Res Lett, DOI 10.1029/2005GL024546

Bush MB, De Oliveira PE, Colinvaux PA, Miller MC, Moreno JE (2004) Amazonian paleoecological histories: one hill, three watersheds. Palaeo 214:459–475

Chiang JCH, Sobel AH (2002) Tropical tropospheric temperature variations caused by ENSO and their influence on the remote tropical climate. J Clim 15:2616–2631

Chiang JCH, Biasutti M, Battisti DS (2003) Sensitivity of the Atlantic Intertropical Convergence Zone to Last Glacial Maximum boundary conditions. Paleoceanography. DOI 10.1029/2003PA000916

Chiang JCH, Bitz CM (2005) Influence of high latitude ice cover on the marine Intertropical Convergence Zone. Clim Dyn. doi: 10.1007/s00382-005-0040-5

Colinvaux PA, De Oliveira PE, Moreno JE, Miller MC, Bush MB (1996) A long pollen record from lowland Amazonia: forest and cooling in glacial times. Science 274:85–88

Colinvaux PA, De Oliveira PE (2001) Palaeoecology and climate of the Amazon basin during the last glacial cycle. J Quat Sci 15:347–356

Cruz FW, Burns SJ, Jercinovic M, Karmann I, Sharp WD, Vuille M (2007) Evidence of rainfall variations in southern Brazil from trace element ratios (Mg/Ca and Sr/Ca) in a Late Pleistocene stalagmite. Geochim Cosmochim Acta 71:2250–2263

Dallenbach A, Blunier T, Fluckiger J, Stauffer B, Chappellaz J, Raynaud D (2000) Changes in the atmospheric CH_4 gradient between Greenland and Antarctica during the last glacial and the transition to the holocene. Geophys Res Lett 27:1005–1008

Felzer B, Webb T, Oglesby RJ (1998) The impact of ice sheets, CO2, and orbital insolation on late quaternary climates: sensitivity experiments with a general circulation model. Quat Sci Rev 17:507–534

Flückiger J, Dallenbach A, Blunier T, Stauffer B, Stocker TF, Raynaud D, Barnola JM (1999) Variations in atmospheric N_2O concentration during abrupt climatic changes. Science 285: 227–230

Haberle SG, Maslin MA (1999) Late Quaternary vegetation and climate change in the Amazon basin based on a 50,000 year pollen record from the Amazon fan, ODP site 932. Quat Res 51:27–38

Hansen J, Lacis A, Rind D, Russell G, Stone P, Fung I, Ruedy R, Lerner J (1984) Climate sensitivity: analysis of feedback mechanisms. In: Hansen J, Takahashi T (eds) Climate processes and climate sensitivity. Geophys Mono 29, Am Geophys Union, Washington, DC, 130–163

Hewitt CD, Mitchell JF (1997) Radiative forcing and response of a GCM to ice age boundary conditions: cloud feedback and climate sensitivity. Clim Dyn 13:821–834

Kageyama M, Braconnot P, Grégoire L, Khodri M, Laîné A, Roche D (2009) Role of CO_2, land ice topography and albedo in the Last Glacial Maximum climate. In prep

Khodri M, Kageyama M, Ramstein G, Braconnot P, Turcq B (2009) Mechanism of climate change over South America during Last Glacial Maximum – Part 1: a multiple coupled ocean-atmosphere model study. Submitted to J Geophys Res

Kim SJ (2004) The effect of atmospheric CO2 and ice sheet topography on Last Glacial Maximum climate. Climate Dyn 22:639–651, doi: 10.1007/s00382-004-0412-2

Koutavas A, Lynch-Stieglitz J, Marchitto TM Jr, Sachs JP (2002) El Nin∼o-like pattern in ice age tropical Pacific sea surface temperature. Science 297:226–230

Koutavas A, Lynch-Stieglitz J (2003) Glacial-interglacial dynamics of the eastern equatorial–Pacific cold tongue–Intertropical Convergence Zone system reconstructed from oxygen isotope records. Paleoceanography 18. doi: 10.1029/2003PA000894

Koutavas A, Lynch-Stieglitz J (2004) Variability of the marine ITCZ over the Eastern Pacific during the past 30,000 years Regional perspective and global context. In: Diaz HF, Bradley RS (eds) The Hadley circulation: present, past, and future. Kluwer Academic Press, Dordrecht

Kubatzki C, Claussen M (1998) Simulation of the global bio-geophysical interactions during the Last Glacial Maximum. Clim Dyn 14:461–471

Lea DW, Pak DK, Peterson LC, Hughen KA (2003) Synchroneity of tropical and high-latitude Atlantic temperatures over the last glacial termination. Science 301 1362–1364

Laîné A, Kageyama M, Braconnot P, Alkama R (2009) Impact of greenhouse gas concentration changes on the surface energetics in the IPSL-CM4 model: regional warming patterns, land/sea warming ratio, glacial/interglacial differences accepted J Clim

Levis S, Foley JA, Pollard D (1999) CO_2, climate, and vegetation feedbacks at the Last Glacial Maximum. J Geophys Res 104:191–198

Leyden B (1985) Late Quaternary aridity and Holocene moisture fluctuations in the Lake Valencia Basin, Venezuela. Ecology 66:1279–1295

Manabe S, Broccoli AJ (1985) The influence of continental ice sheets on the climate of an ice age. J Geophys Res 90:2167–2190

Marti O, Braconnot P, Bellier J, Benshila R, Bony S, Brockmann P, Cadule P, Caubel A, Denvil S, Dufresne JL, Fairhead L, Filiberti MA, Foujols MA, Fichefet T, Friedlingstein P, Goosse H, Grandpeix JY, Hourdin F, Krinner G, Lévy C, Madec G, Musat I, deNoblet N, Polcher J, Talandier C (2005) The New IPSL Climate System Model: IPSL-Cm4, Note du Pôle de Modélisation, n 26, ISSN 1288-1619

MARGO Project Members (2009) Constraints on the magnitude and patterns of ocean cooling at the last glacial maximum. Nat Geosci. doi: 10.1038/NGEO0411

Mayle FE, Burbridge R, Killeen TJ (2000) Millennial-scale dynamics of southern Amazonian rainforest. Science 290:2291–2294

Monnin E, Indermuhle A, Dallenbach A, Fluckiger J, Stauffer B, Stocker TF, Raynaud D, Barnola JM (2001) Atmospheric CO2 concentrations over the last glacial termination. Science 291:112–114 947

Otto-Bliesner BL, Brady EC, Clauzet G, Tomas R, Levis S, Kothavala Z (2006a) Last glacial maximum and Holocene climate in CCSM3. J Clim 19:2526–2544

Otto-Bliesner BL, Schneider R, Brady EC, Kucera M, Abe-Ouchi A, Bard E, Braconnot P, Crucifix M, Hewitt C, Kageyama M, Marti O, Paul A, Rosell-Mele A,′ Waelbroeck C, Weber SL, Weinelt M, Yu Y (2009) A comparison of PMIP2 model simulations and the MARGO proxy reconstruction for tropical sea surface temperatures at last glacial maximum. Clim Dyn. doi: 10.1007/s00382-008-0509-0

Peterson LC, Haug GH, Hughen KA, Rohl U (2000) Rapid changes in the hydrologic cycle of the tropical Atlantic during the last glacial. Science 290:1947–1951

Peltier WR (2004) Global glacial isostasy and the surface of the ice-age Earth: the ICE–5G(VM2) model and GRACE. Annu Rev Earth Planet Sci 32:111–149

Rahmstorf S (2002) Ocean circulation and climate during the past 120,000 years. Nature 419: 207–214

Ramirez E, Hoffmann G, Taupin JD, Francou B, Ribstein P, Caillon N, Ferron FA, Landais A, Petit JR, Pouyaud B, Schotterer U, Simoes JC, Stievenard M (2003) A new Andean deep ice core from Nevado Illimani, (6350 m), Bolivia. Earth Planet Sci Letters 212: 337–350

Santos G, Cordeiro RC, Silva Filho EV, Turcq B, Fifield LK, Gomes PRS, Hausladen A, Sifeddine A (2001) Chronology of atmospheric mercury in Lagoa Da Pata basin, upper Rio Negro region of Brazilian Amazon. Radiocarbon 43(2):801–808

Servain J, Wainer I, McCreary JP Jr, Dessier A (1999) Relationship between the equatorial and meridional modes of climatic variability in the tropical Atlantic, Geophys Res Lett 26: 485–488

Siffeddine A, Martin L, Turcq B, Volkmer-Ribeiro C, Soubiès F, Campello Cordeiro R, Suguio K (2001) Variations of the Amazonian rainforest environment: a sedimentological record covering 30,000 years. Palaeogeogr Palaeoclimatol Palaeoecol 168:221–235

Stott L, Poulsen C, Lund S, Thunell R (2002) Super ENSO and global climate oscillations at millennial time scales. Science 297:222–226

Stott L, Cannariato KG, Thunell R, Haug GH, Koutavas A, Lund S (2004) Decline of surface temperature and salinity in the western tropical Pacific Ocean in the Holocene epoch. Nature 431:56–59

Su HS, Neelin JD (2002) Teleconnection mechanisms for tropical pacific descent anomalies during El Niño. J Atmos Sci 59:2694–2712

Thompson LG, Mosley-Thompson E, Davis ME, Lin PN, Henderson KA, Cole-Dai J, Bolzan JF, Liu K (1995) Late glacial stage and Holocene tropical ice core records from Huascarán, Peru. Science 269:46–50

Thompson LG, Davis ME, Mosley-Thompson E, Sowers TA, Henderson KA, Zagorodnov VS, Lin PN, Mikhalenko VN, Campen RK, Bolzan JF, Cole-Dai J, Francou B (1998) A 25,000-year tropical climate history from Bolivian ice cores. Science 282:1858–1864

van Geel B, van der Hammen T (1973) Upper Quaternary vegetational and climatic sequence of the Fuquene area (Eastern Cordillera, Colombia). Palaeogeogr Palaeoclimatol Palaeoecol 14:9–55

Van der Hammen T, Absy ML (1994) Amazonia during the last glacial. Palaeo 109: 247–261.

Vimeux F, Khodri M (2009) Mechanism of climate change over South America during Last Glacial Maximum – Part 2: New insights to interpret the glacial-interglacial isotopic variation in Andean ice cores. Submitted to J Geophys Res

Wallace JM, Rasmusson EM, Mitchell TP, Kousky VE, Sarachik ES, von Storch H (1998) On the structure and evolution of ENSO-related climate variability in the tropical Pacific: lessons from TOGA. J Geophys Res 103:14241–14260

Wang X, Auler AS, Edwards RL, Cheng H, Cristalli PS, Smart PL, Richards DA, Shen C-C (2004) Wet periods in northeastern Brazil over the past 210 kyr linked to distant climate anomalies. Nature 432:740–743

Wang X, Aluer AS, Edwards RL, Cheng H, I to E, Solheid M (2006) Interhemispheric anti-phasing of rainfall during the last glacial period. Quat Sci Rev 25:3391–3403

Wang X, Edwards RL, Auler AS, Cheng H, Ito E (2007) Millennial-Scale interhemispheric asymmetry of low-latitude precipitation: Speleothem evidence and possible high-latitude forcing. Geophys Monograph Series 173:279–293

Wyputta U, McAvaney BJ (2001) Influence of vegetation changes during the Last Glacial Maximum using the BMRC atmospheric general circulation model. Clim Dyn 17:923–932

Xie PP, Arkin PA (1997) Global precipitation: a 17-year monthly analysis based on gauge observations, satellite estimates, and numerical model outputs. Bull Am Meteorol Soc 78: 2539–2558

Xu KM, Emanuel KA (1989) Is the tropical atmosphere conditionally unstable? Mon Wea Rev 117:1471–1479

Chapter 10
Similarities and Discrepancies Between Andean Ice Cores Over the Last Deglaciation: Climate Implications

Françoise Vimeux

Abstract Andean ice cores extracted from high altitude glaciers have provided a wealth of original information dealing with past climate variability both in tropical and subtropical South America. In this chapter, we focus on the transition between the Last Glacial Maximum (LGM) and the Holocene period as recorded by the isotopic composition of the ice (oxygen 18, $\delta^{18}O$ or deuterium, δD) of three Andean ice cores spanning at least the last ~20,000 years (Sajama, 18°S; Illimani, 16°S; Huascarán, 9°S). We discuss the uncertainties of Andean ice cores dating and compare the three Andean records together and with the isotopic composition of Greenland and Antarctic ice cores (NorthGRIP, 75°N; EPICA Dome C, 75°S). We attribute the common glacial-interglacial isotopic composition increase ($\delta^{18}O$~4–6‰) recorded in Andean ice cores to the enhanced net precipitation lost by airmasses (~+5–7%) at LGM, from the moisture oceanic source to the Andean summits. We discuss the roles of precession and glacial boundary forcings that have been pointed out so far to explain wet conditions in the southern tropics of South America during glacial climate. We also spot that along the deglaciation, strong discrepancies exist between the Sajama ice core and the two other Andean ice cores. A Greenland-like deglacial progression can be observed at Sajama site with a rapid return to near-glacial conditions at around 14 ka, mimicking the Younger Dryas event, whereas an Antarctic-like deglaciation pattern can be identified both at Illimani and Huascarán sites bearing intriguing similarities to the Antarctic Cold Reversal. We discuss different hypotheses including local climate and Pacific influence to examine the possible causes of those discrepancies during the deglaciation.

Keywords Andean ice cores · Polar ice cores · Last Glacial Maximum · Deglaciation · Younger Dryas · Climate reversal · Marine ITCZ

F. Vimeux (✉)
Institut de Recherche pour le Développement (IRD), Laboratoire Hydrosciences Montpellier (HSM) and Laboratoire des Sciences du Climat et de l'Environnement (LSCE), CE Saclay, Orme des Merisiers, Bât. 701, 91191 Gif-sur-Yvette Cedex, France
e-mail: francoise.vimeux@lsce.ipsl.fr

F. Vimeux et al. (eds.), *Past Climate Variability in South America and Surrounding Regions*, Developments in Paleoenvironmental Research 14,
DOI 10.1007/978-90-481-2672-9_10,

10.1 Introduction and Motivations

The transition from the Last Glacial Maximum (hereafter LGM) to the present interglacial period (The Holocene) is the last major global climate change event. This transition is not dull and exhibits significant and abrupt changes that are differently expressed in terms of timing and shape depending on the hemisphere.

This time period is now well documented in high latitudes both in the Northern and Southern hemispheres from polar ice cores (Fig. 10.1). The Younger Dryas

Fig. 10.1 Map showing the different locations cited in the text except the North GRIP site: Cariaco basin (10°N); Huascarán (9°S); Illimani (16°S); Sajama (18°S); Salar de Uyuni (20°S); Santana Cave (24°S); Botuverá Cave (27°S); EPICA Dome C (75°S). The map in background was created using the Online Map Creation available at http://www.aquarius.geomar.de/omc/make_map.html

period (YD) is strongly expressed in Greenland ice cores as an abrupt return to near-glacial conditions in the North Atlantic region between 12.9 and 11.7 ka, occurring right after an abrupt warming at 14.7 ka (the Bølling-Allerød, hereafter BA) and ending gradually in 50 years with a warming leading to the Holocene period (Rasmussen 2006, Steffensen et al. 2008) (Fig. 10.2). In Antarctica, most records indicate a pause during the deglaciation without a return back to glacial conditions and a more complex picture than a basic antiphased behavior (Fig. 10.2). The timing of this event, defined as the Antarctic Cold Reversal (ACR) (Jouzel et al. 1995), has been disputed. Data from Taylor Dome ice core suggest that locally a YD-like pattern could be found (Steig et al. 1998). Synchronisation of Antarctic ice cores using dust records (Mulvaney et al. 2000) and north-south synchronisation of Greenland and Antarctic records, using gas data, suggest either a north-south see-saw with the BA warming as a trigger of the ACR cooling, and the YD cooling associated with the end of the ACR (Blunier et al. 1998) or a more complex picture (Morgan et al. 2001). The Antarctic warming during the YD peaks at around 11 ka (Blunier et al. 1998), forming a clear Holocene optimum that it is not recorded in Greenland records.

At mid-latitudes in the Southern Hemisphere, evidence for a distinct climate reversal during the late glacial period is more complex. Some climate records in New Zealand and Patagonia do not reveal any distinct climate reversal although there is clear evidence of prominent glacial readvances in both the Southern Alps of New Zealand (Denton and Hendy 1994, Ivy-Ochs et al. 1999), and in the Southern Andes (Wenzens 1999, Ackert et al. 2008).

The situation is intriguingly different in tropics and subtropics. In central and northern South America, observations show a consistent picture of enhanced glacial aridity between 5° and 10°N with deglacial steps highly similar to the BA-YD sequence. This is well observed in sea surface temperatures (hereafter, SST) in Cariaco basin (Hughen et al. 1996, Lea et al. 2003), and in palynological studies in Costa Rica and Columbia (Islebe et al. 1995, van der Hammen and Hooghiemstra 1995). Therefore, the climate in the northern tropics of Central and South America sustained cooling and aridification during LGM and fluctuated in step with the northern high latitudes during deglaciation. Further south, in the Amazon basin and the Nordeste, recent studies indicate increased river runoff and more humid conditions during LGM. Paleolakes level reconstructions show clear evidence for wet conditions in the Bolivian Altiplano during LGM (Baker et al. 2001a,b) and also spot major wet episodes occuring between 16.4 and 14.1 ka (Tauca phase) and between around 13 and 11 ka (Coipasa phase) (Placzek et al. 2006).

Therefore, those observations show that most of paleoclimate records in the northern or southern tropical South America exhibit complex deglacial patterns with isotopic or moisture reversals. As mentionned above, polar ice cores have shown that discrepancies and antiphase behavior exist during deglacial progression between high latitudes in both hemispheres. Thus, determining whether the Southern Hemisphere low latitudes follow a North Atlantic or an Antarctic signal remains key to deciphering climate mechanisms invloved in the glacial to interglacial climate change. To help answering this question, we examine in this chapter the isotopic

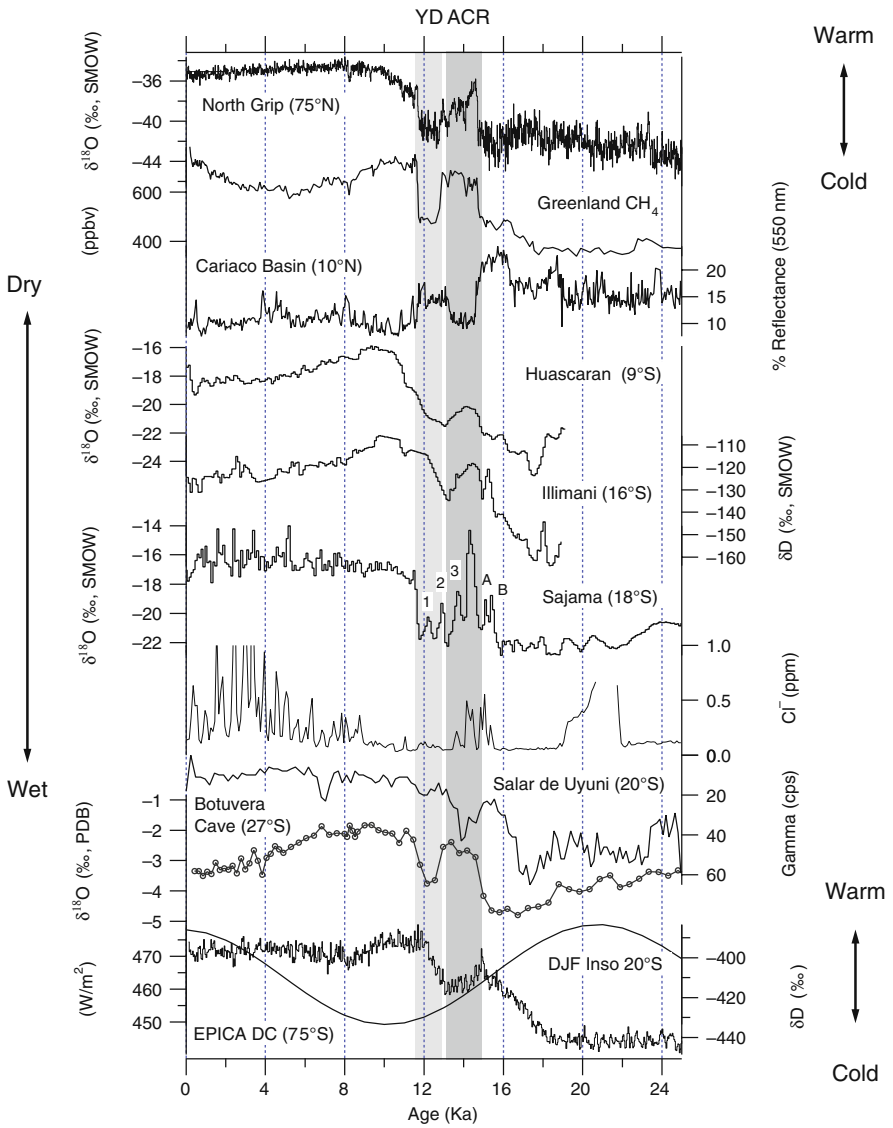

Fig. 10.2 Regional climate records over the last 25,000 years at different latitudes, from top to bottom: NorthGRIP $\delta^{18}O$ (‰, SMOW) (NorthGrip community members 2004); Greenland CH_4 composite (ppbv) (Blunier et al. 2007); Cariaco basin color reflectance 550 nm (Peterson et al. 2000); Huascarán ice $\delta^{18}O$ from core 2 (‰, SMOW) (Thompson et al. 1995); Illimani ice $\delta^{18}O$ (‰, SMOW) (Ramirez et al. 2003); Sajama ice $\delta^{18}O$ (‰, SMOW) (Thompson et al. 1998); Sajama chlorure concentration (ppm) (Thompson et al. 1998); Salar de Uyuni Gamma radiation (c.p.s) (Fritz et al. 2004); Botuverá Cave Bt2 $\delta^{18}O$ (‰, PDB) (Cruz et al. 2005) ; DJF Insolation at 20°S; EPICA Dome C δD (‰, SMOW) (EPICA community members 2004). Each climate records is shown with its timescale as described in the text and references. The ACR and YD bars are defined with the NorthGRIP $\delta^{18}O$ and EPICA Dome C δD respectively

composition of three Andean ice cores spanning the last deglaciation and extracted from (1) Huascarán glacier (9°06'S, 77°36'W, 6048 m) in 1993 where two ice cores reached bedrock at 160.4 m and 166.1 m respectively, reaching back into the Late Glacial Stage (Thompson et al. 1995); (2) the saddle on Illimani (16°37'S, 67°46'W, 6300 m) in June 1999 where two 135 m-long cores cover the whole glacier thickness and contain the climate history of the last 18,000 years (Knüsel et al. 2003, Ramirez et al. 2003) and (3) the ice cap on the highest summit of Bolivia, Sajama (18°06'S, 68°53'W, 6542 m), in June 1997 where the last 25,000 years are recorded in the 132 m-long ice core (Thompson et al. 1998) (Fig. 10.1). We discuss both the LGM to Holocene transition and the intriguing resemblance with polar ice cores (EPICA Dome C, EDC, in Antarctica, EPICA community members 2004 and NorthGRIP in Greenland, NorthGRIP-community members 2004). The choice of those two polar records stands in their high temporal resolution and updated dating.

The goal of this chapter is not to propose new climate mechanisms arising from the comparison of tropical and polar ice cores. Actually, we aim at pointing out the intriguing similarities and discrepancies between ice cores, at listing the limit of such a comparison due to the dating uncertainties of tropical ice cores and at showing that climate mechanisms that have been discussed so far are able to explain a large part of our observations but remain poorly satisfactory to decipher the Pacific from the Atlantic influences on tropical South America climate (see also, Khodri et al., Chapter 9 of this volume).

10.2 Isotopic Composition of Andean Ice Cores: A Common LGM to Holocene Signal, Some Discrepancies Along the Deglaciation

10.2.1 An Important Caveat About Andean Ice Cores Dating

The last deglaciation can be examined with a robust age control in polar regions: they can be synchronised either regionally using aerosol tracers (dust and calcium that are proxies of continental aerosols, or sulphate from volcanism) (Mulvaney et al. 2000) or globally using well-mixed atmospheric gas records (such as CH_4or $\delta^{18}O$ of O_2, hereafter $\delta^{18}O_{atm}$) (Blunier et al. 1998, Loulergue et al. 2008). The error bars on timescale over the last deglaciation vary between 100 and 200 years at NorthGRIP (NorthGRIP community members 2004) and are about 500 years at 15 ka and, at the most, 1000 years at 21 ka at EDC (EPICA community members 2004). The dating of Andean ice cores is much more complex for this time period. Indeed, due to the high accumulation rates in Andean ice cores, the climate variations of the last 1000 years constitute the major part of the ice core (this time period is roughly contained in the upper 115 m and 70 m at Illimani and Sajama, respectively) and between 10,000 and 15,000 years of climate history are compressed in the last few meters of the cores. Consequently, if the dating is relatively accurate at

the surface (about ±2 years over the last decades) and can be estimated downcore to roughly ± 10 years around 100 years BP (Knüsel et al. 2003, comparison of two parallel cores on Illimani), the loss of annual resolution after a few centuries makes it unsuitable to attain an accurate dating for the last deglaciation and errors can attain more than 500 years. We very briefly describe below how the three Andean ice cores spanning the last transition have been dated:

(1) The Sajama record has been dated using different approaches (Thompson et al. 1998 and information extracted from the Data description file available on the National Climatic Data Center web site: http://www.ncdc.noaa.gov/paleo/pubs/thompson1998/sajama.html): (i) annual layer counting for the upper part of the core (the last 100 years), (ii) identification of a ash horizon at around 65 m (Huaynaputina 1600 A.D.), (iii) ten ^{14}C-AMS measurements between around 25 and 131 m on plant material and insect fragments, including two in the deepest part dated at around 24 ka (iv) measurements of $\delta^{18}O_{atm}$ between 56 and 130 m and comparison with the GISP 2 $\delta^{18}O_{atm}$ record, and (v) the use of a age-depth model applied to the full core and accounting for the previous target ages.

(2) The Huascarán record (ice core 2) has also been dated with a combination of different approaches (Thompson et al. 1995 and information extracted from the Age Scale description file available on the National Climatic Data Center web site: http://www.ncdc.noaa.gov/paleo/pubs/thompson1995/huascaran.html): (i) annual layer counting for the upper part (back to 1720 BP), (ii) a cross-correlation with the inverted CaCo3-oxygen isotope record from marine core SU81–18 off Portugal (Bard et al. 1987), (iii) the prominent fall of the isotopic composition of the ice at around 164 m, assumed to be correlated with the Younger Dryas Period and dated at the lowest isotopic value at 12.3–12.4 ka, (iv) $\delta^{18}O_{atm}$ measurements in air bubbles over the 7–15 ka period, and (v) a age-depth model assuming a layer thinning with depth estimated by a two-parameter function and accounting for the target dates.

(3) The Illimani ice core has also been dated with a combination of approaches (Hoffmann et al. 2003, Ramirez et al. 2003): (i) multi-proxy seasonal counting on isotopic and chemical data down to around 80 m, (ii) measurements of $\delta^{18}O_{atm}$ between 131 and 136 m (the last 5 m) showing values ranging from $-0.2‰$ and $+0.8‰$ and thus suggesting an age of about 18 ka for the bottom of the core by comparison with the Vostok $\delta^{18}O_{atm}$ record (Malaizé et al. 1999), (iii) the overall similarity between the Huascarán and Illimani records: sixteen tie points have been selected along the Huascarán profile, only based on the similar shape of the isotopic composition of the ice, with eight points chosen below 133 m, and (iv) a depth-age relationship established using four exponential spline functions and respecting the estimated dating uncertainties of the target points (± 2 years at the surface and ± 200 years at the bottom).

In conclusion, the dating of Andean ice cores is poorly constrained in the deepest part of the cores because of lack of layer counting and numerous absolute age markers. Therefore, the timing of events occuring along the deglaciation remains poorly constrained and has to be taken into account when comparing Andean ice

cores to other paleoclimate reconstructions. However, $\delta^{18}O_{atm}$ and ^{14}C-AMS measurements are robust indications of glacial age for the deepest ice. Therefore, we can reliably discuss both the amplitude and shape of the glacial-interglacial isotopic transition.

10.2.2 The Glacial-Interglacial Transition as Recorded in the Isotopic Composition of Andean Ice Cores

The isotopic composition of Andean ice cores (hereafter, δ_{Andean}) clearly exhibits a common glacial-interglacial shift with lowest values around the LGM and a $\delta^{18}O$ increase from the LGM to the Holocene of 4.6‰, 5.7‰ and 6.1‰ at Illimani, Huascarán and Sajama respectively (the LGM value is calculated over a 1000 year-interval centered around the lowest isotopic value (18.75 ka at Sajama, 17.50 ka at Huascarán, 18.30 ka at Illimani); the Holocene value is calculated over the last 2000 years to reduce the influence of recent trend) (Thompson et al. 1995, 1998, Vimeux et al. in prep.) (Fig. 10.2). No relationship between those three isotopic variations and the drilling sites altitude can be found. It is worth noting that we discuss in this chapter those raw isotopic variations whereas a correction accounting for the change in marine isotopic composition at LGM should be needed. Actually, if this correction can be easily estimated for polar ice cores because roughly related to the degree of airmasses isotopic distillation, the situation in the tropics in much more complex due to the convective precipitation, the intense water vapor recycling and the difficulty to reproduce modern isotopic observations in the Andes with a simple Rayleigh distillation.

Recent studies have focused on exploring the different climate controls on δ_{Andean} using modelling studies, including water stable isotope fractionations (Vuille and Werner 2005, Vuille et al. 2007a,b, Risi et al. 2008) or based on direct modern observations (Hardy et al. 2003, Vimeux et al. 2005, Villacís et al. 2008). These studies conclude that the isotopic composition of Andean precipitation is mainly controlled by local precipitation and rainout upstream (in the Amazon basin and the tropical Atlantic Ocean) at the seasonal and inter-annual timescales. Further, they discuss the possible origin of the precipitation anomalies and so the original, but indirect, cause of the isotopic variability. Part of the precipitation variability originates from a change in location and intensity of the ascending convective branch of the Hadley-Walker cell over tropical South America, affecting the South American Summer monsoon variability. The Hadley-Walker cell motion is perturbed by Pacific SST anomalies and hence by El Niño-Southern Oscillation (Bradley et al. 2003, Vuille et al. 2003a,b, Vuille and Werner 2005, Sturm et al. 2007b). However, Atlantic SST variations also have a large impact on the South American Monsoon. It remains therefore a challenge to separate the Atlantic from the Pacific SST impact when interpreting the isotopic composition of Andean ice. Therefore, we limit here our interpretation of δ_{Andean} in terms of past precipitation variations. Based on modern $\delta^{18}O/P$ calibration in the high altitude Andean region (-0.0575‰ per mm.year^{-1})

(Vimeux et al. 2005) and on an annual precipitation amount of 1500 mm.year^{-1} over the Amazon basin, our observations suggest that the net precipitation changes is higher by about 5−7% at LGM compare with present day. This result is qualitatively in agreement with other paleoclimate reconstructions in the tropical Andes, converging toward wetter conditions at LGM (see also Sylvestre, Chapter 1 of this volume): lower Lake Titicaca level from 24.7 to 21.2 ka (Ybert 1992, Wirrmann et al. 1992, Baker et al. 2001a); presence of lakes in the Coipasa and Uyuni salars between 24.6 and 20.9 ka and 26.1 and 14.9 ka respectively (Sylvestre et al. 1998, Sylvestre 2002, Baker et al. 2001b). Humid conditions during LGM are also indicated in subtropics, along the Atlantic margin (Amazon Fan, Nordeste) (Sylvestre, Chapter 1 of this volume). For example, speleothems extracted in Botuverá (27°S) and Santana (24°S) caves show low $\delta^{18}O$ during LGM that are interpreted as stronger monsoon circulation (Cruz et al., Chapter 2 of this volume). However, past humidity conditions remain unclear in tropical lowlands where an arid corridor is observed from Lake Caço to the lowlands of Bolivia (Sylvestre, Chapter 1 of this volume). This is not in contradiction with our interpretation of Andean ice cores. Actually, δ_{Andean} is an integrated information of all isotopic fractionation that have affected airmasses along their pathway, sustaining a possible mosaic of wetter and dryer continental areas between the Nordeste and the Andes through the Amazon basin. Thus, the δ_{Andean} basically shows the net balance of precipitation change from the moisture source (the tropical Atlantic Ocean) to the Andes via the Amazon basin. Quantitatively, an ongoing study using the coupled climate model HadCm3 confirms a <10% LGM precipitation increase over the Atlantic margin (Nordeste and tropical Atlantic Ocean), overflew by airmasses during the rainy season (Vimeux and Khodri in prep.).

Lastly, it is worth noting that the glacial-interglacial oxygen 18 change recorded in Andean ice cores (4−6‰) is lower but comparable with polar oxygen 18 shift recorded in Greenland (around 8.4‰ at NorthGRIP) or in Antarctica (around 5.3‰ at EDC) (glacial-interglacial polar isotopic shifts are calculated in the same way than Andean ones). This observation has led to a first interpretation of Andean ice cores in terms of local temperature as for polar ice cores (Thompson et al. 1995, 1998). Regardless our knowledge on the climate controls of the isotopic composition of tropical precipitation (see above), it makes no sense to directly compare the raw polar and Andean isotopic shifts because 1- it does not account for the necessary corrections of past marine isotopic composition and moisture source changes and 2- the isotopic composition reflects all the phase changes that have affected the airmasses histories at one given place. For example, we now know that the glacial-interglacial isotopic shift in Greenland includes the effects of a change in precipitation seasonality (Masson-Delmotte et al. 2005). Concerning the role of temperature in the glacial-interglacial isotopic changes, it is now well known that the major part of the polar shift is due to the lower condensation temperature in polar regions during LGM (Jouzel et al. 2003). Concerning tropical regions, Vimeux and Khodri (in prep.) estimate the condensation temperature change at LGM in tropical South America and over the tropical Atlantic Ocean based on basic thermodynamic considerations (the condensation is allowed between the lifting condensation level

and the level of neutral buoyancy). At each level, the condensation temperature is weighted by the amount of condensate water and the mean concensation temperature is obtained by a vertical integration. They show that condensation temperatures were uniformly lower during LGM by about −2 to −4°C from the oceanic moisture source to the Andes, that is unable to explain an isotopic shift of 4–6‰ with our current knowledge of water stable isotopic fractionation (changes in lapse rate are also unable to explain this change, see Vimeux et al. 2005). Obviously, to further investigate the effect of a global cooling on the isotopic composition of tropical precipitation, we will need to examine LGM climate simulations including water stable isotopes and a possible zoom on specific regions.

We discuss in Section 10.3 climate mechanisms that have been pointed out to sustain an increase of moisture in tropical South America in a colder climate. In the next section, we focus on the deglacial progression.

10.2.3 Deglaciation as Recorded in Andean Ice Cores: Deciphering the Greenland and Antarctic Aspects?

We discuss in the previous section the common glacial-interglacial isotopic shift in Andean ice cores. The similarities between Illimani and Huascarán records extend even to the details of the deglaciation history whereas the Sajama record is somewhat different. In this section, we discuss in details the deglacial steps as recorded in those ice cores.

First, on the oriental Cordillera, both the Huascarán and the Illimani isotopic records exhibit a similar deglacial progression both in terms of amplitude and variations. An isotopic minimum is observed at the bottom of both ice cores, dated at 17 and 18 ka respectively, and therefore rather late compare with a "classical" LGM dated at 21 ka. However, as those records do not cover older periods, it is impossible to assert that this is the local isotopic minimum. Then, the isotopic composition increases until an ACR-like interval that can be distinguished between 14.5 and 13 ka in both ice cores, with a comparable $\delta^{18}O$ decrease of about −1.5‰ (Thompson et al. 1995, Vimeux et al. in prep.) (Fig. 10.2). It is worth noting that the local isotopic maximum attained at around 14.5 ka is closer to the $\delta^{18}O$ Holocene level at Illimani than at Huascarán (see Fig. 10.2). The ACR-like interval lag, relatively to the EDC ACR, remains within the 500 years dating uncertainties and thus cannot be discussed (Fig. 10.2). Regardless, at ∼13 ka, the isotopic composition starts increasing simultaneously in EDC and oriental Cordillera ice cores. Whereas the isotopic composition at EDC increases over the YD period and attains a maximum at around 11.5 ka, both Illimani and Huascarán isotopic composition attain a later optimum between 9.5 and 10 ka. The synchronism of this Andean Holocene optimum cannot be discussed as the Huascarán dating was used to construct the age-depth Illimani relationship at that time period (Ramirez et al. 2003). Thus, it is clear that both Illimani and Huascarán isotopic composition mimic the different steps observed in Antarctica along the deglaciation.

In Sajama ice core, located on the occidental Cordillera, the deglacial isotopic variations differ from what it is observed on the oriental Cordillera. This longer record, spanning the last 25,000 years, shows a rather constant isotopic composition from 25 to 15.9 ka whereas both Illimani and Huascarán records show a deglaciation pattern at that time. Then, we can observe an abrupt isotopic increase, attaining a maximum at around 14.3 ka with an isotopic level higher than during the Holocene, followed by a return to LGM conditions (7.9‰ $\delta^{18}O$ drop), mimicking the Greenland BA-YD sequence (Fig. 10.2). It is worth noting that similarly to the NorthGRIP isotopic record, a final abrupt increase of $\delta^{18}O$ at about 11.7 ka leads to the Holocene period with no marked optimum.

Regardless a different general deglacial progression, Illimani and Sajama records show a first $\delta^{18}O$ reversal, leading by about 1000 years the ACR-like and YD-like reversal respectively. At Sajama, this first reversal is actually a double peak (A and B on Fig. 10.2) and corresponds to a 2.2‰-$\delta^{18}O$ fall to be compared with a 7.9‰-$\delta^{18}O$ fall during the YD-like reversal. At Illimani, both isotopic falls have the same amplitude of about 1.5‰. This first isotopic drop could also be seen in Huascarán record but the amplitude is only of about 0.3‰, maybe caused by the isotopic smoothing at that depth. While chemical records are not available for the Illimani ice core, those from Sajama also exhibit this double peak between around 15.8 and 15 ka in chemical concentrations (SO_4^{2-}, Cl^-, NO_3^{2-}) (Fig. 10.2) and in dust profile (Thompson et al. 1998). In addition, in Sajama, three successive isotopic oscillations occur between 14 and 11.7 ka (1, 2 and 3 on Fig. 10.2) that are not recorded in other ice cores. Although the poor dating of the Sajama record, one could see some correlations between those three small isotopic variations and both CH_4 concentration and the NorthGRIP isotopic record (Fig. 10.2).

In summary, the main conclusions arising from Sections 10.2.2 and 10.2.3 are: (1) the common LGM to Holocene isotopic composition shift in Andean ice cores suggests that moister conditions occured at LGM in the Andes and/or upstream, along airmasses trajectories; and (2) the three Andean ice cores show a clear climate reversal along the deglaciation, however the latter is differently expressed depending on the location: Illimani and Huascarán isotopic records exhibit a smooth climate reversal whereas the Sajama ice core shows a BA-YD-like sequence and thus an intriguing resemblance with a North Atlantic signal.

10.3 Discussion in Terms of Global Climate Mechanisms and Local Climate Influences

We first remind the different forcings that can explain the wet conditions in the southern tropics of South America during LGM. We also discuss possible causes for 1- such a reversal climate in the low latitudes during the deglacial progression and 2- such differences between the Sajama record and the two other Andean ice cores.

10.3.1 Influence of Insolation on LGM Precipitation

The net higher precipitation during LGM in tropical southern South America suggested by δ_{Andean} could partly arise from an increase in the strength of the South American Summer Monsoon as a consequence of the austral summer (DJF) insolation maximum 20,000 years ago (mainly controlled by precession) (Fig. 10.2). As explained in Clement et al. (2004), the continent has a larger thermodynamic response to precessional forcing than the ocean, enhancing the land-sea temperature gradient. During LGM, as a response of the insolation maximum, a geographical shift of precipitation from ocean to land is induced by a windstress process. It is nonetheless important to remind that the DJF insolation during LGM is similar to the present DJF insolation and therefore the unique precessional forcing is not able to explain higher precipitation rate during LGM. The glacial forcings have also to be considered and are developped in the next section.

10.3.2 A Mechanism for Wet Southern Tropics and Cold Northern High Latitudes During LGM

Chiang et al. (2003) and Chiang and Bitz (2005) suggest that the glacial boundary conditions could explain part of intense rainfall in the southern tropical South America. According to their study, the huge ice sheet in the high latitudes of the Northern Hemisphere could induce a southward shift of marine ITCZ over the Atlantic Ocean. They show that the marine ITCZ shifts away from the Northern Hemisphere, altering the Hadley circulation with an increased tropical subsidence in the Northern Hemisphere and uplift in the other. They propose the followings steps: the additional ice induces a cooling and drying in the northern high and mid latitudes leading to an anomalous north-south SST gradient that strenghtens windstress and thus a progression of SST cooling towards low latitudes. The cooling in the Northern Hemisphere leads to modify the Hadley cell (increase of subsidence over the Northern Atlantic Ocean and of ascendance over the Southen Atlantic Ocean) and therefore it results in a southward ITCZ shift, favoring additional humidity in the tropical Southern Hemisphere.

Clement et al. (2004) show that both precessional and glacial forcings have a similar importance on the tropical hydrological cycle and are able to account for precipitation changes. However, both previous mechanisms do not involve any shift of the Pacific ITCZ. Indeed, Koutavas and Lynch-Stieglitz (2004) clearly interpret $\delta^{18}O$ and Mg/Ca SST data from eastern equatorial Pacific as a southward migration of the eastern Pacific ITCZ. Such a shift is accompanied by changes in SST structure, affecting the Hadley-Walker circulation and therefore the convective zones in tropical South America. Those Pacific-Atlantic tropical teleconnections and their consequences on tropical South American precipitation are specifically discuss in Khodri et al., Chapter 9 (this volume).

10.3.3 Is a Climate Reversal Expected in the Isotopic Composition of Andean Ice Cores?

The presence of a climate reversal in southern tropics and subtropics during the deglaciation is not intriguing and, as mentionned in the introduction, the most unclear observation is the lack of this reversal in southern mid-latitudes. Indeed, modelling studies proposed that during the Younger Dryas, meltwater input into North Atlantic would lead to a collapse of the thermohaline circulation and thus a southward shift of ITCZ position (Vellinga and Wood 2002, Lea et al. 2003). Such a change, associated to the South American Monsoon system variations at that time, will influence both precipitation rate and convective zones position and thus the isotopic composition of Andean ice cores. Moreover, Leduc et al. (2007) point out that, at millennial timescale, a southerly ITCZ position influences the moisture transport across Central America and acts as an important positive feedback. Thus, we should expect to see a North Atlantic signature during deglaciation in paleoclimate reconstructions of tropical or subtropical rainfall as shown in the Sajama ice core.

However, the isotopic composition of Illimani and Huascarán ice cores do not exhibit any abrupt climate reversal responding in kind with North Atlantic. This is also what we can observe for most of other continental rainfall reconstructions in the Andes or in tropical and subtropical South America offering a sufficient temporal resolution at that time. For example, past moisture reconstructions from Salar de Uyuni (20°S) (Baker et al. 2001b, Fritz et al. 2004) or Botuverá cave (27°S) (Cruz et al. 2005) sites show a smooth climate reversal as in the oriental Cordillera sites (Fig. 10.2), pointing out the peculiar case of the Sajama record. Moreover, the amplitude of the reversal is quite different at Sajama and in the two other ice cores. According to Illimani and Huascarán 1.5‰ reversal, precipitation change should be less than a few percent along airmasses trajectory, assuming an Atlantic moisture source (Vimeux et al. 2005, Vimeux and Khodri in prep.). A similar interpretation of the Sajama 7.9‰ drop (i.e. in terms of regional precipitation with an Atlantic moisture source) would lead to a much more important precipitation rate change.

In the next section, we discuss the potential hypotheses to explain the Sajama case.

10.3.4 The Specificity of Sajama: Local Conditions and/or Pacific Influence?

Different hypotheses based on specific local climate conditions have been pointed out to explain the isotopic record at Sajama. First, the deglaciation progression on the Altiplano was accompanied by large paleolakes appareance/disapearance known as the Tauca and Coipasa events and sustaining a return to wetter conditions. Based on Sajama timescale, we can note that the isotopic composition of the ice starts increasing at 15.9 ka, simulteaneously with dust (Thompson et al. 1998), and around 400 years before the anions concentrations (Cl^-, SO_4^{2-}) (Fig. 10.2). This could be

related to a progressive dryness and a reduction of precipitation. The abrupt $\delta^{18}O$ decrease at 14.3 ka could be concomitant with the Tauca phase although the latter is dated between 16.4 and 14.1 ka (Placzek et al. 2006). In addition, the successive isotopic and chemical oscillations at Sajama between 15.8 and 11.7 ka, missing at both Huascarán and Illimani, could also be related to small paleolake level fluctuations. Indeed, the Sajama site is located eastward, upstream of the paleolakes, and thus might have been more imprinted by precipitation changes overall affecting the Altiplano than Illimani and Huascarán sites. Based on an isotopic gradient of $-0.0575‰$ per mm.year^{-1} for oxygen 18 (Vimeux et al. 2005), and on an annual precipitation amount of 400 mm.year^{-1} in the southern Altiplano basin (17–22°S; 66–77°W) (T. Condom 2002), the 7.9‰ drop at 14.3 ka at Sajama translates into a precipitation increase of about 140 mm.year^{-1} (i.e. one-third more). This interpretation is consistent with hydrological modelling studies showing that 1- paleolakes could appear within a few centuries, suggesting a possible abrupt reorganization of the hydrological cycle on the Altiplano (T. Condom 2002) and 2- the Tauca phase lake level requires an annual mean precipitation of about 700 mm.year^{-1} (assuming colder conditions than nowadays through a lower lake evaporation) (Coudrain et al. 2002). Our estimate, although lower, also confirms the recent results obtained by Blard et al. (2008) showing that the Tauca phase lake is accompanied by an increase of precipitation of about three to four-fold. Of course, in the latter hydrological modelling studies, changes in temperature, lake evaporation and tributaries flow were not fully constrained.

Of course, the local hypotheses mostly exclude any reasons for a Greenland-like shape at Sajama versus an Antartic-like shape at Illimani and Huascarán. We cannot exclude that under different climates, Sajama might also have undergone a stronger Pacific inluence than the two other ice cores. Lake developments during the Tauca phase would correspond with intense and persistent La Nina conditions in central Pacific that could strongly modify moisture supply and moisture source of precipitation on the occidental Cordillera.

10.4 Conclusions

The comparison of the isotopic composition of the three Andean ice cores shows a clear δ_{Andean} increase from the LGM to the Holocene. Based on the modern isotope/climate calibration, this common signal is interpreted as higher net precipitation balance during LGM, upstream the Andes, by about 5–7%. Both glacial boundary conditions and precession forcings are able to explain such a change in precipitation over the tropical Atlantic Ocean and the continental Atlantic margin.

We show that the glacial-interglacial transition exhibits intriguing magnitude and shape resemblance with the polar isotopic glacial-interglacial change although water stable isotopes have a different interpretation at low and high latitudes (precipitation versus temperature). However three effects are still not discussed:

(1) How can tropical SST changes in Pacific and Atlantic have influenced the precipitation regime over tropical South America during LGM? Specifically, we need

to decipher the different causes of precipitation variability. To examine this question for past period and to discuss the stability of teleconnections between Pacific and Atlantic Oceans between LGM and nowadays we need to use past climate simulations using coupled ocean-atmosphere models as it is initiated by Khodri et al., Chapter 9 (this volume).

(2) How is the mean isotopic composition of tropical precipitation affected in a colder climate? Actually, we do not investigate here the effects of a global cooling on the isotopic composition of global precipitation. For this purpose, we need to examine past climate simulations using coupled ocean-atmosphere models equipped with a water stable isotopes module.

(3) At last, we would need more precipitation and temperature archives with an accurate dating in the Andes and upstream to support our interpretation and to further discuss the impacts of the potential climate mechanisms discussed in Section 10.3.

Andean ice cores also show a common deglacial progression with a clear return to near-glacial conditions at around 14 ka. However, the structure of this reversal is quite different at Sajama and in the two other ice cores: although the isotopic composition of the Sajama ice core bears all the marks of a North Atlantic deglacial structure, the Huascarán and Illimani isotopic records are much more comparable both in shape and in amplitude to Antarctic records. The reasons for such discrepancies remain unclear. Indeed, local climate specificities (paleolakes formation, Pacific moisture source more or less active) have been pointed out to explain the Sajama uniqueness although, according to mechanisms pointing out during the YD, the Sajama record is not surprising. Again, additional precipitation archives on the Altiplano (and especially on the Pacific margin and on the occidental Cordillera) with a high temporal resolution will help us to refine our interpretation.

Finally, as a perspective, past climate simulations including water stable isotopes and focusing on tropical South America could help answering part of our questions, especially regarding the importance of the teleconnection mechanisms between both Atlantic and Pacific Oceans.

Acknowledgments I deeply thank Valérie Masson-Delmotte for her fruitful inputs and suggestions as well as Georg Hoffmann for discussions about Andean ice cores discrepancies. Figure 10.1 was created using the Online Map Creation available at http://www.aquarius.geomar.de/omc/make_map.html

References

Ackert RP, Becker RA, Singer BS (2008) Patagonian glacier response during the late glacial-holocene transition. Science 321:392–395

Baker PA, Seltzer GO, Fritz SC (2001a) The history of South American tropical precipitation for the past 25,000 years. Science 291:640–643

Baker PA, Rigsby CA, Seltzer GO et al (2001b) Tropical climate changes at millennial and orbital timescales on the Bolivian Altiplano. Nature 409:698–700

Bard E, Arnold M, Maurice P et al (1987) Retreat velocity of the North Atlantic polar front during the last deglaciation determined by ^{14}C accelerator mass spectrometry. Nature 328: 791–794

Blard PH, Lave J, Farley KA et al (2008) Late glacial paleoclimate of the central Altiplano constrained by cosmogenic He-3 dating and 'clumped-isotope' paleothermometry. Geochimica et Cosmochimica Acta 72:A89

Blunier T, Chappellaz J, Schwander J et al (1998) Asynchrony of Antarctic and Greenland climate change during the last glacial period. Nature 394:739–743

Blunier T, Spahni R, Barnola JM et al (2007) Synchronization of ice core records via atmospheric gases. Clim Past 3:325–330

Bradley RS, Vuille M, Hardy D, Thompson LG (2003) Low latitude ice cores record Pacific sea surface temperatures. Geophys Res Lett 30(4):1174, doi:10.1029/2002GL016546

Chiang JCH, Biasutti M, Battisti DS (2003) Sensitivity of the Atlantic Intertropical Convergence Zone to Last Glacial Maximum boundary conditions. Paleoceanography 18:doi:10.1029/2003PA000916

Chiang JCH, Bitz CM (2005) Influence of high latitude ice cover on the marine Intertropical Convergence Zone. Clim Dyn 25:477–496

Clement AC, Hall A, Broccoli AJ (2004) The importance of precessional signals in the tropical climate. Clim Dyn 22:327–341

Condom T (2002) Dynamiques d'extension lacustre et glaciaire associées aux modifications du climat dans les Andes Centrales, PhD thesis, Université Paris 6

Coudrain A, Loubet M, Condom T et al (2002) Données isotopiques (87Sr/86Sr) et changements hydrologiques depuis 15 000 ans sur l'Altiplano andin. Hydrol Sci 47(2):258–271

Cruz FW, Burns SJ, Karmann I et al (2005) Insolation-driven changes in atmospheric circulation over the past 116,000 years in subtropical Brazil. Nature 434:63–66

Denton GH, Hendy CH (1994) Younger Dryas Age Advance of Franz Josef Glacier in the Southern Alps of New Zealand. Science 264:1434–1437

EPICA community members (2004) Eight glacial cycles from an Antarctic ice core. Nature 429:623–628

Fritz SC, Baker PA, Lowenstein T et al (2004) Hydrologic variation during the last 170,000 years in the southern hemisphere tropics of South America. Quat Res 61:95–104

Hardy DR, Vuille M, Bradley RS (2003) Variability of snow accumulation and isotopic composition on Nevado Sajama, Bolivia. J Geophys Res 108(D22):doi:10.1029/2003JD003623

Hoffmann G, Ramirez E, Taupin JD et al (2003) Coherent isotope history of Andean ice cores over the last century. Geophys Res Lett 30(4):1179, doi:10.1029/2002GL014870

Hughen KA, Overpeck JT, Peterson LC, Trumbore S (1996) Rapid climate changes in the tropical Atlantic region during deglaciation. Nature 380:51–54

Islebe GA, Hooghiemstra H, van der Borg K (1995) A cooling event during the Younger Dryas Chron in Costa Rica. Paleogeogr Paleoclimatol Paleoecol 117:73–80

Ivy-Ochs S, Schlüchter C, Kubik PW, Denton GH (1999) Moraine exposure dates imply synchronous Younger Dryas glacier advance in the European Alps and in the Southern Alps of New Zealand. Geogr Ann 81A:313–323

Jouzel J, Vaikmae R, Petit JR et al (1995) The two-step shape and timing of the last glacial deglaciation in Antarctica. Clim Dyn 11:151–161

Jouzel J, Vimeux F, Caillon N et al (2003) Magnitude of isotope/temperature scaling for interpretation of central Antarctic ice cores. J Geophys Res 108:doi:10.1029/2002JD002677

Knüsel S, Ginot P, Schotterer U et al (2003) Dating of two nearby ice cores from the Illimani, Bolivia. J Geophys Res 108:doi:10.1029/2001JD002028

Koutavas A, Lynch-Stieglitz J (2004) Variability of the marine ITCZ over the eastern Pacific during the past 30,000 years. In: Diaz HF, Bradley RS (eds) The Hadley circulation: Present, past and future. Springer-Kluwer Academic Press, Netherlands

Lea DW, Pak DK, Peterson LC, Hughen KA (2003) Synchroneity of tropical and high latitude Atlantic temperatures over the last glacial termination. Science 301:1362–1364

Leduc G, Vidal L, Tachikawa K et al (2007) Moisture transport across Central America as a positive feedback on abrupt climatic changes. Nature 445:908–911

Loulergue L, Schilt A, Spahni R et al (2008) Orbital and millennial-scale features of atmospheric CH4 over the past 800,000 years. Nature 453:383–386

Malaizé B, Paillard D, Jouzel J, Raynaud D (1999) The Dole effect over the last two glacial-interglacial cycles. J Geophy Res 104:14199–14208

Masson-Delmotte V, Jouzel J, Landais A (2005) GRIP deuterium excess reveals rapid and orbital-scale changes in Greenland moisture origin. Science 309:118–121

Morgan V, Delmotte M, van Ommen T et al (2001) Relative timing of deglacial climate events in Antrctica and Greenland. Science 297:1862–1864

Mulvaney R, Rothlisberger R, Wolff EW et al (2000) The transition from the last glacial period in inland and near-coastal Antarctica. Geophys Res Lett 27:2673–2676

NorthGRIP community members (2004) High resolution climate records of the Northern Hemisphere reaching into last interglacial period. Nature 431:147–151

Peterson LC, Haug GH, Hughen KA, Röhl U (2000) Rapid changes in the hydrologic cycle of the tropical Atlantic during the last glacial. Science 209:1947–1951

Placzek C, Quade J, Patchett PJ (2006) Geochronology and stratigraphy of late Pleistocene lake cycles on the southern Bolivian Altiplano: Implications for causes of tropical climate change. GSA Bulletin 118:515–532

Ramirez E, Hoffmann G, Taupin JD et al (2003) A new Andean deep ice core from Nevado Illimani (6350 m), Bolivia. Earth Planet Sci Lett 212:337–350

Rasmussen SO (2006) A new Greenland ice core chronology for the last glacial termination. J Geophy Res 111:D06102, doi:10.1029/2005JD006079

Risi C, Bony S, Vimeux F (2008) Influence of convective processes on the isotopic composition ($\delta^{18}O$ and δD) of precipitation and water vapor in the Tropics, Part 2: physical interpretation of the amount effect. J Geophys Res 113:D19306, doi:10.1029/2008JD009943

Steffensen JP, Andersen KK, Bigler M et al (2008) High-Resolution Greenland Ice Core Data Show Abrupt Climate Change Happens in Few Years (2008). Science 321:680–684

Steig EJ, Brook EJ, White JWC et al (1998) Synchronous climate changes in Antarctica and the North Atlantic. Science 282:92–95

Sturm K, Hoffmann G, Langmann B (2007a) Climatology of stable water isotopes in South America: comparing general to regional circulation models. J Clim 20:3730–3750, doi:10.1175/JCLI4194.1

Sturm K, Vimeux F, Krinner G (2007b) Intra-seasonal variability in South America recorded in stable water isotopes. J Geophys Res 112:D20118. doi:10.1029/2006JD008298

Sylvestre F, Servant-Vildary S, Servant M (1998) Le Dernier Maximum glaciaire (21 000–17 000 14C ans B.P.) dans les Andes tropicales de Bolivie d'après l'étude des diatomées. Comptes Rendus de l'Académie des Sciences 327:611–618

Sylvestre F (2002) A high resolution diatom-reconstruction between 21 and 17 kyr B.P. from the southern Bolivian Altiplano. J Paleolimnol 27:45–57

Thompson LG, Mosley-Thompson E, Davis ME et al (1995) Late glacial stage and Holocene tropical ice core records from Huascarán, Peru. Science 269:46–50

Thompson LG, Davis ME, Mosley-Thompson E et al (1998) A 25,000-year tropical climate history from Bolivian ice cores. Science 282:1858–1864

van der Hammen T, Hooghiemstra H (1995) The El Abra stadial, a Younger Dryas equivalent in Colombia. Quat Sci Rev 14:841–851

Vellinga M, Wood R (2002) Global climatic impacts of a collapse of the Atlantic thermohaline circulation. Clim Change 54:251–267

Villacís M, Vimeux F, Taupin JD (2008) Analysis of the climate controls on the isotopic composition of precipitation ($\delta^{18}O$) at Nuevo Rocafuerte, 74.5°W, 0.9°S, 250 m, Ecuador. CRAS Géosciences 340:doi:10.1016/j.crte.2007.11.003

Vimeux F, Gallaire R, Bony S et al (2005) What are the climate controls on isotopic composition (δD) of precipitation in Zongo Valley (Bolivia)? Implications for the Illimani ice core interpretation. Earth Planet Sci Lett 240, 205–220

Vimeux F, Ramirez E, Hoffmann G (in prep.) The glacial-interglacial deuterium excess signal in Illimani ice core (16°S, Bolivia)

Vimeux F, Khodri M (in prep.) Mechanism of climate change over South America during Last Glacial Maximum Part 2- New insights to interprete the glacial-interglacial isotopic variation in Andean ice cores

Vuille M, Bradley RS, Werner M et al (2003a) Modeling $\delta^{18}O$ in precipitation over the tropical Americas: Part I. Interannual variability and climatic controls. J Geophys Res 108:4174. doi:10.1029/2001JD002038

Vuille M, Bradley RS, Healy R et al (2003b) Modeling $\delta^{18}O$ in precipitation over the tropical Americas, Part II, Simulation of the stable isotope signal in Andean ice cores. J Geophys Res 108:4175. doi:10.1029/2001JD002039

Vuille M, Werner M (2005) Stable isotopes in precipitation recording South American summer monsoon and ENSO variability: observations and model results. Clim Dyn 25:401–413. doi:10.1007/s00382-005-0049-9

Wenzens G (1999) Fluctuations of outlet and valley glaciers in the Southern Andes (Argentina) during the past 13,000 years. Quat Res 51:238–247

Wirrmann D, Ybert JP, Mourguiart P (1992) A 20,000 years palaeohydrological record from Lake Titicaca. In: Dejoux C, Iltis A (eds) Lake titicaca, a synthesis of limnological knowledge. Kluwer Academic Publisher, Netherlands, pp 40–48

Ybert JP (1992) Ancient lake environments as deduced from pollen analysis. In: Dejoux C, Iltis A (eds) Lake titicaca, a synthesis of limnological knowledge. Kluwer Academic Publisher, Netherlands, pp 49–62

Part III
Characteristics of the Holocene Climate. Focus on Global Events: Are They Widespread, Comparable and Synchroneous in South America?

Chapter 11
Mid-Holocene Climate of Tropical South America: A Model-Data Approach

Pedro L. Silva Dias, Bruno Turcq, Maria Assunção F. Silva Dias, Pascale Braconnot, and Tatiana Jorgetti

Abstract Most of the Early and mid-Holocene paleoclimate studies in tropical South America indicate a drier climate in Amazon and Southeast Brazil and a wetter climate in Venezuela. This pattern has been interpreted as a northward migration of the Intertropical Convergence Zone (ITCZ) due to insolation changes explained by Milancovitch cycles. We show how model simulations and model-data comparisons can help to investigate further the reason of these changes by considering the mid-Holocene period (6 ka). The insolation effect and the vegetation interaction on the seasonal cycle are explored with emphasis on the regional impact on precipitation and on the atmospheric circulation. A major feature of the mean mid-Holocene simulated climate is indeed the decrease of the rainfall in the South Atlantic Convergence Zone (SACZ) region compared to present day, which is confirmed by the proxy data. However, the ITCZ migrates southward during the Southern Hemisphere summer thus enhancing the precipitation in Northeast Brazil. The SACZ and ITCZ displacements are enhanced by the vegetation feedback. The analysis of the transient meridional heat transport and of the baroclinicity of the model climate suggests more intense winter and early spring cold outbreaks in the central region of South America, which seems in agreement with paleoclimate proxies.

Keywords Holocene · Inter tropical convergence zone · Ocean atmosphere general circulation model · South-America · South Atlantic convergence zone

11.1 Introduction

Several Holocene paleoclimate studies in tropical South America indicate a drier climate during Early and mid-Holocene (Absy et al. 1991, Salgado-Labouriau et al. 1997, Ledru et al. 1998, Behling and Hooghiemstra 2000, Freitas et al. 2001,

P.L. Silva Dias (✉)
National Laboratory of Scientific Computing and Institute of Astronomy, Geophysics and Atmospheric Sciences, University of São Paulo, São Paulo, Brazil
e-mail: pldsdias@iag.usp.br

F. Vimeux et al. (eds.), *Past Climate Variability in South America and Surrounding Regions*, Developments in Paleoenvironmental Research 14,
DOI 10.1007/978-90-481-2672-9_11,

Sifeddine et al. 2001, Turcq et al. 2002, Abbott et al. 2003, Cordeiro et al. 2008). This drier paleoclimate has been interpreted as being due to a northward shift of the position of the Inter Tropical Convergence Zone (ITCZ) during the early and mid-Holocene in response to a lower summer insolation in the Southern Hemisphere at that time (Martin et al. 1997, Mayle et al. 2000, Marchant et al. 2001). The ITCZ would have then withdrawn progressively to the south during the last 7000 years (Koutavas and Lynch-Stieglitz 2004).

In the northernmost region of South America a wetter climate and higher riverine discharge has been evidenced by the geochemical composition of Cariaco basin sediments (Haug et al. 2001). A trend toward drier conditions is evident in the data since 5400 years BP. This regional climate changes are also explained by a northern position of the ITCZ during Early to mid-Holocene (Haug et al. 2001), in agreement with the preceding data. This hypothesis clearly links the Monsoon intensity to ITCZ position. This strong link which indeed is observed for present and Holocene climate in North Africa (Braconnot et al. 2000a) is not so clear in South America. Although a relationship exists between the location of the ITCZ and rainfall over Northeast Brazil (Nobre and Shukla 1996) as well as a relationship between interhemispheric SST gradients in the Atlantic Ocean, which controls ITCZ position, and past rainfalls in the Andes (Moura and Shukla 1981, Baker et al. 2001), the precipitations in Amazon and Southeast Brazil during summer are linked to the strong convective activities in Amazon Basin and along the South Atlantic Convergence Zone (SACZ). The SACZ is a low level confluence zone, oriented in the NW/SE direction, which provides a major contribution to the total precipitation in the tropical sector of South America and significantly contributes to the north/south energy exchange in the atmosphere (Kodama 1992, Satyamurti et al. 1998). Although the ITCZ and the SACZ are two different climatic features (Garreaud et al. 2008), their variability are related to each other and to remote forcing (Grimm and Silva Dias 1995). Another indication from Holocene paleoclimate studies is the interpreted changes in cold outbreaks dynamics in Central Brazil (Ledru 1993) and on the central Atlantic coast of Espirito Santo (Martin et al. 1993)

Here we show how climate simulations and the comparisons of the simulated climate with proxy indicators can help to better understand the behaviour of some essential characteristics of the South American paleoclimate. We consider the mid-Holocene climate at 6000 years cal BP (6 ka), which is a period of reference for the Paleoclimate Modeling Intercomparison Project (Joussaume et al. 1999, Braconnot et al. 2007a)

Solar radiation at the top of the atmosphere at 6 ka was significantly different from today due to orbital changes. At 6 ka, during the Northern Hemisphere summer the Earth was closer to the Sun than today. As a result, more (less) energy was available in Northern Hemisphere during summer (winter), which strengthens the temperature contrast between ocean and land. Several studies have been realized during the first phase of the PMIP project considering successively simulations with atmosphere alone model, simulations with coupled ocean-atmosphere model and coupled ocean-atmosphere-vegetation models (Braconnot et al. 2004). Most of the studies focused on Northern Hemisphere where the seasonal cycle is amplified.

Significant changes have been reported in Asia and Africa where the monsoon system was reinforced by an increase of the land-ocean temperature gradient and the resulting increase of the low level convergence in the monsoonal low pressure area (Harrison et al. 1998, Joussaume et al. 1999, Braconnot et al. 1999). The enhanced monsoon contributed to the global energy redistribution at 6 ka (Braconnot et al. 2000a). Although these results are qualitatively in agreement with paleoclimate proxies, the magnitude of the monsoon increase on North Africa is underestimated by all atmosphere alone simulations (Joussaume et al. 1999).

The influence of ocean-atmosphere coupled processes has been first analysed by Kutzbach and Liu (1997) and more recently by Zhao et al. (2005) from several coupled simulations. All the coupled simulations show that the intensity of the hydrological cycle is enhanced at 6 ka and the African summer monsoon is intensified and expanded northward toward the Sahara (Braconnot et al. 2004). The SST responds to insolation forcing with a 2–3 months delay affecting the duration of the monsoonal period which initiates about one month earlier in the coupled simulation while the retreat is slower as compared to the present-day simulation. Another important characteristic of the 6 ka coupled simulation is an amplification of the meridional displacement of the ITCZ (Zhao et al. 2005).

Besides the ocean feedbacks, interactions associated with vegetation changes have been identified in the coupled system (Ganopolski et al. 1998, Braconnot et al. 1999, Diffenbaugh and Sloan 2002). In some regions the vegetation control appeared as important as the insolation effect (Braconnot et al. 1999). The coupling of atmosphere, ocean and vegetation lead to the intensification and enhancement of the northward displacement of the African monsoon thus in better agreement with the paleoclimate data (Braconnot et al. 2004).

Few model studies deal with the South American mid-Holocene climate. Valdes (2000), comparing 19 PMIP atmosphere alone simulations, observed decrease of the amplitude of the temperature seasonal cycle over the continent and weakening of the seasonal precipitation cycle. In most of the continent, during the mid-Holocene, drier conditions were simulated by the mean of the 19 models. The continental mean sea level pressure indicates a small positive anomaly during summer which is consistent with reduced ascent that leads to relatively drier and cooler conditions. Melo and Marengo (2008), using the Atmosphere General Circulation Model from "Centro de Previsão do Tempo e Estudos Climáticos", evidenced, at 6 ka, a weakening of low-level convergence over the Amazon, a decrease of southward moisture transport North of 20°S and an increase of the northerly flow east of the Andes South of 20°S.

In this study, we go one step further and analyse the results of the simulations presented in Braconnot et al. (1999) over South America. Comparison with proxy also allows us to evaluate the simulated changes, and provides new interpretations on the causes of the observed changes in different regions. These simulations consider the coupling between atmosphere and ocean, as well as changes in the vegetation cover. Even though more recent simulations performed as part of the second phase of PMIP consider interactive changes in vegetation, it is not possible from the PMIP2 database to analyse the vegetation feedback because simulations with interactive vegetation and simulations with ocean-atmosphere models do not share the same

control simulation (see Braconnot et al. 2007b for details). A short description of the design and characteristics of the model experiments is provided in Section 11.2. The comparison between the model simulation with the present climate is available in Section 11.3 where we also discuss the main climate differences associated to the insolation changes and the impact of the vegetation changes. Comparison of the model results for the mid-Holocene with paleoclimate proxies are presented in Section 11.4.

11.2 Methodology

The atmospheric model used in this study is the coupled ocean-atmosphere climate model of the Institute Pierre et Simon Laplace – IPSL CM1 (Braconnot et al. 2000b). The atmosphere model resolution is 3.6° in latitude and 5.6° in longitude (50 × 64 grid points) with 11 sigma levels in the vertical. The oceanic component resolution has a 2.4° latitude and 3.9° longitude resolution (76 × 92 grid points) with 31 vertical levels including 10 layers in the upper 100 m. The atmosphere models include a land surface scheme (Noblet-Ducoudre et al. 2000) to compute the water and energy exchanges between land and atmosphere depending on the vegetation type and soil moisture. Changes in the vegetation were accounted for by asynchronously coupling the climate model with BIOME1 (Prentice et al. 1992), which provides the vegetation type as a function of the simulated climate. A complete description of the model and of the experimental design are provided by Braconnot et al. (1999) and Braconnot et al. (2000b). In the present study, all analyses are based on a mean seasonal cycle averaged over at least 50 years of simulation. In the control simulation the vegetation is fixed to the observed modern climatology. This experiment is referred to as CTL. Two mid-Holocene simulations will be explored. The first one only considers the changes in the Earth's orbital parameters prescribed as provided in the Paleoclimate Modeling Intercomparison Project (Joussaume et al. 1999) and includes the biome distribution for present day conditions (referred herein as H1). The second one (H2) also includes changes in vegetation taken from interactive application of BIOME1 vegetation model to the simulated 6 ka climate until equilibrium is reached between vegetation and climate. The present-day and 6 ka BIOME1 vegetation computed for H2 are shown in Fig. 11.1.

11.3 Results

11.3.1 Present Tropical South America Climate as Simulated by IPSL Model (CTL)

Some of the feature of the mid-Holocene climate may be affected by systematic model biases. Therefore it is important to know how the model reproduce the modern climatology before discussing the differences between the past climate and present. The IPSL coupled model has a well-defined precipitation annual cycle

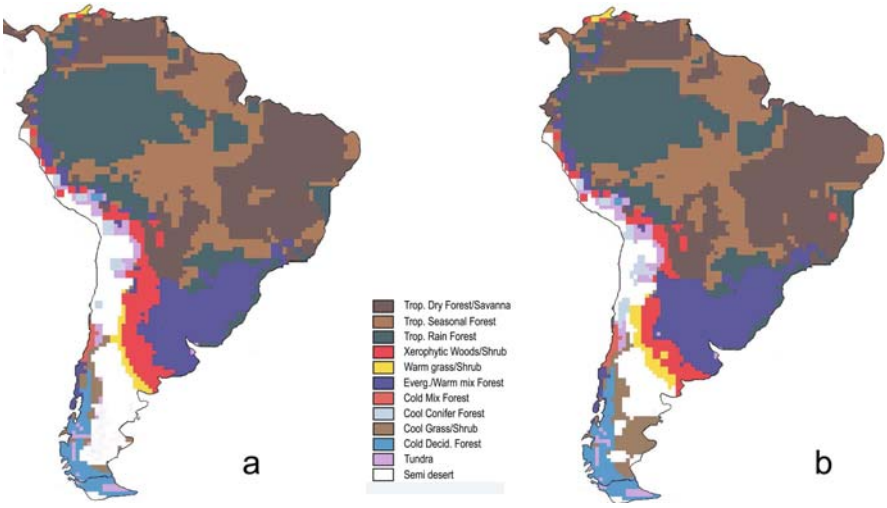

Fig. 11.1 (**a**) Vegetation produced by BIOME1 model with current climate (**b**) Vegetation produced by BIOME1 model with 6 ka simulated climate. This last one is used in H2 simulation

with the development of a very strong SACZ from October to March. This feature well illustrated on Fig. 11.2, which shows the difference between the observed precipitation (*Global Precipitation Climatology Project* /GPCP, Alder et al. 2003) and the CTL mean precipitation for December, January, February (DJF) and June, July, August (JJA). Some of the model drawbacks are commonly found in climate simulations. They concern: (a) excessively dry Amazon region, (b) too much precipitation in the SACZ, (c) excessive precipitation along the eastern slopes of the Andes and over the Bolivian Altiplano, (d) North East (NE) Brazil precipitation above observed values and (e) relatively weak Atlantic ITCZ. The CTL simulation captures the major features of the winter circulation (Fig. 11.2) in South America such as the northward displacement of the ITCZ and the high precipitation associated to the baroclinic zone in the southern portion of South America, along the Andes. However, the model overestimates the precipitation along the eastern slopes of the Andes and the intensity of the ITCZ in the Atlantic Ocean. The simulation properly captures the relative maximum of precipitation along the coast of NE Brazil but fails in reproducing the high levels of precipitation in Central America, particularly over Panama. As a result of the overestimation of the intensity of the precipitation in the Atlantic ITCZ, the trade winds are stronger from the SE in the western Atlantic in the simulated JJA climate (not shown). During winter, the model underestimates the precipitation in northern Argentina, Uruguay and SE Brazil. This is probably related to the lack of sufficiently strong cyclones which typically form in this region from autumn to spring (Gan and Rao 1991). The observed precipitation pattern in the northern portion of the continent is reasonably well reproduced except for some details along the Andes in Colombia.

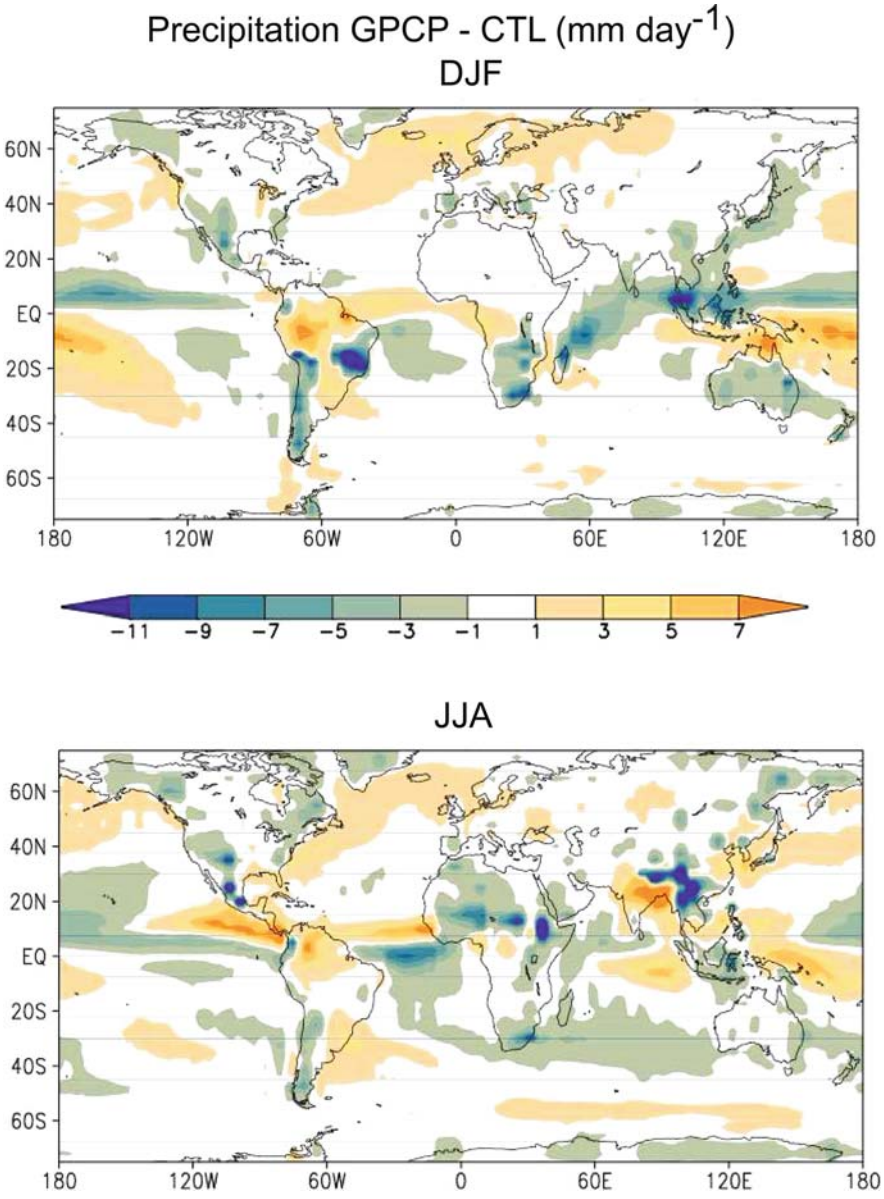

Fig. 11.2 Difference between the observed precipitation (*Global Precipitation Climatology Project*/GPCP, Alder et al. 2003) and the CTL simulation for December-January-February and June-July-August periods

The model summer climate is wetter in the SACZ than observations by a factor of 2–2.5 and drier in the Amazon and Southern Brazil (Gandu and Silva Dias 1998). If the convective scheme does not produce sufficient deep clouds, the tropical atmospheric column is moistened and the so called large-scale precipitation scheme

takes over, producing stratiform precipitation. Thus, the model tends to heat the atmosphere mainly at lower levels, creating a rather persistent low pressure system near the surface which enhances the moisture convergence and in turn, feedback into the stratiform precipitation. This hypothesis is corroborated by the relatively weak upper tropospheric anticyclonic anomaly to the SW of the maximum precipitation in the SACZ region (figure not shown). In the following, we will keep in mind these differences with observations and mainly discuss robust large-scale features.

11.3.2 ITCZ and ZCAS at the Mid-Holocene

The difference between the climatology of H1 and CTL is first discussed in this section. The amplitude of the seasonal temperature cycle is significantly decreased over most of the South American continent (Fig. 11.3). The mean temperature in DJF (JJA) and MAM (SON) in H1 is colder (warmer) compared to CTL. Cooling in H1 is particularly strong in MAM period over the northern and southern sectors of the continent and relatively small in the central region where the SACZ is located during the summer. The cooling in northern Argentina in summer and autumn is particularly strong. The winter and spring warming is stronger along the coast and the Andean region in the spring. There is a slight cooling (approximately 0.2°C) in the annual mean in H1 (mean temperature over the continent of the order of 17.2°C in CTL), which is consistent with the reduction of annual mean insolation within the tropics.

Precipitation differences (Fig. 11.4) between H1 and CTL are also significant. The H1 spring is wetter in central Brazil and the ITCZ precipitation is lower. The SACZ becomes less active in the summer in H1 and displaced to the north while the ITCZ is displaced to the south producing enhanced precipitation in the NE region of Brazil. The ITCZ and the SACZ seem to merge in NE Brazil thus enhancing the precipitation. This phenomenon indicates that the displacement of ITCZ and ZCAS do not follow necessarily the same direction. The autumn climate is also drier in the SACZ region and wetter in the eastern portion of NE Brazil. In the Andes, the Altiplano and eastern slopes are also significantly drier in the present simulation (CTL) than in the 6 ka case (H1). In Southern Hemisphere winter the ITCZ is displaced to the north. The southward (northward) displacement of the ITCZ in summer (winter) is the prevailing feature in the equatorial region. Very small differences in the precipitation regime are found in Southern Brazil, Uruguay, Northern Argentina and Paraguay (just slightly more humid, mainly in the winter period).

These results are in agreement with Valdes (2000) who also observed a dryer climate all over Brazil. This feature is thus a primary climate response to insolation change. Valdes (2000) used PMIP1 atmosphere alone model. The coupled ocean atmosphere model we studied here enhances ITCZ displacements. Most of PMIP2 models, which are also coupled Ocean-Atmosphere models, indicate the same widening of ITCZ range of displacement, suggesting that the feedback from the ocean strongly modulates the location and the size of the ITCZ.

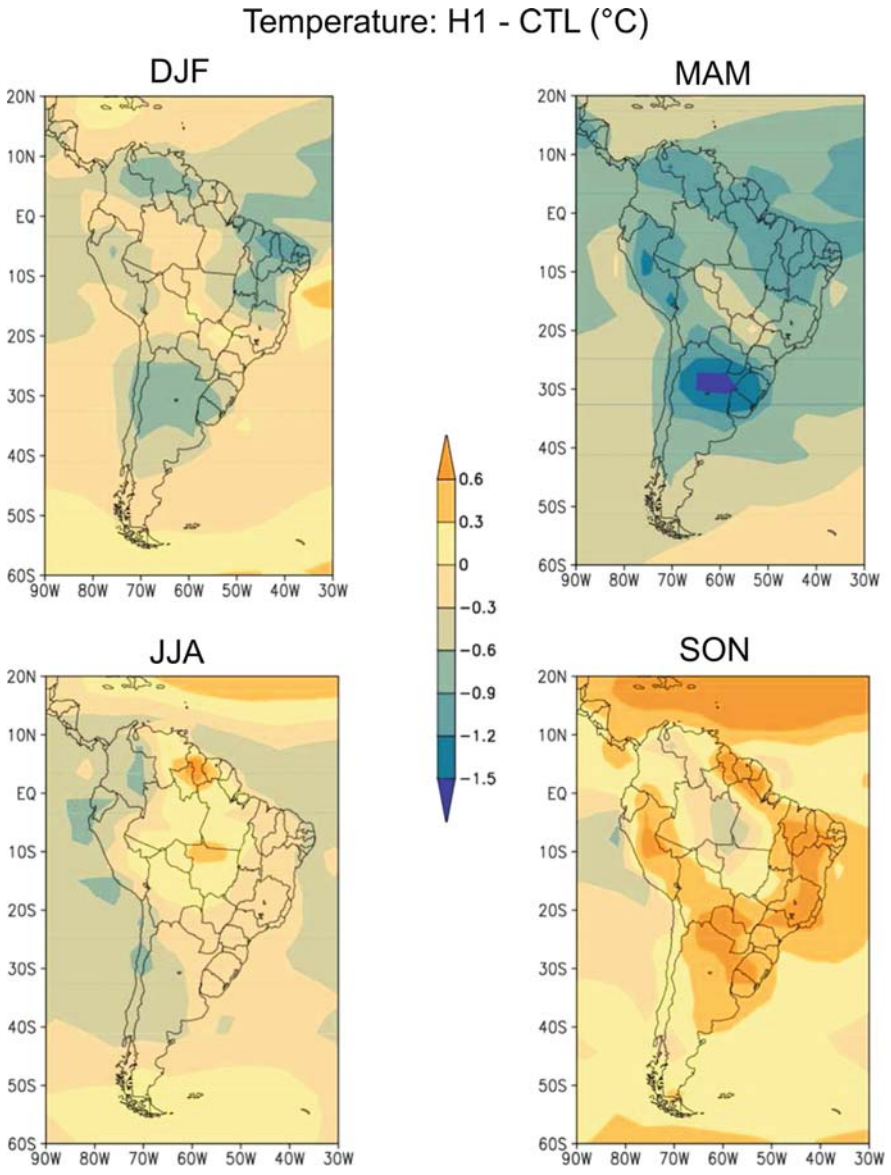

Fig. 11.3 Temperature (°C) difference between CTL and H1 for December-January-February, March-April-May, June-July-August and September-October-November periods

The impact of the vegetation change in H2 provokes an enhancement of the northward displacement of the SACZ and southward migration of the ITCZ during summer compare to H1 (Fig. 11.5). This effect is well depicted by the difference between H2 and H1. The vegetation effect is sufficiently strong in the SACZ to lead

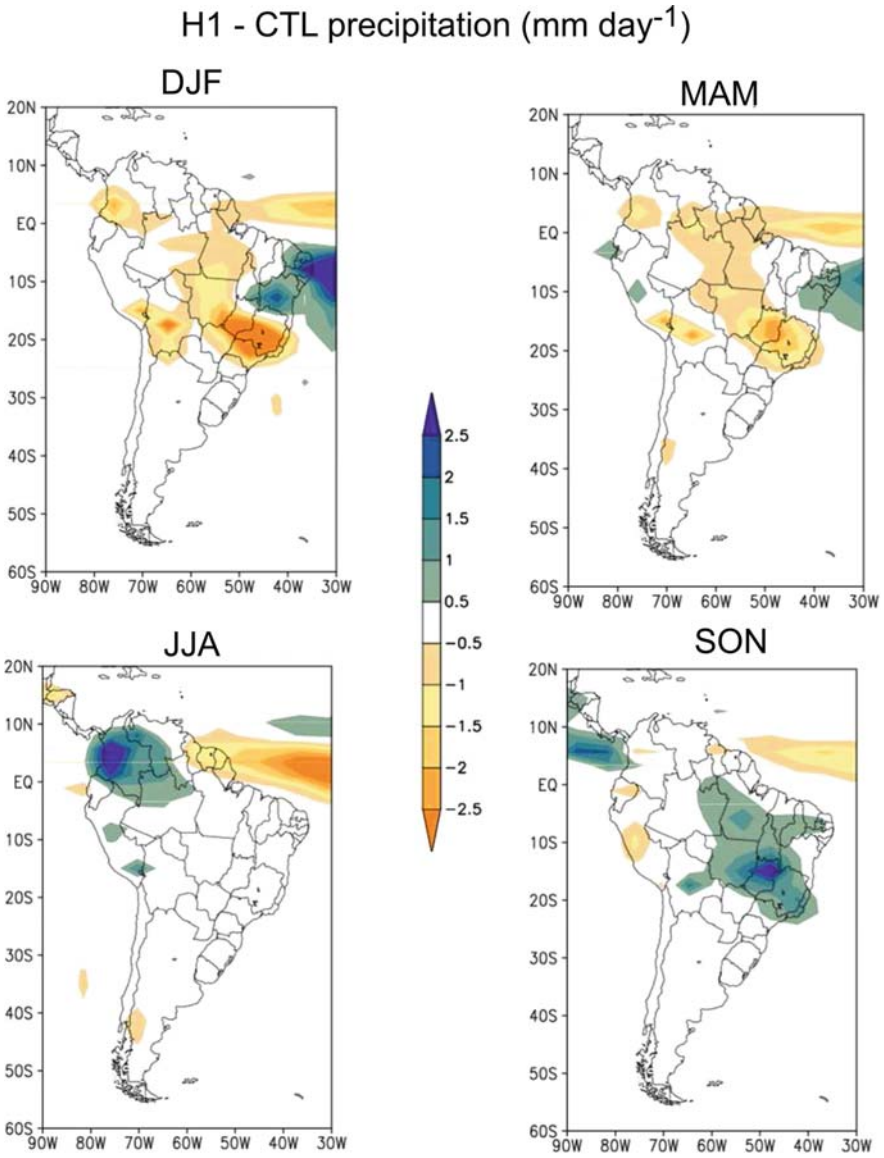

Fig. 11.4 Precipitation difference between H1 and CTL December-January-February, March-April-May, June-July-August and September-October-November periods

to a significant decrease in the summer precipitation. The precipitation regime in NE Brazil is significant in autumn and winter, with relatively more precipitation in JJA in H2 with respect to H1. More precipitation is observed in Central South America during SON, indicating a possible earlier start of the rainy season (Fig. 11.5).

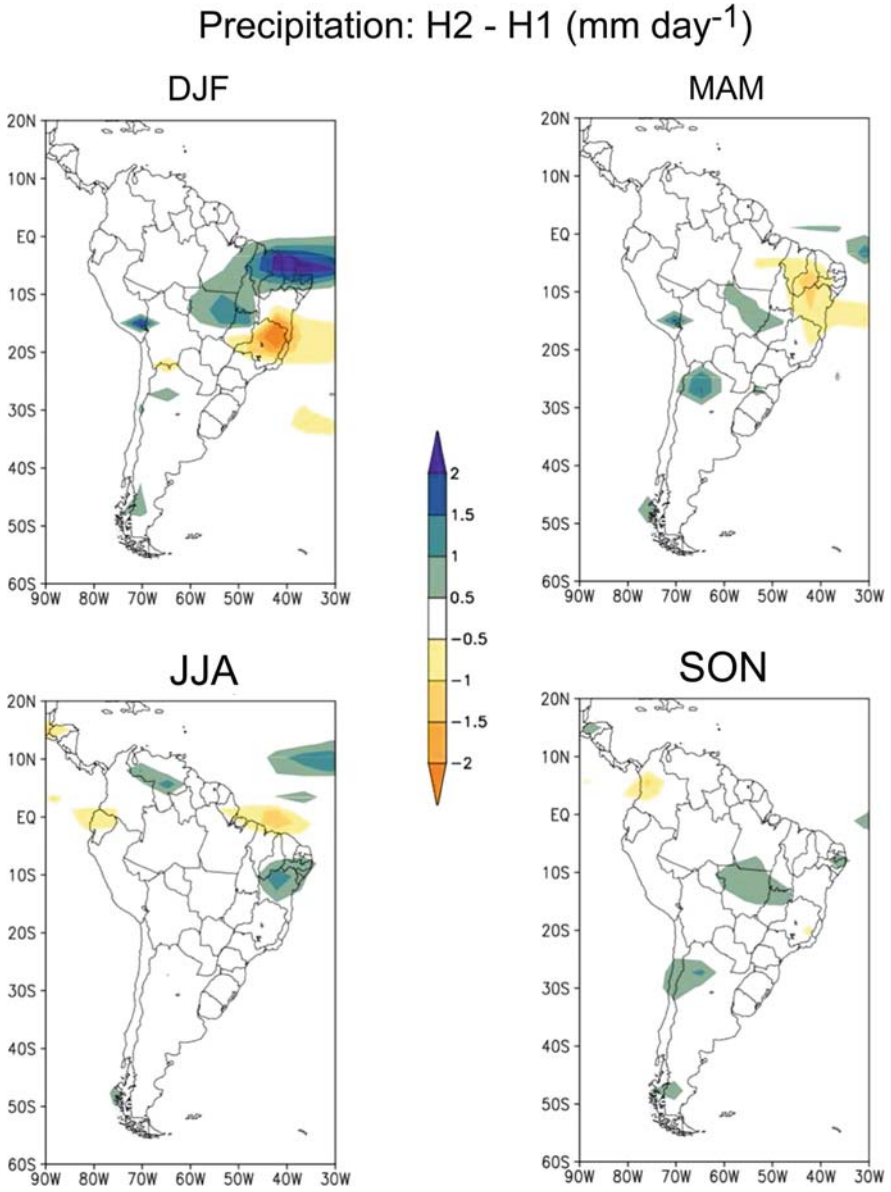

Fig. 11.5 Precipitation difference (mm/day) between H2 and H1 in December-January-February, March-April-May, June-July-August and September-October-November

The vegetation effect leads to increased precipitation in northern Argentina almost throughout the year (small impact in the winter).

Regional vegetation feedbacks due to changes, for example, in albedo, roughness length, and soil moisture are important in paleo-climate simulations, because they

affect both the heat and the water exchanges between the surface and the atmosphere (Dutton and Barron 1996). In the case of the SACZ region (from Southwest Amazon to Southeast Brazil) the observed rainfall reduction cannot be a direct effect of vegetation since there are no changes in the BIOME1 Model (the simulated climate changes are not sufficient to provoke a vegetation change). Thus the observed climate changes are due to a remote effect of the global vegetation change. The weakening of the monsoon circulation associated with the northward displacement of the SACZ is related to an anticyclonic wind anomaly at 850 hPa during the summer and early autumn (Fig. 11.6) and to a more intense westerly flow in H2 than in H1 south to about 40°S. This weakening of the tropical circulation, associated with the precipitation decrease in the SACZ, is probably due to the vegetation changes produced by the model in west Africa and their impact on the Tropical Atlantic SST and the associated strengthening of the SST gradient across 5°N in the Atlantic ocean (Braconnot et al. 2004). In the same manner, the weakening of the trade winds in JJA (Fig. 11.6) is due to the intensification of the African monsoon by the development of vegetation in West Africa arid regions (Braconnot et al. 2004). In Northern Argentina and Northeast Brazil small differences in vegetation are observed (Fig. 11.1). Sensitivity tests would be needed to determine the relative influence of these local vegetation changes.

11.3.3 Atmospheric Mean and Transient Circulation

The reduction of 850 hPa flow intensity over the continent during the mid-Holocene is also and mainly due to the decrease in the seasonal variation of insolation in the Southern Hemisphere producing smaller temperature gradients. Significant changes can be observed at the tropospheric low-level circulation such as the decrease of the intensity of the northwesterly South American Low Level Jet – SALLJ (Marengo et al. 2002) east of the Andes (in DJF and MAM, Fig. 11.7) and of easterly flow in the equatorial region (SON and DJF). The spring and summer main feature in the wind field is the decrease in the intensity of the circulation associated with the subtropical Atlantic High which is associated with the southward displacement of the ITCZ. The decrease in the intensity of the SALLJ has a significant impact in the moisture transport from the Amazon Basin to the northern part of the Plata Basin. The winter low level circulation is characterized by the intensification of the westerly flow towards the northern Andes which provides the moisture explaining the enhanced precipitation in Colombia. We will see later that this increase does not appear in the proxy data, probably because it is, in reality, located more on the North.

However, the transient eddies heat transport shows significant differences between the present and the 6 ka model climate simulations. Figure 11.8 shows the transient meridional heat transport at 20°S 62°W just to the east of the Andes and 20°S 40°W (off the coast of State of Espirito Santo in Brazil). Although the changes in the mean meridional wind (figure not shown) are small, the transient

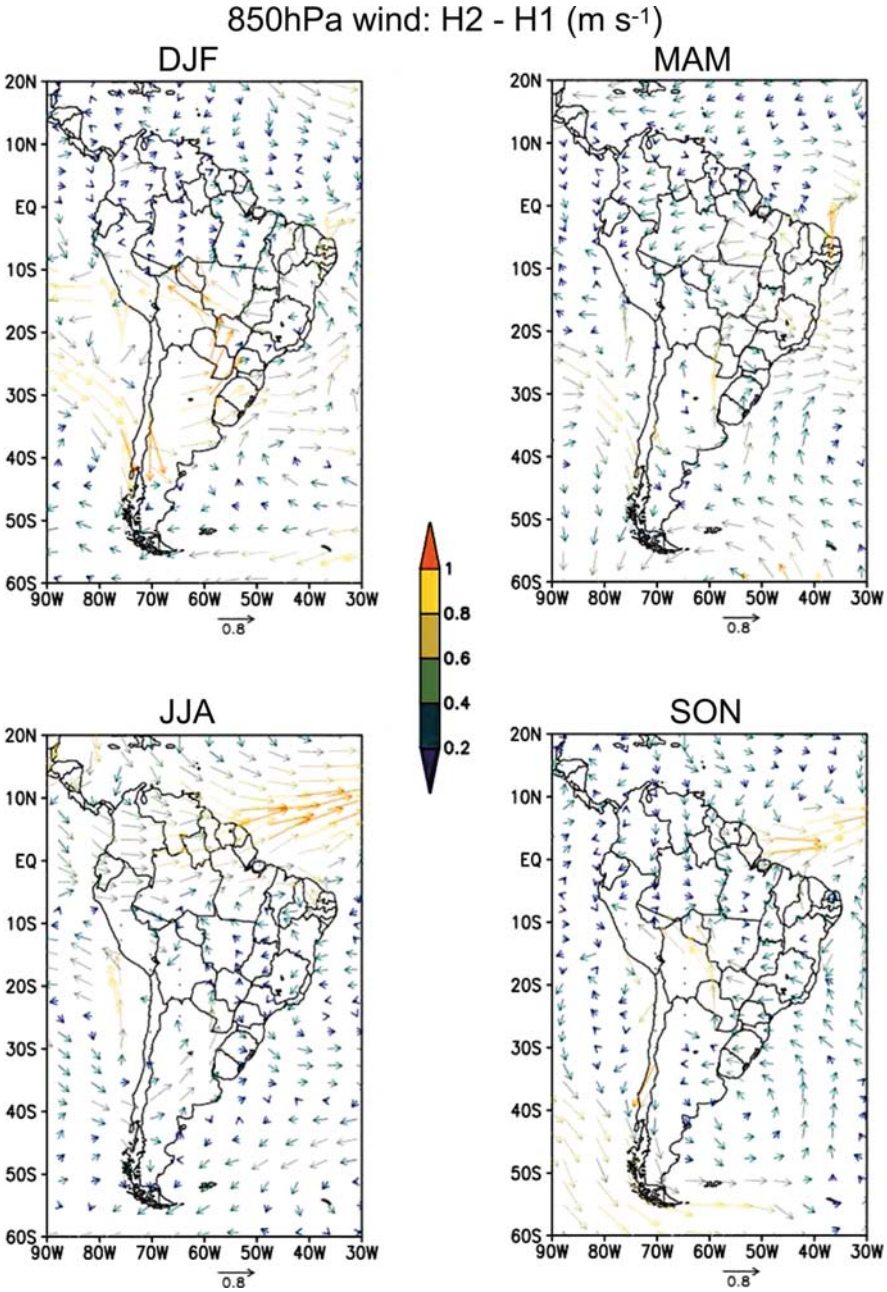

Fig. 11.6 850 hPa wind difference ($m.s^{-1}$) between H2 and H1 in December-January-February, March-April-May, June-July-August and September-October-November

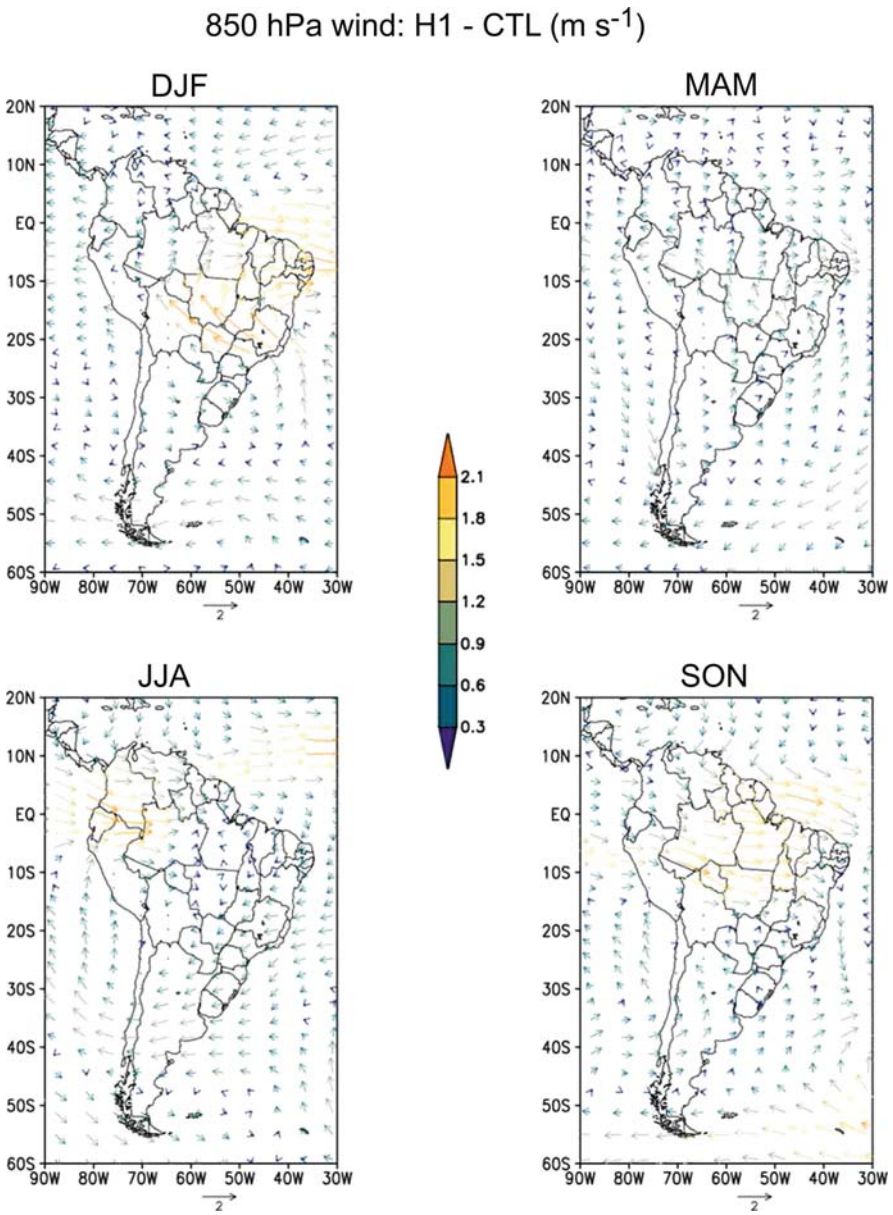

Fig. 11.7 850 hPa wind difference (m.s^{-1}) between H1 and CTL in December-January-February, March-April-May, June-July-August and September-October-November periods

southward (negative in Fig. 11.8) heat transport is significantly lower in H1 off the coast of the State of Espirito Santo during the winter, indicating weaker baroclinic perturbations affecting eastern Brazil in this region. Inversely, the transient meridional heat flux along the Andes in spring (mainly September and October)

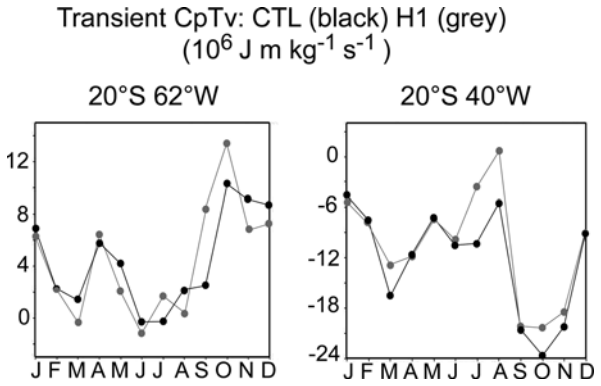

Fig. 11.8 Transient heat transport at 20°S 62°W and 20°S 40°W plotted as a function of months for CTL (*black circles*) and H1 (*grey circles*)

is larger in H1, indicating stronger activity associated with weather systems, suggesting that the cold air outbreaks in Central Brazil could be more intense at the end of the winter/early spring. The zonal flow at 500 hPa is stronger in a broad band between 20 and 35°S in September (Fig. 11.9), supporting enhanced baroclinic

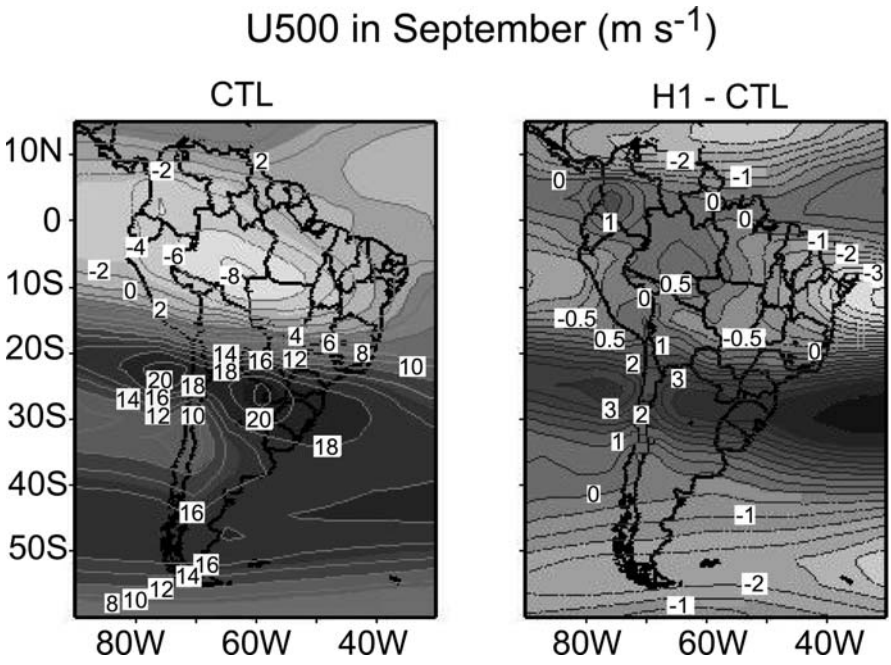

Fig. 11.9 Zonal flow at 500 hPa for the CTL experiment and difference between H1 and CTL in September

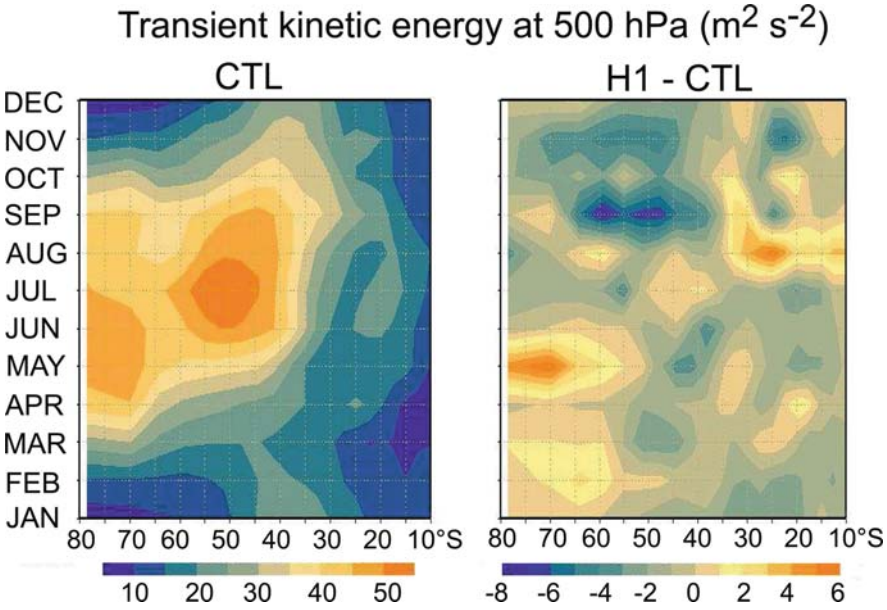

Fig. 11.10 Hovmoller diagram of the transient kinetic energy at the 500 hPa level at 60°W (unit $m^2.s^{-2}$) for the mean CTL annual cycle and the difference between H1 and CTL

instability in this region, which favors the development of low level cyclogenesis. The associated cyclones enhance the northward penetration of cold air masses in the continent.

Another interesting evidence of changes in the transient structure of the weather systems in South America is shown in Fig. 11.10 (transient kinetic energy at the 500 hPa level). The mean CTL annual cycle clearly indicates that the maximum activity occurs from June to November at 35°S and that the tropical intrusion of upper level transients from the south occurs in early spring. The H1 experiment shows significant enhancement of the transient kinetic energy activity in the late winter/early spring and small increase in the autumn. Further south, there is a significant decrease in the transient activity in the spring. Thus, the simulated changes at 6 ka are also significant in the transient activity and therefore in the weather patterns.

A vegetation feedback is identified in the transient meridional heat transport during the winter (Fig. 11.11). A large increase in the magnitude of the heat transport is observed at 20°S and 60°W, near Paraguay and eastern Bolivia. The vegetation feedback in the atmospheric circulation is such that the enhanced upper level flow facilitates the development of transient baroclinic modes which are associated to stronger cyclogenesis and more intense cold outbreaks in the central portion of the continent.

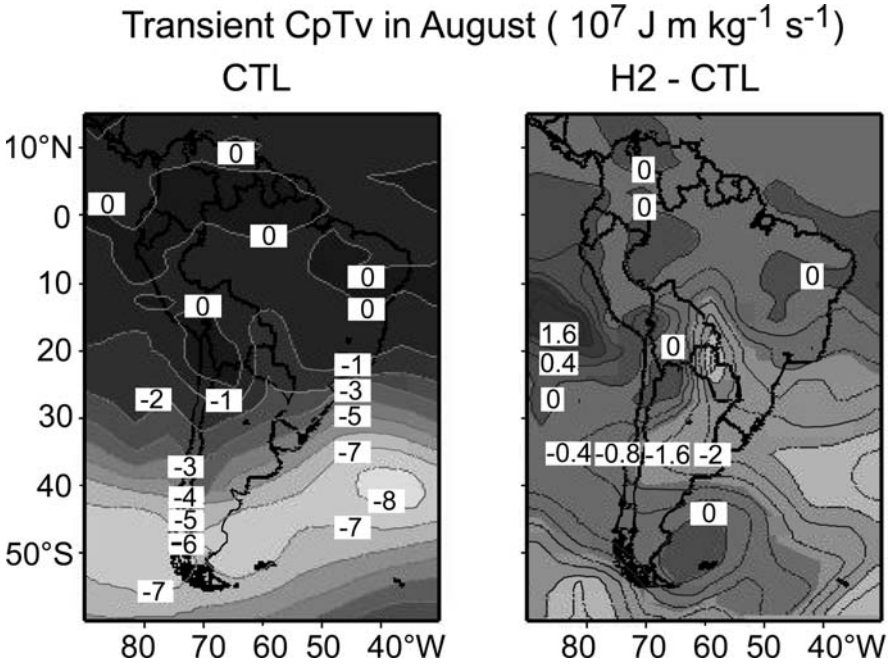

Fig. 11.11 Transient meridional heat transport (units 10^7 J.m.kg^{-1}.s^{-1}) in CTL and difference between H2 and CTL in August

11.4 Comparison with Paleoclimate Data

11.4.1 Precipitation

A major feature of the mean climate change between the CTL and the H1 experiments is the decrease of the rainfall in the SACZ region in the mid-Holocene. This dryness is confirmed by the proxy data (Fig. 11.12). The lakes Dom Helvecio (19°41′S, 42°35′W) and Preta de Baixo (18°25′S, 41°50′W) had water levels lower than present during the mid-Holocene (Turcq et al. 2002). The same is observed at Lagoa Santa (19°38′S, 43°54′W) according to Parizzi et al. (1998). The vegetation reconstructed from palynological studies was more open at Lagoa dos Olhos (19°38′S, 43°54′W – De Oliveira 1992), Morro de Itapeva (22°47′S, 45°28′W – Behling 1997) and Lago do Pires (17°57′S, 42°13′W – Behling 1995a), indicating a dryer climate at 6 ka. It is worth noting that Behling (1995a) interpreted the vegetation change as a result of a longer dry season (approximately 5 months during the mid-Holocene and closer to 4 months at present). The IPSL model indicates a decrease of the summer precipitation in this region but there are no significant indications of a change in the dry season length due to the early start of the rainy season. Another important point is that the vegetation reconstructed by the model (Fig. 11.1) is not significantly changed in this region, i.e. the simulated climate

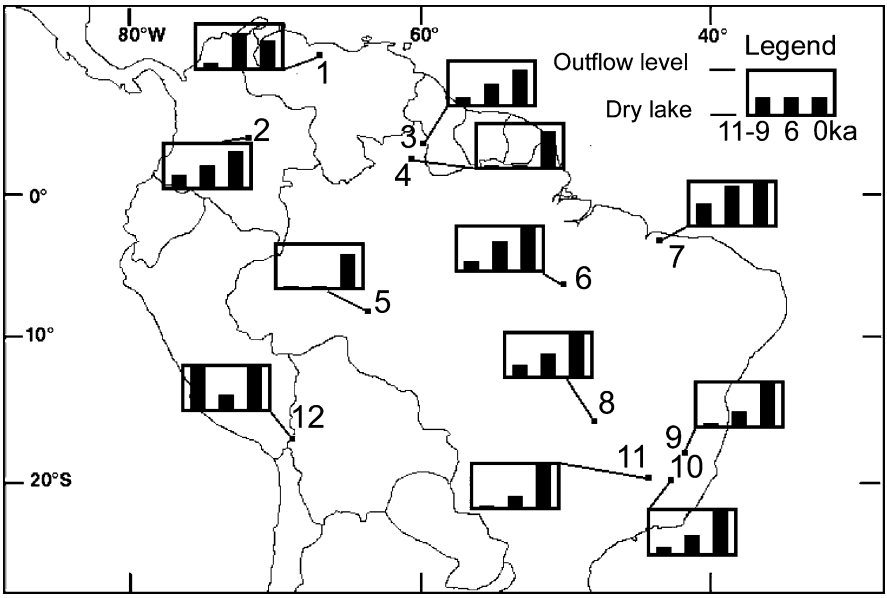

Fig. 11.12 Lake level changes in tropical South America at the beginning of Holocene (11–9 ka), at Middle Holocene (6 ka) and at present. Ages have been calibrated according to Stuiver et al (1998). (*1*) Lake Valencia (Bradbury et al. 1981, Curtis et al. 1999), (*2*) Lake Loma Linda (Behling and Hooghiemstra 2000), (*3*) Lake Caracaranã (Turcq et al. 2002), (*4*) Boa Vista lakes (Simões Filho et al. 1997), (*5*) Humaita lakes (Cordeiro et al unpublished), (*6*) Carajás lake N3 (Cordeiro et al.1997), (*7*) Lake Caçó, (*8*) Aguas Emendadas, (*9*) Lake Agua Preta de Baixo (Turcq et al. 2002), (*10*) Lake Dom Helvecio (Turcq et al. 2002), (*11*) Lake Santa (Parizzi et al. 1998), (*12*) Lake Huinaimarca (Wirrmann and Mourguiart 1995)

change is not strong enough to modify the vegetation classification provided by the BIOME model. However, the proxy data confirms that the tropical rainforest had regressed and thus some cautions must be taken in interpreting the H2 results in that region.

In Northeast Brazil the palynological record of Saquinho (10°24′S, 43°13′W) reveals more developed gallery forests during the mid-Holocene (De Oliveira et al. 1999) indicating a wetter climate, which is also reconstructed by the H1 simulation. It is difficult to assess the results of the changes in vegetation produced in H2 because this region is located in the transition between the wetter and drier areas. More proxy data are necessary in order to evaluate the magnitude and impact of the vegetation change in NE Brazil.

The lake record of Lagoa Feia (47°18′S, 15°34′W – Turcq et al. 2002) as well as the palynological records of Aguas Emendadas (15°S, 47°35′W – Barberi et al. 2000) and Crominia (17°15′S, 42°13′W – Salgado-Labouriau et al. 1997) in the Central region of Brazil (Fig. 11.12) indicates dryer climate conditions during the mid-Holocene. The H1 model shows reduced rainfalls from December to April and

slightly increased precipitation from September to November (Fig. 11.4). These changes are less marked in H2.

In the Southern region of Brazil, where the model indicates a slightly wetter past climate mainly in the H2 experiment (Fig. 11.5), the palynological records show, on the contrary, a reduced forest extension (Behling 1995b) with exception of Serra da Boa Vista (27°42′S, 49°52′W) where a well developed forest was present. This divergence may be related to the mountainous relief of this coastal region. Southward, the Aparados da Serra record (29°13′S, 50°W – Roth 1990) does not evidence any forest change since the mid-Holocene. In the pampas of Argentina (37–38°S, 58–62°W) the pollen indicates a more humid climate during the mid-Holocene (Prieto 1996).

In the northern part of Amazon, in the Roraima state, the Caracaranã Lake (3°51′N, 59°47′W) level was low (Turcq et al. 2002) and the lakes in the Boa Vista region (2°55′N, 50°40′W) have dried (Simões Filho et al. 1997). This is in agreement with the H1 model results (Fig. 11.4). H2 does not significantly change the results in this region. Westward, in the llanos of Colombia (3–5°N, 69–73°W) the forests and arboreal savannas were less developed than present indicating a dryer climate or a longer dry season (Behling and Hooghiemstra 2001). The CTL model indicates less precipitation during the dry season and at the beginning of the rainy season but an increase at the end of the wet period. H2 enhances the effect at the end of the rainy season but has no significant effect in the remaining periods. This result does not seem compatible with the proxy data. In the north, in Venezuela, the paleodata from lake Valencia (Bradbury et al. 1981, Curtis et al. 1999), as well as the marine Cariaco Basin study (Haug et al. 2001) indicate a mid-Holocene wetter climate. The model doesn't reproduce such feature although the Northern position of ITCZ during North Hemisphere summer explains the recorded change. The rainfall increase does not seem to be located at the right place in the model.

11.4.2 Temperature and Cold Outbreaks

The palynological study from Salitre (19°S, 46°46′W) suggests a well-developed forest with cold taxa between 10200 and 7400 cal BP (Ledru 1993). It has been interpreted as a stronger intensity of cold outbreaks during the Holocene. Between 7400 and 6300 cal BP, this forest was replaced by a semi-deciduous forest. Such change in vegetation type may still indicate a cold outbreak influence, since those systems provoke rainfall during the dry season. A higher cold outbreak influence than today, in central Brazil is also reproduced by the model, although the mid-Holocene simulation does not show higher precipitations. In the H2 simulation the transient meridional heat transport indicates an additional increase in cold front intensity in a central South-American region centered in Paraguay and northern Argentina, extending into central Brazil (Fig. 11.11). The reason for this increased penetration of cold air may be partially related to change in vegetation in the Chaco region (Fig. 11.1).

On the central Brazilian coast, the transient meridional heat transport shows, on the contrary, a decrease in cold front influence (Fig. 11.6). This feature seems in a good agreement with the coastal geomorphologic data. Today, in this region, the residual long shore sand transport is always northward due to the southwestern storms generated by the cold outbreaks. During the mid-Holocene several events of erosion due to southward long shore sand transport related to trade winds have been observed (Martin et al. 1993), in agreement with a weaker intensity of transients simulated at 6 ka on Espirito Santo coast (Fig. 11.8).

11.5 Conclusions

The model results of the simulation for the present climate and the mid-Holocene indicate a significant reduction in the seasonal cycle, which is coherent with the orbital forcing. A basic impact of the insolation forcing is the change in the ITCZ location, which is influenced by the coupled ocean-atmosphere system and by the vegetation change. In summary, the following features were observed in the IPSL model simulation for the present and 6 ka climates:

- The simulation of modern precipitation is much larger than observed in the SACZ region and underestimated over the Amazon region;
- At mid-Holocene, the northward displacement of the SACZ and southward migration of the ITCZ during Southern Hemisphere summer is such that the two systems merge, increasing the precipitation in the NE area of Brazil;
- There is a northward migration of ITCZ during mid-Holocene Northern Hemisphere summer.
- The vegetation feedback enhances the impact on the SACZ and ITCZ;
- As a consequence of the ITCZ migration to the south, NE Brazil tends to be cooler in the 6 ka simulation;
- Southern Brazil, Uruguay and NE Argentina are slightly wetter and cooler (mainly in the summer) in the 6 ka simulation;

The northward migration of the SACZ leads to drier condition in SE Brazil that is consistent with paleoclimate proxies, as discussed in Section 11.4. There are observational evidences suggesting a wetter NE Brazil. Thus, the basic model features associated with the northward displacement of the SACZ and southward migration of the ITCZ are consistent with observations. Weakening of the monsoonal circulation in the model is associated with a reduction of the intensity of the upper tropospheric anticyclonic circulation (the Bolivian High).

The largest temperature changes (Fig. 11.3) in the 6 ka simulation are observed in the Atlantic tropical basin. The 6 ka North Atlantic is particularly warmer than in the present simulation and colder to the south, in agreement with other studies (Braconnot et al. 1999, Otto-Bliesner 1999). The warming in the South Atlantic and cooling the North Atlantic are coherent with the insolation effect associated to

the orbital changes. But significant contribution is also associated to the changes in cloud cover in view of the significant displacement of the ITCZ.

The enhanced baroclinicity between 20 and 35°S, mainly during the winter period, as measured by the intensification of the mid-tropospheric zonal flow, leads to the increase of the transient meridional heat transport. Thus, the model results are coherent with a scenario of more intense cold outbreaks on the tropical sector of South America. This effect is enhanced when the vegetation feedback is included in the model.

Acknowledgments Most of this work was made possible thanks to CNPq/IRD grants ("PALEOTROPICA", "CLIMPAST") and to the French LEFE EVE project ECHOS. This work is also part of the PROSUR(IAI) project. FAPESP provided the financial support to Tatiana Jorgetti. The Milenium Institute in Mathematics financed by FINEP/CNPq Brazil is also acknowledged.

References

Abbott MB, Wolfe BB, Wolfe AP et al (2003) Holocene paleohydrology and glacial history of the central Andes using multiproxy lake sediment studies. Palaeogeogr Palaeoclimatol Palaeoecol 194:123–138

Absy ML, Cleef ALM, Fournier M et al (1991) Mise en évidence de quatre phases d'ouverture de la forêt dense dans le sud-est de l'Amazonie au cours des 60 000 dernières années. Première comparaison avec d'autres régions tropicales. C R Acad Sci Paris, t.312 Série II:673–678

Alder RF, Huffman GJ, Chang A et al (2003) The version-2 Global Precipitation Climatology Project (GPCP) monthly precipitation analysis (1979-present). J Hydrometeorol 4(6): 1147–1167

Baker PA, Rigsby CA, Seltzer GO et al (2001) Tropical climate changes at millennial and orbital timescales on the Bolivian Altiplano. Nature 409:698–701

Barberi M, Salgado-Labouriau ML, Suguio K (2000) Paleovegetation and paleoclimate of "Vereda de Aguas Emendadas" central Brazil. J South Am Earth Sci 13:241–254

Behling H (1995a) A high resolution Holocene pollen record from Lago do Pires, SE Brazil: Vegetation, climate and fire history. J Paleolimnol 14:253–268

Behling H (1995b) Investigation into the Late Pleistocene and Holocene history of vegetation and climate in Santa Catarina (S Brazil). Veget Hist Archaeobot 4:127–152

Behling H (1997) Late Quaternary vegetation, climate and fire history from the tropical mountain region of Morro de Itapeva, SE Brazil. Palaeogeogr Palaeoclimatol Palaeoecol 129:407–422

Behling H, Hooghiemstra H (2000) Holocene Amazon rainforest-savanna dynamics and climatic implications: high resolution pollen record from Laguna Loma Linda in eastern Colombia. J Quat Sci 15(7):687–695

Behling H, Hooghiemstra H (2001) Neotropical savanna environments in space and time: Late Quaternary interhemispheric comparisons. In: Markgraf V (ed) Interhemispheric climate linkage in the Americas, Academic, London

Braconnot P, Joussaume S, Marti O (1999) Synergistic feedbacks from ocean and vegetation on the African monsoon response to mid-Holocene insolation. Geophys Res Lett 26:(16)2481–2484

Braconnot P, Marti O, Joussaume S, Leclainche Y (2000a) Ocean feedback in response to 6 kyr BP insolation. J Clim 13:1537–1553

Braconnot P, Joussaume S, de Noblet N, Ramstein G (2000b) Mid-Holocene and Last Glacial Maximum African monsoon changes as simulated within the Paleoclimate Modelling Intercomparison Project. Global Planet Change 26:(1–3)51–66

Braconnot P, Harrison S, Joussaume S et al (2004) Evaluation of coupled ocean-atmosphere simulations of the mid-Holocene. In: Battarbee RW, Gasse F, Stickley CE (eds) Past climate variability through Europe and Africa. Kluwer, Dordrecht

Braconnot P, Otto-Bleisner BL, Harrison S et al (2007a) Results of Pmip2 coupled simulations of the Mid-Holocene and Last Glacial Maximum Part 1: Experiments and Large-Scale Features. Clim Past 3:261–277

Braconnot P, Otto-Bleisner BL, Harrison S et al (2007b) Results of Pmip2 coupled simulations of the Mid-Holocene and Last Glacial Maximum Part 2: Feedbacks with emphasis on the location of the ITCZ and mid-and high Latitudes Heat Budget. Clim Past 3:279–296

Bradbury JP, Leyden B, Salgado-Labouriau ML et al (1981) Late Quaternary environmental history of Lake Valencia, Venezuela. Science 214:1199–1305

Cordeiro RC, Turcq B, Suguio K et al (1997) Holocene environmental changes in Carajás Region (Para, Brazil) recorded by Lacustrine Deposits. Verh Internat Verein Limnol 26: 814–817

Cordeiro RC, Turcq B, Suguio K et al (2008) Holocene fires in East Amazon (Carajás), new evidences, chronology and relation with paleoclimate. Glob Planet Change 61(1–2): 49–62

Curtis JH, Brenner, M, Hodell DA (1999) Climate change in the lake Valencia basin, Venezuela, ~12600 yr BP to present. Holocene 9:609–619

De Oliveira PE (1992) A palynological record of Late Quaternary vegetational and climatic changes in southeastern Brazil, PhD thesis, Ohio State University

De Oliveira PE, Barreto AMF, Suguio K (1999) Late Pleistocene/Holocene climatic and vegetational history of the Brazilian caatinga: the fossil dunes of the middle São Francisco River. Palaeogeogr Palaeoclimatol Palaeoecol 152:319–337

Diffenbaugh NS, Sloan LC (2002) Global climate sensitivity to land surface change: The Mid Holocene revisited. Geophys Res Lett 29(10):1476–1488

Dutton JF; Barron EJ (1996) Genesis Sensitivity to Changes in Past Vegetation. Paleoclimates 1(4):325–354

Freitas HA de, Pessenda LCR, Aravena R et al (2001) Late Quaternary Vegetation Dynamics in the Southern Amazon Basin Inferred from Carbon Isotopes in Soil Organic Matter. Quat Res 55:39–46

Gan MA, Rao VM (1991) Surface cyclogenesis over South America. Mon Wealth Rev 19(5): 1293–1302

Gandu AW Silva Dias PL (1998) Impact of Tropical Heat Sources on the South American Tropospheric Upper Circulation and Subsidence. J Geophys Res 103:6001–6015

Ganopolski A, Kubatski C, Claussen M et al (1998) The influence of vegetation-atmosphere-ocean interaction on climate during the mid-Holocene. Science 280:1916–1919

Garreaud RD, Vuille M, Compagnucci R, Marengo J (2009) Present-day South American climate. Paleogeogr Paleoclimatol Paleoecol (in press)

Grimm AM, Silva Dias PL (1995) Analysis of tropical-extratropical interactions with influence functions of a barotropic model. J Atmos Sci 52(20):3538–3555

Harrison SP, Jolly D, Laarif F et al (1998) Intercomparison of simulated global vegetation distributions in response to 6 kyr BP orbital forcing. J Clim 11:2721–2742

Haug GH, Hughen KA, Sigman DM (2001) Southward migration of the Intertropical Convergence Zone through the Holocene. Science 293:1304–1308

Joussaume S, Taylor KE, Braconnot P et al (1999) Monsoon changes for 6000 years ago: Results of 18 simulations from the Paleoclimate Modeling Intercomparison Project (PMIP). Geophys Res Lett 26(7):859–862

Kodama Y-M (1992) Large-scale common features of sub-tropical precipitation zones (the Baiu Frontal Zone, the SPCZ, and the SACZ). Part I: characteristics of subtropical frontal zones. J Meteorol Soc Japan 70:813–835

Koutavas A, Lynch-Stieglitz J (2004) Variability of the marine ITCZ over the Eastern Pacific during the past 30,000 years Regional perspective and global context. In: Diaz HF, Bradley RS (eds) The Hadley circulation: Present, past, and future. Kluwer Academic Press, Netherlands

Kutzbach JE, Liu Z (1997) Response of the African monsoon to orbital forcing and ocean feedbacks in the middle Holocene. Science 278:440–443

Ledru MP (1993) Late Quaternary environmental and climatic changes in Central Brazil. Quat Res 39:90–98

Ledru MP, Salgado-Labouriau ML, Lorscheitter ML (1998) Vegetation dynamics in southern and central Brazil during the last 10,000 yr B.P. Rev Palaeobot Palynol 99:131–142

Marchant R, Behling H, Berrio JC et al (2001) Mid- to Late-Holocene pollen-based biome reconstructions for Colombia. Quat Sci Rev 20:1289–1308

Marengo JA, Douglas MW, Silva Dias PL (2002) The South American low-level jet east of the Andes during the 1999 LBA-TRMM and LBA-WET AMC campaign. J Geophys Res 107:47.1–47.11

Martin L, Absy ML, Flexor JM et al (1993) Southern Oscillation signal in South American palaeoclimatic data of the last 7000 years. Quat Res 39:338–346

Martin L, Bertaux J, Correge T et al (1997) Insolation control on rainfall decoupling in Tropical South America between 12400 and 8800 cal years BP. Quat Res 47:117–122

Mayle FE, Burbridge R, Killeen TJ (2000) Millenial-scale dynamics of southern Amazon rain forests. Science 290:2291–2294

Melo MLD, Marengo JA (2008) The influence of changes in orbital parameters over South American climate using the CPTEC AGCM: simulation of climate during the mid Holocene. Holocene 18(4):501–516

Moura AD, Shukla J (1981) On the dynamics of the droughts in Northeast Brazil: observations, theory and numerical experiments with a general circulation model. J Atmos Sci 38(12): 2653–2673

Noblet-Ducoudre N, Claussen R, Prentice C (2000) Mid- Holocene greening of the Sahara: first results of the GAIM 6000 year BP Experiment with two asynchronously coupled atmosphere/biome models. Clim Dyn 16:643–659

Nobre P, Shukla J (1996) Variations of sea-surface temperature, wind stress and rainfall over the tropical Atlantic and South America. J Clim 9:2464–2479

Otto-Bliesner BL (1999) El Niño/La Niña and Sahel precipitation during the middle Holocene. Geophys Res Lett 26(1):87–90

Parizzi MG, Salgado-Labouriau ML, Kohler CH (1998) Genesis and environmental history of Lagoa Santa, SE Brazil. Holocene 8(3):311–321

Prentice IC, Cramer W, Harrison SP et al (1992) A Global Biome model based on plant physiology and dominance, soil properties and climate. J Biogeogr 19:117–134

Prieto AR (1996) Late Quaternary vegetational and climatic changes in the Pampa grassland of Argentina. Quat Res 45:73–88

Roth L (1990) Palinologia de uma turfeira do Parque Nacional de Aparados da Serra, Planalto Leste do Rio Grande do Sul, Brasil. Thesis. Universidade Federal do Rio Grande do Sul, Porto Alegre

Salgado-Labouriau ML, Casseti W, Ferraz-Vincentini KR et al (1997) Late Quaternary vegetational and climatic changes in Cerrado and palm swamp from central Brazil. Palaeogeogr Palaeoclimatol Palaeoecol 128:215–226

Satyamurti P, Nobre CA, Silva Dias P (1998) South America. In: Karoly D, Vincent DG (eds) Meteorology of the Southern Hemisphere. Meteorological Monograph, vol 27. American Meteorological Society, Boston, pp 119–139

Sifeddine A, Martin L, Turcq B et al (2001) Amazon rainforest variations. A sedimentological records covering 30 000 years BP. Palaeogeogr Palaeoclimatol Palaeoecol 168:221–235

Simões Filho FFL, Turcq B, Carneiro Filho A Souza AG (1997) Registros sedimentares de lagos e brejos dos campos de Roraima: Implicações paleoambientais ao longo do Holoceno. In: Barbosa RJ, Ferreira EJG, Castellon EG (eds) Ocupação humana, ambiente e ecologia em Roraima. INPA, Manaus

Stuiver M, Reimer PJ, Bard E et al Plicht JVD, Spurk M (1998) INTCAL 98 Radiocarbon Age Calibration 24,000-0 cal BP. Radiocarbon 40:1041–1083

Turcq B, Cordeiro RC, Albuquerque ALS et al (2002) Accumulation of organic carbon in five Brazilian lakes during the Holocene. Sediment Geol 148(1–2):319–342

Valdes PJ (2000) South American palaeoclimate model simulations: How reliable are the models? J Quat Sci 15(4):357–368
Wirrmann D, Mourguiart P (1995) Late Quaternary spatio-temporal limnological variations in the Altiplano of Bolivia and Peru. Quat Res 43:344–354
Zhao Y, Braconnot P, Marti O et al (2005) A multi-model analysis of the role of the ocean on the African and Indian monsoon during the mid-Holocene. Clim Dyn 25:777–800

Chapter 12
Millennial-Scale Ecological Changes in Tropical South America Since the Last Glacial Maximum

Dunia H. Urrego, Mark B. Bush, Miles R. Silman, Alexander Correa-Metrio, Marie-Pierre Ledru, Francis E. Mayle, Gina Paduano, and Bryan G. Valencia

Abstract An analysis of rates of ecological change (RoC) from thirteen pollen records from tropical South America is presented here. The analysis aims to identify the periods of fastest change since the last glacial maximum (LGM) and possible driving mechanisms. Despite rapid cooling periods, region-wide profound droughts, fire and human disturbances, RoC analysis showed that the speed of these climate changes never exceed the species response capabilities. Our results legitimize concerns regarding the resilience of species to accommodate future change and emphasize the urgency for integrative environmental measures.

Keywords Rates of ecological change · Climate change · Eastern Andes · Western Amazonia

12.1 Introduction

Human modifications of the landscape coupled with the indirect effects of human-induced pollution resulting in climate change pose synergistic threats to wildlife. While tropical ecosystems have been forced to accommodate prior environmental change (Colinvaux and De Oliveira 2000, Bush et al. 2004b, Mayle et al. 2004, Jansen et al. 2007), it is possible that modern rates of change are so rapid, and ensuing community disruption so severe, that we are poised on the brink of a major extinction event (Brooks et al. 2002, Thomas et al. 2004). While tropical ecosystems are known to be influenced by current climate change (Pounds 2001, Pounds et al. 2006), there are few data regarding tropical past rates of ecological changes and how they compare with modern ones. Under current and projected future climatic conditions, improbably fast migration rates will be required for species to track their fundamental niches (Malcolm et al. 2006). This scenario is further complicated by

D.H. Urrego (✉)
Department of Biological Sciences, Florida Institute of Technology, Melbourne, FL 32901, USA
e-mail: durrego@fit.edu

F. Vimeux et al. (eds.), *Past Climate Variability in South America and Surrounding Regions*, Developments in Paleoenvironmental Research 14,
DOI 10.1007/978-90-481-2672-9_12,

human-induced changes of landscapes such as land use, reduced habitat availability, and barriers to dispersal.

Assessments of rates of ecological changes in Europe and North America showed that temperature and atmospheric CO_2 fluctuations account for the greatest rates of post-LGM (last glacial maximum) ecological change (Jacobsen et al. 1987, Huntley 1990, Williams et al. 2001, Shuman et al. 2005). In temperate systems the rates of ecological change were probably slower than those of climatic fluctuations induced by the meltwater pulse at c. 14 ka, the Younger Dryas (12.5–11 ka), and the 8.2 ka cooling event (all ages are expressed in thousand of calibrated years BP and abbreviated as ka). Consequently, species may have existed in non-equilibrial assemblages, giving rise to the peak occurrence of no-analog communities (e.g. Williams et al. 2004). Orlóci et al. (2006) detected a strong correlation between species compositional change and the Vostok temperature record in several sites worldwide, including two records from eastern South America. Studies from gallery forest and savanna systems in southeastern Amazonia reveal what appears to be an accelerating rate of ecological change within the last 4000 years (Behling et al. 2005, Behling et al. 2007). These increases were correlated with the intensification of human occupation and human-induced fires in the region. However, an integrative regional analysis for western Amazonia, the area with the highest biodiversity, is lacking.

The extent of Holocene ecological variability in tropical South America was traditionally considered small relative to Quaternary glacial and interglacial fluctuations. This idea of relative Holocene stability was founded mostly on high-latitude evidence of stable temperatures since c. 10 ka (Alley 2004). Recent tropical evidence suggested that Holocene environmental change was greater than traditionally thought and that it correlated with abrupt changes in precipitation and increased human occupation (Mayle et al. 2000, De Freitas et al. 2001, Burbridge et al. 2004, Bush et al. 2004b, Mayle and Power 2008). From these observations, Holocene rates of environmental change were hypothesized to be greater than those of the Late Pleistocene.

The purpose of this chapter is to review post-LGM rates of ecological change from western Amazonian and eastern Andean records. We aim to identify periods when the fastest environmental changes took place, and discern whether patterns of change are the same in lowland and high-elevation systems. An analysis of the possible driving mechanisms behind fast rates of change is also presented. In particular, we consider the effects of post-LGM rising temperatures, the role of abrupt cooling events like the Younger Dryas (YD) and the 8.2 ka events, the influence of mid-Holocene dry episodes, and the importance of fire and human occupation as modifying aspects of the landscape.

12.2 Rate-of-Change Analysis

Paleoecological records offer an invaluable opportunity to answer questions regarding the speed of past ecological changes and to improve our understanding of past climate and human-induced variability in western Amazonia and the eastern

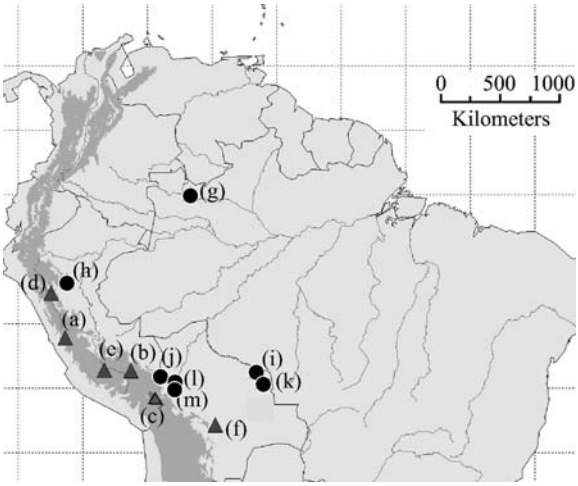

Fig. 12.1 Geographic location of sites used for the rates of change (RoC) analysis: Anden records (*dots*, *a–f*) and western Amazonian records (*triangles*, *g–m*). (*a*) Junin; (*b*) Caserococha; (*c*) Titicaca; (*d*) Chochos; (*e*) Pacucha; (*f*) Siberia; (*g*) Pata; (*h*) Sauce; (*i*) Bella Vista; (*j*) Consuelo; (*k*) Chaplin; (*l*) Chalalan; (*m*) Santa Rosa

Andes (Orlóci et al. 2002). The rates of change (RoC) are defined here as the amount of ecological change per time unit, determined from pollen records. It is comparable with velocity of change previously calculated by Orlóci et al. (2002). Fossil pollen extracted from lacustrine sediments reflects the community composition around the lake and allows statistical comparisons to be made within and between records (e.g. Birks and Birks 1980). In these analyses, plant compositional changes were derived from fossil pollen analyzed at discrete points in time, herein called time slices. We calculated RoC as the dissimilarity between pollen assemblages from two adjacent time slices divided by the time interval between them. Records were used where the chronology was sufficiently robust to allow pausible linear interpolations between dates and where sample intervals were relatively brief (Figs. 12.1 and 12.2). The underlying assumptions of such analyses were that sedimentation was continuous between time slices and that ecological change was continuous between samples. The RoC analysis was only attempted for core sections meeting these basic requirements. Age models constructed by original authors were used when provided. In records where only radiocarbon dates were available, age models were calculated based on calibrated ages using Calib 5.0.2 (Stuiver and Reimer 1993, Stuiver and Reimer 2005) with linear interpolation between dates.

The dissimilarity between time slices was calculated as the Euclidean distance among scores on the first three axes derived from ordination analyses (Hill and Gauch 1980). This dissimilarity measure represented the geometric (Pythagorean) distance between two samples in the ordination space and corresponded to the change in the forest composition during a given time interval. The units of these dissimilarity measures were fractions of each dataset's total variability, which facilitates relative comparisons among time slices within the same record. However, it should be noted that comparisons among records were done based on the trend of RoC, as comparisons of the absolute magnitudes are meaningless. The DCA was

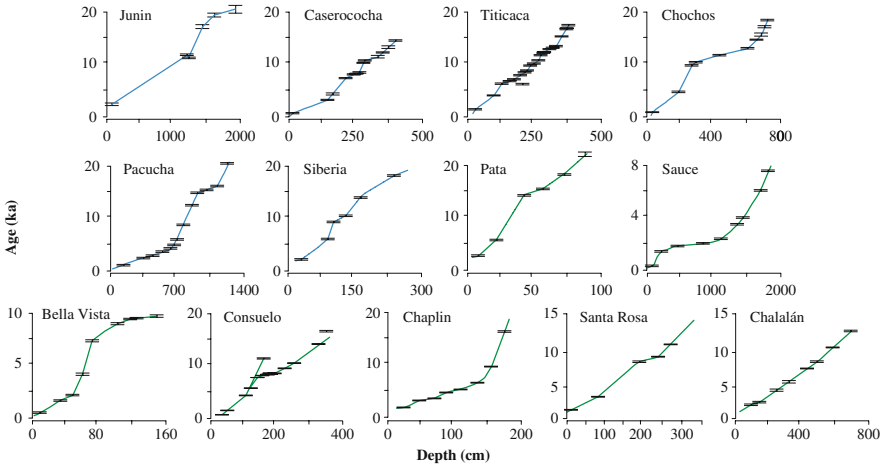

Fig. 12.2 Age-depth curves and age error for thirteen paleoecological records used in the RoC analysis (see Table 12.1 for source and site description)

performed on reduced pollen percentage matrices for thirteen paleoecological sites from western Amazonia and the eastern Andes (Table 12.1 and Fig. 12.1). For all ordinations, iterations were run until a stable solution was reached. The reduced pollen percentage matrices resulted from applying an abundance and persistence filter that preserves the main variability of pollen datasets, while eliminating the noise caused by rare taxa (after Birks and Birks 1980). This filter retained terrestrial taxa with at least 1% (abundance) and occurring in at least 5 time slices per record (persistence). Spores and shoreline elements were excluded to avoid masking terrestrial-vegetation changes. The decision for non-woody taxa such as Cyperaceae was based on their role in the specific modern ecosystems of each site. Cyperaceae were included in the analysis for sites where they were known to be important components of the terrestrial vegetation (e.g. Titicaca, Chaplin and Bella Vista) but excluded for sites where they mostly represent shoreline vegetation (e.g. Consuelo, Pata, Chalalán).

12.3 Paleoecological Records

The RoC analysis is based on thirteen pollen records from western Amazonia and the eastern Andes spanning at least the last 18 ka (Fig. 12.2 and Table 12.1). Andean sites lie on the eastern slopes of the Andes and parts of the Altiplano ranging from 2900 to 4100 m elevation (Table 12.1). Lowland sites include pollen records between the Equator (Lake Pata in Northwestern Brazil) and 14°S (Lakes Chaplin and Bella Vista in eastern Bolivia) and from 100 m elevation to the modern lower limit of permanent cloud cover (Lake Consuelo 1360 m.a.s.l.) (Table 12.1).

Table 12.1 Description of pollen records from western Amazonia and the eastern Andes used for the rates of change analysis (see Fig. 12.2 for geographic location)

Site*	Latitude	Longitude	Altitude (m.a.s.l.)	Wet-season precipitation (mm)†	Annual precipitation (mm/year)†	No. of taxa included in analysis	Source
Junin[a]	11°05′S	76°22′W	4100	156	945	49	Hansen et al. 1984
Caserococha[b]	13°39′S	71°17′W	3980	142	726	20	Paduano 2001
Titicaca[c]	16°20′S	65°59′W	3810	190	1136	35	Paduano et al. 2003
Chochos[d]	7°38′S	77°28′W	3285	180	1176	46	Bush et al. 2005
Pacucha[e]	13°36′S	73°19′W	3050	168	911	42	Valencia 2006
Siberia[f]	17°50′S	64°43′W	2920	142	730	49	Mourguiart and Ledru 2003
Pata[g]	0°16′N	66°41′W	300	363	2893	22	Bush et al. 2004a
Sauce[h]	6°43′S	76°13′W	600	161	1419	153	Correa-Metrio 2006
Bella Vista[i]	13°37′S	61°33′W	170	276	1562	35	Mayle et al. 2000, Burbridge et al. 2004
Consuelo[j]	13°57′S	68°59′W	1360	362	2395	70	Bush et al. 2004b, Urrego 2006
Chaplin[k]	14°28′S	61°04′W	175	256	1445	26	Mayle et al. 2000, Burbridge et al. 2004
Chalalán[l]	14°25′S	67°55′W	330	278	1883	34	Urrego 2006
Santa Rosa[m]	14°28′S	67°52′W	350	279	1902	36	Urrego 2006

*Nomenclature as in Figs. 12.1 and 12.2; [a–f] high-elevation Andean records; [g–m] lowland western Amazonian records; † annual precipitation and precipitation wettest quarter from WorldClim dataset (Hijmans et al. 2005)

12.3.1 Andean vs Western Amazonian Changes

Our RoC analysis illustrated clear differences between the timing and intensity of ecological changes in lowland and high-elevation sites during the past 18 ka (Fig. 12.3). Fluctuations in RoC were mostly concentrated in the Holocene period in lowland records while montane sites showed conspicuous oscillations both during the Holocene and the Late Pleistocene. In Lake Junin, located at 4100 m elevation, peaks in RoC occurred between 13 and 11 ka (Fig. 12.3a). This period of rapid change coincided with the final ice retreat identified from moraine patterns in the lake's catchment (Hansen et al. 1984). Lake Caserococha showed the fastest RoC during the Pleistocene-Holocene transition between 13.1 and 8.5 ka (Fig. 12.3b). These fluctuations that began 12.9 ka and lasted until 8.5 ka, pre-date the Younger Dryas (YD) cooling event (12.5–11 ka), suggesting that this relatively short-cooling was not the mechanism behind them (Paduano 2001). Mid-Holocene lowstands were also reported for Lake Caserococha but were not detected as periods of increased changes in the terrestrial vegetation. Lake Titicaca showed relatively steady RoC during the Late Pleistocene (Fig. 12.3c). Although a series of pulses were revealed around the YD episode, these changes have been attributed to the onset of postglacial fires rather than cooling (Paduano et al. 2003). During the Holocene, however, two periods of increased change were observed. The first period dated between 8 and 6 ka, when several peaks in the RoC were associated with reduced-moisture episodes (Paduano et al. 2003, Theissen et al. in press). The second period of increased change took place in the Late-Holocene and corresponded to a shift toward weedy vegetation associated with human activities (Paduano et al. 2003). Timing of this change coincided with the onset of Quinoa cultivation in southern Peru (Chepstow-Lusty et al. 2003).

Laguna de Chochos (3285 m) showed marked oscillations during deglacial phases from c. 14.5 to 11 ka (Fig. 12.3d), while the highest RoC occurred during the early Holocene. Late-Pleistocene peaks coincided with a drought period that lowered lake level between c. 9 and 7.2 ka (Bush et al. 2005). During this period, a *Polylepis* forest dominated the landscape and fire frequency increased at Chochos. At c. 1 ka this record showed a marked increase in RoC, probably related to human occupation of the site (Bush et al. 2005). Human intervention was also inferred to account for the highest RoC in Lake Pacucha (3050 m) (Valencia 2006) between c. 6 and 3 ka (Fig. 12.3e). Increased abundance of *Ambrosia* and Amaranthaceae-Chenopodiaceae were attributed to the construction of agricultural terraces and Quinoa cultivation by pre-Colombian peoples (Chepstow-Lusty and Winfield 2000, Valencia 2006). Between 12 and 6 ka, two periods of reduced precipitation at Lake Pacucha were evidenced from the replacement of *Isöetes* and *Myriophyllum* by Cyperaceae in the shoreline vegetation (Valencia 2006), reduction of freshwater diatoms, and increased calcium carbonate in the sediments (Hillyer et al. 2009). However, the RoC based on terrestrial vegetation did not differ from that of the background (Fig. 12.3e) suggesting that the terrestrial vegetation response to drought was gradual and that the most significant moisture-balance change occurred as a result of a reduction in wet-season precipitation (Valencia

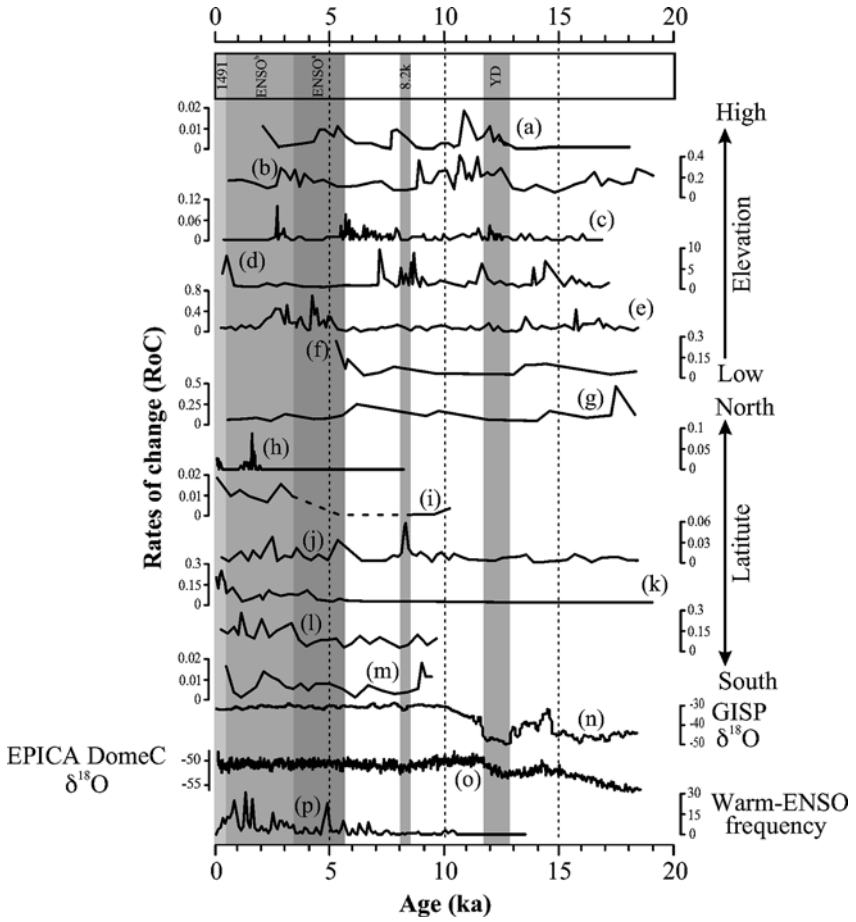

Fig. 12.3 Rates of change from several lacustrine pollen records over the past 18 ka (see Table 12.1 for source and site description). Eastern Andean records plotted on an elevational gradient (a–f); from high to low elevation: (*a*) Junin; (*b*) Caserococha; (*c*) Titicaca; (*d*) Chochos; (*e*) Pacucha; (*f*) Siberia. Western Amazonian records plotted on a latitudinal gradient (g–m), from North to South: (*g*) Pata; (*h*) Sauce; (*i*) Bella Vista; (*j*) Consuelo; (*k*) Chaplin; (*l*) Chalalán; (*m*) Santa Rosa. Other records plotted for comparison: temperature reconstruction based on stable isotope analysis, (*n*) from GISP (Alley 2004), (*o*) from EPICA Dome C (Monnin et al. 2001); (*p*) number of warm-ENSO events (Moy et al. 2002); YD: Younger Dryas (Broecker 1998); 8.2k: 8.2-ka cooling events (Alley et al. 1997); ENSO^a: period of modern-frequency warm-ENSO events (Sandweiss et al. 1996); ENSO^b: period of intensified warm-ENSO events (Sandweiss et al. 1996); 1491: onset of European colonization. RoC are based on detrended correspondence analyses performed on percentage pollen data and Euclidean distance among ordination axes. Note that RoC scales are relative to total variance within each dataset

2006). In the Lake Siberia record, trends of community change resemble those of lowland records, which may be related to sharing the same Amazonian moisture sources. Post-LGM changes in Siberia were minimal, with slightly increased RoC

between 18 and 16 ka (Fig. 12.3f). This increase was mostly driven by a downslope migration of the puna-cloud forest limit, characterized by the colonization of *Polylepis-Acaena* (Mourguiart and Ledru 2003). No evidence of drought-caused increases of RoC was observed during the mid-Holocene in Siberia. However, a close examination of charcoal peaks in Siberia (Mourguiart and Ledru 2003, Fig. 12.1) showed a rough coincidence in timing with low lake-level stands in Pacucha (Valencia 2006, Hillyer et al. 2009), suggesting that increased fires may be related to reduced moisture availability in the region. Highest RoC between c. 7 and 5 ka coincided with increased fire frequency associated with the beginning of human activities (Mourguiart and Ledru 2003) or possibly with intensified ENSO activity as proposed by Haberle and Ledru (2001). Unfortunately, in the Siberia record the top 30 cm of the sediment column were lost during coring, hence no record was available for the past 5 ka.

Unlike Andean records which have highest RoC in the Late Pleistocene, records from lowland western Amazonia showed high RoC concentrated in the Holocene (Fig. 12.3 g–m). A few minutes North of the Equator, Lake Pata showed a large Pleistocene RoC peak, not observed in any of the other lowland records (Fig. 12.3 g). This prominent peak was centered around 18 ka and was probably associated with post-LGM temperature increase (Bush et al. 2004a). Following this period of substantial forest change, the Pata record showed another increase in RoC around 6 ka that coincided with increases of herbaceous understory elements suggesting a less dense forest canopy consistent with a reduction in precipitation (Mayle and Power 2008). RoC changes in the Pata record were derived from large time intervals (i.e. as much as 3000 years), hence its low sensitivity to short-lived events such the YD and 8.2 ka events.

Lake Sauce (6°S) provided a high-resolution Holocene record characterized by relatively constant RoC throughout the early and mid-Holocene (Fig. 12.3 h). These virtually constant RoC did not mean that the forest was unchanged, but rather that the speed of these changes was roughly constant. Analyses of El Niño Southern Oscillation (ENSO) activity suggested increased frequency after c. 5.5 ka (Fig. 12.3 p, Sandweiss et al. 2001) and strengthening of the oscillation in the last 1500 years (Fig. 12.3p, Moy et al. 2002). However, the existing records accounted for variability in the warm-phase, El Niño portions of the cycle. The multiproxy record of Lake Sauce showed a strong correlation with the frequency and intensity of both cold and warm ENSO phases in western Amazonia (Correa-Metrio 2007). From 1.8 to 1.1 ka, the high RoC in Sauce (Fig. 12.3 h) coincided with a period that apparently had c. 30 strong El Niño and La Niña events per century; the highest concentration in the last 6 ka (Correa-Metrio 2007). Enhanced ENSO activity in the mid-Holocene was hypothesized to have induced the most rapid changes in terrestrial vegetation in Sauce within the last 6 ka (Correa-Metrio 2007).

The RoC for Lake Bella Vista between 8.5 and 3 ka were plotted as a discontinuous line because we could not establish whether a marked reduction in sedimentation was associated with a sedimentary hiatus (Fig. 12.3i). High RoC are concentrated during the past 3 ka in Bella Vista and sustained until the present. Such large community changes in the Bolivian lowlands were attributed to a reduction in open savannas as forests expanded in response to a gradual increase in mean annual

precipitation (Mayle et al. 2000, Burbridge et al. 2004). The trend of forest expansion is evident in the Lake Chaplin data (Fig. 12.3 k), with the onset of high RoC at c. 3 ka and an intensification of community change around 1 ka. The greater sensitivity of Lake Chaplin, compared with Bella Vista, to Late-Holocene forest expansion may be explained by its proximity to the southern limit of Amazonian forest (i.e. 30 km as opposed to 120 km for Lake Bella Vista) (Mayle et al. 2000, Burbridge et al. 2004). In Lake Consuelo, RoC showed significant differences between the Pleistocene and Holocene periods (Fig. 12.3j). Variability in Pleistocene RoC was much less than that of the Holocene, despite an almost complete forest turnover between 20 and c. 12 ka (Bush et al. 2004b). Even with a 5.5°C Pleistocene cooling relative to modern, the deglacial warming resulted in incremental rather than sudden changes in forest composition. During the Holocene, a significant change in sedimentation rates was identified based on radiocarbon dating of two parallel cores from Lake Consuelo and was attributed to a period of reduced precipitation in the region (Urrego 2006). The effect of this episode on both lake level and forest composition was greater than that caused by any ecological change associated with the LGM or deglaciation. Within the last 3.5 ka, RoC were more variable, with the largest spike around 2.2 ka (Fig. 12.3j). Overall, the results from the RoC analysis of Lake Consuelo suggested that moisture availability, possibly mediated through cloud cover, played the most significant role in rapid ecological change in this system (Bush et al. 2004b).

Also in the western Amazonian lowlands, Lakes Chalalán and Santa Rosa lie c. 450 km West of Chaplin and Bella Vista. RoC in Chalalán and Santa Rosa showed oscillations throughout the Holocene, with a generally increasing trend toward the present (Fig. 12.3 l–m). Lake Santa Rosa showed a peak in RoC during the early stages of the lake, which may be associated with rapid changes in the forest edge due to the stabilization of a new permanent water body (Fig. 12.3m). This tendency was not observed in Lake Chalalán and was attributable to bathymetric differences between these lakes. Today, Santa Rosa is much shallower than Chalalán and has a flat bottom with gentle side slopes. This bathymetric morphology makes its record more sensitive to changes in the forest-edge vegetation. The RoC in Lake Chalalán were relatively small between 8 and 3 ka (Fig. 12.3 l), despite pollen evidence of drier or more-seasonal conditions (Urrego 2006). This evidence included increased abundance of dry forest elements but not a complete replacement of the mesic vegetation. These data suggested that the reduction in precipitation may have been more marked in the wet-season than in the dry season (Urrego 2006). Both the Chalalán and Santa Rosa records suggested that the regional mid-Holocene dry event documented elsewhere (Mayle et al. 2000, Bush et al. 2005) had only a modest influence on these forests. Late-Holocene RoC showed a few shifts in community composition associated with increased precipitation and possibly human disturbance in the last millennium (Urrego 2006).

12.3.2 Drivers of Change

Post-LGM vegetation responses to climate changes in tropical South America remain controversial on issues such as deglacial timing (Seltzer et al. 2002,

Thompson 2005), the effect of warming and moisture fluctuations (Maslin and Burns 2000, Harrison et al. 2003, de Toledo and Bush 2007, Mayle et al. 2007), and the effect of ENSO anomalies on the eastern flank of the Andes (Vuille et al. 2003). Whether rapid cooling events such as the Younger Dryas and the 8.2 ka event are detectable in the southern Neotropics remains to be resolved (Thompson et al. 1998, Alley et al. 2003, Paduano et al. 2003). Fire is another important process driving ecological change in almost all records from the Andes and western Amazonia at millennial timescales. In this section, we discuss these climatic and physical mechanisms focusing on their role in shaping terrestrial plant communities.

12.3.2.1 Temperature

After the LGM, the most important temperature-driven global oscillation associated with the glacial period was probably the onset of deglaciation. The LGM global chronozone is defined as being between 24 and 18 ka (Mix et al. 2001). However, in the Andes and western Amazonia, deglaciation probably began between 22 and 19 ka (Rodbell 1993, Mark et al. 2002, Seltzer et al. 2002, Bush et al. 2004b, Smith et al. 2005). While deglacial warming started some 5000 years earlier in the Neotropics than at Northern high latitudes, the process continued until c. 11 ka (Blunier and Brook 2001, Grootes et al. 2001). From the available paleoecological data, it seems probable that although there was an initial warming as early as 22 ka, this did not become a sustained trend until ca. 18 ka (Bush et al. 2004b). Our RoC analysis begins at 18 ka and a strong response to warming is evident in Lakes Pata (Fig. 12.3 g) and Caserococha (Fig. 12.3 c). At other sites the deglacial signature is more gradual and lacks defined peaks of change.

After the deglaciation, two important post-glacial global temperature reversals were the YD and the 8.2 ka event. The YD was the most significant rapid cooling period that occurred during the last deglaciation in the North Atlantic region, and was clearly recorded in the isotopic temperature reconstruction from GISP (Fig. 12.3n, Alley 2004). The RoC calculated from GISP showed rapid temperature changes before and after the YD (Fig. 12.3 n) indicating the abrupt nature of this episode. In tropical South America, the signal of the YD differed between the northern and central Andes. In the northern Andes of Colombia, this temperature reversal was ubiquitously recorded as a 4 to 6°C cooling (van der Hammen and Hooghiemstra 1995), while in the central Andes and western Amazonia, the impact of the YD remains unclear. In our analysis, high RoC around the YD were observed in Lake Junin, Caserococha and Chochos (Figs. 12.3a,b,d), although rapid cooling has not been suggested as the cause for these changes (Bush et al. 2005). A somewhat uncertain chronology around the YD in the Lake Junin record prevented us from establishing a definitive relationship at this site. At Caserococha and Chochos relatively robust chronologies (Fig. 12.2) and 100- and 200-year resolution, respectively, make these sites appropriate for an investigation of the YD. In Chochos, the RoC signal lagged by c. 1000 year the onset of the YD, while in Caserococha rapid RoC preceded the event. In the three lowland records presented here that span the YD period, no change in RoC was observed that coincided with the event. The

records from Lakes Pata, Chaplin and Consuelo showed relatively low changes during the temperature reversal, indicating that the YD either had no influence on the vegetation of western Amazonia or that it was too short to be recorded. Alternatively, this pattern could be due to poor dating or low sampling resolution. Overall, we were not able to identify changes in Andean or Amazonian records that were directly attributable to the YD event.

The 8.2 ka event was a short-lived cooling event triggered by freshwater inputs to the North Atlantic (Ellison et al. 2006), similar to the YD in its interhemispheric signature although much shorter in duration (c. 200 years) (Alley et al. 1997). No linkage between this rapid episode and terrestrial ecological changes in tropical South America has yet been documented. The marine sedimentary record from the Cariaco Basin reveals the presence of the 8.2 ka event when sedimentary changes suggested a period of enhanced winds or decreased precipitation (Hughen et al. 1996, Alley et al. 2003). Due to the short duration of this temperature reversal, high-resolution, well-dated records are necessary to discern its influence. Furthermore, sedimentation rates need to be high enough to capture such short events. Despite these limitations, we feel it is important to discuss potential linkages between community changes in tropical South America and the 8.2 ka event given the growing evidence of its signature in other tropical systems (Lamb et al. 1995, Mulitza and Rühlemann 2000, Thompson et al. 2002, Lachniet et al. 2004). Within our study region, records with sampling resolution and sedimentation rates high enough to reveal the effects of this event are available from Lakes Titicaca, Chochos and Pacucha.

RoC between 9 and 8 ka in Titicaca were low and preceded a period of increased variability (Fig. 12.3c). In Lake Chochos, the 8.2 ka event fell within a phase of enhanced variability of RoC, although it did not seem to have produced a particular oscillation (Fig. 12.3d). On the other hand, while RoC from terrestrial vegetation in Pacucha did not reveal significant changes around the event, other proxies, e.g. diatoms and $CaCO_3$ concentrations, reflected an increase in lake level consistent with increased precipitation (Hillyer et al. 2009).

12.3.2.2 Precipitation

The most prominent reduced-precipitation event that has been documented in post-glacial tropical South America is the Mid-Holocene Dry Episode (MHDE) (Mayle and Power 2008). This event has been recorded in several sites both in the northern Andes (Berrio et al. 2002), central Andes (Abbott et al. 1997, Seltzer et al. 1998, Baker et al. 2001, Rowe et al. 2002, Paduano et al. 2003, Theissen et al. in press) and western Amazonia (Mayle et al. 2000, De Freitas et al. 2001, Bush 2005), suggesting that it was regionally widespread. However, the timing and duration of the MHDE were not synchronous among records. In the Andean records used here, the influence of mid-Holocene dry conditions were clear in RoC from Lakes Junin, Caserococha, Titicaca, Chochos and Consuelo (Fig. 12.3). The weakness, or lack of, the MHDE signal in Lake Siberia, could be explained by the buffering effect of a semi-permanent cloud cover. Lake Consuelo, on the other hand, is

presently located right at the lower cloud-base limit (i.e. 1400 m elevation), which may have been displaced upslope as moisture availability was reduced during the mid-Holocene. In Lakes Pacucha, Chalalán, and Santa Rosa the influence of MHDE has been correlated with decreased wet-season precipitation and subtle forest compositional changes (Urrego 2006, Valencia 2006), but not with a complete terrestrial vegetation turnover. This observation could explain the absence of a conspicuous increase of RoC in the records corresponding to the MHDE (Fig. 12.3e,l,m).

Despite the evidence of a regional mid-Holocene dry phase in tropical South America, the driving forces behind this event have yet to be clarified. Hypothesized driving mechanisms include precessional fluctuations in solar forcing of the South American low-pressure systems (Lamb et al. 1995, Seltzer et al. 2000, Garreaud et al. 2003, Harrison et al. 2003, Theissen et al. 2008) and changes in tropical Pacific circulation and millennial-scale fluctuations of ENSO frequency (Sandweiss et al. 1996, Andrus et al. 2002, Riedinger et al. 2002). The RoC analysis could shed light on the effects of this regional drought on the vegetation but does not reveal the mechanism underlying the MHDE in western Amazonia or the eastern Andes. In general, the RoC data identified the MHDE as being a time of substantial and rapid community change in many of the systems studied.

Regarding ENSO, the analysis of community RoC in Lake Sauce supported the correlation with enhanced frequency of both warm and cold ENSO hypothesized by Correa-Metrio (2007). The onset of increased fire frequency in Siberia could also be correlated with intensified ENSO warm-phases since c. 5 ka (Haberle et al. 2001).

12.3.2.3 Fire

Fire has been an important natural mechanism in Andean and western Amazonian sites well before humans occupied the landscape. For instance at Lake Titicaca, fire has been a modifying component of the landscape for 370,000 years (Hanselman 2007). In Lakes Chochos and Siberia, Pleistocene and Holocene vegetation changes were attributed to increased fire frequency (Bush et al. 2005). Similarly, records from Chalalán and Santa Rosa in western Amazonia, showed rapid changes in RoC that correlate with increased fire intensity (Urrego 2006). In general, fluctuations in fire regimes at these sites could be responsible for the large amount of local variability detected in the RoC analysis, indicating the major role that fire has played in shaping tropical South American vegetation.

12.3.2.4 Human Disturbance

Records of human occupation in western Amazonia (Piperno 1990, Bush et al. 2007, de Toledo and Bush 2007) and the eastern Andes (Chepstow-Lusty et al. 2003) date back at least 7 ka and 12 ka, respectively, but only intensify during the Late Holocene. The overall RoC trend observed in both regions was of enhanced variability during last few millennia (Fig. 12.3), consistent with human-derived

modifications of the landscape. The lowland sites of Pata and Consuelo have no known history of human occupation (Bush et al. 2004a), and the Chaplin and Bella Vista records exhibit low late-Holocene charcoal concentrations during a time of forest expansion (Mayle et al. 2000, Burbridge et al. 2004).

Human intervention included deforestation, introduction of weeds, slash and burn, and agricultural practices, indicating that these are not new problems facing the Andes and Amazonia (Willis et al. 2004). Human influence was suggested for Lake Chochos as a deforestation signal as early as 6 ka (Bush et al. 2005) and at Lake Titicaca as an increase in weedy vegetation documented at c. 3.1 ka (Paduano et al. 2003). In Lake Siberia, the onset of human occupation was inferred at c. 7 ka when fire frequency increased (Mourguiart and Ledru 2003) and RoC also rose (Fig. 12.3f). In Lake Pacucha, high RoC at c. 5 ka resulted from an increase in Quinoa and *Ambrosia* (Valencia 2006) both of which are reported as important agroforestry elements of pre-Incan cultures (Chepstow-Lusty et al. 2003).

Our results support theories of human population demise following European colonization of the new world (Roosevelt et al. 1996, Denevan 2003, Heckenberger et al. 2003). RoC increase around 400–500 year BP, which we interpret to indicate the recovery of plant communities following abandonment at Chochos, Sauce, Chalalán and Santa Rosa (Fig. 12.3). Similarly, we expect a second peak during the last two centuries as human populations and European influence expanded exponentially in the region. However, the temporal resolution of most of the records is not high enough to reveal this change. The best evidence for this post-conquest population recovery and landscape change is found in the RoC from Sauce (Fig. 12.3 h), where the paleoecological record has decadal resolution during the past 1000 years.

12.4 Overview

Paleoecological records from the eastern Andes and lowland western Amazonia show great variability both during the Pleistocene and the Holocene. Despite the scattered network of records, RoC peaks appear to be frequent during both the Pleistocene and Holocene in the Andes while being more concentrated in the Holocene period at lowland sites. In light of these differences, we hypothesize that the lack habitat availability makes montane systems like the Andes more sensitive to climate change than the Amazon lowlands. In the lowlands, species have been able to migrate in any direction as local conditions became unfavorable, e.g. species no longer within their bioclimatic envelope. Such migrations could have led populations to migrate in terms of macrotopography, i.e. elevationally within the Andes, or in microtopography, i.e. from terra firme to gallery forests. In the Andes, an upslope migration of species due to warming results in less occupiable space because mountains are effectively cone shaped. In areas where large high-elevation plateaus exist, they lie above modern tree line and could only be occupied by trees if warming is accompanied by increased moisture. Consequently, as migration proceeds

habitat suitable for forest would inexorably decrease, increasing the vulnerability of populationss and species to extinction. If true, our hypothesis would have large implications for the conservation of tropical South American ecosystems in the light of future climate change.

Fluctuations in terrestrial plant assemblages are the result of multiple driving mechanisms, including temperature and precipitation changes, fire frequency and ENSO. The marked response to short-sharp cooling events, e.g. the YD and 8.2 ka events, observed at high latitude was not evident in our study area. However, we recognize that the number of suitable records to detect such fine-scale variability is still small. We predict that further high-resolution examination of tropical South American records with high sedimentation rates may reveal pulses of change caused by events like the YD. Evidence of the MHDE is regionally consistent but its impact on ecosystems differed at the local scale according to the extent to which sites were buffered from moisture deficit. While in Lake Consuelo, mid-Holocene dry events were associated with the lifting of the cloud base and vegetation changes indicative of lowered lake levels, in Lakes Pacucha, Chalalán, and Santa Rosa, the changes were not as pronounced. In the two latter sites, reduction of wet-season precipitation has been hypothesized to produce the observed changes. Impacts of MHDE are evident virtually in all records from the eastern Andes and western Amazonia, although the driving mechanisms behind its occurrence remain unclear. The only records with a sedimentation rate and depositional regime suitable to study ENSO variability in the region are those of Lake Sauce, Peru (Correa-Metrio 2007, and Pallcacocha) Ecuador (Rodbell et al. 1999, Moy et al. 2002). Those records depict a consistent image of ENSO variability with Lake Sauce providing the first detailed reconstruction of La Niña-dominated phases.

Overall, the RoC analysis showed that the timing of major changes in forest composition was essentially local rather than regional, making widespread patterns the exception rather than the norm. In the eastern Andes and western Amazonia, fire may be a major driver at the local scale, as it was recorded and correlated with changes in all sites with the exception of those from hyper-humid locales (i.e. Pata). Many records show accelerated RoC during the past 3000 years attributable to intensification of human activities. A clear outcome of this analysis is that ecological rates of change from both eastern Andean and the western Amazonian ecosystems have kept pace with the rates of climate changes since the LGM. Such coupling has been possible because rates of climatic change did not exceed the species response capability. Anticipated rates of warming for the next century (IPCC 2002) are likely to challenge the ability of species to keep pace with the geographic movement of their climatic envelope (Malcolm et al. 2006). Landscapes modified by human activities will add barriers impeding needed migration and may trigger an extinction event (Brooks et al. 2002). Our results legitimize concerns regarding the resilience of species to accommodate future change and emphasize the urgency for effective and prompt conservation measures, and the reduction of greenhouse gas emissions.

References

Abbott MB, Seltzer GO, Kelts KR, Southon J (1997) Holocene paleohydrology of the tropical Andes from lake records. Quat Res 47:70–80

Alley RB (2004) GISP2 Ice Core Temperature and Accumulation Data. IGBP PAGES/World Data Center for Paleoclimatology Data Contribution Series #2004-013, NOAA/NGDC Paleoclimatology Program, Boulder CO, USA

Alley RB, Marotzke J, Nordhaus WD et al (2003) Abrupt Climate Change. Science 299:2005–2010

Alley RB, Mayewski PA, Sowers T et al (1997) Holocene climatic instability: A prominent, widespread event 8200 yr ago. Geology 25:483–486

Andrus CFT, Crowe DE, Sandweiss DH et al (2002) Otolith $d^{18}O$ Record of Mid-Holocene Sea Surface Temperatures in Peru. Science 295:1508–1511

Baker PA, Seltzer GO, Fritz SC et al (2001) The history of South American tropical precipitation for the Past 25,000 years. Science 291:640–643

Behling H, Pillar VD, Bauermann SG (2005) Late Quaternary grassland (Campos), gallery forest, fire and climate dynamics, studied by pollen, charcoal and multivariate analysis of the Sao Francisco de Assis core in western Rio Grande do Sul (southern Brazil). Rev Palaeobot Palynol 133:235–248

Behling H, Pillar VD, Müller SC, Overbeck GE (2007) Late-Holocene fire history in a forest-grassland mosaic in southern Brasil: Implications for conservation. Appl Veg Sci 10:81–90

Berrio JC, Hooghiemstra H, Behling H et al (2002) Late-Quaternary savanna history of the Colombian Llanos Orientales from Lagunas Chenevo and Mozambique a transect synthesis. Holocene 12(1):35–48

Birks HJB, Birks HH (1980) Quaternary palaeoecology. University Park Press, Baltimore

Blunier T, Brook EJ (2001) Timing of Millennial-scale climate change in Antarctica and Greenland during the last glacial period. Science 291:109–112

Broecker WS (1998) Paleocean circulation during the last deglaciation: A bipolar seesaw? Paleoceanography 13:119–121

Brooks TM, Mittermeier RA, Mittermeier CG et al (2002) Habitat loss and extiction in the hotspots of Biodiversity. Conserv Biol 16:909–923

Burbridge RE, Mayle FE, Killeen TJ (2004) Fifty-thousand-year vegetation and climate history of Noel Kempff Mercado National Park, Bolivian Amazon. Quat Res 61:215–230

Bush MB (2005) Holocene climates of the lowland tropical forests. In: Mackay A, Battarbee R, Birks J, Oldfield F (eds) Global Change in the Holocene. Academic Press, New York, pp 293–306

Bush MB, De Oliveira PE, Colinvaux PA et al (2004a) Amazonian paleoecological histories: One hill, three watersheds. Palaeogeogr Palaeoclimatol Palaeoecol 214(4):359–393

Bush MB, Hansen BCS, Rodbell DT et al (2005) A 17 000-year history of Andean climate and vegetation change from Laguna de Chochos, Peru. J Quat Sci 20:703–714

Bush MB, Silman MR, de Toledo MB et al (2007) Holocene fire and occupation in Amazonia: Records from two lake districts. Phil Trans R Soc B 362(1478):209–218

Bush MB, Silman MR, Urrego DH (2004b) 48,000 years of climate and forest change in a biodiversity hot spot. Science 303:827–829

Chepstow-Lusty A, Frogley MR, Bauer BS et al (2003) A late Holocene record of arid events from the Cuzco region, Peru. J Quat Sci 18:491–502

Chepstow-Lusty A, Winfield M (2000) Inca Agroforestry: Lessons from the Past. Ambio 29:322–328

Colinvaux PA, De Oliveira PE (2000) Palaeoecology and climate of the Amazon basin during the last glacial cycle. J Quat Sci 15:347–356

Correa-Metrio A (2007) Reconstruccion de la sucesion y los cambios ambientales durante el Holoceno en la cuenca del Lago Sauce, Nororiente del Perú. Escuela de Geociencias. Medellin, Universidad Nacional de Colombia. MSc:120

De Freitas HA, Pessenda LCR, Aravena R et al (2001) Late Quaternary vegetation dynamics in the southern Amazon Basin inferred from carbon isotopes in soil organic matter. Quat Res 55:39–46

de Toledo MB, Bush MB (2007) A mid-Holocene environmental change in Amazonian savannas. J Biogeogr 34:1313–1326

Denevan WM (2003) Cultivated landscapes of native Amazonia and the Andes. Oxford University Press, Oxford, England

Ellison CRW, Chapman MR, Hall IR (2006) Surface and deep ocean interactions during the cold climate event 8200 years ago. Science 312:1929–1932

Garreaud R, Vuille M, Clement A (2003) The climate of the Altiplano:observed current conditions and mechanisms of past changes. Palaeogeogr Palaeoclimatol Palaeoecol 194:5–22

Grootes PM, Steig EJ, Waddington ED et al (2001) The Taylor Dome Antarctic ^{18}O Record and Globally Synchronous Changes in Climate. Quat Res 56:289–298

Haberle SG, Hope GS, van der Kaars WA (2001) Biomass burning in Indonesia and Papua New Guinea: Natural and human induced fire events in the fossil record. Palaeogeogr Palaeoclimatol Palaeoecol 171:259–268

Haberle SG, Ledru MP (2001) Correlations among charcoal records of fires from the past 16,000 years in Indonesia, Papua New Guinea, and Central and South America. Quat Res 55:97–104

Hanselman JA (2007) A 370,000-yr history of vegetation and climate change around Lake Titicaca (Bolivia/Peru). Biological Sciences. Melbourne, FL, Florida Institute of Technology. PhD:210

Hansen BCS, Wright HEJ, Bradbury JP (1984) Pollen studies in the Junín area, Central Peruvian Andes. Geol Soc Am Bull 95:1454–1465

Harrison SP, Kutzbach JE, Liu Z et al (2003) Mid-Holocene climates of the Americas: A dynamical response to changed seasonality. Clim Dyn 20:663–688

Heckenberger MJ, Kuikuro A, Kuikuro UT et al (2003) Amazonia 1492: Pristine forest or cultural Parkland. Science 301:1710–1714

Hijmans RJ, Cameron SE, Parra JL et al (2005) Very high resolution interpolated climate surfaces for global land areas. Int J Climatol 25:1965–1978

Hill MO, Gauch HG (1980) Detrended correspondence analysis: An improved ordination technique. Vegetatio 42:47–58

Hillyer R, Bush M, Valencia BG et al (2009) A 24,000-year paleolimnological history from the Peruvian Andes. Quat Res 71:71–82

Hughen KA, Overpeck JT, Peterson LC, Trumbore S (1996) Rapid climate changes in the tropical Atlantic region during the last deglaciation. Nature 380:51–54

Huntley B (1990) European post-glacial forests: Compositional changes in response to climatic change. J Veg Sci 1:507–518

IPCC (2002) Climate change and biodiversity. Geneva-Switzerland, p 85

Jacobsen GL Jr, Webb III T, Grimm EC (1987) Patterns and rates of vegetation change during the deglaciation of eastern North America. In: Ruddiman WF, Wright HE Jr (eds) North America and Adjacent Oceans during the last deglaciation. Geological society of America, Boulder, CO, pp 277–288

Jansen E, Overpeck J, Briffa KR et al (2007) Paleoclimate. Climate Change 2007: The Physical Science Basis. In: Solomon S, Qin D, Manning M, Chen Z, Marquis M, Averyt KB, Tignor M, Miller HL (eds) Contribution of Working Group I to the Fourth Assessment of the IPCC. Cambridge University Press, Cambridge, UK and New York, USA

Lachniet MS, Asmerom Y, Burns S et al (2004) Tropical Response to the 8200 yr cold event? Speleothem isotopes indicate a weakened early Holocene monsoon in Costa Rica. Geology 32:957–960

Lamb HF, Gasse F, Benkaddour A et al (1995) Relation between century-scale Holocene arid intervals in tropical and temperate zones. Nature 373:134–137

Malcolm JR, Liu C, Neilson RP et al (2006) Global warming and extinctions of endemic species from biodiversity hotspots. Conserv Biol 20(2):538–548

Mark BG, Seltzer GO, Rodbell DT, Goodman AY (2002) Rates of Deglaciation during the Last Glaciation and Holocene in the Cordillera Vilcanota-Quelccaya Ice Cap Region, Southeastern Peru. Quat Res 57:287–298

Maslin MA, Burns SJ (2000) Reconstruction of the Amazon Basin Effective Moisture Availabillity over the Past 14,000 Years. Science 290:2285–2287

Mayle FE, Beerling DJ, Gosling WD, Bush MB (2004) Responses of Amazonian ecosystems to climatic and atmospheric carbon dioxide changes since the Last Glacial Maximum. Phil Trans R Soc B 359(1443):499–514

Mayle FE, Burbridge R, Killeen TJ (2000) Millennial-Scale Dynamics of Southern Amazonian Rain Forests. Science 290:2291–2294

Mayle FE, Langstroth RP, Fisher RA, Meir P (2007) Long-term forest-savannah dynamics in the Bolivian Amazon: Implications for conservation. Phil Trans R Soc Lond B 362:291–307

Mayle FE, Power MJ (2008) Impact of a drier early-mid Holocene climate upon Amazonian forests. Phil Trans R Soc B 363(1498):1829–1838

Mix A, Bard E, Schneider R (2001) Environmental processes of the Ice Age: Land, oceans, glaciers (EPILOG). Quat Sci Rev 20(4):627–657

Monnin E, Indermühle A, Dällenbach A et al (2001) Atmospheric CO2 Concentrations over the Last Glacial Termination. Science 291:112–114

Mourguiart P, Ledru MP (2003) Last Glacial Maximum in an Andean cloud forest environment (Eastern Cordillera, Bolivia). Geology 31:195–198

Moy CM, Seltzer GO, Rodbell DT, Anderson DM (2002) Variability of El Niño/Southern Oscillation activity at millenial timescales during the Holocene epoch. Nature 420:162–165

Mulitza S, Rühlemann C (2000) African monsoonal precipitation modulated by interhemispheric temperature gradients. Quat Res 53:270–274

Orlóci L, Pillar VD, Anand M (2006) Multiscale analysis of palynological records: New possibilities. Community Ecol 7:53–67

Orlóci L, Pillar VD, Anand M, Behling H (2002) Some interesting characteristics of the vegetation process. Community Ecol 3:125–146

Paduano G (2001) Vegetation and fire history of two tropical Andean lakes, Titicaca (Peru/Bolivia), and Caserochocha (Peru) with special emphasis on the Younger Dryas chronozone. Department of Biological Sciences. Melbourne, Florida Institute of Technology:319

Paduano GM, Bush MB, Baker PA et al (2003) A vegetation and fire history of Lake Titicaca since the Last Glacial Maximum. Palaeogeogr Palaeoclimatol Palaeoecol 194:259–279

Piperno DR (1990) Aboriginal agriculture and land usage in the Amazon Basin, Ecuador. J Archaeol Sci 17:665–677

Pounds JA (2001) Climate and amphibian declines. Nature 410:639–640

Pounds JA, Bustamante MR, Coloma LA et al (2006) Widespread amphibian extinctins from epidemic disease driven by global warming. Nature 439:161–167

Riedinger MA, Steinitz-Kannan M, Last WM, Brenner M (2002) A 6100 ^{14}C yr record of El Nino activity from the Galapagos Islands. J Paleolimnol 27:1–7

Rodbell DT (1993) Subdivision of late Pleistocene moraines in the Cordillera Blanca, Peru, based on rock weathering features, soils and radiocarbon dates. Quat Res 39:133–143

Rodbell DT, Seltzer GO, Anderson DM et al (1999) An ~15,000-year record of El Niño-driven alluviation in southwestern Ecuador. Science 283:516–520

Roosevelt AC, Lima da Costa M, Lopes Machado C et al (1996) Paleoindian cave dwellers in the Amazon: The peopling of the Americas. Science 272:373–384

Rowe HD, Dunbar RB, Mucciarone DA et al (2002) Insolation, Moisture Balance and Climate Change on the South American Altiplano since the Last Glacial Maximum. Clim Change 52:175–199

Sandweiss DH, Maasch KA, Burger RL et al (2001) Variation in Holocene El Niño frequencies:Climate records and cultural consequences in ancient Peru. Geology 29:603–606

Sandweiss DH, Richardson JBI, Reitz EJ et al (1996) Geoarchaeological evidence from Peru for a 5000 years B.P. onset of El Niño. Science 273:1531–1533

Seltzer G, Rodbell D, Burns S (2000) Isotopic evidence for late Quaternary climatic change in tropical South America. Geology 28(1):35–38

Seltzer GO, Cross S, Baker P et al (1998) High-resolution seismic reflection profiles from Lake Titicaca, Peru/Bolivia. Evidence for Holocene aridity in the tropical Andes. Geology 26:167–170

Seltzer GO, Rodbell DT, Baker PA et al (2002) Early warming of tropical South America at the last glacial-interglacial transition. Science 296:1685–1686

Shuman B, Bartlein PJ, Webb III T (2005) The magnitudes of millennial- and orbital-scale climatic change in Eastern North America during the late-quaternary. Quat Sci Rev 24:2194–2206

Smith JA, Seltzer GO, Farber DL et al (2005) Early local last glacial maximum in the tropical Andes. Science 308:678–681

Stuiver M, Reimer PJ (1993) Extended ^{14}C database and revised CALIB radiocarbon calibration program. Radiocarbon 35:215–230

Stuiver M, Reimer PJ (2005) CALIB Radiocarbon Calibration Program. Version 5.0.1html

Theissen KM, Dunbar RB, Rowe HD, Mucciarone DA (2008) Multidecadal-to century-scale arid episodes on the northern Altiplano during the middle Holocene. Palaeogeogr Palaeoclimatol Palaeoecol 257:361–376

Theissen KM, Dunbar RB, Rowe HD, Mucciarone DA (in press) Multidecadal-to century-scale arid episodes on the northern Altiplano during the middle Holocene. Palaeogeogr Palaeoclimatol Palaeoecol:doi:10.1016/j.palaeo.2007.09.011

Thomas CD, Cameron A, Green RE et al (2004) Extinction risk from climate change. Nature 427:145–148

Thompson LG (2005) Tropical ice core records: Evidence for asynchronous glaciations on Milankovitch timescales. J Quat Sci 20:723–733

Thompson LG, Davis ME, Mosley-Thompson E et al (1998) A 25,000-year tropical climate history from Bolivian ice cores. Science 282:1858–1864

Thompson LG, Mosley-Thompson E, Davis ME et al (2002) Kilimanjaro ice core records: Evidence of Holocene climate change in tropical Africa. Science 298:589–593

Urrego DH (2006) Long-term vegetation and climate change in Western Amazonia. Biological Sciences. Melbourne, FL, Florida Institute of Technology. Doctor of Philosophy:278

Valencia BG (2006) Late Quaternary Vegetation and Climate Change in the Southern Andes of Peru. Biological Sciences. Melbourne, FL, Florida Institute of Technology: 80

van der Hammen T, Hooghiemstra H (1995) The El Abra stadial, a Younger Dryas equivalent in Colombia. Quat Sci Rev 14:841–851

Vuille M, Bradley RS, Werner M et al (2003) Modeling $\delta^{18}O$ in precipitation over the tropical Americas: 2. Simulation of the stable isotope signal in Andean ice cores. J Geophys Res 108:4175

Willis KJ, Gillson L, Brncic TM (2004) How "virgin" is virgin rainforest? Science 304:402–403

Williams JW, Shuman BN, Webb III T (2001) Dissimilarity analyses of late-Quaternary vegetation and climate in eastern North America. Ecology 82:3346–3362

Williams JW, Shuman BN, Webb III T et al (2004) Late Quaternary vegetation dynamics in North America: Scaling from taxa to biomes. Ecol Monogr 74:309–334

Chapter 13
The Nature and Origin of Decadal to Millennial Scale Climate Variability in the Southern Tropics of South America: The Holocene Record of Lago Umayo, Peru

Paul A. Baker, Sherilyn C. Fritz, Stephen J. Burns, Erik Ekdahl, and Catherine A. Rigsby

Abstract This paper serves two purposes: to review current ideas about the nature and forcing of decadal to millennial scale precipitation variation in the southern tropics of South America during the late Quaternary and to present a new methodology for the reconstruction of precipitation as applied to a Holocene stable isotopic record of carbonate sediments in a tropical Andean lake, Lago Umayo, Peru. The basic thesis of the first part of the paper is that, although modern instrumental records suffice for deducing climate variability at decadal and shorter time scales, these records cannot adequately characterize the nature and forcing of lower-frequency climate variation. Understanding the nature of multi-decadal to millennial-scale climate variation and the mechanisms of large abrupt climate change is best derived from paleoclimatic time series. Tropical Atlantic sea-surface temperature variation is a significant control on tropical South American paleoclimate at these longer time scales. In the second part of the paper, an original method is presented for quantitatively reconstructing precipitation. This method utilizes the well-known relationship between the stable isotopic composition of precipitation and the amount of precipitation, a relationship that is highly significant in many tropical locales. Due to many simplifying assumptions, the reconstruction should be considered to be tentative.

A ~12% increase in precipitation (~570 to 650 mm a^{-1}) at 4750 cal year BP is consistent with the 6% increase in summer insolation at this latitude over the same period. However, the increase in precipitation was neither unidirectional nor gradual. Instead, every 240 years on average, precipitation increased or decreased by at least ~8% for periods lasting on average 100 years. The largest of these events had ~15% positive or negative departures from the long-term mean precipitation. These southern tropical wet events apparently coincided with periods of low sea-surface temperatures in the high-latitude North Atlantic, supporting a hypothesis of a tropical North Atlantic sea-surface temperature

P.A. Baker (✉)
Division of Earth and Ocean Sciences, Duke University, Durham, NC 27708, USA
e-mail: pbaker@duke.edu

F. Vimeux et al. (eds.), *Past Climate Variability in South America and Surrounding Regions*, Developments in Paleoenvironmental Research 14,
DOI 10.1007/978-90-481-2672-9_13,

control on tropical South American precipitation at decadal to millennial scales.

Keywords Paleoclimate · Precipitation · Oxygen isotopes · Tropical South America

13.1 Introduction

The modern climate of tropical South America is known only from a short, sparse, and incomplete instrumental record. In fact, there is only one weather station within the entire Amazon basin (Manaus, Brazil) with a century of complete precipitation data. Although the instrumental data that do exist may suffice for deducing modern climate variability at decadal and shorter time scales, they are clearly insufficient for understanding lower-frequency climate variability of the region and for elucidating mechanisms of large, abrupt climate changes that are, until now, only observable in the paleoclimatic record.

Discounting long-term secular trends, the instrumental record of South American climate displays three main continent-wide patterns of variability related to three main modes of climate variability (recently reviewed by Garreaud et al. 2008): (1) El Niño-Southern Oscillation (ENSO), (2) the Pacific Decadal Oscillation (PDO), and (3) the Southern Annular Mode (SAM) or Antarctic Oscillation (AAO). However, there is some evidence suggesting that these patterns of variability are not independent of each other. For example, the first two modes, ENSO and PDO, have similar spatial patterns of forcing and produce very similar spatial patterns of precipitation anomalies (see Fig. 10 of Garreaud et al. 2008). Although the forcing footprint of the SAM mode is quite different from that of the other two modes (Fig. 6 of Garreaud et al. 2008), the SAM also produces a similar spatial pattern of precipitation response (albeit of reversed sign) when compared with the other two modes.

Furthermore, in most regions of the South American continent these three remote forcings account for only a small part of the total climate variability. For example, for the period 1950–1999, ENSO variability explains a maximum of two-thirds of the inter-annual variability of precipitation in some regions of southern tropical South America (Garreaud et al. 2008), yet over most of the continent, south of the equator, precipitation variability is not significantly correlated with ENSO. Furthermore, because ENSO forcing is non-stationary in time and space, the spatio-temporal patterns of its teleconnection are also non-stationary. For example, Torrence and Webster (1999) showed that the periods 1875–1920 and 1960–1990 were periods of relatively high ENSO variability (high variance of the Southern Oscillation (SOI) and Nino-3 indices), whereas 1920–1960 was a period of low ENSO variability and a period of low coherency between ENSO and Indian monsoonal precipitation. In the North Atlantic region, Sutton and Hodson (2003) showed that ENSO had a significant impact on climate variability during some time periods, but during the period 1910–1960, this influence waned. Aceituno and Montecinos (1993) illustrated the non-stationarity of the ENSO teleconnection in

South America, with several examples showing the changing correlation between SOI and annual precipitation. As in the Asian monsoonal and North Atlantic regions, Aceituno and Montecinos (1993) found that 1920–1960 was a period of insignificant correlation between SOI and regional precipitation at sites scattered throughout southern tropical South America. Hastenrath and co-workers (2004) also found that the correlation between SOI and wet-season precipitation on the South American Altiplano changed from insignificant during the period 1915–1957 to significant (at the 95% level) during the period 1958–1984. These studies all illustrate the perils of too narrowly interpreting past climate variability based solely upon lessons drawn from the short and imperfect instrumental record (what Seager and Battisti (2007) refer to as "limitations of the ENSO blueprint").

The spatio-temporal patterns of variability derived from statistical analyses of climate depend on the particular climate variable being analyzed, the period of the record being considered, and the boundaries of the domain under consideration. For example, a significant pattern of climate variability, not found in continent-wide analyses, emerges when analysis of precipitation variability is limited to the tropical sector of South America (e.g. EOF-3 of Liu 2008). On roughly decadal timescales, small, but persistent, sea-surface temperature (SST) anomalies (superimposed upon much larger intra-annual variability) develop in the northern and southern tropical Atlantic. These SST anomalies (not completely independent of ENSO forcing) are, in part, maintained by regional wind-evaporation-SST feedback (Chang et al. 1997). The SST anomalies produce anomalous north-south shifts of the ITCZ and its embedded atmospheric circulations toward the warmer hemisphere (e.g. Chiang and Koutavas 2004). The SST and circulation anomalies are associated with significant perturbations of precipitation along the northeastern coastal region of South America (e.g. Hastenrath and Greischar 1993, Nobre and Shukla 1996) and throughout the entire Amazon basin south of the equator (Zeng et al. 2008). In boreal winter, tropical Atlantic SST anomalies may be organized into an alternating zonal SST anomaly pattern that extends into higher northern and southern latitudes of the Atlantic and that varies on decadal timescales (Xie and Tanimoto 1998, Xie and Carton 2004).

Atlantic variability, although significant, is not a dominant factor in forcing tropical South American climate variability during the instrumental period. However, there is a great deal of evidence pointing towards a much more important role for the Atlantic in forcing large, persistent, and sometimes abrupt, climate changes in tropical South America in the past, perhaps in synchrony with yet larger-scale ocean-atmosphere regime shifts. In the instrumental period, annual SST anomalies in the northern tropical Atlantic are rarely greater than 1 K (and their correlations with higher-latitude North Atlantic SSTs are only marginally significant), thus we might expect relatively weak forcing of terrestrial climate variability. However, paleoceanographic studies reveal past periods of much larger decreases (relative to today) of northern tropical Atlantic SST. For example, during the Last Glacial Maximum, SSTs in the northern tropical Atlantic were on average about 3 K lower than modern, while SSTs in the southern tropical Atlantic and the northern subtropical gyre were similar to modern (Mix et al. 1999). Northern tropical Atlantic SST

apparently cooled in concert with high latitude North Atlantic SST, while SST in the sub-tropical gyre did not change, in effect causing a persistent and greatly amplified North Atlantic SST tripole. Paleoceanographic evidence is consistent with a similar SST pattern in the North Atlantic during all of the Pleistocene (glacial stages, stadials, and Heinrich events) and Holocene (Bond events) cold events. Irrespective of other forcings (global temperature, insolation, land-surface changes, etc.), the great difference between these past Atlantic SSTs and modern Atlantic SSTs must have forced a very large increase (decrease) in southern (northern) tropical South American precipitation, relative to modern, during the North Atlantic cold events. Large precipitation increases in the southern tropics of South America synchronous with cold events in high northern latitudes have been observed at multi-decadal to millennial time scales in lake and ice-core paleoclimate records from the Altiplano of Peru and Bolivia (Baker et al. 2001a,b, 2005, Hoffmann et al. 2003, Ramirez et al. 2003), speleothem records from the exit region of the South American summer monsoon (Cruz et al. 2005, 2006, Wang et al. 2006, 2007) and from the Nordeste (Wang et al. 2004), and paleoceanographic records of discharge offshore of the Nordeste (Arz et al. 1998, Jennerjahn et al. 2002). Precipitation decreases during North Atlantic cold events have been observed in northern tropical South America in the records from the Cariaco Basin (Black et al. 1999, 2004, Haug et al. 2001, 2003, Peterson et al. 2000, Peterson and Haug 2006).

Climate model simulations provide strong support for both the sensitivity of tropical South American precipitation to North Atlantic SST (e.g. Harris et al. 2008, Zeng et al. 2008) and the postulated linkage between North Atlantic cold events, north tropical Atlantic cold SSTs, and tropical South American precipitation. Broccoli and co-workers (2006) pointed out that many different climate simulations by different groups (e.g. Vellinga and Wood 2002,; Chiang and Bitz 2005, Zhang and Delworth 2005) using models of different complexities and a variety of forcing and boundary conditions, all produce increased (decreased) precipitation south (north) of the equator in tropical South America during North Atlantic cold events. These simulations, no matter what the original intent of the modelers (for example Vellinga and Wood 2002, were addressing future climate change scenarios), are relevant to all of the Quaternary-age North Atlantic cold periods that we previously listed. The relationship between tropical South American precipitation and tropical Atlantic SST is the most robust result of all of these simulations and is completely consistent with paleoclimate results from the region. Furthermore, the near global-scale, the amplitude, and the abruptness of both simulated and observed past climate changes seem to require a major atmospheric reorganization perhaps into an alternate state as envisioned by Seager and Battisti (2007).

In this paper, our purposes are two-fold. First, we briefly review the studies most relevant to the proposition of tropical Atlantic control on tropical South American paleoclimate through the late Pleistocene and Holocene (with emphasis on the latter). Then we present new results from a study of stable oxygen isotopic ratios of carbonate sediments in Lago Umayo (Peru), that aims to quantify past changes in precipitation amount in order to clarify the amplitude and duration of Holocene climate variation in the southern tropical Andes. The novel aspect of this

reconstruction is the methodology for quantitatively reconstructing precipitation. Specifically, we introduce an equation that relates the stable isotopic composition of precipitation and the amount of precipitation, a relationship that is highly significant in many tropical locales, into the standard equation for determining the isotopic balance of a lake. Our original approach allows the direct calculation of precipitation amount. However, because we do not have sufficient knowledge of the climate and hydrology of the modern Lago Umayo watershed, we have chosen to make several simplifying assumptions for our calculations. Thus, our approach is meant to be demonstrative more than definitive and the results of our reconstruction should be considered to be tentative.

13.2 Precipitation in Tropical South America During the Late Quaternary and its Relationship to Tropical Atlantic Variability

In this section, we discuss a selection of paleoclimatic records that we believe most accurately reflect the large-scale patterns of precipitation change in tropical South America through the late Quaternary. These reconstructions share the characteristics of accurate dating and high fidelity recording of precipitation.

Long paleoclimatic records demonstrate that orbital control of insolation has played a major role in forcing precipitation in both northern and southern tropical South America. In southern tropical South America, the water level of Lake Titicaca, reconstructed from chemical, isotopic, and paleoecological measurements of deep drill cores (Fritz et al. 2007), rose during global glacial stages and fell dramatically during interglacial stages, although, the extent to which this water balance reflects global temperature change or regional precipitation change is still an open question. Nevertheless, the Lake Titicaca drill core record is the first southern tropical record in South America to clearly indicate that the largest amplitude changes in water balance during the late Quaternary occur on 100,000 year time scales. This finding has implications for the ongoing debate about climate variability and the origin of species in the neotropics.

On precessional timescales (order 10^4 years), the regional-scale patterns of precipitation are more clear-cut. Precipitation changes in the northern and southern tropics of South America are generally in phase with summer insolation maxima (in the respective hemispheres), thus anti-phased with each other. In the southern tropics, several records clearly demonstrate the coherence between summer insolation and the abundance of summer monsoonal precipitation. For example, widespread drying across the southern tropics during the early and middle Holocene (e.g. Cross et al. 2000, Seltzer et al. 2000, Mayle and Power 2008) (Fig. 13.1) broadly coincided with the summer insolation minimum centered at 10,000 years BP when top-of-the-atmosphere insolation was 7% lower at 20°S than its maximum during the Last Glacial Maximum at 20,000 years BP (data from Berger and Loutre 1991). For reference, this change in summer insolation of 34 W m^{-2} is about 20% of the total intra-annual range of insolation, thus, it is no surprise that insolation variability is

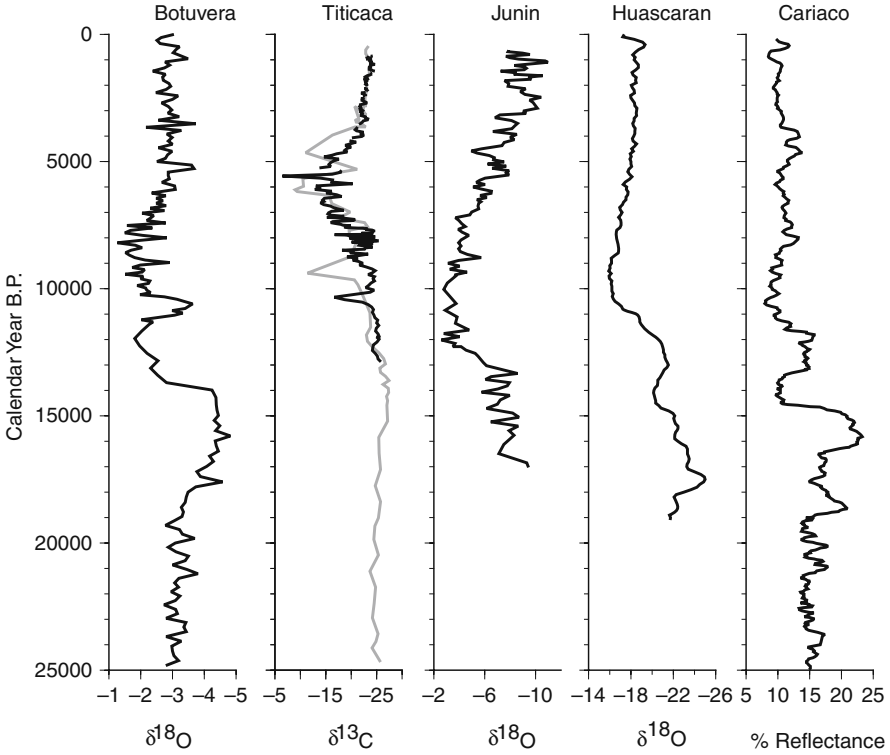

Fig. 13.1 Late Glacial to Holocene paleoclimate time series from selected sites in tropical South America. These records are described in more detail in the text. All figures (with the exception of Cariaco) are aligned with wetter conditions to the right and drier conditions to the left. From left to right, data are the Botuvera speleothem record (Cruz et al. 2006); Lake Titicaca carbon isotopes of organic carbon (Bakert al. 2001a, 2005); Lago Junin oxygen isotopes in carbonate sediments (Seltzer et al. 2000); Huascaran oxygen-isotopic values (Thompson et al. 1995); Cariaco reflectance in sediments (Peterson et al. 2000). In general, relatively wet (dry) conditions prevailed in the southern (northern) tropics during the Last Glacial Maximum and the late Holocene, and relatively dry (wet) conditions prevailed in the southern (northern) tropics during the early and mid Holocene

capable of forcing large changes in precipitation amount. Throughout the tropics, it is almost universally observed that $\delta^{18}O$ of precipitation is a measure of the amount of "rain out" from the atmosphere of moisture along its advective pathway from the evaporation source to the site of precipitation (e.g. Dansgaard 1964, Rozanski et al. 1993, Vuille et al. 2003a, Vimeux et al. 2005). Although changing circulation trajectories and changing moisture sources can surely complicate its interpretation, we accept that $\delta^{18}O$ in past precipitation, derived either from its direct measurement in ice cores or less direct deduction from measurements in speleothems or lacustrine carbonates, is a valid proxy for past precipitation amount. Thus, the nearly exact correspondence between stable oxygen isotopic variations recorded by speleothem

carbonates from Botuverá cavern in the southern subtropics of Brazil (27°S) and summer insolation for the past 116,000 years (Cruz et al. 2006), is strong confirmation that summer insolation is a major control on South American summer monsoonal precipitation, thus, total annual precipitation.

On sub-orbital time-scales, several studies have shown that throughout the southern South American tropics, precipitation amount is elevated during North Atlantic cold events (Baker et al. 2005). Again the speleothem records illustrate this best for the late Pleistocene. For the past 210,000 years, speleothem growth, signifying wet conditions, observed in a cave in the Nordeste of Brazil at 10°S, occurred only during North Atlantic cold events (Wang et al. 2004). Farther south at Botuverá cavern, Cruz and co-workers (2006, 2007) noted negative departures of $\delta^{18}O$, signifying increased precipitation, coincident with each of the last 10 Heinrich events and the Younger Dryas. The precise anti-correlation at millennial time-scales between the late Pleistocene $\delta^{18}O$ records of Botuverá cavern in the South American monsoon and Hulu cave located in the Asian monsoon (Wang et al. 2006) is a remarkable paleoclimate result and supports the proposed relationship between subtropical South American precipitation increases and both northern monsoon dry periods and North Atlantic cold events.

There are surprisingly few high-resolution Holocene-age paleoclimate records in tropical South America. Three of particular interest are from the Cariaco Basin off the north coast of Venezuela (Black et al. 1999, 2004, Haug et al. 2001, 2003, Peterson et al. 2000, Peterson and Haug 2006), Laguna Pallcacocha in the southern Ecuadorian Andes (Rodbell et al. 1999, Moy et al. 2002), and the Quelccaya ice core from the Cordillera Oriental of southern Peru (Thompson et al. 1985).

Laguna Pallcacocha is thought to be primarily a record of ENSO variability and amplitude, in which individual El Niño events are recorded by alluvial deposition into the lake basin (Rodbell et al. 1999). Although Laguna Pallcacocha records some variability at millennial timescales, the climatic interpretation of this variability is not clear. Moy and co-workers (2002) suggest two alternatives: millennial variability may be related to North Atlantic cold events (Bond et al. 2001) or may be somehow intrinsic to ENSO.

The Quelccaya ice core record (Thompson et al. 1985) is one of the most valuable tropical South American paleoclimate archives, because it preserves ice layers that have been accurately annualized to at least 500 year BP. The climatic interpretation of Quelccaya has been controversial, however, with disagreement arising about the fidelity of the annual accumulation data (e.g. Hastenrath et al. 2004, Vimeux et al. 2008) and the climatic significance of the stable oxygen isotopic ratios (Thompson et al. 2000, Vuille et al. 2003a,b, Hoffmann et al. 2003, Hastenrath et al. 2004, Vimeux et al. 2005, Sturm et al. 2007). We accept the standard interpretation mentioned previously (Dansgaard 1964, Rozanski et al. 1993), that $\delta^{18}O$ of tropical precipitation is largely a measure of the amount of precipitation rainout between source (the Atlantic Ocean and the Amazon) and the final sink (Quelccaya). Thus, the isotopic record of Quelccaya, like that of Botuverá cave, is a regional-scale measure of past precipitation.

Perhaps the most salient feature of the Quelccaya $\delta^{18}O$ record is its highly significant and persistent, decadal-scale (12–14 years) variability and the correlation of that variability with the low-frequency variability of tropical North Atlantic SST (Melice and Roucou 1998). This study implies that for the past half millennium there has been significant quasi-periodic, decadal variability of precipitation amount over southern tropical South America, and this precipitation has varied inversely with tropical North Atlantic SST on decadal timescales.

The Cariaco sediment record indicates that the northern tropics of South America were dry during North Atlantic cold events throughout the entire last glacial and the Holocene (Fig. 13.1), including the Younger Dryas and the Little Ice Age (Peterson et al. 2000, Haug et al. 2001). Peterson and Haug (2006) illustrated the similarity over the last several centuries between the time series of titanium concentrations in Cariaco sediments (a well-established proxy measure of runoff from northern continental South America) and the Quelccaya $\delta^{18}O$ record indicating that even at decadal -to-multidecadal timescales precipitation in northern and southern tropical South America was anti-phased and correlated with North Atlantic SST.

13.3 Reconstruction of Holocene Precipitation in the Northern Altiplano, Lago Umayo, Peru

Many of the studies discussed previously have endeavored to reconstruct a history of precipitation with high temporal resolution. However, none of these studies actually quantify the amount of past precipitation. In this section, we present new chemical, stable isotopic, and paleobiotic data determined on a lacustrine sediment core, and we advance a original methodology for calculation of mean annual precipitation. We apply this method to produce a ca. 7000 year-long, high-resolution (sub-decadal, on average) record of precipitation in the southern tropical Andes of Peru. Here we again caution that our results depend upon simplifying assumptions that are difficult to test. Thus our precipitation reconstruction should be considered to be tentative.

13.3.1 Regional Setting of Lago Umayo

Lago Umayo (15.44°S, 70.10°W, ~3880 masl) is located just to the west of Lake Titicaca, approximately 17 km northwest of the city of Puno, Peru (Fig. 13.2). Two main rivers, the Rio Vilque and Rio Challamayo, flow into the lake, and the lake drains via the Rio Ilpa into Lake Titicaca. The watershed area is approximately 975 km^2. Lago Umayo has a surface area of about 40.0 km^2 not including the island in its center that occupies 1.05 km^2. No bathymetric charts of the lake have been published; the greatest depth of the lake is over 20 m.

Temperature and precipitation data, recorded by SENAMHI, Peru, are available for Puno, Peru, from two stations Salcedo (15.88°S, 70.00°W, 3840 masl) and Puno (15.83°, 70.01°, 3812 masl) that together span the period from 1932 to the present.

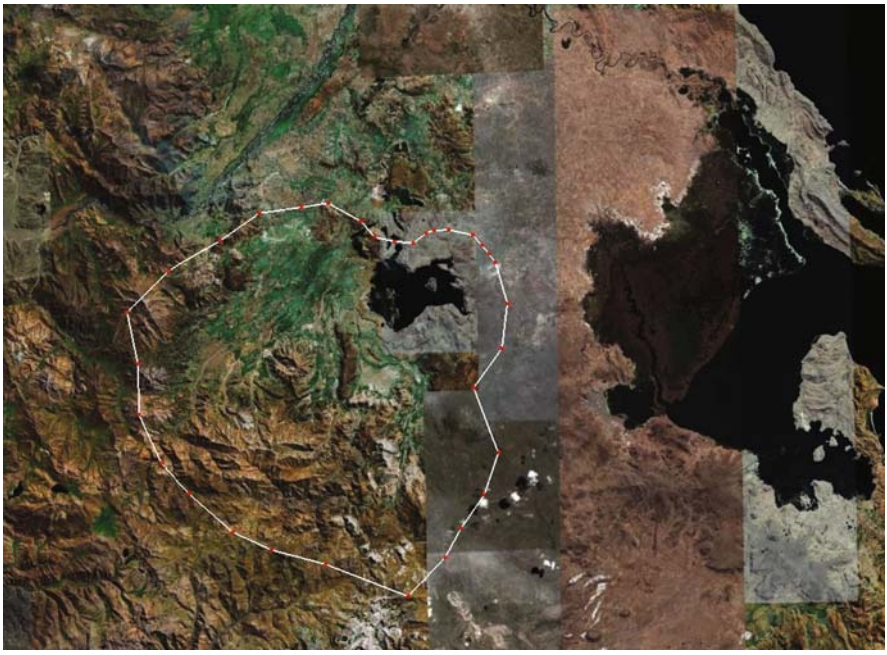

Fig. 13.2 Lago Umayo watershed in *white outline*. The image is from Google Earth and has dimensions of 85 km (E-W) and 60 km (N-S)

Mean annual precipitation (MAP) for the period 1960–1990 was 717 mm at Puno and 753 mm at Salcedo (INTECSA 1993). Mean annual temperature (MAT) for 1960–1990 was 8.5°C at Puno and 8.4°C at Salcedo. At both stations, 87% of MAP occurs during the wet half-year of November through April. The driest year on record was 1940/41. Other dry years were 1965/6, 1982/3, 1991/2, and 1997/9. Three of these (40/41, 82/83, and 97/98) were El Niño years, but the other two (65/66 and 91/92) were years of an essentially "neutral" Pacific. The decade from 1936 to 1945 is noteworthy, because precipitation was significantly below normal for these consecutive ten years.

Spatial gradients exist in the regional precipitation and temperature fields. In general, precipitation totals and temperatures decrease with increasing distance (and often increasing elevation) from Lake Titicaca. Compared to Puno and Salcedo on the shore of Lake Titicaca, MAP for the period 1960–1990 was 599 mm at Juliaca (15.5°S, 70.2°W, 3825 masl) about 25 km west of Lake Titicaca and 648 mm at Umayo. Lago Umayo is approximately midway between Juliaca and Puno, approximately 12 km west of Lake Titicaca.

Because of the tropical, high-altitude setting of the region, the diurnal temperature range is far greater than the seasonal temperature range. For example, at Juliaca the mean monthly diurnal temperature range is 17.8°C and at Puno it is 11.7°C (because of its closer proximity to the moderating influences of Lake Titicaca),

whereas the total annual range of mean monthly temperatures at Juliaca is 5.9°C (coldest month is July, warmest is December) and at Puno it is only 4.3°C. The mean annual value of relative humidity at Puno is 49%. The highest mean monthly values of relative humidity occur in wet season: >60% from January through March. The lowest mean monthly values of relative humidity occur in dry season: <45% from May through October. Although top-of-atmosphere (TOA) radiation is significantly greater in the summer than in the winter, the greater cloudiness of the summer wet season cancels much of this intra-annual variation. The Penman equation yields values of potential evapo-transpiration in reasonable agreement with observed values in the Titicaca watershed (INTECSA 1993), even in the absence of wind, humidity, and solar radiation data (Garcia et al. 2004).

The level of the surface of Lake Titicaca has been measured at Puno since 1915 (SENAMHI, Peru). This level fluctuates by about 1 m each year, rising following the wet season of peak riverine input and falling more steadily throughout the year due to evaporative loss from the lake surface and (much less) outflow into the Rio Desaguadero. On inter-annual timescales, the level of the lake has varied by about 6 m, attaining a recorded high of 3812.48 masl in 1986 following three anomalously wet years and a recorded low of 3806.26 masl in 1943 as a result of extended drought. The value of the lake-level time series as a measure of effective moisture and wet season precipitation has been discussed in several previous studies (including Melice and Roucou 1998, Baker et al. 2001a, Hastenrath et al. 2004). Here we utilize lake-level rise from October to March of the following year (the wet season spans the calendar year) as a regional measure of the wet season precipitation amount.

The Quelccaya ice core as an archive of past climate is particularly relevant to our present study because its location (13.9°S, 70.8°W, 5670 masl) is just to the north of the Lake Titicaca watershed about 200 km north of our study site. The inverse correlation between the annual $\delta^{18}O$ measurements of Quelccaya and the total wet season precipitation for the same year in Puno is significant at the 99.9% level (Fig. 13.3,

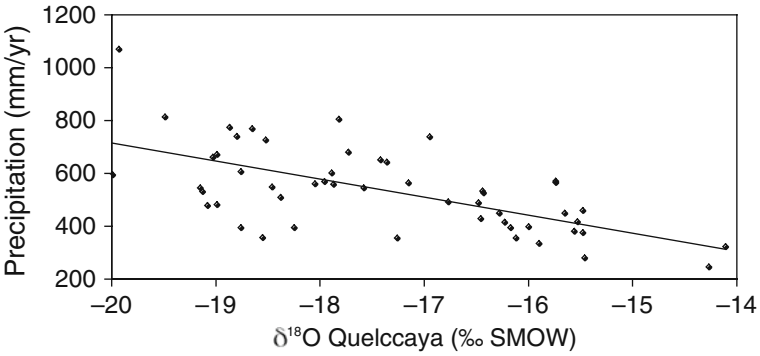

Fig. 13.3 Wet season (November-April) precipitation in Puno is inversely correlated with $\delta^{18}O$ of ice of the same year from Quelccaya (n=66, $r^2 = 0.403$, $p < 0.001$)

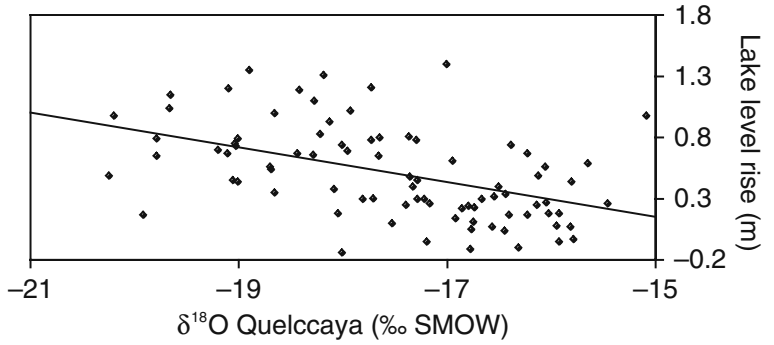

Fig. 13.4 The stable isotopic composition of Quelccaya ice core (Thompson et al. 2006) is significantly inversely correlated with the lake level rise of Lake Titicaca from October of the preceding year to March of the same year ($r^2 = 0.2393$, $n = 85$, $p < 0.001$)

$r^2 = 0.403$). If we compare the annual $\delta^{18}O$ measurements of Quelccaya to the October-March rise of Lake Titicaca for the same year (Fig. 13.4), again the inverse correlation is highly significant ($r^2 = 0.239$). The latter correlation would likely be higher except for a discrepancy between the $\delta^{18}O$ values of the different Quelccaya cores (Thompson et al. 2006). We speculate that the discrepancy may arise from dating errors of $\pm$ 1 year. Thus, when we compute 5-year moving averages of the $\delta^{18}O$ and lake level records (Fig. 13.5), the correlation between the two time series improves ($r^2 = 0.686$). Vimeux and co-workers (2005) demonstrated that δD values of precipitation from the nearby Zongo Valley, Bolivia, correlate even more highly with rainout over the "upstream" Amazon basin.

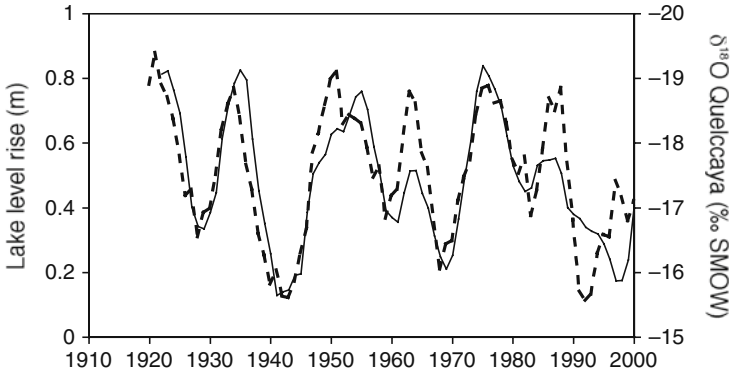

Fig. 13.5 Five-year moving averages of the time series (1915–2000) of $\delta^{18}O$ Quelccaya (*solid line*, data from Thompson et al. 2006) and lake level rise of Lake Titicaca (*dotted line*). Note that the $\delta^{18}O$ scale is reversed such that more depleted values plot with a lake-level rise of greater magnitude ($r^2 = 0.686$, $n = 81$, $p < 0.001$)

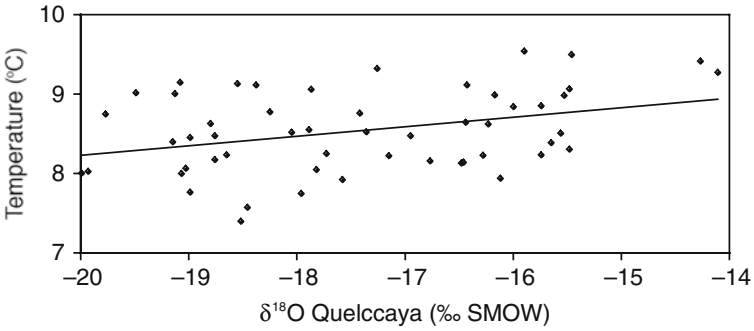

Fig. 13.6 Mean annual temperature (July-June) in Puno is positively correlated with $\delta^{18}O$ of ice of the same year from Quelccaya (n=53, $r^2 = 0.125$, $p < 0.05$)

Our findings agree with the conclusion of Hastenrath et al. (2004) that negative departures of $\delta^{18}O$ in Quelccaya ice are accompanied by large-scale circulation departures that favor more abundant precipitation over the southern tropical Andes: from a paleoclimate perspective we conclude that $\delta^{18}O$ is a reasonable predictor of precipitation amount in the southern tropical Andes and the adjacent Amazon basin. Previously, it has been assumed that $\delta^{18}O$ in Quelccaya ice was inversely correlated with regional temperature (as it is in high latitude ice cores), thus negative departures of $\delta^{18}O$ from mean values were taken to indicate periods of below-normal temperature. In fact, there is a *positive,* but only weakly significant, correlation between mean annual temperature in Puno and $\delta^{18}O$ in Quelccaya ice (Fig. 13.6).

13.3.2 Methods

Overlapping sediment cores were taken in 2001 in the eastern part of the lake in ~10.5 m water depth using a Russian peat corer. The lithology of each core segment was described in the laboratory, and a 7.07 m composite core sequence was constructed from the overlapping drives based on visual correlation of distinctive sedimentary features. The composite core sequence was sampled continuously at 1-cm resolution for diatom enumeration and stable carbon and oxygen isotopic composition of the carbonate fine fraction ($CaCO_3$ content of the sediments ranged from 28 to 100 wt% with a mean (SD) of 68.3 (10.2) wt%.).

Prior to isotopic analysis, all recognizable coarse shells and shell fragments were hand-picked from the dried sediment sample. The stable oxygen and carbon isotopic compositions of calcium carbonate in the fine fraction of the sediment were analyzed with an on-line, automated, carbonate preparation system linked to a Finnigan Delta XL ratio mass spectrometer in the Department of Geosciences at University of Massachusetts. Ratios are reported relative to the PDB standard. The reproducibility for the $\delta^{18}O$ and $\delta^{13}C$ determinations of standard materials is respectively 0.08‰ and 0.05‰.

Sediments for diatom analysis were prepared following standard methodology (Battarbee 1986). A weighed aliquot of sediment was chemically digested with cold 10% hydrochloric acid and hydrogen peroxide to remove carbonate and organic material, respectively. Cleaned material was settled onto cover slips, dried, and mounted using Zrax, a high refractive-index diatom mounting material. Diatom valves were identified using differential interference contrast on a Zeiss Axioskop microscope with an oil immersion objective. At least 300 valves were counted per slide, and species abundances are expressed as a percentage of the total number of identified diatom valves. Diatom species were categorized as freshwater or saline and as planktic or benthic, based on known ecological affinities (Servant-Vildary and Roux 1990, Sylvestre et al. 2001, Tapia et al. 2003).

A chronology for the core was constructed using 10 accelerator mass spectrometry ^{14}C dates. ^{14}C dates were calibrated using CALIB 5.0.2 (Stuiver and Reimer 1993) using the Southern Hemisphere calibration (McCormac et al. 2004). The age-depth relationship was constructed by fitting a fifth-order polynomial through the calibrated ages (see Ekdahl et al. 2008 for more detailed information on age model construction).

13.3.3 The Oxygen Isotopic Model

The stable oxygen isotopic composition of a through-flow lake at hydrologic and isotopic steady state is given by Gat (1995):

$$\delta_{\text{lake}} = \delta_{\text{i}} + [(1 - \text{h})(\varepsilon^* + \text{C}_{\text{k}})]/[\text{h} + (1 - \text{h})(\text{Q}_{\text{i}}/\text{Q}_{\text{e}})] \quad (1)$$

where:

δ_{i} is the stable oxygen isotopic composition of the influx and is assumed to have the same value as precipitation, δ_{P} (‰, SMOW);
ε^* is the temperature-dependent oxygen isotopic separation factor for the equilibrium between water liquid and water vapor (‰);
$\text{C}_{\text{K}} = 14.2$ (‰) is a constant associated with kinetic fractionation during the non-equilibrium evaporation of water (Vogt 1978);
h is fractional relative humidity;
Q_{i} is the flux of water into the lake from direct precipitation and river runoff (m a^{-1}) normalized to the surface area of the lake;

$$\text{Q}_{\text{i}} = \text{P} + \text{Pf}(\text{S}_{\text{W}}/\text{S}_{\text{L}})$$

where:

P is the precipitation rate (m a^{-1}), assumed constant throughout the watershed;
$\text{S}_{\text{W}}/\text{S}_{\text{L}}$ is the ratio of the surface area of the watershed to the surface area of the lake;

f is the fraction of precipitation falling on the land that contributes to runoff (the remainder is assumed to be returned to the atmosphere by non-fractionating evapotranspiration);

Q_e is the evaporative flux of water vapor from the lake surface to the atmosphere (m a^{-1}), again normalized to the surface area of the lake.

In order to apply our model to the paleoclimate of the Umayo watershed, we assume constant values for h, f, Q_e, S_L/S_W, and surface air temperature T. These are determined from present-day values of mean annual climatology (in the case of h, Q_e, f, and T_A) or hypsometry (for S_L/S_W). The surface water temperature of the lake T_w is assumed to be 2 K warmer than the surface air temperature T_A, similar to the difference observed at nearby Lake Titicaca (Carmouze 1992). ε^* is a known function of T_w (Kelvin), and here we use the formulation of Majoube (1971) to determine its value:

$$\mathrm{In}\alpha_{I-V} = 1137T_W^{-2} - 0.4516T_W^{-1} - 0.00207$$

where $\alpha_{l\text{-}v}$ is the equilibrium isotopic fractionation factor between water liquid and water vapor and is related to ε^* by:

$$\varepsilon^* = 1000(\alpha - 1).$$

We use the equation of O′Neil et al. (1969) to determine values for δ_{lake} from stable isotopic analysis of the fine fraction of the carbonate sediments δ_c:

$$\delta_{lake} = \delta_c - 2.78 \times 10^6 T_W^{-2} - 2.89$$

Finally, following the discussion of the previous section, we use our observed relationship between precipitation amount and stable isotopic composition of precipitation to write an expression for $\delta_P = \delta_i$:

$$\delta_i = -14.126P - 7.317$$

Substituting into (1) and rearranging, we can solve the quadratic equation for precipitation that depends only on temperature and δ_{lake} (Fig. 13.7).

In order to improve upon our present approach, it will be most important to quantitatively reconstruct (1) water paleo-temperature and (2) evaporative flux, using only variables that can be realistically deduced from the paleoclimate record. Delclaux and co-workers (2007) recently determined that the Abtew model of evaporation, containing net solar radiation as its only climate variable, produced an excellent fit with instrumental data on the evaporative flux from the surface of Lake Titicaca.

How appropriate is it to use a steady-state model (1) to deduce past climate? In brief, to our knowledge hydrologic steady-state (dV/dt = 0, the volume of the lake remains unchanged through time) is today maintained in Lago Umayo with only

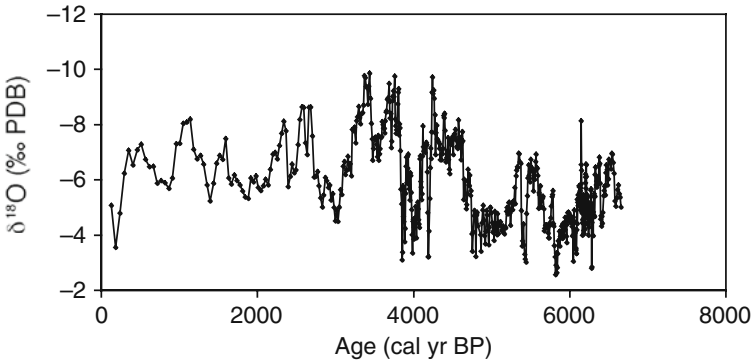

Fig. 13.7 Stable oxygen isotopic composition of carbonate fine fraction of Lago Umayo. Note that the $\delta^{18}O$ axis is reversed such that enriched values plot lower on the axis

minor changes in its lake level from year-to-year. Our sedimentological analysis indicates no unconformities during the period of the record, that is the lake level certainly never fell by more than 10 m even when the lake was apparently closed (in the early Holocene). The diatom evidence presented below supports the argument that since the middle Holocene the lake has been relatively fresh and overflowing, thus near its present volume. The stable isotopic evidence itself, specifically the low rate of $\delta^{18}O$ change (on order of 0.02‰ a^{-1}), argues that the assumption of isotopic steady-state is also valid for our application.

13.3.4 Model Results and Validation

Our first attempt at the quantitative isotopic reconstruction of precipitation (Fig. 13.8) spans 6529 years of record from 6656 to 127 cal year BP. The reconstructed long-term mean annual precipitation is 600±130 (±2σ) mm a^{-1}. Precipitation increased about 12% over the duration of the record from the early Holocene to near modern. But this increase was neither linear nor gradual, rather it occurred abruptly at about 4750 cal year BP. A second attribute of the precipitation time series is its large-amplitude variability. Thus, over the portion of the record from 6656 to 3000 cal year BP where the resolution is highest, averaging 6.5 year/sample, there are about 15 events with amplitude >1σ, an average frequency of about 240 year and an average duration of about 100 years. The largest amplitude events between 5000 and 3000 year BP were ∼15% positive or ∼15% negative departures of mean annual precipitation from the prevailing mean, often sustained over two to three centuries. These large sustained changes of precipitation would have had a major impact on the natural biota and early human occupants of the region. For reference, our analysis of data from the United Nations Food and Agriculture Organization (FAO; not shown) indicates that modern agricultural yields of

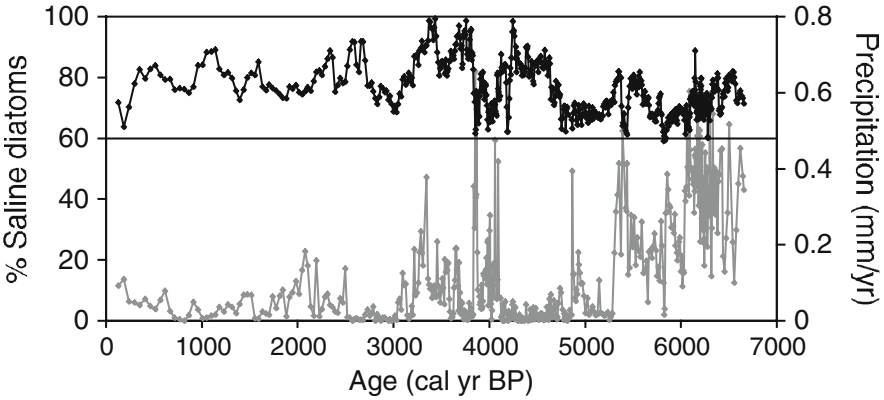

Fig. 13.8 Time series of the mean annual precipitation (*black line and diamonds*) calculated from the isotopic analysis of carbonate sediments from Lago Umayo. Also shown are abundances of saline diatoms as a percentage of the total diatom assemblage (*gray line and diamonds*) (See Ekdahl et al. 2008 for complete species compositional data). The black horizontal line represents closed basin lake conditions: when precipitation falls below 480 mm a^{-1}, Lago Umayo becomes a closed basin lake and its salinity rises. This calculation of precipitation assumed constant relative humidity of 0.5 and constant air temperature of 8.0°C (see text for more details)

quinoa and potatoes on the Altiplano are adversely impacted by this magnitude of climate anomaly even if sustained for only one summer.

At times in its past, Lago Umayo was a closed basin, and there was no outflow into its only outlet, the Rio Ilpa. These endorheic conditions took place during periods of negative water balance, most likely due to lower precipitation. As long as closed-basin conditions persisted, the soluble constituents of inflowing rivers and direct precipitation accumulated in the lake, and the salinity of the lake rose. Our isotopic model is an easy way to identify the timing of these closed-basin, dry phases. Thus, given closed basin conditions $Q_i = Q_e$ and equation (1) simplifies to:

$$\delta_{lake} - \delta_i = (1 - h)(\varepsilon^* + C_K)$$

The rate of increase of the salinity of the lake is easily estimated by assuming constant salt content of the tributary rivers. Because all of this salt remained in the lake during the closed basin period, the salt content of the lake would have increased at roughly 15 mg l^{-1} a^{-1}. Within a century of the lake becoming (and remaining) closed, its salinity would have increased to about 1.5 g l^{-1} (in addition to its original salt content), well within the salinity optimum of the dominant saline diatoms. In fact, the measured abundances of saline diatoms demonstrate exactly the expected response (Fig. 13.8). During periods when the calculated mean annual precipitation was sustained at a value near that calculated for closed-basin conditions, the abundance of saline diatoms increased rapidly. During subsequent periods of increased precipitation, flushing and freshening of the lake led to decreased abundances of saline diatoms. The agreement between the saline diatom abundance data and the carbonate isotope data provides strong independent confirmation for our methodology.

13.4 Discussion

With few exceptions (e.g. Baker et al. 2005, Ekdahl et al. 2008), the forcing of Holocene climate variability in the southern tropics of South America has previously been ascribed to orbital and ENSO mechanisms. Indeed, as introduced previously, it is clear that insolation forcing of the South American summer monsoon is largely responsible for the early Holocene drier climate and late Holocene wetter climate of the region. And on inter-annual timescales, it is likely that ENSO variability played a role in forcing past precipitation variability in the southern tropics much as it does today (e.g. Rodbell et al. 1999, Moy et al. 2002, Bradley et al. 2003, Theissen et al. 2008). But, as we have shown (Fig. 13.8), between these orbital and inter-annual timescales, there is large amplitude precipitation variation at decadal-to-centennial-to-millennial timescales. We believe that much of this variation is forced by northern tropical Atlantic SST change, the plausibility of which is documented in both empirical (e.g. Nobre and Shukla 1996, Zeng et al. 2008) and modeling studies (Harris et al. 2008).

During the instrumental period, throughout most of the northern tropical Atlantic, SST is largely determined by surface ocean-atmosphere heat exchange (e.g. Yu et al. 2006), a significant portion of which is due to latent heat exchange driven by surface winds (e.g. Carton et al. 1996, Chang et al. 1997). In the boreal winter, coincident with the wet season in the southern tropics of South America, SST anomalies in the northern tropical Atlantic are significantly correlated with high-latitude North Atlantic SST anomalies (forming the North Atlantic SST tripole). These Atlantic SST anomalies co-vary with the atmospheric North Atlantic Oscillation (e.g. Seager et al. 2000) at its characteristic decadal-scale periodicity (Hurrell and van Loon 1997). These relationships suggest the possibility that on longer timescales, low temperatures in the high-latitude North Atlantic accompanied by high surface pressures in the Bermuda High and stronger northeasterly trades, can cause anomalously cold SSTs in the tropical North Atlantic and a southward shift of the mean annual position of the ITCZ. The anomalously strong northeasterly trades should also bring about increased moisture convergence in the Amazon Basin and increased precipitation in the southern tropics of South America, including much of the Amazon and tropical Andes. In fact, Curtis and Hastenrath (1999), examining reanalysis data from 1958 to 1997, documented an example of such a long-term increase of the Atlantic northeasterly trades that supported a long-term increase in moisture convergence in the Amazon region. The trend observed by Curtis and Hastenrath (1999) also coincided with a nearly 40 year period of increasing winter NAO index (Hurrell and Van Loon 1997).

In agreement with this hypothesized mechanism, the centennial-scale wet periods that we reconstruct at Lago Umayo, correlate reasonably well with North Atlantic cold periods reconstructed by Bond et al. (2001) in the North Atlantic (Fig. 13.9). We believe that the lack of a more perfect correlation between these two time series is due to problems in the age models of both records.

We can also reconstruct past precipitation amount from southern tropical Andean ice core records if we assume, as we have done in this study, a constant relationship

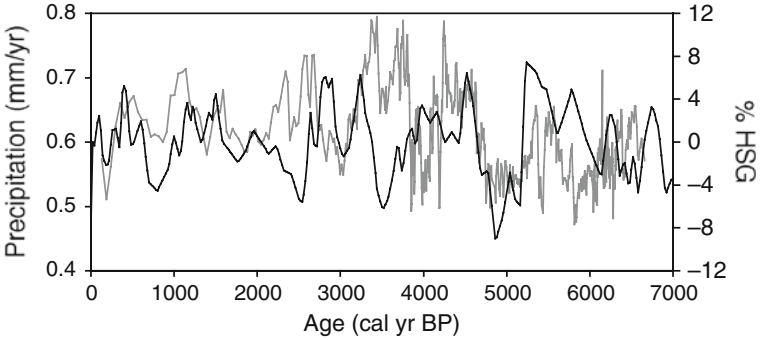

Fig. 13.9 Altiplano precipitation (*gray line*) and hematite-stained grains (HSG) in the North Atlantic (*black line*). Their reasonable correspondence supports the hypothesized role of North Atlantic SST in forcing Altiplano precipitation. HSG data are from Bond et al. (2001)

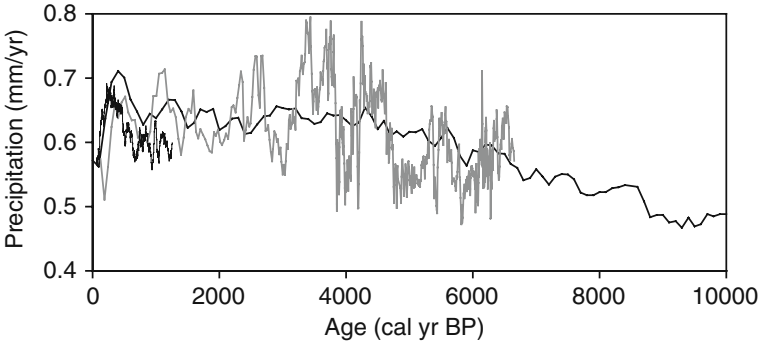

Fig. 13.10 Time series of wet-season precipitation reconstructed from Quelccaya ice core (*black line*, 50-year moving average, Thompson et al. 1985), Huascaran ice core (low-resolution curve, *black line*, centennial averages, Thompson et al. 1995), and Lago Umayo sediments (*gray line*)

between local precipitation and its isotopic composition. Using this approach, precipitation determined from both the Quelccaya and Huascaran ice cores (Fig. 13.10) agrees reasonably well with that from Lago Umayo. The Huascaran data are reported as centennial averages (Thompson et al. 1995), thus they average out all higher-frequency variability. Furthermore, the age model for the Huascaran ice core is constructed without any absolute age dates for all of the Holocene with the exception of the last century.

13.5 Conclusions

Atlantic variability is not a dominant factor in forcing the climate of tropical South America during most of the instrumental period, but with few exceptions (e.g. 2005), over this interval, annual SST anomalies are relatively small. On multi-decadal to

millennial time scales, past SST anomalies were much larger and therefore might have played a much larger role in forcing climate variability. We reviewed a number of paleoclimatic time series from continental South America, as well as climate model simulations, that support a significant influence of Atlantic SST variation on precipitation in tropical South America during the late Quaternary.

Our reconstruction of precipitation at decadal scale over the last ~7000 years from the oxygen isotopic composition of carbonates in from lake sediments in the northern Altiplano of the southern tropical Andes, is consistent with previous regional reconstructions that show a secular increase in precipitation from the mid Holocene to the present day. Our quantitative reconstruction of this trend suggests a ~12% increase in precipitation (from ~560 to 650 mm a^{-1}), coincident with the 6% increase in summer insolation at this latitude over the same period. The increase in precipitation was neither uni-directional nor gradual. Instead, every 240 years on average, precipitation increased or decreased by at least ~8% for periods lasting on average 100 years. The largest of these events had ~15% positive or negative departures from the long-term mean precipitation. These southern tropical wet events apparently occurred during periods when SSTs in the high-latitude North Atlantic were low, corroborating the hypothesis of an Atlantic SST control on tropical South American precipitation. Further testing of this hypothesis will require better-dated records of both Atlantic SST and of Andean or Amazonian precipitation.

References

Aceituno P, Montecinos A (1993) Circulation anomalies associated with dry and wet periods in the South American Altiplano. In: Fourth International Conference on Southern Hemisphere Meteorology and Oceanography, American Meteorological Society, Boston, MA

Arz HW, Patzold J, Wefer G (1998) Correlated millennial-scale changes in surface hydrography and terrigenous sediment yield inferred from Last-Glacial marine deposits off Northeastern Brazil. Quat Res 50:157–166

Baker PA, Seltzer GO, Fritz SC et al (2001a) The history of South American tropical precipitation for the past 25,000 years. Science 291:640–643

Baker PA, Rigsby CA, Seltzer GO et al (2001b) Tropical climate changes at millennial and orbital timescales on the Bolivian Altiplano. Nature 409:698– 700

Baker PA, Fritz SC, Garland J, Ekdahl E (2005) Holocene hydrologic variation at Lake Titicaca, Bolivia/Peru, and its relationship to North Atlantic climate variation. J Quat Sci 20: 655–662

Battarbee RW (1986) Diatom analysis. In: Berglund, B (ed) Handbook of Holocene palaeoecology and palaeohydrology. Wiley, New York, pp 527–570

Berger A, Loutre MF (1991) Insolation values for the climate of the last 10 million years. Quat Sci Rev 10:297–317

Black DE, Peterson LC, Overpeck JT (1999) Eight centuries of North Atlantic ocean atmosphere variability. Science 286:1709–1713

Black DE, Thunell RC, Kaplan A et al (2004) A 2000-year record of Caribbean and tropical North Atlantic hydrographic variability. Paleoceanography 19:PA2022. doi:10.1029/2003PA000982

Bond G, Kromer B, Beer J et al (2001) Persistent solar influence on North Atlantic climate during the Holocene. Science 294:2130–2136

Bradley RS, Vuille M, Hardy D, Thompson LG (2003) Low latitude ice cores record Pacific sea surface temperatures. Geophys Res Lett 30:doi:10.1029/2002GL016546

Broccoli AJ, Dahl KA, Stouffer RJ (2006) Response of the ITCZ to Northern Hemisphere cooling. Geophys Res Lett 33:L01702, doi:10.1029/2005GL024546

Carmouze JP (1992) The energy balance. In: Dejoux C, Iltis A (eds) Lake Titicaca, a Synthesis of Limnological Knowledge. Kluwer, Dordrecht

Carton JA, Cao X, Giese BS, Silva AM (1996) Decadal and interannual SST variability in the tropical Atlantic Ocean. J Phys Oceanogr 26:1165–1175

Chang P, Ji L, Li H (1997) A decadal climate variation in the tropical Atlantic Ocean from thermodynamic air-sea interactions. Nature 385:516–518

Chiang JCH, Bitz CM (2005) Influence of high latitude ice cover on the marine Intertropical Convergence Zone. Clim Dyn 25:477–496

Chiang JCH, Koutavas A (2004) Tropical flip-flop connections. Nature 432:684–685

Cross SL, Baker PA, Seltzer GO, Fritz SC, Dunbar RB (2000) A new estimate of the Holocene lowstand level of Lake Titicaca, central Andes, and implications for tropical palaeohydrology. Holocene 10:21–32

Cruz FWJ, Burns SJ, Karmann I et al (2005) Insolation-driven changes in atmospheric circulation over the past 116,000 years in subtropical Brazil. Nature 434:63–66

Cruz FW, Burns SJ, Karmann I, Sharp WD, Vuille M (2006) Reconstruction of regional atmospheric circulation features during the late Pleistocene in subtropical Brazil from oxygen isotope composition of speleothems. Earth Planet Sci Lett 248:495–507

Cruz FW, Burns SJ, Jercinovic M et al (2007) Evidence of rainfall variations in Southern Brazil from trace element ratios (Mg/Ca and Sr/Ca) in a Late Pleistocene stalagmite. Geochimica et Cosmochimica Acta 71:2250–2263

Curtis S, Hastenrath S (1999) Trends of upper-air circulation and water vapour over equatorial South America and adjacent oceans. Int J Climatol 19:863–876

Dansgaard W (1964) Stable isotopes in precipitation. Tellus 16:436– 468

Delclaux F, Coudrain A, Condom T (2007) Evaporation estimation on Lake Titicaca: A synthesis review and modeling. Hydrol Process 21:1664–1677

Ekdahl E, Fritz SC, Baker PA et al (2008) Holocene multi-decadal to millennial-scale hydrologic variability on the South American Altiplano. Holocene 18:867–876

Fritz SC, Baker PA, Seltzer GO et al (2007) Quaternary glaciation and hydrologic variation in the South American tropics as reconstructed from the Lake Titicaca drilling project. Quat Res 68:410–420

Garcia M, Raes D, Allen R, Herbas C (2004) Dynamics of reference evapotranspiration in the Bolivian highlands (Altiplano). Agric For Meteorol 125:67–82

Garreaud RD, Vuille M, Compagnucci R, Marengo J (2008) Present-day South American climate. Palaeogeogr Palaeoclimatol Palaeoecol in press. doi:10.1016/j.palaeo.2007.10.032

Gat JR (1995) Stable isotopes and the water balance of fresh and saltwater lakes. In: Lerman A, Imboden DM, Gat JR (eds) Physics and chemistry of lakes. Springer-Verlag, Berlin

Harris PP, Huntingford C, Cox PM (2008) Amazon Basin climate under global warming: The role of the sea surface temperature. Phil Trans R Soc B 363:1753–1759

Hastenrath S, Greischar L (1993) Circulation mechanisms related to Northeast Brazil rainfall anomalies. J Geophys Res Atmos 98(D5):5093–5102

Hastenrath S, Polzin D, Francou B (2004) Circulation variability reflected in ice core and lake records of the southern tropical Andes. Clim Change 64:361–375

Haug GH, Hughen, KA, Sigman DM et al (2001) Southward migration of the Intertropical Convergence Zone through the Holocene. Science 293:1304–1308

Haug GH, Gunther D, Peterson LC et al (2003) Climate and the collapse of Maya civilization. Science 299:1731–1734

Hoffmann G, Ramirez E, Taupin JD et al (2003) Coherent isotope history of Andean ice cores over the last century. Geophys Res Lett 30:doi:10.1029/2002GL014870

Hurrell JW, van Loon H (1997) Decadal variations in climate associated with the North Atlantic Oscillation. Clim Change 36:301–326

INTECSA (1993) Estudio de Climatologia. Plan director global binacional de proteccion - prevencion de inundaciones y aprovechamiento de los recursos del Lago Titicaca, Rio Desaguadero, Lago Poopo y Lago Salar de Coipasa (Sistema T.D.P.S). INTECSA, AIC, CNR

Jennerjahn TC, Ittekkot V, Arz HW et al (2002) Asynchronous terrestrial and marine signals of climate change during Heinrich events. Science 306:2236–2239

Liu J (2008) Interannual to decadal variability of precipitation in tropical South America and its relationship to the Tropical Atlantic and Pacific Oceans. Unpublished M.S. Thesis, Duke University

Majoube M (1971) Fractionnement en oxygène-18 et en deutérium entre l′eau et sa vapeur. J Chem Phys 197:1423–1436

Mayle FE, Power MJ (2008) Impact of a drier Early–Mid-Holocene climate upon Amazonian forests. Phil Trans R Soc B 363:1829–1838

McCormac FG, Hogg AG, Blackwell PG et al (2004) SHCal04 Southern Hemisphere calibration 0–1000 cal BP. Radiocarbon 46:1087–1092

Melice JL, Roucou P (1998) Decadal time scale variability recorded in the Quelccaya summit ice core $\delta^{18}O$ isotopic ratio series and its relation with the sea surface temperature. Clim Dyn 14:117–132

Mix AC, Morey AE, Pisias NG, Hostetler SW (1999) Foraminiferal faunal estimates of paleotemperature: Circumventing the noanalog problem yields cool ice age tropics. Paleoceanography 14:350–359

Moy CM, Seltzer GO, Rodbell DT, Anderson DM (2002) Variability of El Niño/Southern Oscillation activity at millennial timescales during the Holocene epoch. Nature 420:162–165

Nobre P, Shukla J (1996) Variations of sea surface temperature, wind stress and rainfall over the tropical Atlantic and South America. J Clim 9:2464– 2479

O′Neil JR, Clayton RN, Mayeda TK (1969) Oxygen isotope fractionation between divalent metal carbonates. J Chem Phys 51:5547–5558

Peterson LC, Haug GH, Hughen KA, Rohl U (2000) Rapid changes in the hydrologic cycle of the tropical Atlantic during the Last Glacial. Science 290:1947–1951

Peterson LC, Haug GH (2006) Variability in the mean latitude of the Atlantic Intertropical Convergence Zone as recorded by riverine input of sediments to the Cariaco Basin (Venezuela). Palaeogeogr Palaeoclimatol Palaeoecol 234:97–113

Ramirez E, Hoffman G, Taupin JD et al (2003) A new Andean deep ice core from Nevado Illimani (6350 m), Bolivia. Earth Planet Sci Lett 212:337–350

Rodbell D, Seltzer GO, Anderson DM (1999) An 15,000-year record of El Niño-driven alluviation in southwestern Ecuador. Science 283:516–520

Rozanski K, Araguas-Araguas L, Gonfiantini R (1993) Isotopic patterns in modern global precipitation. In: Swart PK, Lohmann KC, MacKenzie J, Savin S (eds) Climate change in continental isotopic records. AGU, Washington, DC

Seager R, Kushnir Y, Visbeck M et al (2000) Causes of Atlantic Ocean climate variability between 1958 and 1998. J Clim 13:2845–2862

Seager R, Battisti, DS (2007) Challenges to our understanding of the general circulation: Abrupt climate change. In: Schneider T, Sobel AH (eds) The global circulation of the atmosphere. Princeton University Press, Princeton

Seltzer G, Rodbell D, Burns S (2000) Isotopic evidence for late Quaternary climatic change in tropical South America. Geology 28:35–38

Servant-Vildary S, Roux M (1990) Multivariate analysis of diatoms and water chemistry in Bolivian saline lakes. Hydrobiologia 197:267–290

Stuiver M, Reimer PJ (1993) Extended ^{14}C data base and revised CALIB ^{14}C age calibration program. Radiocarbon 35:215–230

Sturm C, Hoffmann G, Langmann B (2007) Simulation of the stable water isotopes in precipitation over South America: Comparing regional to global circulation models. J Clim 20:3730–3750

Sutton RT, Hodson DLR (2003) Influence of the ocean on North Atlantic climate variability 1871–1999. J Clim 16:3296–3313

Sylvestre F, Servant-Vildary S, Roux M (2001) Diatom-based ionic concentration and salinity models from the south Bolivian Altiplano (15–23 degrees South). J Paleolimnol 25:279–295

Tapia PM, Fritz SC, Baker PA (2003) A late Quaternary diatom record of tropical climate history from Lake Titicaca (Peru and Bolivia). Palaeogeogr Palaeoclimatol Palaeoecol 194:139–164

Theissen KM, Dunbar RB, Rowe HD, Mucciarone DA (2008) Multidecadal- to century-scale arid episodes on the northern Altiplano during the middle Holocene. Palaeogeogr Palaeoclimatol Palaeoecol 257:361–376

Thompson LG, Mosley-Thompson E, Bolzan JF, Koci BR (1985) A 1500-year record of tropical precipitation in ice cores from the Quelccaya ice cap, Peru. Science 234:361–364

Thompson LG, Mosley-Thompson E, Davis ME et al (1995) Late Glacial stage and Holocene tropical ice core records from Huascaran, Peru. Science 269:46–50

Thompson LG, Mosley-Thompson E, Henderson KA (2000) Ice-core palaeoclimate records in tropical South America since the Last Glacial Maximum. J Quat Sci 15:377–394

Thompson LG, Mosley-Thompson E, Brecher HH et al (2006) Abrupt tropical climate change: Past and present. Proc Natl Acad Sci 103:10536–10543

Torrence C, Webster PJ (1999) Interdecadal changes in the ENSO-monsoon system. J Clim 12:2679–2690

Vellinga M, Wood RA (2002) Global climatic impacts of a collapse of the Atlantic thermohaline circulation. Clim Change 54:251–267

Vimeux F, Gallaire R, Bony S et al (2005) What are the climate controls on δD in precipitation in the Zongo Valley (Bolivia): Implications for the Illimani ice core interpretation. Earth Planet Sci Lett 240:205–220

Vimeux F, Ginot P, Schwikowski M et al (2008) Climate variability during the last 1000 years inferred from Andean ice cores: A review of methodology and recent results. Palaeogeogr Palaeoclimatol Palaeoecol:doi:10.1016/j.palaeo.2008.03.054, in press

Vogt HJ (1978) Isotopentrennun bei der Verdunstun von Wasser. Thesis, Institute of Environmental Physics, University of Heidelberg, 78 pp

Vuille M, Bradley R, Werner M et al (2003a) Modeling $\delta^{18}O$ in precipitation over the tropical Americas: 1. interannual variability and climatic controls. J Geophys Res 108:doi:10.1029/2001JD002038

Vuille M, Bradley R, Healy R et al (2003b) Modeling $\delta^{18}O$ in precipitation over the tropical Americas: 2. Simulation of the stable isotope signal in Andean ice cores. J Geophys Res 108:doi:10.1029/2001JD002039

Wang X, Auler AS, Edwards RL et al (2004) Wet periods in northeastern Brazil over the past 210 kyr linked to distant climate anomalies. Nature 432:740–743

Wang X, Auler AS, Edwards R et al (2006) Interhemispheric anti-phasing of rainfall during the last glacial period. Quat Sci Rev 25:3391–3403

Wang X, Auler AS, Edwards RL (2007) Millennial-scale precipitation changes in southern Brazil over the past 90,000 years. Geophys Res Lett 34:L23701, doi:10.1029/2007GL031149

Xie SP, Tanimoto Y (1998) A pan-Atlantic decadal climate oscillation. Geophys Res Lett 25: 2185–2188

Xie SP, Carton JA (2004) Tropical Atlantic variability: Patterns, mechanisms, and impacts. In: Wang C, Xie SP, Carton JA (eds) Earth climate: The ocean-atmosphere interaction. Geophysical Monograph, 147, AGU, Washington, DC

Yu L, Jin X, Weller RA (2006) Role of net surface heat flux in seasonal variations of sea surface temperature in the tropical Atlantic Ocean. J Clim 19:6153–6169

Zeng N, Yoon J, Marengo J, (2008) Causes and impacts of the 2005 Amazon drought. Environ Res Lett 3:doi:10.1088/1748–9326/3/1/014002

Zhang R, Delworth TL (2005) Simulated tropical response to a substantial weakening of the Atlantic thermohaline circulation. J Clim 18:1853–1860

Chapter 14
Hydrological Variability in South America Below the Tropic of Capricorn (Pampas and Patagonia, Argentina) During the Last 13.0 Ka

Eduardo L. Piovano, Daniel Ariztegui, Francisco Córdoba, Marcela Cioccale, and Florence Sylvestre

Abstract New limnogeological results (Laguna Mar Chiquita, 30°S) at the middle latitudes in the subtropical Pampean plains of Southern South America are used to establish comparisons with records spanning Late Glacial times and the Holocene covering the Northern Andean Patagonia and the Extra Andean Southern Patagonia. Historical and archaeological data were also used to enlarge existing environmental reconstructions in the central plains of Southern South America. Two groups of climate records – at both sides of the Arid Diagonal- can be distinguished according to their hydrological response during dominant warm or cold climatic phases. The first group includes records from the Pampean region and allows to reconstruct the past activity of the South America Monsoonal System. The second group includes archives of the Patagonian climate, as well as the Salinas del Bebedero, and provides a record of past changes in the strength and latitudinal position of the Southern Westerlies.

Keywords Pampean lakes · Late-Pleistocene/Holocene hydrological reconstruction · Arid Diagonal · South American Monsoon System vs. Westerlies

14.1 Introduction

The reconstruction of Late Pleistocene and Holocene environmental variability across the subtropical Pampean plains of Southern South America (SSA) – i.e., south of the Tropic of Capricorn (i.e., 23° 25′S) and east of the Andes- have been hampered by the paucity of complete and well-dated paleoclimate archives. Despite that the last decade has been marked by a substantial increase of paleoclimatic studies in South America, ongoing paleoenvironmental research clearly shows the

E.L. Piovano (✉)
CICTERRA-CONICET, Universidad Nacional de Córdoba, Av Velez Sarsfield 1611, X5016GCA, Córdoba, Argentina
e-mail: epiovano@efn.uncor.edu

F. Vimeux et al. (eds.), *Past Climate Variability in South America and Surrounding Regions*, Developments in Paleoenvironmental Research 14,
DOI 10.1007/978-90-481-2672-9_14,

necessity to analyze past climate variability from a more regional prospective (e.g., LOTRED- SA initiative). To insert the results of single environmental archives in a more regional context is critical to answer some basic and often intriguing questions dealing with the occurrence, timing and frequency of climate fluctuations since the Last Glacial Maximum. The PAGES-sponsored initiative PEP I (Pole Equator Pole through the Americas) represents a milestone using this research strategy (Markgraf et al. 2000, Markgraf 2001) gathering for the first time a limited number of available paleolimnogeological records across the Americas (e.g., Ariztegui et al. 2001, Bradbury et al. 2001, Fritz et al. 2001). Since this early effort a substantial increase in limnogeological studies is shown by the starting of several new research programs (i.e., PALEO-PAMPAS at the middle latitudes or PALATo, PaLaTra, SALSA and the ongoing ICDP-sponsored PASADO in the Argentinean Patagonia).

Results of these investigations point out that SSA climate archives show a complex pattern of timing and climate interactions throughout the Holocene. The precise chronology and magnitude of some of these climatic shifts is still a mater of debate. The new datasets, however, show the advantage of using regional high-resolution multi-proxy climate reconstructions to obtain more realistic past climate scenarios. This downscaling approach is better than the early "smoothed" reconstructions obtained by using paleoenvironmental data at a hemispheric or sub-hemispheric scale. Following this idea, the study of paleoenvironmental records in the Pampean Plains of SSA became critical for comparing latitudinal paleo-circulation dynamics and the hydroclimatic response during the Late Pleistocene and throughout the Holocene. Recent paleoclimate reconstructions show regional contrasting patterns in hydrological responses between the Pampas and Patagonia at both sides of the Arid Diagonal (AD) (Piovano et al. 2006b) (Fig. 14.1). The AD is a narrow band, with precipitation less than 250 mm/year, sited at the boundary or transition between two different atmospheric circulations systems given by the Atlantic and Pacific dominant source of moisture (Bruniard 1982, Schäbitz and Liebricht 1998, Mancini et al. 2005). Numerous paleohydrological reconstructions suggest dominant wet conditions during cold phases -such as those occurred during the middle Holocene or the Little Ice Age (LIA)- in regions located West and South of the AD, like Patagonia or even the Central Andes, with a dominant Pacific source of moisture. For the same climate phase dry conditions can be proposed across the subtropical low-lands east of the AD, under the influence of an Atlantic summer rain regime (Fig. 14.1a). Conversely, extensive dryness across Patagonia and wet conditions in the Pampas can be inferred during warm climate phases such as the Medieval Climatic Anomaly (MCA) or the last part of the 20th century.

In this chapter we present new paleohydrological results at the middle latitudes in the subtropical plains of South America (Laguna Mar Chiquita, 30°S) to further establish comparisons with published limnogeological records spanning Late Glacial times and the Holocene covering the Northern Andean Patagonia and the Extra Andean Southern Patagonia (Fig. 14.1). We also include historical data when available to blend both natural and historically-recorded climate archives in an attempt to enlarge existing environmental reconstructions especially during both the MCA and the LIA in the central plains of Southern South America.

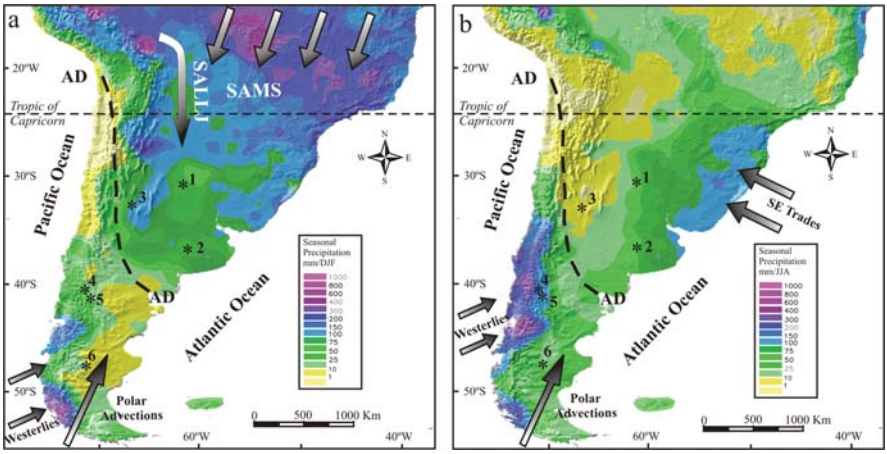

Fig. 14.1 Main components of the seasonal atmospheric circulation patterns in South America (SASM: South American Summer Monsoon, SALLJ: South American Low Level Jets). The numbers refer to the location of the reviewed lakes; (*1*) Laguna Mar Chiquita; (*2*) Lagunas Encadenadas del Oeste system (LEO system); (*3*) Salina del Bebedero; (*4*) Lago Mascardi; (*5*) Lago Frías; and (*6*) Lago Cardiel. AD and dashed-line indicates the position of the Arid Diagonal. (**a**) Austral summer precipitation (DJF, December-January-February) GPCC Full Data Product Version 4 Gauge-Based Analysis 0.5 degree precipitation for seasonal (DJF) 2001–2002 in mm month. (**b**) Austral winter precipitation (JJA, June-July-August) GPCC Full Data Product Version 4 Gauge-Based Analysis 0.5 degree precipitation for seasonal (JJA) 2001 in mm month

14.2 Modern Climate of Southern South America

South America climate distribution is closely linked to the particularly tapered shape and topography of the continent combined with the meridional location and height of the Andes, global circulation cells, ocean currents and the proximity of large bodies of water (Cerveny 1998). The source regions for water vapour and dominant circulations in SSA are: (a) the Pacific Ocean and the Westerly circulation belt in Patagonia and Southern Chile; (b) the south-east trade wind circulation associated with the subtropical South Atlantic anticyclone bringing moisture into the subtropics east of the Andes; and (c) meridional transport of water vapour from the humid lowlands of Brazil and Bolivia to the subtropics (Fig. 14.1). A recent overview on present-day South America climate has been summarized by Garreaud et al. (in press).

A major feature of the seasonal climate variability in South America is the development of a monsoon-like system (Vera et al. 2006) which extends southward from the tropical continental region during the austral summer. It connects the tropical Atlantic Inter Tropical Convergence Zone (ITCZ) with the South Atlantic Convergence Zone (SACZ) via large-scale atmospheric circulation containing a low-level jet (Fig. 14.1a). The South American low-level jet (LLJ) starts in the northern part of South America at the foot of the Andes and driven by the Chaco Low provides moisture for South Eastern South America (SESA) (Nogués-Paegle and Mo 1997,

Labraga et al. 2000) and largely determines the hydrological balance of the region (Berbery and Collini 2000, Saulo et al. 2000, Berbery and Barros 2002). Austral summer precipitation maxima (Fig. 14.1a) and dry winters (Fig. 14.1b) characterize a large area east of the Andes between 22°S and 40°S, where the only external sources of water vapour for rainfall are the Atlantic Ocean and the tropical latitudes (Doyle and Barros 2002). Other important climatic features are the episodic incursions of polar air outbreaks east of the Andes (Marengo and Rogers 2001, Garreaud et al. in press) and El Niño teleconnections controlling precipitation and the hydrology of major fluvial systems (Aceituno 1988, Depetris et al. 1996, Silvestri 2004, Boulanger et al. 2005).

The dominant atmospheric feature south of the 40°S is the strong influence of the Westerly circulation belt or Southern Westerlies (SW) largely controlling the precipitation pattern along the Southern Andes (Prohaska 1976, Garreaud et al. in press) (Fig. 14.1). In the Argentinean Patagonia, the west wind zone forms a straight band, with a northern limit running from the Andean valleys in northern Neuquén at about 37°S to the Atlantic Ocean coast at 41°S. Northwards of 37°S the average height of the Andes increases notably (Aconcagua, 6959 masl at 33°S) blocking the effect of the SW and, therefore, the moistured Pacific air. Precipitation over extratropical South America presents a marked asymmetry with wet conditions to the west of the Andes and dry conditions to the east due to the strong rain-shadow effect (Garreaud et al. in press)

As previously mentioned an outstanding climatic and geographic South American feature is the "Arid Diagonal" (Bruniard 1982) corresponding to a narrow band with very low precipitations, typically less than 250 mm/year, that crosses the continent from northern Peru to the northernmost influence of the SW storm tracks at the Patagonian Atlantic coast (Fig. 14.1). In Argentina, this band extends from ca. 40° to 42°S in the Atlantic coast to the north up to 27°S along the eastern flank of the Andes. Regions at both sides of the AD are characterized by different moisture sources: the subtropical summer rain regime towards the north and east (Atlantic influence) while western and south-western areas are mainly dominated by winter precipitation maxima (Pacific influence) (Fig. 14.1). Changes in vegetation and climatic conditions inferred from pollen records allowed to assess the displacement and location of the AD during the mid-Holocene (Mancini et al. 2005).

14.3 Paleoclimate Archives

In this section we examine and compare new and published limnogeological records spanning Late Glacial times and the Holocene south of the Tropic of Capricorn and east of the Andes. The records cover a wide geographical range and climate regimes in the subtropical Pampean plains, the Northern Andean Patagonia and the Extra Andean Southern Patagonia (Fig. 14.1). Historical and archaeological records from the central plains of Argentina were additionally considered to enlarge existing environmental reconstructions corresponding to the last two millennia. Radiocarbon ages from Laguna Mar Chiquita are presented in Table 14.1while the remaining

Table 14.1 Radiocarbon dates for the core TMC02-2 from Laguna Mar Chiquita

Samples	Depth (cm)	N° laboratory	Material	δ^{13}C/PDB (‰)	^{14}C age year BP	Error	cal ^{14}C AD/BC *a	cal ^{14}C BP *b
TMC02-2 131.5	131.5	Beta-206364	organic sediment	−17.5	1200	40	AD 920–960 (95%)	1062
TMC-02-161.5	161.5	ETH-26692	bulk sediment	−19.7	1590	60	AD 372–612 (98.2%)	1475
TMC-02-181	181.0	ETH-26694	bulk sediment	−24.1	4220	95	BC 3034–2561 (98.2%)	4746
TMC02-2 243.5	243.5	Beta-206365	organic sediment	−21.0	11,100	70	BC 11,250–10,940 (95%)	12,938

*a: calibrated ages obtained using Calib rev 5.0.1 (Reimer et al. 2004).
*b: calibrated ages obtained following Bard et al. (1998).

ages were taken from published data and original papers are cited for details. All the cal BP ages (cal ka and cal a) were obtained following Bard et al. (1998). AD radiocarbon ages where obtained using Calib rev 5.0.1 (Reimer et al. 2004).

14.3.1 Subtropical Latitudes: Pampean Plains

Located eastward of the Andes the Pampean plain in Argentina (Fig. 14.1) is a flat and low area with an altitude ranging between 80 and 400 masl and extending to the south up to ca. 40°S. This extensive and geomorphologically very uniform area is characterized by widespread Late Pleistocene-Holocene loess deposits (for a review see Zárate 2003). We have selected Laguna Mar Chiquita (30°S) as a representative paleoclimate record of the northern pampas (Piovano et al. 2002, 2004a,b, 2006b) and the Salinas del Bebedero (33°S) in the SW margin of the plains (González 1994, González and Maidana 1998, García 1999).

Laguna Mar Chiquita (30°54′S-62°51′W) is a shallow saline lake (ca. 10 m maximum water depth) in the subtropical Pampean plains of Argentina (see location in Fig. 14.1) located at the lowermost end of a large catchment area covering ca. 37570 km^2. Variability in precipitation and river discharge during the 20th century has triggered sharp lake-level fluctuations, making Laguna Mar Chiquita a sensitive hydroclimatic indicator at middle latitudes in South America. The Amazon basin is the principal source of moisture for this portion of South America (Rao et al. 1996) and low-level jets variability largely controls the hydrological balance of the region (e.g., Berri and Inzunza 1993, Nogués-Paegle and Mo 1997, Saulo et al. 2000). Historical and instrumental data show that during dry intervals (i.e., prior to the 1970s), the lake surface was reduced to ∼1000 km^2 whereas covered up to ∼6000 km^2 during periods with a positive hydrological balance (Fig. 14.2a). At present, the lake is at a highstand becoming not only the largest saline lake in South America but also one of the largest in the world. The lake ecosystem, that includes a large wetland in the northern area, is protected by the Ramsar Convention on Wetlands (http://www.ramsar.org/).

Well dated short-cores allowed a calibration of the lake sedimentary, isotope and biological response to the last 100 years of documented lake levels changes. The comparison among these sedimentological and geochemical features, their stable isotope compositions, diatom assemblages, pigments and biomarkers shows a coherent picture that further allows us to formulate a well constrained multiproxy model for the basin (Fig. 14.2b,c; Piovano et al. 2002, 2004a,b, Lucatto et al. 2007, Varandas da Silva et al. 2008, Coianiz et al. 2008). The chronology was developed by combining ^{210}Pb (Piovano et al. 2002) and ^{14}C-AMS radiocarbon dating techniques (Table 14.1). The most recent age control based on the concentration of radionuclides ^{210}Pb was extrapolated downward up to an evaporitic layer that is present in all the retrieved cores, giving an age of AD 1767. Radiocarbon ages on organic remains (Table 14.1) of longer sedimentary cores allowed the reconstruction of lake-level variations prior to the 18th century, covering regional hydrological changes since the Last Glacial Maximum.

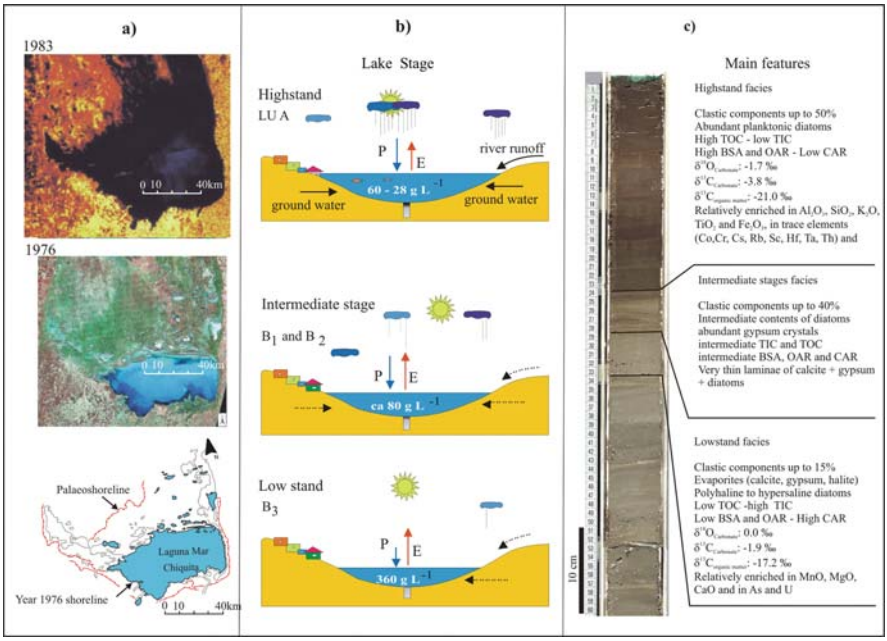

Fig. 14.2 (**a**) Satellite images showing Laguna Mar Chiquita surface variations between 1976 and 1983 (images from http://conae.gov.ar; see Fig. 14.1 for lake location). The scheme on the bottom left shows the extension of the lake (in blue) and paleoshorelines mapped from a 1976 satellite image. The present-day lake shoreline matches the position of the mapped paleoshorelines. (**b**) Laguna Mar Chiquita hydrological model and associated lake-level changes. P-E arrows represent the precipitation (P) evaporation (E) balance; the relative length of the arrows indicates the predominance of either P or E. Higher river runoff and groundwater inputs are indicated by solid arrows, whereas dotted arrows display comparatively low inputs. Lake water salinity is displayed in g L^{-1}. (**c**) Sedimentary, isotopical and geochemical datasets for core TMC-00-I showing conspicuous changes during historically documented low, intermediate and highstands (Modified from Piovano et al. 2002, 2004b, Sylvestre et al. in prep.) TOC: total organic carbon, TIC: total inorganic carbon, BSA: bulk sediment accumulation rate, OAR: organic accumulation rate, CAR: carbonate accumulation rate, REE: rare earth elements. Isotope ratios are average values

A semi-quantitative estimation of paleolake-levels using the carbon isotope composition of organic matter as a hydrological proxy (see Piovano et al. 2004a) shows a pattern of alternating lake highstands and lowstands during the past ca. 13.0 cal ka of reconstructed variability (Fig. 14.3). This reconstruction was further confirmed by modelling variations in bulk sediments elemental composition using ultra high resolution μXRF (Lucatto et al. 2007). The limnogeological record of closed lakes, like Laguna Mar Chiquita, usually contains a clear signature of past variations in the regional hydrological balance but they frequently enclose hiatus due to subaerial lake-floor exposures during pronounced droughts. The analyzed hydroclimatic record of Laguna Mar Chiquita indicates the onset of a highstand and therefore a positive hydrological balance at ca. 13.0 cal ka BP (at level 243.5 cm, Fig. 14.3). This early wet phase follows extremely dry conditions recorded by the

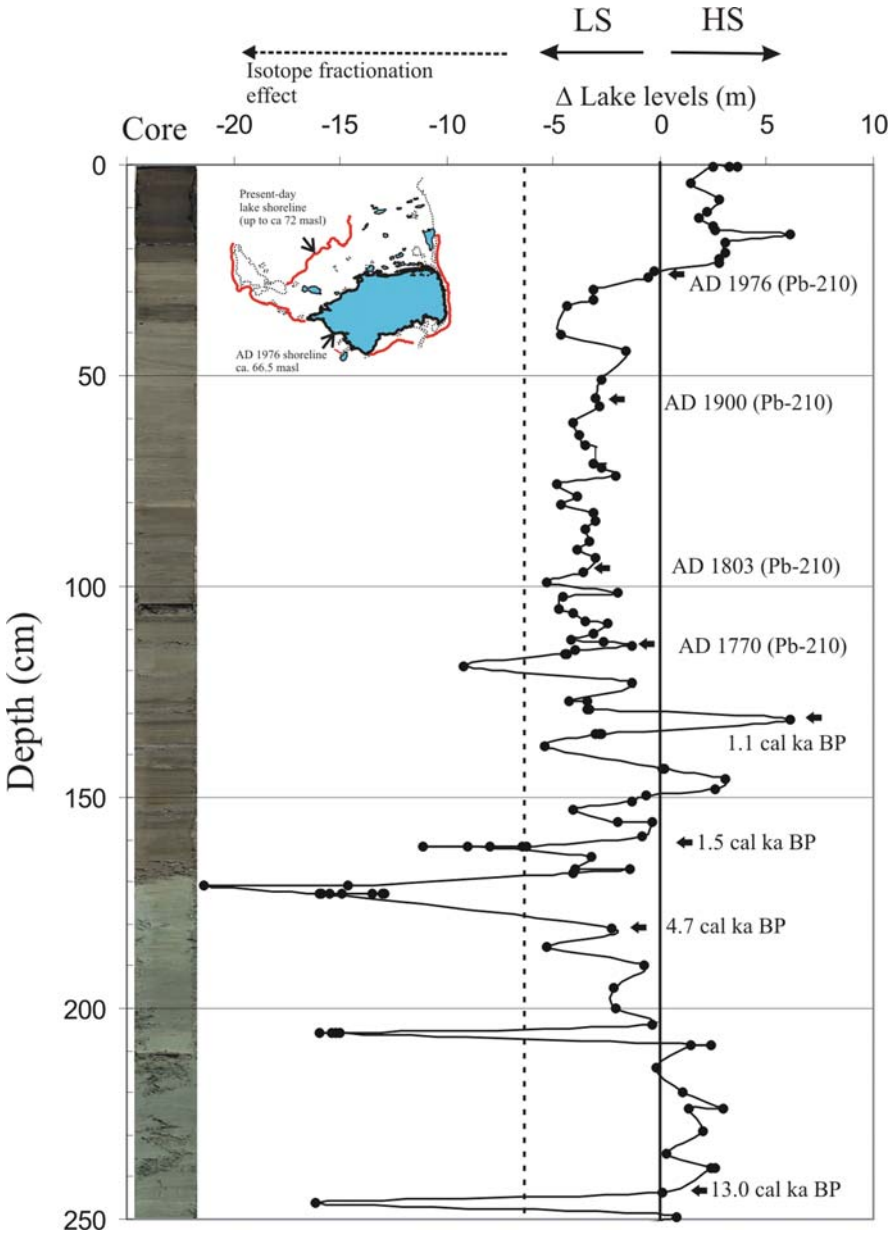

Fig. 14.3 Quantitative paleo-lake level reconstruction based on the isotopic composition of organic matter ($\delta^{13}C$) on core TMC-02-2 following Piovano et al. (2004a). Photograph of the analized core on the left side of the figure. Δ lake level is expressed as a deviation of the 66.5 masl shoreline. Δ lake level = 0 is an intermediate lake-level stage that matches the AD 1976–1977 shoreline elevation (66.5 masl). Positive values represent highstands (lake surface beyond the AD 1976 shoreline position in the scheme) and negative values indicate lowstands (lake surfaces below the

development of discrete levels of evaporates and comparatively more positive isotope composition of both carbonates and organic matter indicating the dominance of evaporation over precipitation throughout the catchment. This wet phase extends along the Early Holocene until a hydrological reversal to an extremely dry phase. Although the age of the onset of this dry phase (level 210 cm, Fig. 14.3) is still unknown, its most intensive magnitude was dated around 4.7 cal Ka BP (level 181 cm, Fig. 14.3). Dry conditions, triggering the precipitation of evaporates and the development of sedimentary hiatuses, were mostly dominant from the Middle Holocene until the middle of the first millennia when less extreme lowstands can be inferred by 1.5 cal Ka BP (AD 372–612; level 161.5 cm, Fig. 14.3) or two highstands, one of them by 1.1 cal Ka BP (AD 920–960; level, 131.5 cm, Fig. 14.3). The timing of the droughs for both the first and second millennia are poorly resolved due to the occurrence of several sedimentary hiatuses indicated by gypsum-halite layers.

In the middle part of the 18th century (∼A.D. 1770), sedimentation became more constant and a good chronology has been established for this later part of the sequence based on ^{210}Pb dates (Piovano et al. 2002). The palaeohydrological record indicates dry conditions since ∼A.D. 1770 but less extreme than the early part of the sequence with the occurrence of short-lived humid pulses during the second half of the 19th century (A.D. 1850–1870). This lowstand has been associated with the LIA whereas the lake level remained very low until the last quarter of the 20th century.

Salina del Bebedero (33° 20′S, 66° 45′W – 380 masl) is a playa complex located close to the SW margin of the Chaco-Pampean plains (see Fig. 14.1). Past connections of the salina with an inflow fed by Pacific moisture and Andean ice-melt water (Rio Desagüadero fluvial system) triggered highstand phases matching cooling global episodes (González 1994, González and Maidana 1998, García 1999). Today and following the river diversion the salina is only fed by local rainfall with Atlantic provenance and a dominant negative hydrological balance that allows the development of a temporary and very shallow lake with water-depth up to 0.5 m (González 1994).

The presence of paleoshorelines located up to 25 m above the present-day salina floor, in addition to sedimentological features as well as changes in diatom and charophyte assemblages provide clear evidence of recurring lake highstands since the Late Pleistocene until the LIA (González 1994, García 1998, González and Maidana 1998) (Fig. 14.4). Several pulses of lake highstands took place during the Late Pleistocene with the last highstand event dated at 13.5 cal Ka BP (González 1994). This increase in lake level seems to be triggered by local rainfall during a

Fig. 14.3 (continued) AD 1976 shoreline position in the scheme). Cal a BP are calibrated radiocarbon ages (Table 14.1) whereas years AD are derived from the ^{210}Pb chronology (Piovano et al. 2002). Arrows indicate dated level. Lake levels below -6 m are not realistic and are interpreted as a statistical artefact of the equation for reconstruction paleo-lake levels (see Piovano et al. 2004a) due to super heavy organic carbon isotope compositions during high evaporative phases

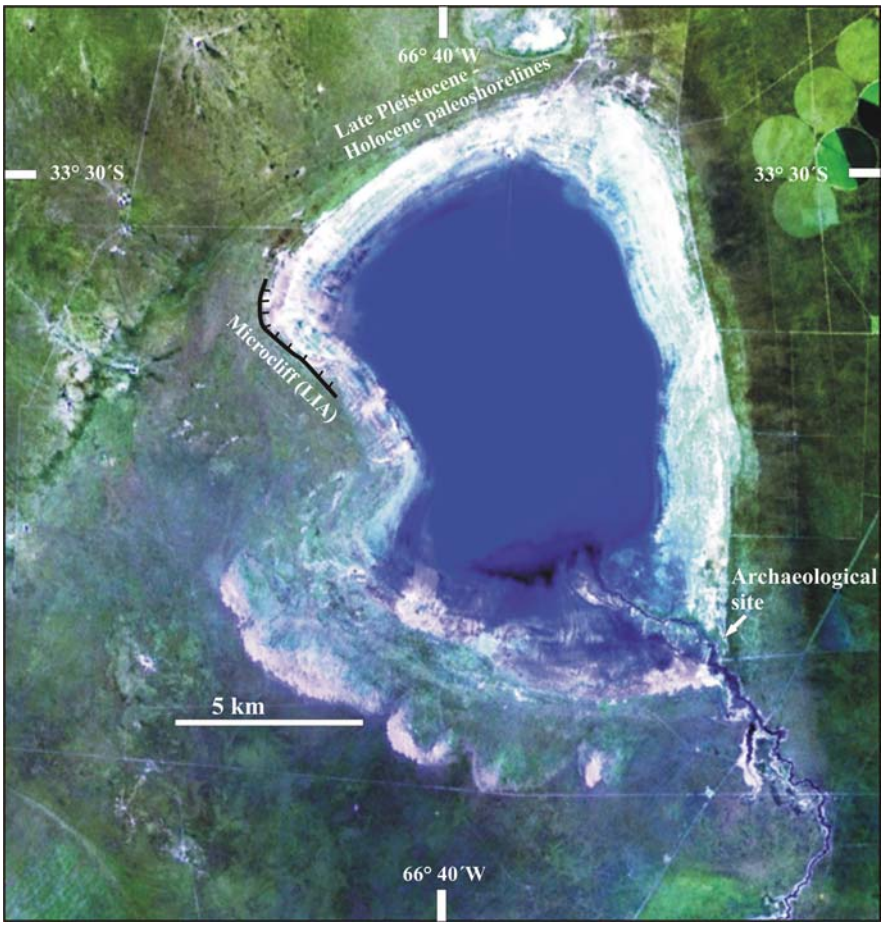

Fig. 14.4 Paleoshorelines at Salina del Bebedero (modified from González and Maidana 1998, see Fig. 14.1 for lake location). Geomorphological evidence of Late Pleistocene and Holocene Lacustrine Stages (in the sense of González 1994, González and Maidana 1998). A paleoshoreline at 6 m above the present-day salina floor (380 masl) is overlapping the archaeological site (indicated in the figure) dated between 10.1 and 9.5 cal Ka BP. The microcliff correspond to the LIA highstands. The satellite image is a Landsat 5–7 processed for agricultural use (obtained at http://conae.gov.ar)

warm episode (González and Maidana 1998). Several lacustrine phases, most of them undated yet, took place during the Holocene. The oldest highstand record presents a magnitude of around 6 m above the present-day lake floor and is overlapping an archaeological site dated between 10.1 and 9.5 cal Ka BP (González 1994). Two subsequent highstands (+10 and +6 m over the salar floor) took place during the LIA at 550 and 334 cal a BP, respectively (1280/1420 and AD 1443/1656). The two pulses during the LIA indicate the existence of a dry episode between these two well defined highstands. Historical documents, however, appears to indicate a high

lacustrine stage (+5/+6 m over the salar floor) from the 18th to the 19th century associated to late LIA times (González 1994).

14.3.2 Argentinean Patagonia and Extra-Andean Patagonia

In the southernmost continental portion of South America, the Andes are separated as Cordillera Patagónica Septentrional extending from 39° to 45°S whereas south of 45°S they form the Cordillera Patagónica Austral. East of the Andes Patagónicos Australes (Southern Andes), the Patagonian Plateau or Meseta Patagónica Austral is mainly formed by extended basaltic plateaux.

In recent years there has been a major increase of limnogeological studies across different areas of Patagonia holding multiproxy results and relatively well-resolved chronologies (e.g., Ariztegui et al. 2008). We have selected the following records, (a) Lago Frias (40°S; Ariztegui et al. 2007) and Lago Mascardi (41° S; Ariztegui et al. 1997) in Northern Patagonia; and (b) Lago Cardiel (49°S; Stine and Stine 1990, Gilli et al. 2001, Gilli 2003, Markgraf et al. 2003, Gilli et al. 2005a,b) in the Patagonian Plateau (see lake locations in Fig. 14.1). Other outstanding lacustrine records are Laguna Potrok Aike (52°S) providing continuous multi-millennial sediment records in the dry steppe of southeastern Patagonia (Haberzettl et al. 2005, Zolitschka et al. 2006, Mayr et al. 2007, Haberzettl et al. 2008) and Lago Fagnano (54°S) in Tierra del Fuego (Waldmann et al. 2007, Waldmann et al. in press). Lakes Fagnano and Potrok Aike most probably represent the southermost continuous continental records outside Antarctica since the Last Glacial Maximum and for the last hundred of thousands years, respectively.

Lago Mascardi (41°S, 71°W; 800 masl) 30 km^2 and 218 m maximum water depth, is fed directly by turbid glacial melt water from the Tronador ice-cap. Its sedimentary record (Fig. 14.5a) provides a continuous archive of the unstable conditions that characterized the Late Glacial-Holocene transition in northern Patagonia with an unprecedent chronological resolution at this latitude in the eastern side of the Andes. Changes in the sedimentary, geochemical and biological record of this lacustrine basin indicate a sharp stepwise climatic evolution that conflict with early reconstructions suggesting a smooth warming of the region during the transition. Four environmental phases were identified and associated with mass balance variations of the Tronador ice-cap using a multiproxy approach that includes grain-size variations, quantity and quality of the organic fraction, pollen and chironomid remains (Ariztegui et al. 1997, Massaferro and Corley 1998). Between ca. 15.2 and 13.3 cal ka BP there was a climatic amelioration showed by a relative increase in the sedimentary organic matter and grain size, reaching maximum values at ca. 14.5 cal Ka BP. The later indicates a substantial retreat of the Tronador ice-cap in phase with the climatic amelioration that occurred during the Bolling-Alleröd interval in the Northern Hemisphere. A subsequent phase is characterized by small grain size, similar to that observed during the Late Glacial and has been attributed to increasing erosion due to a glacier advance. A sharp decrease in the quality of the

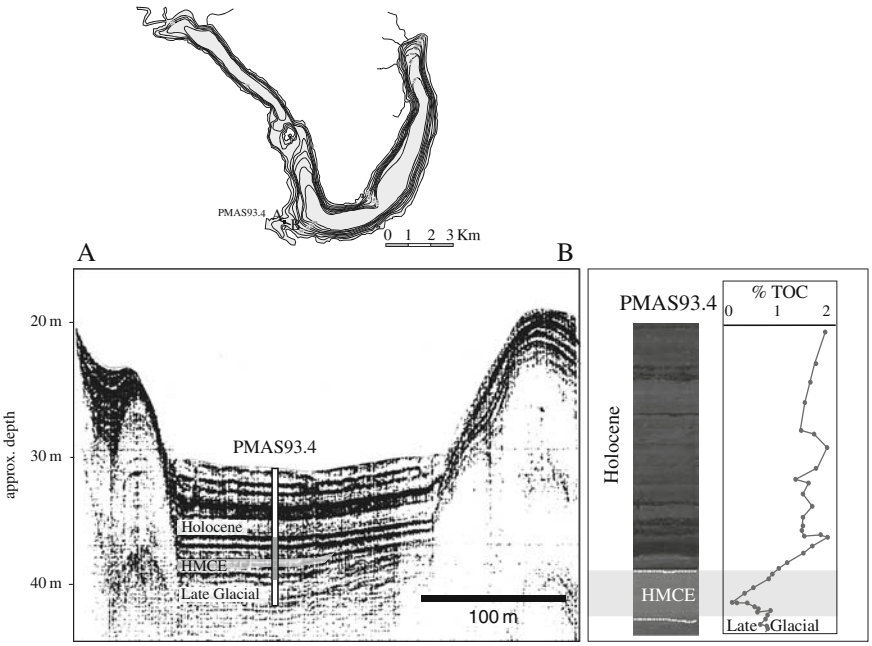

Fig. 14.5 (**a**) Lago Mascardi bathymetric map and seismic profile showing distinctive seismic facies for both Late Glacial and Holocene sediments (see Fig. 14.1 for lake location). (**b**) The light gray zone indicates the Huelmo-Mascardi Cold Event (HMCE) that is visualized in core PMAS93.4 (located in this seismic section) by both increasing quality of the lamination and total organic carbon content

organic matter and in the pollen influx together with changes in chironomid assemblages point towards a cooling phase. The excellent chronology of these changes and their synchronism with the equivalent Huelmo site in the western side of the Andean Cordillera (Moreno et al. 2001) allowed to define the Huelmo-Mascardi Cold Event (HMCE) that encompass the European Younger Dryas chronozone and the Gerzensee/Killamey oscillation and intervening warm spell (Hajdas et al. 2003) (Fig. 14.5b). The early Holocene in Lago Mascardi is marked by warming temperatures and further retreating ice showed by a grain size increase which is considered to reflect a retreat of the Tronador ice-cap during the early Holocene. The climate record corresponding to the rest of the Holocene shows an increasing trend in the abundance of chironomid, that is affected by both climatic and volcanic forcings (Massaferro and Corley 1998). Neither the MCA nor the LIA have been identified so far in this record due to the lack of the appropriated chronological resolution. The nearby Lago Frías record, however, contains a detailed archive of the most recent climate fluctuations in Northern Patagonia.

Lago Frias (40°S, 71°W, 790 masl) is an elongated proglacial lake (4.1 km long, 1.1 km wide; 75 m max. water-depth) located at ca. 7.5 km north of the Frías glacier, one of the Argentinean tongues of the Tronador ice cap (Fig. 14.6). This lacustrine

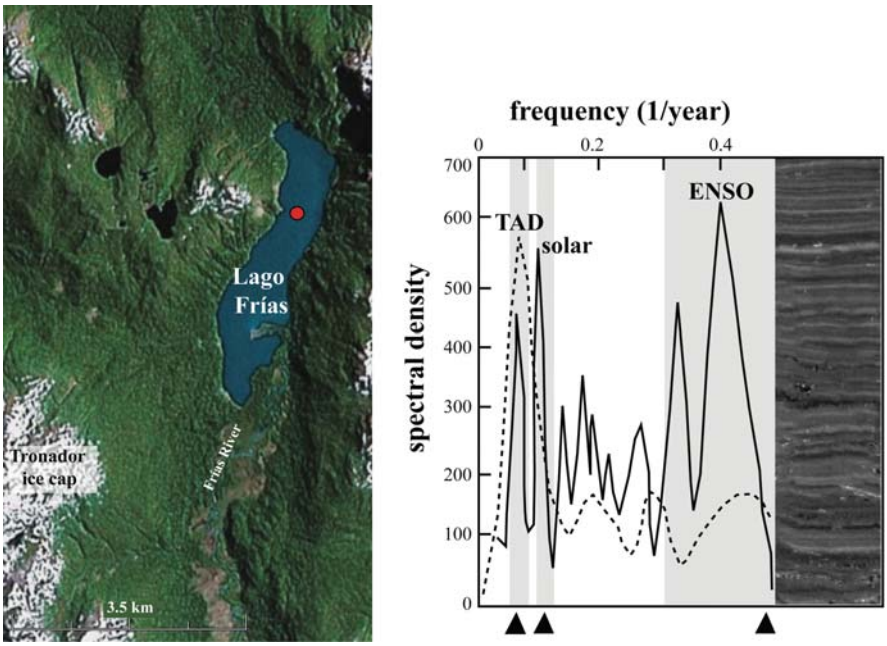

Fig. 14.6 Satellite image showing the location of Lago Frías and the Tronador ice cap. The statistical analyses of annually deposited sediments in Lago Frias (see Fig. 14.1 for lake location in South America) indicate a dominant but not exclusive ENSO signal (see text for discussion)

basin contains a pelagic sequence often affected by mass wasting events (Chapron et al. 2006, Ariztegui et al. 2007). Meteorological, historical and dendrochronological data from the Frías valley show a sharp ENSO impact on local climate (Villalba et al. 1990, 1998). Combining instrumental and historical information with event stratigraphy and radioisotopic data in a well-laminated sedimentary core allowed to generate a robust chronology that confirms the annual character of the lamination. Glacier re-advances have been recorded as a better development of sediment lamination. Variations in the thickness of the clay lamina of a continuous laminated sequence have been related to changes in winter precipitation covering the last ~200 years. A change in the quality of the lamination dated at AD 1873 is in concert with the tree-ring derived cold and rainy period ending in AD 1873 previously assigned to the LIA. Substantial variations in precipitation became evident through changes in lamination from the period AD 1873 to 1909. The most recent formation of push-moraines, between AD 1968 and 1977, is shown by an increase in the lamination index what confirms the sensitivity of this record to changes in glacier activity. Statistical analyses of this dataset indicate an ENSO signal that plays a dominant role in the development of the lamination (Ariztegui et al. 2007). This signal was previously identified in the Frías valley using tree-rings (Villalba et al. 1990 and 1998) and more recently in the sedimentary sequence of Lago Puyehue on the Chilean side

of the Andes (Boës and Fagel 2008). Dendrochronological studies allowed matching cold intervals with higher rainfall and, thus, glacial re-advances (Villalba et al. 1990) that are also recorded through a better development of the lamination along the lacustrine record (Ariztegui et al. 2007). The Lago Frías laminated sequence shows additional frequencies superimposed on the decadal ENSO variations that can be related to both, the eleven years solar cycles, and to a less extend the Tropical Atlantic Dipole (TAD; Ariztegui et al. 2007). Thus, the Lago Frías record provides new insights about the complexity of the various forcing mechanisms behind glacier advances during the LIA in Northern Patagonia. It further higlights the role of precipitation that probably ruled the most recent variation of the glacier equilibrium line.

Lago Cardiel (49°S, 71°W, 276 masl) is located in the Extra-Andean Patagonian plateau of Argentina. It is a closed-lake with a maximum water depth of 76 m occupying a tectonic depression of ca. 20 km of diameter (Gilli et al. 2001). At present, this very arid but sensitive rain-shadow area east of the Andes is seasonally influenced by the Southern Westerlies, therefore the lake provides an ideal location to trace changes in their strength and influence on the local sedimentological regime through time (Gilli et al. 2005a, Stine and Stine 1990, Stine 1994).

The multiproxy analyses of sedimentary cores combined with seismic stratigraphy data indicate substantial lake-level changes during the late Pleistocene and Holocene (Gilli et al. 2001, 2005a,b, Markgraf et al. 2003) (Fig. 14.7). A very shallow lake existed during the starting of the deglaciation until the occurrence of a few hundred years desiccation period after 13.2 cal ka BP. The latter resulted in a peaty, gravelly layer that can also be observed in the seismic (Gilli et al. 2005b). A major change in the hydrological balance followed this desiccation phase. This sequence is found throughout the entire basin implying a large lake level rise after ca. 12.6 cal ka BP up to at least the modern lake level. This transgression of almost +80 m occurred very fast within a few hundred years and it was discontinuous. The occurrence of buried beach ridges during this transgression points towards a stepwise character of the lake level rise since only such a mechanism could allow their preservation preventing their erosion by wave action (Gilli et al. 2005b). Subsequently, the lake level receded but never drops significantly below modern level (Gilli et al. 2005a; Markgraf et al. 2003). High sedimentation rates dominate the north-eastern part of the basin permitting the detailed study of laminated sediments covering the last ca. 1800 years with variable degree of development and thickness (Gilli et al. 2005a,b). Variations in magnetic susceptibility and in trace element content indicate increasing influx of iron oxyhydroxides to the basin during summer that appears as a dark lamina (Ariztegui et al. 2004). Image analyses in the laminated sections of the core show a conspicuous frequency of changes that can be attributed to ENSO as a dominating forcing mechanism behind their formation. These changes in lamination thickness have been related to local wind activity which is directly induced to either intensification or weakening of the westerly storm tracks. It further provides an independent proxy for wind intensity confirming previous studies that were based on indicators at a lower time resolution such as seismic stratigraphy, stable isotopes and pollen analysis (Gilli 2003, Gilli et al. 2005b, Markgraf et al. 2003). All these proxies

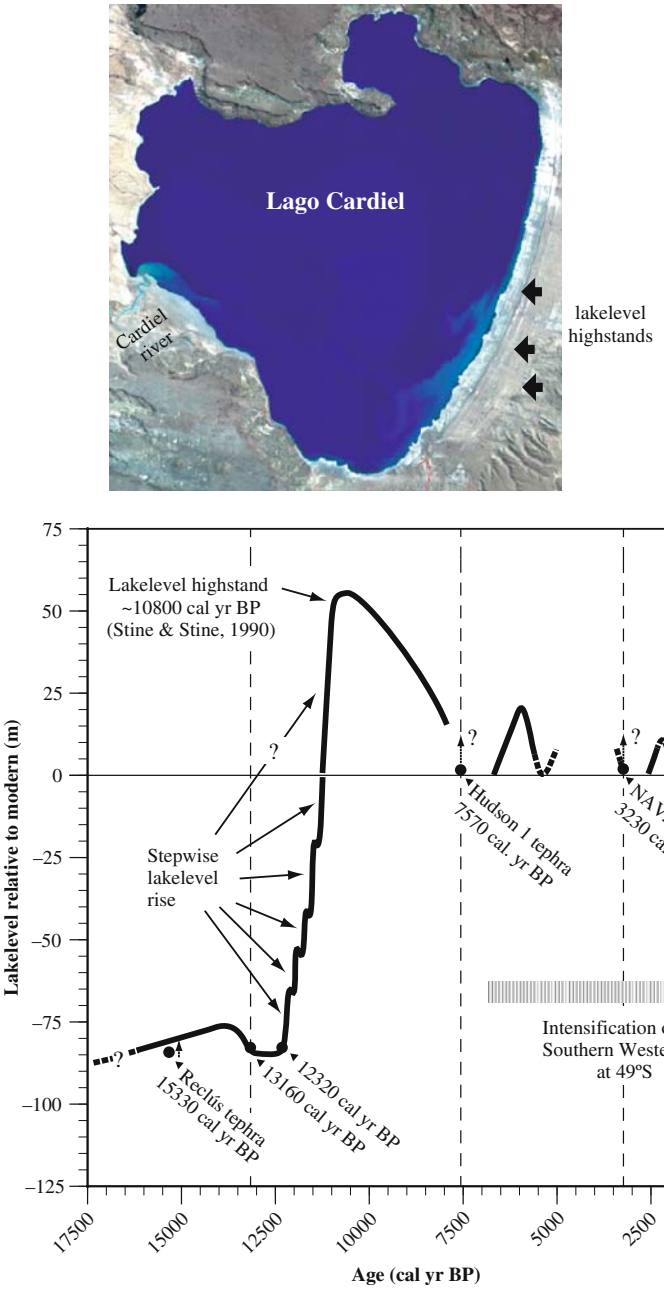

Fig. 14.7 Satellite image of Lago Cardiel in the extra Andean Patagonia and the reconstructed lake level curve using a limnogeological approach (after Gilli et al. 2005a, Ariztegui et al. 2008). See text for discussion

indicate a strong dominance of wind (i.e., precipitation) during the last 2000 years and thus, the thermally defined periods of Medieval Warm Period (MWP) and the Little Ice Age (LIA) are not clearly expressed in the record. Gilli (2003) noticed that the high variability documented in most of the proxies during this interval is a characteristic pattern for many paleoenvironmental records in the circum-South Pacific for the last 3000 years and can be partially explained by an ENSO intensification (Aceituno 1988).

14.3.3 Archeological and Historical Sources of Climate Variability in Central Argentina

The MCA (Stine 1994, Villalba 1994) and the LIA (Villalba 1994, Luckman and Villalba 2001) are very well represented across Patagonia by a wide range of climate archives (i.e., tree-rings, glacial features, archeological sites, paleolimnological records) (Stine 1994, Villalba 1994, Favier-Dubois 2003, 2007, Mauquoy et al. 2004, Haberzettl et al. 2005, Mayr et al. 2005, 2007, Meyer and Wagner 2008, Moy et al. 2008). Conversely, the number of high resolution climate reconstructions across the Pampean plains spanning the last millennium is still scarce. With the exception of the semiquantitative hydrological reconstruction from the Laguna Mar Chiquita (Fig. 14.3) that allows to establish a hydrological comparison between the MCA and LIA, there is a general lack of calibrated hydroclimatic reconstructions to compare the intensity of a certain hydroclimatic phase.

For the period coeval to the MCA several climatic indicators suggest warm and wet conditions for the Pampean plains tentatively between 1400 and 800 a BP with important soil development and formation of swamps in depressions (Carignano 1999, Iriondo 1999). The wet period, particularly between 1410 and 1068 cal a BP, was interrupted by dry-phases as can be recognized in the Laguna Mar Chiquita paleohydrological reconstruction (Fig. 14.3, see level 140 cm). Archaeological sources indicate an increase in the human occupation of this area ca. 1000 a BP, characterized by a mixed subsistence strategy based on hunter-gathering complemented by agriculture, as well as village lifestyle and pottery manufacture, established NW of Mar Chiquita before the Spanish Conquer at about 1573 AD (Laguens and Bonnin in press). During this time, the cultivation line was displaced several kilometers into the present-day playa complex pointing toward more favorable condition for human expansion by 1000 a BP (Laguens and Bonnin 1987, Cioccale 1999). With the exception of the Mar Chiquita paleohydrological reconstruction, no other well dated episodes are available to better constrain the duration of this wet and warm phase during the MCA in center Argentina.

Climate during the LIA in the central region of Argentina was more arid and colder than today (Politis 1984, Cioccale 1999, Iriondo 1999, Piovano et al. 2002, 2004a; Laguens and Bonnin in press). On the loessic plain the hydrological deficit triggered recessions of fluvial and lacustrine systems as become evident through the analysis of Jesuit cartography (Fig. 14.8). Present-day rivers feeding Laguna Mar Chiquita (i.e., río Suquia and Xanaes) infiltrated before reaching the lake, which

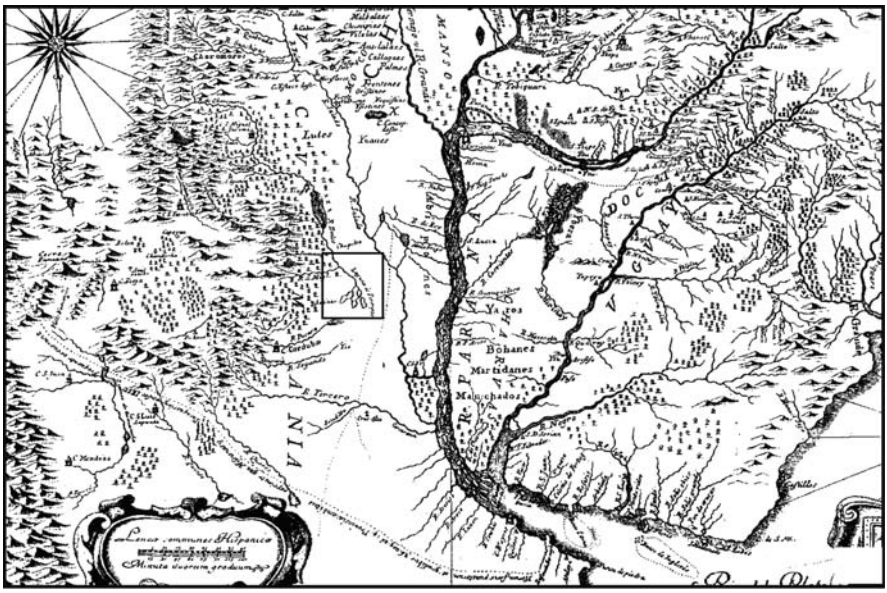

Fig. 14.8 The Jesuit cartography from AD 1732 (taken from Furlong Cardiff 1937) shows a marked reduction in the length of the active channels as well as a decrease or absence of lakes and swamps associated to a dry phase. The square in the center of the map shows that Laguna Mar Chiquita is mapped as small and isolated water bodies (named Laguna de Los Porongos)

was formed by several minor lakes partially covered by dunes (Furlong Cardiff 1937, Parras 1943) instead of a main water body like the present. Archaeological evidences point toward two cold pulses, separated by a comparatively "warmer and wetter" phase during the LIA in the central region of Argentina (Cioccale 1999). The first cold pulse extended from the first decades of the 15th century until the end of the 16th century. Archaeological sources indicate for the 15th century a generalized crisis of the indigenous system that was dramatically increased by the invasion of Spanish conquerors at the end of the 16th century (Laguens and Bonnin in press). This period characterized by high demographic pressure and little development of agricultural practices, coeval with conspicuous environmental changes due to extensive droughts (Laguens and Bonnin 1987, Laguens 1993, Laguens and Bonnin in press). In addition, a widespread record of droughts in the regions north and east of Mar Chiquita (i.e., Tucumán and Santa Fé Provinces) can be reconstructed by the end of the 16th century (Prieto and Jorba 1990, López de Albornoz 1997).

In comparison to central Argentina, the southernmost portion of the subtropics, close to the Lagunas Encadenadas system (37°S; see Fig. 14.1), were under more severe droughts that resulted in frequent dust storms, sand dunes reactivations, desiccated lakes, and pervasive cattle mortality. An interesting archeological-proxy data is provided by the characteristics of the infrastructure for storing food built by

the indigenous (Laguens 1993, Cioccale 1999). The indigenous built underground spaces for food conservation locally named "hornitos". Two different generations of "hornitos" can be recognized for the period before and after AD 1550. More recent "hornitos" are comparatively bigger than the early ones due to the necessity of increasing the storing capacity. This change is interpreted as a strategy of minimizing risks due to environmental crisis (Laguens 1993).

The intermediate period, spanning from the end of the 16th until the beginning of the 17th century, was characterized by comparatively more positive hydrological balances as suggested by the cartography that shows lake expansions and more defined fluvial systems (Furlong Cardiff 1937). Under this climatic scenario, the Spanish conquer expanded all over the region (Laguens and Bonnin in press). Historical data make references to a general increase in precipitations with a peak between AD 1650–1600 and AD 1720–1740 (Pietro and Jorba 1990). Historical records from the Extinguished Council of Buenos Aires indicate that during the 16th and 17th century the climate was similar to present. Records from AD 1589 to AD 1697 show that 85% of the years were "normal" (Politis 1984).

The second cold pulse started during the first part of the 18th century and lasted until the end or even the middle of the 19th century (Cioccale 1999). This pulse was the coldest and driest part of the LIA. In comparison with the 12th century, the 18th century was characterized by the occurrence of extreme events of droughts or floods for a wide region, according to historical sources (Prieto and Herrera 2001). The Jesuit cartography (Furlong Cardiff 1937) shows a marked reduction in the length of the active channels as well as a decrease or absence of lakes and swamps associated to a dry phase (Fig. 14.8). Historical data also reveal a marked water deficit during the 18th and beginning of the 19th century (Prieto and Jorba 1990). Proceedings of the Extinguished Council of Buenos Aires indicate dryer and cooler conditions than today for the 73% of the years between AD 1698 and 1791 (Politis 1984). Intensive droughts were recorded in the decade of 1770 with a maximum during 1780–1790 in central, west and NW Argentina (Prieto and Herrera 2001).

Extreme and generalized droughts also occurred during the first half of the 19th century from AD 1800 to AD 1810 and from AD 1827 to AD 1832. The last period, namely "the Great Drought" or "Gran Seca", was very well described by Darwin (1860). In his report Darwin mentioned . . .*During this time so little rain fell, that the vegetation, even to the thistles, failed; the brooks were dried up, and the whole country assumed the appearance of a dusty high-road. Very great numbers of birds, wild animals, cattle, and horses perished from the want of food and water. . . The smaller streams in the Pampas were paved with a breccias of bones*. . .. In contrast, the second half of the 19th century, was characterized by an increase of the flood frequency (Moncaut 2003) but always under a dominant negative hydrological balance. Darwinś descriptions make reference that . . .*subsequently to the drought of 1827 to 1832, a very rainy season followed which caused great floods. Hence it is almost certain that some thousands of the skeletons were buried by the deposits of the very next year. What would be the opinion of a geologist, viewing such an enormous collection of bones, of all kinds of animals and of all ages, thus embedded in one thick earthy mass? Would he not attribute it to a flood having swept over the surface of the land, rather than to the common order of things.*

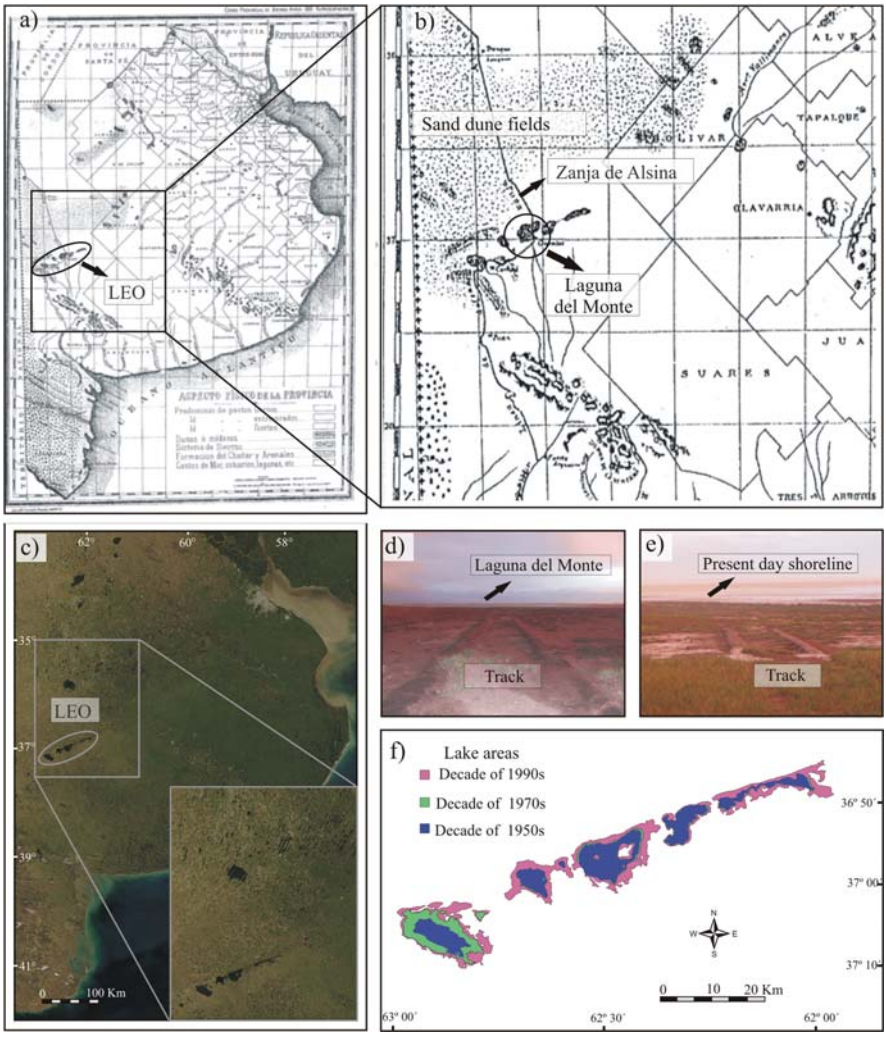

Fig. 14.9 Contrasting hydrological scenario between the end of the LIA and the present-day situation in the Southern Pampean Plain. (**a**) Historical map of the region from AD 1881 (courtesy of the Museo Regional Dr. Adolfo Alsina). (**b**) An enlargement of a portion of the map showing a reduced lacustrine system (LEO system) and extensive sand dunes fields. The "Zanja de Alsina" was built as a boundary between Indian domains (to the West) and areas controlled by the Argentinean government (to the East) during the namely "Conquest of the Desert" in 1877. (**c**) and (**d**) Photographs showing the remains of a dirty-road running next to the "Zanja Alsina" used to cross the Laguna del Monte during the end of the 19th century. At present the track is interrupted by the most recent lake level increase of Laguna del Monte. (**e**) Satellite image showing the present-day conditions. (**f**) Lake area decadal variability of the LEO system during the 20th century

A map from 1881 and a recent satellite image offers a comparison between the contrasting hydrological scenario, during the LIA (Fig. 14.9a,b) and the present-day situation (Fig. 14.9c,d,e,f) in the LEO system, at the southern border of the subtropical plains. The expansion of the sand dune field, reduced lake extensions

and a dirty-road (see "Zanja Alsina" in Fig. 14.9b) crossing a lake was used for travelling across western Buenos Aires Province illustrate the negative hydrological balance during the end of the 19th century. Figures 14.8d,e (AD 2006) shows the old track interrupted by the lake level increase of Laguna del Monte after the 70s (Córdoba et al. 2006).

14.4 Discussion

Limnogeological records south of 30° S in Southern South America show substantial regional hydrological variability since Late Glacial times and overall the Holocene at both sides of the AD. Today, the south-eastern part of the AD (Bruniard 1982) represents the austral border of the subtropics, a very sensitive area to past and present atmospheric circulation changes. It also represents the limit between two main geographical domains in South America: the Pampas and Patagonia. The south-eastern portion of the AD is located along the border of two different circulation systems corresponding to the southernmost influence of the subtropical low-level jet associated to the South America Monsoonal System (SAMS) (Berri and Inzunza 1993, Nogués-Paegle and Mo 1997, Zhou and Lau 1998, Vera et al. 2006) and the northern border of the Southern Westerlies (Prohaska 1976, Garreaud et al. in press) (Fig. 14.1).

Two groups of climate records can be distinguished according to their hydrological response during dominant warm or cold climatic phases. The first group includes records from the Pampean region with the exception of Salina del Bebedero that is mostly controlled by Pacific moisture. This "Pampean group" – with an Atlantic source of moisture – allows to reconstruct the past activity of the SAMS (Piovano et al. 2006b). The second group includes the Salinas del Bebedero and Patagonian climate archives and provides a record of past changes in the strength and latitudinal position of the Southern Westerlies (Markgraf et al. 1992, Gilli et al. 2005a,b, Mayr et al. 2007).

14.4.1 Climatic Driven Hydrological Changes in Southern South America (South of 30°S). From the Late Glacial Times Until the Little Ice Age and the 20th Century

Paleoenvironmental data covering the Last Glacial Maximum show extensive dry conditions for both the Pampas (Muhs and Zárate 2001, Prieto et al. 2004, Piovano et al. 2006b, Zech et al. 2008) and Patagonian region (Ariztegui et al. 1997, Bradbury et al. 2001, Gilli et al. 2001) excepting at Salinas del Bebedero where large amounts of seasonal meltwater from Andean fluvial system triggered high lake levels (González 1994, González and Maidana 1998, García 1999). Model simulations of Last Glacial Maximum westerlies in the subtropics are consistent

with comparatively more humid conditions in agreement with the paleohydrological reconstructions from Salina del Bebedero (Wainer et al. 2005). Following the Last Glacial Maximum extensive dry conditions, the hydrological shift toward positive balances noted in Mar Chiquita and starting by 13.0 cal Ka BP (Fig. 14.3), is also evident through paleoshorelines above the present floor of Salina del Bebedero dated at 13.5 cal Ka BP. This synchronic and in phase hydrological response of both systems (Mar Chiquita and Bebedero) confirm previous assumptions (González and Maidana 1998) pointing toward a precipitation increase with an Atlantic source as the triggering mechanism of the 13.5 cal Ka BP highstand in Bebedero. The duration of the 13.0 cal Ka BP wet and warm phase recorded in Mar Chiquita is still unknown. However, it can probably span the Early Holocene as proposed for different latitudes across the central plains of Argentina (e.g., Zárate et al. 2000, Prieto et al. 2004, Zech et al. 2008). The precipitation and temperature increase covering the Late Glacial-Early Holocene was also identified in the southernmost subtropical region of the Pampean Plains (Zech et al. 2008) suggesting the development of a regional wet phase by a monsoonal circulation strengthening. A climatic amelioration after full-glacial times is further evident at different latitudes in Patagonia as shown in the records of Lago Mascardi (Ariztegui et al. 1997) and Lago Cardiel (Gilli et al. 2005b), respectively. High lake levels associated to a pluvial phase between 13.2 and 11.8 Ka BP (TL and $^{230}Th/^{234}U$ ages) were also proposed for the Extra-Andean Patagonia along 41°S (Tatur et al. 2002) suggesting for this time in-phase conditions for the Pampean region and Patagonia.

The paleohydrological reconstruction in Laguna Mar Chiquita indicates that the wet and warm phase was interrupted by a hydrological reversal to a super-dry phase with an extreme magnitude around 4.7 cal Ka BP. The general drying was dominant until the middle of the first millennia when less extreme lowstands can be inferred (Fig. 14.3). Dry conditions during the Mid Holocene have been widely recognized across the subtropical Pampean plains (Muhs and Zárate 2001, Prieto et al. 2004, Mancini et al. 2005) pointing toward a regional magnitude of the cold and dry climatic event.

The cold and dry Middle Holocene phase is consistent with a reduced latitudinal convey of moisture from the tropics to the subtropics as a consequence of a weakened Monsoonal circulation. The present-day South American Monsoon circulation and austral summer precipitation in SESA are both highly related to changes in the thermal contrast between the continent and the adjacent oceanic regions (Vera et al. 2006). Rainfall variability in a broad region of South Eastern South America is related to both variations in the position of the South Atlantic Convergence Zone (SACZ) and to the sea surface temperature (SST). Colder than usual SST anomalies to the south of the mean SACZ position are also accompanied by lower than usual rainfall in SESA (Barros et al. 2000) and Central-western Argentina (Compagnucci et al. 2002) due to a decrease of low level jet moisture contribution (Doyle and Barros 2002).

Conversely, lake systems fed by dominant Pacific-source moisture (i.e., Bebedero and Patagonian lakes) did not experience the general dry-phase in comparison to those from the Pampean region. The Late-Pleistocene-Holocene transition warming

is recorded both in Lago Mascardi and Cardiel while the lake levels never dropped significantly during the whole Holocene (Gilli et al. 2001, Markgraf et al. 2003). Hydrological proxies from the Lago Cardiel record indicate an strengthening of the Southern Westerlies after 6.8 cal Ka BP caused by an increase in the temperature gradient as a result of an enhanced influence of the Southeast Pacific anticyclone, larger Antartic sea-ice extend (Gilli et al. 2005b) and the effect of changes in insolation (Markgraf 1998). The intensified strengthening of the Southern Westerlies after 6.8 cal Ka BP is coeval with weakened Monsoonal circulation in the Subtropics that triggered the Middle Holocene dry period, pointing toward the development of a hydrological anti-phasing at both sides of the Arid Diagonal.

Several climate indicators (lake sediments, historical documents and archaeological data) also indicate the hydrological anti-phasing during the MCA and the LIA. High lake levels in Mar Chiquita after 1475 cal a BP and by 1060 cal a BP and archaeological reconstruction indicate wet and warm conditions across the Pampean region for the period prior and synchronous to the MCA (Villalba 1994). Paleohydrological reconstructions indicate that the MCA wet phase had a magnitude equivalent to the present-day one; however, it was not uniform and included a dry, and therefore cooler, phase between 1475 cal a BP and 1060 cal a BP. In contrast, there are multiple evidence of increased aridity during the MCA overall Patagonia as well as all the regions under the influence of latitudinal shifts of the Southern Hemisphere westerlies (Villalba et al. 1990, Favier-Dubois 2003, Jenny et al. 2003, Mauquoy et al. 2004, Haberzettl et al. 2005, Boës and Fagel 2008, Mayr et al. 2007, Meyer and Wagner 2008, Moy et al. 2008).

Paleohydrological proxies for the cold period corresponding to the LIA indicate opposite hydroclimatic conditions in the Pampean region and Patagonia, respectively. Several proxies in the Laguna Mar Chiquita record as well a high number of historical sources signify an intense drying northward the Arid Diagonal due to a diminished meridional transport of moisture into the subtropics. Conversely, high lake levels can be inferred both in Northern and Southern Patagonia (Stine and Stine 1990, Haberzettl et al. 2005, Ariztegui et al. 2007, among others) as well as in the Salina del Bebedero (González 1994, González and Maidana 1998).

Following the scenario of summer precipitation in the subtropics, the lake-levels increase in Lake Mar Chiquita during the MCA can be interpreted as a response to increased summer moisture convergence. Hence, these more humid conditions are the result of increasing low-level jet moisture transport associated with a weaker SACZ seasonal development. In contrast, colder SST anomalies during the LIA were accompanied by lower precipitations due to a decreased low level jet moisture as identified during present-day cold phases (Doyle and Barros 2002). The link between Southern Hemisphere Westerlies variability and precipitation fluctuation in Patagonia for the MCA and LIA can be possibly explained by changes in the extension of the sea ice south of South America (Meyer and Wagner 2008). The dry phase during the MCA is associated with a decreased SHW activity due to a southward shift of the storm track as the result of a decrease in sea ice cover. During the LIA the volume of sea ice increased again and the SHWs shifted further northward increasing precipitation (Meyer and Wagner 2008).

14.4.2 The 20th Century Climate Variability

The 20th century climate variability shows contrasting hydroclimatic patterns at both sides of the AD. The regions located northward of it were affected by long drought intervals throughout the first three quarters of the 20th century followed by a humid phase since the 70s. This most recent wet phase seems to be linked to both long-term trends and El Niño-Southern Oscillation (ENSO) interannual teleconnections (e.g., Boulanger et al. 2005). The wet spell has not finished yet and resulted in a general increase of precipitations and streamflows in the Río de la Plata basin (Genta et al. 1998, Robertson and Mechoso 1998, García and Mechoso 2005, Pasquini and Depetris 2007), central Argentina (Piovano et al. 2004a; Pasquini et al. 2006), and central western Argentina (Compagnucci et al. 2002, Pasquini et al. 2006) triggering a widespread lake level increase across the pampean plains (Piovano et al. 2002, 2004a, 2006a; Córdoba et al. 2006). In contrast, linear trends in regionally-averaged annual and seasonal temperature and precipitation records in northwestern Patagonia (between ca. 38° and 45°S) indicate significant warming and decreasing precipitation over the 20th century (Masiokas et al. 2008). Negative correlation between regional annual streamflow variations and both annual and seasonal precipitation and temperature records over the 1912–2002 period point toward the opposite influence of this variables on river discharges (Masiokas et al. 2008). At a higher fluvial-catchment scale, the hydrological analyses of the rivers draining Patagoniaś Atlantic seaboard show a negative trend in some austral summer months (Pasquini and Depetris 2007). A clear warming trend is also evident at southern latitudes from 46° to 55°S that is intensified at higher latitudes (Villalba et al. 2003).

These results suggest the development of anti-phasing hydrological balances when the most recent hydroclimatic scenario of Patagonia is compared to the dominant situation in the Pampean region. The coeval and in phase sequence of the 20th century hydrological variability shown by Laguna Mar Chiquita water-levels, regional instrumental record of precipitation and discharges from large-scale fluvial systems (e.g., Río Paraná; Río Paraguay) highlight that the Mar Chiquita paleoclimatic record can be further extrapolated to a wider region of South Eastern South America east of the Andes (Piovano et al. 2004a, Sylvestre et al. in prep.).

14.5 Final remarks

Paleohydrological changes occurred in the Pampean region after Late Glacial times can be fairly reconstructed from the Laguna Mar Chiquita paleolimnological record (30°S). The matching 20th century hydrological variability between Laguna Mar Chiquita and large-scale fluvial systems (e.g., Río Paraná; Río Paraguay) remarks the value of Laguna Mar Chiquita record for reconstructing past South American Monsoon System activity. Work on progress also shows the potential of the Lagunas Encadenadas del Oeste system (37°S) for recording the hydroclimatic variability in the southernmost influence of the SAMS in the vicinity of the Arid Diagonal.

Instrumental record suggests the development of anti-phasing hydrological balances when the 20th century hydroclimatic scenario of Patagonia is compared to the dominant situation in the Pampean region. Multiproxy paleohydrological reconstructions in Patagonia and the Pampean plains further indicate the development of the anti-phasing hydrological response after the middle Holocene when took place a synchronic intensification of the Southern Westerlies and weakened Monsoonal circulation. The anti-phasing cold/wet vs. cold/dry hydrological conditions at different latitudes reveal that increased rainfall triggered by intensified Westerlies in Patagonia are synchronous with a diminished advection of humidity from the tropics to the subtropics. This results show that paleolimnological studies along the subtropical plains of South America are critical for obtaining more realistic regional reconstructions of past climate variability. The initiative followed by the PALEOPAMPAS programme will help to disentangle the role of the subtropics as forcing factors of changes in the atmospheric circulation in South America.

Acknowledgments Part of this study was supported by Argentina through funding of CONICET (PIP 5947; PIP 112-200801-00808), FONCYT (PICT Nº 25594 and PICT 2006-00625) and SECyT (UNC), PID 2008 (Ministerio de Ciencia y Tecnologia de la Provincia de Córdoba). We acknowledge financial support from the Swiss National Foundation (projects NF21-37689.93, NF2100-050862.97/1, NF200021-1006668/1 and NF200020-111928/1 to D. Ariztegui). The research leading to these results has received funding from the European community's seventh Framework Programme (FP7/2007–2013) under Grant Agremment N°212492 (CLARIS LPB. A Europe-SouthAmerica Network for Climate Change Assesment and Impact Studies in La Plata Basin). We thank Jorge Chiesa for fruitful comments on Salina del Bebedero and Emmanuel Chapron for his constructive comments during the review.

References

Aceituno P (1988) On the functioning of the Southern Oscillation in the South American sector. Part 1: Surface climate. Mon Weather Rev 116:505–524

Ariztegui D, Bianchi M, Masaferro J et al (1997) Interhemispheric synchrony of Late-glacial climatic instability as recorded in proglacial lake Mascardi, Argentina. J Quat Sci 12:333–338

Ariztegui D, Anselmetti FS, Kelts K et al (2001) Identifying paleoenvironmental change across South and North America using high-resolution seismic stratigraphy in lakes. In: Markgraf V (ed) Interhemispheric Climate Linkages. Academic Press, New York

Ariztegui D, Waldmann N, Gilli A, Anselmetti FS (2004) Sedimentary Iron Oxyhydroxides Fluxes in Lago cardiel (Argentina): Estimating Late Holocene Wind Intensity in Southernmost Patagonia. EOS Trans AGU, 85, AGU Fall Meet. Suppl., San Francisco, USA.

Ariztegui D, Bösch P, Davaud E (2007) Dominant ENSO frequencies during the Little ice Age (LIA) in Northern Patagonia as shown by laminated sediments in proglacial Lago Frias (Argentina). Quat Int 161:46–55

Ariztegui D, Anselmetti F, Gilli A, Waldmann N (2008) Late Pleistocene environmental changes in Patagonia and Tierra del Fuego – A limnogeological approach. In: Rabassa J (ed) The Late Cenozoic of Patagonia and Tierra del Fuego. Developments in Quaternary Sciences Series 11. ISBN 978-0-444-52954-1. Elsevier Science

Bard E, Arnold M, Hamelin B et al (1998) Radiocarbon calibration by means of mass spectrometric $^{230}Th/^{234}U$ and ^{14}C ages of corals. An updated data base including samples from Barbados, Mururoa and Tahiti. Radiocarbon 40:1085–1092

Barros V, González M, Liebmann B, Camilloni I (2000) Influence of the SACZ and South Atlantic sea surface temperatura on interanual summer rainfall variability in Southeastern South America. Theor Appl Climatol 67:123–133

Berbery EH, Barros V (2002) The hydrologic cycle of the La Plata basin in South America. J Hydrometeorol 3:630–645
Berbery EH, Collini A (2000) Springtime precipitation and water vapour flux over southeastern South America. Mon Weather Rev 128:1328–1346
Berri GJ, Inzunza J (1993) The effect of the low-level jet on the poleward water vapour transport in the central region of South America. Atmos Environ 27A:335–341
Boës X, Fagel N (2008) Relationships between southern Chilean varved lake sediments, precipitation and ENSO for the last 600 years. J Paleolimnol 39:237–252
Boulanger J-P, Leloup J, Penalba O et al (2005) Observed precipitation in the Paraná-Plata hydrological basin : Long-term trends, extreme conditions and ENSO teleconnections. Clim Dyn 24:393–413
Bradbury JP, Grosjean M, Stine S, Sylvestre F (2001) Full and late glacial lake records along the PEP1 Transect: Their role in developing interhemispheric palaeoclimate interactions. In: Markgraf V (ed) Interhemispheric Climate Linkages. Academic Press, New York
Bruniard E (1982) La diagonal árida Argentina: un límite climático real. Revista Geográfica 95:5–20
Vera C, Higgins W, Amador J et al (2006) Toward a unified view of the American monsoon systems. J Clim Special Section:4977–5000
Carignano CA (1999) Late Pleistocene to recent climate change in Córdoba Province, Argentina: Geomorphological evidence. Quat Int 57–58:117–134
Cerveny RS (1998) Present climates of South America. In: Hobbs JE, Lindesay JA, Bridgman HA (eds) Climates of the southern continents: Present, past and Future. John Wiley, Hoboken, NJ
Chapron E, Ariztegui D, Mulsow S (2006) Impact of 1960 major subduction earthquake in Northern Patagonia (Chile-Argentina). Quat Int 158:58–71
Cioccale M (1999) Climatic fluctuation in the Central region of Argentina in the last 1000 years. Quat Int 62:35–47
Coianiz L, Ariztegui D, Piovano E (2008) Lacustrine Organic Matter (LOM) in a saline to hypersaline system: Tracking the relationship between modern depositional environments and organic matter formation and distribution. EGU2008-A-07779
Compagnucci RH, Agosta EA, Vargas WM (2002) Climatic change and quasi-oscillations in central-west Argentina summer precipitation: Main features and coherent behaviour with southern African region. Clim Dyn 18:421–435
Córdoba F, Piovano E, Pasquini A (2006) The 20th-century limnological and rainfall variation across the Pampean plains of central Argentina. Reconstructing Past Regional Climate Variations in South America over the late Holocene: A new PAGES iniciative. International Symposium. Malargue, Argentina. Abstracts:49
Darwin C (1860) A Naturalist´s Voyage Round the World. The Voyage of the Beagle First Edition. Chapter VII:142–143. (The Project Gutenberg EBook, http://www.darwinsgalapagos.com/Darwin_voyage_beagle/darwin_beagle_title.html)
Depetris PJ, Kempe S, Latif M, Mook WG (1996) ENSO controlled flooding in the Paraná River (1904–1991). Naturwissenschaften 83:127–129
Doyle M, Barros VR (2002) Midsummer low-level circulation and precipitation in subtropical South America and related sea surface temperature anomalies in the South Atlantic. J Clim 15:3394–3410
Favier-Dubois C M (2003) Late Holocene climatic fluctuations and soil genesis in southern Patagonia: Effects on the archaeological record. J Archaeol Sci 30:1657–1664.
Favier-Dubois C (2007) Soil genesis related to medieval climatic fluctuations in southern Patagonia and Tierra del Fuego (Argentina): Chronological and paleoclimatic considerations. Quat Int 162–163:158–165
Fritz SC, Metcalfe SE, Dean W (2001) Holocene climate patterns in the Americas inferred from paleolimnological records. In: Markgraf V (ed) Interhemispheric Climate Linkages. Academic Press, New York
Furlong Cardiff G (1937) Cartografía Jesuítica del Río de La Plata, Buenos Aires. Publ Inst Invest Hist LXXI:125 pp

García A (1999) Quaternary charophytes from Salina del Bebedero, Argentina: Their relation with extant taxa and palaeolimnological significance. J Paleolimnol 21:307–323

García NO, Mechoso CR (2005) Variability in the discharge of South American rivers and in climate. Hydrol Sci 50:459–478

Garreaud R, Vuille M, Compagnucci R, Marengo J (in press) Present-day South America Climate. Palaeogeogr Palaeoclimatol Palaeoecol doi: 10.1016/ j. palaeo. 2007. 10. 032< http:// dx. doi. org/ 10. 1016/ j. palaro. 2007. 10. 032>

Genta JL, Perez Iribarren G, Mechoso C (1998) A recent increasing trend in the streamflow of rivers in Southeastern South America. J Clim 11:2858–2862

Gilli A (2003) Tracking late Quaternary environmental change in southernmost South America using lake sediments of Lago Cardiel (49°S), Patagonia, Argentina. Unpublished PhD dissertation, ETH-Zürich (Switzerland)

Gilli A, Anselmetti FS, Ariztegui D et al (2001) Tracking abrupt climate change in the Southern Hemisphere: A seismic stratigraphic study of Lago Cardiel, Argentina (49°S). Terranova 13:443–448

Gilli A, Ariztegui D, Anselmetti FS et al (2005a) Mid-Holocene strengthening of the Southern Westerlies in South America – Sedimentological evidences from Lago Cardiel, Argentina (49°S). Glob Planet Change 49:75–93

Gilli A, Anselmetti FS, Ariztegui D et al (2005b) Seismic stratigraphy, buried beach ridges and contourite drifts: The Late Quaternary history of the closed Lago Cardiel basin, Argentina (49°S). Sedimentology 51:1–23

González MA (1994) Salinas del Bebedero basin (República Argentina). In: Kelts K, Gierlowski-Kordesch E (eds) Global Inventory of Lacustrine Basins. Cambridge University Press, Cambridge, UK

González MA, Maidana N (1998) Post-Wisconsinian paeoenvironments at Salinas del Bebedero basin, San Luis, Argentina. J Paleolimnol 20:353–368

Haberzettl T, Fey M, Lücke A et al (2005) Climatically induced lake level changes during the last two millennia as reflected in sediments of Laguna Potrok Aike, southern Patagonia (Santa Cruz, Argentina). J Paleolimnol 33:283–302

Haberzettl T, Kück B, Wulf S et al (2008) Hydrological variability in southeastern Patagonia and explosive volcanic activity in the southern Andean Cordillera during Oxygen Isotope Stage 3 and the Holocene inferred from lake sediments of Laguna Potrok Aike, Argentina. Palaeogeogr Palaeoclimatol Palaeoecol 259:213–229

Hajdas I, Bonani G, Moreno PI, Ariztegui D (2003) Precise radiocarbon dating of Late-Glacial cooling in mid-latitude South America. Quat Res 59/1:70–78

Iriondo M (1999) Climatic changes in the South American plains: Record of a continent-scale oscillation. Quat Int 57–58:93–112

Jenny B, Wilhelm D, Valero-Garcés B (2003) The Southern westerlies in Central Chile: Holocene precipitation estimates based on a water balance model for Laguna Aculeo (33°50⁄S). Clim Dyn 20:269–280

Labraga JC, Frumento O, López M (2000) The atmospheric water vapor cycle in South America and the tropospheric circulation. J Clim 13:1899–1915

Laguens A (1993) Locational structure of archaeological underground storage pits in northwest Córdoba, Argentina. Revista do Museo de Arq. e Etnol. S. Paulo 3:17–33

Laguens A, Bonnin M (1987) Espacio, paisaje y recursos. Estrategias indígenas alternativas y complementarias en la cuenca del Río Copacabana. Sitio el Ranchito. 1000 a.C–1600 d.C. Publicaciones XLV, Instituto de Antropología. Universidad Nacional de Córdoba, pp 159–201

Laguens A, Bonnin M (in press) Arqueología de Córdoba. Las sociedades indígenas de las Sierras Centrales de Argentina. Universidad Nacional de Córdoba. Argentina

López de Albornoz C (1997) Crisis agrícolas y crisis biológicas en la jurisdicción de San Miguel de Tucumán durante la segunda mitad del Siglo XVIII. In: García Acosta V (ed) Historia y Desastres Naturales en América Latina. Volumen II; LA RED/CIESAS/ITDG, Lima,

Perú, (2- 26). Red de Estudios Sociales en Prevención de Desastres en América Latina. http://www.desenredando.org
Lucatto G, Ariztegui D, Piovano EL (2007) Authigenic versus allogenic mineralization in a closed lacustrine basin – A Late Glacial and Holocene record of E/P changes in subtropical South America. 4th International Limnogeology Congress. International Association of Limnogeology, Barcelona, España, Wed-P51:157
Luckman BH, Villalba R (2001) Assessing the synchroneity of glacier fluctuations in the western cordillera of the Americas during the last millennium. In: Markgraf V (ed) Interhemispheric Climate Linkages. Academic Press, New York
Mancini MV, Paez MM, Prieto AR (2005) Mid-Holocene climatic variability reconstruction from pollen records (32°–52°S, Argentina). Quat Int 132:47–59
Marengo JA, Rogers JC (2001) Polar air outbreaks in the Americas: Assessments and impacts during modern and past climates. In: Markgraf V (ed) Interhemispheric Climate Linkages. Academic Press, New York
Markgraf V (1998) Past climate of South America. In: Hobbs JE, Lindesay JA, Bridgman HA (eds) Climate of the southern continents: Present, past and future. John Wiley & Sons Ltd, Hoboken, NJ
Markgraf V (2001) Interhemispheric Climate Linkages. Academic Press, New York
Markgraf V, Dodson JR, Kershaw AP (1992) Evolution of late Pleistocene and Holocene climates in the circum-South Pacific land areas. Clim Dyn 6:193–211
Markgraf V, Baumgartner TR, Bradbury JP et al (2000) Paleoclimate reconstruction along the Pole-Equator-Pole transect of the Americas (PEP 1). Quat Sci Rev 19:125–140
Markgraf V, Bradbury JP, Schwalb A et al (2003) Holocene palaeoclimates of southern Patagonia: limnological and environmental history of Lago Cardiel, Argentina. Holocene 13:581–591
Masiokas MH, Villalba R, Luckman B et al (2008) 20th-century glacier recession and regional hydroclimatic changes in northwestern Patagonia. Glob Planet Change 60:85–100
Massaferro J, Corley J (1998) Environmental disturbance and chironomid palaeodiversity: 15 kyr BP of history at Lake Mascardi, Patagonia, Argentina. Aquatic Conserv Mar Freshw Ecosyst 8:315–323
Mauquoy D, Blaauw M, van Geel B et al (2004) Late Holocene climatic changes in Tierra del Fuego based on multiproxy analyses of peat deposits. Quat Res 61:148–158
Mayr C, Fey M, Haberzettl T et al (2005) Palaeoenvironmental changes in southern Patagonia during the last millennium recorded in lake sediments from Laguna Azul (Argentina). Palaeogeogr Palaeoclimatol Palaeoecol 228:203–227
Mayr C, Wille M, Haberzettl T et al (2007) Holocene variability of the Southern Hemisphere westerlies in Argentinean Patagonia (52°S). Quat Sci Rev 26:579–584
Meyer I, Wagner S (2008) The little ice age in southern Patagonia: Comparison between downscaled model output of a GCM simulation. PAGES News 16:12–13
Moncaut CA (2003) Inundaciones y sequías tienen raíces añejas en la pampa bonaerense (1576–2001). In: Maiola OC, Gabellone NA, Hernández MA (eds) Inundaciones en la región pampeana. Editorial Universidad Nacional de La Plata, Chapter 1, pp 27–47
Moreno PI, Jacobson GL, Lowell TV, Denton GH (2001) Interhemispheric climate links revealed by a late-glacial cooling episode in southern Chile. Nature 409:804–808
Moy C, Dunbar R, Moreno P et al (2008) Isotopic evidence for hydrologic change related to the westerlies in SW Patagonia, Chile, during the last millennium. Quat Sci Rev 27:1335–1349
Muhs DR, Zárate M (2001) Late Quaternary eolian records of the Americas and their paleoclimatic significance. In: Markgraf W (ed) Interhemispheric climate linkages. Academic Press, New York
Nogués-Paegle J, Mo KC (1997) Alternating wet and dry conditions over South America during summer. Mon Weather Rev 125:279–291
Parras P (1943) Diario y Derrotero de sus viajes. Solar Ed. Bs. As 251 pp
Pasquini A, Depetris P (2007) Discharge trends and flow dynamics of South American rivers draining the southern Atlantic seaboard: An overview. J Hydrol 333:385–399

Pasquini A, Lecomte K, Piovano E, Depetris PJ (2006) Recent rainfall and runoff variability in central Argentina. Quat Int 158:127–139
Piovano E, Ariztegui D, Damatto Moreira S (2002) Recent environmental changes in Laguna Mar Chiquita (Central Argentina): A sedimentary model for a highly variable saline lake. Sedimentology 49:1371–1384
Piovano E, Ariztegui D, Bernasconi SM, Mckenzie JA (2004a) Stable isotope record of hydrological changes in subtropical Laguna Mar Chiquita (Argentina) over the last 230 years. Holocene 14:525–535
Piovano E L, Larizatti FE, Favaro D et al (2004b) Geochemical response of a closed-lake basin to 20th century recurring droughts/wet intervals in the subtropical Pampean plains of South America. J Limnol 63:21–32
Piovano E, Villalba R, Leroy S (2006a) Holocene environmental catastrophes in South America: From the Lowlands to the Andes, Quat Int 158:1–3
Piovano EL, Ariztegui D, Cioccale M et al (2006b) Reconstrucciones paleolimnológicas desde el Ultimo Máximo Glacial en el sur de Sudamérica: Megasistemas en antifase hidrologica? III Congreso Argentino de Cuaternario y Geomorfología, Tomo II:659–669
Politis G (1984) Climatic variations during historical times in Eastern Buenos Aires Pampas. Argentina. Quat South Am Antarc Penins 2:133–161
Prieto AR, Blasi AM, De Francesco CG, Fernández C (2004) Environmental history since 11,000 14-C y B.P. of the northestern Pampas, Argentina, from alluvial sequences of the Lujan River. Quat Res 62:146–161
Prieto M del R, Jorba RA (1990) Las anomalías climáticas en la Cuenca del Plata y NOA y sus consecuencias socioeconómicas. Siglos XVI-XVII y XVIII. Leng. Revista Argentina de Geografía 1:41–103
Prieto M del R, Herrera RG (2001) De sequías, hambrunas, plagas y "otras varias y continuas calamidades acaecidas en la jurisdicción de Córdoba" durante el siglo XVIII. Cuadernos de Historia, Serie Ec. y Soc., Nº4, Secc. Art., Universidad Nacional de Córdoba, pp 131–158
Prohaska F (1976) The climate of Argentina, Paraguay and Uruguay. In: Schwerdfeger W (ed) Climates of Central and South America. Elsevier, Amsterdam
Rao VR, Cavalcanti IF, Hada K (1996) Annual variation of rainfall over Brazil and water vapor characteristics over South America. J Geophys Res 101:26539–26551
Reimer PJ, Baillie MGL, Bard E et al (2004) IntCal04 Terrestrial Radiocarbon Age Calibration, 0–26 cal kyr BP. Radiocarbon 46:1029–1059
Robertson AW, Mechoso C (1998) Interannual and decadal cycles in river flows of Southeastern South America. J Clim 11:2570–2581
Saulo AC, Nicolini M, Chou SC (2000) Model characterization of the South American low-level flow during the 1997–1998 spring-summer season. Clim Dyn 16:867–881
Schäbitz F, Liebricht H (1998) Landscape and climate development in the south-eastern part of the "Arid Diagonal" during the last 13,000 years. Bamberger Geographische Schriften Bd 15 S:371–388
Silvestri G (2004) El Niño signal variability in the precipitation over southeastern South America during the austral summer. Geophys Res Lett 31:L18206
Stine S (1994) Extreme and persistent drought in California and Patagonia during mediaeval time. Nature 369:546–549
Stine S, Stine M (1990) A record from Lake Cerdiel of climate change in southern South America. Nature 345:705–708
Tatur A, del Valle R, Bianchi MM et al (2002) Late Pleistocene palaeolakes in the Andean and Extra-Andean Patagonia at mid-latitudes of South America. Quat Int 89:135–150
Varandas da Silva L, Piovano EL, Azevedo D, Aquino Neto F (2008) Quantitative evaluation of the sedimentary organic matter in Laguna Mar Chiquita, Argentina. Org Geochem 39:450–464
Villalba R (1994) Tree-ring and glacial evidence for the Medieval Warm Epoch and the Little Ice Age in Southern South America. Clim Change 26:183–197
Villalba R, Leiva J, Rubulls S et al (1990) Climate, Tree-Ring and Glacial Fluctuations in the Río Frías Valley, Río Negro, Argentina. Arc Alp Res 22:215–232

Villalba R, Cook ER, Jacoby GC et al (1998) Tree-ring based reconstructions of northern Patagonia precipitation since AD 1600. Holocene 8/6:659–674

Villalba R, Lara A, Boninsegna J et al (2003) Large-scale temperature changes across the Southern Andes: 20th-century variations in the context of the past 400 years. Clim Change 59:177–232

Zech W, Zech M, Zech R et al (2008) Late Quaternary palaeosol records from subtropical (38°S) to tropical (16°S) South America and palaeoclimatic implications. Quat Int:doi:10.1016/j.quaint.2008.01.005a

Wainer I, Clauzet G, Ledru M-P et al (2005) Last Glacial Maximum in South America: Paleoclimate proxies and model results. Geophys Res Lett 32:L08702

Waldmann N, Ariztegui D, Anselmetti FS et al (in press) Lago Fagnano (Tierra del Fuego, Argentina) – A continuous archive of paleoclimate and tectonic activity since the Late Glacial. Geologica Acta

Waldmann N, Ariztegui D, Anselmetti FS et al (2007) Climate vs. tectonics at the end of the world: The Lago Fagnano sedimentary record, Tierra del Fuego, southernmost South America. EOS Trans AGU, 87(52), Fall Meet. Suppl., Abstract PP31C-1763

Zárate M (2003) Loess of southern South America. Quat Sci Rev 22:1987–2006

Zárate M, Kemp R, Espinosa M, Ferrero L (2000) Pedosedimentary and palaeoenvironmental significance of a Holocene alluvial sequence in the southern Pampas Argentina. Holocene 10:481–488

Zhou J, Lau K-M (1998) Does a monsoon climate exist over South America? J Clim 11:1020–1040

Zolitschka B, Schäbitz F, Lücke A et al (2006) Crater lakes of the Pali Aike Volcanic Field as key sites for paleoclimatic and paleoecological reconstructions in southern Patagonia, Argentina. J South Am Earth Sci 21:294–309

Chapter 15
Climate Change in Southern South America During the Last Two Millennia

Christopher M. Moy, Patricio I. Moreno, Robert B. Dunbar, Michael R. Kaplan, Jean-Pierre Francois, Ricardo Villalba, and Torsten Haberzettl

Abstract Paleoclimate records from southern South America can be used to address important questions regarding the timing and nature of late-Holocene climate variability. During the last 30 years, many areas of southern South America have experienced rapid climatic and ecological changes that are driven by global and hemispheric-scale ocean-atmosphere processes. In order to place these recent changes in a longer-term context, we first present an overview of the modern climate processes relevant for the interpretation of paleoclimate records in southern South America, and then review records that have been developed from various archives that span the last two thousand years. Multiple paleoclimate records provide evidence for an overall decrease in temperature and an increase in westerly wind intensity that culminates in the last few hundred years during the time of the European Little Ice Age. We also find evidence for aridity generally coincident with the Medieval Climate Anomaly in several paleoclimate archives. Although much work has been done in this region, high-resolution well-dated archives are still needed from sensitive locations to improve our understanding of past and present climate change. From the paleoclimate records that we have compiled, we infer that warming, retreat of glaciers, and reconfiguration of precipitation patterns during the past century is unique within the context of the last 2000 years.

Keywords South America · Patagonia · Paleoclimate · Southern Hemisphere Westerlies · Little Ice Age

15.1 Introduction

Southernmost South America is an important venue for examining the timing and nature of past climate change. The region of Patagonia including Tierra del Fuego spans ~15° of latitude and represents the southernmost continuous landmass outside

C.M. Moy (✉)
Department of Geological and Environmental Sciences, 450 Serra Mall, Braun Hall (Bldg. 320), Stanford University, Stanford, CA 94305-2115 USA
e-mail: moyc@stanford.edu

F. Vimeux et al. (eds.), *Past Climate Variability in South America and Surrounding Regions*, Developments in Paleoenvironmental Research 14,
DOI 10.1007/978-90-481-2672-9_15,

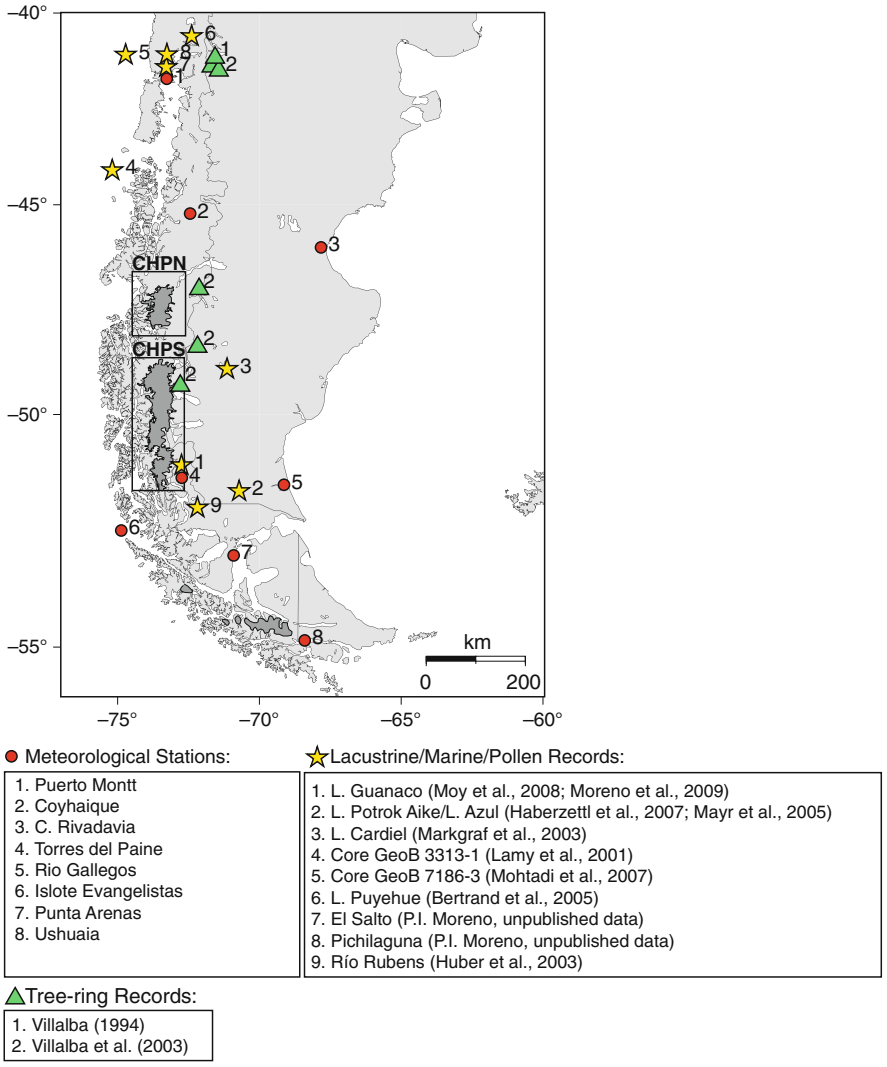

Fig. 15.1 Map of southern South America highlighting meteorological stations and the locations of paleoclimate records referenced in this paper. The black rectangle highlights the modern ice extent (*grey* regions) of the Campo de Hielo Patagónico Norte (CHPN) and Sur (CHPS) or northern and southern Patagonian ice fields

of Antarctica (Fig. 15.1). The N-S oriented Andes have an average elevation of 2500 m in southern South America, and are a significant topographical divide that establishes sharp climate and vegetation gradients from west to east. The geography and climate of southern South America support a diverse array of natural climate archives, such as glaciers and ice caps, tree rings, and lake sediments that can be used to better understand how climate has changed in the past.

The present-day climate of the region is influenced by processes that originate in the high latitudes and the tropics, most notably the Southern Annual Mode (SAM) or the Antarctic Oscillation (AAO) and the El Niño-Southern Oscillation (ENSO). Both of these large-scale ocean-atmosphere processes play a role in altering not only temperatures at seasonal to interannual timescales, but also precipitation amount and distribution through changes in the strength and latitudinal position of the southern westerlies (Garreaud et al. 2008). Southern South America is unique in that it is the only large landmass that extends through the core of the modern westerly wind field at ~50°S (Fig. 15.2) permitting the study of past westerly wind variability using terrestrial climate archives.

The modern instrumental record of temperature and precipitation in Patagonia is short (typically less than 50 years), discontinuous, and spatially limited. Despite these shortcomings, modern observations suggest patterns that are of paleoclimate significance. Over the last 30 years, a strengthening of atmospheric circulation in the high southern latitudes is evident in direct instrumental observations (Marshall 2003) and wind fields derived from reanalysis data sets (Thompson and Wallace 2000), reflecting a trend towards the positive mode or phase of the SAM. An increase in summer air temperature in southern Patagonia, concurrent with a decrease in summer temperatures in coastal areas in northern Patagonia, is observed during the same period (Carrasco et al. 2008, Villalba et al. 2003). The trend in the SAM towards positive index values has significant implications for the global carbon cycle, in particular the rates of CO_2 exchange between the ocean and atmosphere in the high southern latitudes (Canadell et al. 2007, Le Quéré et al. 2007, Lovenduski et al. 2007). The regional pattern of summer warming and cooling in recent decades has implications for understanding the mechanisms of past, present, and future climate change.

In addition to modern climate change observed in instrumental records, paleoclimate records provide evidence of climate variations during the last 2000 years. For instance, there have been significant changes in ENSO event frequency and magnitude in the tropics during the last 2000 years (Cobb et al. 2003, Moy et al. 2002, Rein et al. 2004). Within the last 1000 years, Northern Hemisphere climatic events such as the Little Ice Age (LIA), from 380 to 50 calendar years before present (cal year BP, where 1950 = 0 cal year BP) (Matthews and Briffa 2005), and the Medieval Climate Anomaly (MCA), between 950 and 750 cal year BP, have been identified in paleoclimate records throughout both hemispheres (Stine 1994). However, these events are regionally complex (Bradley et al. 2003, Jones and Mann 2004) and their timing, magnitude, and nature have not been clearly delineated in southern South America. In addition, changes in glacial ice extent evident in both the northern and southern Patagonian ice fields are related to Neoglaciation, which has been recognized throughout the Southern Hemisphere, beginning ~5400 cal year BP and ending with the recent retreat from LIA ice positions (Clapperton and Sugden 1988, Hodell et al. 2001, Porter 2000, Schaefer et al., 2009). These climatic events and trends set the stage for our understanding of climate variability during the last 2000 years.

Here, we review the record of paleoclimate change in Patagonia during the last 2000 years. We first present an overview of the modern climate of the region and

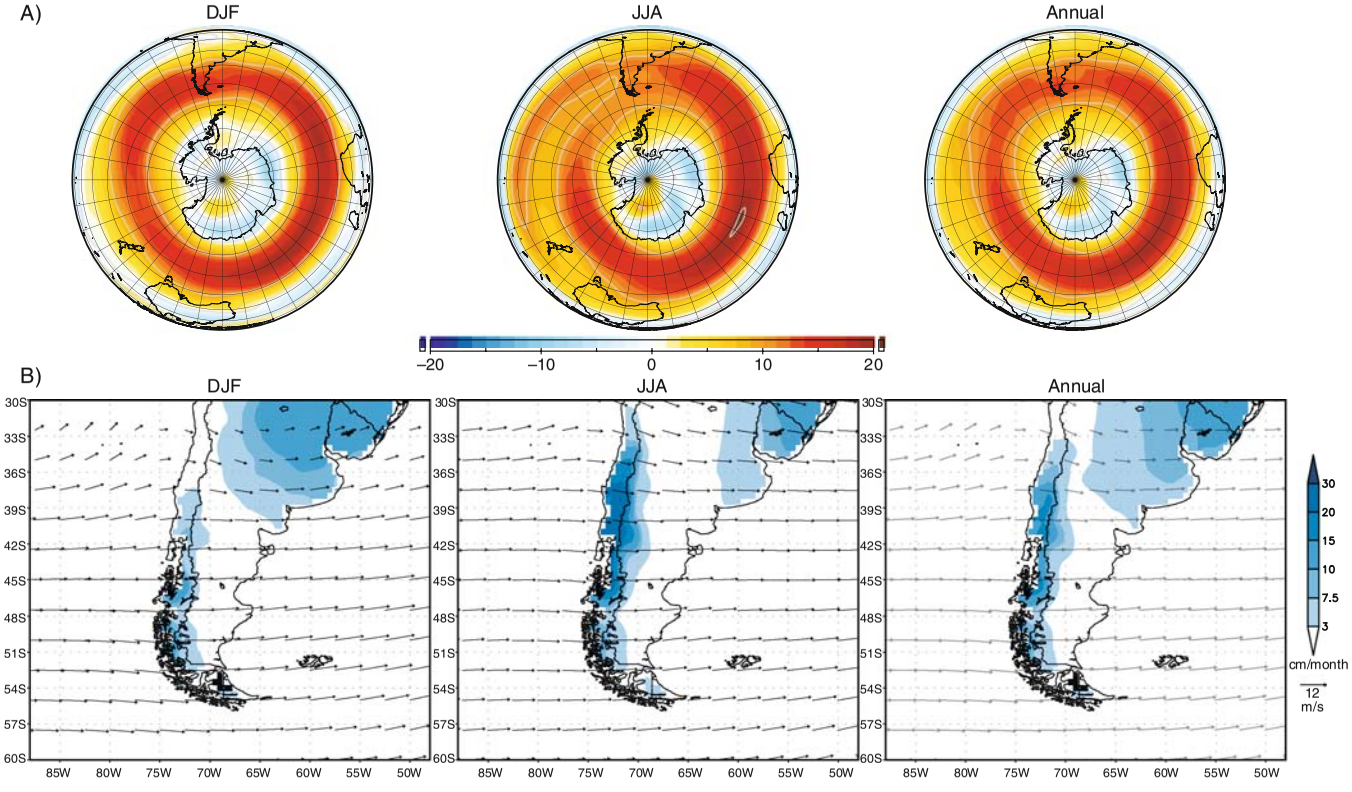

Fig. 15.2 Annual and seasonal composite means of atmospheric circulation and precipitation in southern South America from 1980 to 2006. (**A**) Summer (DJF), winter (JJA), and annual composite averages of 700 hPa zonal wind speed (m/s) from the NCEP-NCAR reanalysis. During DJF the westerlies are strongest and shifted poleward over southern Patagonia, which is in contrast to the winter months (JJA), which exhibit reduced wind strength and northward expansion of the wind field. (**B**) summer (DJF), winter (JJA), and annual composite averages of U. Delaware surface precipitation rate (cm/month) and 700 hPa wind vectors in southern South America. The 700 hPa wind vectors (reference arrow at right of plot) show strong westerly flow during all seasons in southern South America. Note that the location of maximum precipitation in (**B**) follows the seasonal migration of the 700 hPa westerly wind maximum in (**A**)

focus on the interannual linkages between tropical and high-latitude forcing mechanisms that are important for the interpretation of paleoclimate records. We then present results from a lake sediment record from Lago Guanaco, which is located within the modern westerly wind maximum (∼50°S), and highlight late-Holocene changes in moisture balance related to the westerlies. We incorporate existing paleoclimate records from Patagonia, which include lake sediment, pollen and charcoal, geomorphologic (glacial and lake level), tree-ring, and marine data in order to answer the following questions:

1. Can we identify global climate events (such as the Northern LIA and MCA) in southern South America? If so, is the timing and nature of these past changes synchronous and of the same sign/direction throughout Patagonia?
2. How has the strength and latitudinal position of the Southern Hemisphere westerly wind field changed during the last 2000 years? Can we identify trends in climate or climate variability that place the modern conditions in perspective?
3. What are potential forcing mechanisms of climate change in southernmost South America at centennial and millennial timescales? Are there links between past climate variability observed in this region with both tropical and high-latitude records of climate change during the last 2000 years?

15.2 Climatology

To place paleoclimate records in a proper context, we provide a brief summary of present-day climate, including the general atmospheric circulation, the relationship between wind and precipitation, seasonal and interannual variability, and potential tropical and high latitude forcing mechanisms. We focus on interactions between atmospheric circulation and precipitation because the two often exhibit strong correlations in southern South America, and this modern link between precipitation and zonal atmospheric flow is commonly used in paleoclimate studies to identify past changes in the intensity and latitudinal position of the westerlies. More extensive reviews on extratropical climate variability in South America, which discuss variations in the thermal and precipitation fields, can be found in Garreaud and Aceituno (2007) and Garreaud et al. (2008).

15.2.1 Co-Variability of Wind and Precipitation

Southern South America is an excellent place to investigate past variations in the Southern Hemisphere westerlies for three reasons: First, it is the only significant continental landmass that intersects the region of maximum zonal flow in the Southern Hemisphere (Fig. 15.2). The strongly oceanic nature of the mid- to high southern latitudes leads to the high zonal symmetry observed in both lower and upper level zonal wind on monthly to interannual timescales. One advantage of this zonal structure is that a meridional transect through the core of the westerlies at a given location has relevance across a range of longitudes.

Second, atmospheric circulation in the southern mid-latitudes is maintained by strong thermal gradients in the troposphere and in sea-surface temperatures (SST) over the Pacific Ocean. The strong atmospheric pressure gradient drives geostrophic flow and promotes baroclinic instability and the formation of transient eddies (Garreaud and Aceituno 2007). These eddies in turn produce frontal systems in the form of migratory surface cyclones and anticyclones that drift eastward and are "steered" by the 700 hPa winds along storm tracks located poleward of the upper-level jet (Garreaud 2007, Trenberth 1991). Increasing wind intensity or strength of zonal flow increases baroclinic instability, which increases the succession of extratropical cyclones circling the Southern Ocean and impinging on the South American continent (Garreaud 2007).

Third, topography and the general circulation are closely related in that the southern Andes are the only formidable obstacle to tropospheric flow in the Southern Hemisphere. The uplift of air over the cordillera produces significant amounts of orographic precipitation (>10000 mm/year), while farther to the east, subsidence produces an overall drying effect in Argentine Patagonia and the Atlantic seaboard (Garreaud et al. 2008). Orographic precipitation on the windward side of the Andes increases with both altitude and overall westerly wind strength to produce extreme environmental and climatological gradients. For example, at 50°S, annual precipitation ranges from 3000 mm/year at western coastal sites, to 6000 mm/year at sea level on the western slope of the Andes, to an estimated 8000–10000 mm/year along the crest of the cordillera, rapidly decreasing to less that 500 mm/year east of Punta Arenas and 200–300 mm/year on the Atlantic seaboard (Garreaud et al. 2008, Schneider et al. 2003, Villalba et al. 2003). At lat. 41°S, annual precipitation ranges from 1800 mm/year in Puerto Montt, up to 4000 mm/year on the continental divide, and falls to less than 1000 mm/year in Bariloche (Villalba et al. 2003).

15.2.2 Seasonal Variations in Wind and Precipitation

Figure 15.2 displays the annual cycle of precipitation and low-level winds (700 hPa) in southern South America. We use the University of Delaware global precipitation data set derived from surface instrumental data from the NOAA GHCN network and the climate archive compiled by Legates and Willmott (1990). Wind vectors represent the long-term mean of annual, summer, and winter wind magnitude and direction at 700 hPa derived from the NCEP-NCAR reanalysis (Kalnay et al. 1996). During the austral summer (DJF), low level winds are strongest and situated in their most poleward or southern position of the year at approximately 50°S (Fig. 15.2). During austral winter (JJA), the low-level winds weaken, especially in Southern Patagonia, and the main axis of the wind field migrates north. The northward migration is mainly due to seasonal changes in SST and the northward migration of the anticyclonic high pressure cell situated in the southeastern Pacific Ocean. Through the seasonal cycle, the main locus of precipitation largely follows the mean zonal wind maximum (Fig. 15.2). In southern Patagonia, precipitation is more evenly distributed throughout the year with a small maximum during the Austral autumn. In

contrast, precipitation in northern Patagonia is more seasonal with higher amounts during JJA when the subtropical high and the jet are located farther to the north (Fig. 15.2).

15.2.3 Correlation Between Zonal Wind and Precipitation

To highlight the relationship between precipitation and wind in southern South America, we calculate the annual spatial correlation between precipitation derived from 8 meteorological stations and the zonal wind at 700 hPa from the NCEP-NCAR reanalysis (Fig. 15.3). Monthly precipitation values for the selected locations were obtained from the NOAA GHCN, Dirección Meteorológica de Chile, Dirección General de Aguas, and the Servicio Hidrográfico de la Armada de Chile (SHOA) for the period from 1980 to 2003 (Table 15.1). We selected this 23 year period because the meteorological stations have good data coverage and it postdates the inclusion of satellite sounder data into the NCEP-NCAR reanalysis (Marshall 2003). Precipitation at Puerto Montt, Coyhaique, Torres del Paine and Islote Evangelistas exhibit an overall positive correlation with zonal wind speed that extends throughout much of the Southern Hemisphere, indicating that precipitation at annual timescales at a particular site is related to the atmospheric circulation over a significant portion of the Southern Hemisphere. The positive correlation extends to locations on the eastern side of the range: precipitation falling at Coyhaique and Torres del Paine exhibits significant positive correlations with the westerlies similar to I. Evangelistas, which is the westernmost site. The latitude of maximum positive correlation varies with location. For example, the correlation between precipitation and wind at Puerto Montt is most positive at ~40°S, reflecting the seasonal delivery of precipitation during the austral winter when the westerlies are shifted to the north. Two of the eastern Atlantic coastal locations, Comodoro Rivadavia and Río Gallegos, exhibit either negative or little correlation between zonal wind and precipitation, and this may reflect contribution of precipitation from the Atlantic Ocean. Mayr et al. (2007) present meteorological data from a station close to Laguna Potrok Aike, which is located in the Argentine steppe midway between the Andean divide and Río Gallegos on the Atlantic coast. There, higher rainfall is associated with easterly winds and the greater input of Atlantic moisture when the zonal westerlies are weak.

15.2.4 El Niño-Southern Oscillation (ENSO) Variability

ENSO plays a role in driving interannual climate variability in southern South America. NCEP reanalysis data indicate high annual correlations between a multivariate ENSO index (Wolter and Timlin 1993, Wolter and Timlin 1998) and zonal wind speed, precipitation and surface air temperature from 1980 to 2006 (Fig. 15.4). When averaged over the year, an ENSO warm event (positive multivariate ENSO index values) is associated with an overall decrease in the strength of

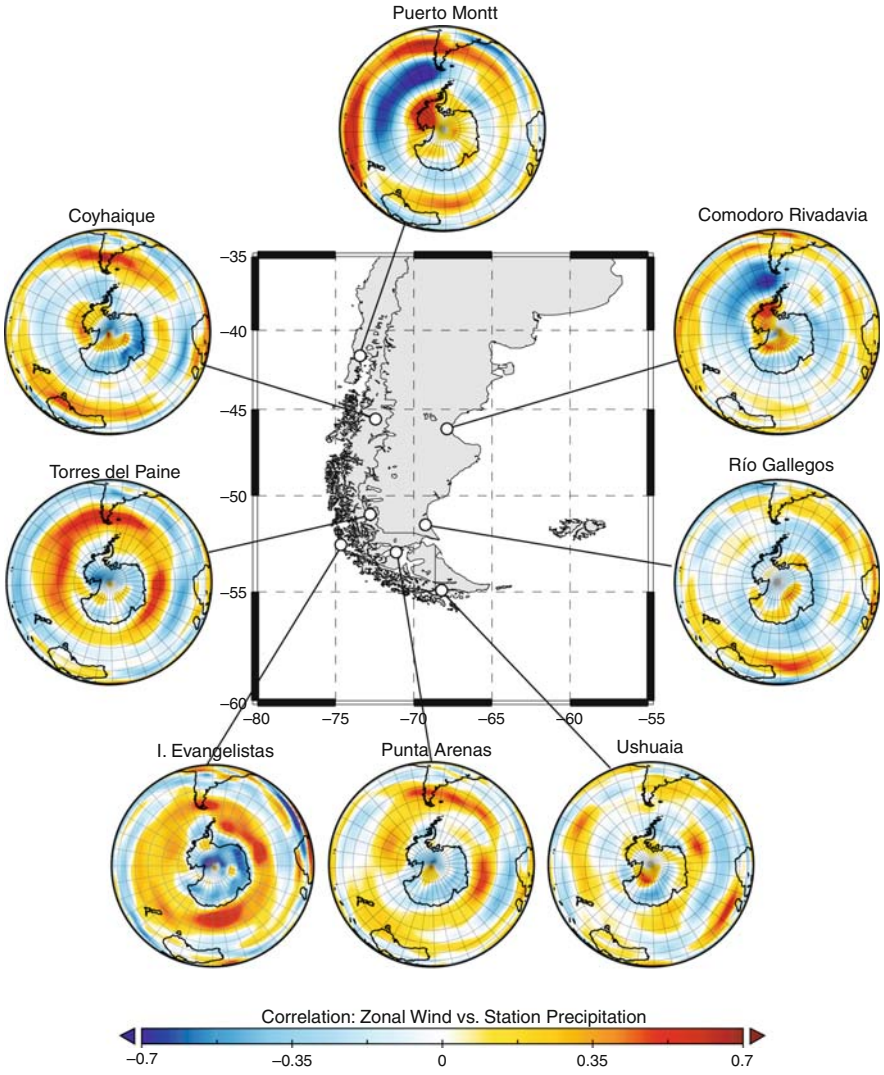

Fig. 15.3 Annual correlation between NCEP-NCAR reanalysis 700 hPa zonal wind in the Southern Hemisphere and selected precipitation records from Patagonia and Tierra del Fuego for the years 1983–2003 (Table 15.1). Meteorological stations proximal to the Andean divide exhibit positive correlations with atmospheric circulation, whereas locations closer to the Atlantic coast exhibit weak or negative correlations with the wind field. Color bar at base of map refers to correlation value (r value)

the wind field and a slight reduction in precipitation in western Patagonia. Northern Patagonia exhibits an overall reduction in summer precipitation and warmer surface air temperatures. The Pacific-South American (PSA) pattern of circulation is responsible for these observations largely through a wave train that extends from the western tropical Pacific to the mid to high southern latitudes (Mo 2000). Of

Table 15.1 Location and sources of monthly precipitation data obtained from meteorological stations in southern South America (see Fig. 15.1). The station data were used to evaluate the relationship between zonal wind and precipitation at annual timescales throughout Patagonia (Fig. 15.3) for the period 1983 to 2003

No.	Name	Latitude	Longitude	Elevation (m)	Source
1	Puerto Montt	−41.40	−73.10	81	Dirección Meteorológica de Chile
2	Coyhaique	−45.60	−72.10	311	Dirección Meteorológica de Chile
3	Commodoro Rivadavia	−45.80	−67.50	46	NOAA GHCN
4	Torres del Paine	−51.18	−72.97	25	Direccion General de Aguas
5	Río Gallegos	−51.60	−69.30	19	NOAA GHCN
6	Islote Evangelistas	−52.39	−75.10	52	Servicio Hidrográfico de la Armada de Chile (SHOA)
7	Punta Arenas	−53.00	−70.90	97	Dirección Meteorológica de Chile
8	Ushuaia	−54.80	−68.30	14	NOAA GHCN

particular relevance is the frequent occurrence of long-lived, tropospheric deep anticyclonic anomalies east of the southern tip of South America (centered at 50°S, 100°W) during El Niño years. These so-called blocking anticyclones at high latitudes are responsible for an equatorward migration of the storm track thus reducing precipitation over Patagonia.

Schneider and Geis (2004) and Fogt and Bromwich (2006) observe a non-stationary ENSO teleconnection with the high southern latitudes over decadal timescales. Specifically, relatively low correlations between meteorological variables and the southern oscillation index (SOI) during the 1980s increased after 1990. Using reanalysis data in a domain over the Southern Ocean, Fogt and Bromwich (2006) note that the Southern Annular Mode (SAM) plays an important role in modulating the strength of the ENSO signal in Western Antarctica and over the Pacific sector of the Southern Ocean: the ENSO teleconnection was particularly strong during periods when the SAM and the SOI index were positively correlated.

15.2.5 Southern Annular Mode (SAM)/Antarctic Oscillation (AAO) Variability

The Southern Annular Mode (SAM) or the Antarctic Oscillation (AAO) is the leading mode of atmospheric circulation in the high southern latitudes and plays a significant role in altering climate on seasonal and interannual timescales (Thompson

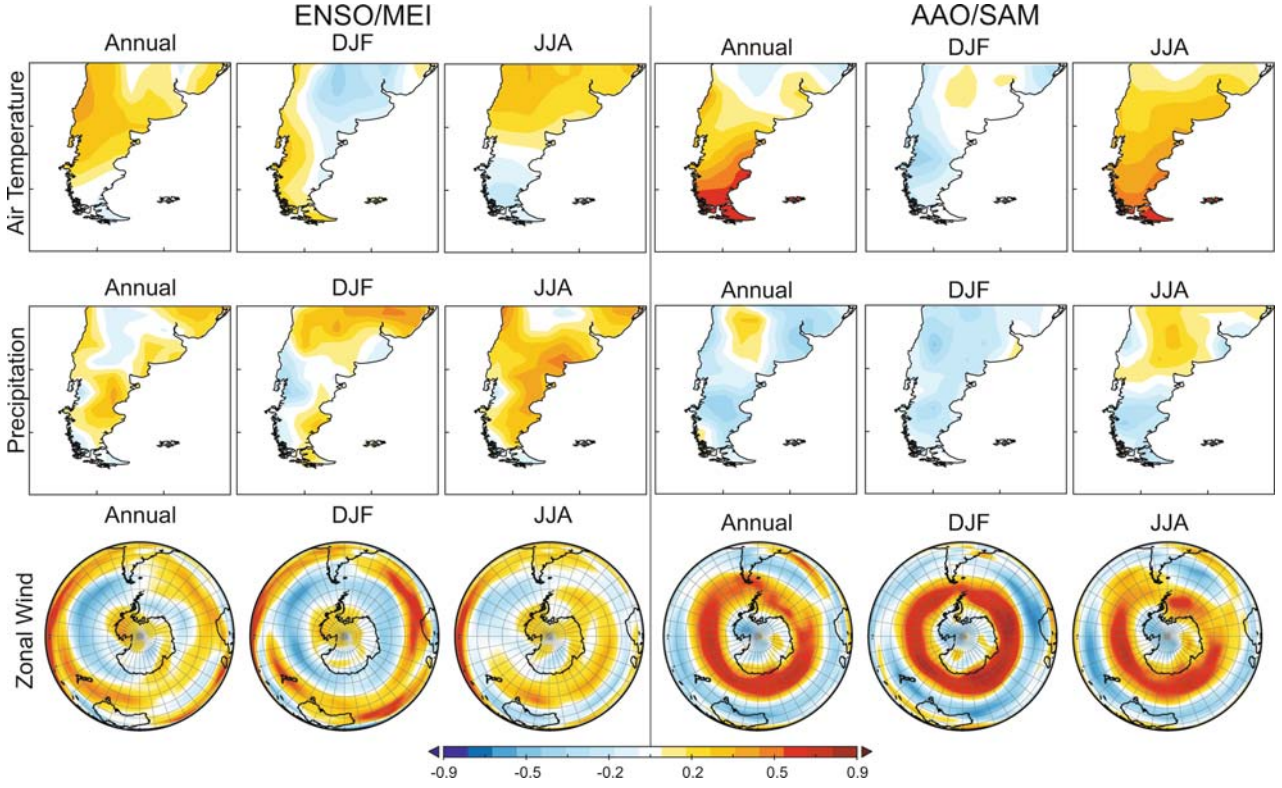

Fig. 15.4 Annual and seasonal correlations between NCEP surface air temperature, enhanced CMAP precipitation (Xie and Arkin 1997) and NCEP 700 hPa zonal wind (Kalnay et al. 1996) with indices of tropical (Multivariate ENSO Index) and high latitude (Southern Annular Mode) climate variability (1980–2006). Among the correlations presented here, most significant is the positive correlation between the SAM and the 700 hPa winds over the Southern Ocean and surface air temperature over southernmost South America. Most significant with respect to ENSO, are the negative correlations between the multivariate ENSO index (MEI) and the strength of the westerlies over the Pacific sector of the Southern Ocean and precipitation in western Patagonia during summer months (DJF)

and Wallace 2000). The SAM has been identified in both reanalysis and instrumental data, and the index is commonly defined as the leading empirical orthogonal function (EOF) of the 700 hPa geopotential height anomalies poleward of 20°S. The positive phase of the SAM is characterized by positive anomalies in atmospheric pressure over the mid-latitudes, negative pressure anomalies over Antarctica, and a strengthening of the atmospheric flow over the Southern Ocean across all longitudes (Marshall 2003). Figure 15.4 shows seasonal and annual spatial correlations of the SAM with zonal wind (NCEP), precipitation (CMAP) and air temperature (NCEP) from 1980 to 2006. Coincident with the positive phase of the SAM and relevant for interpreting paleoclimate archives from southern South America is an intensification and poleward shift of the westerlies, positive air temperature anomalies that increase with latitude, and a reduction in precipitation, particularly in northern Patagonia. Kwok and Comiso (2002) note that during the last two decades there has been a greater tendency towards the positive phase of the SAM and the negative phase of the Southern Oscillation. The Authors argue that the warming of air temperatures around the Antarctic Peninsula, adjacent ocean, and southernmost South America is a response due to the combined response of ENSO and the SAM. Although the SAM appears to be an important modulator of climate in southern South America, a number of questions remain concerning the origin or processes responsible for its long-term variability and trends. The recent increasing trend in the SAM, for example, has been attributed to such things as reductions in stratospheric ozone concentrations over the Antarctic continent (Thompson and Solomon 2002), increases in atmospheric CO_2 (Marshall 2003), and natural climate variability (Jones and Widmann 2004).

In summary, the meridional lay-out of southern South America allows the reconstruction of past variations in the strongly zonal westerly wind field. In many locations proximal to the Andes, zonal flow is positively correlated with precipitation. As a result of seasonal shifts in the latitudinal position of the westerlies, these correlations are seasonally dependent, with stronger correlations occurring during the summer in southern Patagonia and during the winter in northern Patagonia. Some of the stations east of the Andean divide (Torres del Paine and Coyhaique) show high variability in annual precipitation that is consistent with stations to the west of the Andean divide (I. Evangelistas). Farther to the east on the Atlantic coast and in central Argentine Patagonia, precipitation increases during periods of reduced westerly flow. Interannual climate variability in Patagonia is controlled, in part, by teleconnections with the tropics related to ENSO and variations in the SAM. These teleconnections manifest as anomalies in low-level wind strength, surface air temperature and precipitation. The strongest teleconnection in southern South America appears to be related to the SAM, where increasing surface air temperatures and poleward shifted westerlies coincide with the positive phase of the index.

15.3 Lake Sediment Records

15.3.1 Lago Guanaco

Moy et al. (2009) and Moreno et al. (2009) combined stable isotope and pollen data from Lago Guanaco, a small lake located in Torres del Paine National Park (51°S), to investigate past variations in atmospheric circulation (Fig. 15.1). The lake is located in the core of the modern wind field and precipitation falling in the region is well-correlated to the strength of the westerlies (Fig. 15.3). In addition, Lago Guanaco is an alkaline lake that preserves biogenic carbonate (bivalves, ostracodes, and *Chara* calcite) and it is situated close to the precipitation-controlled forest-steppe ecotone in southwest Patagonia. Two factors make Lago Guanaco an important site for reconstructing past changes in the westerlies. First, a strong positive correlation exists between precipitation and the strength of the westerly winds; increases in annual and seasonal precipitation correspond with increases in zonal wind speed across the Southern Hemisphere (Fig. 15.3). Second, two independent methods are available to evaluate changes in hydrology related to the westerlies. The first relies on reconstructing past changes in moisture balance by analyzing the oxygen isotopic composition ($\delta^{18}O$) of biogenic carbonates recovered from sediment cores. The second method utilizes a paleovegetation index that monitors zonal migrations of the boundary between the *Nothofagus* forests to the west and the Poaceae-dominated steppe to the east. Because this ecotone is controlled by moisture availability, increases in precipitation expand the forest to the east at the expense of the steppe.

Moy et al. (2008) collected a series of undisturbed sediment-water interface cores from Lago Guanaco and picked *Pisidium* sp. bivalves and extracted fine-fraction carbonate (<63 μm) from the sediment. The $\delta^{18}O$ of these two carbonate phases are shown in Fig. 15.5. Freshwater bivalves have been shown to precipitate their shell carbonate at or very close (within 1‰) to oxygen isotopic equilibrium (Dettman et al. 1999, Moreno et al. 2009, von Grafenstein et al. 1999), while the fine-fraction carbonate is likely derived from *Chara* growing in the littoral regions of the lake

Fig. 15.5 Compilation of paleoclimate proxies derived from Lago Guanaco (paleovegetation index and biogenic carbonate $\delta^{18}O$) and Siple Dome, Antarcica (Na^+). Concomitant increases in *Pisidium* $\delta^{18}O$ (**C**) and the *Nothofagus*/Poaceae ratio (**A**) are indicative of increased wind, enhanced evaporative conditions, and increased precipitation during the last 500 years and provide evidence for an enhancement of Southern Hemisphere circulation during the LIA. High $\delta^{18}O$ values and reduced paleovegetation index values centered at 800 cal year BP reflect increases in aridity coincident with the MCA. The variations observed in the Guanaco record show a strong similarity to the first EOF of Na+ concentration from Siple Dome, Antarctica (Kreutz et al. 1997) calculated using a 25- (*solid line*) and 115-year (*dashed line*) window (**B**). The vertical dashed line is the calculated break in slope that Kreutz et al. (1997) use to identify the start of the LIA, the red rectangle corresponds to drought termination in central Patagonia inferred from radiocarbon-dated trees exposed in Patagonia lakes (Stine 1994), and the triangles at the base of the plot refer to median calibrated ages used in the Lago Guanaco age model. The paleovegetation index declines at ~150 cal year BP due to widespread clearance of the Nothofagus forest for livestock grazing

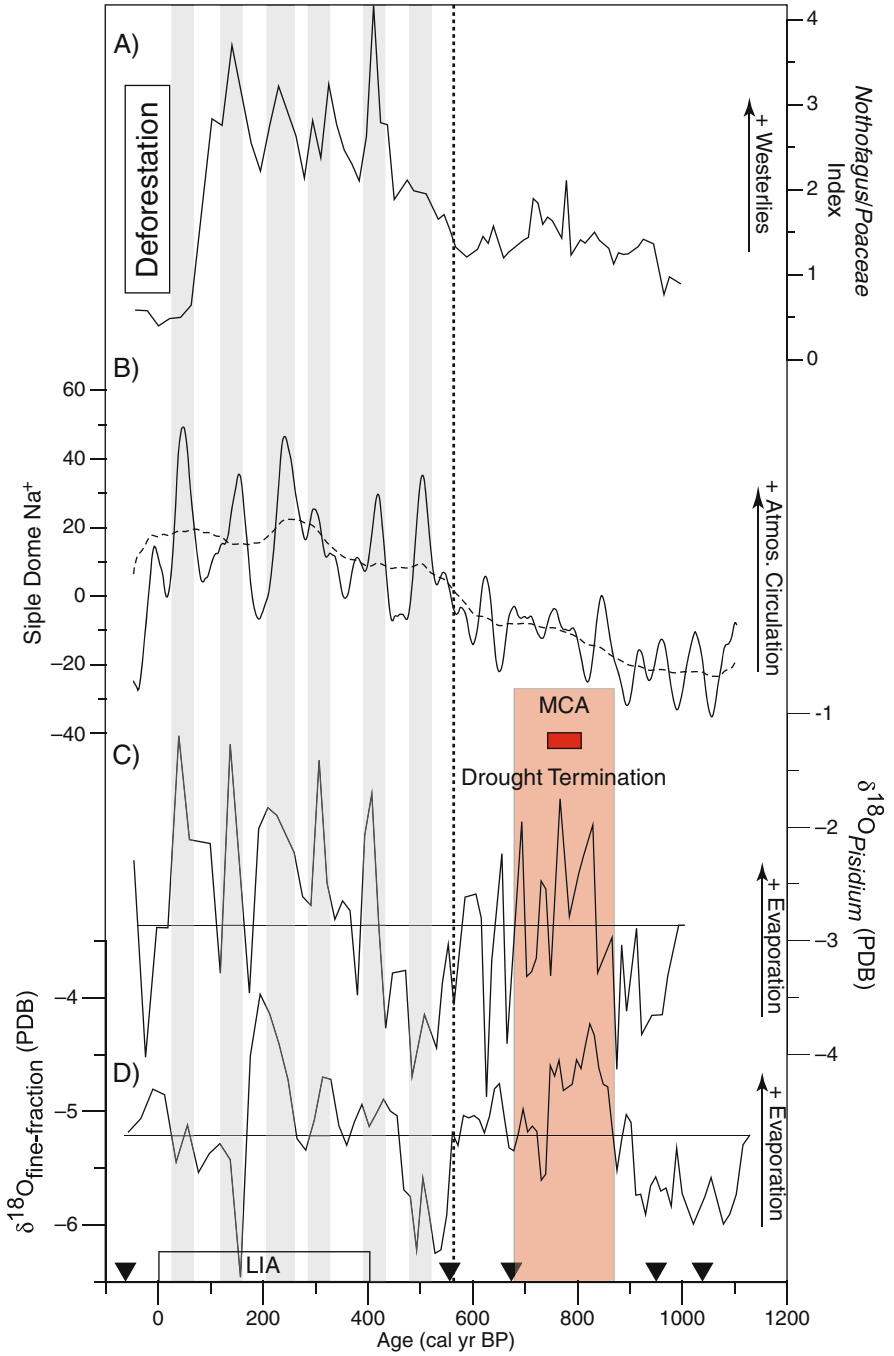

Fig. 15.5 (continued)

and is offset from equilibrium values by >2‰ (Moy et al. 2008). Despite these differences, however, we generally see similar variations in both isotope stratigraphies during the last 1200 years over centennial timescales (Fig. 15.5). Minor divergences between the two isotopic profiles, especially on shorter timescales such as during the last 200 years, may be related to seasonal changes in fine-fraction calcification.

The annual weighted average of the isotopic composition of precipitation entering the lake is ~–10.5‰ based on data from IAEA/WMO stations in Punta Arenas and Coyhaique, and the average isotopic composition of groundwater measured from a nearby well in January 2007 was –13.9‰. In contrast to these hydrologic inputs, the measured $\delta^{18}O$ of the lake water during January 2007 was –4.05‰ VSMOW and average core-top $\delta^{18}O$ value for PS0711SC is –3.7‰ VPDB. The > 6‰ discrepancy indicates a significant isotopic enrichment of $\delta^{18}O$ due to evaporative effects. Today, the lake level is ~1.5 m below a spillway that drains water to Lago Sarmiento and is hydrologically closed. Evaporation is the major mechanism for water loss, and evaporative processes dominate the $\delta^{18}O$ signal in the *Pisidium* and fine-fraction carbonate (Leng and Marshall 2004, Moy et al. 2008).

We compile the oxygen isotopic data from *Pisidium* and the fine-fraction carbonate (Moy et al. (2008); Fig. 15.5) to illustrate changes in hydrologic balance in the last millennium. The two profiles exhibit similar variability over the last 1200 years, and the Authors identify two periods of above-average $\delta^{18}O$ values between 900 and 600 cal year BP and between 400 and 0 cal year BP. Centered on 1100 and 500 cal year BP are two century-long intervals of below average $\delta^{18}O$. The periods of above-average $\delta^{18}O$ are indicative of increased evaporative processes coincident with the MCA and the LIA.

Moreno et al. (2009) calculated a paleovegetation index based on the ratio of *Nothofagus*/Poaceae pollen to identify changes in the relative abundance of forest and steppe. Positive anomalies indicate dominance of *Nothofagus* forests and negative anomalies indicate steppe. During the last two millennia, increases in the paleovegetation index occurred at 1300 and 570 cal year BP. High positive anomalies between 570 and 100 cal year BP are interpreted as an eastward expansion of the *Nothofagus* forest during LIA due to increased precipitation and westerly atmospheric flow (Fig. 15.5). The large decrease in the last 100 years is attributed to forest clearance by European settlers and is coincident with high charcoal concentrations and of the presence of the introduced herb *Rumex acetosella*.

Combining the paleovegetation index and the oxygen isotope data from the two carbonate fractions provides new insight into past variations in the westerlies. During the MCA, above-average $\delta^{18}O$ values indicating aridity are associated with relatively dry centennial-scale phases inferred from the paleovegetation index. Peak isotopic values at Lago Guanaco that span 200 years and are centered on ~800 cal year BP, coincide with the age of submerged tree stumps from two Patagonian lakes that have been interpreted to indicate drought termination during and after the MCA (Stine 1994).

During LIA time, a significant and complex change takes place in the relationship between the $\delta^{18}O$ and the paleovegetation index. Moy et al. (2008) observe

an increase in both parameters that is interpreted as an increase in the strength of the westerlies at this latitude. The reasoning is that increased wind stress on the lake would increase isotopic fractionation through evaporative effects. At the same time, stronger westerlies would also increase precipitation and promote forest expansion, increasing the paleovegetation index. At multi-decadal timescales, consistent variations in the *Pisidium* $\delta^{18}O$ values and paleovegetation index may reflect the enhanced delivery of *Nothofagus* pollen to the coring site during periods of increased westerly wind speeds. The paleovegetation index are highest during the LIA than any other time in the last 5000 years suggesting that westerly wind strength culminated during this time (Moreno et al. 2009).

Moy et al. (2008) compared the results from Lago Guanaco with the record of Na^+ from the Siple Dome ice core in western Antarctica, which reflects enhanced atmospheric circulation and delivery of sea salt derived Na^+ to the coring site (Kreutz et al. 1997). To identify important multi-decadal and longer variations in this time series, the first EOF with 25- and 115-year windows were calculated using singular spectrum analysis (SSA) (Ghil et al. 2002) (Fig. 15.5). The Na^+ time series in Siple Dome exhibits significant multi-decadal variability between 550 and 0 cal year BP that is superimposed upon a long-term trend of increasing values. The increase in Na^+ coincides with the prominent increase in the paleovegetation index, and high values in *Pisidium* $\delta^{18}O$ data at L. Guanaco, all three records exhibit sustained high values until ~150 cal year BP, when the pollen index values decline due to widespread forest clearance. Although the Guanaco *Pisidium* $\delta^{18}O$ and the Siple Dome record (25-year window) show consistent in-phase multi-decadal variations during the LIA, the inherent uncertainty in the calibrated radiocarbon chronology precludes a close evaluation of this relationship.

In summary, we highlight two important findings regarding climate change in southern Patagonia during the last millennium. A period of aridity (reduced westerlies) coincides with the timing of the MCA and an extended period of increased evaporation and precipitation occurs during the LIA. The former interval reflects periods of aridity in the region, whereas the latter indicates an overall increase in the strength of atmospheric circulation in the high southern latitudes.

15.3.2 Laguna Potrok Aike

Directly to the east of Lago Guanaco in Argentine Patagonia, a number of paleoclimate archives have been derived within the project SALSA (South Argentinean Lake Sediment Archives and modeling). Sediment sequences have been recovered from lakes within the Pali Aike volcanic field, including Laguna Potrok Aike (Haberzettl et al. 2007, Haberzettl et al. 2005, Mayr et al. 2007, Wille et al. 2007), Laguna Azul (Mayr et al. 2005), and from the tarn Laguna de las Vizcachas on the Meseta de las Vizcachas (Fey et al. In Press). Based on seismic stratigraphy, Laguna Potrok Aike has a ~300-m-thick sediment sequence (Anselmetti et al. 2009). Because the lake is located beyond the late-Quaternary ice limit, Laguna Potrok Aike has the potential to provide a long record (i.e. multiple glacial cycles)

of climate change in Southern Patagonia and has been drilled by the International Continental Scientific Drilling Program (ICDP) in late 2008.

Haberzettl et al. (2005, 2008) combined geochemical, palynological, and physical property data from sediment cores collected in the 100-m-deep central basin and in the littoral zone of Laguna Potrok Aike and inferred changes in lake level during the last ~2000 years. By combining the different proxies, namely wt.% total inorganic carbon, Ti, C/N, and $\delta^{13}C$, the Authors highlight a period of lowered lake levels between 720 and 470 cal year BP and a period of increased lake levels and relatively moist conditions between ~450 and 0 cal year BP. The former period is attributed to aridity during the MCA, while the latter is related to relatively wet conditions during the LIA. Similarly, in Laguna Azul, Mayr et al. (2005) identify a sequence of hydrologic changes between 550 and 250 cal year BP (dry) and 250 and 50 cal year BP (wet) also using a multi-proxy approach but focusing on the $\delta^{13}C$ of bulk organic matter. Both studies suggest that changes in the strength of the southern westerlies during the last two millennia caused the lake-level variations. Although the late Holocene wet and dry periods interpreted from Laguna Potrok Aike and Laguna Azul generally mirror results from Lago Guanaco, the modern relationship between wind and precipitation indicates that intervals of enhanced westerly intensity should produce wetter conditions in western Patagonia and drier conditions in the east (Mayr et al. 2007, Moy et al. 2008). Therefore, westerly-driven wet/dry cycles should be antiphased between the L. Potrok Aike/L. Azul and Lago Guanaco records. Yet geochemical proxies from these three lakes suggest that both east and west Patagonia were wet during the LIA and dry during the MCA, yielding opposite interpretations of westerly wind behavior. This discrepancy will best be reconciled by the establishment of additional weather stations in southern Patagonia and by the development of additional paleoclimate reconstructions from the Patagonian interior.

15.3.3 Lago Cardiel

Past climate change and related lake level variations have also been reconstructed at Lago Cardiel (49°S; Fig. 15.1), located in central Patagonia and on the eastern Andean slope. Lago Cardiel is a large closed-basin lake with a modern surface area of 370 km^2 and a maximum water depth of 76 m (Markgraf et al. 2003). Galloway et al. (1988) and Stine and Stine (1990) reconstructed former lake high stands by radiocarbon dating both sediments and tufas exposed in stream cuts and strandlines encircling the modern lake. An impressive shoreline transgression was centered at ~10500 cal year BP, when the lake surface was > 50 m above the 1990 lake level. During the late Holocene, Stine and Stine (1990) document smaller (< 10 m) variations in lake level and identify 4 transgressions during the last 2000 years centered at ~2000, ~1200, ~800 and ~200 cal year BP. The 1990 lake level is considered a relatively low elevation for the Holocene and the culmination of a regression that began ca. AD 1940 (Markgraf et al. 2003). Recently, the lake has risen at least 4 m since this 1990 position, possibly as a result of ENSO-induced precipitation (Markgraf et al. 2003).

Gilli et al. (2001 and 2005) compared seismic surveys of the sediment stratigraphy and the physical properties from a number of cores from Lago Cardiel to identify variations in climate during the Holocene, and Markgraf et al. (2003) presented geochemical and paleoenvironmental (diatoms and pollen) data collected from multiple coring sites within the lake. These studies characterize the last 2000 years of climate history as highly variable with alternating wet and dry periods, possibly related to the increase in ENSO variability. The Holocene chronology is derived from two tephra found in the sediment cores: the older tephra is derived from Volcán Hudson at ~7500 cal year BP (Naranjo and Stern 1998) and the younger is from the Northern Austral Volcanic Zone (NAVZ) at ~3200 cal year BP (Markgraf et al. 2003). Radiocarbon dates on carbonate and organic fractions preserved in the sediment cores provide a range of ages that are older than the tephrochronology by >3000 years (Gilli et al. 2005). The offset has been attributed to two processes: a variable reservoir effect that is dependent on lake volume and contamination from the erosion of older sediment within the watershed. Unfortunately, the two ages that constrain the Holocene tephrochronology make it difficult to compare results with other paleoclimate records.

15.4 Pollen and Charcoal Records

Pollen records derived from lakes and bogs represent one of the most abundant paleoclimate archives in southern South America. Since the pioneering work by Auer (1933, 1958), many studies have reconstructed the ecological and climatic history over a range of time periods (Heusser 1966, Heusser and Heusser 2006, Heusser et al. 1999, Markgraf 1993, Markgraf et al. 2003, Moreno 2004, Moreno et al. 1999, Villagrán 1985, 1988). However, few palynological records in Patagonia have adequate chronology and sampling resolution to address environmental changes of the past 2000 years. Two records from small closed-basin sites located in the rainforest-dominated region of the Chilean channels and the Andean region of Central Patagonia (~45°S) (Szeicz et al. 2003, 1998) are exceptional because they link changes in vegetation changes and fire regimes (inferred from the presence of charcoal particles in the sediments) on decadal timescales over the last millennium. These records indicate little or no variation in the vegetation and fire regime since ~1900 cal year BP, with the exception of a decline in forest dominance associated with European settlement and forest clearance by ~1890 AD.

Pollen records from southern Patagonia (50–52°S) show a varied response to climate change during the last 2000 years. High-resolution pollen and plant macrofossil records from the Río Rubens bog (Huber and Markgraf 2003), located in the deciduous forest zone of Southern Patagonia (51.5°S) east of the Andes, indicate the presence of *Nothofagus* forests (probably *N. pumilio*) with little or no variations in vegetation since ~5000 cal year BP. Intense fires at ~350 cal year BP led to the expansion of grasslands with exotic species of European origin (*Rumex acetosella*). Likewise, a pollen record from Lago Potrok Aike (Haberzettl et al. 2005), directly east in the Patagonian steppe, shows dominance of steppe herbs and shrubs over the last ~1900 years and the expansion of *Rumex acetosella* at ~1850 AD. The

pollen record from Lago Guanaco (Fig. 15.5) shows a pulse of forest expansion starting at 1300 cal year BP and increasing between 570 and 70 cal year BP. The data are interpreted as evidence of an eastward shift of the forest-steppe ecotone and an intensification and/or latitudinal shift of the westerly winds (see previous discussion). The fact that L. Potrok Aike, Rio Rubens bog, and Lago Guanaco lie within 200 km of each other, but show different signals, can be attributed to the location of the records in different ecological environments (i.e. steppe vs. forest), the depositional environment (lake vs. bog), chronologic control, and local differences in the sensitivity of the forest-steppe ecotone to changes in precipitation (Moreno et al. 2009). In addition, a complicating factor for the interpretation of pollen records from Patagonia is that the palynomorph *Nothofagus dombeyi*-type includes species found in a broad range of habitats and climatic regimes (*N. antarctica, N. betuloides, N. dombeyi, N. nitida, N. pumilio*), including azonal habitats such as wetlands. By dwelling on the surface or the periphery of fens and bogs, species such as *Nothofagus antarctica* can impose a biased palynological signal in the sedimentary record that overrides the extralocal or regional one. Future regional-scale interpretations of past vegetation and climate change in Patagonia should take these issues into account.

The occurrence of natural fires depends on the accumulation, quality, and spatial/temporal continuity of biomass, their desiccation, and ignition sources. The stratigraphic analysis of charcoal particles allows reconstruction of past fire regimes, and thus allows inferences to be drawn about past variability in hydrologic balance, seasonality, and ignition sources at multiple scales of analysis. Charcoal records from the rainforest region of NW Patagonia (∼41°S) indicate the culmination of a multi-millennial increase in fire activity that started at ∼3000 cal year BP (Whitlock et al. 2007) and peaked ∼1100 years ago. Macroscopic charcoal records from two closed-basin lakes (Pichilaguna and El Salto) in the Longitudinal Valley of the Chilean Lake District indicate centennial-scale variations (Fig. 15.6), including periods of high charcoal abundance between ∼1200–1000 and 500–250 cal year BP, and low values between 900–500 and 250–0 cal year BP. A palynological site from Isla Grande de Chiloé shows changes in forest composition that suggests high levels of disturbance in the last 500 years (Abarzua and Moreno 2008). This increase was followed by high levels of charcoal from recent European-set burning. The climatic significance of the latter remains unclear as the disturbance signal in the vegetation overrides or obscures a genuine climatic response. A high-resolution study of a 600-year old sedimentary record from Lago Puyehue by Bertrand et al. (2005) revealed a distinctive peak in terrigenous supply between 450 and 250 cal year BP, which was interpreted as a prominent wet phase followed by a steady decline toward the present. This putative wet phase was contemporaneous with intense fire activity in Pichilaguna and El Salto, thus suggesting that fire activity in the Longitudinal Valley of the Lake District between 500 and 250 cal year BP was caused by humans, or mechanisms other than increased precipitation can account for increased terrigenous supply to Lago Puyehue. Additional high-resolution precisely dated paleoclimate records from this area are needed to solve this apparent mismatch.

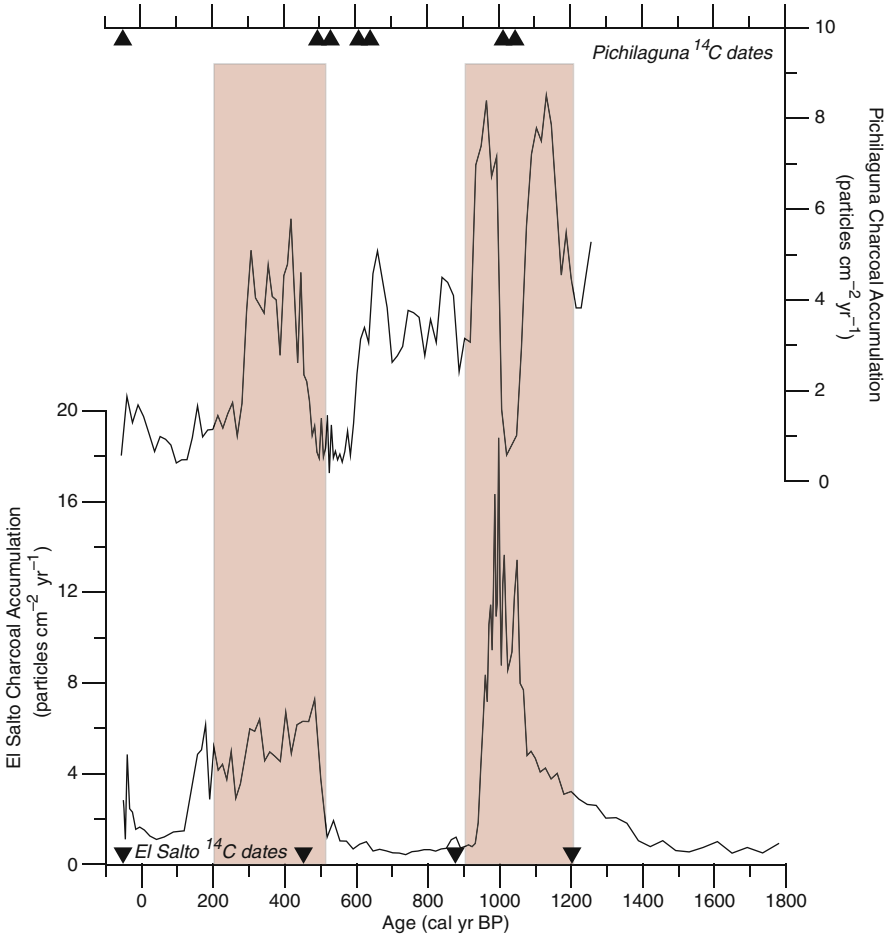

Fig. 15.6 Charcoal accumulation rates from Pichilaguna and El Salto highlight the last ~1200 cal year BP of fire history in the Chilean Lake District (42°S). These two records display alternating periods of high charcoal abundance between ~1200–1000 and 500–200 cal year BP (vertical red bars), and intervals with relatively low values between 900–500 and 200–0 cal year BP. Black triangles refer to median calibrated radiocarbon ages used in the chronology

15.5 Glacier Records

The Campo de Hielo Patagónico Norte (CHPN) and Sur (CHPS) are the most prominent glacial features in southern South America, and when combined, they represent the largest and most extensive areas of ice in the Southern Hemisphere outside Antarctica (Casassa et al. 1998). The northern and southern ice fields have aerial extents of ~4200 and ~13000 km^2, respectively (Rignot et al. 2003). The CHPN has average elevations between 1000 and 1500 m from west to east and the CHPS has average elevations of 1500 to 2000 m (Aniya 1988, Aniya et al. 1996, Rivera et al. 2007, Warren and Sugden 1993). Both ice fields have exten-

sive outlet glaciers that terminate in the Chilean fjords, into freshwater lakes, or on land (Casassa et al. 2002). The Southern Hemisphere westerlies transport massive amounts of precipitation to both ice sheets (present-day accumulation rates of up to 10 m water equivalent per year), but the eastern outlet glaciers terminate in areas that receive a fraction of the amount received in the west or at the divide (Rivera et al. 2007). Because of the difficulty of field work and obtaining clear satellite imagery in this very wet region, the high-elevation ice fields remain relatively poorly studied.

20th century research indicates that climate *in general* has been the dominant driver of glacial changes but the nature of the terminal environment, and other "non-climate effects" are important second-order controls for particular glaciers (Harrison et al. 2007, Naruse 2006, Rignot et al. 2003, Warren and Sugden 1993). Patagonian glaciers are sensitive climate proxies that respond to temperature (<0.5°C) and precipitation, with the former being relatively most important for most glaciers in the latter part of the 1900s (Rignot et al. 2003, Rivera and Casassa 2004). Many outlet glaciers radiating from the ice fields have been retreating from their LIA maximum positions since the late 19th century, (Harrison et al. 2007). Recent work has focused on quantifying the rate of ice-volume loss, which has increased relatively rapidly towards the present and are considered large enough to account for ~6% of recent global sea level rise (Rignot et al. 2003).

Clapperton and Sugden (1988), Porter (2000), and Glasser et al. (2004) reviewed the history of glacial ice activity in southern South America in the mid and late Holocene. Given the remoteness of glaciers in Patagonia, only a few areas have been investigated in detail. Paleoclimate knowledge is based largely on the research of Mercer (1965, 1968, 1970, 1976, 1982), Porter (2000), Röthlisberger (1986), Malagnino and Strelin (1992), Aniya (1995), Aniya et al. (1996), Strelin and Malagnino (2000), and Harrison et al. (2007). Most of the data for glacial ice expansion is derived from radiocarbon-dated glacial deposits on outlet and satellite glaciers in the northern and southern Patagonian ice fields. In addition to radiocarbon chronologies, lichenometry (Harrison et al. 2008) and tree-ring derived chronologies (Harrison et al. 2007, Koch and Killian 2005, Villalba 1994) have been used to date recent (last millennium) moraine deposits. Cosmogenic surface-exposure ages have been used to date middle Holocene and older deposits in southern South America (Douglass et al. 2005).

Porter (2000) highlighted some of the challenges that must be considered when interpreting and identifying the timing of past glacial ice extents. Radiocarbon age-dating of glacial deposits can be challenging due to the difficulty of finding suitable or relevant organic material. Minimum or maximum limiting ages may not closely constrain the timing of ice advance, and organic material may be remobilized or contaminated by younger material. Also, many studies rely on single minimum or maximum age limits for the timing of a glacial advance. Modern process studies show, internal ice instabilities due to changes in the calving environments in lakes and fjords, in addition to rockfall deposits on glacier ablation areas, are secondary mechanisms that should also be considered when interpreting past changes in ice extent (Porter 2000). In addition to these local or site-specific challenges, whether temperature or precipitation is the primary climate mechanism driving past changes in ice extent has been questioned. Glasser et al. (2002) suggested that outlet

glaciers on the eastern side of the Andes may be particularly sensitive to changes in precipitation, largely due to the steep rainfall gradient that exists from west to east across the topographic divide. However, eastern outlet glaciers, from the ice fields at least, are also ultimately nourished by the high ice accumulation areas on the divide and ablation areas on the eastern side still occur in areas classified as much wetter than semi-arid (e.g., see weather data listed above for Torres del Paine). In addition, because the westerlies are driven by atmospheric and oceanic temperature gradients, increases in accumulation in the past may have been coupled with reductions in temperature (see above), facilitating ice expansion. Nonetheless, glacial response and its relative magnitude to a climatic change may vary across the Andean divide, and evidence from multiple sites (and with multiple chronostratigraphies) is needed to provide a robust chronology of glacial response to climate change (Porter 2000).

Evidence from radiocarbon-dated deposits from outlet and satellite glaciers from the northern and southern Patagonian ice fields indicates that Neoglaciation in southern South America began, and was most extensive, in the mid Holocene ca. ~5400 cal year BP (e.g., Mercer 1976). Mercer described advances from his work in the Patagonian ice fields at ~4600 cal year BP, ~2500 cal year BP, and during the last few hundred years. The Mercer chronology was replaced with the four event Clapperton and Sugden (1988) and Aniya (1995) model, which had glacial maxima at ~3800 cal year BP, ~2700–1900 cal year BP, ~1400–1200 cal year BP, and the last few hundred years (also see Porter 2000).

We compiled radiocarbon and tree-ring evidence for glacial advances during the last 2000 years in Patagonia (In Fig. 15.7 and Table 15.2). We calibrated the radiocarbon ages using the Southern Hemisphere calibration curve (McCormac et al. 2004) and present the results in calendar year BP to facilitate comparison with other paleoclimate records presented in this review. Many of the ages presented here reflect a minimum age of ice advance (i.e., the radiocarbon dates were either derived from peat that started growing after the ice retreated or from deposits on top of the moraine). When the ages are combined, we identify three periods of increased glacial ice extent in Patagonia and Tierra del Fuego during the last 2000 years centered on 1300 cal year BP, 600 cal year BP, and between 400 and 50 cal year BP (Fig. 15.7).

15.6 Tree-Ring Records

Tree-ring records from southern South America represent the most broadly distributed and annually resolved paleoclimate archives. Tree-ring networks derived from sensitive locations can be used to reconstruct large-scale atmospheric circulation patterns at annual to multi-decadal timescales (Aravena et al. 2002, Lara et al. 2001, Lara and Villalba 1993, Lara et al. 2008, Villalba 1990, 1991, 1994). Records from southernmost South America, for example, are well-poised to reconstruct climate variability related to the SAM and therefore can significantly expand our understanding of the potential magnitude of change and timescales of variability (Villalba 2007).

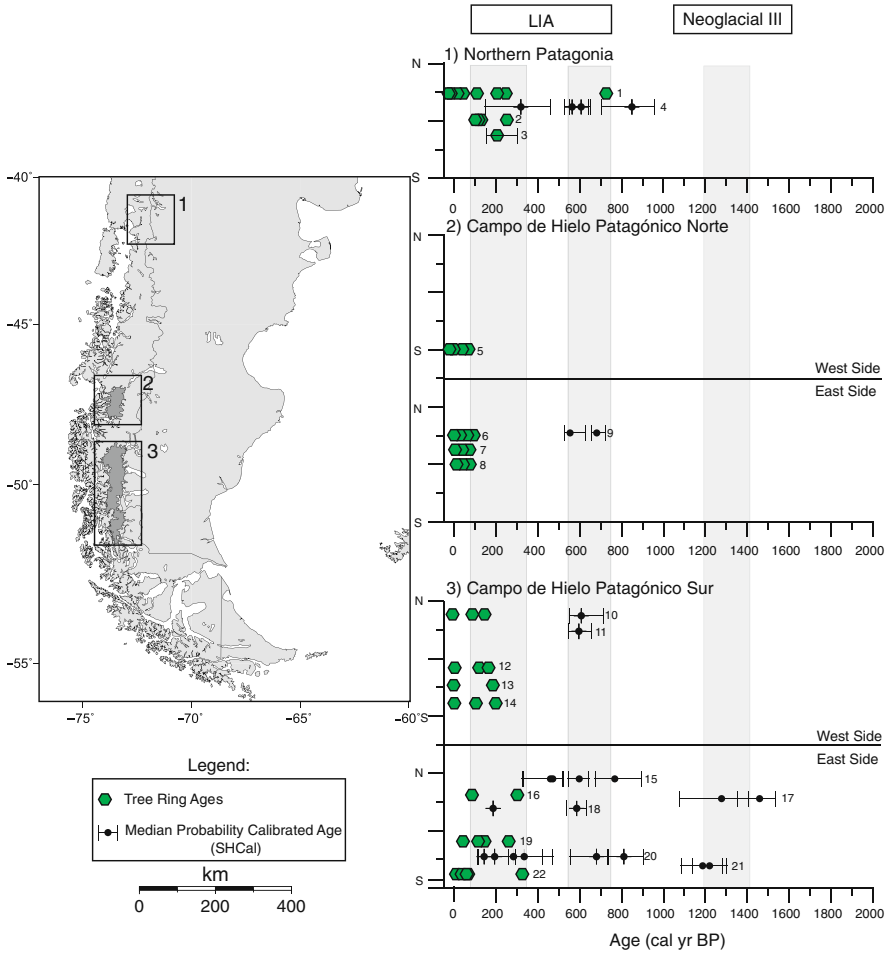

Fig. 15.7 Summary of glacial advances in southern South America during the last 2000 years. Glacial activity derived from tree rings and from radiocarbon dates on glacial deposits are shown for three regions. We calibrated the ages published in the literature using the Southern Hemisphere calibration curve (McCormac et al. 2004), show the median probability age along with the 1-sigma range, and plot the data on the calibrated age scale (cal year BP). See Table 15.2 for data sources, locations, and references for the dated glacial deposits. We highlight three periods of enhanced glacial activity (vertical bars): (1) between 1400 and 1200, (2) 550 and 750, and (3) 400 and 50 cal year BP. Ice generally began retreating from LIA ice positions in the late 19th century (Harrison et al. 2007, Villalba et al. 2005)

Villalba et al. (2003) compiled a network of tree-ring records derived from upper treeline locations in northern and southern Patagonia to investigate changes in temperature during the last four centuries (Fig. 15.8). These records were processed to highlight multi-decadal variations in mean annual temperature, and therefore, are especially useful for placing the modern temperature observations in a longer context that can be compared with paleoclimate records from these regions. In Fig. 15.8,

Table 15.2 Compilation of calibrated radiocarbon dates and tree ring ages for timing of glacial activity in southern South America. T, R, L refer to tree-ring, radiocarbon, and lichenometry age dating techniques, respectively and CHPN and CHPS refer to Campo de Hielo Patagónico Norte (CHPN) and Sur (CHPS)

Figure 7 References	Glacier name	Location	References	Latitude	Type	Median calibrated age (SHCal) or tree-ring age	1 sigma range for ^{14}C
1	Frías	Mt. Tronador	Villalba (1990)	−40.17	T	>714	–
1	Frías	Mt. Tronador	Villalba (1990)	−40.17	T	312	–
1	Frías	Mt. Tronador	Villalba (1990)	−40.17	T	228	–
1	Frías	Mt. Tronador	Villalba (1990)	−40.17	T	203	–
1	Frías	Mt. Tronador	Villalba (1990)	−40.17	T	111	–
1	Frías	Mt. Tronador	Villalba (1990)	−40.17	T	69	–
1	Frias	Mt. Tronador	Villalba (1990)	−40.17	T	36	–
1	Frías	Mt. Tronador	Villalba (1990)	−40.17	T	−2	–
1	Frías	Mt. Tronador	Villalba (1990)	−40.17	T	−27	–
1	Frías	Mt. Tronador	Villalba (1990)	−40.17	T	250	–
3	Río Manso	Mt. Tronador	Lawrence and Lawrence (1959)	−41.0	T	250	–
3	Río Manso	Mt. Tronador	Lawrence and Lawrence (1959)	−41.0	T	135	–
3	Rio Manso	Mt. Tronador	Lawrence and Lawrence (1959)	−41.0	T	117	–
3	Río Manso	Mt. Tronador	Lawrence and Lawrence (1959)	−41.0	T	103	–
4	Río Manso	Mt. Tronador	Rabassa et al. (1984)	−41.0	T,L,R	180−300	–
2	Río Manso	Mt. Tronador	Röthlisberger (1986)	−41.0	R	822	685−927
2	Río Manso	Mt. Tronador	Röthlisberger (1986)	−41.0	R	590	535−633
2	Río Manso	Mt. Tronador	Röthlisberger (1986)	−41.0	R	549	515−624
2	Río Manso	Mt. Tronador	Röthlisberger (1986)	−41.0	R	315	152−451
5	Gualas and Reicher	CHPN	Harrison and Winchester (1998)	−46.5	T	74	–
5	Gualas and Reicher	CHPN	Harrison and Winchester (1998)	−46.5	T	41	–
5	Gualas and Reicher	CHPN	Harrison and Winchester (1998)	−46.5	T	−4	–
5	Gualas and Reicher	CHPN	Harrison and Winchester (1998)	−46.5	T	−20	–
6	Soler	CHPN	Sweda (1987)	−47.0	T	100−90	–
6	Soler	CHPN	Sweda (1987)	−47.0	T	60−50	–

Table 15.2 (continued)

Figure 7 References	Glacier name	Location	References	Latitude	Type	Median calibrated age (SHCal) or tree-ring age	1 sigma range for ^{14}C
6	Soler	CHPN	Sweda (1987)	−47.0	T	40−30	–
6	Soler	CHPN	Sweda (1987)	−47.0	T	10−0	–
7	Arco, Arenales, and Colonia	CHPN	Harrison and Winchester (2000)	−47.25	T	75	–
7	Arco, Arenales, and Colonia	CHPN	Harrison and Winchester (2000)	−47.25	T	45	–
7	Arco, Arenales, and Colonia	CHPN	Harrison and Winchester (2000)	−47.25	T	5	–
8	Nef	CHPN	Winchester et al. (2001)	−47.2	T	87	–
8	Nef	CHPN	Winchester et al. (2001)	−47.2	T	66	–
8	Nef	CHPN	Winchester et al. (2001)	−47.2	T	15	–
9	Soler	CHPN	Glasser et al. (2002)	−47.0	R	553	525–625
9	Soler	CHPN	Glasser et al. (2002)	−47.0	R	680	660–720
10	Ofhidro Norte	CHPS	Mercer (1970)	−48.4	R	697	570–765
10	Ofhidro Norte	CHPS	Mercer (1970)	−48.4	T	95	–
10	Ofhidro Norte	CHPS	Mercer (1970)	−48.4	T	100	–
10	Ofhidro Norte	CHPS	Mercer (1970)	−48.4	T	155	–
11	Ventisquero Bravo	CHPS	Röthlisberger (1986)	−48.0	R	600	555–650
11	Ventisquero Bravo	CHPS	Röthlisberger (1986)	−48.0	R	Modern (< 200 cal year BP)	–
11	Ventisquero Bravo	CHPS	Röthlisberger (1986)	−48.0	R	Modern (< 200 cal year BP)	–
12	Bernardo	CHPS	Mercer (1970)	−48.6	T	175	–
12	Bernardo	CHPS	Mercer (1970)	−48.6	T	140–130	–
12	Bernardo	CHPS	Mercer (1970)	−48.6	T	10–0	–
13	Témpano	CHPS	Mercer (1970)	−48.65	T	200–180	–
13	Témpano	CHPS	Mercer (1970)	−48.65	T	10–0	–

Table 15.2 (continued)

Figure 7 References	Glacier name	Location	References	Latitude	Type	Median calibrated age (SHCal) or tree-ring age	1 sigma range for ^{14}C
14	Hammick	CHPS	Mercer (1970)	−48.8	T	200	–
14	Hammick	CHPS	Mercer (1970)	−48.8	T	110	–
14	Hammick	CHPS	Mercer (1970)	−48.8	T	10–0	–
15	Ventisquero Huemul	CHPS	Röthlisberger (1986)	−48.0	R	604	555–650
15	Ventisquero Huemul	CHPS	Röthlisberger (1986)	−48.0	R	202	145–310
15	Ventisquero Huemul	CHPS	Röthlisberger (1986)	−48.0	R	332	154–453
15	Ventisquero Huemul	CHPS	Röthlisberger (1986)	−48.0	R	446	332–501
15	Ventisquero Huemul	CHPS	Röthlisberger (1986)	−48.0	R	469	334–529
15	Ventisquero Huemul	CHPS	Röthlisberger (1986)	−48.0	R	480	341–527
15	Ventisquero Huemul	CHPS	Röthlisberger (1986)	−48.0	R	775	681–900
16	Narvarez	CHPS	Mercer (1968)	−48.0	T	300	–
16	Narvarez	CHPS	Mercer (1968)	−48.0	T	70	–
17	Upsala	CHPS	Aniya (1995)	50.0	R	1464	1358–1539
17	Upsala	CHPS	Aniya (1995)	50.0	R	1283	1083–1413
18	Ventisquero Frances	CHPS	Röthlisberger (1986)	−51.0	R	Modern (< 200 cal year BP)	–
18	Ventisquero Frances	CHPS	Röthlisberger (1986)	−51.0	R	606	559–649
19	Grey	CHPS	Marden and Clapperton (1995)	−51.5	T	290–225	–
19	Grey	CHPS	Marden and Clapperton (1995)	−51.5	T	145	–
19	Grey	CHPS	Marden and Clapperton (1995)	−51.5	T	105	–
19	Grey	CHPS	Marden and Clapperton (1995)	−51.5	T	< 60	–
20	Ventisquero Perro	CHPS	Röthlisberger (1986)	−51.0	R	Modern (< 200 cal year BP)	–
20	Ventisquero Perro	CHPS	Röthlisberger (1986)	−51.0	R	226	148–320
20	Ventisquero Perro	CHPS	Röthlisberger (1986)	−51.0	R	312	152–446
20	Ventisquero Perro	CHPS	Röthlisberger (1986)	−51.0	R	361	289–492

Table 15.2 (continued)

Figure 7 References	Glacier name	Location	References	Latitude	Type	Median calibrated age (SHCal) or tree-ring age	1 sigma range for ^{14}C
20	Ventisquero Perro	CHPS	Röthlisberger (1986)	−51.0	R	691	571–744
20	Ventisquero Perro	CHPS	Röthlisberger (1986)	−51.0	R	816	743–904
21	Tyndall	CHPS	Aniya (1995)	−51.6	R	1226	1145–1308
21	Tyndall	CHPS	Aniya (1995)	−51.6	R	1193	1091–1288
22	Lengua	Gran Campo Nevado	Koch and Killian (2005)	−53.0	T	322	–
22	Lengua	Gran Campo Nevado	Koch and Killian (2005)	−53.0	T	77	–
22	Lengua	Gran Campo Nevado	Koch and Killian (2005)	−53.0	T	64	–
22	Lengua	Gran Campo Nevado	Koch and Killian (2005)	−53.0	T	48	–
22	Lengua	Gran Campo Nevado	Koch and Killian (2005)	−53.0	T	38	–
22	Lengua	Gran Campo Nevado	Koch and Killian (2005)	−53.0	T	9	–

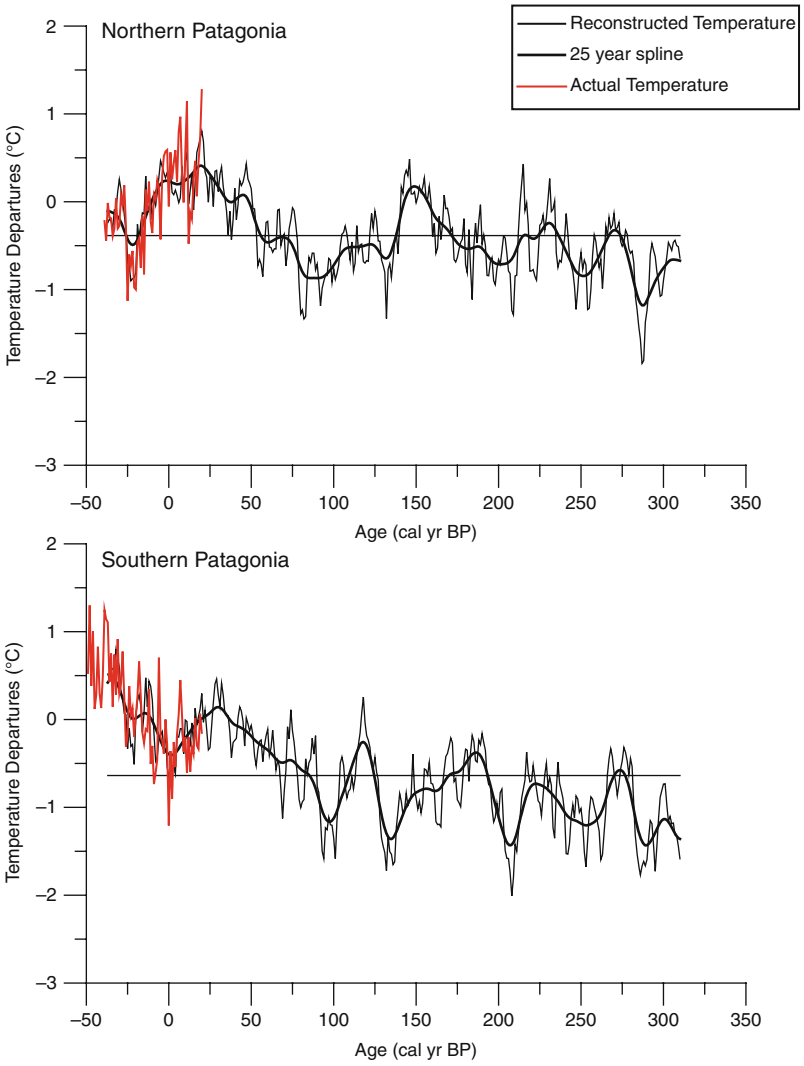

Fig. 15.8 Villalba et al. (2003) tree-ring derived temperature reconstruction for northern and southern Patagonia during the last four centuries derived from upper treeline locations (Fig. 15.1). The annually resolved temperature reconstructions are displayed along with a 25-year spline (*heavy dark lines*), and actual temperatures (*red lines*) from meteorological stations. The horizontal line represents the reconstructed mean. Both temperature reconstructions show a positive trend in temperature over the last 300 years, but there are differences in the timing of decadal variations and the short-term trend in temperature over the last ~50 years

we show the results from the northern and southern Patagonian tree-ring networks. There are some important similarities and differences between the two locations: although there is a clear positive trend in temperature between 1850 and 1920, the two records diverge (as does the instrumental record) during the last 50 years. In

addition, some of the multi-decadal variability observed in the records is not temporally consistent between northern and southern Patagonia. Some of the differences may be related to the different climatic forcing mechanisms between these two sites. When the northern Patagonia time series is regressed onto SST fields in the southern Pacific and the Atlantic basins, the variability is most strongly correlated with tropical and subtropical SST variability and is similar to the spatial SST structure of the PDO. In contrast, temperature variability in southern Patagonia is related to SST variability in the southern Atlantic Ocean and when regressed on a global field, the spatial structure is similar to the global warming mode of SST (Villalba et al. 2003). The Villalba et al. (2003) temperature reconstruction highlights three important points for our understanding of climate change in southern South America: (1) the period from 1850 to 1875 (100 to 75 cal year BP) marks a turning point in which temperatures begin to climb towards present day values, (2) the temperatures observed within the last 50 years are unprecedented with respect to the last 350 years (Villalba et al. 2003), (3) the multi-decadal temperature variations observed in the Northern Patagonia tree-ring reconstruction corresponds with detailed records of Frías glacier retreat rate (41°S), re-emphasizing the role temperature plays in controlling ice extent in Patagonia (Villalba et al. 2005).

In northern Patagonia, Villalba et al. (1990 and 1994) reconstructed summer temperature variations from a network of sites located in the Río Alerce valley in Argentina (∼41°S). The ∼1200 year reconstruction reveals two relatively cool periods from 1050 to 880 cal year BP and from 680 to 290 cal year BP with an intervening warm period between 870 and 700 cal year BP. The decadal variability in this record is similar to winter precipitation reconstructed from central Chile where warm summers in northern Patagonia correspond with wet winters in central Chile (Boninsegna 1990). Villalba (1994) interprets the consistency of the records as a shared response to ENSO variability during the last millennium.

Recent work by Villalba et al. (2008) has reconstructed past variations in the SAM index using tree-ring chronologies from a network of temperature- and precipitation-sensitive sites in Tasmania, New Zealand, and southern South America. Depending on which season is considered, the reconstructed record captures 47–51% of the total variance in the instrumental SAM index. The most significant result of the reconstruction is the large departure in SAM index values that begins in 1950 and extends to present day, which reflects the shift toward the positive phase of the SAM observed in instrumental records. The 1950 shift reflects the beginning of a major reorganization of atmospheric circulation in the high southern latitudes that is unprecedented within the last 350 years of the reconstruction (Villalba et al. 2008).

15.7 Marine Records

Marine sediment records from the Chilean continental shelf offer a unique opportunity to track changes in oceanic circulation and the response of continental weathering to atmospheric circulation. Lamy et al. (2001) and Lamy et al. (2002)

document changes in sea surface temperature (SST), sea surface salinity (SSS), productivity and precipitation-induced runoff during the last ~8000 cal year BP using a sediment core collected from the Chilean continental shelf at 41°S (Fig. 15.1). Combined alkenone and stable isotope analyses identified an overall decline in SST (~1°C) and SSS (~1 PSU) during the last 2000 years. This decline is coincident with an increase in biogenic opal and wt.% C, which was interpreted as an increase in productivity (Fig. 15.9). To investigate changes in weathering related to precipitation, Lamy et al. (2001) examine the Fe content of the bulk sediment and suggest that higher iron contents in the offshore core reflects greater erosion and runoff in the high Andes, where volcanic source rocks have high Fe content. Reduced Fe content in the sediment core is attributed to sediment derived from mixed sources including the Andes and the Chilean Coastal Range, the latter having relatively low Fe and apparently more sensitivity to rainfall variations than the Andes. Low Fe content in the sediment core is evidence of northward-shifted westerlies that enhanced precipitation in the Coastal Range and effectively diluted the contribution of the Andean source rocks, whereas high Fe content is attributed to a southward-shifted westerlies and a larger contribution of Andean-sourced sediment. Clay mineralogy was used to further this hypothesis. From the Fe profile, the Authors interpret significant changes in rainfall during the mid to late Holocene. Higher Fe counts centered at ~1700 and 700 cal year BP suggest reduced precipitation and southward-shifted westerlies, and two intervening periods centered on 1200 and 300 cal year BP imply northward shifted westerlies and increased precipitation on the continent east of the sediment core location. Lamy et al. (2001) identify arid and southward-shifted westerlies during the MCA (~700 cal year BP) and cooler and equatorward-shifted westerlies during the LIA (~300 cal year BP). Taken together, Lamy et al. (2002) argue that the declining SST, SSS, and Fe concentration at the coring site during the last 2000 years indicates an overall northward extension of the Antarctic Circumpolar Current and the westerlies.

Farther to the south (44°S), Mohtadi et al. (2007) use a similar suite of marine proxies to identify a northward shift in water mass properties (hydrography) and atmospheric circulation related to the westerlies and the Antarctic Circumpolar Current (ACC) between 1300 and 750 cal year BP. The 2° shift in latitude is associated with an overall decline in SST and SSS and increases in diatom concentration and the $\delta^{13}C$ of foraminifera. Taken together, Mohtadi et al. (2007) argued that the northward migration of cooler water and enhanced runoff from westerly-derived precipitation increased productivity between 1300 and 750 cal year BP

Fig. 15.9 (continued) inferred from the Fe profile. Higher Fe counts centered at ~1700 and 700 cal year BP are interpreted as reflecting reduced precipitation and southward-shifted westerlies, while two intervening periods centered on 1200 and 300 cal year BP suggest northward shifted westerlies and increased precipitation. Triangles at the top and at the base of the plot refer to median calibrated radiocarbon ages used in the GeoB 7186-3 and the GeoB 3313-1 chronologies

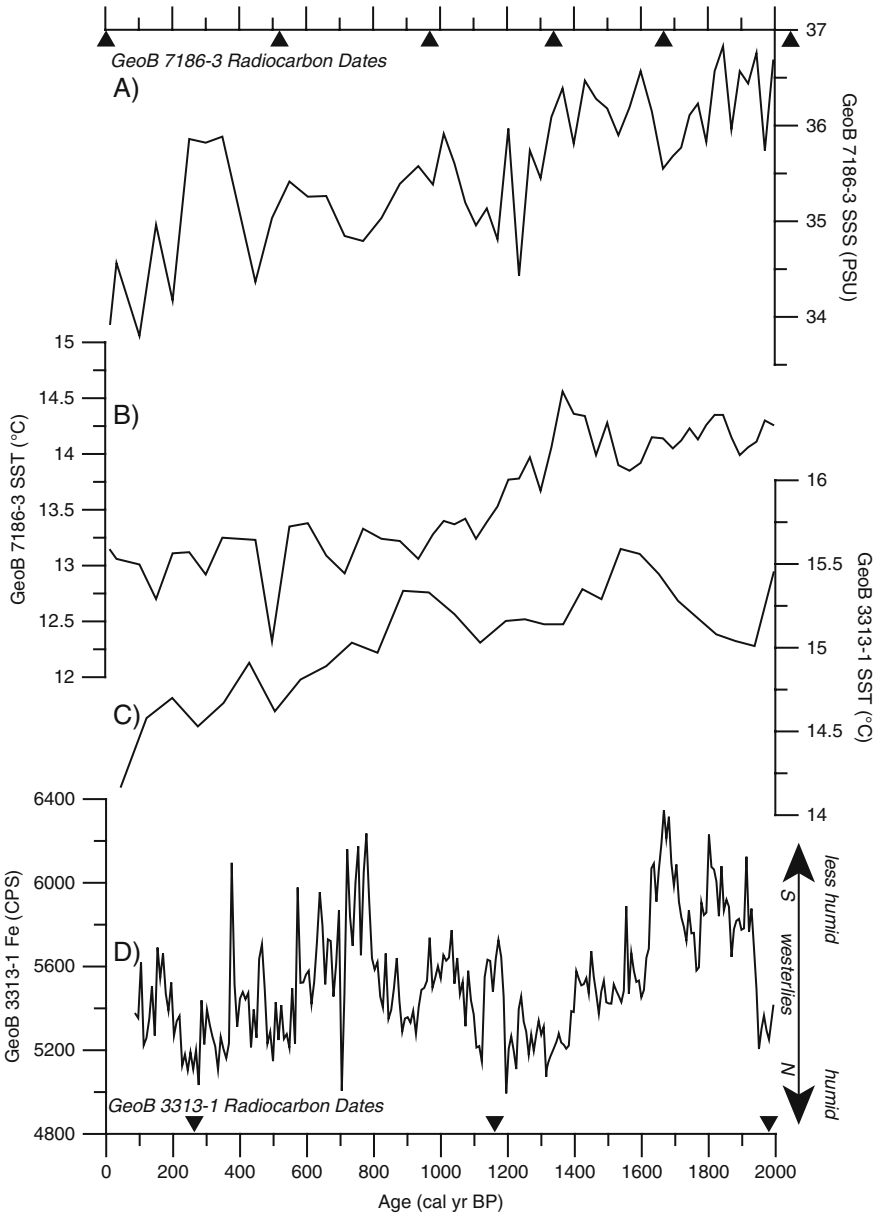

Fig. 15.9 Compilation of marine paleoclimate records from the Chilean continental shelf during the last 2000 years. (**A**) Alkenone-based sea surface salinity (SSS) and (**B**) sea surface temperature (SST) from core GeoB 7186-3 (44°S) (Mohtadi et al. 2007). (**C**) Alkenone-based SST reconstruction and (**D**) Fe content from core GeoB 3313-1 (41°S) (Lamy et al. 2001, Lamy et al. 2002). The SST and SSS reconstructions show an overall decline in sea surface temperature (SST) and sea surface salinity (SSS) that together have been interpreted to reflect a northward migration in the ACC during the last 2000 years. Changes in continental weathering related to westerly precipitation are

and further argued that the northward migration in the westerlies and the ACC is the result of a period of more La Niña-like conditions in the tropical Pacific Ocean.

15.8 Summary and Directions for Future Research

Understanding the last 2000 years of climate variability in southern South America is important because it provides information on processes influencing climate in the mid-latitudes of the Southern Hemisphere and enables us to place the rapid climate changes at present within a broader context. Over the last decade, numerous studies suggest that the southern westerlies play a role in the global carbon cycle, largely through air-sea gas exchange in the Southern Ocean, (Le Quéré et al. 2007, Lovenduski et al. 2007, Sigman and Boyle 2000, Toggweiler et al. 2006). Furthermore, increased atmospheric greenhouse gases in recent decades may at least be partly responsible for the tendency toward the positive phase of the SAM and increasing westerly wind intensity over the Southern Ocean (Kushner et al. 2001, Stone et al. 2001). Paleoclimate studies from southern South America offer one of the best opportunities to gain a better understanding of the natural processes influencing the strength and position of the southern westerlies because such data extend beyond the short record provided by instrumental and reanalysis data sets. In this section we summarize important aspects of climate variability during the last 2000 years in southern South America and highlight relevant paleoclimate records in Fig. 15.10.

1) The modern interannual climate variability, as revealed by instrumental and reanalysis data sets, is influenced by large-scale climate phenomena that originate in the high latitudes (SAM) as well as the tropics (ENSO). The apparent coupling between ENSO and the SAM (Fogt and Bromwich 2006, L'Heureux and Thompson 2006), influences teleconnections, and therefore, the overall climate system response in southern South America. The correlation between precipitation and the zonal winds is generally strong in southern South America and offers an important tool for reconstructing past variability in the wind field using paleoenvironmental records. However, the topography of the Andes and potential advection of moisture from the Atlantic produce heterogeneities in the precipitation-atmospheric circulation relationship in some areas in Southern Patagonia that bears further investigation.
2) Lacustrine sediment records provide continuous high-resolution time series that can be used to infer past variability of the westerlies with centennial- to millennial-scale resolution. Isotopic records from closed-basin lakes, in particular, are sensitive to changes in moisture balance, and when combined with other proxy data, can yield information regarding effective moisture and westerly wind strength. The late-Holocene record from Lago Guanaco in SW Patagonia, for example, suggests a significant increase in atmospheric circulation during the

last few hundred years, i.e., the LIA time in the Northern Hemisphere. Additional lacustrine records from Potrok Aike and Lago Cardiel all point toward increased variability in moisture balance/lake levels during the last 2000 years. Comparing the Guanaco and Potrok Aike records show consistent dry and wet intervals that are associated with the MCA and the LIA, respectively.

3) Radiocarbon-dated glacial deposits, primarily associated with outlet glaciers from the Northern and Southern Patagonian icefields, provide evidence for changes in glacial ice extent during the last two millennia. Holocene glacier records are hampered by a lack of chronologies and existing ages are spatially sporadic and often only provide "minimum- or maximum-limits". Taken at face value, a compilation of radiocarbon dates from the margins of the two ice sheets indicate expanded ice at ~1200 and ~600 cal year BP and more than once during the last 400 years. The pollen record from Lago Guanaco indicates that the millennial-scale variations in late Holocene ice extent observed in southern Patagonia glacier records are related to the overall strength of the westerlies at the latitude of the lake (51°S) (Moreno et al. 2009). Owing to its location in the lowlands directly east of the Andes, the Lago Guanaco record monitors past changes in the forest-steppe ecotone, which responds primarily to changes in precipitation of westerly origin. As pointed out by Moreno et al. 2009, the palynological evidence cannot exclude the likely possibility that increases in westerly wind variability were coincident with reductions in temperature. Tree-ring ages from moraines in Patagonia indicate, on average, ice retreat occurring since the late 19th century positions or LIA time. The most extensive ice advance of the mid- to late Holocene occurred at the start of Neoglaciation, ~5400 cal year BP. Mercer (1970) pointed out the trend of ice extent has decreased in South America during the Neoglacial. Patagonian glaciers responded primarily to temperature and secondarily to precipitation (e.g., Rignot et al. 2003, Cassasa 2003). Thus, future studies can maximize insight into former Patagonian climate by combining glacial changes with other precipitation sensitive proxies (e.g., pollen and isotopes), and tree-ring research.
4) Tree-rings offer excellent potential to investigate interannual to decadal variations in climate, and modern calibration with instrumental records allow the quantification of the magnitude of temperature and precipitation changes during the last millennium. Patagonian tree ring records provide evidence for warm dry conditions during the MCA centered between 870 and 700 cal year BP. Temperature reconstructions from northern and southern Patagonia indicate that 1850 to 1875 (100–75 cal year BP) marks an important turning point after which temperatures begins to climb towards present day values. In addition, temperature and atmospheric circulation as revealed in the reconstructed SAM index, indicates that the last 50 years are unprecedented within the context of the last 350 (Villalba et al. 2003).
5) Marine records from the Chilean continental shelf provide evidence of changes in ocean hydrography and productivity, in addition to, providing a monitor of terrestrial run-off related to westerly-derived precipitation. A Holocene record

obtained from ~41°S indicates declining SST and SSS, in combination with increased continental run-off during the last 2000 years (Lamy et al. 2001, Lamy et al. 2002). The Authors interpret these changes as a northward shift in both the westerlies and the ACC, which decreased SST and increased productivity through the delivery of nutrient-rich waters and the introduction of micronutrients from continental run-off. The marine records are important for our understanding of climate change in southern South America because they best illustrate the latitudinal coupling of SST gradients in the subtropical Pacific with latitudinal variations in atmospheric circulation (the westerlies).

We have assembled in Fig. 15.10 the proxy records that best summarize the key aspects of climate change in southern South America and address the research questions presented in the introduction of this chapter. Multiple paleoclimate archives from southern South America indicate an overall decrease in temperature and increase in westerly wind intensity during the last 2000 years that culminates between 400 and 50 cal year BP or European LIA time (Fig. 15.10). The marine records from the Chilean continental shelf document a ~1.5°C (Lamy et al. 2001) and a ~1°C (Mohtadi et al. 2007) SST cooling since 2000 cal year BP that culminates within the last 100 years (Fig. 15.10) that is interpreted as a northward shift in the Antarctic Circumpolar Current. Lake sediment records from southern Patagonia (Guanaco and Potrok Aike) and long tree-ring temperature reconstructions from northern Patagonia document aridity and warmer temperatures, respectively, between 900 and 700 cal year BP that is generally coincident with the timing of the MCA. The pollen and isotopic records from Guanaco indicate a significant increase in westerly wind strength within the last 2000 years that is coincident with the LIA. The culmination in strength in Lago Guanaco is similar in timing to the Siple

Fig. 15.10 Summary of paleoclimate records from southern South America and Antarctica. (**A**) Alkenone-based SST reconstruction from the Chilean continental shelf in northern Patagonia 45°S (Mohtadi et al. 2007). (**B**) Southern Patagonia 25-year spline tree-ring temperature reconstruction and actual temperature (*red line*) from Villalba et al. (2003). The horizontal line represents the reconstructed mean. Coldest reconstructed temperatures occur at the oldest part of the reconstruction (300–350 cal year BP) and increase abruptly after 100 cal year BP. (**C**) Fe record from the Chilean continental shelf reflecting changes in westerly-derived precipitation (Lamy et al. 2001). (**D**) Bivalve $\delta^{18}O$ (Moy et al. 2008) and (**E**) *Nothofagus*/Poaceae paleovegetation index (Moreno et al. 2009) from Lago Guanaco showing changes in evaporation and westerly-derived precipitation. Peak paleovegetation index and $\delta^{18}O$ values occur during LIA time (~400–100 cal year BP). (**F**) First EOF of Siple Dome Na^+ (Kreutz et al. 1997) calculated using a 25- (*solid line*) and 115-year (*dashed line*) window. Na^+ values culminate over a 300 year period centered on 200 cal year BP similar to the paleoclimate proxies from Lago Guanaco. The three vertical blue bars reflect periods of increased ice extent in CHPN, CHPS, and northern Patagonia glaciers identified in Fig. 15.7. The red rectangle labeled "1" refers to period of warm reconstructed summer temperatures in northern Patagonia (Villalba 1994) and the red rectangle labeled "2" indicates timing of drought termination in southern Patagonia (Stine 1994) and both events are generally coincident with inferred aridity and reduced westerlies from Lago Guanaco (**D**) and the Fe record from GeoB 3313-1 (**C**) and represents the MCA in Patagonia

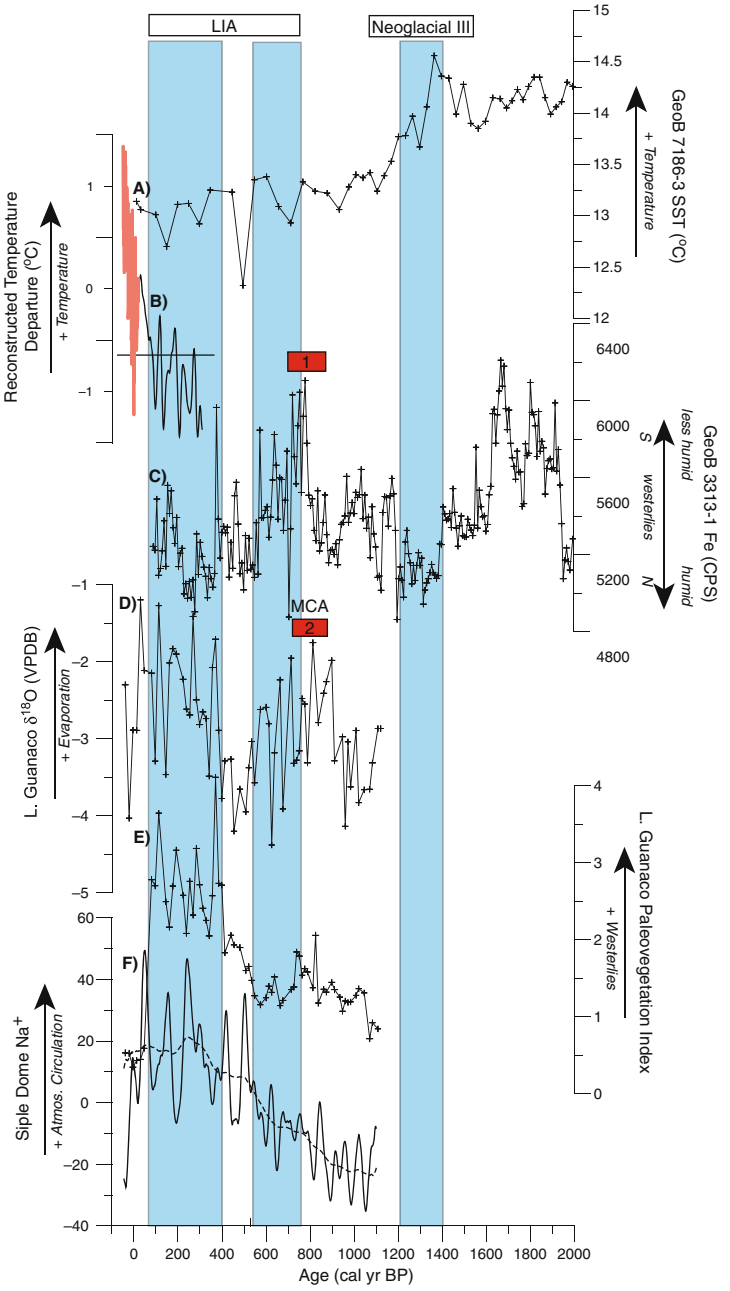

Fig. 15.10 (continued)

Dome record, indicating that atmospheric circulation increased throughout the high southern latitudes from 400 to 50 cal year BP. Tree ring records from northern and southern Patagonia indicate a shift towards warmer temperatures that begins at 1875 AD, is cotemporaneous with ice retreat from LIA ice positions, and represents the inception of warmer temperatures in southern Patagonia that exceed reconstructed temperatures during the last 350 years.

Future paleoclimate research in southern South America can work towards improving our current understanding of past climate and ecological change. The incorporation of new analytical techniques for proxy development and chronology refinement, in addition to, regional-scale multi-proxy reconstructions can significantly contribute to our understanding of past climate change. Chronologies can be improved by incorporating more high-quality radiocarbon dates from resistant and relevant organic fractions such as pollen and charcoal. Higher quality radiocarbon chronologies will facilitate comparisons with other paleoclimate records and provide a better understanding of the timing and variability of past climate change. Similarly, improved cosmogenic dating techniques can be further applied to Holocene glacial deposits (e.g., Schaefer et al. 2009). Marine paleoclimate records must apply a reservoir age correction to radiocarbon dates to account for the difference in ^{14}C content between the surface water and the atmosphere at a given location. The correction is often assumed to be constant over long periods of time (e.g. Holocene and late glacial timescales) despite evidence for significant changes in ocean circulation that would work to alter the past surface water ^{14}C content. Relatively new methods that measure ^{226}Ra in barite (van Beek et al. 2002), which as an independent chronometer, can be used in conjunction with radiocarbon dates to get a better understanding of past Holocene reservoir ages. The application of this technique along the Chilean continental margin could vastly improve marine chronologies and make them directly comparable to terrestrial records. The incorporation of relatively new isotopic and geochemical proxies for lake settings, such as the δD of terrestrial leaf waxes (Huang et al. 2002, Huang et al. 2004) and the TEX_{86} paleotemperature proxy (Tierney et al. 2008) can be combined and used to deconvolve seasonal variations in moisture balance and quantify past changes in temperature. However, modern calibration studies, that have yet to be undertaken in Patagonia, are required in order for these new methods to be interpreted correctly. Finally, multi-proxy regional reconstructions that combine multiple paleoclimate data sets from climatically relevant areas such as the Long-Term climate REconstruction and Dynamics of (southern) South America project (LOTRED) can be used to better understand past variations in climate. This project aims to build a database of paleoclimate proxy data from southern South America for the last 2000 years and to use these data to reconstruct past climate variability along multiple spatial and temporal scales.

Acknowledgments C. Moy acknowledges support from a U.S. State Department Fulbright to Chile, Department of Energy Global Change Education Program Graduate Fellowship, and a Stanford School of Earth Sciences McGee grant. P.I. Moreno acknowledges support from the Institute of Ecology and Biodiversity P05-002, contract PFB-23 and Fondecyt # 1040204, 1070991, and

1080485. T. Haberzettl acknowledges the support provided by Le Fonds québécois de la recherche sur la nature et les technologies (FQRNT). Helpful discussions with Rene Garreaud significantly improved the quality of this manuscript. We thank Andres Rivera for providing precipitation data from I. Evangelistas, which was collected by the Servicio Hidrográfico de la Armada de Chile (SHOA), and the Direccion General de Aguas (DGA) for the use of Torres del Paine meteorological data. We also thank Antje Schwalb and Cathy Whitlock for providing constructive reviews that greatly improved an earlier version of this manuscript. Figures 15.3 and 15.4 were constructed from NCEP-NCAR reanalysis data available at the NOAA/ESRL Physical Sciences Division, Boulder Colorado from their Web site at http://www.cdc.noaa.gov/. Southern South America base maps (Figs. 15.1, 15.3, and 15.7) were created using an online version of Generic Mapping Tools (GMT) at http://www.aquarius.ifm-geomar.de/.

References

Abarzua AM, Moreno PI (2008) Changing fire regimes in the temperate rainforest region of southern Chile over the last 16,000 yr. Quat Res 69:62–71

Aniya M (1988) Glacier inventory for the Northern Patagonia Icefield, Chile, and variations 1944/45 to 1985/86. Arc Antarct Alp Res 20:179–187

Aniya M (1995) Holocene glacial chronology in Patagonia: Tyndall and Upsala Glaciers. Arc Alp Res 27:311–322

Aniya M, Sato H, Naruse R et al (1996) The use of satellite and airborne imagery to inventory outlet glaciers of the Southern Patagonia Icefield, South America. Photogramm Eng Remote Sens 62:1361–1369

Anselmetti FS, Ariztegui D, de Baptist M et al (2009) Environmental history of Southern Patagonia unravelled by the seismic stratigraphy of Laguna Potrok Aike. Sedimentology 56:873–892

Aravena JC, Lara A, Wolodarsky-Franke A et al (2002) Tree-ring growth patterns and temperature reconstruction from Nothofagus pumillo (Fagaceae) forests at the upper tree line of southern Chilean Patagonia. Rev Chil Hist Nat 75:361–376

Auer V (1933) Verschiebungen der Wald-und Steppengebiete Feuerlands in postglazialer Zeit. Acta Geogr 5

Auer V (1958) The Pleistocene of Fuegopatagonia, part II: The history of the flora and vegetation. Ann Acad Sci Fenn 50:1–239

Bertrand S, Boes X, Castiaux J et al (2005) Temporal evolution of sediment supply in Lago Puyehue (Southern Chile) during the last 600 yr and its climatic significance. Quat Res 64:163–175

Boninsegna JA (1990) Santiago de Chile winter rainfall since 1220 as being reconstructed by tree rings. Quat South Am Antarct Peninsula 6:67–87

Bradley RS, Briffa KR, Cole J et al (2003) The climate of the last millennium. In: Alverson KD, Bradley RS, Pederson TF (eds) Paleoclimate, global change and the future. Springer-Verlag, New York, pp 105–141

Canadell JG, Le Quere C, Raupach MR et al (2007) Contributions to accelerating atmospheric CO2 growth from economic activity, carbon intensity, and efficiency of natural sinks. Proc Natl Acad Sci USA 104:18866–18870

Carrasco JF, Osorio R, Casassa, G (2008) Secular trend of the equilibrium-line altitude on the western side of the southern Andes, derived from radiosonde and surface observations. J Glaciol 54:538–550

Casassa G, Espizua L, Francau B et al (1998) Glaciers in South America. In: Haeberli W, Hoezle M, Suter S (eds) Into the second century of world wide glacier monitoring: Prospects and strategies. UNESCO Studies and Reports in Hydrology, Zurich, pp 125–146

Casassa G, Rivera A, Aniya M, Naruse R (2002) Current knowledge of the Southern Patagonian Icefield. In: Casassa G, Sepulveda FV, Sinclair RM (eds) The Patagonian Icefields: A

unique laboratory for environmental and climate change studies. Kluwer Academic/Plenum Publishers, New York, pp 67–83
Clapperton CM, Sugden DE (1988) Holocene glacier fluctuations in South America and Antarctica. Quat Sci Rev 7:185–198
Cobb KM, Charles CD, Cheng H, Edwards RL (2003) El Niño/Southern Oscillation and tropical Pacific climate during the last millennium. Nature 424:271–276
Dettman DL, Reische AK, Lohmann KC (1999) Controls on the stable Isotope composition of seasonal growth bands in fresh-water bivalves (unionidae). Geochimica et Cosmochimica Acta 63:1049–1057
Douglass DC, Singer BS, Kaplan MR et al (2005) Evidence of early Holocene glacial advances in southern South America from cosmogenic surface-exposure dating. Geology 33:237–240
Fey M, Korr C, Maidana NI et al (2009) Palaeoenvironmental changes during the last 1600 years inferred from the sediment record of a cirque lake in southern Patagonia (Laguna las Vizcachas, Argentina). Palaeogeography Palaeoclimatology Palaeoecology. (DOI:10.1016/j.palaeo.2009.01.012). Article in press; corrected proof available online (05/2009).
Fogt RL, Bromwich DH (2006) Decadal Variability of the ENSO Teleconnection to the high-latitude South Pacific governed by coupling with the southern annular mode. J Clim 19: 979–997
Galloway RW, Markgraf V, Bradbury JP (1988) Dating shorelines of lakes in Patagonia, Argentina. J South Am Earth Sci 1:195–198
Garreaud R (2007) Precipitation and circulation covariability in the extratropics. J Clim 20:4789–4797
Garreaud R, Vuille M, Compagnucci R, Marengo J (2008) Present-day South American Climate. Palaeogeography Palaeoclimatology Palaeoecology. (DOI:10.1016/j.palaeo.2007.10.032). Article in press; corrected proof available online (05/2009).
Garreaud RD, Aceituno P (2007) Atmospheric circulation over South America: Mean features and variability. In: Veblen T, Young K, Orme A (eds) The physical geography of South America. Oxford University Press, Oxford, England
Ghil MR, Allen M, Dettinger MD et al (2002) Advanced spectral methods for climatic time series. Rev Geophys 40:3.1–3.41
Gilli A, Anselmetti FS, Ariztegui DF et al (2001) Tracking abrupt climate change in the Southern Hemisphere: A seismic stratigraphic analysis of Lago Cardiel, Argentina (49°S). Terra Nova 13:443–448
Gilli A, Ariztegui D, Anselmetti FS et al (2005) Mid-Holocene strengthening of the Southern Westerlies in South America – Sedimentological evidences from Lago Cardiel, Argentina (49S). Glob Planet Change 49:75–93
Glasser NF, Hambrey MJ, Aniya M (2002) An advance of Soler Glacier, North Patagonian Icefield at c. AD 1222–1342. Holocene 12:113–120
Glasser NF, Harrison S, Winchester V, Aniya M (2004) Late Pleistocene and Holocene palaeoclimate and glacier fluctuations in Patagonia. Glob Planet Change 43:79–101
Haberzettl T, Corbella H, Fey M et al (2007) Lateglacial and Holocene wet-dry cycles in southern Patagonia: Chronology, sedimentology and geochemistry of a lacustine record from Laguna Portok Aike, Argentina. Holocene 17:297–310
Haberzettl T, Fey M, Lücke A et al (2005) Climatically induced lake level changes during the last two millennia as reflected in sediments of Laguna Potrok Aike, southern Patagonia (Santa Cruz, Argentina). J Paleolimnol 33:283–302
Haberzettl T, Kück B, Wulf S et al (2008) Hydrological variability in southeastern Patagonia and explosive volcanic activity in the southern Andean Cordillera during Oxygen Isotope Stage 3 and the Holocene inferred from lake sediments of Laguna Potrok Aike, Argentina. Palaeogeogr Palaeoclimatol Palaeoecol 259:213–229
Harrison S, Glasser N, Winchester V et al (2008) Glaciar León, Chilean Patagonia: Late-Holocene chronology and geomorphology. Holocene 18:643–652

Harrison S, Winchester V (1998) Historical fluctuations of the Gualas and Reicher Glaciers, North Patagonian Icefield, Chile. Holocene 8:481–485
Harrison S, Winchester V (2000) Nineteenth and twentieth century glacier fluctuations and climatic implications in the Arco and Colonia valleys, Hielo Patagónico Norte. Arct Antarct Alp Res 32:55–63
Harrison S, Winchester V, Glasser N (2007) The timing and nature of recession of outlet glaciers of Hielo Patagónico Norte, Chile, from their Neoglacial IV (Little Ice Age) maximum positions. Glob Planet Change 59:67–78
Heusser CJ (1966) Late-Pleistocene pollen diagrams from the Province of Llanquihue, southern Chile. Proc Am Philos Soc 110:269–305
Heusser CJ, Heusser LE (2006) Submillennial palynology and palaeoecology of the last glaciation at Taiquemo (similar to 50,000 cal yr, MIS 2–4) in southern Chile. Quat Sci Rev 25:446–454
Heusser CJ, Heusser LE, Lowell TV (1999) Paleoecology of the southern Chilean Lake District-Isla Grande de Chiloé during middle-Late Llanquihue glaciation and deglaciation. Geogr Ann Ser A Phys Geogr 81 A:231–284
Hodell DA, Kanfoush SL, Shemesh A et al (2001) Abrupt cooling of Antarctic surface waters and sea ice expansion in the South Atlantic sector of the Southern Ocean at 5000 cal yr B.P. Quat Res 56:191–198
Huang Y, Shuman B, Wang Y, Webb T (2002) Hydrogen isotope ratios of palmitic acid in lacustrine sediments record late Quaternary climate variations. Geology 30:1103–1106
Huang Y, Shuman B, Wang Y, Webb T (2004) Hydrogen isotope ratios of individual lipids in lake sediments as novel tracers of climatic and environmental change: A surface sediment test. J Paleolimnol 31:363–375
Huber UM, Markgraf V (2003) European impact on fire regimes and vegetation dynamics at the steppe-forest ecotone of southern Patagonia. Holocene 13:567–579
Jones JM, Widmann M (2004) Atmospheric science: Early peak in Antarctic oscillation index. Nature 432:290–291
Jones PD, Mann ME (2004) Climate over past millennia. Rev Geophys 42:1–42
Kalnay E, Kanamitsu M, Kistler R et al (1996) The NCEP/NCAR 40-year Re-analysis Project. Bull Am Meteorol Soc 77:437–471
Koch J, Killian, R (2005) 'Little Ice Age' glacier fluctuations, Gran Campo Nevado, southernmost Chile. Holocene 15:20–28
Kreutz KJ, Mayewski PA, Meeker LD et al (1997) Bipolar changes in atmospheric circulation during the little ice. Sci 277:1294–1296
Kushner PJ, Held IM, Delworth TL (2001) Southern Hemisphere Atmospheric Circulation Response to Global Warming. J Clim 14:2238–2249
Kwok R, Comiso JC (2002) Spatial patterns of variability in Antarctic surface temperature: Connections to the Southern Hemisphere Annular Mode and the Southern Oscillation. Geophys Res Lett 29:1–4
L'Heureux ML, Thompson DWJ (2006) Observed relationships between the El Niño–Southern Oscillation and the extratropical zonal-mean circulation. J Clim 19:276–287
Lamy F, Hebbeln D, Röhl U, Wefer G (2001) Holocene rainfall variability in southern Chile: A marine record of latitudinal shifts of the southern westerlies. Earth Planet Sci Lett 185:369–382
Lamy F, Ruhlemann C, Hebbeln D, Wefer G (2002) High- and low-latitude climate control on the position of the southern Peru-Chile Current during the Holocene. Paleoceanography 17:1028
Lara A, Aravena JC, Villalba R et al (2001) Dendroclimatology of high-elevation Nothofagus pumilio forests at their northern distribution limit in the central Andes of Chile. Can J For Res 31:925–936
Lara A, Villalba R (1993) A 3620-year temperature record from Fitzroya cupressoides tree rings in southern South America. Science 260:1104–1106
Lara A, Villalba R, Urrutia R (2008) A 400-year tree-ring record of the Puelo River summer-fall streamflow in the Valdivian Rainforest eco-region, Chile. Clim Change 86:331–356

Lawrence DB, Lawrence EG (1959) Recent glacier variations in southern South America. In: Technical Report, Office of Naval Research. American Geographical Society, New York
Le Quéré C, Rodenbeck C, Buitenhuis ET et al (2007) Saturation of the Southern Ocean CO2 Sink Due to Recent Climate Change. Science 316:1735–1738
Legates DR, Willmott CJ (1990) Mean Seasonal and Spatial Variability Global Surface Air Temperature. Theor Appl Climatol 41:11–21
Leng MJ, Marshall JD (2004) Palaeoclimate interpretation of stable isotope data from lake sediment archives. Quat Sci Rev 23:811–831
Lovenduski NS, Gruber N, Doney SC, Lima ID (2007) Enhanced CO2 outgassing in the Southern Ocean from a positive phase of the Southern Annular Mode. Glob Biogeochem Cycles 21:GB2026 1–14
Malagnino EC, Strelin, JA (1992) Variations of Upsala Glacier in southern Patagonia since the late Holocene to the present. In: Naruse R, Aniya M (eds) Glaciological researches in Patagonia, 1990. Japanese Society of Snow and Ice, Japan, pp 61–85
Markgraf V (1993) Paleoenvironments and Paleoclimates in Tierra-Del-Fuego and Southernmost Patagonia, South-America. Palaeogeogr Palaeoclimatol Palaeoecol 102:53–68
Markgraf V, Bradbury JP, Schwalb A et al (2003) Holocene palaeoclimates of southern Patagonia: Limnological and environmental history of Lago Cardiel, Argentina. Holocene 13:581–591
Marshall GJ (2003) Trends in the Southern Annualar Mode from observations and Reanalysis. J Clim 16:4134–4143
Matthews JA, Briffa KR (2005) The 'Little Ice Age': Re-evaluation of an evolving concept. Geogr Ann 87:17–36
Mayr C, Fey M, Haberzettl T et al (2005) Palaeoenvironmental changes in southern Patagonia during the last millennium recorded in lake sediments from Laguna Azul (Argentina). Palaeogeogr Palaeoclimatol Palaeoecol 228:203–227
Mayr C, Wille M, Haberzettl T et al (2007) Holocene variability of the Southern Hemisphere westerlies in Argentinean Patagonia (52°S). Quat Sci Rev 26:579–584
McCormac FG, Hogg AG, Blackwell PG et al (2004) SHCal04 Southern Hemisphere Calibration 0–11.0 cal kyr BP. Radiocarbon 46:1087–1092
Mercer JH (1965) Glacier variations in Southern Patagonia. Geogr Rev 55:390–413
Mercer JH (1968) Variations in some Patagonian glaciers since the late-glacial. Am J Sci 266: 91–109
Mercer JH (1970) Variations of some Patagonian glaciers since the Late Glacial: II. Am J Sci 269:1–25
Mercer JH (1976) Glacial history of southernmost South America. Quat Res 6:125–166
Mercer JH (1982) Holocene glacial variations in southern South America. Striae 18:35–40
Mo K (2000) Relationships between low-frequency variability in the southern hemisphere and sea surface temperature anomalies. J Clim 13:3599–3610
Mohtadi M, Romero OE, Kaiser J, Hebbeln D (2007) Cooling of the southern high latitudes during the Medieval Period and its effect on ENSO. Quat Sci Rev 26:1055–1066
Moreno PI (2004) Millennial-scale climate variability in northwest Patagonia over the last 15000 yr. J Quat Sci 19:35–47
Moreno PI, Francois JP, Villa-Martinez R, Moy CM (2009) Millennial-scale variability in Southern Hemisphere westerly wind activity over the last 5000 years in SW Patagonia. Quat Sci Rev 28:25–38
Moreno PI, Lowell TV, Jacobson GL, Denton GH (1999) Abrupt vegetation and climate changes during the last glacial maximum and last termination in the Chilean Lake District: A case study from Canal de la Puntilla (41 degrees s). Geogr Ann Ser A Phys Geogr 81A:285–311
Moy CM, Dunbar RB, Moreno P et al (2008) Isotopic evidence for hydrologic change related to the westerlies in SW Patagonia, Chile, during the last millennium. Quat Sci Rev 27: 1335–1349
Moy CM, Seltzer GO, Rodbell DT, Anderson DM (2002) Variability of El Niño/Southern Oscillation activity at millennial timescales during the Holocene epoch. Nature 420:162–165

Naranjo JA, Stern CR (1998) Holocene explosive activity of Hudson Volcano, southern Andes. Bull Volcanol 59:291–306
Naruse R (2006) The response of glaciers in South America to environmental change. In Knight P (ed) Glaciers and Earth's changing environment. Blackwell, Oxford, pp 231–238
Porter SC (2000) Onset of Neoglaciation in the Southern Hemisphere. J Quat Sci 15:395–408
Rabassa J, Brandani A, Boninsegna JA, Cobos DR (1984) Cronologia de la "Pequeña Edad del Hielo" en los glaciares Rio Manso y Castafio Overo, Cerro Tronador, Provincia de Rio Negro. 9no. Congreso Geologico Argentino Actas 3:624–639
Rein B, Luckge A, Sirocko F (2004) A major Holocene ENSO anomaly during the Medieval period. Geophys Res Lett 31:L17211 1–4
Rignot E, Rivera A, Casassa G (2003) Contribution of the Patagonia Icefields of South America to Sea Level Rise. Science 302:434–437
Rivera A, Benham T, Casassa G et al (2007) Ice elevation and areal changes of glaciers from the Northern Patagonia Icefield, Chile. Glob Planet Change 59:126–137
Rivera A, Casassa G (2004) Ice elevation, areal, and frontal changes of glaciers from national park Torres del Paine, Southern Patagonia Icefield. Arct Antarct Alp Res 36:379–389
Röthlisberger E (1986) 1000 Jahre Gletschergeschichte der Erde. Verlag Sauerlander, Salzburg
Schaefer JM, Denton GH, Kaplan MR et al (2009) High-frequency Holocene glacier fluctuations in New Zealand differ from the northern signature. Science 324:622–625
Schneider C, Geis D (2004) Effects of El Niño-Southern Oscillation on southernmost South America precipitation revealed from NCEP-NCAR reanalysis and weather station data. Int J Climatol 24:1057–1076
Schneider C, Glaser M, Kilian R et al (2003) Weather observations across the southern Andes at 53 °S. Phys Geogr 24:97–119
Sigman DM, Boyle EA (2000) Glacial/interglacial variations in atmospheric carbon dioxide. Nature 407:859–869
Stine S (1994) Extreme and persistent drought in California and Patagonia during mediaeval time. Nature 369:546–549
Stine S, Stine M (1990) A record from Lake Cardiel of climate change in southern South America. Nature 345:705–708
Stone, DA, Weaver AJ, Stouffer RJ (2001) Projection of climate change onto modes of atmospheric variability. J Clim 14:3551–3565
Strelin JA, Malagnino EC (2000) Late Glacial history of Lago Argentino, Argentina, and age of the Puerto Bandera moraines. Quat Res 54:339–347
Sweda T (1987) Recent retreat of Soler Glacier, Patagonia as seen from vegetation recovery. Bull Glacier Res 4:119–124
Szeicz JM, Haberle SG, Bennett KD (2003) Dynamics of North Patagonian rainforests from fine-resolution pollen, charcoal and tree-ring analysis, Chonos Archipelago, Southern Chile. Austral Ecol 28:413–422
Szeicz JM, Zeeb BA, Bennett KD, Smol JP (1998) High-resolution paleoecological analysis of recent disturbance in a southern Chilean Nothofagus forest. J Paleolimnol 20:235–252
Thompson DWJ, Solomon S (2002) Interpretation of recent Southern Hemisphere climate change. Science 296:895–899
Thompson DWJ, Wallace JM (2000) Annular modes in the extratropical circulation. Part II: Trends. J Clim 13:1018–1036
Tierney JE, Russell JM, Huang Y et al (2008) Northern Hemisphere Controls on Tropical Southeast African Climate During the Past 60,000 Years. Science 322:252–255
Toggweiler JR, Russell JL, Carson SR (2006) Midlatitude westerlies, atmospheric CO_2, and climate change during the ice ages. Paleoceanography 21:PA2005
Trenberth KE (1991) Storm Tracks in the Southern Hemisphere. J Atmos Sci 48:2159–2178
van Beek P, Reyss JL, Paterne M et al (2002) ^{226}Ra in barite: Absolute dating of Holocene Southern Ocean sediments and reconstruction of sea-surface reservoir ages. Geology 30:731–734

Villagrán C (1985) Análisis palinológico de los cambios vegetacionales durante el Tardiglacial y Postglacial en Chiloé, Chile. Revista Chilena de Historia Natural 58:57–69
Villagrán C (1988) Late Quaternary vegetation of Southern Isla Grande de Chiloé, Chile. Quat Res 29:294–306
Villalba R (1990) Climatic fluctuations in northern Patagonia during the last 1000 years as inferred from tree-ring records. Quat Res 34:346–360
Villalba R (1991) Latitude of the surface high-pressure belt over western South America during the last 500 years as inferred from tree-ring analysis. Quat South Am Antarct Peninsula 7:305–327
Villalba R (1994) Tree-ring and glacial evidence for the Medieval Warm Epoch and the Little Ice Age in southern South America. Clim Change 26, 183–197
Villalba R (2007) Tree-ring evidence for tropical-extratropical influences on climate variability along the Andes in South America. PAGES Newsl 15:23–25
Villalba R, Boninsegna JA, Lara A et al (2008) A dendrochronological approach to estimates of past changes in the Antarctic Oscillation. In: Documenting, understanding and projecting changes in the hydrological cycle in the American Cordillera, IAI CRN 2047, Second Science Meeting. San Carlos, Argentina
Villalba R, Lara A, Boninsegna JA et al (2003) Large-scale temperature changes across the southern Andes: 20th-century variations in the context of the past 400 years. In: Climatic change climate variability and change in high elevation regions: Past, Present and Future, 25–28 June 2001, vol 59. Davos, Switzerland, pp 177–232
Villalba R, Masiokas MH, Kitzberger T, Boninsegna JA (2005) Biogeographical consequences of recent climate changes in the Soutern Andes of Argentina. In: Huber UM, Bugmann HKM, Reasoner MA (eds) Global change and mountain regions: An overview of current knowledge. Advances in global change research. Springer, New York, 650 pp
von Grafenstein U, Erlenkeuser H, Trimborn, P (1999) Oxygen and carbon isotopes in modern fresh-water ostracod valves: Assessing vital offsets and autoecological effects of interest for paleoclimate studies. Palaeogeogr Palaeoclimatol Palaeoecol 148:133–152
Warren C, Sugden D (1993) The Patagonian icefields: A glaciological review. Arct Antarct Alp Res 25:316–331
Whitlock C, Moreno PI, Bartlein, P (2007) Climatic controls of Holocene fire patterns in southern South America. Quat Res 68:28–36
Wille M, Maidana NI, Schäbitz F et al (2007) Vegetation and climate dynamics in southern South America: The microfossil record of Laguna Potrok Aike, Santa Cruz, Argentina. Rev Palaeobot Palynol 146:234–246
Winchester V, Harrison S, Warren CR (2001) Recent retreat of Glaciar Nef, Chilean Patagonia, dated by lichenometry and dendrochronology. Arct Antarct Alp Res 33:266–273
Wolter K, Timlin MS (1993) Monitoring ENSO in COADS with a seasonally adjusted principal component index. In: N. NOAA/N MC/CAC (ed) Proceedings of the 17th Climate Diagnostics Workshop, Norman, OK, pp 52–57
Wolter K, Timlin MS (1998) Measuring the strength of ENSO events – how does 1997/98 rank? Weather 53:315–324
Xie P, Arkin PA (1997) Global Precipitation: A 17-year monthly analysis based on gauge observations, satellite estimates, and numerical model outputs. Bull Am Meteorol Soc 78:2539–2558

Chapter 16
The Little Ice Age in Southern South America: Proxy and Model Based Evidence

Inka Meyer and Sebastian Wagner

Abstract In this chapter climatic changes over southern South America during the last millennium with focus on the period of the Little Ice Age (LIA 1550–1800 AD) are investigated. Results presented are based on proxy and modelling evidence. Proxy studies include a variety of different sites, ranging from geomorphological, lacustrine, pollen to tree ring reconstructions. These different sources of evidence are combined into a multi-proxy network. Based on this network, spatio-temporal climatic changes in southern South America are assessed for the last millennium. A climate model simulation of the last millennium is used to investigate the influence of external forcing parameters, such as solar, volcanic and greenhouse gases on the local climate in southern South America. To compare proxy-based results and the output of the global climate model on a common basis, conceptual and quantitative downscaling and upscaling models are established. Based on these methodological approaches both reconstruction methods indicate a period of wetter conditions in south-eastern South America during the period of the LIA. Investigating the driving mechanisms for hydrological changes during the LIA, large-scale atmospheric circulation changes of the Southern Hemispheric Westerlies (SHWs) over southern South America are indicated in modelling results. Changes of the SHWs during the LIA also fit into the spatial pattern indicated by different proxies with wetter conditions and cooler temperatures in south-eastern South America accompanied with drier and warmer conditions to the north.

Keywords Climate modelling · Downscaling · Little Ice Age · Southern South America · Southern Westerlies

16.1 The Little Ice Age

During earth history climate variations occur at various time scales (cf. Crowley 2000, Jones et al. 2001). The strength, spatial extension and duration of these

I. Meyer (✉)
Marum – Centre for Marine Environmental Sciences, University of Bremen, Bremen, Germany
e-mail: minka@marum.de

F. Vimeux et al. (eds.), *Past Climate Variability in South America and Surrounding Regions*, Developments in Paleoenvironmental Research 14,
DOI 10.1007/978-90-481-2672-9_16,

anomalous climatic periods vary strongly. In the Holocene several short term climate changes have occurred. The period of the "Little Ice Age" (hereafter LIA, ~1550–1850 AD) is one of the most prominent examples for a short term climatic anomaly during the late Holocene.

The exact strength and duration of the LIA varies, depending on the specific site. Even more important for the definition of the LIA is the climatic indicator used for analysis, e.g. related to meteorological (temperature, precipitation), geomorphological (moraines, lake levels) or biological (tree-rings) evidence.

In the Northern Hemisphere the period of the LIA is well documented, especially in Europe and North America. Here a huge variety of historical reports, archaeological, botanical and glaciological indicators, and also meteorological observations are available (e.g. Lamb 1965, Grove 1988, Daley 1998, Fagan 2000, Glaser 2001). This empirical evidence indicates cooler and wetter conditions over many parts of the Northern Hemisphere. For example, records from England and the Netherlands point to an unusually often freezing of canals and rivers (Joussaume 1996). Also expanded sea ice conditions around Iceland and Greenland were recorded (Grove 1988). Another climatic characteristic of this time is the increasing number of great storm floods around the North Sea due to changes in atmospheric circulation (Lamb 1984).

Although a lot of studies provide information on the climatic conditions during the LIA, only few studies investigate potential forcing mechanisms of this climatic anomalous period (Houghton 1994). A prominent forcing factor possibly explaining the lower temperature over the Northern Hemisphere during the LIA relates to changes in solar activity. Solar activity and therefore incoming solar radiation are characterized by regular and recurrent cycles. A prominent feature of solar activity changes relates to the 11-year sunspot-cycle. In the study of Joussaume (1996) the author finds indications that a low number of sunspots is related to cold climate conditions. Within the period of the LIA several periods with an anomalous low number of sunspots occurred. These periods are related to the Wolf, the Spörer, the Maunder and the Dalton Minimum. The period with no sunspots at all was the period of the Maunder Minimum from 1645 to 1715 AD (Lean et al. 1995). For the Maunder Minimum proxy and modelling studies point to a prominent influence of the anomalous low solar forcing causing lower temperatures over many regions (Eddy 1976, Zorita et al. 2004).

A second forcing factor potentially causing lower temperature relates to an increase in volcanic activity. Changes of volcanic activity are for example recorded in ice cores of Greenland and Antarctica. Based on these reconstructions the period between 1300 and 1700 AD shows an intense volcanic activity (Bradley 1985). The climatic effects of explosive volcanism relate to the release of great amounts of ash, dust and sulphuric aerosols into the stratosphere, reducing the amount of incoming sunlight over several years, reducing the heating of earth surface (cf. Joussaume 1996, Kirchner et al. 1999, Robock 2000). After strong volcanic eruptions the temperature could drop by roughly about 0.5–1 K (Joussaume 1996). One of the most intensive volcanic eruptions during the LIA was the eruption of the Tambora (Indonesia) in 1815. The following two years have been anomalously cold. The year

1816 became known for as "The year without summer" (Lamb 1970). Even though there is a connection between volcanism and climate, the effect of volcanism on climate is not strong enough to cause a long-term climatic change explaining the lower temperatures during the period of the LIA (Houghton 1994).

A third theory deals with changes in ocean circulations. For example, Lund et al. (2006) assumes that the Gulfstream was around 15–25% weaker during the LIA compared with modern times. This triggered a decline in northward heat transport and caused a cooling in northern and western Europe. It is hypothesised that similar variations could have happened also in other ocean basins. However this theory is still heavily contested (Joussaume 1996).

Since a single forcing mechanism discussed above is not able to explain the variety of climatic conditions during the LIA one might speculate on a combination of different external and internal climate forgings. In the following chapter a more detailed overview of the climate over southern South America will be presented.

16.2 The Climate of Southern South America

For a more detailed understanding of global climate, knowledge and explanations of past and present climatic change and variability over the Southern Hemisphere are of specific importance. Compared to the Northern Hemisphere, for the Southern Hemisphere, and here especially for the mid- and high latitudes, comparatively few studies on the climate for the last millennium are available. This relates to the large oceanic areas and to the sparse settlement of these regions, the poor quality of the instrumental data and the small number of meteorological stations (Villalba et al. 2003).

Due to the small size of the southern South America, the landmass does not heat up during austral summer as much, as for example the large Eurasian and North American continents. The proximity of southern South America to the Pacific and Atlantic Ocean causes cold summers and mild winters (Zolitschka et al. 2006). South of 40°S, strong westerly winds, the Southern Hemisphere Westerlies (SHWs), are the most important climatic feature of southern South America.

As a result of the large oceanic areas in the Southern Hemisphere and the cold Antarctic continent, the mean atmospheric circulation is more zonally symmetric compared to the Northern Hemisphere (Cerveny 1998). The near-surface SHWs are characterized by high wind speeds with mean annual values of 7.4 ms^{-1}. Maxima wind speeds are observed during austral summer (Baruth et al. 1998). The high wind speeds over southern South America during summer are the result of the southward displacement in the position of the SHWs.

The SHWs are the thermo-dynamical result of mass and energy exchanges between equator and pole. Here a crucial region is the middle and upper troposphere over the mid-latitudes regions where meridional temperature gradients are strongest. In these regions wind systems with wind speeds between 200 and 500 km/h, the jet streams, establish. These jet streams are vital for the understanding of the extra-tropical atmospheric circulation: Over the Northern Hemisphere

the jet streams show an asymmetric annular structure due to the presence of the Mountain chains of the Rocky Mountains and the Himalayas. Over the Southern Hemisphere the jet streams show a more annular structure because only very few areas are covered with high mountain chains into mid-latitudes. Moreover, meridional temperature gradients are much steeper over the Southern Hemisphere due to the lower temperatures over Antarctica compared to the Arctic. The jet stream systems on both hemispheres are subject to changes in incoming solar radiation and thus show seasonal movements. These movements follow changes of the Innertropical Convergency Zone (ITCZ). Because the extra-tropical westerly winds are the near-surface manifestation of the jet streams, these winds are also subject to latitudinal seasonal movements. Due to the different regions in the troposphere with highest wind speeds, ranging from the upper tropospheric jet streams over the mid-latitudes to the near-surface westerlies in mid- and high latitudes, the definition of the SHWs is not consistent (cf. also discussion in Wagner et al. 2007).

As an exception to most regions over the Southern Hemisphere, the longitudinal oriented mountain chain of the Andes Mountains plays an important role for the distribution of precipitation over southern South America. The high mountain chain induces a pronounced trans-Andean precipitation gradient with 4000–6000 mm/year along the western slope of the Andes Mountains, to 200 mm/year in the eastern parts of Patagonia. The decreasing amount of precipitation is also reflected in vegetation patterns, ranging from rain forests in the western parts to semiarid steppe in the eastern parts (Weischet 1996).

16.3 Proxy Data in Southern South America

Due to its outstanding geographical position southern South America offers a unique opportunity to reconstruct past climates using continental proxies, for example related to lake sediments, ice caps and pollen spectra (Zolitschka et al. 2006, Villalba 1994). In addition, southern South America is the only landmass extending into latitudes comparable to the well studied areas of Europe and North America. It thus offers the opportunity for comparative, interhemispheric studies of paleo-climatic and environmental conditions (Galloway et al. 1988, Markgraf 1993). These comparisons are however complicated by the large oceanic areas in the Southern Hemisphere, exerting an important influence on the climate and consequently also the proxies in these latitudes. For southern South America, instrumental measurements are only available since 1950 AD and therefore proxy based reconstructions need to be taken into account for the analysis of climate variability. In the following a series of different proxies and derived results related to climate variability during the period of the LIA will be presented.

16.3.1 Dendroclimatological Evidence

The climate of Patagonia is mainly controlled by the atmospheric circulation of the mid latitudes. Therefore dendrochronological investigations basically provide the opportunity to reconstruct atmospheric circulation changes in this area. In the wetter

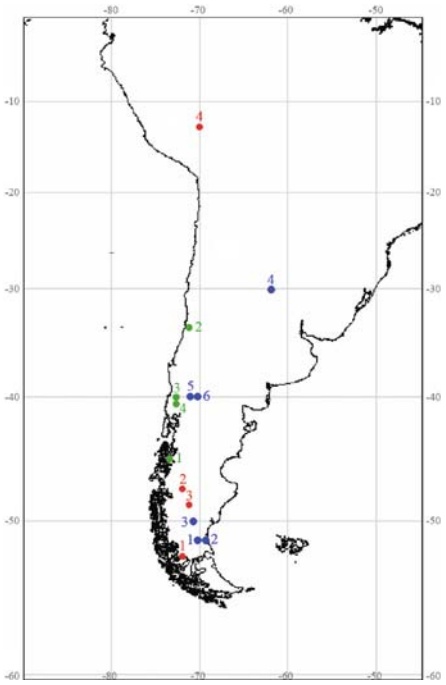

Fig. 16.1 Geographic position of proxy sites discussed in this study. The *Laguna Potrok Aike (52°S, 70°W)* is used as reference site in south-eastern Patagonia for statistical downscaling of the large-scale atmospheric circulation provided by the ECHO-G climate model simulation for the last millennium

parts of southern South America along the west coast of the Andes Mountains, several tree ring studies were carried out to reconstruct precipitation and temperature variations. For different proxy site locations displayed in Fig. 16.1 results are presented in the following section.

Boninsegna (1988) used tree rings to reconstruct variations in winter precipitation in Chile (Santiago de Chile, 33°S, 71°W). Tree-ring records from *Austrocedrus chilensis* indicate increases in precipitation between 1220–1280 AD and 1450–1550 AD. A decrease in precipitation is determined between 1280–1450 AD and 1570–1650 AD compared with the long term mean. For the eastern Andes Mountains, Villalba (1990) used *Fitzroya cupressoides* to reconstruct summer temperature deviations for the Andes in the region of northern Patagonia (41°S, 72°W) with respect to the most recent period. Here several climatic episodes can be distinguished in the tree ring record: A long, cold and moist period was found from 1270 to 1670 AD, with a temperature minimum around 1340 and 1650 AD. These cold phases are synchronous with two main LIA events recorded in the Northern Hemisphere. At the western side of Andes in the region of southern Chile, Lara and Villalba (1993) used alerce trees (*Fitzroya cupressoides*) to reconstruct mean summer temperatures for southern Chile. The record shows cooler temperatures between 1490 and 1700 AD, corresponding to the period of the LIA. For Chiloé Island,

Table 16.1 Temporal coherence between humid/dry periods in Chile with warm/cool periods in Patagonia

Chile: 1220–1280 → humid	Patagonia: 1080–1250 → warm
Chile: 1450–1550 → humid	Patagonia: 1380–1520 → warm
Chile: 1280–1450 → dry	Patagonia 1270–1380 → cool
Chile: 1570–1650 → dry	Patagonia 1520–1650 → cool

located at 44°S, 73°W, Boninsegna (1995) reconstruct summer precipitation by analysing tree ring information contained in *Pilgerodendron uviferum*. Wetter conditions are indicated between 1600–1620 AD and 1670–1690 AD. Drier conditions prevail between 1720–1740 and 1770–1790.

A comparison between reconstructed summer temperatures in northern Patagonia, 41°S, (Villalba 1990) and precipitation in central Chile, 33°S, (Boninsegna 1988) indicate a positive relation, i.e. humid phases in Chile are accompanied by warm periods in Patagonia and vice versa. (cf. Table 16.1). To explain this phenomenon, Lamy et al. (2001) propose as driving mechanism an equatorward shift of the SHWs during cooler episodes, resulting in increased rainfall over the western side of the Andes Mountains.

16.3.2 Lacustrine Investigations

High-resolution lacustrine records also provide an opportunity to investigate climatic changes based on information contained in lake sediments (e.g. mineralogical properties, pollen and organic matter) and geomorphological evidence (e.g. lake terraces). In the following sections results found for different lakes in southern South America are presented.

Lake terraces and sediments of the crater lake Laguna Potrok Aike (52°S, 70°W) are used to reconstruct lake level changes. Based on these reconstructed lake levels, hypotheses on changes for both, local and large scale atmospheric phenomena can be drawn. These hypotheses relate for example on precipitation changes in south-eastern Patagonia and changes in the position of the SHWs, respectively. Specifically for the last millennium, a terrace above the modern lake level indicates moister conditions compared to present-day at Laguna Potrok Aike (Haberzettl et al. 2005). Also at Lago Cardiel, further to the north (49°S, 71°W) lake level terraces were analysed. Similar to results from Laguna Potrok Aike, lake terraces at Lago Cardiel indicate wetter conditions together with high lake levels during LIA compared to modern times (Stine and Stine 1990). In the lake Laguna Azul (52°S, 69°W) a prominent shift in carbon isotope records occurred between AD 1670 and AD 1890 pointing to cooler climate conditions with higher lake levels (Mayr et al. 2005). Based on varved lake sediments from Lago Puyehue (40°S, 72°W), Boës and Fagel (2008) investigate changes in precipitation and the influence of the El Nino Southern Oscillation (ENSO) in South America. Between ∼1510 and ∼1730 AD they identify more humid conditions compared with modern values. During the period ∼1630

to ~1730 AD the reconstructed lake level seems to be higher than the present-day lake level. Investigations on varve thicknesses and physical properties are carried out for a sediment core of Lago Frías (40°S, 71°W) (Ariztegui et al. 2007). In this core a variable sedimentation as a direct response to climatic changes is indicated. The period of the LIA is reflected with an increasing varve thickness and clearly discernible laminated layers.

Different results are found for Laguna Mar Chiquita (30°S, 62°W) in Argentina. At this site the LIA is characterized by drier conditions and with lower lake levels (Piovano et al. 2002).

All lacustrine investigations support the hypothesis of a northward shift of the SHWs during the LIA. Both, results from Laguna Potrok Aike and Lago Cardiel indicate cooler and wetter conditions during the period of LIA (~1480–1900 AD). For Laguna Azul, δ^{13}Corg-analysis indicates wetter and cooler conditions together with high lake levels during the LIA (~1670–1890 AD). Opposite to the lakes in southern Patagonia, studies at Laguna Mar Chiquita indicate low lake levels during the LIA. A mechanism potentially explaining the climatic anomalous period at Laguna Mar Chiquita relates to a northward shift of the SHWs causing a decrease in precipitation and lower lake levels.

16.3.3 Pollen Analysis

Besides analysis of lake terraces and isotopic signatures, also pollen composition contained in sediment cores was analysed at Laguna Azul and Laguna Potrok Aike. In the sediment record of Laguna Azul continuous high amounts of Andean forest pollen were found. The high amount of pollen in the sediment core are caused by the prevailing SHWs, carrying pollen from the Andean forests, located approximately 160 km to the west, into the lakes (Mayr et al. 2005). During the period of the LIA the amount of Andean pollen taxa decreases while the amount of Patagonian steppe pollen increases. The main cause for the observed variations in the pollen composition is variability in the strength of the SHWs. Mayr et al. (2007) therefore suggest Andean pollen taxa as a proxy for the intensity of the SHWs. Contemporaneous with the reduced input of Andean pollen taxa (mainly *Nothofagus*) into the lakes due to weaker SHWs, the Patagonian steppe vegetation was growing faster due to higher precipitation. Similar observations are found at Laguna Potrok Aike. Here after 1410 AD an increasing amount of pollen from the dry steppe (mainly *Poaceae*) is deposited in the sediments. These taxa represent the regional and dominant vegetation surrounding the lake (Haberzettl et al., 2005, Mayr et al. 2007). In contrast to these results, Moy et al. (2008) found an increasing amount of *Nothofagus* pollen during the LIA in a sediment core from Lago Guanaco (51°S, 71°W). The authors propose an expansion of the Andean forest vegetation driven by increased humidity. As driving mechanism for vegetation changes they propose an intensification and a poleward shift of the SHWs during the LIA.

16.3.4 Ice Cores and Glacio-Geomorphological Evidence

In southern Patagonia two large icefields are located, the North and South Patagonian Icefield. Here numerous studies have been carried out (Glasser et al. 2004). In the following a selection of their results will be given.

Most studies about glacier fluctuations during the LIA are carried out for the North Patagonian Icefield. Harrison and Winchester (1998) investigate moraines and reconstruct past tree lines. All glaciers reach their maximum extension around 1870 AD. Afterwards glaciers moved back to their present position (Harrison and Winchester 1998, Harrison et al. 2006). Harrison et al. (2006) study a total of twelve valleys in the North Patagonian Icefield. In eight of the valleys moraines were dated back to the period of the LIA. In 1976, Mercer investigated glacier fluctuations at the North Patagonian Icefield. Similar to glacier advances in the Northern Hemisphere during the LIA, several neoglacial advances can be found in South America, too. According to ^{14}C measurements, glacial advances started between 1222 and AD 1342 AD (Glasser et al. 2001). Based on these results the author proposes the onset of the LIA during this time period.

For the South Patagonian Icefield, Mercer (1965) dated various moraines. He concludes that all glacier advances in the South Patagonian Icefield take place at the same time during the LIA. The maximum extension of most glaciers occurred between 1750 and 1800 AD (Mercer 1970). South of the Patagonian Icefields, the Gran Campo Nevado (53°S, 73°W) is located. It is a small ice cap ($\sim$200 km^2) in the southern Andes Mountains. Similar to moraine datings in the North and South Patagonian Icefields a series of glacier advances is dated between 1280 AD and 1460 AD, corresponding to an early period of the LIA (Koch and Kilian 2005).

The most studied glaciated site in South America is the Quelccaya Ice Cap in tropical Peru (14°S, 70°W; 55 km^2). It is the only tropical ice cap in the world (Clapperton 1983). Thompson et al. (1986) analysed two ice cores containing climatic information for the last millennium. Dating is based on several volcanic ash layers. Inferred from lower $\delta^{18}O$-values and changes in electric conductivity records, Thompson et al. (1986) dated the period of the LIA between 1530 and 1900 AD. However, recent studies show that the interpretation of isotopic variations found in ice cores from tropical and subtropical South America is far more complex. Vimeux et al. (2005) propose that changes in $\delta^{18}O$-values in most sites in the Andes are related to regional precipitation changes and not to temperature changes. According to Vuille and Werner (2005) lower $\delta^{18}O$-values indicate wet conditions, whereas higher $\delta^{18}O$-values are related to drier conditions. Moreover, it should be mentioned that the climatic conditions in tropical Peru are very different to climate conditions in the southern part of Patagonia. The latter is of specific importance when comparing tropical with extra-tropical proxies.

As summary for proxy data it can therefore be concluded that dendroclimatological investigations show wetter conditions during the LIA in Patagonia. Additionally, lacustrine investigations indicate also wetter conditions and lower temperatures. Regions to the north however indicate a decrease in precipitation,

reflected e.g. in lower lake levels. Pollen-based results from Patagonia point to vegetation-type changes from dry to wet species. Moreover, geomorphological analysis of glaciers and moraines in Patagonia also indicate expanded glaciation during the LIA.

16.4 Climate Modelling Studies for Southern South America

For the period of the LIA modelling studies have been carried out by Meyer and Wagner (2008), analysing precipitation changes in south-eastern Patagonia. For other periods modelling studies have been carried out by De Melo and Marengo (2008) for the mid-Holocene with a global Atmosphere-Ocean General Circulation Model (AOGCM). For the most recent times and a future greenhouse gas (GHG) scenario, Solman et al. (2007) and Nunez et al. (2008) carried out simulations with a regional model for South America.

A study analysing transient coupled AOGCM simulations also focusing on climatic changes over southern South America during the mid-Holocene was carried out by Wagner et al. (2007). This study discusses physical mechanisms linking changes in external orbital forcings on changes in SHWs and precipitation in south-eastern Patagonia. Because the methods related to climate modelling used in the studies of Wagner et al. (2007) and Meyer and Wagner (2008) are the same, results for mid-Holocene and LIA conditions over south-eastern Patagonia can be compared on a conceptually sound basis (cf. Section 16.4.2).

The reason why only few modelling studies for southern South America are available in the historical and plaeoclimate context, might relate to the fact that only few proxy data exist that are suitable for comparative studies. These comparative studies are however of vital importance (i) to test the quality of climate models in reproducing past climates and (ii) to check, whether proxy-based hypotheses are physically consistent with large-scale climate forcings.

The following section presents the main ideas underlying the reconstruction of the paleo-climate in south-eastern Patagonia. This approach is then used for investigations on hydrological and large-scale climate changes in southern South America during the last millennium.

16.4.1 Reconstructing Local Climatic Changes by Means of Statistical Analysis

Large-scale hypotheses about past atmospheric changes are usually derived from local proxy data, for example contained in lake sediments. These sediments contain indirect information on local climate changes, i.e. related to hydrological changes. To compare results based on proxy information and global climate models it is therefore necessary to close the gap between the skilful scale of the AOGCM, the large scale, and the skilful scale of the proxy, the local sale. With this approach it is

then possible to compare results on a common basis. Therefore the AOGCM output related to large-scale sea level pressure (SLP) needs to be downscaled to the local scale by means of statistical and/or dynamical models. This step is of specific importance in regions with complex terrain, because AOGCMs do usually not resolve small-scale topographic features important for regional climatic effects, as for example the Andes Mountains in southern South America. It should be noted here that it is of importance to conceptually and technically separate the two models mentioned above: The *numerical* global climate model (AOGCM,) driven with changes in external parameters (i.e. solar, volcanic, GHG) and the *statistical* downscaling model for the estimation of local precipitation changes. Both models are however interrelated in that the large-scale output (e.g. SLP) from the numerical climate model is used as input for the statistical downscaling model.

An example of the application of statistical downscaling is presented in the study of Wagner et al. (2007). Here links between SHWs and precipitation changes in south-eastern Patagonia have been assessed by setting up statistical downscaling models using recent observational data of large-scale sea level pressure (SLP) provided by NCEP/NCAR reanalysis (Kistler et al. 2001) and local precipitation extracted from the VASCLIMO data set (Beck et al. 2004). The downscaling approach used is principal component regression (PCR) analysis. The PCR approach has extensively used in climate research for climate reconstruction and prediction (cf. Luterbacher et al. 2002). The basis of the PCR model forms a multiple regression analysis. A specific feature of the PCR is a spatio-temporal pre-filtering of the predictand time series, i.e. the SLP fields. In other words, the PCR model does not contain time series for every single grid point of the SLP fields, but contains information about the temporal evolution of the most important SLP variability patterns, the so called Empirical Orthogonal Functions (EOFs). The temporal evolution of the EOF patterns is reflected in the principal components (PCs). Once the PCR model has been set up using observational or reanalysis data and its performance has been tested in an independent period, it can be applied on the AOGCM output, i.e. the modelled SLP fields. To guarantee that the modelled PCs really represent the evolution of the observed EOF patterns used for the set up of the PCR model, the observed EOF patterns are projected onto the modelled SLP anomaly fields. This results in PCs entering the PCR model as predictands for the climate model simulation. A shortcoming of this approach is that it implicitly assumes a constant temporal relationship between the predictands (SLP) and predictors (precipitation is south-eastern Patagonia).

Based on the statistical downscaling model, results indicate a moderate connection between SHWs changes and precipitation changes in south-eastern Patagonia on a monthly time scale. The physical mechanisms controlling precipitation changes could be explained by changes in the SHWs concerning a blocking of the westerly winds. During these blocking episodes humid air masses from the South Atlantic are advected into south-eastern Patagonia and lead to precipitation. In the following section results for local precipitation based on the statistical approach described in this section and large-scale atmospheric circulation changes including the SHWs are presented.

16.4.2 Changes of Precipitation and Southern Westerlies During the LIA

The statistical relationships described in the last section have been used for reconstructing precipitation changes in the last millennium. First results based on statistical downscaling have already been discussed in the study of Meyer and Wagner (2008). Here the output of an AOGCM simulation with ECHO-G, forced with changes in solar, volcanic and GHG changes (cf. von Storch et al. 2006) has been used for statistically downscaling precipitation in south-eastern Patagonia and to investigate latitudinal shifts of the SHWs.

For their study Wagner et al. (2007) and Meyer and Wagner (2008) use the coupled atmosphere-ocean model ECHO-G (Legutke and Voss 1999). The ECHO-G model is a coupled atmosphere-ocean general circulation model. It consists of the atmospheric part ECHAM4 (Roeckner et al. 1996) and the oceanic part HOPE-G (Wolf et al. 1997). The horizontal resolution is $3.75° \times 3.75°$ for the atmosphere and $2.8° \times 2.8°$ for the ocean. The vertical resolution is 19 levels for the atmosphere, from earth's surface up to a height of approximately 10 hPa. The ocean consists of 20 irregularly spaced levels. Both model components are linked by the OASIS coupler, allowing an interactive exchange of latent and sensible heat and moisture fluxes between atmosphere and ocean.

The ECHO-G model is externally forced by changes in solar and volcanic activity and changes in GHGs. Changes in solar activity have been reconstructed by means of information contained in ice cores as production rates of ^{10}Be. Here an important relates to long-term changes in solar activity. The scaling of the solar forcing was estimated by scaling changes of ^{10}Be such that the difference in solar activity between present-day and Maunder Minimum – a period without any sunspots – is 0.35%. The volcanic forcing has been implemented indirectly as changes in solar activity, assuming an integrated cooling effect of volcanic aerosols released by explosive volcanism (Robock 2000). Changes in GHG concentrations (CO_2, CH_4, N_2O) have been derived from air trapped in Antarctic ice cores (Etheridge et al. 1996).

Results for downscaled precipitation are given in Fig. 16.2 for austral summer (DJF). Here changes in precipitation relative to the period 1960–1990 are displayed. During the period of the LIA, indicated with the light blue shading, an increase in precipitation (+3.44 mm/mon) is clearly discernible. This precipitation difference is statistically significant at the 5% level. Uncertainties not included in the precipitation difference relate to (i) the statistical downscaling model used, (ii) internal climatic variability, (iii) the reconstruction of external forcings, and (iv) the coupled AOGCM used. Among other factors, these different sources of uncertainty might explain inconsistencies between hypotheses derived from proxy data and results based on this model study.

A first uncertainty related to statistical downscaling assumes that the basic relationships between the atmospheric circulation and precipitation in south-eastern Patagonia derived from present-day observational data is constant over time. This assumption is only hard to verify, because no observational data from the period of

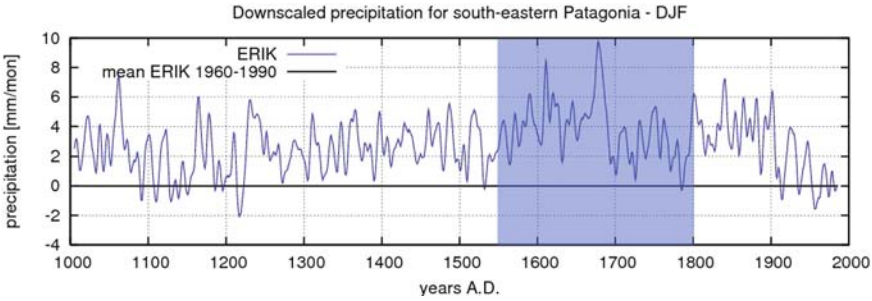

Fig. 16.2 Downscaled precipitation changes for south-eastern South America for austral summer (DJF). Note the increase in precipitation during the LIA (light blue area) compared to the period 1960–1990. The large-scale SLP fields used for downscaling are from a simulation with the coupled global atmosphere-ocean general circulation model ECHO-G forced with changes in solar, volcanic activity and changes in greenhouse gas concentrations

the LIA in southern South America are available. A second source of uncertainty related to statistical downscaling pertains to the downscaling model used. In the present analysis the PCR downscaling approach is used. This method has the disadvantage that the amount of variability is reduced for the predictor variable and hence reconstructed precipitation variations are smaller than in the observational period. This reduction of variance is of specific importance when the predictand variable (i.e. precipitation) is only weakly linked to the predictor variable (i.e. SLP) and therefore the amount of variance not explained (i.e. the residuals) is large. For south-eastern Patagonia this relationship is only moderate in strength and for DJF the statistical downscaling model using SLP represents only 10% of the precipitation variability in the observational period. However, more importantly the statistical model reflects the main physical mechanisms linking atmospheric circulation anomalies to precipitation changes in south-eastern Patagonia. The main cause for the moderate performance of the regression model is possibly related to the usage of monthly mean fields, not reflecting important short-lived circulation anomalies, as for example polar outbreaks.

Uncertainties related to natural climate variability are also an important point, especially when only a single realisation of the climate model simulation. To estimate uncertainties related to natural or internal climate variability it would be necessary to carry out more simulations (so called ensemble simulations). Using this approach, the climate model is forced with the same external climate forcings but with different initial conditions. Using coupled AOGCMs the most important factor are different initial conditions of the oceanic state. The most important factors are related to differences in sea surface temperatures and oceanic sea ice coverage. These initial conditions might influence the evolution of global and regional climates for decades or even centuries. Due to the high computational costs of multicentennial AOGCM simulations it is currently only possible to carry out one or two simulations driven with the same external forcings.

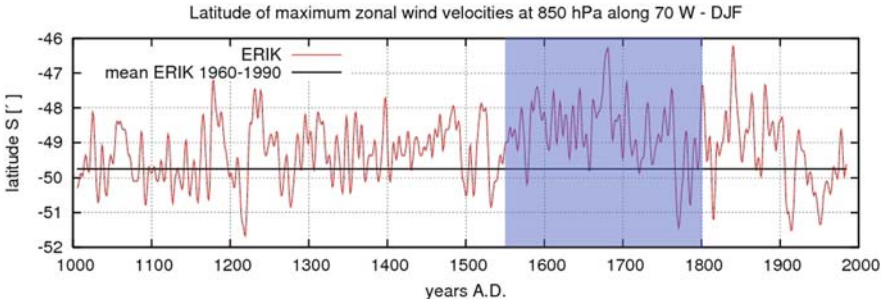

Fig. 16.3 Changes in the latitude of maximum zonal winds at the 850 hPa level (approx. 1500 m height) over southern South America along 70°W for austral summer (DJF). Note the northward shift in SHWs during the period of the LIA (*grey area*) compared to the period 1960–1990. The wind fields are from the ECHO-G simulation of the last millennium forced with changes in solar, volcanic activity and changes in greenhouse gas concentrations

Uncertainties in the external forcing relate to the scaling of the amplitude of the ^{10}Be values. In the literature a range between 0.15 and 0.6% is discussed (cf. Bard et al. 2000). This scaling is of specific importance, especially for regions showing high connections to changes in solar activity. The volcanic forcing also includes uncertainties, for example related to the amplitude of the volcanic outbreaks and the scaling and translation of sulphuric ash contained in ice cores into changes in optical depths in the stratosphere (cf. Robock 2000).

The LIA is not only reflected in changes in local-scale precipitation but also in latitudinal changes of maximum near-surface wind-speeds, reflecting changes in SHWs (cf. Fig. 16.3). Wagner et al. (2007) already noted that different definitions for the SHWs can be found in the literature. In the study the 850 hPa level is used because (i) very specific surface effects of the are excluded and (ii) the level is not located too high above the surface and is therefore thought to represent near-surface westerlies best. For comparison purposes this definition will also be used here. According to Fig. 16.3, during the period of the LIA a northward shift in the SHWs in DJF compared to period 1960–1990 can be seen. The statistically significant at the 5% level northward shift of 1.1° in latitude leads to a decrease in maximum wind speeds over south-eastern Patagonia. This observation is also in accordance with results derived from statistical downscaling models, linking high precipitation over south-eastern Patagonia with reduced SHWs and vice versa.

The complex nature of the interplay between externally forced and internally generated climate variability possibly results in different forcings mechanisms of SHW changes. In the study of Wagner et al. (2007), changes in meridional temperatures gradients between the mid-Holocene and pre-industrial times are used to explain changes in SHWs. Accordingly, changes in the equator-to-pole temperature gradient, caused by changes in orbital forcing are used to explain changes in high and mid tropospheric southern jet streams. The jet streams also control the position of the near-surface SHWs. A similar mechanism could also be proposed for the LIA,

although differences in external forcings between the LIA and present times are not as large as for the time period of the mid-Holocene minus present day.

Moreover, also the glaciation in southern South America was different in the mid-Holocene compared to the LIA. The extent of the glaciated area could however have a second order-impact on the SHWs, because of indirect feedbacks (ice-albedo feedback) or more localized wind systems at glaciated sites, for example related to catabatic winds.

Another mechanism, not yet investigated in detail, relates to changes in oceanic sea ice south of South America. The conceptual model, justifying oceanic sea ice as candidate explaining the position of the SHWs relates to the modification of atmosphere-ocean heat- and freshwater fluxes. These sensible and feasible heat flux changes might change lower tropospheric temperature gradients, which themselves could feed back on the middle and high troposphere.

16.5 Conclusions and Outlook

In this chapter climatic changes of the last 1000 years for southern South America with focus on the period of the Little Ice Age (LIA) were presented. In order to test if and to which extent the LIA could be identified in southern South America, results from a transient climate simulation are compared with different proxy based reconstructions.

Comparison between proxy-based reconstructions and downscaled results from the AOGCM simulation show that both, model and proxy data, indicate a climatically anomalous period between the 1550 and 1800 AD for the southern South America. This supports the hypothesis that the LIA is also reflected in hydrological variables over parts of the Southern Hemisphere (cf. Meyer and Wagner 2008).

An important point related to the physical mechanisms leading to this climatic anomalous period of the LIA are related to changes in the SHWs. The SHWs play an important role controlling precipitation patterns and variability in southern South America. Changes in the latitudinal position of the SHWs can also be used to explain the hydrological pattern indicated by the multi-proxy network during the LIA: Due to the more northerly position of the SHWs during DJF in the period of the LIA, the southeastern parts of Patagonia yield more precipitation compared to recent times (cf. Fig. 16.2). This is caused by an easterly advection of humid air masses from the South Atlantic penetrating into south-eastern Patagonia. Likewise, regions to the north experience drier conditions due to the lee-effect of the Andes Mountains that is amplified by the stronger SHWs over these latitudes during the LIA (cf. Fig. 16.3).

A mechanism explaining precipitation changes during DJF are changes in the position of maximum zonal winds. This explanation is motivated by results found for the mid-Holocene in the study of Wagner et al. (2007). Here increases in precipitation are linked to movements in the position of the SHWs. In the LIA this movement during DJF is also evident, albeit weaker in amplitude. The weaker amplitude might relate to the fact that also changes in external forcing between the

mid-Holocene (mostly orbital) and the LIA (mostly solar and volcanic) are weaker, because orbitally induced insolation changes and changes in solar activity differ by one order of magnitude. In other words, changes in the insolation forcing during the mid-Holocene and present day are 10 times larger than those exerted by solar activity changes between the LIA and present day.

Results presented here from the modelling point of view only relate to austral summer (DJF). In order to better compare model based results with proxy data or derived hypotheses it might be necessary to look into other seasons. Also proxy data usually do not represent mean annual conditions. Therefore it could be that some of the putative inconsistencies between model based results and proxy data are related to the season problem.

A conclusion that might also be drawn from our analyses encompasses a temporal and spatial inhomogeneous manifestation of the LIA in southern South America. Dynamically this relates to the semi-arid and arid climate, especially east of the Andes. From present-day semi-arid and arid climates, the high temporal and spatial variability, especially in hydrological variables is a prominent regional feature. From the modelling point of perspective it is not possible to reproduce these very localized processes with a coupled AOGCM. Also applying statistical downscaling on the AOGCM output only yields moderate performance of downscaling models when establishing links between large-scale atmospheric circulation and local precipitation.

Future investigations will analyse the driving mechanisms responsible for the hydrological anomalous period of the LIA in southern South America in greater detail. Moreover, an ensemble of simulations carried out on the new generation of super computers will help to assess the trustworthiness and validity of results presented is this study. Analysis related to proxy data will comprise quantitative approaches in the upscaling of local proxy information. Both reconstruction approaches, i.e. proxy and model simulations, will then yield new results together with confidence intervals allowing the assessment of uncertainties and the potential range of climate change in the last millennium over southern South America.

Acknowledgments We thank the anonymous reviewer and Francoise Vimeux for their very valuable suggestions for improvement of the manuscript. The climate simulation of the last millennium with ECHO-G was carried out on a NEC-SX6 at the German Climate Computer Center (DKRZ).

References

Ariztegui D, Bösch P, Davaud E (2007) Dominant ENSO frequencies during the Little Ice Age in Northern Patagonia: The varved record of proglacial Lago Frías, Argentinia. Quat Int 161: 46–55

Bard E, Raisbeck G, Yiou F, Jouzel J (2000) Solar irradiance during the last 1200 years based on cosmogenic nuclides. Tellus 52B:985–992

Beck C, Grieser J, Rudolf B (2004) A new monthly precipitation climatology for the global land areas for the period 1951 to 2000. Tech. Rep. 18, Global Precipitation Climatology Centre c/o Deutscher Wetterdienst

Boës X, Fagel N (2008) Relationships between southern Chilean varved lake sediments, precipitation and ENSO for the last 600 years. J Paleolimnol 39:237–252

Boninsegna JA (1988) Santiago de Chile Winter Rainfall since 1220 as being Reconstructed by Tree Rings. Quat South Am Antarct Peninsula 6:67–87

Boninsegna JA (1995) South American dendrochronological records. In: Bradley RS, Jones PD (eds) Climate since A.D. 1500. Routledge, London

Bradley RS (1985) Quaternary Paleoclimatology. Methods of Paleoclimatic Reconstruction, Allen & Unwin, London

Cerveny RS (1998) Present Climates of South America. In: Hobbs JE, Lindesay JA, Bridgeman HA (eds) Climates of the Southern Continents – Present, Past and Future. John Wiley & Sons Ltd, Chichester

Clapperton CM (1983) The Glaciation of the Andes. Quart Sci Rev 2:83–155

Crowley TJ (2000) Causes of Climate Change over the past 1000 years. Science 289:270–277

Daley A (1998) The little Ice Age; was it big enough to be global. www.jrscience.wcp.muohio.edu, 20.05.2007

De Melo MLD, Marengo JA (2008) The influence of changes in orbital parameters over South American climate using the CPTEC AGCM: Simulation of climate during the mid Holocene. Holocene 18:501–516

Eddy JA (1976) The maunder minimum. Science 192:1189–1202

Etheridge D, Steele LP, Langenfelds RL, Freandcey RJ, Barnola JM, Morgan VI (1996) Natural and anthropogenic changes in atmospheric CO_2 over the last 1000 years from air in Antarctic ice and firn. J Geophys Res 101:4115–4128

Baruth B, Endlicher W, Hoppe P (1998) Climate and desertification processes in Patagonia. Bamberger Geographische Schriften 15:307–320

Fagan B (2000) The Little Ice Age: How Climate Made History 1300–1850. Basic Books, New York

Galloway RW, Markgraf V, Bradbury JP (1988) Dating shorelines of lakes in Patagonia, Argentina. J South Am Earth Sci 1:195–198

Glaser R (2001) Klimageschichte Mitteleuropas. 1000 Jahre Wetter, Klima, Katastrophen. Wissenschaftliche Buchgesellschaft, Darmstadt

Glasser NF, Hambrey MJ, Aniya M (2001) An advance of Soler Glacier, North Patagonian Icefield, at c. AD 1222–1342. Holocene 12(1):113–120

Glasser NF, Harrison S, Winchester V, Aniya M (2004) Late Pleistocene and Holocene palaeoclimate and glacier fluctuations in Patagonia. Glob Planet Change 43:79–101

Grove JM (1988) The little Ice Age. Methuen, London

Haberzettl T, Fey M, Lücke A, Maidana N, Mayr C, Ohlendorf C, Schäbitz F, Schleser GH, Wille M, Zolitschka B (2005) Climatically induced lake level changes during the last two millennia as reflected in sediments of Laguna Potrok Aike, southern Patagonia (Santa Cruz, Argentina). J Paleolimnol 33:283–302

Harrison S, Winchester V (1998) Historical fluctuations of the Gualas and Reicher Glaciers, North Patagonian Icefield, Chile. Holocene 8(4):481–485

Harrison S, Glasser N, Winchester V, Haresign E, Warren C, Jansson K (2006) A glacial lake outburst flood associated with recent mountain glacier retreat, Patagonian Andes. Holocene 16(4):611–620

Houghton J (1994) Globale Erwärmung. Fakten, Gefahren und Lösungswege. Springer-Verlag, Berlin

Jones PD, Osborn TJ, Briffa KR (2001) The evolution of climate over the last millennium. Science 292:662–667

Joussaume S (1996) Klima- Gestern, Heute, Morgen. Springer Verlag, Berlin

Kirchner I, Stenchikov GL, Graf H-F, Robock A, Antuña C (1999) Climate model simulation of winter warming and summer cooling following the 1991 Mount Pinatubo volcanic eruption. J Geophys Res 104(D16):19,039–19,055

Kistler R, Kalnay E, Collins W, Saha S, White G, Woollen J, Chelliah M, Ebisuzaki W, Kanamitsu M, Kousky V, van den Dool H, Jenne R, Fiorino M (2001) The NCEP/NCAR 50-year reanalysis: Monthly means CD ROM and documentation. Bull Am Meteorol Soc 82:247–267

Koch J, Kilian R (2005) "Little Ice Age" glacier fluctuations, Gran Campo Nevado, southernmost Chile. Holocene 15(1):20–28

Lamb HH (1965) The Early Medival Warm Epoch And Its Sequel. Palaeogeogr Palaeoclimatol Palaeoecol 1:13–37

Lamb HH (1970) Volcanic Activity And Climate. Palaeogeogr Palaeoclimatol Palaeoecol 10: 203–230

Lamb HH (1984) Some Studies of the Little Ice Age of Recent Centuries and its Great Storms. In: Mörner N-A, Karlén W (eds) Climatic changes on a yearly to millenial basis. D. Reidel, Dordrecht

Lamy F, Hebbeln D, Röhl U, Wefer G (2001) Holocene rainfall variability in southern Chile: A marine record of latitudinal shifts of the Southern Westerlies. Earth Planet Sci Lett 185: 369–382

Lara A, Villalba R (1993) A 3620-year temperature record from *Fitzroya cupressoides* tree ring in Southern South America. Science 260:1104–1106

Lean J, Beer J, Bradley R (1995) Reconstruction of solar irradiance since 1610: Implications of climate change. Geophys Res Lett 22(23):3195–3198

Legutke S, Voss R (1999) The Hamburg atmosphere-ocean coupled model ECHO -G. Technical Report 18, German Climate Computer Center (DKRZ), (available online http://www.mad.zmaw.de/fileadmin/extern/documents/reports/ReportNo.18.pdf)

Lund C, Lynch-Stieglitz J, Curry WB (2006) Gulf Stream weakened in 'Little Ice Age'. Nature 444:601–604

Luterbacher JE, Xoplaki D, Dietrich R, Rickli J, Jacobeit C, Beck D, Gyalistras C, Schmutz H Wanner (2002) Reconstruction of sea level pressure fields over the Eastern North Atlantic and Europe back to 1500. Clim Dyn 18:545–561

Markgraf V (1993) Paleoenvironments and paleoclimates in Tierra del Fuego and southernmost Patagonia, South America. Palaeogeogr Palaeoclimatol Palaeoecol. 102:53–68

Mayr C, Fey M, Haberzettl T, Janssen S, Lücke A, Maidana N, Ohlendorf C, Schäbitz F, Schleser GH, Struck U, Wille M, Zolitschka B (2005) Palaeoenvironmental changes in southern Patagonia during the last millennium recorded in lake sediments from Laguna Azul (Argentina), Palaeogeogr Palaeoclimatol Palaeoecol 228:203–227

Mayr C, Wille M, Haberzettl T, Fey M, Janssen S, Lücke A, Ohlendorf C, Oliva G, Schäbitz F, Schleser GH, Zolitschka B (2007) Holocene variability of the Southern Hemisphere westerlies in Argentiniean Patagonia (52°S). Quat Sci Rev 26:579–584

Mercer JH (1965) Glacier Variations In Southern Patagonia. Geogr Rev 55:390–413

Mercer JH (1970) Variations of some Patagonian glaciers since the Late glacial: II. Am J Sci 269:1–25

Mercer JH (1976) Glacial history of southernmost South America. Quat Res 6:125–166

Meyer I, Wagner S (2008) The Little Ice Age in southern Patagonia: Comparison between paleoecological reconstructions and downscaled model output of a GCM. PAGES news 16(2):12–13

Moy CM, Dunbar RB, Moreno PI, Francois J-P, Villa-Martínez R, Mucciarone DM, Guilderson TP, Garreaud RD (2008) Isotopic evidence for hydrologic change related to the weterlies in SW Patagonia, Chile, during the last millennium. Quat Sci Rev 27:1335–1349

Nunez MN, Solman SA, Cabre MF (2008) Regional climate change experiments over southern South America. II: Climate change scenarios in the late twenty-first century. Clim Dyn. doi:10.1007/s00382-008-0449-8

Piovano EL, Ariztegui D, Damatto Moreiras S (2002) Recent environmental changes in Laguna Mar Chiquita (central Argentina): A sedimentary model for a highly variable saline lake. Sedimentology 49:1371–1384

Robock A (2000) Volcanic eruptions and climate. Rev Geophys 38:191–219

Roeckner E, Arpe K, Bengtsson L, Christoph M, Claussen M, Dümenil L, Esch M, Giorgetta M, Schlese U, Schulzweida U (1996) The atmospheric general circulation model ECHAM4: Model description and simulation of present-day climate. Technical Report 218, Max Planck Institut für Meteorologie

Solman SA, Nunez MN, Cabre MF (2007) Regional climate change experiments over southern South America. I: Present climate. Clim Dyn 30:533–552

Stine S, Stine M (1990) A record from Lake Cardiel of climate change in southern South America. Nature 345:705–708

Thompson LG, Mosley-Thompson E, Dansgaard W, Grootes PM (1986) The little Ice Age as recordet in the Stratigraphy of the tropical Quelccaya. Science 234:361–364

Villalba R (1990) Climatic Fluctuations in Northern Patagonia during the Last 1000 Years as Inferred from Tree-Ring Records. Quat Res 34:346–360

Villalba R (1994) Tree-Ring and Glacial Evidence for the Medival Warm Epoch and the Little Ice Age in Southern South America. Clim Change 26:183–197

Villalba R, Lara A, Bonninsegna JA, Masiokas M, Delgano M, Aravena J, Roig FA, Schmelter A, Wolodarsky A, Ripalta A (2003) Large-Skale Temperature Changes Across The Southern Andes: 20th-Century Variations In The Context Of The Past 400 Years. Clim Change 59: 177–232

Vimeux F, Gallaire R, Bony S, Hoffmann G, Chiang JCH (2005) What are the climate controls on δD in precipitation in the Zongo Valley (Bolivia)? Implications for the Illimani ice core interpretation. Earth Planet Sci Lett 240:205–220

von Storch H, Zorita E, Jones JM, Dmitriev Y, González, F, Tett SFB (2004) Reconstructing past climate from noisy data, Science 306:679–682

Vuille M, Werner M (2005) Stable isotopes in precipitation recording South American summer monsoon and ENSO variability: Observations and model results. Clim Dyn 25:401–413

Wagner S, Widmann M, Jones J, Haberzettl T, Lücke A, Mayr C, Ohlendorf C, Schäbitz F, Zolitschka B (2007) Transient simulations, empirical reconstructions and forcing mechanisms for the Mid-Holocene hydrological climate in Southern Patagonia. Clim Dyn 29:333–355

Weischet W (1996) Regionale Klimatologie. Teil 1. Die NeueWelt: Amerika, Neuseeland, Australien: Teubner Studienbücher der Geographie, Stuttgart

Wolf J, Maier-Reimer E, S. Legutke (1997) The Hamburg Primitive Equation Model HOPE. Technical Report 18, German Climate Computer Center (DKRZ)

Zolitschka B, Schäbitz F, Lücke A, Corbella H, Ercolano B, Fey M, Haberzettl T, Janssen S, Maidana N, Mayr C, Ohlendorf C, Oliva G, Paez MM, Schleser GH, Soto J, Tiberi P, Wille M (2006) Crater lakes of the Pali Aike Volcanic Field as key sites for paleoclimatic and paleoecological reconstructions in southern Patagonia, Argentina. J South Am Earth Sci 21:294–309

Zorita E, von Storch H, González-Rouco F, Cubasch U, Luterbacher J, Legutke S, Fischer-Bruns I, Schlese U (2004) Climate evolution in the last five centuries simulated by an atmosphere-ocean model: Global temperatures, the North Atlantic Oscillation and the Late Maunder Minimum. Meteorologische Zeitschrift 13(4):271–228

Index

A

Accelerator mass spectrometry, 135, 313
Adiabatic heating, 162
Africa, 4, 102, 208–209, 260, 261, 269
AGCM, 5, 165, 215, 216, 217
Albedo, 62, 145, 215, 217, 218, 219, 225, 228, 232, 233, 234, 235, 268, 408
Alkenones, 131, 135, 136, 138, 139, 140, 141, 142, 143, 144, 146, 381, 382, 385
Altiplano, 12–13, 14, 19, 48, 50, 64–65, 73, 74, 75, 81, 90, 96–97, 106, 107, 194, 195, 201, 203, 204, 206, 214–215, 241, 250–251, 252, 263, 265, 286, 303, 304, 308–317, 318f, 319
Amazon basin, 4–5, 11–12, 16–17, 19–20, 30–31, 33, 34–35, 47, 48–49, 50, 55, 64–65, 98–99, 102–103, 104, 105, 107, 194–195, 196–197, 198, 201, 203, 204, 206, 207, 214–215, 216–217, 227–228, 230, 231, 234, 235, 241, 245–246, 260, 269, 302, 303, 311, 312, 317, 328
Amazon fan, 16, 91, 98–99, 104, 106, 107, 108, 214, 246
Amazonia, 6, 10, 11–12, 19, 38, 90, 98–100, 101, 102–105, 108–109, 196–197, 203, 207, 219, 224, 228, 229, 230, 284–285, 286, 287, 288–291, 292–295, 296, 319
AMS, 66, 115, 135, 244, 245, 328
Andes, 6, 10, 12–14, 16, 18, 19, 20, 31, 33, 54, 61–81, 90, 96, 97, 101, 107, 118–119, 133–134, 194–195, 196–197, 198, 201, 203, 204, 206, 241, 245, 246, 247, 248, 250, 251, 252, 260, 261, 263, 265, 269–273, 285, 286, 287t, 292–296, 304–305, 307, 308, 312, 317, 319, 323–324, 325–328, 333–334, 336, 345, 354, 358, 363, 369–370, 373, 381, 383, 384, 398, 399–400, 402, 404, 408, 409
Antarctica, 81, 133, 139, 140, 143–145, 149, 151, 241, 243, 246–247, 333, 354, 361, 363, 364, 367, 370, 371–372, 385, 396–397, 398
Antarctic Circumpolar Current (ACC), 130, 132, 381, 385
Antarctic Cold Reversal (ACR), 72, 81, 143, 241, 242, 247, 248
Antarctic Oscillation (AAO), 169, 302, 355, 361–363
Argentina, 9t, 10, 14–15, 62, 64, 76–78, 263, 265, 268, 269, 276, 277, 323–346, 380, 401
Arid diagonal, 65, 74, 324, 325, 326, 344, 345
Atacama, 9, 14, 19, 138, 149–151
Atlantic forest, 89, 100–101, 107
Atlantic Meridional Overturning Circulation (AMOC), 143, 215

B

Baroclinic instability, 160, 227, 230, 233, 358
Bella Vista, 8, 11–12, 92, 98, 99, 214, 285, 286, 287, 289, 290–291, 295
Biomes, 11, 31, 54, 89, 93, 94, 95, 101, 102, 106, 107, 108, 262, 263, 269, 275
Bolivia, 8t, 9t, 12–14, 16–17, 19, 62, 64, 68–74, 90, 91, 92t, 99, 214–215, 243, 246, 273, 286, 304, 311, 325
Bolivian high, 49, 63, 64, 73, 201, 204
Bølling-Allerød (BA), 121, 235, 241, 248
Botuverá, 8, 12, 32, 35, 36, 38, 41, 42–43, 46, 48, 51, 53, 240, 242, 246, 250, 306, 307
Boundary layer, 203, 228, 230, 232, 234
Brazil, 8t, 10, 11–12, 16, 17, 18–19, 20, 29–55, 73, 91t, 92t, 99, 100–101, 107–108, 162–164, 171, 172–173, 177, 178, 181–183, 184, 185–186, 203, 204, 205, 206, 207, 209, 214–216, 217, 227, 228, 229, 230, 231, 232, 260, 263, 264–265,

F. Vimeux et al. (eds.), *Past Climate Variability in South America and Surrounding Regions,* Developments in Paleoenvironmental Research 14,
DOI 10.1007/978-90-481-2672-9_BM2, © Springer-Verlag Berlin Heidelberg 2009

267, 269–273, 275–276, 277, 286, 302, 307, 325

C
^{13}C, 38
^{14}C, 6, 13, 66, 71, 72, 73, 76, 77, 114, 115, 125, 135, 244, 245, 313, 327, 328, 371, 375, 376, 377, 378, 387, 402
Caço, 8, 11–12, 16–17, 70, 91, 92, 100, 106, 244, 246, 275, 293, 296, 307, 312
Campos, 91, 92, 95, 100, 101, 105, 107
Cape-Horn Current (CHC), 132
Carajas, 8, 11, 92, 98, 214, 275
Cardiel, 9, 16, 325, 333, 336, 337, 343, 344, 354, 368–369, 384, 399, 400–401
Cariaco, 8, 11, 17–19, 32, 45, 48, 51, 115, 117, 135, 209, 214, 235, 240, 241, 242, 260, 276, 293, 304, 306, 307, 308
Cari Laufquen, 9, 16
Caserococha, 285, 286, 287, 288, 289, 292–294
Central America, 4, 11, 13, 62, 113–126, 214–215, 250, 263
Central Andes, 12–14, 18–19, 62, 197, 203, 204, 206, 292–293, 324
Cerro Aconcagua, 63–64
Chaco, 31, 263
Chaco Low, 6–10, 63, 64–65, 201, 205, 325–326
Chalalán, 285, 286, 287, 289, 291, 294, 295, 296
Chaplin, 8, 11–12, 91, 98, 99, 104, 105, 107, 285, 286, 287, 289, 291, 293, 295
Charcoal, 90–93, 94, 105, 106, 113, 116, 117, 290, 295, 357, 366, 369–371, 369, 370, 371, 387
Chile, 9t, 12–14, 16, 62, 74, 75–76, 78, 81, 129–151, 208, 325, 359, 361t, 380, 399–400
Chilean lake district, 9, 15, 63, 76, 81, 141–142, 370, 371
Chochos, 285, 286, 287, 288–290, 292–294, 295
Clausius-Clapeyron, 229, 234
Cloud forest, 12, 91, 95, 96–97, 100, 105, 106, 290
CO_2, 16, 17, 38, 39, 47, 89, 90, 93, 101, 102, 103, 104, 105, 106, 107, 108, 130, 144, 145, 215, 218, 284, 355, 363, 405
Coipasa phase, 73–74, 241
Colombia, 11, 91, 100, 101–102, 162–164, 214, 263, 269, 276, 292–293
Colônia, 8, 12, 376
Consuelo, 90, 91, 96–97, 285, 286, 287, 289, 291, 293–294, 295, 296
Cordillera occidental, 64–65, 75
Cordillera oriental, 64–65, 80, 307
Cosmogenic nuclides, 66
Coupled model, 216, 224, 262
Coyhaique, 354, 359, 360, 361, 363, 366

D
Dansgaard/Oeschger, D/O events, 30, 48, 235
Deforestation, 202, 295, 365
Deglaciation, 13–14, 70, 71, 76, 78, 79, 90, 116, 119, 141, 142, 145, 235, 239–252, 291, 292, 336
Deuterium, 140
Diatoms, 12, 113, 121, 288, 293, 312, 313, 315, 316, 328, 331, 369, 381
Dome C, 130, 140, 143, 144, 149, 240, 242, 243, 289
Dronning Maund Land, 139, 143
Dry forest vegetation, 95, 99, 100, 101, 102, 103, 104, 106, 108, 291
Dry grassland, 101, 106
Dunes, 339, 341
Dust deposition, 50

E
Easterlies, 11, 74, 165
Ecological changes, 283–296, 387
Ecosystems, 3, 4, 16, 17, 20, 90, 93, 99, 100, 101, 102, 103, 104, 107, 108, 142, 283, 286, 296, 328
Ecuador, 8, 11, 162, 206, 296, 307
Eddies, 227, 269, 358
El Niño-Southern Oscillation (ENSO), 5, 6, 33, 34, 53, 74, 133, 151, 159, 161, 164, 171, 173, 175, 206, 213, 227, 232, 235, 245, 290, 302, 307, 309, 326, 345, 355, 359, 361, 400
El Pinal, 91, 100, 101, 107, 214
El Valle, 8, 11, 119, 120, 121, 123, 214
EPICA, 130, 139, 140, 141, 143, 147, 149, 240, 242, 243–244
Equilibrium-line altitude (ELA), 14, 65, 118, 125, 126
Evaporation, 19, 33, 107, 173, 175, 194, 198, 199, 200, 202, 203, 207, 251, 303, 306, 313, 314, 329, 331, 365, 366, 367, 385, 386
Exposure ages, 66, 67–79, 80, 372
Extra-tropics, 19, 227
Extreme events, 340

F
Feedback, 55, 62, 145, 170, 175, 186, 201, 202, 207, 215, 227, 230, 231, 234, 250,

253, 259, 261, 265, 268, 273, 277, 303, 408
Fire, 89–109, 116, 142, 284, 288, 290, 292, 294, 295, 296, 369–370, 371
Floods, 161, 178, 340, 396
Forcing orbital, 3, 125, 277, 403, 407
Fossil pollen, 90, 98, 100, 101, 103, 107, 113, 116, 117, 119, 120, 285
Frias, 325, 333, 334–336, 375, 380, 399, 401
Fuquene, 8, 11, 91, 97–98, 106, 214

G

General circulation model, 5, 17, 30, 34, 145, 215, 217, 261, 403, 405, 406
GeoB, 131–132, 134, 135, 146–147, 148–149, 150, 151, 354, 381, 382, 385, 386
GeoB 3202–1, 8
GeoB 3229–2, 8
GeoB 3302–1, 9
Geochemistry, 38
Geomorphology, 15, 62, 67–68, 277, 328, 332, 396, 399, 400, 402–403
GISP, 45, 244, 289, 292–293
Glacial advance, 62, 70, 71–73, 74, 75, 78–79, 81, 119, 372–373, 374, 402
Glaciers, 13–14, 15, 16, 61, 62, 63–64, 65, 68, 70, 72–73, 75, 76, 78, 79, 80, 81, 113, 118, 126, 136, 141, 143, 243, 333–336, 354, 371–373, 375, 376, 377, 378, 380, 384, 385, 402, 403
Grassland, 12, 17, 31, 54, 91, 92, 97, 100, 101, 102, 105, 106, 107, 119, 369
Greenhouse gases, 62, 79, 80, 145, 217, 218, 229, 234, 383
Greenland, 45, 50, 51, 117, 121, 139, 141, 143–144, 218, 235, 241, 242, 243, 246–248, 396–397
Groundwater, 35, 39, 44, 329, 366
Guanaco, 354, 357, 364–368, 370, 383–384, 385–387, 401
Guatemala, 113–126

H

Hadley cell, 18, 31, 48, 51, 123, 151, 161, 162, 170, 173, 177, 213, 216, 217, 224, 227, 228, 230, 231, 232, 233, 234, 235, 249
Hadley circulation, 18, 51, 53, 161–165, 167, 169, 172, 216, 222, 224, 227, 233, 249
Heinrich events, 19, 29, 43, 44, 48, 51, 55, 79, 123, 124, 304, 307
Holocene, 13, 30, 31, 43, 48–49, 53, 54–55, 73–74, 97–98, 102, 114, 118, 120–121, 122, 125, 129–151, 194, 195, 205, 206–207, 208, 213–215, 240, 241, 243–248, 251, 259–278, 284, 288–290, 291, 293–296, 301–319, 323–324, 326–328, 331, 332–334, 336–338, 342, 343–344, 346, 357, 368, 369, 372, 373, 381, 383–384, 385, 387, 396, 403, 407, 408–409
Huara Loma Valley, 71
Huascarán, 8, 13, 130, 147, 149–151, 214, 240, 242, 243, 244, 245, 247, 248, 250, 251, 252, 306, 318
Huelmo, 9, 15, 334
Humboldt current, 10, 130
Humidity, 3, 17, 18, 20, 64, 118, 175, 195, 198, 203, 204, 216, 228, 229, 246, 249, 310, 313, 316, 346, 401
Hydrological cycle, 29, 30, 33, 145, 249, 251, 261
Hydrology, 38, 151, 186, 214, 305, 326, 364

I

Ice caps, 33, 118, 243, 333, 334, 335, 402
Ice core, 8, 9, 13, 19, 33, 34, 45, 50, 54, 62, 103, 117, 121, 130, 139, 140, 141, 143, 144, 145, 147, 149, 151, 218, 239–252, 304, 306–307, 310, 311, 312, 317–318, 367, 396, 399, 402–403, 405, 407
Ice sheets, 3, 15, 16, 90, 123, 131, 132, 134, 136, 137, 138, 141, 142, 149, 213, 215, 216, 217, 218, 227, 233, 234, 235, 249, 372, 384
Illimani, 9, 13, 214, 240, 242, 243–244, 245, 247, 248, 250, 251, 252
Insolation, 17, 29, 30, 31, 42, 43, 44, 46, 47, 48, 49, 52, 53, 54, 55, 62, 73, 78, 80, 121, 122, 123, 124, 125, 145, 193, 195, 215, 218, 242, 249, 260, 261, 262, 265, 269, 277, 301, 304, 305, 307, 317, 319, 344, 409
Instrumental records, 302, 303, 345, 346, 355, 379, 380, 384
Intertropical Convergence Zone (ITCZ), 3, 4, 17, 29, 30, 32, 48, 51, 73, 151, 197, 214

L

Lago Buenos Aires (LBA), 63, 65, 76–78
Lake sediments, 5, 62, 76, 79, 113, 319, 328, 344, 354, 357, 364–369, 385, 398, 400, 403
La Niña, 34, 133, 151, 164, 206, 251, 290, 296, 383
Last Glacial Maximum (LGM), 3–17, 19, 30, 55, 61–81, 89–109, 113–126, 130–131, 132, 134, 136, 137, 138, 139–140,

213–235, 240, 283–296, 303–304, 305–307, 324, 328, 333, 342–343
Last millennia, 50
Lejia, 9, 14
Little Ice Age (LIA), 308, 324, 338, 342–344, 355, 395–409
Llanos, 91, 100, 101, 107, 276
Loess, 328
Lowland, 16, 17, 19, 33, 90, 91, 92, 98–101, 102, 103, 106, 107, 108, 113–126, 203, 204, 246, 284, 286, 287, 288, 289, 290, 291, 292, 295, 325, 384
  forest, 106, 107
Low level jet, 6, 34, 51, 64, 201, 269, 325, 328, 343, 344

M
Madden-Julian Oscillation, 179, 181, 205
Magnetic susceptibility, 71, 115, 116, 117, 135, 336
Mar Chiquita, 9, 15, 324, 325, 326–328, 329–331, 338–339, 343, 344, 345, 399, 401
MARGO, 217, 224, 225, 226, 234, 235
Marine Isotope Stage (MIS), 44, 50, 52, 53, 54, 62, 78, 80, 116, 119, 121, 137
Marine sediments, 75, 78, 130, 131, 139, 293, 380
Mascardi, 325, 333–334, 343, 344
Maunder minimum, 396, 405
Medieval climate anomaly, 355
Medieval warm period, 338
Meridional mode, 208, 215, 216, 234
Meteoric water line, 35
Mexico, 116, 118, 119, 121, 124, 126
Mg/Ca, 31, 38–39, 40, 44–47, 49, 50, 52, 55, 139, 146, 249
Middle Holocene, 146, 148, 149, 150, 151, 275, 305, 315, 324, 331, 343, 344, 346, 372
Mid-Holocene Dry Episode (MHDE), 284, 293, 294, 296
Milankovitch cycles, 48
Millennial scale, 18, 19, 29–55, 72, 79, 80, 136, 139, 143, 149, 283–296, 301–319, 383, 384
Milluni Valley, 70–71
Miscanti, 9, 14
Modeling, 3, 16, 17, 19, 31, 51, 73, 75, 138, 160, 161, 173, 207, 260, 262, 317, 367
Moist adiabat, 220, 222
Moist instability, 230
Monsoon, 3, 5, 6, 18, 30, 31, 32, 33, 34, 38, 39, 44, 45, 47, 48, 49, 51, 52, 54, 55, 73, 164, 178, 195, 197, 202, 203, 204, 206, 207, 208, 215, 216, 219, 235, 245, 246, 249, 250, 260, 261, 269, 304, 307, 317, 325, 343, 345
Moraines, 54, 64, 65, 67, 68, 70, 72, 73, 74, 75, 76, 78, 80, 119, 288, 372, 373, 402
Multiproxy studies, 336

N
Nordeste, 11–12, 16–17, 194, 205–206, 207, 208, 209, 214–216, 217, 227, 228, 229, 230, 231, 232, 234, 241, 246, 304, 307
North Atlantic, 4–5, 6, 17–19, 34–35, 49–50, 51–53, 55, 72, 73, 123, 144, 185, 205–206, 207, 208, 215–216, 241–243, 248, 250, 252, 277–278, 292–293, 302–304, 307, 308, 317, 318, 319
  deep water, 4
  oscillation, 6, 34, 317
  surface Water, 4
NorthGRIP, 242, 243–244, 246, 248

O
^{18}O, 38, 310
OAGCM, 215, 216, 217
Obliquity, 218
Ocean-atmosphere interactions, 162, 175
Ocean Drilling Project (ODP), 8, 11–12, 45, 98, 99, 129–151, 214
Ostracods, 364
Oxygen isotopic model, 313–315

P
Pacific Decadal Oscillation (PDO), 6, 302
Pallcacocha, 296, 307
Pampean lakes, 323
Pampean plains, 323–324, 326–333, 338, 341, 343, 345, 346
Panama, 8, 11, 119, 120, 121, 123, 214, 263
Paramo grasslands, 119
Parana Plata basin, 10, 15
Pata, 8, 11, 16–17, 91, 98–99, 106, 107, 108–109, 214, 285, 286, 289, 290, 292, 293, 295, 296
Patagonia, 16, 62, 65, 67, 77–78, 80, 81, 142–143, 205, 241, 323–346, 353–354, 355–357, 358–359, 360–361, 362, 363, 364, 367–368, 369–370, 372, 373, 374–380, 383–384, 385–387, 398–401, 402–403, 404, 405–406, 407, 408
Patagonian Andes, 65, 76–79
Patagonian Ice Sheet (PIS), 131, 132, 134, 135, 136, 137, 138, 141, 142

Peru, 8t, 12–14, 33, 62, 64, 68–74, 91t, 130–131, 132–133, 138, 139, 162–164, 206, 214f, 288, 296, 301–319, 326, 402
Peru-Chile Current (PCC), 130, 131, 132, 138, 139, 148, 151
Petén Itzá, 113–126
PMIP, 260, 261, 265
Polar air masses, 124
Pollen, 5, 11–12, 15, 16–17, 19, 54, 75, 76, 90–91, 93, 94, 95–101, 103, 104, 106, 107–108, 113–114, 116–118, 119, 120, 125, 131, 135, 136, 137, 142–143, 194, 276, 285, 286, 287, 289, 291, 326, 333–334, 336, 354, 357, 364, 366, 367, 369–371, 384, 385, 387, 398, 399, 400, 401, 403
Potential temperature, 219, 220, 221, 226, 227, 228, 230, 233
Potrok Aike, 333, 354, 359, 367–368, 369–370, 384, 385–387, 399, 400–401
Precession, 17, 30, 47, 48, 121, 122, 218, 249, 251
Productivity, 105, 138, 148, 149
Proxies, 4, 6, 17, 18, 20, 26, 62, 125, 148
Puerto Montt, 133, 134, 354, 358, 359, 360, 361
Puno, 308, 309–310, 312

Q

Quaternary, 13, 15, 62, 80, 99, 100–101, 126, 131, 284, 304, 305–308, 319, 367
Quebrada del Torro, 9
Quelccaya, 33, 307, 308, 310–311, 312, 318, 399, 402

R

Radiocarbon, 15, 71, 73, 76, 77, 78, 114, 135, 139, 140, 146, 199, 291, 327, 328, 368
Rainforest, 12, 17, 19, 31, 48, 91, 98, 99, 100, 101, 102, 104, 105, 106, 108, 275, 369, 370
Rainforest leaf area index (LAI), 104
Reservoir effects, 73, 142, 369
Residence time, 39
Rio Gallegos, 354, 359, 360, 361
Rio Suturi Valley, 71
River discharge, 328, 345
Rossby wave, 160, 161, 165, 166, 167, 168, 169, 170, 171, 172, 175, 178, 179, 185, 206

S

Sajama, 9, 13, 96, 151, 214, 240, 242, 243–244, 245, 247, 248, 250–251, 252
Salar, 9, 12–13, 14, 19, 32, 50, 63, 64, 73, 91, 96–97, 240, 242, 246, 250, 332–333
Salcedo, 308, 309
Salinas del Bebedero, 9, 16, 325, 328, 331–333, 342–343, 344
Salinity, 134, 151, 155, 316, 329, 381, 382
  sea surface, 4, 5, 10, 30, 48, 64, 74, 107, 131, 135, 160, 162, 205, 219, 222, 241, 301, 303, 343, 358, 381, 382, 406, 407
San Francisco Valley, 69, 70–71, 73
Santa Maria, 9, 15
Santana, 8, 12, 32, 35, 36–37, 38, 39, 40, 41, 42–43, 47, 48, 49, 240, 246
Santa Rosa, 285, 286, 287, 289, 291, 294, 295, 296
Savanna, 11, 17, 31, 54, 90, 92, 98, 99, 100, 102, 103, 104, 105, 107, 108, 276, 284, 290
Sea level, 5, 14, 65, 67, 90, 94, 95, 108, 113, 119, 173, 218, 261, 358, 372, 404
Sea surface temperature, 4, 5, 6, 10, 30, 48, 64, 74, 107, 123, 131, 135, 160, 162, 205, 215, 219, 222, 241, 301, 303, 358, 381, 406
Solar activity, 396, 405, 407, 409
South American Summer Monsoon (SAMS), 3, 6, 31, 33, 38, 39, 47, 51, 54, 73, 195, 245, 249, 304, 307, 317, 325
South Atlantic Convergence Zone (SACZ), 6, 47, 179, 196, 219, 260, 325, 343
South Eastern South America (SESA), 325–326, 343, 345, 395, 406
Southern Annular Mode (SAM), 169, 302, 361–363
Southern Brazil, 10, 12, 16–17, 20, 34–35, 46f, 47, 48–49, 50, 51–53, 54, 55, 177, 178, 203, 206, 216, 264–265, 277
Southern hemisphere, 4–5, 15, 30–31, 44, 48–49, 54, 55, 72, 123–124, 130, 131, 133, 141, 143–144, 162, 169–171, 172, 179–181, 195, 204, 205, 216, 230, 240, 241–243, 249, 260, 265, 269, 277, 313, 344, 355, 357, 358, 359, 360, 364, 371–372, 373, 374, 383, 397, 398, 408
Southern Oscillation Index (SOI), 303, 361
Southern Westerly Wind belt (SWW), 130, 131, 132, 133, 138, 140, 144, 145, 149, 150, 151
Speleothems, 5, 8, 12, 17, 29–55, 73, 194, 214, 246, 304, 306–307
Sr/Ca, 31, 38–39, 40, 44–47, 49, 50, 52, 55
Stable isotopes, 31, 33, 34, 41, 245, 247, 251, 252, 289, 336, 364, 381

Stalagmites, 12, 36, 38, 39, 42–43, 44, 45, 46, 47, 49, 53
Static stability, 216, 217, 219, 220, 221, 222, 224, 226, 228, 230, 232, 234, 235
Subsidence, 18, 51, 161, 162, 164, 173, 176, 177, 183, 206, 209, 213, 216, 217, 227, 230, 232, 233, 234, 249, 358
Subtropical high pressure cell, 133
Subtropical jet, 167, 169, 176, 231, 234
Surface exposure dating, 14, 61–81

T
Tauca phase, 19, 73, 241, 251
Teleconnection, 49, 80, 159–186, 208–209, 213–235, 249, 252, 302, 326, 345, 361, 363, 383
Tephra, 369
Termination, 1, 134, 139, 141–146
Thermohaline circulation, 215, 250
Tierra del Fuego, 62, 65, 76–79, 333, 353–354, 360, 373
Time-series, 54
Titicaca, 9, 12–13, 63, 71, 91, 96–97, 106, 214, 246, 285, 286, 287, 288, 289, 293–294, 295, 305, 306, 308, 309, 310, 311, 314
Torres del Paine, 63, 77, 78, 354, 359, 360, 361, 363, 364, 373, 388
Trade winds, 10, 161, 173, 263
Transfer functions, 97, 136
Tree line, 107, 295, 402
Tree rings, 33, 335, 338, 354, 357, 372, 373–380, 384, 385, 387, 396, 399
Tropical lowland, 16–17, 19–20, 90, 246
Tropics
  -high latitudes, 161–169
  -tropics, 161–169, 175, 183
Troposphere, 161, 162, 166, 173, 203, 218, 221, 224, 227, 228, 231, 235, 358, 397, 398, 408

U
Umayo, 301–319
Upwelling, 132, 133, 138, 142, 145, 150, 222
Uranium, 41, 46
Uyuni, 9, 12–13, 19, 32, 50, 63, 64, 73, 91, 96–97, 240, 242, 246, 250

V
Vegetation, 11, 20, 54, 89–109, 114, 116, 118, 119, 122, 123, 124, 142, 200, 202, 215, 218, 260, 261, 262, 263, 266, 268, 269, 273, 274, 275, 277, 278, 286, 288, 290, 291, 293, 294, 295, 296, 340, 354, 364, 366, 367, 369, 370, 385, 386, 398, 401, 403
  model, 90, 93, 97, 99, 101, 103, 107, 108, 260, 262
Velocity potential, 219, 223, 224, 226, 227
Venezuela, 4–5, 8, 11, 30, 48–49, 115, 162–164, 172–173, 205–206, 214, 235, 276, 307

W
Walker cell, 162, 164, 183, 245
Walker circulation, 161, 162, 164, 168, 173, 183, 206, 217, 222, 224, 227, 228, 231, 232, 233, 234, 249
Warm pool, 145, 146, 147, 151, 162, 217
Water stable isotopes, 245, 247, 251, 252
Westerlies, 10, 15, 16, 19, 65, 75, 76, 78, 79, 81, 124, 125, 148, 169, 170, 178, 185, 336, 337, 342, 344, 346, 355, 357, 359, 363, 364, 365, 367, 368, 372, 381, 383, 384, 385, 386, 397, 398, 407
Woodland, 100, 101, 102

Y
Younger Dryas (YD), 71–72, 124, 142, 240, 244, 250, 284, 288, 289, 292, 307, 308, 334

Z
Zongo Valley, 69, 70–71, 311